SELF-HEALING ABILITY AND BEHAVIOUR OF CEMENTED PASTE BACKFILL

Submitted by

Weizhou Quan

Under the supervision of

Dr. Mamadou Fall

Thesis submitted to the University of Ottawa
in partial fulfillment of the requirements for the
Doctorate in Philosophy degree in Civil Engineering

Department of Civil Engineering
Faculty of Engineering
University of Ottawa

Abstract

Cemented paste backfill (CPB), as an innovative cementitious material, has been extensively employed to cost-effectively manage mine wastes, ensure workplace safety, and improve mine productivity in the mining industry from a sustainable perspective. CPB is an engineered mixture typically consisting of dewatered tailings (70-85 wt.%), hydraulic binder (3-7 wt.%), and water to achieve a homogeneous paste. It is usually prepared in a plant located at the surface of a mine site and transported to refill the underground mined-out stopes and voids.

CPBs are designed to satisfy an adequate load-bearing capacity for safe mining operations. The primary geotechnical performance criterion of CPB is mechanical stability, which ensures resistance against deformation and prevents failure, thereby stabilizing surrounding rock masses. In parallel, the low permeability of CPB, as an essential environmental design criterion, plays a pivotal role in ensuring structural stability and long-term durability by minimizing the migration of aggressive chemicals or contaminants that could otherwise weaken the CPB structure and pollute groundwater systems. Upon placement, both mechanical and permeability properties are governed by complex multiphysical processes, including thermal (T), hydraulic (H), mechanical (M), and chemical (C) processes. However, cracks may initiate in the CPB matrix as a result of various factors, such as shrinkage, sulphate attack, initial structural defects, excessive overburden pressure, stresses induced by surrounding rocks and ground movement, rock bursts, or combined effects of these conditions, during the curing stage under the interaction of the multiphysical processes. The progressive generation and propagation of cracks can severely deteriorate the integrity of the CPB matrix, impairing its mechanical stability, environmental performance, and serviceability. Moreover, CPB structures often extend tens to hundreds of meters underground in at least one dimension, which makes manual maintenance and repair of cracks in CPB structures infeasible in practical manners. Given that, self-healing in CPB has been proposed as a promising strategy to mitigate crack-induced deterioration. Yet, existing studies are scarce, focusing primarily on autonomous self-healing with externally added agents, while the intrinsic autogenous self-healing behaviour of CPB remains unexplored. Furthermore, the effects of different factors (e.g., multiphysical THMC factors) on the autogenous self-healing capacity and performance of CPBs have not been comprehensively evaluated, presenting a critical research gap.

This Ph.D. study addresses this gap through a series of systematic experiments investigating the autogenous self-healing behaviour of CPB under a wide range of factors/conditions, including age of cracking, pre-cracking level, crack width, self-healing period, thermal (e.g., healing/curing temperature), hydraulic (e.g., drainage condition), mechanical (e.g., different crack-inducing stresses), chemical (e.g., sulphate content), as well as addition of mineral additives (e.g., blast furnace slag and fly ash). Self-healing efficiency was evaluated based on crack closure observations, recovery of mechanical properties (e.g., uniaxial

compressive strength, deviator stress, indirect tensile strength), recovery of permeability (e.g., hydraulic conductivity), changes in physical properties (e.g., porosity, void ratio), and characterization of self-healing products. Results demonstrate that CPB exhibits a promising autogenous self-healing capability, which is mainly attributed to the precipitation of self-healing products, primarily consisting of C-S-H, $CaCO_3$, $Ca(OH)_2$, ettringite, and/or gypsum (under sulphate exposure). The relative proportions of these products vary considerably under different self-healing conditions. Both the age of cracking and the self-healing period significantly influence the self-healing efficiency of CPBs. The initiated cracks within the CPB matrix can ameliorate the hydration reactions, favouring the self-healing performance. Elevated curing temperatures (e.g., 35 °C and 50 °C) significantly accelerate the self-healing process via enhanced binder hydration, whereas low temperatures (e.g., 2 °C) exhibit negligible self-healing performance. Internal sulphate exposure exerts either positive or negative effects depending on sulphate concentration and self-healing duration. Improved drainage enhances self-healing performance through the combined effects of increased hydration and microstructural refinement. In the same way, shear cracks generated under confinement and tensile cracks with small apertures show favourable healing performance due to advantageous crack geometry within the matrix. Moreover, the impacts of incorporating mineral additives (e.g., blast furnace slag and fly ash) on self-healing performance are reflected in their contributions to binder hydration mechanisms and associated microstructural modifications. To validate and extend these findings, natural mine tailings with diverse mineralogical compositions were also tested under site-specific CPB formulations.

The findings of this research provide fundamental insights into the autogenous self-healing mechanisms of CPB, with significant implications for improving structural design, mechanical stability, permeability, durability, and environmental performance under field-relevant conditions. This work also demonstrates a comprehensive scientific basis for linking laboratory observations to engineering practice and for advancing the long-term sustainability of CPB systems in underground mining.

Acknowledgement

First and foremost, I would like to express my deepest gratitude to my supervisor, Dr. Mamadou Fall, for his invaluable guidance, encouragement, and patience throughout my doctoral studies. His passion, dedication, perseverance, and rigorous approach to research have profoundly shaped this dissertation and my way of thinking as a researcher, and they will continue to inspire me throughout my life. I feel truly fortunate to have had the opportunity to learn from him.

I would also like to extend my sincere gratitude to my doctoral committee members: Dr. Hassan Aoude, Dr. Rozalina Dimitrova, Dr. Muslim Majeed from the University of Ottawa, and Dr. Shahid Azam from the University of Regina. Their careful evaluation and constructive advice have greatly improved not only this dissertation but also my broader understanding of the field.

My thanks also go to Mr. Jean Claude Célestin, the technical officer of the Geotechnical Engineering Laboratory at the University of Ottawa, for his essential support and assistance throughout this research. I am especially thankful to my colleagues, Hongbin Liu, Zhe Liu, Feifan Wang, and Vyom Abhinav, for their friendship, late-night discussions, shared frustrations, and countless hours we spent together in the lab and office. Their companionship made the demanding times more manageable and the joyful moments more memorable. I am also grateful to Dr. Hassan Aoude, with whom I have worked on departmental work over the past years; even a simple compliment or kind word from him was often enough to encourage me when things felt overwhelming.

Most importantly, I owe my deepest gratitude to my family and friends. To my parents, Yong Quan and Xiaoling Hu, who have always loved and supported me in every way they could, I am because you are. To my grandparents, whose legacy of love inspires me every day and will forever be cherished in my heart. To my buddies, Guanhua Xun, Yupiao Zou, Chongyang Bi, Shuai Tian, Shuo Fang, Jingyi Chen, Quan Zhang, and Jinqiao Wang, who stand by me not only as supporters of my academic journey but also as companions in countless experiences beyond academia. You have been my unwavering source of strength, and all of you complete me.

Finally, I want to acknowledge myself for holding on through countless moments of self-doubt, embracing the challenges, and continuing to shape my story with patience and determination.

“你当时相信的那些事情 会在如今变成美丽风景”

Table of Contents

List of Figures

List of Tables

List of Symbols and Abbreviations

G_s	Specific gravity
C_u	Coefficient of uniformity
C_c	Coefficient of curvature
e	Void ratio
n	Porosity
w/c	Water-to-cement ratio
w/b	Water-to-binder ratio
c/a	Cement-to-additive ratio
σ_v	Vertical stress
C-S-H	Calcium silicate hydrate
CH	Calcium hydroxide
CC	Calcite
C_3A	Tricalcium aluminate
C_2S	Dicalcium silicate
C_3S	Tricalcium silicate
CPB	Cemented paste backfill
AMD	Acid mine drainage
UCS	Uniaxial compressive strength
SS	Shear stress
TS	Tensile stress
PCI	Portland cement Type I
GU	General use
ST	Silica tailings
NT	Natural tailings
PSD	Particle size distribution
PWP	Pore water pressure
XRD	X-ray diffraction
TG	Thermo-gravimetric
DTG	Differential thermo-gravimetric
SEM	Scanning electron microscopy
EDS	Energy dispersive spectroscopy

FTIR	Fourier transform infrared spectroscopy
XR-μCT	X-ray micro-computed tomography
MIP	Mercury intrusion porosimetry
VWC	Volumetric water content
RD	Relative density
SSA	Specific surface area
LOI	Loss on ignition
IC	Initial curing
k_{sat}	Saturated hydraulic conductivity
HCRR	Hydraulic conductivity recovery ratio
CCS	Changes in compressive strength
CMS	Changes in mechanical strength
PC	Pre-cracking
SCM	Supplementary cementitious material

Chapter 1 Introduction

1.1 Background

Mining, as a fundamental engineering field, is indispensable for the modern civilization and economic development of many nations across the world. Moreover, the significantly increasing consumption and demand of mineral resources push the mining industry towards deep areas as surface and near-surface mineral resources are depleted (Dong et al., 2019; Ranjith et al., 2017). As an illustration, the Kidd Creek Mine in Canada extends to 3,014.3 m below the surface, making it the deepest base-metal mine in the world, while the Mponeng Gold Mine in South Africa holds the overall record as the world's deepest mine, reaching about 4,000 m and in some areas descending even further to nearly 4,100 m. Add to that, the minerals and metals production in Canada contributed directly $109 billion in 2022, which accounts for 6% of the total gross domestic product (GDP) (Natural Resources Canada, 2024). However, an enormous amount of mining waste (i.e., tailings) would be produced during the mining operation and mineral processing (Franks et al., 2011). According to the UN Environment Programme, approximately 223 billion tonnes (534 billion cubic meters) of waste tailings were present in active, inactive, and abandoned tailings storage facilities (TSFs) as of 2019, with an estimated additional 40 to 50 billion tonnes likely to be generated over the next five years as demonstrated in Figure 1-1 (World Mine Tailings Futures, 2020).

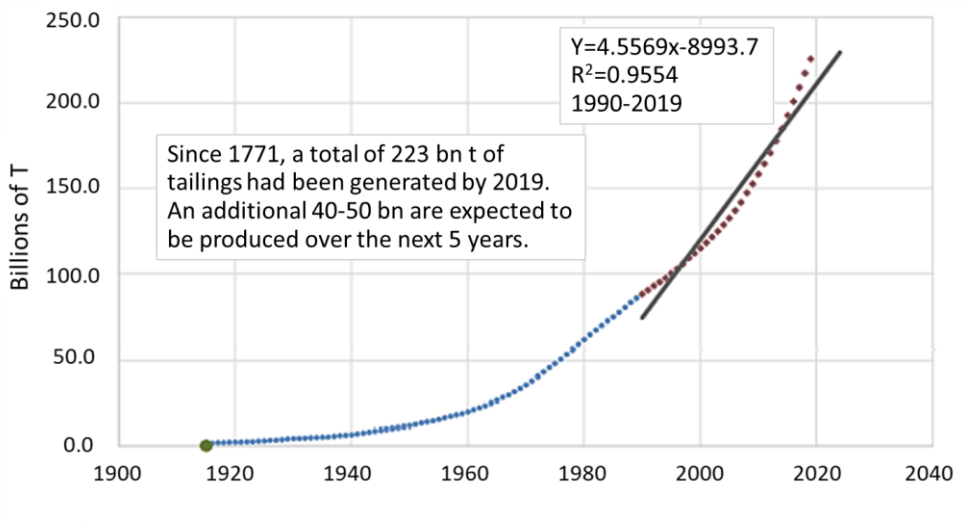

Figure 1-1. Cumulative tailings depositions 1915-2019 (adapted from World Mine Tailings Futures, 2020)

Mining waste management methods generally include surface and underground disposal. Surface disposal refers to an approach in which tailings are disposed of in TSFs, such as a dam, pond, or impoundment, usually termed a tailings dam or tailings pond. The tailings are transported and stored in the slurry phase, consisting of approximately 25-30% solids

(Adiansyah et al., 2015), or through co-disposal techniques (mixing of tailings and waste rocks) (Yilmaz, 2011; Mark, 2006). However, the surface disposal methods have substantial potential to induce significant environmental impacts on the nearby communities and ecosystem, such as mine tailings dust (Entwistle et al., 2019), tailings dam failure (Deng et al., 2017; Vanden Berghe et al., 2011; Davies, 2001), acid mine drainage (AMD) (Naidu et al., 2019; Kalin et al., 2006), etc. Moreover, the capacity of the tailings impoundment is insufficient to meet the requirements of expanding the production of minerals, and the discharged tailings further generate environmental issues, such as water pollution, landslides, leaching, and dust, in the fields of the environment, economy, and society. The mining industry developed a more effective alternative means of tailings disposal-underground disposal, including cemented hydraulic, rock, and paste backfills, which can fill underground mined-out voids (stopes) and dispose of the mining tailings properly (Sveinson, 1999; Grice, 1998; Stone, 1993). Among them, cemented paste backfill (CPB), standing as an innovative engineered mixture, has been implemented in many modern mines around the world, especially in Canada and Australia (Yumlu, 2010; Grice, 1998).

CPB is a cementitious material consisting of waste tailings (75-85% solids by weight), hydraulic binder (3-7% by dry total paste weight), and water. The use of CPB enables the possibility of placing up to 60% of generated tailings back into the underground, thus reducing the need for surface tailings impoundment space and rehabilitation expenses (Yilmaz et al., 2005). In addition, in the design of CPBs, the added hydraulic binder (i.e., Portland cement) not only favours the strength development of CPB structure, satisfying the mechanical requirements to provide ground support and a safe working surface for machinery and personnel but also reduces the permeability of the CPB matrix, acting as a barrier to inhibit the oxygen diffusion and underground water seepage, which in turn, reduce the formation of AMD by increasing acid neutralization potential. Furthermore, the placement of CPBs underground enhances the ore/pillar recovery to improve productivity and reduce the ore dilution and loss rate (Coates, 1981), delivering enhanced profitability.

1.2 Problem Statement and Knowledge Gaps

The components of a CPB are combined and mixed in a plant usually located at the surface of a mine and transported to the underground by pumping and/or gravity (Belem & Benzaazoua, 2008), where the CPB will fill the mining cavities or stopes and perform the roles mentioned above. Upon placement, CPBs must meet certain load requirements to ensure a safe underground working environment for all mining activities. Mechanical stability stands as the critical geotechnical performance criterion for CPB, with uniaxial compressive strength (UCS) serving as the most important parameter used in mines to evaluate the structural integrity of CPB. In addition to mechanical stability, environmental considerations are also essential in the design of CPB, particularly the sensitivity of CPB to AMD and its potential to release contaminants into mining areas or groundwater systems. The susceptibility of CPB to AMD primarily depends on the reactivity of the tailings, which

is influenced by the type and quantity of present sulphide minerals, as well as the permeability of the CPB matrix. The ease with which fluids, such as air and water, can infiltrate and flow through the CPB system impacts this reactivity and can be assessed through the measurement of its hydraulic conductivity (Fall et al., 2009). Furthermore, it is known that the aforementioned mechanical and hydraulic properties of CPBs are dominated by the thermal (**T**, e.g., geothermal gradient, hydration heat, heat transfer), hydraulic (**H**, e.g., suction, pore water pressure (PWP) development, water drainage), mechanical (**M**, e.g., in-situ stress, CPB self-weight, filling rate and strategy), and chemical processes (**C**, e.g., binder reactions, contamination dissolution, and precipitation) upon being placed into stopes (Aldhafeeri & Fall, 2017; Cui & Fall, 2015; Ghirian & Fall, 2015).

During the curing phase, cracks can form in the CPB material or structure ascribed to several factors, such as excessive stresses generated by the pressure of the CPB overburden, stresses induced by the closure of rock walls adjacent to or surrounding the CPB structures, rock bursts, shrinkage, etc. (as illustrated in Figure 1-2 and explicated in Section 2.5.1). The presence of cracks in CPBs tends to weaken the integrity and mechanical strength of the structures as well as increase their permeability properties, thus severely compromising their safety, serviceability, durability, and environmental performance. These weaknesses have been of deep concern to researchers and practitioners, especially with the current trend of deep mining, where the stresses induced by rock wall closure and the intensity and frequency of rock bursts are higher. In addition, CPB structures vary from a few tens to several hundred meters underground in at least one dimension, which makes manual maintenance and repair of cracks in CPB structures infeasible in practical manners. As the problem that frequently appears in conventional cementitious materials (e.g., concrete and mortar), it is well known that these cementitious materials have a self-healing capability, which mainly refers to the material having the ability to repair cracks automatically, without external diagnosis or human intervention. Many studies have been conducted on cementitious materials to investigate the self-healing (autogenous healing) behaviour and ability, such as concrete (De Belie et al., 2018; Neville, 2002), mortar (Suleiman & Nehdi, 2021; De Nardi et al., 2017), high-performance fiber reinforced cementitious composites (Cuenca & Ferrara, 2017; Ferrara et al., 2017), and engineered cementitious composites (Yang et al., 2011; Yang et al., 2009), to address crack induced problems. However, no studies have been conducted to date on the self-healing (autogenous healing) ability and behaviour of CPB and its impact on the recovery of mechanical and permeation properties of CPB. In addition, due to the significant differences between CPB and conventional cementitious materials, such as lower cement content and higher water-to-cement ratio in CPB, and the differing particle size distributions between tailings and aggregates, the existing findings of conventional cementitious materials cannot be directly applied to CPB materials. It is essential to bridge this research and technology gap for the reasons outlined above.

Therefore, to ensure a cost-effective and safe design, as well as to enhance the durability and environmental performance of CPB structures, this study conducts a comprehensive experimental investigation to examine the effects of crack damage level, age of cracking, crack with, self-healing period, temperature, water drainage, crack-inducing stresses, and sulphate concentration on the self-healing (autogenous healing) behaviour and capacity of the CPB. Furthermore, the hydraulic binder (i.e., Portland cement in this study) is partially substituted with fly ash and blast furnace slag to explore the impact of these mineral additives on the self-healing performance of CPB.

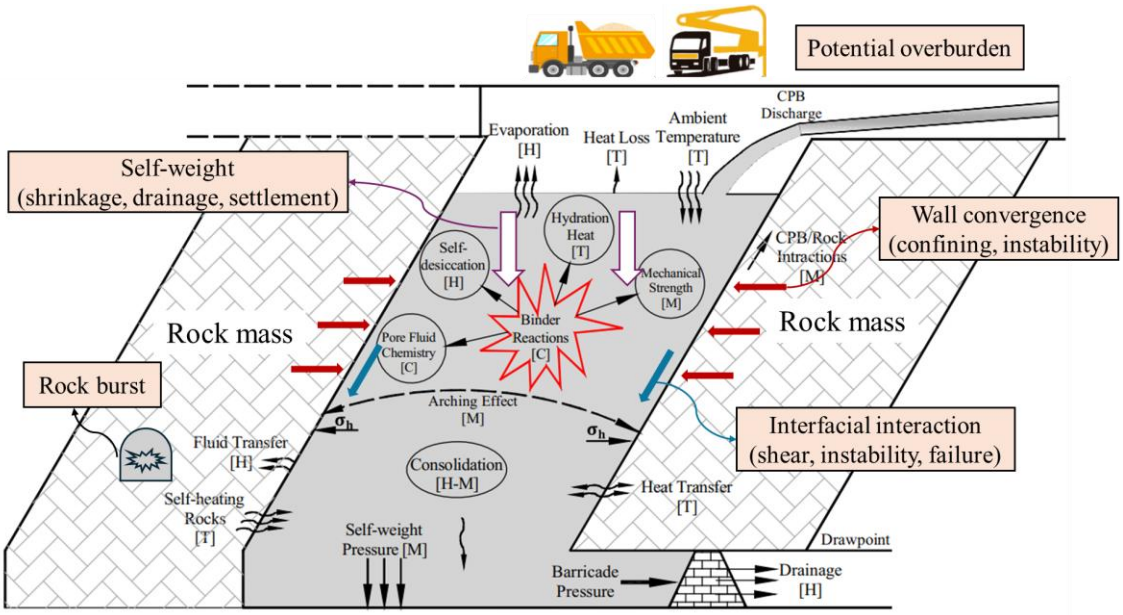

Figure 1-2. Schematic diagram illustrating various THMC processes and the factors that induce cracks in a backfill structure (adapted from Ghirian & Fall, 2015).

1.3 Objectives

The main objectives of this doctoral research are to conduct a comprehensive investigation into the self-healing (autogenous healing) behaviour of CPB subjected to various thermal, hydraulic, mechanical, and chemical conditions, as well as to assess the effects of mineral additives, all while considering the multiphysical processes involved. This study holds significant implications with respect to the structural design, mechanical stability, permeability, and durability of CPB exposed to practical conditions, providing a profound understanding of the autogenous self-healing mechanism within the CPB matrix and valuable guidance for engineering practice. The explicit objectives of this study are as follows:

- To investigate the existence of self-healing (autogenous healing) behaviour in CPB material at different curing ages and to understand the self-healing mechanisms, while evaluating the self-healing efficiency of CPB material through its recovery of mechanical and permeation properties, as well as crack closure ability.

- To study the effects of various multiphysical loading factors on the self-healing behaviour of CPB at the experimental level. The sub-objectives are achieved by the following studies of:
  i) The effect of chemical factors (sulphate concentrations) on the self-healing capacity and mechanisms of CPB from the early to advanced self-healing period.
  ii) The effect of thermal factors (healing/curing temperatures) on the self-healing efficiency in CPB with different self-healing periods.
  iii) The effect of hydraulic factors (drainage conditions) on the self-healing efficiency in CPB across different self-healing periods.
  iv) The effect of mechanical factors (cracks induced by different types of loading stresses) on the self-healing efficiency with different self-healing periods.
- To explore the variations in the self-healing capacity of CPB resulting from the incorporation of mineral additives, and to examine their contributions to the binder hydration and microstructural alterations, as evidenced by the recovery of mechanical strength and permeability properties.
- To provide technical information that enhances the comprehensive understanding of the self-healing behaviour and capacity of CPB material, as well as to offer fundamental insights for the maintenance and repair of cracked CPB, improving the durability and environmental performance of CPB structures.

1.4 Research Approaches and Methods

A comprehensive experimental investigation program, including the specific research approach and methods, is established and schematically represented in Figure 1-3 to achieve the aforementioned main objectives. This study consists of the following phases:

- **Phase I** includes the definition of the problem statement and research objectives, highlighting the research gap in the CPB study and outlining the primary goals to address this knowledge gap.
- **Phase II** involves a literature review of the theoretical and technical background of this study, as well as a comprehensive literature review of the existing state-of-the-art literature related to the self-healing properties of cementitious materials. This phase is essential in identifying the most effective testing procedures and methods to monitor and evaluate the performance of the CPB during its self-healing process under various conditions.
- **Phase III** comprises the experimental work in this research, which consists of three stages of experiments.

  Stage 1: This stage includes a pre-requisite study to demonstrate the presence of autogenous self-healing behaviour in the CPB materials. The CPB specimens are pre-cracked at three different initial curing (IC) periods (i.e., 3, 7, and 28 days) with five

different pre-cracking levels (i.e., 30%, 50%, 75%, 90%, or 100% of compressive strength in the pre-peak phase after IC) by the compression loading. UCS, saturated hydraulic conductivity, and porosity/void ratio tests are performed on the control and healed pre-cracked specimens to monitor the self-healing capability after the self-healing period of 1, 7, 28, and 90 days. Meanwhile, the healing performance of microcracks is observed using a digital microscope. Furthermore, analytical techniques, including X-ray diffraction (XRD), scanning electron microscopy-energy dispersive spectroscopy (SEM-EDS), thermogravimetric analysis (TGA), etc., are conducted to examine the microstructural changes and characterize the self-healing products.

Stage II: This stage incorporates the study of the effects of thermal (T, healing/curing temperature), hydraulic (H, drainage condition), mechanical (M, crack-inducing stresses), and chemical (C, sulphate concentration) conditions on the self-healing behaviour and capacity of CPB, respectively. On the basis of *Stage I*, the initial curing period of 7 days for the studied CPB specimens is adopted before the pre-cracking process. As the cracks start to appear on the CPB specimens only when the pre-cracking level reaches 75%, the pre-cracking levels of 75% and 90% are implemented to initiate the cracks. Additionally, the tests evaluating self-healing efficiency in the recovery of mechanical and hydraulic properties are conducted at the designated self-healing periods of 7, 28, and 90 days. One batch of experiments is conducted to study the effect of temperature (T) on the self-healing performance of CPB with the healing/curing temperature of 2°C, 20°C, 35°C, and 50°C. Moreover, the hydraulic (H) effect on the self-healing behaviour is investigated through a batch of CPB specimens under three different drainage conditions (i.e., full drainage, half drainage, and no drainage), under which the volumetric water content is also monitored. In addition, the tests concerning the effects of the mechanical (M) factor refer to the tests conducted on the specimens pre-cracked under the uniaxial compression, triaxial compression, and indirect tensile loading, respectively. Furthermore, the effect of the chemical (C) factor on the self-healing capacity and mechanism is carried out on the specimens with different sulphate concentrations of 0, 5000, 15000, and 25000 ppm.

Stage III: This stage explores the variation in the self-healing capacity of CPB when the hydraulic binder (i.e., Portland cement) is partially replaced with mineral additives (i.e., blast furnace slag and fly ash).

- **Phase IV** incorporates the comprehensive analysis of the experimental results and the evaluation of the self-healing performance in the CPB with respect to the tested conditions. The findings in this study provide an innovative perspective on CPB durability and serviceability research, and recommendations for the maintenance of CPB structures containing cracks will be provided for the practical problems that on-site operators and engineers may face in practice.

1.5 Thesis Organization

This thesis is organized into eight main chapters, as presented in Figure 1-4. Below is a brief overview of each chapter:

Chapter 1 provides a general introduction to this study, including the research problem and its significance, the primary objectives of the study, the employed theoretical knowledge and methodology, and a brief overview of the thesis structure.

Chapter 2 delves into the theoretical and technical background of the post-mining backfilling techniques, with an emphasis on the practice of the CPB technique. This chapter depicts the design of the CPB mixture and its distribution system. The main geotechnical features of CPB are described with a focus on its physical, mechanical, and hydraulic properties. Moreover, background information on cement hydration within the CPB matrix as well as the multiphysical (THMC) impacting processes, is provided. In addition, the factors that induce the formation of cracks within the CPB structure are also clarified.

Chapter 3 is a comprehensive literature review of the existing literature related to the research topic in this study. This chapter covers i) the use of the CPB technique and its fundamental properties, ii) scenarios inducing the formation of cracks in CPB structures, iii) self-healing approaches in cementitious materials and their impacting factors, iv) methods to evaluate the self-healing efficiency, and v) current studies on the self-healing behaviour of CPB. The information given in this chapter is essential for better identification and understanding of the research gap.

Chapters 4 through 6 follow a paper-based thesis format. Note that each technical paper includes sections for introduction, materials and methods, results and discussions, and conclusions. While some information may be repeated across chapters, it is necessary to present the key findings of the Ph.D. research within each paper.

Chapter 4 focuses on investigating the autogenous self-healing behaviour in the CPB materials (**Technical paper I**), in which the effect of curing age before pre-cracking and the effect of pre-cracking levels are examined.

Chapter 5 dedicates attention to the effects of multiphysical (THMC) factors on the self-healing behaviour and capacity of CPB, consisting of four technical papers. Section 5.2 reveals the effect of sulphate concentration (factor **C**) on the self-healing performance of CPB (**Technical paper II**). Section 5.3 discusses the impact of healing/curing temperature (factor **T**) on the self-healing performance of CPB (**Technical paper III**). The effects of water drainage (factor **H**) and crack-introducing stresses (factor **M**) are presented in Sections 5.4 and 5.5 (**Technical papers IV** and **V**, respectively).

Chapter 6 narrows the scope to the self-healing performance of CPB when it contains mineral additives (i.e., blast furnace slag and fly ash) (**Technical paper VI**).

Chapter 7 synthesizes the key results and findings in compliance with the primary objectives of the study, and provides a comprehensive understanding of the autogenous self-healing behaviour in CPB under various conditions, indicating significant impacts and practical implications concerning CPB structure design, mechanical stability, and durability. The chapter also articulates the research's key innovations and original contributions, underscoring how these findings advance current knowledge and practice.

Chapter 8 provides the overall conclusions and suggestions for the maintenance of the CPB structure. It also outlines the main limitations of the research and provides guidance for future investigations aimed at further advancing the understanding and practical implementation of self-healing in CPB.

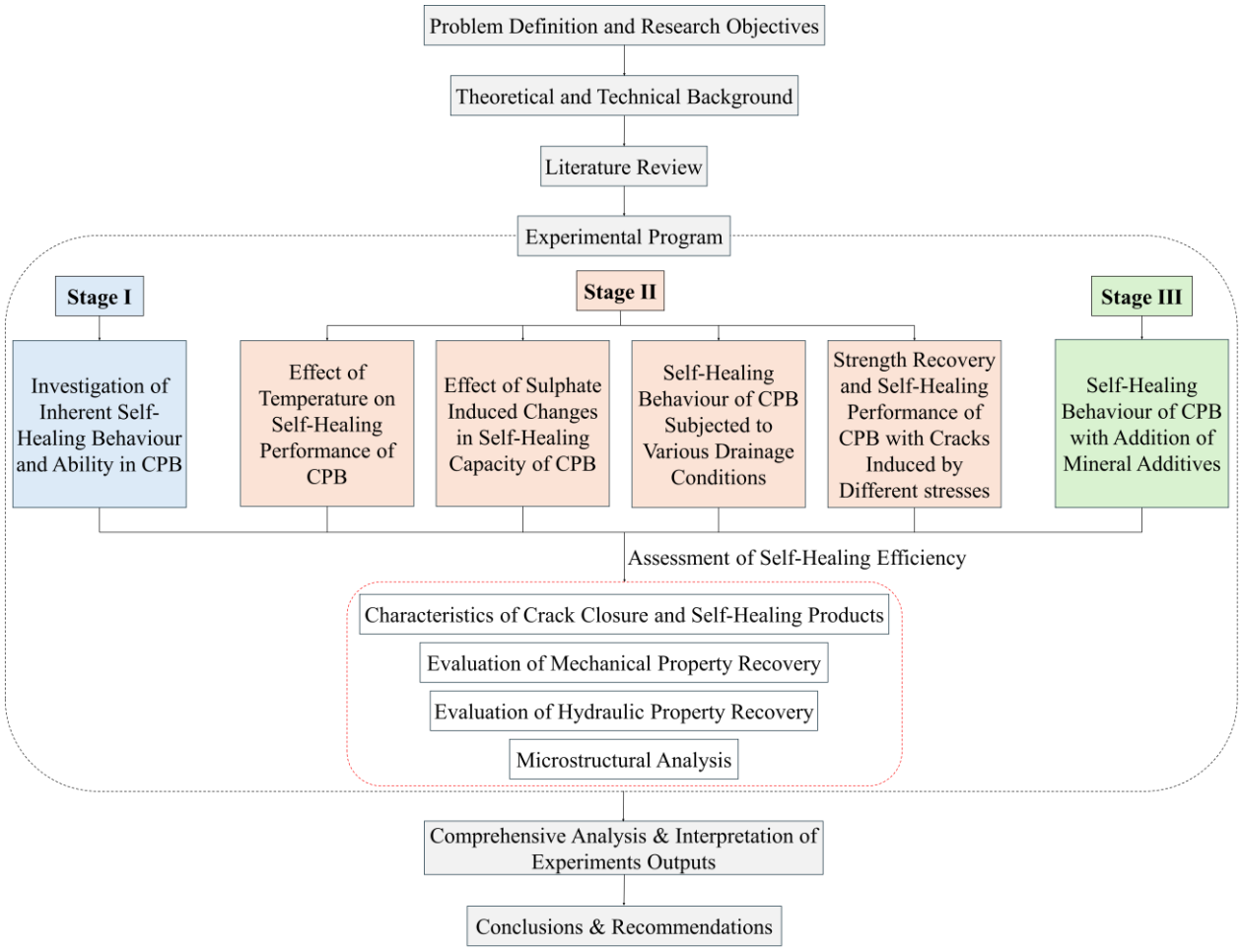

Figure 1-3. Research and study approach.

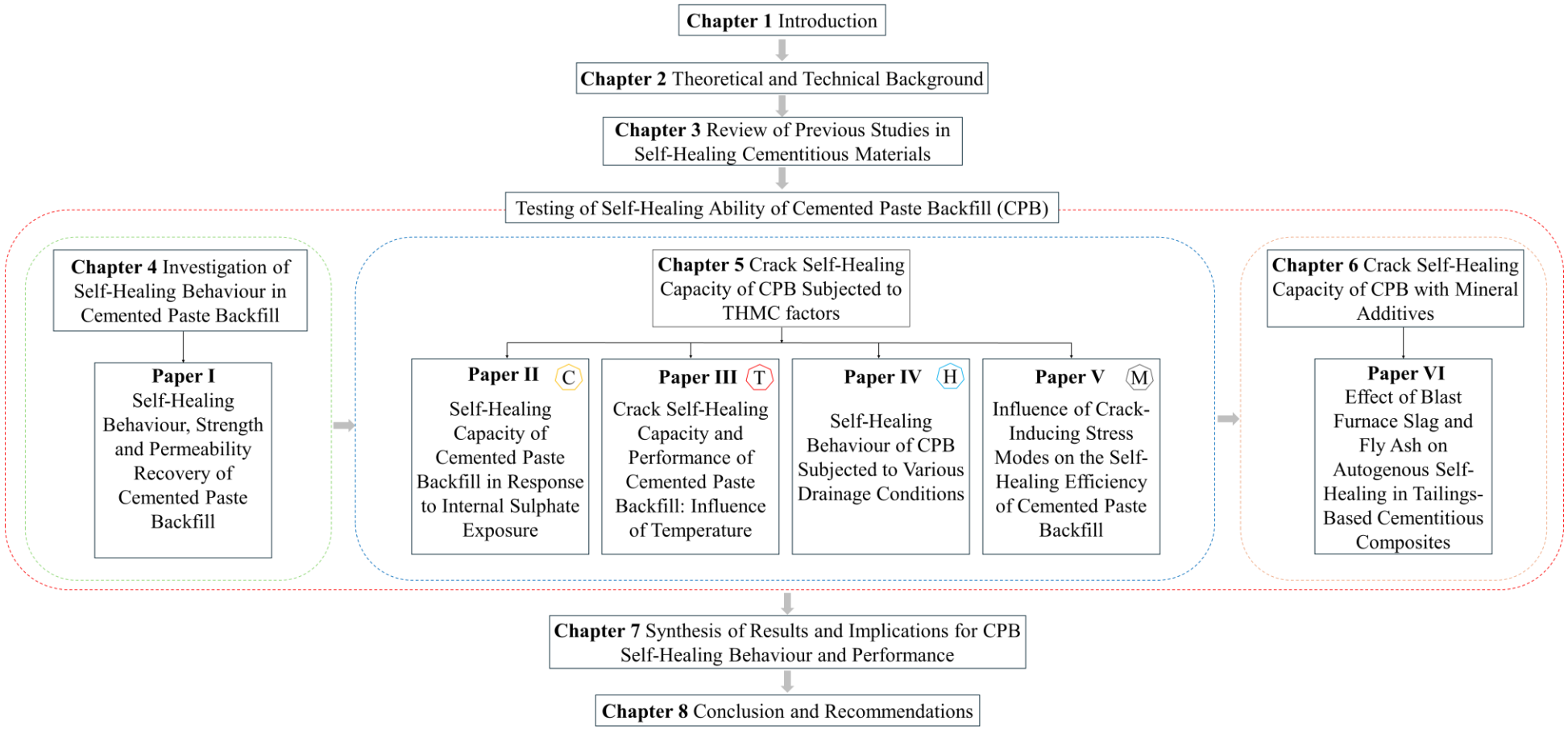

Figure 1-4. Tasks and organization of the thesis.

1.6 References

Adiansyah, J. S., Rosano, M., Vink, S., & Keir, G. (2015). A framework for a sustainable approach to mine tailings management: disposal strategies. Journal of cleaner production, 108, 1050-1062.

Aldhafeeri, Z., & Fall, M. (2017). Sulphate induced changes in the reactivity of cemented tailings backfill. International Journal of Mineral Processing, 166, 13-23.

Belem, T., & Benzaazoua, M. (2008). Design and application of underground mine paste backfill technology. Geotechnical and Geological Engineering, 26, 147-174.

Coates, D. F. (1981). Caving, subsidence, and ground control. Rock Mechanics Principles, CANMET, Department of Energy, Mines and Resources, Canada, 5-1.

Cuenca, E., & Ferrara, L. (2017). Self-healing capacity of fiber reinforced cementitious composites. State of the art and perspectives. KSCE Journal of Civil Engineering, 21(7), 2777-2789.

Cui, L., & Fall, M. (2015). A coupled thermo–hydro-mechanical–chemical model for underground cemented tailings backfill. Tunnelling and Underground Space Technology, 50, 396-414.

Davies, M. P. (2001). Impounded mine tailings: What are the failures telling us?. CIM Bulletin, 94.

De Belie, N., Gruyaert, E., Al-Tabbaa, A., Antonaci, P., Baera, C., Bajare, D., ... & Jonkers, H. M. (2018). A review of self-healing concrete for damage management of structures. Advanced materials interfaces, 5(17), 1800074.

De Nardi, C., Cecchi, A., Ferrara, L., Benedetti, A., & Cristofori, D. (2017). Effect of age and level of damage on the autogenous healing of lime mortars. Composites Part B: Engineering, 124, 144-157.

Deng, D. Q., Liu, L., Yao, Z. L., Song, K. I., & Lao, D. Z. (2017). A practice of ultra-fine tailings disposal as filling material in a gold mine. Journal of Environmental Management, 196, 100-109.

Dong, L., Tong, X., Li, X., Zhou, J., Wang, S., & Liu, B. (2019). Some developments and new insights of environmental problems and deep mining strategy for cleaner production in mines. Journal of Cleaner Production, 210, 1562-1578.

Entwistle, J. A., Hursthouse, A. S., Marinho Reis, P. A., & Stewart, A. G. (2019). Metalliferous mine dust: Human health impacts and the potential determinants of disease in mining communities. Current Pollution Reports, 5, 67-83.

Fall, M., Adrien, D., Célestin, J. C., Pokharel, M., & Touré, M. (2009). Saturated hydraulic conductivity of cemented paste backfill. Minerals engineering, 22(15), 1307-1317.

Ferrara, L., Krelani, V., Moretti, F., Flores, M. R., & Ros, P. S. (2017). Effects of autogenous healing on the recovery of mechanical performance of High Performance Fibre Reinforced Cementitious Composites (HPFRCCs): Part 1. Cement and Concrete Composites, 83, 76-100.

Franks, D. M., Boger, D. V., Côte, C. M., & Mulligan, D. R. (2011). Sustainable development principles for the disposal of mining and mineral processing wastes. Resources policy, 36(2), 114-122.

Ghirian, A., & Fall, M. (2015). Coupled behavior of cemented paste backfill at early ages. Geotechnical and geological engineering, 33, 1141-1166.

Grice, T. (1998). Underground mining with backfill. 2nd Annual Summit œ Mine Tailings Disposal Systems, Brisbane, Nov, 24-25.

Kalin, M., Fyson, A., & Wheeler, W. N. (2006). The chemistry of conventional and alternative treatment systems for the neutralization of acid mine drainage. Science of the total environment, 366(2-3), 395-408.

Mark, R. (2006). Closure of tailings facilities: Current practice review and guidelines for success.
Naidu, G., Ryu, S., Thiruvenkatachari, R., & Choi, Y. J. S., & Vigneswaran, S. (2019). A critical review on remediation, reuse, and resource recovery from acid mine drainage. Environmental Pollution, 247, 1110-1124.
Neville, A. (2002). Autogenous healing—a concrete miracle?. Concrete international, 24(11), 76-82.
Ranjith, P. G., Zhao, J., Ju, M., De Silva, R. V., Rathnaweera, T. D., & Bandara, A. K. (2017). Opportunities and challenges in deep mining: a brief review. Engineering, 3(4), 546-551.
Stone, D. M. R. (1993). The optimization of mix designs for cemented rockfill. In Minefill (Vol. 93, pp. 249-253).
Suleiman, A. R., & Nehdi, M. L. (2021). Effect of autogenous crack self-healing on mechanical strength recovery of cement mortar under various environmental exposure. Scientific Reports, 11(1), 7245.
Sveinson, S. (1999). Characterisation of tailings for paste backfill system design (Doctoral dissertation, University of British Columbia).
Vanden Berghe, J. F., Ballard, J. C., Pirson, M., & Reh, U. (2011). Risks of Tailings Dams Failure. Geotechnical Safety and Risk. ISGSR 2011, 209-216.
World Mine Tailings Futures. (2020). STATE OF WORLD MINE TAILINGS PORTFOLIO 2020. Retrieved from https://worldminetailingsfailures.org/
Yang, Y., Lepech, M. D., Yang, E. H., & Li, V. C. (2009). Autogenous healing of engineered cementitious composites under wet–dry cycles. Cement and Concrete Research, 39(5), 382-390.
Yang, Y., Yang, E. H., & Li, V. C. (2011). Autogenous healing of engineered cementitious composites at early age. Cement and concrete research, 41(2), 176-183.
Yilmaz, E. (2011). Advances in reducing large volumes of environmentally harmful mine waste rocks and tailings. Gospodarka Surowcami Mineralnymi-Mineral Resources Management, 89-112.
Yilmaz, E., Kesimal, A., Ercikdi, B., Benzaazoua, M., Belem, T., & Bussière, B. (2005). Short and long terms strength performances of cemented paste backfill. In 19th Int. Mining Congress and Fair of Turkey, MCET2005 (pp. 11-17).
Yumlu, M. (2010). Mining with paste fill. In AusIMM Cobar Mining Seminar, 26p.

Chapter 2 Theoretical and Technical Background

2.1 Introduction

This chapter provides a review of the theoretical and technical background on the fundamental design of the CPB technique, primary binder hydration mechanisms within its matrix, multiphysical impacts on the development of geotechnical properties of CPB, and the crack-inducing factors in the CPB structures. Specifically, the fundamental principle of backfilling technology is provided in Section 2.2, which specifies its corresponding advantages and disadvantages in mining waste management, with an emphasis on the CPB technique, including its recipe design, preparation, distribution, and environmental performance. Subsequently, multiphysical (THMC) impacting factors that govern the geotechnical features of CPB are reviewed in Section 2.3. Following this, a detailed introduction to the cement hydration mechanism, which dominates the mechanical response of the CPB matrix, is presented in Section 2.4. Furthermore, the potential factors inducing the cracks in the CPB structure are discussed in Section 2.5. By reviewing the established literature and technical advancements, this chapter offers a comprehensive understanding of the theoretical and technical dimensions of the current CPB study, ensuring that this study is grounded in both sound theory and robust technical mining practices.

2.2 Backfill Technology

Mining activities typically generate vast quantities of solid wastes, such as tailings and crushed rocks, positioning the mining industry as one of the world's largest waste producers, with approximately 65-80 billion tons of waste generated annually (Adiguzel et al., 2022; Jones & Boger, 2012). The surface disposal of mining wastes poses significant threats to the environment, society, and economy, including heavy metal mobilization, acid mine drainage, water pollution, landslides, leaching, and dust generation. With the expansion of the mining industry, insufficient disposal impoundments, and the resulting environmental challenges, the industry faces growing pressure to develop and adopt sustainable waste management practices of cemented backfills.

2.2.1 Backfilling Types

Backfills are essential for filling the voids left by ore body extraction in underground mines. They provide structural support to the surrounding rock, prevent surface subsidence, and minimize the potential for ground movements. In addition, backfilling helps restore the original rock stress conditions, contributing to the long-term stability of the mine. From an environmental perspective, backfilling plays a crucial role by utilizing tailings and other waste materials, thus reducing the need for surface disposal and lessening the environmental footprint of mining operations. Mine cemented backfills can be primarily classified into three categories: cemented hydraulic fill (CHF), cemented rockfill (CRF), and cemented paste backfill (CPB). The selection of a specific backfill method in underground mining is influenced by several factors, such as the type of mine, stope geometry, mining depth, availability of resources, and the associated cost of backfilling, which remains a key consideration in the decision-making process (Landriault, 2001).

2.2.1.1 Cemented hydraulic fill (CHF)

Hydraulic fill (HF) was the first continuous method of mine backfilling in the mining industry to backfill underground stopes/voids with materials transported as a slurry by gravity through boreholes and pipelines (Martic et al., 2014; Grice, 1998). This fill material, conventionally composed of unclassified tailings or tailing sands mixed with water, is deposited into mined-out areas to provide ground support and minimize surface subsidence. The water content in hydraulic fill is relatively high, where water serves as the medium for transporting materials, allowing them to flow and settle in place. Once the slurry reaches the designated area, the excess transport water is drained out through embedded drainage systems, such as sumps or drainage pipes, to prevent waterlogging and facilitate the settlement of fill materials. Moreover, CHF, a major step forward by incorporating the binders (i.e., cement), is a mixture of classified tailings, binders (3-5%), and water, with a range of solid density of 50-70% (Sivakugan et al. 2013, Béket Dalcé et al. 2019), which has a similar grain size distribution to that of HFs (Rankine et al., 2007). The addition of cement enhances the structural integrity of the backfill, enabling it to achieve higher strength and mechanical stability. This makes CHF particularly suitable for use in areas where significant load-bearing capacity is required, such as beneath active mining levels, while also contributing to effective waste disposal and reducing environmental impacts. However, the permeable barricades need to be constructed to retain the backfill and allow the drainage of excess transport water from HFs before the placement, resulting in an increase in the costs of backfilling operations. Add to that, excess transport water accumulated in the stopes would lead to water ponding, which increases the possibility of pipe erosion and potentially causes barricade failure if the water is not promptly pumped out of the mine. Barricade failures, along with the associated hazards of backfill inrush, present significant safety risks that demand careful management and proactive mitigation to address these critical concerns effectively (Grice, 1998).

2.2.1.2 Cemented rockfill (CRF)

CRF, also known as consolidated rock fill, is a material composed of aggregates (e.g., rock fragments), water, and a hydraulic binder (e.g., cement) in proportions of 1-6% (Jiang et al., 2019; Emad et al., 2015). CRF is generally prepared by transporting the rock fills to the stope and mixing with CHF with a ratio of 1:1 to 3:1 (RF:CHF) by weight. During the hydration process, the CHF binds solid particles and fills the voids between the aggregates. Various factors, constituting grain size distribution of aggregates, binder content, segregation, mixing ratio, method of placement (e.g., backfill raise and impact damage), and water quality, dominate the properties of CRFs (Yu, 2021; Bloss, 1992). Unlike CHF systems, CRF does not require a drainage system, as the water within the mix does not seep out. The primary advantage of CRF lies in its cost-effectiveness due to its relatively low cement consumption (typically 4-6%). In addition, CRF structures exhibit superior geotechnical features, such as compressive strength, modulus of elasticity, cohesion, and angle of friction, compared to any other types of fill using the same content of hydraulic binder (Jiang et al., 2019; Peterson, 1996; Farsangi, 1996). These characteristics make CRF capable of withstanding active pressures, providing ground support, and enhancing wall rock stability (Emad et al., 2015). However, the preparation of CRF involves the crushing of quarried rock, which significantly

increases the costs related to transportation, surface production, and haulage. Moreover, the limited utilization of waste tailings in the CRF system leaves a substantial amount of tailings requiring disposal impoundment, thereby failing to fully address environmental concerns (Shrestha, 2008).

2.2.1.3 Cemented paste backfill (CPB)

Paste fill, as a viable alternative to hydraulic slurry and rock fill, was introduced in the mid-1970s while describing surface disposal of concentrated tailings using pipeline reticulation (Robinsky 1975, 1978) and was first produced at the Bad Grund Mine in Germany in 1979 (Rankine & Sivakugan, 2007). With the development of paste in the decades, paste fill has become the most prevalent backfilling method for larger projects mining massive ore bodies employing sublevel mining systems (Emad et al., 2015). Due to the demand for specific geotechnical loading requirements, hydraulic binders (typically cement) are also introduced to paste fills such as CPB. As an engineered mixture composed of waste tailings (75-85% solids by weight), a hydraulic binder (3-7% by dry total paste weight), and water, CPB has been implemented in many modern mines around the world (Grice, 1998). The paste fills can obtain a similar strength to rock backfills by using less cement than hydraulic backfills. It utilizes the full range of tailings, which decreases the quantity of tailings to be disposed of compared to hydraulic fill and rock fill systems (Emad et al., 2015), reducing the surface tailings pond accumulation and the costs associated with constructing and reclaiming tailings ponds during mining. In comparison, rock and hydraulic fills prefer less solid content or a larger size distribution of tailings. In the same way, the decant water from paste fills can be virtually eliminated, which lowers costs and reduces associated problems with barricade setup, shortening the mining cycle and speeding up production. Furthermore, the existing borehole delivery systems of slurry fills can also be applied to the paste backfill delivery. The paste backfill system is less complex than the rock and hydraulic fill systems in the preparation and distribution design. Therefore, CPB can not only solve the safety and environmental issues caused by mine production and tailings discharge but also maximize the recovery of resources, which is of great significance for the development of sustainable mining.

2.2.2 Background of Cemented Paste Backfill

The practice of using CPBs to fill extracted stopes has become more commonplace worldwide, particularly in Canada and Australia (Yumlu, 2010). The use of CPB enables the possibility of placing up to 75% of generated tailings back into the underground, thus reducing the need for surface tailings impoundment space and rehabilitation expenses (Ercikdi et al., 2015). For instance, the Doyon mine extracts and treats 3000 tonnes of gold ore daily. Approximately 60% of the produced tailings after cyanidation are used as CPB for underground operation. The placement of CPBs underground not only reduces the surface tailings impoundment but also enhances the ore/pillar recovery to improve productivity and reduce the ore dilution and loss rate (Coates, 1981), thus resulting in more profits.

2.2.2.1 CPB mixture design

CPB is usually prepared using dewatered (thickened) tailings with a solid percentage of 70-85 wt.%, hydraulic binder (typically 3-7 wt.%), and mined processed/fresh water (15-25%) (Fall et al., 2005;

Belem et al., 2000). Considerations of various factors, such as geomechanical properties, rheological properties, and environmental performance, are required in the design and optimization of CPB mixtures to satisfy the required target design criteria (Ghirian & Fall, 2017; Belem & Benzaazoua, 2008).

First of all, the mechanical stability of CPB stands as the most crucial performance property, which is predominantly governed by the hydraulic binder (typically Portland cement (PC)) used in the preparation of CPB mixtures. The mechanical properties of CPB are attributed to the hydration products (e.g., calcium silicate hydrates, ettringite, and calcium hydroxide) formed by the hydraulic reactions of added binders, which determine the ultimate strength of CPBs. Generally, the more cement that is added, the greater the strength that can be attained. However, the cost of binders in the CPB mixture accounts for up to 75% of the backfilling operations, which makes it an economically inefficient choice for the mining industry (Hassani et al., 2007; Grice, 1998). In addition, the PC is susceptible to sulfate attacks when sulfide-rich tailings are used, undermining the strength development of the CPB structures (Ercikdi et al., 2009). Given that, researchers have found that PC can be partly substituted or blended with other binders or additives, such as fly ash, slag, or lime, to reduce costs, enhance strength development, and achieve other desirable properties. Ercikdi et al. (2009) investigated that even with lower cement percentages, the mechanical strength was still retained when pozzolanic minerals and chemical additives were used as an alternative binder in the CPB mixture. Also, alkali-activated slag cement can prevent mechanical strength loss under aggressive conditions, and its cost is considerably lower than that of PC (Xue et al., 2018). Similarly, fly ash is usually used to achieve benefits, such as reducing the cement content to reduce costs, improving the workability and rheological properties, and ensuring the required long-term strength in backfill. Thus, the partial replacement of cement or blending with mineral additives not only reduces the cost of CPBs but also lowers the overall energy required to produce cementitious materials, as well as decreases carbon dioxide emissions (Nwankwo et al., 2020).

Additionally, the impact of rheological properties on CPB is crucial in determining the design of distribution and placement systems, such as tank dewatering systems, retention time, backfill formation rates, and underflow discharge systems, which influence flow resistance and pipeline pressure loss. Paste backfill typically generates higher pipeline pressure than slurry backfill, necessitating stronger pipeline support. Previous studies have revealed that several factors, including cement content, particle size distribution (PSD) of tailings, water-to-cement (w/c) ratio, and tailings density, significantly affect the rheology of CPBs (Benzaazoua et al., 2004; Fall et al., 2008). In particular, the proportion of fine particles (less than 20 μm) in the tailings strongly influences the slump, strength gain, porosity, pore size distribution, and water drainage ability of the CPB (Fall et al., 2005). CPBs made from fine tailings usually exhibit lower strength. In most cases, the CPB mixture must contain at least 15% by weight of particles less than 20 μm in diameter to retain sufficient water forming a paste (Kesimal et al., 2005). Besides, waste rocks and admixtures (e.g., superplasticizers) can be used to improve the PSD and consistency to optimize the properties of CPBs (Hane et al., 2017; Yang et al., 2018). Add to that, extra water is usually added to ensure the pumpability of the CPB, resulting in a volumetric water content that

consistently exceeds the hydration requirements of the cement (Belem and Benzaazoua, 2008), which is significantly higher than that of concrete. Increasing the w/c ratio reduces the number of particle-particle contacts and increases the thickness of the lubricating film around the particles, facilitating particle sliding and thus reducing the yield stress (increasing fluidity) of the CPB mixtures (Zhao et al., 2020). However, a higher w/c ratio inversely impacts the strength development of the CPBs (Galaa et al., 2011; Yılmaz et al., 2014).

Furthermore, the quality of the mixed water affects the hydration of the binders within the CPB matrix. Freshwater, which contains minimal concentrations of chemicals, is typically used in laboratory preparations of CPBs to eliminate the effects of soluble chemicals on performance. However, heavy metals and chemicals, such as zinc, lead, sulfate, etc., would be present in the mine process water. For instance, the existence of sulfate salts or the low pH of acidic water would deteriorate the cementitious bonds within the CPB structures, resulting in a reduction in strength, durability, and stability (Belem and Benzaazoua, 2008).

Last but not least, environmental protection is a critical consideration in all mining activities, necessitating efforts to minimize the environmental impact of waste at every stage of the process. Tailings management is a key aspect of waste management. Traditionally, mining industries have used waste rock as underground support and for waste disposal. The introduction of hydraulic slurry backfills reduced the volume of surface tailings by sending coarse tailings underground, but fine particles were excluded. These leftover fine particles have caused significant environmental issues, such as leaching from tailings ponds, landslides, and dust pollution. The adoption of CPB offers several environmental benefits. It creates a safer material for underground backfill and surface disposal, reduces the accumulation of tailings in ponds, and potentially eliminates the need for impoundments for reactive tailings. At the same time, mining is a commercial venture, and profitability is essential for sustaining operations. Backfilling often represents a substantial portion of mining costs. These costs are influenced not only by material expenses but also by site-specific factors. For instance, the location of the mine plays a crucial role; remote mines far from supply sources may face significantly higher transportation costs. Additionally, in such remote locations, electricity expenses can be considerable, especially if hydroelectric power is unavailable.

2.2.2.2 CPB mixture preparation

Tailings discharged from milling processes usually have a low solid concentration of 35-60%. These tailings are initially sent to a hydrocyclone and thickener for desliming, where a part of the fine particles is eliminated at the overflow and the solid concentration is increased to approximately 75%, meeting the minimum requirement for CPB preparation (Ghirian, 2016). To date, two main techniques of tailings dewatering are commonly utilized, including the two-stage dewatering system, which combines a high-efficiency thickener followed by a vacuum filter, and the one-stage thickening process using a deep cone thickener (DCT) (Wang et al., 2014; Schoenbrunn, 2011). The DCT can simplify the traditional dewatering process while achieving an adequate underflow concentration. In contrast, the two-stage thickening method is often associated with high costs, increased energy consumption, and reduced system reliability, particularly when processing

tailings with large quantities of fines (Wu et al., 2015). After thickening, the tailings report to the holding tank. From the holding tank, the thickened tailings are fed by gravity to the disc filter to decrease the number of ultrafine particles (i.e., particles less than 5 μm in size) in tailings (Fang, 2021). The tailings are discharged and weighed on a belt conveyor, then transported to a screw mixer, where the tailings are combined with the predetermined quantity of binder, water, and other admixtures to create the final CPB mixture. The processes are schematically represented in Figure 2-1.

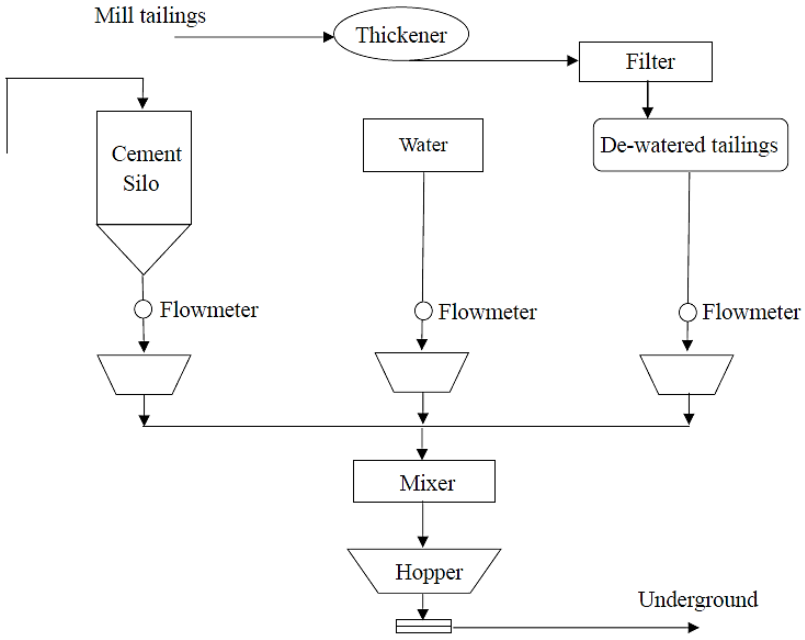

Figure 2-1. Design flowchart of backfill preparation system (Quan, 2021).

2.2.2.3 CPB mixture distribution and placement

The distribution and placement system aims to transport the homogeneous CPB mixtures from the ground surface mixing plant to the underground stopes/voids. The fresh CPB mixture is typically transported through a network of pipelines to the designated backfill area, which may include vertical boreholes (gravity-driven) and/or horizontal pipelines (pumping), as illustrated in Figure 2-2. To maintain the flowability of the paste and prevent blockages, the rheological behaviour of the non-Newtonian fluid CPB mixture, such as slump, viscosity, and yield stress, is determined to optimize the design of the pipeline system. In practice, the standard slump test is a common method to measure the rheological properties of the CPB in the mining industry due to its simplicity, which can measure the consistency of the CPB mixture for transportability (Deng et al., 2018; Belem & Benzaazoua, 2008; Clark et al., 1995). The desirable slump of paste backfill is in the range of 150 mm to 250 mm to ensure that the paste has adequate flowability for pumping and placement while maintaining sufficient stability to prevent segregation or excessive water bleeding (Landriault et al., 1997). Moreover, to comprehensively assess the rheological behaviour of the CPB mixture, tests such as yield stress, viscosity, and vane shear are conducted to determine the required pressure

gradient for pumping systems or the maximum horizontal distance achievable in gravity-driven systems, both of which are critical for the performance of pipeline transport and material placement (Saremi, 2024). Moreover, additional factors such as mine layout, stope geometry, flow rates, pump selection, pipe diameter, etc., should be considered to accommodate the specific requirements of each mining operation.

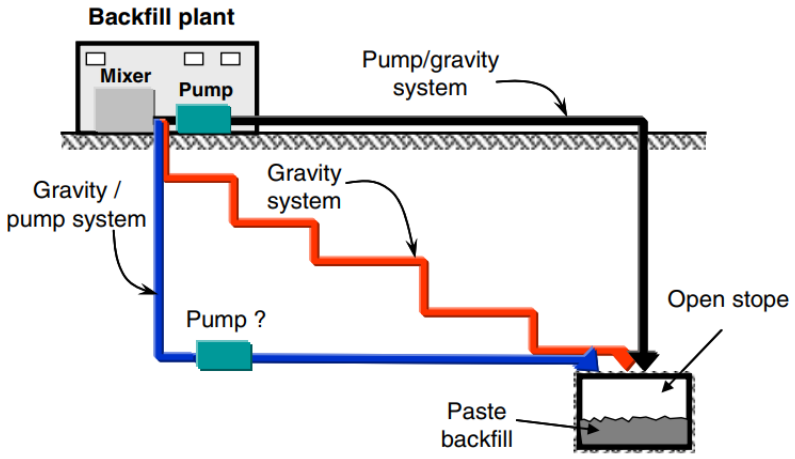

Figure 2-2. Schematic representation of backfill delivery system (Belem & Benzaazoua, 2008).

2.3 Background of Cement Hydration

2.3.1 Portland Cement

Portland cement has been the most widely used material in engineering construction since its inception, owing to its advantages such as ease of preparation, high compressive strength, adaptability to various shapes, and durability (Mehta, 1999). According to ASTM C150/C150M, Portland cement (PC) can be categorized into five types: Type I, II, III, IV, and V. Type I and II are designed for general use, Type III favours the early strength development, Type IV is characterized by a low heat of hydration, and Type V provides high sulfate resistance. Among these, ordinary Portland cement (OPC or Type I) is commonly employed as a hydraulic binder in the preparation of CPBs, primarily contributing to the development of properties within the CPB structure through bonding tailings particles and hydration products (Fall et al., 2009). Moreover, numerous studies have explored the partial replacement of OPC in CPB mixtures with pozzolanic materials such as blast furnace slag and fly ash (Behera et al., 2021; Bull & Fall, 2020; Zhao et al., 2020; Jiang et al., 2019; Belem et al., 2000). This approach not only reduces the costs associated with OPC usage in mine backfilling operations but also enhances the mechanical and rheological properties of CPBs.

2.3.2 Hydration Process

Ordinary Portland cement (OPC) primarily comprises lime (CaO), silica (SiO_2), alumina (Al_2O_3), iron oxide (Fe_2O_3), magnesium oxide (MgO), and sulfur trioxide (SO_3). The first three components predominantly influence the properties of cement, while the remaining components exert secondary effects (Rankin, 1915). During clinker production, these oxides interact at high

temperatures in a kiln, resulting in the formation of key crystalline phases: tricalcium silicate (C_3S), dicalcium silicate (C_2S), tricalcium aluminate (C_3A), and tetracalcium aluminoferrite (C_4AF) with typical constitution approximately of 26-53%, 16-54%, 3-15%, and 8-12% of the clinker composition, respectively, which also govern the chemical, physical, and mechanical properties of hardened cement paste through hydration reactions (Cui, 2017; Telschow et al., 2012; Hansen et al., 1973). When OPC is mixed with water, hydration reactions start immediately to produce three primary hydration products, including calcium silicate hydrate (C-S-H), calcium hydroxide ($Ca(OH)_2$ or CH), and calcium sulfoaluminate (ettringite, $3CaO{\cdot}Al_2O_3{\cdot}3CaSO_4{\cdot}31H_2O$). C-S-H, formed from the hydration of C_3S and C_2S, is the primary binding and strength-conferring product, accounting for approximately 60% (by volume) of the total hydration products in hardened cement. It is characterized by its amorphous and poorly crystalline nature (Ghirian, 2016). CH, a by-product of hydration, constitutes around 20% (by volume) of the total hydration products and is identified by its thin to large hexagonal crystal structure (Double, 1983). Ettringite, formed from the reaction of tricalcium aluminate (C_3A) with gypsum, is a needle-like crystalline compound responsible for controlling the setting time of cement paste. A schematic representation of the Portland cement hydration process and the morphology of hydration products are shown in Figure 2-3 and Figure 2-4.

The hydration process of Portland cement involves a series of chemical reactions between the cement particles (e.g., clinkers, gypsum) and water, which results in the hardening and strength development of the cementitious material. In addition, the hydration of cement is an exothermic process that generates a considerable amount of heat (Swaddiwudhipong et al., 2002). This intricate process can be divided into four key phases (Aldhafeeri, 2018; Scrivener et al., 2015; Bullard et al., 2011; Ylmén et al., 2009; Gartner et al., 2002; Neville, 1995).

i) ***Initial reaction/Pre-induction phase***: The hydration process immediately begins when water is introduced to cement. During the first 30 minutes, rapid reactions occur between tricalcium aluminate (C_3A) and water, leading to significant heat release. The dissolution of aluminates, gypsum, and a portion of tricalcium silicate (C_3S) also takes place. Additionally, alkali sulfates (i.e., Na_2SO_4 and K_2SO_4) and gypsum ($CaSO_4$) dissolve, releasing ions such as K^+, Na^+, Ca^{2+}, OH^-, and SO_4^{2-} into the pore water. These ions react with C_3A to form ettringite, while a small amount of C_3S and dicalcium silicate (C_2S) react to produce initial calcium silicate hydrate (C-S-H) gel and calcium hydroxide (CH). Both reactions are exothermic, generating the first heat peak, as shown in Figure 2-5.

ii) ***Slow reaction/Dormant phase***: Following the initial reactions, the generated ettringite and C-S-H gel precipitate onto the surfaces of unhydrated C_3S and C_2S particles. This precipitated layer acts as a barrier, inhibiting further water ingress and temporarily slowing down the hydration reactions. This phase, which lasts approximately 30 minutes to 3 hours, generates minimal heat. It provides the necessary workability of the cement paste, allowing it to be placed and compacted before hardening begins.

iii) ***Acceleration phase***: At the end of the dormant phase, the protective barrier on the cement particles destabilizes due to chemical and physical changes. Factors such as osmotic stresses from high ion concentrations (i.e., Ca^{2+}, OH^-), increased kinetic energy from rising temperatures, and pressure-induced cracking due to the volume expansion of hydration products (i.e., C-S-H and CH) contribute to the breakdown of this layer. The exposure of unhydrated particles to water allows hydration to resume at an accelerated rate, particularly the reaction of C_3S. During this phase, the formation of C-S-H gel and CH increases significantly, accompanied by a peak in heat generation. This stage also leads to pore structure refinement and the setting of the cement paste.

iv) ***Deceleration phase***: As the hydration progresses, the availability of water and unhydrated cement particles decreases, which decelerates the reaction rate. The produced hydration products continue to fill the pore spaces, further refining the pore structures. Heat generation declines but persists at a low level over time. During the later stages, the hydration of C_2S becomes more prominent, contributing to long-term strength development, which can continue for years as long as unhydrated particles and moisture are available.

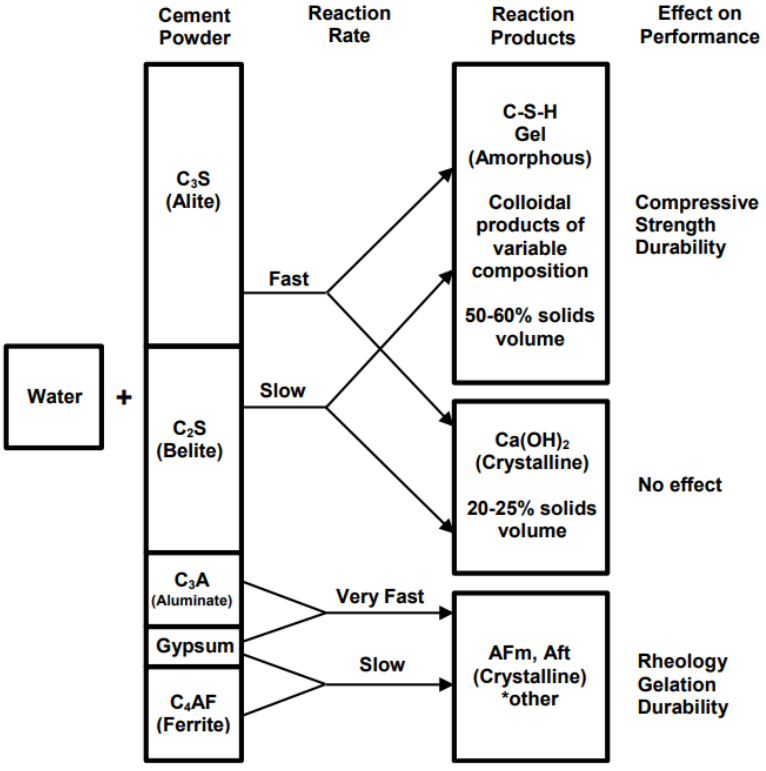

Figure 2-3. Schematic diagram of cement hydration processes (Ghirian, 2016).

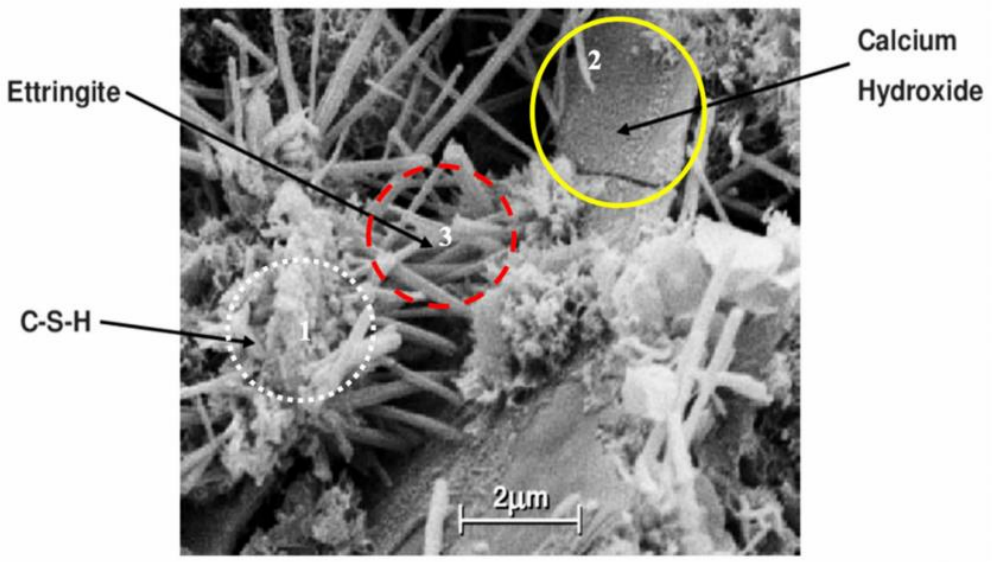

Figure 2-4. Morphology of cement hydration products (Othman et al., 2023).

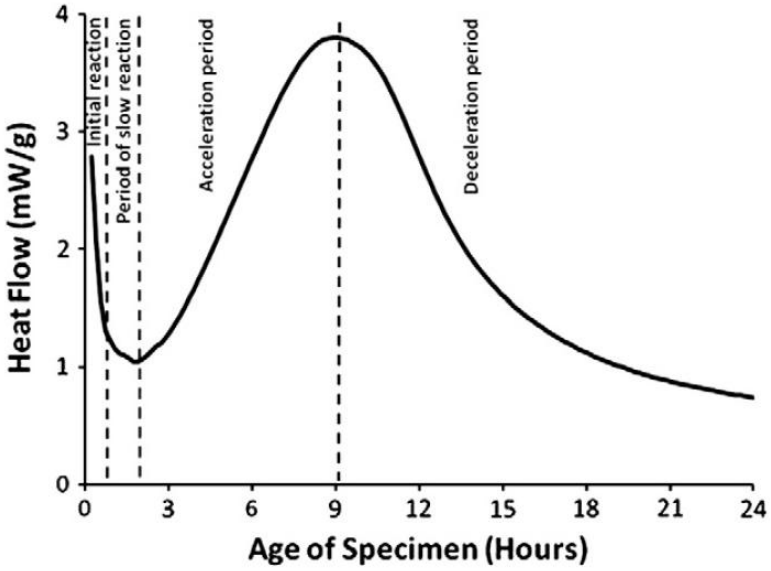

Figure 2-5. Rate of cement hydration subjected to curing time (Bullard et al., 2011)

2.4 Properties Development of CPB

CPB structure serves as the structural support in the underground mined voids, where its ability to withstand stresses from overburden, overlying or surrounding rock masses, or ground movement is essential for maintaining the stability of the mine site. A thorough understanding of the properties of CPB and the factors influencing them is crucial for optimizing its performance and ensuring the reliability of the designed backfill structure. This section provides a comprehensive overview of the primary properties of CPB, including the physical, thermal (T), hydraulic (H), mechanical (M),

and chemical (C) characteristics, as well as an analysis of the factors influencing these properties and their interactions.

2.4.1 Physical Properties and Influencing Factors

The physical properties of CPB, such as porosity (or void ratio), density (or unit weight), water content, and degree of saturation, significantly influence its geotechnical performance. Numerous laboratory and in situ studies (Liu et al., 2018; Ghirian & Fall, 2015; Yilmaz et al., 2011; Fall et al., 2005; le Roux et al., 2005; Pierce, 1999) have explored the evolution of these properties during the curing process. These studies have identified that the physical properties of CPB are influenced by various individual or combined factors, including tailings characteristics (e.g., fineness, density, mineralogy), mixing recipe (e.g., binder content, binder type, w/c ratio), backfilling strategies, and curing conditions (e.g., temperature, curing stress, drainage conditions).

Tailings, as the primary constituent of CPB, determine the key properties, such as particle size distribution and mineralogy, which affect the microstructure, density, cohesion, and strength development within the matrix. Fall et al. (2005) evaluated the impact of tailings particle size and density on CPB quality and found that fine tailings (<20 μm) significantly increase porosity and change the pore size distribution, reducing water drainage and strength development while increasing water demand for a given consistency. Specifically, the overall porosity and void ratio are increased when increasing the portion of fine tailings used for the mixture, thus contributing to the reduced strength gain. In addition, the presence of sulphide minerals in tailings adversely affects the strength and durability of the CPB through two primary mechanisms. First, high sulfate content inhibits binder hydration, particularly during the early hydration of C_3A. Second, the formation of expansive minerals such as ettringite and gypsum causes volumetric expansion, generating pressure and microcracks, which degrade the CPB matrix. The combined effect of reduced hydration and the formation of expansive minerals results in significantly increased porosity, decreased mechanical strength, and compromised long-term stability. However, under controlled conditions, the precipitation of expansive minerals can refine the pore structure (i.e., porosity reduction with lower sulfate content) and positively contribute to strength development.

The components of the designed CPB, such as binder content and type, also play a critical role in determining the physical properties. OPC is the typical binder used in the preparation of CPB in the mining industry, while other minerals, such as fly ash, silica fume, and blast furnace slag, are also added to reduce the binder consumption and enhance strength. For example, Yilmaz et al. (2011) reported that increasing binder content (i.e., OPC-slag at a ratio of 20:80 wt.%) refines porosity and reduces average pore diameter due to the formation of more hydration products. Qi et al. (2005) investigated the compressive strength and microscopic characteristics of CPB by employing fly ash at an early age (up to 28 days). The results revealed that the porosity decreases and the compressive strength of CPB increases with the increase of fly ash dosage, ascribed to the higher pozzolanic activity and fewer large pores. Add to that, the enhancements of high pozzolanic content also improve resistance to sulphate attack, contributing to the long-term stability of CPB, particularly when sulphide tailings are incorporated (Kesimal et al., 2005).

Water content in CPB mixtures is another critical factor influencing their physical properties. Additional water is typically added to ensure workability and pumpability during the design and preparation of CPB. However, increasing the w/c ratio reduces particle-particle contact and increases the thickness of the lubricating film, decreasing the yield stress (increasing fluidity) of the mixture (Zhao et al., 2020). Despite its benefits for handling, high water content often exceeds the hydration requirements of cement, leading to increased porosity and reduced strength (Belem and Benzaazoua, 2008). Lowering the w/c ratio generally reduces porosity and improves compressive strength by filling capillary voids with hydration products, which dominate CPB strength development (Yılmaz et al., 2014; Yilmaz et al., 2011). Moreover, water quality plays a critical role; while freshwater minimizes chemical interference, mine process water containing heavy metals or sulfates can attack cementitious bonds, deteriorating CPB microstructure, strength, and stability (Belem and Benzaazoua, 2008).

Due to challenges associated with in situ sampling and testing, such as limited access to backfilled stopes, operational interruptions, costs, and safety concerns, data on in situ physical properties of CPB are limited (le Roux et al., 2005; Pierce, 1999). To simulate field conditions, Ghirian and Fall (2013, 2014) developed a curing cell system at the University of Ottawa that accounts for curing stress, time, filling rate, and drainage conditions, integrating multiphysical THMC processes. Their findings revealed that the application of curing stress reduces porosity regardless of drainage conditions or filling rates. This reduction is attributed to the densification of the CPB matrix under stress. Additionally, under drainage conditions, the removal of excess water facilitates a faster settlement of suspended solids and denser packing of the CPB matrix while under pressure, resulting in a further decreased porosity and void ratio.

2.4.2 Mechanical Properties and Influencing Factors

The mechanical properties of CPB are among the most critical design criteria, as CPB structures must meet specific loading requirements to ensure a safe underground working environment for mining activities (Fall et al., 2010). Extensive research has been conducted using various tests, including uniaxial compressive strength (UCS), triaxial compression, direct shear, indirect tensile, and consolidation tests, to evaluate the mechanical characteristics of CPB. These studies focus on parameters, such as different strength measures, stress-strain behaviour, modulus of elasticity, Poisson's ratio, cohesion, and internal friction angle. A comprehensive understanding of these mechanical properties is essential for designing reliable CPB structures and assessing their short- and long-term performance after placement.

Triaxial shear tests are widely employed to evaluate the shear strength, cohesion, internal friction angle, and failure envelope of CPB materials under various influencing factors, including tailings characteristics (e.g., particle size distribution; Wu et al., 2018), binder type and content (Behera et al., 2020; Belem et al., 2002; de ARAÚJO et al., 2017), curing conditions (Wang et al., 2020), and drainage conditions (e.g., temperature and drainage; Xiu et al., 2022). For instance, Fall et al. (2007) conducted triaxial compression tests varying the curing time and confinement ratio (the ratio of confinement stress to UCS). Their findings indicated that deviator stress (peak stress) increased

with a higher confinement ratio, though the rate of increase diminished at higher confinement levels. They also observed that an increase in confinement reduced the elastic modulus, a relationship influenced by the UCS of the CPB. Based on their results, a formula was proposed to predict the effect of confinement on the elastic modulus. Xiu et al. (2022) further explored the mechanical parameters of CPB using triaxial compression tests, analyzing the results within the Mohr-Coulomb criterion framework to assess the effects of drainage conditions and curing temperatures. The study revealed that higher lateral constraints led to a linear increase in peak deviator stress and an exponential increase in ultimate axial strain, accompanied by an enhanced elastoplastic stage. Additionally, they reported that prolonged curing time, elevated curing temperatures, and drained curing conditions significantly improved peak deviator stress and cohesion but reduced the internal friction angle. These findings imply the critical role of shear mechanical parameters in influencing vertical stress distribution within CPB structures. Direct shear tests have also been utilized to measure the shear strength parameters at CPB-rock and CPB-CPB interfaces (Guo et al., 2020; Xu et al., 2019; Nasir & Fall, 2008). For example, Koupouli et al. (2006) examined the shear strength of CPB-CPB and CPB-rock wall interfaces at short curing times (≤7 days) and found that the mobilized shear strength at the CPB-CPB interface was higher than at the CPB-rock interface under identical normal stress, regardless of cement content. Fang (2021) extended this work by conducting a series of laboratory tests to evaluate the effects of sulfate content, temperature, curing stress, drainage conditions, interface roughness, and their interactions (THMC effects) on the shear behaviour of CPB-rock interfaces. These studies provide valuable insights into the stability of backfill structures and contribute to their improved design.

The tensile strength of CPB is an important property for evaluating its ability to resist cracking and failure under tensile stresses, which are frequently encountered in underground mining environments. Both direct tensile test and indirect (Brazilian) tensile test have been employed to evaluate the tensile strength of CPBs (Guo et al., 2021; Pan & Grabinsky, 2021; Jafari & Grabinsky, 2021; Johnson et al., 2015). Among these methods, the indirect tensile test is more commonly used for brittle materials like CPB due to its simplicity in specimen preparation and the practicality of utilizing standard compression testing equipment. Tang et al. (2023) conducted a comparative study on the tensile strength of cemented tailings backfill (CTB) using both Brazilian and direct tensile tests. Their results revealed similar trends in tensile strength across variations in binder content, solid mass content, and curing time for both methods. However, tensile strength values obtained from the Brazilian test were generally lower due to the influence of the Poisson effect. To address this discrepancy, the authors proposed a linear correlation to enhance the accuracy of Brazilian test results for field applications.

The UCS test is the most widely used method to evaluate the mechanical performance of CPB at mines due to its simplicity, cost-effectiveness, and efficiency (Fall et al., 2010; Belem & Benzaazoua, 2008). The required UCS of a CPB structure largely depends on its intended purpose and the geotechnical loading requirements under varying geological conditions. For instance, CPB used for underground disposal or stope backfilling generally requires low compressive strength (e.g., 150-300 kPa), whereas backfill designed for free-standing or roof support typically demands

higher compressive strength, ranging from 1 to 4 MPa (Belem & Benzaazoua, 2008; Fall et al., 2005; Grice, 1998). Numerous studies have investigated the factors influencing the short- and long-term compressive strength development of CPB, which can be broadly categorized into two categories: internal factors, including tailings characteristics (e.g., particle size distribution, compositions), binder type and content, w/c ratio (water content), mixing water; and external factors, including curing time, curing conditions (e.g., curing stress, temperature, humidity), drainage conditions, and backfilling strategies (e.g., placement method, filling rate).

The characteristics of tailings, including particle fineness, density, and sulphide content, significantly influence the UCS evolution of CPB. Specifically, the proportion of fine particles (< 20 μm) strongly affects strength development, porosity, pore size distribution, and water drainage ability (Fall et al., 2005). CPBs with higher fine particle content generally exhibit lower strength. A minimum fine particle content of 15% by weight is typically required to retain sufficient water for paste formation. Additionally, the chemical composition of the tailings plays a pivotal role. For example, sulphide minerals can oxidize in the presence of oxygen and water, producing sulphate ions that inhibit binder hydration and promote the formation of expansive secondary minerals like ettringite, which can weaken the CPB matrix (Fall & Pokharel, 2010; Benzaazoua et al., 2002). On the other hand, reactive aluminosilicates in the tailings may enhance strength through pozzolanic reactions with lime released during cement hydration (Ouffa et al., 2020; Hadi et al., 2018). Factors such as the pH of tailings and contaminants, including heavy metals and organic compounds, further influence hydration, setting time, and mechanical properties (Kasap et al., 2022; Kesimal et al., 2005).

The development of mechanical properties in CPB is driven by the hydration products (e.g., calcium silicate hydrates, ettringite, and calcium hydroxide) formed by binder reactions, typically using OPC. Increasing the binder content generally enhances strength, but the cost of the binder can account for up to 75% of backfilling operations, making cost optimization essential. Consequently, studies have explored partially replacing OPC with supplementary materials such as slag or fly ash. For example, Jiang et al. (2020) found that replacing OPC with alkali-activated slag significantly increased strength after 28 days of curing, achieving UCS values of 3 MPa with an 8% binder content. Similarly, fly ash replacement has been shown to improve strength due to enhanced bonding between tailings particles and binder hydration products (Zhou et al., 2021; Zhao et al., 2020).

The w/c ratio also dominates the strength development of CPB. The reduction in w/c would result in an increase in strength regardless of the binder content. This enhancement in strength is mainly attributed to the decreased overall porosity of the backfill and the higher binding between particles, thus contributing to the rapid strength development (Fall et al., 2008; Galaa et al., 2011; Yılmaz et al., 2014). Additionally, the chemistry of mixing water can impact hydration. For instance, high sulphate concentrations in water can inhibit early-stage cement hydration, delaying strength development (Fall & Pokharel, 2010; Pokharel & Fall, 2013). In contrast, water containing

chlorides may promote early hydration but can compromise long-term durability due to corrosion (Ouyang et al., 2022; Tian et al., 2023).

External factors, such as environmental and operational conditions during curing, significantly influence the mechanical properties of CPB. Curing stress enhances particle packing, accelerates binder hydration, and promotes the formation of hydration products, resulting in a refined microstructure, reduced porosity, and increased compressive strength (Yilmaz et al., 2011, 2014). Additionally, it is noted that the drainage of excess pore waters within fresh CPB mixture contributes to the strength increment as the drainage of excess pore water results in the reduction in the total porosity and void ratio of backfilling, thereby increasing the strength. Moreover, the increase in curing temperature accelerates the hydration process. The enhanced cement hydration produces more hydration products, refining the pore structure and enhancing cohesion and strength (Fall et al., 2010). Furthermore, faster filling rates generally result in higher UCS values due to increased particle packing density under curing stress (Ghirian & Fall, 2016). However, rapid filling can generate high PWPs during the early stages, reducing effective stress and inhibiting binder hydration. Moreover, rapid loading can cause microcracking at points of contact between cement hydration products, compromising the structural integrity of CPB.

In summary, understanding and optimizing the mechanical properties of CPB allow for more efficient material use and cost reduction. For example, tailoring the mix design to achieve adequate strength without excessive binder content can lower material costs while maintaining performance. Thus, the mechanical properties of CPB are not only fundamental to ensuring its structural integrity but also critical for the overall efficiency, safety, and sustainability of mining operations.

2.4.3 Thermal Properties and Influencing Factors

The thermal properties and processes of CPB materials can be classified into two main categories: intrinsic thermal properties and external thermal factors. Intrinsic thermal properties, such as thermal conductivity, specific heat capacity, and thermal expansion, are inherent to the composition and structure of the CPB. These properties are influenced by various factors, such as binder type and content, tailings mineralogy, curing age, curing temperature, porosity, and degree of saturation, which govern the heat transfer, retention, and expansion behaviour of the CPB matrix.

Thermal conductivity is a key intrinsic property of CPB, reflecting its ability to transfer heat. Célestin and Fall (2009) conducted a study using a KD2 thermal properties analyzer to quantitatively investigate the effects of different influencing factors on the thermal conductivity of CPB by using a KD2 thermal properties analyzer. The results revealed that CPBs with higher quartz content exhibit greater thermal conductivity due to the high thermal conductivity of quartz (7.7 W/(m·K)), which is significantly higher than that of other minerals commonly found, such as amphibole (3.46 W/(m·K)), feldspar (2.25 W/(m·K)), and mica (2.03 W/(m·K)). Additionally, components such as water (0.56-0.64 W/(m·K)) and Portland cement (0.3-1.3 W/(m·K)) contribute much lower conductivity in the CPB mixture (Wolterbeek & Hangx, 2023). The study also demonstrated that the thermal conductivity of CPB decreases as the content of fine-grained tailings

increases. Increased tailings fineness reduces the gradation and packing density of the material, resulting in higher porosity and void ratios. This increased porosity introduces more void spaces filled with air or water, which have significantly lower thermal conductivity, thereby reducing the overall thermal conductivity of CPB (Ghirian & Fall, 2013; Célestin & Fall, 2009). However, the mixing parameters, such as binder type and content, water content, and the presence of sulphate, appear to have a minor influence on the thermal conductivity of CPBs. Furthermore, Célestin and Fall (2009) observed that thermal conductivity decreases as specimen temperature increases. Notably, a significant drop in thermal conductivity occurs when temperatures exceed 50°C. This phenomenon is attributed to accelerated hydration at higher temperatures, which increases the water consumption rate. Simultaneously, elevated temperatures enhance water evaporation. The combined effects of self-desiccation and evaporation reduce the degree of saturation within the CPB matrix, leading to the partial replacement of water in voids with air. Since air has an extremely low thermal conductivity (0.025 W/(m·K)) under ambient conditions, this substitution markedly lowers the overall thermal conductivity of CPB.

On the other hand, external thermal factors, such as geothermal gradients, ambient temperature fluctuations, and heat generated during binder hydration, significantly impact the thermal performance of CPB under site-specific conditions. Among them, the exothermic reactions during binder hydration are the primary source of heat within CPB structures. During the curing process, a considerable amount of heat is released (Nasir & Fall, 2009). Given the large dimensions of underground CPB structures, this heat is effectively retained, and when combined with heat generated during pipeline transportation, the temperature within the CPB structure can rise substantially, reaching up to 50°C or even higher (Fall et al., 2010; Thompson et al., 2012). As previously discussed, the binder hydration process highly depends on various factors, including binder dosage, water content, curing conditions, backfilling strategy, etc. Then, the geological conditions significantly impact the temperature due to the geothermal gradients. The exposed rock mass can be the heat load source in any deep-level mining operation, which means those near geothermal sources would experience higher temperature levels with deeper mines (Menéndez et al., 2019; Wagner, 2023). Additionally, the geographical location of a mine affects the thermal behaviour of backfill structures, especially those situated at relatively shallow depths. In such cases, the regional climate and ambient conditions can have a noticeable impact on CPB temperature (Sheshpari, 2015; Fall et al., 2010). Moreover, self-heating caused by the exothermic reactions of sulphide minerals, either within the backfill or in the surrounding rock mass, can further raise temperatures (Rosenblum et al., 2001). However, human-induced heat sources, such as machinery operation and blasting activities, typically have a minor influence on the thermal behaviour of large-scale CPB structures due to their transient and localized nature (Fall et al., 2010).

The effects of temperature on CPB materials have been extensively studied (Jiang et al., 2020; Zhao et al., 2020; Aldhafeeri et al., 2016; Fall et al., 2010; Nasir & Fall, 2010). For example, it has been demonstrated that moderate temperature increases (below 35°C) can enhance the compressive and split tensile strengths, shear stress at the CPB-rock interface, modulus of elasticity, and microstructure of CPB specimens. This improvement is primarily attributed to the accelerated

cement hydration process (Fall et al., 2010; Fang & Fall, 2018). Furthermore, the increasing temperatures would increase yield stress and viscosity of the CPB mixture, which are not favourable to the transportation process (Wu et al., 2013). This deterioration occurs as a result of the coupled effects: (i) the decomposition of hydration products, (ii) the development of microcracks at the interfaces between tailings and the cement matrix, and (iii) the formation of larger cracks due to the excessive water vapor pressure at temperatures exceeding 400°C. These factors collectively contribute to the structural weakening and failure of the CPB material.

2.4.4 Hydraulic Properties and Influencing Factors

The primary hydraulic properties and processes in CPB materials include hydraulic conductivity and the generation of pore water pressure (PWP), both of which are critical for understanding water movement and stability in CPB systems.

Hydraulic conductivity determines the rate at which water flows through the CPB matrix and is a key indicator of the permeability and integrity of the material. Studies have been conducted to investigate the evolution of hydraulic conductivity (i.e., saturated hydraulic conductivity, k_{sat}) of CPBs subjected to different factors, such as mix components, porosity, binder content, sulphate presence, curing time, curing temperature, mechanical damage, etc. The hydraulic conductivity of CPB is highly dependent on the binder dosage and type. Increased cement dosage reduces hydraulic conductivity by increasing the precipitation of hydration products, which contributes to microstructure refinement (Fall et al., 2009). The type of binder also influences hydraulic conductivity. For instance, partial replacement with slag introduces both filler and pozzolanic effects, with the impact varying based on curing time (Wu et al., 2019; Alhomair et al., 2017; Fall et al., 2009). As aforementioned, a lower w/c ratio accelerates binder hydration at early ages, refining pore structures, blocking pore connectivity, and reducing permeability while increasing strength.

Curing conditions also play a significant role. Hydraulic conductivity decreases as curing temperature increases, primarily due to accelerated hydration and pore filling (Pokharel & Fall, 2013; Fall et al., 2009). The presence of sulphates introduces positive and negative effects. At early curing stages (0-28 days), CPBs with high sulphate concentrations (i.e., 15,000-25,000 ppm) exhibit higher hydraulic conductivity because sulphates inhibit cement hydration, resulting in a more porous matrix. Over time, CPBs with high sulphate content show reduced hydraulic conductivity due to the precipitation of secondary hydrated minerals in the capillary pores, including gypsum and ettringite. However, at advanced curing stages (e.g., 90 days), the formation of excessive amounts of expansive minerals (ettringite, gypsum) in the CPB with high sulphate contents exert excessive pressure in the CPB structure, resulting in the formation of microcracks, thus causing an increase in the permeability of the CPBs (Li & Fall, 2016; Pokharel & Fall, 2013). The coupled effects of sulphate and temperature on hydraulic conductivity have also been studied. Higher curing temperatures typically reduce hydraulic conductivity by enhancing hydration and pore filling, except in high-sulphate environments (25,000 ppm at 50°C), where destabilization of ettringite and sulphate adsorption by C-S-H gel led to increased hydraulic conductivity (Pokharel

& Fall, 2013). During the service life of CPB, cracks can form in the structures due to internal and external factors (see Section 2.5.1), compromising mechanical stability and increasing permeability. Increased permeability provides preferential pathways for aggressive agents (e.g., oxygen, ions) that facilitate acid mine drainage (AMD) and contamination of mine areas and/or groundwater systems.

PWP is a reliable indicator for the assessment of mechanical strength, liquefaction potential, and the stability of barricades in CPB structures. PWP evolution occurs immediately after placement because the confined water within the backfill material cannot dissipate quickly. Laboratory and field studies have been conducted to monitor PWP behaviour (Al-Moselly & Fall, 2024; Wang et al., 2022; Xiu et al., 2022; Helinski et al., 2011; Thompson et al., 2012). Several factors can impact the magnitude and dissipation of PWP, including mix design (e.g., water content, binder type, and dosage), tailings properties (e.g., particle size and mineralogy), and curing/placement conditions (e.g., curing temperature, stope geometry, and drainage conditions). Upon placement, CPB is typically saturated with high initial PWP due to its water content and overburden pressure from surrounding rock or additional backfill layers. Efficient drainage is essential for the reduction of PWP and increases in effective stress, which favour consolidation and strength development (Ghirian & Fall, 2013; Fahey et al., 2010). Conversely, poor drainage conditions retain water within the low-permeability CPB matrix, causing prolonged elevated PWP (Al-Moselly, 2024). Sustained high PWP would reduce effective stress, delay hydration reactions, and increase the risk of structural instability, deformation, or liquefaction. Furthermore, inadequate drainage can result in uneven PWP dissipation, leading to localized zones of weakness or cracks within the CPB structure.

2.4.5 Chemical Properties and Influencing Factors

The chemical properties of CPB are fundamental to its durability, strength development, and overall performance in underground environments. These properties are primarily influenced by interactions among the binder, water, and tailings, as well as the chemical reactions that occur during the hydration process. In other words, the chemical characteristics of CPB significantly affect the coupled thermal, hydraulic, and mechanical behaviours as previously discussed.

The hydration of cement binders in CPB results in the formation of hydration products such as C-S-H, CH, and ettringite, which fill pore spaces within the CPB matrix. These hydration products contribute to strength development and permeability reduction. The specific chemical reactions involved in binder hydration are detailed in Section 2.3. The mineral composition of the tailings has a profound influence on the chemical behaviour of CPB. For example, high sulphate concentrations can lead to sulphate attack, where C_3A and CH react with sulphate ions to form expansive minerals, such as ettringite and gypsum. The excessive expansive minerals in the capillary pores can induce microcrack formation and weaken the CPB structure (Pokharel & Fall, 2013; Fall et al., 2009). Similarly, acidic tailings can lower the pH of the curing environment ($pH<7$), hindering hydration reactions and accelerating the deterioration of the backfill matrix (Kasap et al., 2022; Zhang et al., 2021). CPBs containing high concentrations of acidic tailings experience more complex hydration processes. Acidic ions reduce pH and gradually increase

sulphate content, significantly lowering the alkalinity of the curing environment. Over time, this results in the dissolution of CH and the destruction of C-S-H, ultimately diminishing the strength and permeability of CPB (Kasap et al., 2022; Dashti & Nematzadeh, 2020; Dong et al., 2019).

In the same way, the chemistry of the mixing water also significantly impacts the hydration process and the resulting chemical properties of CPB. Fresh water, with its neutral pH and low dissolved ion content, is considered ideal for CPB preparation as it minimizes interference with cement hydration and the formation of hydration products. However, mine process water is often preferred for its practicality and sustainability in mining operations. Mine process water usually contains dissolved ions and contaminants, such as sulphates, chlorides, heavy metals, and organic matter, which can alter CPB properties (Zhou et al., 2021; Wu et al., 2015; Rubashkina & Kostina, 2023). For example, chlorides can accelerate the corrosion of reinforcing materials within the backfill (Xu et al., 2022; Wang et al., 2021), while dissolved gases such as CO_2 and variations in pH can further disrupt hydration reactions and compromise the durability of CPB (Chen et al., 2022).

Changes in ion concentration within the CPB pore fluid can be monitored using electrical conductivity (EC), a measure of the chemical characteristics of the pore solution, particularly the ion composition and concentration (Jafari et al., 2023; Xiapeng et al., 2019; Ghirian & Fall, 2017). During the early stages of hydration, the EC value is typically high due to the rapid dissolution of cement particles and the release of ions, such as calcium, hydroxide, and sulphates, into the pore water. As hydration progresses, these ions are consumed to form solid hydration products like C-S-H and ettringite, leading to a gradual decline in EC over time (Liu & Fall, 2022). The mixing water, such as freshwater or sulphate-rich mine process water, also influences EC. For instance, CPB prepared with mine process water often exhibits higher EC due to the elevated concentrations of sulphates and other dissolved ions (Li & Fall, 2016). In addition to ion concentrations, factors such as pore structure, degree of saturation, and temperature also impact EC by affecting ion mobility and pore connectivity. Monitoring EC provides valuable insights into chemical evolution, hydration progress, and interactions between the constituents within the CPB matrix, making it a useful indicator for the evaluation of the long-term stability and performance of CPB structures.

2.4.6 Coupled Multiphysical (THMC) Processes

The fundamental properties and factors affecting CPB performance provide a basis for understanding its behaviour. However, in underground applications, CPB operates as a complex geotechnical system where thermal (T), hydraulic (H), mechanical (M), and chemical (C) properties and processes are intricately interconnected. These coupled THMC interactions, as illustrated in Figure 2-6, critically influence the performance, stability, and durability of CPB structures.

Thermal (T) processes: The thermal behaviour of CPB involves heat generation, transfer, and advection, all of which play a significant role in determining the overall performance. Cement hydration, an exothermic reaction, generates heat that accelerates the production of hydration products. This, in turn, contributes to pore refinement and improves the mechanical strength of the

CPB. Additionally, the heat generated during hydration interacts with the surrounding rock mass and pore water, influencing water evaporation rates and altering pore water movement. These thermal changes lead to the rapid development of PWP and suction within the matrix. Furthermore, temperature increases affect chemical processes by altering the concentration of ions in the pore water, further influencing the microstructural and mechanical properties of CPB.

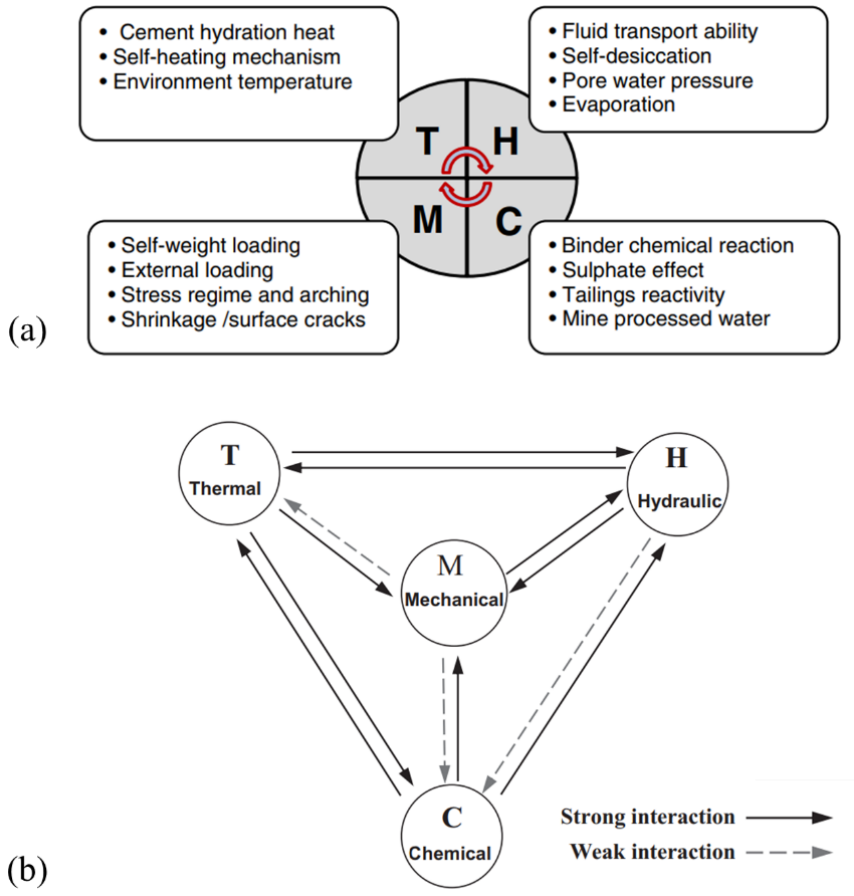

Figure 2-6. (a) Primary coupled THMC factors impacting the behaviour of CPB structures; (b) Primary multi-physics THMC processes and their interactions (Ghirian & Fall, 2013 and 2017).

Hydraulic (H) processes: Hydraulic processes such as permeability and PWP development are strongly linked to the thermal and mechanical behaviour of CPB. Water within the CPB matrix moves through capillary pores during curing, while hydration products precipitate to fill these pores. This reduces both permeability and PWP. As hydration progresses or water evaporates due to elevated temperatures, desaturation occurs, leaving voids filled with air. This desaturation reduces the thermal conductivity of the CPB. Moreover, as water is removed through drainage or evaporation, the remaining pore water becomes concentrated with dissolved ions. This increase in ion concentration intensifies chemical interactions, further impacting the long-term stability and durability of the CPB.

Mechanical (M) processes: The mechanical properties of CPB, such as its compressive strength, elasticity, and stress response, interact with the chemical and hydraulic processes. During placement, the curing stress facilitates the consolidation of the backfill by draining excess water and compacting particles, which reduces pore water pressure and increases effective stress. This process enhances hydration, reduces permeability, and improves the mechanical strength of CPB. However, excessive stress may lead to microcrack formation within the matrix, which can create pathways for fluid flow and increase permeability. Additionally, the curing stress has insignificant effects on the rate of hydration reactions, as the stress in the field backfill is insufficient.

Chemical (C) processes: Chemical reactions, particularly cement hydration and interactions with impurities in tailings or mixing water, play a vital role in the evolution of CPB. The binder hydration process generates hydration products (e.g., C-S-H, CH), which enhance the bonding between the particles and increase the mechanical strength of CPB. The precipitation of hydrates filling in the voids also decreases the overall porosity and void ratio, thus reducing the permeability of the CPB matrix. As the hydration reactions progress, the released heat increases the temperature of CPB, which, in turn, further facilitates the hydration process. However, the presence of sulphates, chloride ions, or other contaminants can interfere with the hydration process. Additionally, the pH of the CPB, which is influenced by the chemical composition in the mixing water and tailings, affects the solubility and formation of various minerals, further influencing the strength development and durability.

2.5 Cracks Generation in CPB Structure

2.5.1 Crack-inducing Factors

The properties of CPB mixtures are dominated by a wide range of factors, including physical, thermal, hydraulic, mechanical, and chemical characteristics, as extensively discussed in the previous section. The application of CPB in refilling underground extracted goaf not only stabilizes the surrounding geological structures and ensures a safe working environment for mining operations but also significantly reduces the surface disposal of tailings, mitigating environmental pollution and ecological damage. However, as an engineered cementitious material, cracks may form in CPB matrices as a similar challenge arises in other conventional cementitious materials (e.g., concrete, mortar, engineered cementitious composites) (Choi et al., 2017; Ohno & Ohtsu, 2010; Yıldırım et al., 2015).

The generation and propagation of cracks in CPB structures (Song et al., 2022; Zhou et al., 2021; Cao et al., 2019; Liu et al., 2019; Aldhafeeri & Fall, 2016; Ghirian & Fall, 2014; Fall et al., 2009; Fall & Benzaazoua, 2005) can be induced by internal factors, such as shrinkage (self-desiccation), sulphate attack and initial structural defects, external factors, such as the overburden pressure (self-weight pressure, loads from mining activities (i.e., machinery), early application of load, and uneven load distribution), stresses induced by the closure of rock walls or ground movement, and rock bursts, or coupled effects of these conditions, as illustrated in Figure 1-2. In practical applications, defects such as joints or fissures are inevitable within CPB structures during

placement (Song et al., 2022). Under external stresses, these defects acting as zones of stress concentration are more susceptible to stress concentration, where the propagation and expansion of cracks will be accelerated within the matrices.

Although CPB structures are designed to meet the geotechnical loading requirements for underground stability, with dimensions often spanning tens to hundreds of meters, the abovementioned crack-inducing factors may not immediately lead to catastrophic structural failure or collapse. However, over time, the accumulation of degradation and the propagation of micro- and macro-cracks can compromise the integrity of the CPB matrix. This progressive deterioration may impair the durability and environmental performance of CPB, posing challenges to its long-term functionality and stability.

2.5.2 Crack Damage Evolution

For CPB structures in underground mines, the CPB material at a given depth is significantly influenced by compressive, shear, and tensile stresses, as previously discussed. The stability of the CPB structure is closely tied to the accumulation of cracks and other forms of damage within the material, which develop and propagate progressively under external loads until structural failure occurs. The generation, propagation, and interaction of microcracks within the CPB, driven by external stresses, ultimately determine the macroscopic deformation and failure characteristics of the material (Zhou et al., 2021). Understanding the stress-strain behaviour of CPB is crucial for gaining insights into the mechanisms of crack initiation and propagation within the matrix. This knowledge is essential for evaluating the structural behaviour and overall stability of the CPB under various loading conditions.

UCS is considered one of the most important parameters in the design and optimization of CPB operations for underground mining due to its simplicity and cost-effectiveness (Fall et al., 2010). Generally, the stress-strain curve of CPB under compression loading can be divided into four main stages as illustrated in Figure 2-7 (Wang et al., 2024; Zhang et al., 2022; Wang et al., 2021; Zhou et al., 2021; Fall et al., 2007). Stage I (segment AB): compaction stage. During this stage, the primary micro-voids and cracks in the CPB matrix are gradually compacted in the axial direction, resulting in a concave-shaped curve. The energy from the applied load is mainly used to compress the internal pore structure of the CPB sample. Once the pore structure is compacted, the energy input begins to be stored in the CPB sample as elastic energy. Stage II (segment BC): linear elastic stage. In this stage, the curve exhibits a relatively linear upward trend, indicating that the CPB is in the elastic range. No cracks initiate or propagate, and the volume strain increases gradually. The strain remains reversible if the external load is removed during this phase. At this stage, elastic energy accumulates quickly, while dissipated energy remains minimal. Stage III (segment CD): yield stage (crack initiation and propagation). As the applied load increases, the stress exceeds the elastic limit (i.e., the crack-initiation strength, point C), causing the deformation to transition into elastoplastic behaviour. In this stage, elastic energy accumulation slows, and energy is gradually dissipated as plastic energy. Cracking begins inside the sample, with primary microcracks expanding and new cracks initiating and propagating. The crack-initiation strength marks the

critical stress at which the CPB sample begins to experience damage, while the stress at endpoint D represents the peak stress of the sample. Stage IV (segment DE): post-peak stage. Upon reaching the peak stress, the CPB sample becomes destabilized as the applied stress exceeds its pressure-bearing capacity. The elastic energy of the sample decreases to its minimum, and the rate of energy dissipation slows down. Despite the decrease in the strength of the tested sample, residual strength from friction between failure surfaces prevents a sudden drop in the stress curve after peak stress. The increasing deformation contributes to the further propagation and opening of the cracks formed earlier.

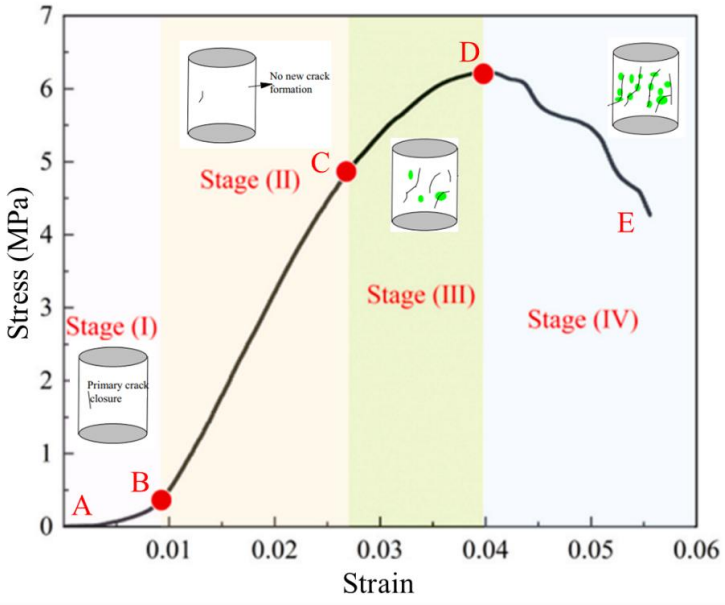

Figure 2-7. Schematic representation of CPB stress-strain curve under compression loading (adapted from Wang et al., 2024; Zhou et al., 2021).

Shear stress may arise at the interface between CPB and surrounding rock walls, particularly under conditions of differential rock movement, rock wall convergence, or fault slip, which can impose lateral constraint stress on the CPB structure. To account for these stress conditions, triaxial shear tests are commonly used to evaluate the mechanical behaviour and deformation characteristics of CPB under confining pressures. The failure patterns of CPB samples subjected to triaxial compression can generally be categorized into four types: single shear cracks, which form along one direction due to shear stress; parallel shear cracks, where multiple cracks form in parallel under relatively uniform shear stress conditions; conjugate shear cracks, which develop as pairs at opposite angles, typically at approximately 45° relative to the stress direction; and mixed shear cracks, where the cracks exhibit a combination of shear and tensile components (Yang et al., 2020). The stress-strain curve (deviator stress versus axial strain) for CPB under triaxial compression can generally be divided into three main stages, as illustrated in Figure 2-8 (Xiu et al., 2022; Jafari et al., 2021; Zhang & Li, 2021; Yang et al., 2020; Pierce, 1999). In the initial linear elastic stage, the relationship between deviator stress and axial strain is linear, and the CPB material exhibits elastic

deformation, where the stress increases rapidly, and the deformation is reversible upon removal of the external load. As the stress increases, the material enters the elastoplastic stage, where it begins to yield and exhibit irreversible deformation. During this stage, new cracks initiate and interconnect with existing microcracks, gradually extending and aligning with the direction of stress. The deviator stress continues to rise but deviates from linearity, and the curve reaches its peak value, corresponding to the shear strength or failure point of the CPB sample. The application of confining pressure enhances the friction between fractured surfaces, increasing the deviator stress and contributing to the strain-hardening behaviour observed during this stage (Fall et al., 2007). In the post-peak or failure stage, which follows the peak stress, the CPB sample enters the softening phase, where deviator stress begins to decrease as large-scale cracks propagate and coalesce, ultimately leading to structural failure. This phase is characterized by the transition to residual strength, which reflects the ability of the material to resist further deformation despite extensive cracking (Jafari et al., 2021). These stages provide critical insights into the deformation and failure mechanisms of CPB under shear loading and the influence of confining pressure on its overall behaviour.

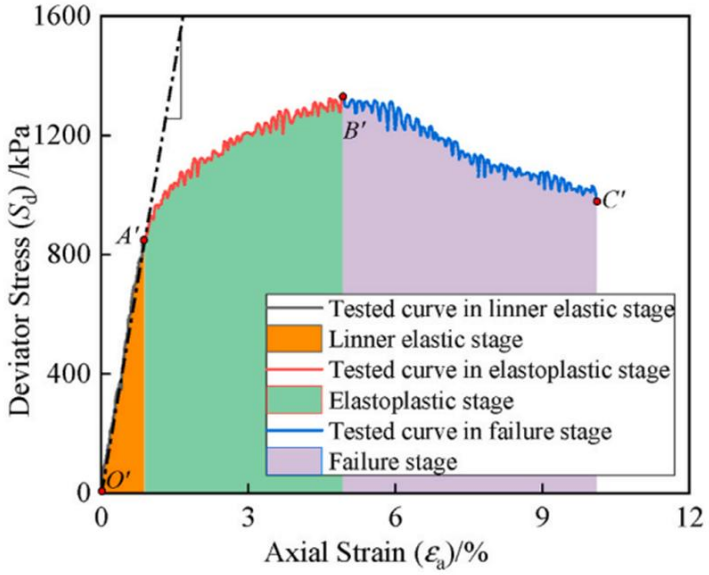

Figure 2-8. Schematic representation of CPB stress-strain curve under triaxial shear test (adapted from Xiu et al., 2022).

CPB exhibits brittle behaviour under tensile stress, characterized by minimal plastic deformation prior to failure. Its inherently low tensile strength makes CPB susceptible to crack initiation under tensile stresses, especially in underground stopes where factors such as shrinkage, differential settlement, or uneven loading are prevalent. To assess the tensile strength of CPB, indirect tensile strength (ITS) tests, such as the Brazilian tensile strength (BTS) test, are commonly employed due to their simplicity, efficiency, and reliability. These tests reduce the risk of premature failure by ensuring uniform stress distribution across the sample and are especially suited for brittle materials like CPB. The ITS test setup is straightforward, requiring only standard compression testing equipment and cylindrical specimens. Figure 2-9 shows the typical stress-strain curve of a brittle

material under tensile loading. This curve can generally be divided into four stages (Li et al., 2022; Chen et al., 2019), which are comparable to those observed under compressive and triaxial shear loading: (i) the linear elastic stage (segment *O*A), where stress increases proportionally with strain; (ii) the nonlinear stage (segment AB), where microcracks begin to form and initiate; (iii) the fracture and failure stage (segment BC), marked by stress drop and macrocrack formation; and (iv) the post-failure stage (segment CD), during which residual strength persists due to frictional interactions along fracture surfaces. In the tensile stress-strain curve of CPB, the stage of crack initiation and propagation is notably brief due to the brittleness of the material and low fracture energy. When the tensile stress approaches or exceeds the bond strength at weak points, such as voids or particle interfaces, microcracks rapidly form and coalesce into macrocracks. During ITS testing with flat loading plates, cracks typically originate at the center of the disc, propagate toward the edges, and ultimately cause a complete fracture of the sample, as shown in Figure 2-10. The crack propagation path follows the loading direction, and the development of a straight crack is directly related to the stress propagation pattern within the material (Xiao et al., 2022).

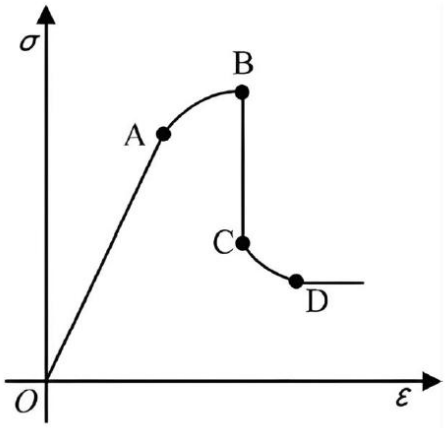

Figure 2-9. Typical indirect tensile stress-strain curve of brittle materials (Li et al., 2022)

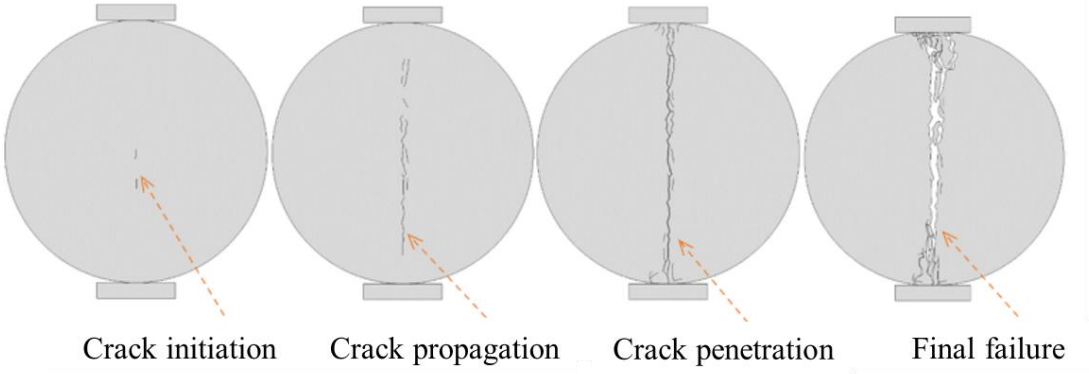

Figure 2-10. Failure process of disc CPB sample under indirect (Brazilian) tensile test using flat loading plates (Xiao et al., 2022).

2.5.3 Impacts of Crack Damage

The presence of defects and cracks significantly diminishes the load-bearing capacity of CPB, undermining its ability to support overburden pressures and resist mining-induced stresses. Song et al. (2022) examined the impact of prefabricated fractures on the mechanical performance of CPB using UCS tests. Their findings demonstrated that pre-existing fractures reduce the mechanical properties of CPB and promote crack propagation, typically originating at fracture tips and ultimately leading to macro-failure of the samples. Similarly, Zhao et al. (2023) introduced varying degrees of initial defects in CPB by incorporating different concentrations of air-entraining agents (AEA). They observed that an increase in medium- and large-sized voids reduced the density of the CPB microstructure, leading to lower UCS and elastic modulus. Comparable detrimental effects of cracks on mechanical performance have also been reported in other cementitious materials, including concrete, mortar, and engineered cementitious composites (ECC) (Lu et al., 2018; Wu et al., 2012; Turatsinze et al., 2007; Zhang, 1997; Vecchio & Collins, 1993). Cracks in CPB compromise its structural integrity by weakening its ability to evenly distribute loads, increasing the risk of instability in stopes. Over time, this loss of cohesion can result in partial or complete failure of backfill structures, jeopardizing the stability of surrounding rock masses and creating stress concentration zones that further propagate cracks. These instabilities would disrupt mining operations, necessitating costly remedial actions such as re-grouting, additional backfill placement, or reinforcement of adjacent areas. Moreover, cracks complicate controlled excavation for re-mining purposes by introducing unpredictable fragmentation patterns, which can further escalate operational costs and reduce overall mining efficiency.

In addition to mechanical degradation, cracks can significantly increase the hydraulic conductivity of CPB, particularly when crack damage exceeds 80% of the corresponding UCS (Fall et al., 2009). The interconnected crack networks facilitate fluid transport, allowing water and oxygen to infiltrate the backfill structure. Oxygen ingress accelerates sulfide oxidation, leading to acid mine drainage (AMD) formation, which weakens the CPB matrix (Aldhafeeri & Fall, 2016). Furthermore, cracks act as pathways for contaminants, such as residual tailings or process chemicals, to escape into surrounding groundwater, posing environmental risks. Over time, water flow through cracks can erode the CPB material, exacerbating instability and reducing long-term durability.

Cracking in CPB structures also poses significant durability and safety challenges in cold regions, where water retained in cracks expands during freeze-thaw cycles, intensifying crack damage and further compromising structural integrity (Hou et al., 2020; Wu et al., 2020; Chang, 2016). These repeated cycles reduce the CPB's durability and performance, increasing the potential of structural failure in such problematic environments.

Overall, the formation and propagation of cracks significantly impair the integrity of CPB structures by reducing mechanical strength, increasing permeability, and diminishing service life, durability, and environmental performance. From a safety perspective, cracked CPB structures pose significant hazards to underground workers by increasing the risk of collapse. Cracks near barricades, in particular, can lead to uneven loading and potential barricade failure, resulting in

widespread instability. Therefore, mitigating cracks in CPB structures is critical to ensuring the safety, economic efficiency, and environmental sustainability of mining operations, particularly in deep and geologically complex underground environments.

2.6 Conclusions

This chapter provides a comprehensive summary of the theoretical and technical background of the CPB technique with a focus on its role as an innovative cementitious engineering material in the mining industry. The literature review explores the mechanisms governing CPB property development and its dominant multiphysical THMC processes and factors. Furthermore, it identifies the factors contributing to crack formation in CPB structures, along with the mechanisms of crack evolution and their impacts on CPB performance. Self-healing has been proposed as a promising and efficient method to mitigate crack damage within the CPB matrix. However, to date, no previous studies have been conducted to explore the self-healing (autogenous healing) behaviour and capacity of CPB materials. To bridge this knowledge gap, a comprehensive study on the self-healing (autogenous healing) behaviour of CPB is conducted in this Ph.D. research.

2.7 References

Adiguzel, D., Tuylu, S., & Eker, H. (2022). Utilization of tailings in concrete products: A review. Construction and Building Materials, 360, 129574.

Aldhafeeri, Z. (2018). Reactivity of cemented paste backfill (Doctoral dissertation, Université d'Ottawa/University of Ottawa).

Aldhafeeri, Z., & Fall, M. (2016). Time and damage induced changes in the chemical reactivity of cemented paste backfill. Journal of Environmental Chemical Engineering, 4(4), 4038-4049.

Aldhafeeri, Z., Fall, M., Pokharel, M., & Pouramini, Z. (2016). Temperature dependence of the reactivity of cemented paste backfill. Applied geochemistry, 72, 10-19.

Alhomair, S. A., Gorakhki, M. H., & Bareither, C. A. (2017). Hydraulic conductivity of fly ash-amended mine tailings. Geotechnical and Geological Engineering, 35, 243-261.

Al-Moselly, Z. (2024). Multiphysics investigation of the geotechnical behaviour of cemented paste backfill with superplasticizer (Doctoral dissertation, Université d'Ottawa| University of Ottawa).

Al-Moselly, Z., & Fall, M. (2024). Investigating Pore Water Pressure Development in Paste Backfill Under Conditions Mimicking Field Loading. Geotechnical and Geological Engineering, 1-24.

Behera, S. K., Ghosh, C. N., Mishra, D. P., Singh, P., Mishra, K., Buragohain, J., & Mandal, P. K. (2020). Strength development and microstructural investigation of lead-zinc mill tailings based paste backfill with fly ash as alternative binder. Cement and Concrete Composites, 109, 103553.

Behera, S. K., Mishra, D. P., Singh, P., Mishra, K., Mandal, S. K., Ghosh, C. N., ... & Mandal, P. K. (2021). Utilization of mill tailings, fly ash and slag as mine paste backfill material: Review and future perspective. Construction and Building Materials, 309, 125120.

Béket Dalcé, J., Li, L., and Yang, P. 2019. Experimental Study of Uniaxial Compressive Strength (UCS) Distribution of Hydraulic Backfill Associated with Segregation. Minerals (2075-163X), 9(3): 147–147.

Belem, T., & Benzaazoua, M. (2008). Design and application of underground mine paste backfill technology. Geotechnical and Geological Engineering, 26, 147-174.

Belem, T., Benzaazoua, M., & Bussière, B. (2000, October). Mechanical behaviour of cemented paste backfill. In Proc. of 53rd Canadian Geotechnical Conference, Montreal (pp. 373-380).
Benzaazoua, M., Belem, T., & Bussiere, B. (2002). Chemical factors that influence the performance of mine sulphidic paste backfill. Cement and concrete research, 32(7), 1133-1144.
Benzaazoua, M., Fall, M., & Belem, T. A contribution to understanding the hardening process of cemented pastefill. Miner. Eng., 17 (2004), 141-152.
Bloss, M. L. (1992). Prediction of cemented rock fill stability: design procedures and modelling techniques.
Bull, A. J., & Fall, M. (2020). Thermally induced changes in metalloid leachability of cemented paste backfill that contains blast furnace slag. Minerals Engineering, 156, 106520.
Bullard, J. W., Jennings, H. M., Livingston, R. A., Nonat, A., Scherer, G. W., Schweitzer, J. S., ... & Thomas, J. J. (2011). Mechanisms of cement hydration. Cement and concrete research, 41(12), 1208-1223.
Cao, S., Yilmaz, E., Song, W., Yilmaz, E., & Xue, G. (2019). Loading rate effect on uniaxial compressive strength behavior and acoustic emission properties of cemented tailings backfill. Construction and Building Materials, 213, 313-324.
Célestin, J. C. H., & Fall, M. (2009). Thermal conductivity of cemented paste backfill material and factors affecting it. International Journal of Mining, Reclamation and Environment, 23(4), 274-290.
Chang, S. (2016). Strength and Deformation Behaviour of Cemented Paste Backfill in Sub-Zero Environment (Doctoral dissertation, Université d'Ottawa/University of Ottawa).
Chen, Q., Zhu, L., Wang, Y., Chen, J., & Qi, C. (2022). The carbon uptake and mechanical property of cemented paste backfill carbonation curing for low concentration of CO2. Science of The Total Environment, 852, 158516.
Chen, X., Shi, X., Zhou, J., & Yu, Z. (2019). Influence of polypropylene fiber reinforcement on tensile behavior and failure mode of tailings cemented paste backfill. IEEE Access, 7, 69015-69026.
Choi, S.-G., Wang, K., Wen, Z., & Chu, J. (2017) Mortar crack repair using microbial induced calcite precipitation method. Cem. Concr. Compos., 83, 209-221.
Clark, C. C., Vickery, J. D., & Backer, R. R. (1995). Transport of total tailings paste backfill: results of full-scale pipe test loop pumping tests.
Coates, D. F. 1981. Caving, subsidence, and ground control. Rock Mechanics Principles, CANMET, Department of Energy, Mines and Resources, Canada, 5-1.
Cui, L. (2017). Multiphysics modeling and simulation of the behavior of cemented tailings backfill (Doctoral dissertation, Université d'Ottawa/University of Ottawa).
Cui, L., & Fall, M. (2015). A coupled thermo–hydro-mechanical–chemical model for underground cemented tailings backfill. Tunnelling and Underground Space Technology, 50, 396-414.
Dashti, J., & Nematzadeh, M. (2020). Compressive and direct tensile behavior of concrete containing Forta-Ferro fiber and calcium aluminate cement subjected to sulfuric acid attack with optimized design. Construction and Building Materials, 253, 118999.
de ARAÚJO, E. E. B., Simon, D., de FRANÇA, F. A. N., de Freitas Neto, O., & dos Santos Jr, O. F. (2017). Shear strength of a cemented paste backfill submitted to high confining pressure. Applied Mechanics and Materials, 858, 219-224.
Deng, X. J., Klein, B., Hallbom, D. J., de Wit, B., & Zhang, J. X. (2018). Influence of particle size on the basic and time-dependent rheological behaviors of cemented paste backfill. Journal of Materials Engineering and Performance, 27, 3478-3487.

Dong, L., Tong, X., Li, X., Zhou, J., Wang, S., & Liu, B. (2019). Some developments and new insights of environmental problems and deep mining strategy for cleaner production in mines. Journal of Cleaner Production, 210, 1562-1578.

Double, D. D. (1983). New developments in understanding the chemistry of cement hydration. Philosophical Transactions of the Royal Society of London. Series A, Mathematical and Physical Sciences, 310(1511), 53-66.

Emad, M. Z., Mitri, H., & Kelly, C. (2015). State-of-the-art review of backfill practices for sublevel stoping system. International Journal of Mining, Reclamation and Environment, 29(6), 544-556.

Ercikdi, B., Kesimal, A., Cihangir, F., Deveci, H., & Alp, İ. (2009). Cemented paste backfill of sulphide-rich tailings: Importance of binder type and dosage. Cement and concrete composites, 31(4), 268-274.

Ercikdi, B., Külekci, G., & Yılmaz, T. (2015). Utilization of granulated marble wastes and waste bricks as mineral admixture in cemented paste backfill of sulphide-rich tailings. Constr. Build. Mater., 93, 573-583.

Fahey, M., Helinski, M., & Fourie, A. (2010). Consolidation in accreting sediments: Gibson's solution applied to backfilling of mine stopes. Géotechnique, 60(11), 877-882.

Fall, M., & Benzaazoua, M. (2005). Modeling the effect of sulphate on strength development of paste backfill and binder mixture optimization. Cement and Concrete Research, 35(2), 301-314.

Fall, M., & Pokharel, M. (2010). Coupled effects of sulphate and temperature on the strength development of cemented tailings backfills: Portland cement-paste backfill. Cement and concrete composites, 32(10), 819-828.

Fall, M., Adrien, D., Célestin, J. C., Pokharel, M., & Touré, M. (2009). Saturated hydraulic conductivity of cemented paste backfill. Minerals engineering, 22(15), 1307-1317.

Fall, M., Belem, T., Samb, S., & Benzaazoua, M. (2007). Experimental characterization of the stress–strain behaviour of cemented paste backfill in compression. Journal of materials science, 42, 3914-3922.

Fall, M., Benzaazoua, M., & Ouellet, S. (2005). Experimental characterization of the influence of tailings fineness and density on the quality of cemented paste backfill. Minerals engineering, 18(1), 41-44.

Fall, M., Célestin, J. C., Pokharel, M., & Touré, M. (2010). A contribution to understanding the effects of curing temperature on the mechanical properties of mine cemented tailings backfill. Engineering Geology, 114(3-4), 397-413.

Fang, K. (2021). Testing and multiphysics modelling of the shear behaviour of rock-cemented paste backfill interface (Doctoral dissertation, Université d'Ottawa/University of Ottawa).

Farsangi, P. N. (1996). Improving cemented rockfill design in open stoping.

Galaa, A. M., Thompson, B. D., Grabinsky, M. W., & Bawden, W. F. (2011). Characterizing stiffness development in hydrating mine backfill using ultrasonic wave measurements. Canadian geotechnical journal, 48(8), 1174-1187.

Gartner, E. M., Young, J. F., Damidot, D. A., & Jawed, I. (2002). Hydration of Portland cement. Structure and performance of cements, 2, 57-113.

Ghirian, A. (2016). Coupled thermo-hydro-mechanical-chemical (THMC) processes in cemented tailings backfill structures and implications for their engineering design (Doctoral dissertation, Université d'Ottawa/University of Ottawa).

Ghirian, A., & Fall, M. (2013). Coupled thermo-hydro-mechanical–chemical behaviour of cemented paste backfill in column experiments. Part I: Physical, hydraulic and thermal processes and characteristics. Engineering Geology, 164, 195-207.
Ghirian, A., & Fall, M. (2014). Coupled thermo-hydro-mechanical–chemical behaviour of cemented paste backfill in column experiments: Part II: Mechanical, chemical and microstructural processes and characteristics. Engineering Geology, 170, 11-23.
Ghirian, A., & Fall, M. (2015). Coupled behavior of cemented paste backfill at early ages. Geotechnical and geological engineering, 33, 1141-1166.
Ghirian, A., & Fall, M. (2016). Strength evolution and deformation behaviour of cemented paste backfill at early ages: Effect of curing stress, filling strategy and drainage. International Journal of Mining Science and Technology, 26(5), 809-817.
Ghirian, A., & Fall, M. (2017). Properties of cemented paste backfill. Paste Tailings Management, 59-109.
Grice, T. (1998). Underground mining with backfill. 2nd Annual Summit œ Mine Tailings Disposal Systems, Brisbane, Nov, 696, 24-25.
Guo, L., Peng, X., Zhao, Y., Liu, G., Tang, G., & Pan, A. (2022). Experimental study on direct tensile properties of cemented paste backfill. Frontiers in Materials, 9, 864264.
Guo, S., Fall, M., & Haruna, S. (2020). Interface shear behavior of cementing underground mine backfill. International Journal of Geomechanics, 20(12), 04020230.
Hadi, M. N., Al-Azzawi, M., & Yu, T. (2018). Effects of fly ash characteristics and alkaline activator components on compressive strength of fly ash-based geopolymer mortar. Construction and Building Materials, 175, 41-54.
Hane, I., Belem, T., Benzaazoua, M., & Maqsoud, A. (2017). Laboratory characterization of cemented tailings paste containing crushed waste rocks for improved compressive strength development. Geotechnical and Geological Engineering, 35, 645-662.
Hansen, T.C., Radjy, F., Sellevold, E.J., 1973. Cement paste and concrete. Annu Rev Mater Sci 3, 233-268.
Hassani, F., Razavi, S. M., & Isagon, I. (2007). A study of physical and mechanical behaviour of gelfill. CIM Bull, 100(1).
Helinski, M., Fahey, M., & Fourie, A. (2011). Behavior of cemented paste backfill in two mine stopes: measurements and modeling. Journal of geotechnical and geoenvironmental engineering, 137(2), 171-182.
Hou, C., Zhu, W., Yan, B., Guan, K., & Du, J. (2020). The effects of temperature and binder content on the behavior of frozen cemented tailings backfill at early ages. Construction and Building Materials, 239, 117752.
Jafari, M., & Grabinsky, M. (2021). Effect of hydration on failure surface evolution of low sulfide content cemented paste backfill. International Journal of Rock Mechanics and Mining Sciences, 144, 104749.
Jafari, M., Grabinsky, M., & Yue, W. (2023). Integrated interpretation of electrical conductivity changes, heat generation, and strength development in the first week in cemented paste backfill. Geotechnical Testing Journal, 46(3), 559-578.
Jafari, M., Shahsavari, M., & Grabinsky, M. (2021). Drained triaxial compressive shear response of cemented paste backfill (CPB). Rock Mechanics and Rock Engineering, 54, 3309-3325.
Jiang, H., Fall, M., Li, Y., & Han, J. (2019). An experimental study on compressive behaviour of cemented rockfill. Construction and Building Materials, 213, 10-19.

Jiang, H., Han, J., Li, Y., Yilmaz, E., Sun, Q., & Liu, J. (2020). Relationship between ultrasonic pulse velocity and uniaxial compressive strength for cemented paste backfill with alkali-activated slag. Nondestructive Testing and Evaluation, 35(4), 359-377.

Jiang, H., Qi, Z., Yilmaz, E., Han, J., Qiu, J., & Dong, C. (2019). Effectiveness of alkali-activated slag as alternative binder on workability and early age compressive strength of cemented paste backfills. Construction and Building Materials, 218, 689-700.

Jiang, H., Yi, H., Yilmaz, E., Liu, S., & Qiu, J. (2020). Ultrasonic evaluation of strength properties of cemented paste backfill: Effects of mineral admixture and curing temperature. Ultrasonics, 100, 105983.

Johnson, J. C., Seymour, J. B., Martin, L. A., Stepan, M., Arkoosh, A., & Emery, T. (2015, June). Strength and elastic properties of paste backfill at the Lucky Friday Mine, Mullan, Idaho. In ARMA US Rock Mechanics/Geomechanics Symposium (pp. ARMA-2015). ARMA.

Jones, H., & Boger, D. V. (2012). Sustainability and waste management in the resource industries. Industrial & Engineering Chemistry Research, 51(30), 10057-10065.

Kasap, T., Yilmaz, E., & Sari, M. (2022). Physico-chemical and micro-structural behavior of cemented mine backfill: Effect of pH in dam tailings. Journal of Environmental Management, 314, 115034.

Kesimal, A., Yilmaz, E., Ercikdi, B., Alp, I., & Deveci, H. (2005). Effect of properties of tailings and binder on the short-and long-term strength and stability of cemented paste backfill. Materials Letters, 59(28), 3703-3709.

Koupouli, N. J., Belem, T., Rivard, P., & Effenguet, H. (2016). Direct shear tests on cemented paste backfill–rock wall and cemented paste backfill–backfill interfaces. Journal of rock mechanics and geotechnical engineering, 8(4), 472-479.

Landriault, D. (2001). Backfill in underground mining. Underground mining methods: engineering fundamentals and international case studies, 601-614.

Landriault, D., Verburg, R., Cincilla, W., & Welch, D. (1997, April). Paste technology for underground backfill and surface tailings disposal applications. In Short course notes, Canadian Institute of Mining and Metallurgy, Technical workshop œ april (Vol. 27, p. 1997).

le Roux, K., Bawden, W. F., & Grabinsky, M. F. (2005). Field properties of cemented paste backfill at the Golden Giant mine. Mining Technology, 114(2), 65-80.

Li, W., & Fall, M. (2016). Sulphate effect on the early age strength and self-desiccation of cemented paste backfill. Construction and building materials, 106, 296-304.

Li, Z., Shi, X., & Chen, X. (2022). Effect of rice straw on tensile properties of tailings cemented paste backfill. Applied Sciences, 12(1), 526.

Liu, L., Fang, Z., Qi, C., Zhang, B., Guo, L., & Song, K. I. (2018). Experimental investigation on the relationship between pore characteristics and unconfined compressive strength of cemented paste backfill. Construction and Building Materials, 179, 254-264.

Liu, L., Zhu, C., Qi, C., Zhang, B., & Song, K. I. (2019). A microstructural hydration model for cemented paste backfill considering internal sulfate attacks. Construction and Building Materials, 211, 99-108.

Liu, S. G., & Fall, M. (2022). Fresh and hardened properties of cemented paste backfill: Links to mixing time. Construction and Building Materials, 324, 126688.

Lu, C., Li, V. C., & Leung, C. K. (2018). Flaw characterization and correlation with cracking strength in Engineered Cementitious Composites (ECC). Cement and Concrete Research, 107, 64-74.

Ma, Q., Liu, G., Yang, X., & Guo, L. (2023). Physical model investigation on effects of drainage condition and cement addition on consolidation behavior of tailings slurry within backfilled stopes. International Journal of Minerals, Metallurgy and Materials, 30(8), 1490-1501.

Martic, Z., Gelson, J., Bras, H., Xu, Q., & Brosko, W. (2014, May). New perspectives for cemented hydraulic fill with chemical technologies. In Mine Fill 2014: Proceedings of the Eleventh International Symposium on Mining with Backfill (pp. 295-308). Australian Centre for Geomechanics.

Mehta, P. K. (1999). Advancements in concrete technology. Concrete International, 21(6), 69-76.

Menéndez, J., Ordóñez, A., Álvarez, R., & Loredo, J. (2019). Energy from closed mines: Underground energy storage and geothermal applications. Renewable and Sustainable Energy Reviews, 108, 498-512.

Nasir, O., & Fall, M. (2008). Shear behaviour of cemented pastefill-rock interfaces. Engineering Geology, 101(3-4), 146-153.

Nasir, O., & Fall, M. (2009). Modeling the heat development in hydrating CPB structures. Computers and Geotechnics, 36(7), 1207-1218.

Nasir, O., & Fall, M. (2010). Coupling binder hydration, temperature and compressive strength development of underground cemented paste backfill at early ages. Tunnelling and Underground Space Technology, 25(1), 9-20.

Neville, A. M. (1995). Properties of concrete.

Nwankwo, C. O., Bamigboye, G. O., Davies, I. E., & Michaels, T. A. (2020). High volume Portland cement replacement: A review. Construction and Building materials, 260, 120445.

Ohno, K., & Ohtsu, M. (2010) Crack classification in concrete based on acoustic emission. Constr. Build. Mater., 24, 2339-2346.

Othman, R., Putra Jaya, R., Duraisamy, Y., Sulaiman, M. A., Chong, B. W., & Ghamari, A. (2023). Efficiency of waste as cement replacement in foamed concrete—A review. Sustainability, 15(6), 5163.

Ouffa, N., Benzaazoua, M., Belem, T., Trauchessec, R., & Lecomte, A. (2020). Alkaline dissolution potential of aluminosilicate minerals for the geosynthesis of mine paste backfill. Materials Today Communications, 24, 101221.

Ouyang, S., Huang, Y., Wu, L., Yin, W., Yang, X., Wang, J., ... & Lei, Y. (2022). Effects of chlorides on setting time, hydration heat and hydration products of fresh slurry of cemented paste backfill. Case Studies in Construction Materials, 17, e01462.

Pan, A. N., & Grabinsky, M. W. (2021). Tensile strength of cemented paste backfill. Geotechnical Testing Journal, 44(6), 1886-1897.

Peterson, S. M. (1996). Cemented rockfill optimization in vertical block mining.

Pierce, M. E. (1999). Laboratory and numerical analysis of the strength and deformation behaviour of paste backfill. Queen's University at Kingston.

Pokharel, M., & Fall, M. (2013). Combined influence of sulphate and temperature on the saturated hydraulic conductivity of hardened cemented paste backfill. Cement and Concrete Composites, 38, 21-28.

Qi, T., Feng, G., Zhang, Y., Guo, J., & Guo, Y. X. (2015). Effects of fly ash content on properties of cement paste backfilling. Journal of Residuals Science & Technology, 12(3), 133-141.

Quan, W. (2021). Experimental optimization of drilling, rock strength and backfilling for mining by drilling applications (Doctoral dissertation, Memorial University of Newfoundland).

Rankin, G. A. (1915). The Constituents of Portland Cement Clinker. Industrial & Engineering Chemistry, 7(6), 466-474.

Rankine, R. M., & Sivakugan, N. (2007). Geotechnical properties of cemented paste backfill from Cannington Mine, Australia. Geotechnical and Geological Engineering, 25, 383-393.
Rankine, R., Pacheco, M., & Sivakugan, N. (2007). Underground mining with backfills. Soils and Rocks, 30(2), 93-101.
Robinsky, E. I. (1975). Thickened discharge. A new approach to tailings disposal.
Robinsky, E. I. (1978, May). Tailings disposal by the thickened discharge method for improved economy and environmental control. In Tailings Disposal Today, Proceedings of the Second International Tailings Symposium, Denver, Colorado, USA (pp. 75-92).
Rosenblum, F., Nesset, J., & Spira, P. (2001). Mineral Processing v Evaluation and control of self-heating in sulphide concentrates. Cim. Org, 94.
Rubashkina, T. I., & Kostina, M. A. (2023). Usability of Chloride Mine Water in Preparing Cemented Paste Backfill. Journal of Mining Science, 59(3), 410-416.
Saremi, A. (2024). Multiscale and Multiphysics Investigation of the Geotechnical Behaviour of Nano-Cemented Paste Backfill Plug (Doctoral dissertation, Université d'Ottawa| University of Ottawa).
Schoenbrunn, F. (2011, April). Dewatering to higher densities-an industry review. In Paste 2011: Proceedings of the 14th International Seminar on Paste and Thickened Tailings (pp. 19-23). Australian Centre for Geomechanics.
Scrivener, K. L., Juilland, P., & Monteiro, P. J. (2015). Advances in understanding hydration of Portland cement. Cement and Concrete Research, 78, 38-56.
Sheshpari, M. (2015). A review of underground mine backfilling methods with emphasis on cemented paste backfill. Electronic Journal of Geotechnical Engineering, 20(13), 5183-5208.
Shrestha, B. K. (2008). Properties of cemented rockfill at Diavik Mine.
Sivakugan, N., Rankine, K., Lovisa, J., and Hall, W. 2013. Flow Rate Computations in Hydraulic Fill Mine Stopes. Indian Geotechnical Journal, 43(3): 195–202.
Song, X., Hao, Y., Wang, S., Zhang, L., Liu, W., & Li, J. (2022). Mechanical properties, crack evolution and damage characteristics of prefabricated fractured cemented paste backfill under uniaxial compression. Construction and Building Materials, 330, 127251.
Song, X., Li, J., Wang, S., Zhou, S., Liu, W., Zhai, Y., & Hao, Y. (2022). Study of mechanical behavior and cracking mechanism of prefabricated fracture cemented paste backfill under different loading rates from the perspective of energy evolution. Construction and Building Materials, 361, 129737.
Swaddiwudhipong, S., Chen, D., & Zhang, M. H. (2002). Simulation of the exothermic hydration process of Portland cement. Advances in cement research, 14(2), 61-69.
Tang, G., Guo, L., Liu, G., & Yang, X. (2023, April). Determination of the relationship between direct tensile test and Brazilian splitting test of cemented tailings backfill. In Paste 2023: Proceedings of the 25th International Conference on Paste, Thickened and Filtered Tailings (pp. 98-111). University of Alberta, Edmonton, and Australian Centre for Geomechanics, Perth.
Telschow, S., Frandsen, F., Theisen, K., & Dam-Johansen, K. (2012). Cement Formation A Success Story in a Black Box: High Temperature Phase Formation of Portland Cement Clinker. Industrial & engineering chemistry research, 51(34), 10983-11004.
Thompson, B. D., Bawden, W. F., & Grabinsky, M. W. (2012). In situ measurements of cemented paste backfill at the Cayeli Mine. Canadian Geotechnical Journal, 49(7), 755-772.

Tian, Y., Zhang, G., Ye, H., Zeng, Q., Zhang, Z., Tian, Z., ... & Wang, J. (2023). Corrosion of steel rebar in concrete induced by chloride ions under natural environments. Construction and Building Materials, 369, 130504.

Turatsinze, A., Bonnet, S., & Granju, J. L. (2007). Potential of rubber aggregates to modify properties of cement based-mortars: improvement in cracking shrinkage resistance. Construction and Building Materials, 21(1), 176-181.

Vecchio, F. J., & Collins, M. P. (1993). Compression response of cracked reinforced concrete. Journal of structural engineering, 119(12), 3590-3610.

Wagner, H. (2013). The management of heat flow in deep mines. Mining Report, 149(2), 88-100.

Wang, B., Yang, L., Li, Q., Shu, X., & Kang, M. (2024). Mechanical behavior, acoustic emission and principal strain field evolution properties of layered cemented paste backfill under unconfined compression. Construction and Building Materials, 415, 135111.

Wang, C., Harbottle, D., Liu, Q., & Xu, Z. (2014). Current state of fine mineral tailings treatment: A critical review on theory and practice. Minerals Engineering, 58, 113-131.

Wang, J., Fu, J., & Song, W. (2020). Mechanical properties and microstructure of layered cemented paste backfill under triaxial cyclic loading and unloading. Construction and Building Materials, 257, 119540.

Wang, J., Zhang, C., Fu, J., Song, W., & Zhang, Y. (2021). Effect of water saturation on mechanical characteristics and damage behavior of cemented paste backfill. Journal of Materials Research and Technology, 15, 6624-6639.

Wang, S., Wang, F., Yin, D., Jiang, T., & Zhang, Z. (2021). Experimental study on mechanical properties of paste backfill with flue-gas desulphurisation gypsum under combined action of dry–wet cycles and chloride erosion. Minerals, 11(8), 882.

Wang, Y., Na, Q., & Zhang, L. (2022). Monitoring of in-situ properties for cemented tailings backfill that under drainage condition. Construction and Building Materials, 356, 129254.

Wolterbeek, T. K. T., & Hangx, S. J. T. (2023). The thermal properties of set Portland cements–a literature review in the context of CO2 injection well integrity. International Journal of Greenhouse Gas Control, 126, 103909.

Wu, A. X., Miao, X. X., Liu, X. H., Wang, Y. M., Wang, C. L., & Zhang, J. J. (2015, April). Paste backfill system design and commissioning at Chambishi Copper Mine. In Paste 2015: Proceedings of the 18th International Seminar on Paste and Thickened Tailings (pp. 301-308). Australian Centre for Geomechanics.

Wu, A., Wang, Y., Wang, H., Yin, S., & Miao, X. (2015). Coupled effects of cement type and water quality on the properties of cemented paste backfill. International journal of mineral processing, 143, 65-71.

Wu, H. L., Jin, F., Ni, J., & Du, Y. J. (2019). Engineering properties of vertical cutoff walls consisting of reactive magnesia-activated slag and bentonite: workability, strength, and hydraulic conductivity. Journal of Materials in Civil Engineering, 31(11), 04019263.

Wu, J., Feng, M., Chen, Z., Mao, X., Han, G., & Wang, Y. (2018). Particle size distribution effects on the strength characteristic of cemented paste backfill. Minerals, 8(8), 322.

Wu, M., Johannesson, B., & Geiker, M. (2012). A review: Self-healing in cementitious materials and engineered cementitious composite as a self-healing material. Construction and Building Materials, 28(1), 571-583.

Xiao, P., Zhao, G., & Liu, H. (2022). Failure transition and validity of Brazilian disc test under different loading configurations: a numerical study. Mathematics, 10(15), 2681.

Xiapeng, P., Fall, M., & Haruna, S. (2019). Sulphate induced changes of rheological properties of cemented paste backfill. Minerals Engineering, 141, 105849.

Xiu, Z., Wang, S., Ji, Y., Wang, F., & Ren, F. (2022). Experimental study on the triaxial mechanical behaviors of the Cemented Paste Backfill: Effect of curing time, drainage conditions and curing temperature. Journal of Environmental Management, 301, 113828.

Xu, G., Fan, K., Wang, K., & Ning, J. (2022). Paste backfill corrosion mechanisms in chloride and sulfate environments. Minerals, 12(5), 551.

Xu, W., Han, M., & Li, P. (2020). Influence of freeze–thaw cycles on mechanical responses of cemented paste tailings in surface storage. International Journal of Mining, Reclamation and Environment, 34(5), 326-342.

Xu, X., Fall, M., Alainachi, I., & Fang, K. (2019). Characterisation of fibre-reinforced backfill/rock interface through direct shear tests. Geotechnical Research, 7(1), 11-25.

Yang, L., Xu, W., Yilmaz, E., Wang, Q., & Qiu, J. (2020). A combined experimental and numerical study on the triaxial and dynamic compression behavior of cemented tailings backfill. Engineering Structures, 219, 110957.

Yang, L., Yilmaz, E., Li, J., Liu, H., & Jiang, H. (2018). Effect of superplasticizer type and dosage on fluidity and strength behavior of cemented tailings backfill with different solid contents. Construction and Building Materials, 187, 290-298.

Yıldırım, G., Keskin, Ö. K., Keskin, S. B., Şahmaran, M., & Lachemi, M. (2015) A review of intrinsic self-healing capability of engineered cementitious composites: Recovery of transport and mechanical properties. Constr. Build. Mater., 101, 10-21.

Yilmaz, E., Belem, T., & Benzaazoua, M. (2014). Effects of curing and stress conditions on hydromechanical, geotechnical and geochemical properties of cemented paste backfill. Engineering Geology, 168, 23-37.

Yilmaz, E., Belem, T., Bussière, B., & Benzaazoua, M. (2011). Relationships between microstructural properties and compressive strength of consolidated and unconsolidated cemented paste backfills. Cement and concrete composites, 33(6), 702-715.

Ylmén, R., Jäglid, U., Steenari, B. M., & Panas, I. (2009). Early hydration and setting of Portland cement monitored by IR, SEM and Vicat techniques. Cement and Concrete Research, 39(5), 433-439.

Yu, T. R. (2021). Some factors relating to the stability of consolidated rockfill at Kidd Creek. In Innovations in Mining Backfill Technology (pp. 279-286). CRC Press.

Zhang, C., Fu, J., Song, W., Kang, M., Li, T., & Wang, N. (2022). Analysis on mechanical behavior and failure characteristics of layered cemented paste backfill (LCPB) under triaxial compression. Construction and Building Materials, 324, 126631.

Zhang, J. P. (1997). Diagonal cracking and shear strength of reinforced concrete beams. Magazine of Concrete Research, 49(178), 55-65.

Zhang, Q. L., Li, Y. T., Chen, Q. S., Liu, Y. K., Feng, Y., & Wang, D. L. (2021). Effects of temperatures and pH values on rheological properties of cemented paste backfill. Journal of Central South University, 28(6), 1707-1723.

Zhang, Z., & Li, J. (2021). Experimental investigation on strength and failure characteristics of cemented paste backfill. Frontiers in Materials, 8, 792561.

Zhao, K., Zhou, Y., Yin, S., Yan, Y., Wu, J., Zhao, H., & Wang, S. (2023). Effect of initial defects on the microstructure, mechanics, and energy dissipation characteristics of cemented paste backfill. Materials Today Communications, 35, 105785.

Zhao, Y., Taheri, A., Karakus, M., Chen, Z., & Deng, A. (2020). Effects of water content, water type and temperature on the rheological behaviour of slag-cement and fly ash-cement paste backfill. International Journal of Mining Science and Technology, 30(3), 271-278.

Zhou, N., Dong, C., Zhang, J., Meng, G., & Cheng, Q. (2021). Influences of mine water on the properties of construction and demolition waste-based cemented paste backfill. Construction and Building Materials, 313, 125492.

Zhou, Y., Yu, X., Guo, Z., Yan, Y., Zhao, K., Wang, J., & Zhu, S. (2021). On acoustic emission characteristics, initiation crack intensity, and damage evolution of cement-paste backfill under uniaxial compression. Construction and Building Materials, 269, 121261.

Chapter 3 Background on Self-healing Behaviour and Review of Previous Studies on Self-healing of Cementitious Materials

3.1 Introduction

Self-healing can be defined as the ability of a material that is able to heal/repair/recover its properties from damage automatically by itself without any external intervention (Ghosh, 2009) or refers to a process that can sense, diagnose, and heal/repair/recover a damaged condition without intervention. This ability or process is also termed self-repairing, autonomic-healing, or autonomic-repairing, typical for plants and animals in nature. Damaged skin may heal itself on trees and animals, a typical example of self-healing behaviour. One's hand is injured with a small cut and treated with a bandage. The bandage protects the cut, allowing the body to self-heal with fewer disturbances. The body stops the bleeding and then regrows tissue over the wound part over a timescale (Cremaldi and Bhushan, 2018). As for the plants, it is the formation of internal impervious boundary walls that protects the plants from further damage (Biggs, 1985), allowing the tissues to self-heal.

Cementitious material, especially concrete, has been the most widely used construction material since the invention of Portland cement in the 1820s because of its outstanding advantages, including high compressive strength, good molding performance, low material cost, etc. (Wang et al., 2019; Van Tittelboom and De Belie, 2013). However, it is known that concrete has limited tensile strength, which makes it sensitive to crack formation due to load or deformation-induced stresses. The concrete structures and even infrastructures may suffer severe deterioration during service life. Once the crack is introduced within the concrete structure, the microcracks may expand into macrocracks, reducing the bearing capacity and durability of the concrete structure. Moreover, the cracks in the structure provide pathways for aggressive gases or liquids penetrating the matrix, such as sulfate and chloride ions. As a result, the service life of the concrete structure is significantly reduced due to the further damage induced by reinforcement corrosion and concrete carbonation.

To optimize the properties of concrete structures, modern techniques have enabled concrete design with low porosity, higher strength, and high resistance. Still, the formation of cracks is inevitable due to shrinkage, loading, thermal expansion, phase expansion during freezing and thawing, or creep, even though cracks in concrete can be reduced. Therefore, inspection and maintenance are of great importance in addressing the crack problems of concrete structures. However, the implementation of continuous maintenance is complex due to limitations, such as the difficulty of detecting internal cracks, the inability to enter narrow spaces, insufficient funds to repair extensive infrastructure, and significant inconvenience when infrastructure has to be closed down. As reported, the costs related to maintenance and repair work account for half of the annual construction budget in Europe (Cailleux and Pollet, 2009). In addition, the total direct cost of corrosion was determined to be $276 billion per year, which was 3.1% of the U.S. GDP, of which infrastructure-related costs represent a sizeable portion, even though it was from 1999 to 2001. The overall dollar impact of corrosion on highway bridges was considerable and is estimated to be an average of $8.29 billion annually (Yunovich and Thompson, 2003). In the United Kingdom, repair

and maintenance accounted for almost 45% of the UK's activity in the construction and building industry (Woudhuysen and Abley, 2004). Therefore, even if such maintenance work is theoretically feasible, the expense and labor involved in diagnostic and repair procedures for large-scale infrastructures may be prohibitive.

Under such circumstances, smart materials with the ability to self-heal, self-repair, autonomic-healing, or autonomic-repairing have attracted more attention from researchers. The organisms in nature inspired the development of self-healing concrete. The self-healing behaviour or autogenous healing of cracks in fractured concrete was noticed by the French Academy of Science in 1836, and it is already in water-retaining structures, culverts, and pipes (Van Breugel, 2007). The initially observed self-healing behaviour is owing to the inherent self-healing potential in the traditional concrete structure. Generally, traditional concrete mixtures are made with a water/cement ratio between 0.4 and 0.55. Nevertheless, only 70% of cement will hydrate in practice during the early curing period. The remaining 30% of cement will stay unhydrated in the mixture. If cracks form within the structure, the hydration reaction will resume with unhydrated cement particles when exposed to penetrating moisture or water. Then, the delayed hydration products will precipitate and fill the gaps to heal the cracks (see Figure 3-1). After that, Hyde and Smith (1889), Hearn and Morley (1997), and Glanville (1926) investigated self-healing behaviour more systematically. The difference between self-healing and self-sealing was also distinguished. In the process of self-healing, the inherent or original mechanical property can be restored, while there is no mechanical recovery. The flourishing research has extended the study of self-healing behaviour from concrete to other cementitious materials, such as high-performance concrete, high-performance fiber-reinforced cementitious composites (HPRFCCs), engineered cementitious composites (ECCs), etc. Besides, the research on self-healing agents/materials development has also attracted significant attention, which will be discussed in the later sections.

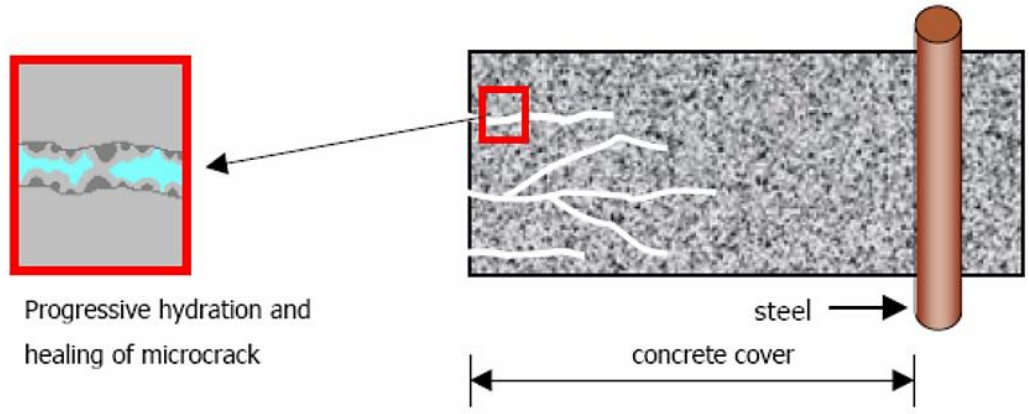

Figure 3-1. Healing of cracks in concrete due to delayed hydration (Van Breugel, 2007).

Taking advantage of self-healing behaviour reduces the cost and the requirement for labor, which is an effective approach to maintaining or repairing cracks in cementitious infrastructures. When the crack occurs, the self-healing system embedded in the cementitious structure will automatically

heal the crack, thus restoring the function of the structure, enhancing its durability, and prolonging the longevity of service life.

3.2 Self-healing Approaches in Cementitious Materials

The development of the self-healing cementitious material mechanism is inspired by different materials in nature. For instance, damaged skins of trees or injured skins and tissues of human and animal bodies can autonomously heal themselves based on nutrient uptake. Similarly, essential products or additions act as nutrients in cementitious materials with self-healing capability, enabling these materials to heal or restore inherent properties. The self-healing approaches of cementitious materials can be roughly divided into two categories: autogenous healing and autonomous healing (Blaiszik et al., 2010).

3.2.1 Autogenous Healing

Generally, conventional cementitious matrix (i.e., concrete) contains approximately 20-30% unhydrated cement particles after curing. When cracks occur, the unhydrated cement within the matrix can come into contact with inflowing water or vapor, and the hydration reaction would be stimulated again, resulting in delayed hydration products, which contribute to the crack closure. This mechanism has been known since 1836 (Hearn and Morley, 1997) and is called autogenous healing. Autogenous healing is the self-healing process in which cracks are healed by healing products that are produced by delayed hydration of unhydrated cement particles and carbonation of calcium hydroxide within the cementitious matrix, and materials are not intentionally added into the matrix or designed for self-healing (Cuenca and Ferrara, 2017). Autogenous healing can be mainly attributed to two chemical mechanisms (Ramm and Biscoping, 1998; Edvardsen, 1999): i) hydration of unhydrated cement particles and ii) dissolution and subsequent carbonation of calcium hydroxide. The calcium hydroxide $Ca(OH)_2$ is a cement hydration product precipitating on the crack surfaces. The calcium ions are liberated and dissipated along the cracking surfaces by dissolving in water. Then, the free calcium ions from cement hydration react with the carbonate ion CO_3^{2-} or bicarbonate ion HCO_3^- from dissolved carbon dioxide CO_2 to form the self-healing product calcite $CaCO_3$, growing on both surfaces of the cracks and finally filling the crack gaps (Wu et al., 2012). The chemical reaction process is as follows:

$$H_2O+CO_2 \Leftrightarrow H_2CO_3 \Leftrightarrow H^++HCO_3^- \Leftrightarrow 2H^++CO_3^{2-} \quad (3\text{-}1)$$

$$Ca^{2+}+CO_3^{2-} \Leftrightarrow CaCO_3 \quad (3\text{-}2)$$

$$Ca^{2+}+HCO_3^- \Leftrightarrow CaCO_3+H^+ \quad (3\text{-}3)$$

In the chemical mechanisms, the content of unhydrated cement particles dominates the efficiency of self-healing by autogenous healing. Cement hydration is the primary mechanism in young cementitious materials. At later ages, calcite precipitation becomes the primary mechanism for the self-healing process (Neville, 2002). Besides the chemical mechanism, the physical mechanism (i.e., swelling of calcium silicate hydrates) and mechanical mechanism (i.e., loose particles broken from the fracture surface or impurities in ingress water) also produce autogenous healing. A

schematic overview of the main mechanisms that lead to autogenous healing is presented in Figure 3-2.

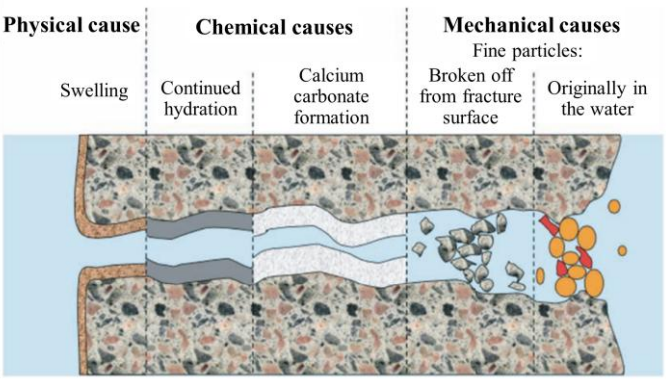

Figure 3-2. Mechanisms leading to autogenous healing (De Rooij et al., 2013)

Although debates exist about the main mechanism of autogenous healing, a consensus is that researchers commonly identify the essential presence of water. Some researchers (Lee et al., 2010a; Lee et al., 2010b; Kim et al., 2011; Lopez-Tendero et al., 2011; Snoeck et al., 2012; Snoeck et al., 2014) added superabsorbent polymers (SAP) into the cementitious mixtures to provide additional water. SAP can absorb a large amount of liquid and swell to form an insoluble gel in the matrix. In the hydration stage, the absorbed liquid can be released from the SAP. The shrunk SAP particles produce small macro-pores around themselves. When the cracks propagate through the pores, liquid ingress will make the SAP swell again, leading to a physical blocking effect. In the dry periods, the absorbed water will be released from the SAP to activate autogenous healing. However, the pores induced by swelling SAP can undermine the mechanical strength of the matrix structure.

Additionally, autogenous healing has excellent potential for long-term healing (Wu et al., 2012) by partially substituting the cement with mineral admixtures, such as fly ash, silica fume, and blast furnace slag, which are pozzolanic and latent hydraulic materials (Li et al., 2002; Yang et al., 2007; Şahmaran et al., 2008; Termkhajornkit et al., 2009; Zhou et al., 2011; Na et al., 2012; Van Tittelboom et al., 2012). For example, fly ash is an industrial byproduct of coal combustion and is usually considered a waste material. Initially, fly ash was used to replace cement to reduce the proportion of Portland cement in concrete, which optimizes costs and environmental friendliness (Yu et al., 2017). Thomas (2007) stated that fly ash could contribute to long-term strength development in concrete, resulting in greater compressive strength at later ages due to the pozzolanic activity to produce C-S-H and C-A-H gels. Besides, the secondary hydration of fly ash at later ages also favors self-healing behaviour. Termkhajornkit et al. (2009) investigated the self-healing possibility of fly ash-cement systems and found that the fly ash-cement system performed the self-healing ability for cracks that occur from shrinkage, and the self-healing ability increased with the increasing fraction of fly ash. In the same way, blast furnace slag (slag), as an industrial by-product, has been used to replace cement clinker in cementitious materials (i.e., concrete) to enhance the chloride and sulphate resistance, and to improve the durability of the infrastructures (Özbay et al., 2013; Li et al., 2012; Aïtcin, 2007). Since the latent character of slag, a significant

amount of slag particles can remain unreacted in slag cement paste even at long-term curing stages, which provides a substantial potential for self-healing. For instance, Huang et al. (2014) investigated the self-healing process in blast furnace slag cement paste activated with a saturated $Ca(OH)_2$ solution. The findings revealed that the slag cement paste with a high slag concentration has a greater potential for self-healing than cement paste, with the reaction products C-S-H, ettringite, hydrogarnet, and OH-hydrotalcite forming in cracks. Nguyễn et al. (2018) compared the self-healing properties of cement-based and alkali-activated slag-based fiber-reinforced composites with controlled crack width. The results indicated that alkali-activated slag-based composites outperformed cement-based composites in reducing relative crack widths but were less effective in recovering resonant frequency. Similarly, mortar mixtures containing blast furnace slag demonstrated a significantly enhanced self-healing capacity, which effectively reduces chloride penetration and improves structural durability (Darquennes et al., 2016).

Furthermore, other mineral admixtures (cementitious materials), such as expansive agents, geo-materials, and crystalline admixtures, have been investigated in previous studies not only to improve the properties of cementitious infrastructure but also to promote the self-healing performance of cementitious materials by the formation of calcite, C-S-H, ettringite, and portlandite (Sisomphon et al., 2013; Lee and Ryou, 2016). When a crack forms, the unreacted mineral admixtures can contact the ingress water, the active components react with water, and the ions or compounds in the matrix form healing products to heal the cracks. Expansive agents, composed of calcium sulfoaluminate ($Ca_4(AlO_2)_6SO_4$), calcium oxide (CaO), and anhydrite ($CaSO_4$), react with $Ca(OH)_2$ to form expansive healing products, such as ettringite, magnesium hydrate, magnesium carbonate, and calcite, which have larger volumes than the reactants, leading to crack filling and closure. The MgO is typically used to optimize the shrinkage performance of concrete and promote self-healing capacity in cementitious materials. Sherir et al. (2017) presented the self-healing performance of ECCs produced with the expansive agent MgO. The results showed that the ECCs with MgO tended to recover original mechanical properties by healing microcracks. Additionally, Ahn (2008a) prepared modified concrete beams using 10% expansive agent addition (CaO and $CaSO_4$) and found that the concrete beam incorporating expansive agent could completely heal the crack width of 220 μm after one month, compared to the normal concrete beam, which only achieved partial healing. However, the expansion property in geo-materials is not quite the same as in expansive agents. Most of the volume expansion in geo-materials to fill cracks is caused by the swelling of the materials after absorbing water, though active substances, such as SiO_2 and Al_2O_3, can react to produce healing products with large volumes. Ahn and Kishi (2010) demonstrated that a geo-material containing SiO_2 of 71.3% and Al_2O_3 of 15.4% when added to the expansive material, could form a geo-polymer via polymerization of aluminate and silicate complexes. Montmorillonite, feldspar, and quartz are also parts of the geo-materials. The swelling behaviour of geo-material is mainly caused by the swelling of montmorillonite, which is a swelling clay mineral. Since montmorillonite is a 2:1 layer consisting of an octahedral sheet sandwiched between two silica sheets, it can swell 15-18 times its dry size when wetted by water (Ahn and Kishi, 2010). What's more, crystalline admixtures (CA), consisting of substances that react with

cement constituents and form calcium silicate hydrates and are already employed for the reduction of concrete porosity and water permeability of concrete, can also effectively serve as self-healing engineering additions (Li and Li, 2011). The commonly contained materials are Na_2CO_3, $NaHCO_3$, Li_2CO_3, Na_2FPO_3, sodium silicate, colloidal silica, ethyl silicates, etc. (Wang et al., 2019). Roig-Flores et al. (2016) compared the effect of a CA on self-healing behaviour in early-age concrete under three different exposure conditions. The results showed that specimens with crystalline admixtures yielded healing ratios with lower standard deviations than those for control specimens, thus increasing the reliability of healing. Additionally, Jaroenratanapirom and Sahamitmongkol (2011) studied the self-healing performance of mortar using different additives: fly ash, silica fume, expansive admixture, limestone powder, and CAs. They reported that CAs showed the best performance in closing cracks with the crack width range of 0-0.05 m, becoming inefficient for wider cracks. This limit can be eliminated when CAs are combined with expansive admixtures (i.e., CSA). Complete self-healing for cracks up to 400 μm can be achieved under water immersion after 30 days of curing (Sisomphon et al., 2012).

3.2.2 Autonomous Healing

Self-healing can also be autonomous by incorporating a self-healing mechanism inside the cementitious materials produced by reactions of specific agents intentionally added to produce self-healing behaviour, as illustrated in Figure 3-3. In autonomous healing, the material used to heal or close cracks does not originate from the matrix itself but from other external sources, including directly added or embedded in capsules, crystalline admixtures, sodium silicate, adhesives, and bacteria. The activation methods can be crack propagation, contact with air or water, other agents, and external changes (i.e., temperature and humidity). Consequently, the efficiency of autonomous healing highly depends on the crack width, which is consistent with the autogenous healing, encapsulation method (spherical or tabular), and the amount of deposited healing agents inside the matrix.

Autonomous healing relies on embedding engineered additives in cementitious materials to provide self-healing capacity (De Belie et al., 2018). Another reason for embedding additions is to protect healing agents during the mixing procedure and to activate them only at the required moment. The capsules vary from macroscale to microscale, inspired by the cells, seeds, and birds' eggs in nature (Hemsley and Griffiths, 2000). For these aims, several encapsulation techniques have been developed, either for chemical agents or bacteria. There are two main systems for encapsulation: single-component embedded systems and multi-component embedded systems. In the encapsulation system, capsules could be spherical or cylindrical in shape. Microscale encapsulation (microencapsulation) generally has a diameter below 1 mm, a popular technique for producing autonomous healing in cementitious materials (De Belie et al., 2018). In this method, the microcapsules are embedded in the cementitious matrix during the mixing procedure. They should be broken upon rupture, crack formation, and propagation, thereby releasing the embedded healing agent via capillary effects (Wu et al., 2012) and even regaining mechanical strength. Then, there are four healing strategies for the released healing agent: reaction activated by water, heat, air, or

radiation, reaction with cementitious matrix, reaction with a second component present in the matrix, and reaction with a second component embedded in additional microcapsules. For instance, Dry (1994 and 2000) embedded cylindrical glass capsules filled with cyanoacrylate as a healing agent. Upon the crack formation and propagation, the released cyanoacrylate contacted the air, starting the healing process. Add to that, Yang et al. (2011) developed a new family of self-healing materials that are expected to offer potential synergy with microfibers in arresting cracks formed in cementitious materials. In their study, the healing agent methyl methacrylate (MMA) and catalyst triethyl borane (TEB) were microencapsulated, respectively, through an interfacial self-assembly process and sol-gel reaction. A crack was expected to rupture both agents, and a polymerization reaction was triggered to fill the crack when the healing agent was in contact with the catalyst. Though various microencapsulation techniques are available, the specific technique is sometimes only suited for particular types of materials. Several factors should be considered for the determination of the microencapsulation technique and wall matrix, including critical properties of the core material, microcapsule size, permeability of the shell, encapsulation efficiency, resistance of the capsules to compounding with the matrix, difference in the toughness properties and interfacial interactions between the microcapsule and polymer matrix, and processing parameters of the self-healing composite system (Zhu et al., 2015). Additionally, macroscale encapsulation (macroencapsulation) was first carried out by Dry (1993 and 1994), who proposed polypropylene and glass fibers with mono- or multi-component methyl methacrylate core for concrete crack repairing. Macroscale encapsulation is also classified as located capsules (Roig-Flores et al., 2021). In microencapsulation, the tubes and capsules are placed in the molds before pouring the cementitious materials, which means the prediction of crack formation and propagation is required to ensure the system's validity. The concept of microencapsulation is similar to vascular-based self-healing.

A vascular-based self-healing concept in cementitious materials is inspired by the animal blood-vessel system that transports blood around the body and the plant vascular tissue system (xylem and phloem networks) that transports nutrients and water. The vascular network developed in cementitious materials consists of artificially manufactured channels through which healing agents can be delivered to the cementitious matrix, connecting the interior and the exterior of the structure. This method allows an increase in the amount of healing agents that can be released to the target cracks, theoretically, even with no limit from an external supply source. The delivery system can be divided into two categories: a one-channel vascular system, when a single component healing agent is needed, and a multi-channel vascular system, when two or more healing agents are required. Regarding the one-channel vascular system, Joseph et al. (2010), for example, used cyanoacrylates (CA) as a healing agent encapsulated in glass tubes. The capillary glass tubes were open to the atmosphere on one side and plugged with wax on the other to maximize the provision of healing agents. Upon the cracking of tubes under loads, an additional healing agent could be delivered to the inside matrix to heal wider cracks. The additional healing agents were supplied by human intervention in the previous study, and they can also be achieved through gravitational force action (Mihashi et al., 2000) or a vacuum pump (Dry, 1994). Furthermore, Dry and McMillan (1996) used

a three-part methylmethacrylate adhesive system (multi-channel vascular system). The adhesive was released from hollow glass tubes coated with a brittle breakable sealer. The three-part adhesive system was made up of MMA, cumene hydroperoxide, and cobalt neodecanoate, the latter two components being the initiators that cause the MMA to polymerize or harden. Due to the chemical instability of the two initiators, the three-part system was reduced to a two-part system by pre-mixing either of the initiators with the MMA. Instead of using capillary glass tubes, rounded steel rods were cast in the concrete and pulled out after 24 h of curing, leaving small channels through the length of the sample.

Apart from the aforementioned methods, functional materials, such as shape memory alloy or shape memory polymer, are also incorporated in the self-healing cementitious materials. When cracks are initiated, the shape memory materials with a shorter predefined memorized shape than the current state will contract or shrink in a restrained condition; thus, a shrinking force will be generated, leading to the closure of cracks (Wu et al., 2012). Among many types of shape memory alloys (SMA), Nitinol is the most commonly used SMA due to its superior thermo-mechanical and thermo-electrical properties, shape memory effect, and superelasticity (Duerig et al., 2013). Shape memory materials can be activated upon heating or electricity to control cracks. Kuang and Ou (2008a) utilized SMA wires and an adhesive to develop a smart self-repairing concrete beam. The results demonstrated that the SMA wires added self-restoration capacity to concrete beams, the deflection of the beams reversed, and the crack almost closed after unloading. Sakai et al. (2003) investigated the self-restoration of a concrete beam using superelastic SMA wires. The results revealed that the mortar beam with SMA wires recovered almost completely after incurring an extremely large crack. Furthermore, shape memory polymers (SMP) are also incorporated into self-healing cementitious materials. The cracks occur within the matrix due to early age shrinkage, thermal effects and/or mechanical loading, then the shrinkage mechanism in the embedded shape memory polymer tendon (or tendons) is activated by heating, which results in crack closure and compressive stresses being developed across the closed crack faces (Wu et al., 2012).

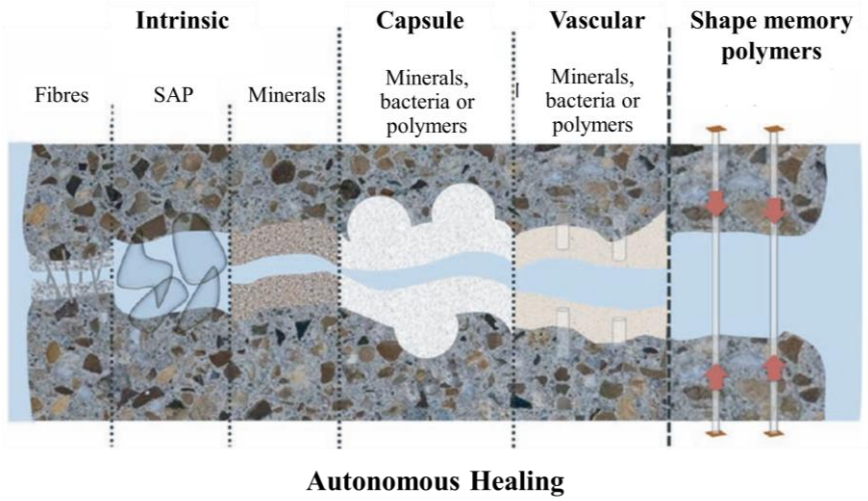

Figure 3-3. Mechanisms leading to autonomous healing (De Rooij et al., 2013)

Although previous studies have explored autonomous healing in conventional cementitious materials, the understanding of autonomous healing in CPB remains limited. Xiang et al. (2023a) utilized waste porous ceramic (WPC) as a bacterial carrier to embed Sporosarcina pasteurii, achieving self-healing in backfill paste. The results demonstrated that the embedded biosolution could be released from WPC upon crack formation, with initial crack widths of less than 1 mm, achieving a 100% self-healing ratio in crack closure after 28 days. Additionally, Xiang et al. (2023b) proposed a bacterial mixture of Sporosarcina pasteurii and Pseudomonas denitrificans pre-embedded in polypropylene-fiber reinforced backfill to enhance the self-healing capacity without the need for additional carriers.

3.2.3 Discussions

Autogenous healing is an intrinsic property of cementitious materials that enables them to heal or repair small cracks through delayed hydration of unhydrated cementitious particles. The efficiency of autogenous healing significantly depends on the age of the cementitious material, the presence of water or moisture, and the crack width. Numerous investigations have been conducted to explore methods or materials to increase healing efficiency. The basic method is to lower the water-to-cement ratio to increase the content of cementitious material, in which the higher amount of unhydrated particles in the matrix can contribute to autogenous healing at later ages. Additionally, mineral admixtures (i.e., blast furnace slag, fly ash, silica fume, crystalline additive, etc.) are introduced to enhance autogenous healing. However, disadvantages still exist in autogenous healing, such as insufficient exposure conditions, higher content of cementitious material resulting in an increased hydration heat, shrinkage and crack risk, loss of workability, and inadequate ability to fill large cracks.

In contrast to autogenous healing, autonomous healing is able to embed different unconventional engineered admixtures in the composite to trigger and develop the self-healing process, such as encapsulation and vascular methods. The encapsulation method can protect healing agents during the mixing procedure and activate them only at the critical moment of rupture. The vascular-based method allows an increase in the number of healing agents that can be released to the target cracks, theoretically, even with no limit from an external supplying source. Based on theory and results obtained from small-scale laboratory studies, autonomous self-healing should be an efficient self-healing process. Nevertheless, the survival rate of capsules is low during the mixing procedure, and the workability will be decreased if the number of capsules increases. If a bacterial healing agent is adopted, the bacterial nutrients slow down or even completely hinder the hydration of cementitious material, leading to lower strength values. When considering the application in engineering practice, the autonomous healing process is relatively complex and expensive to be applied on a full scale.

Generally, the approach of autogenous healing appears to be more feasible, efficient, cost-effective, safer, and simpler to implement than the approach of autonomous healing for real-life applications.

3.3 Factors Affecting Self-healing in Cementitious Materials

3.3.1 Age of Pre-cracking

Due to different exposure conditions in engineering practice, the cracking time within cementitious materials and the quantity of unhydrated cementitious particles cannot be predicted. The interest in studying the influence of pre-cracking age/time on self-healing behaviour attracts increasing attention. Qian et al. (2015) investigated the self-healing potential of early-age cracks in cement-based materials incorporating the bacteria that could produce carbonic anhydrase. In their study, cement-based material specimens were pre-cracked at ages 7, 14, 28, and 60 days to study the self-healing ability influenced by cracking time. It was shown that the self-healing effect was excellent for cracking at the early age of 7 days, and the self-healing agent lost the repair effect when the cracking age was more than 60 days. Thus, the self-healing efficiency of cracks drops when the cracking age increases. Similarly, Luo et al. (2015) concluded that the crack healing ratio of specimens dropped significantly along with the extension of cracking age. When the cracking age was more than 60 days, the crack healing ratio was very small. Furthermore, Heide and Schlangen (2007) found a better recovery of flexural strength in concrete beams pre-cracked at earlier ages and an apparent decrease in strength recovery with increasing specimen age when making the first crack.

3.3.2 Crack Width

Previous studies have implied the need for crack width control to attain effective self-healing in cementitious materials. Generally, autogenous healing can be effective for crack widths up to 200 μm (Talaiekhozani and Abd Majid, 2014). However, with the increase in crack width, self-healing behaviour will become more and more difficult (Sahmaran et al., 2015). Qian et al. (2015) investigated the influence of crack width on the healing rate with crack widths from 0.1 to 1 mm. The experimental results indicated that the cracks below 0.4 mm were almost completely closed. It was concluded that crack width influenced self-healing effectiveness significantly. As for engineered cementitious composites, Yang et al. (2009) observed that when the crack width exceeds 150 μm, the specimen resonant frequency remains unchanged even after exposure to wet-dry cycle conditions. The resonant frequency and the permeability measurements suggest that autogenous self-healing within cement-based materials in both mechanical and transport properties can be achieved, provided that damage must be restricted to very tight crack widths, below 150 μm and preferably below 50 μm, at least under 10 wet/dry cycles exposure regime. However, the extremely tight crack width is challenging to attain reliably in most conventional concrete materials, even when steel reinforcement is used.

3.3.3 Exposure/Self-healing Condition

When cementitious material specimens are pre-cracked, they will be exposed to the corresponding prescribed conditions for the self-healing process. Different exposure conditions are adopted either for their good compatibility in combination with the healing agent or as representative of the intended field of application (Ferrara et al., 2018). Various exposure conditions have been

investigated on cementitious materials, including open air, immersion in water, wet/dry cycles, freeze/thaw cycles, Ca^{2+} and CO_2 concentrations, controlled temperature and relative humidity, etc., in the studies of cementitious materials (i.e., concrete, mortar, ECCs, etc.). For most techniques, the presence of free water or a humid environment is required to produce significant self-healing (Snoeck et al., 2014).

3.3.4 Self-healing Duration

Healing duration or curing time for the self-healing process also plays an essential role in the self-healing behaviour of cementitious materials. Ferrara et al. (2017) conducted a thorough characterization of the self-healing capacity of high-performance fiber-reinforced cementitious composites under different exposure conditions (water immersion, exposure to humid or dry air, and wet/dry cycles) and exposure times (from one month to two years). The experimental results illustrated that the specimens immersed in water, together with specimens exposed to 90% RH, were able to gain the highest recovery trend after much longer exposure times, even though the strength of the healed specimen was slightly higher than that of the virgin specimen. However, the specimens exposed to open air performed no further significant improvement with prolonged exposure time after an initial appreciable healing rate. As for the specimens immersed in water, water could penetrate deeper into cracks, promoting and prolonging the delayed hydration of unhydrated particles. Similar performance was also observed by Ferrara et al. (2016a and 2016b). The recovery of mechanical performance continued even after relatively long exposure times, up to the complete closure of cracks.

3.4 Methods for Characterization of Self-healing Behaviour

In a self-healing system, it is essential to measure or evaluate its feasibility and healing efficiency. Healing may occur on the surface crack or internal crack, resulting in different healing efficiency. A thorough evaluation or assessment of the healing efficiency of a self-healing system in cementitious materials is significantly crucial. Therefore, different techniques have been put forward to assess the changes in microstructure and evaluate the recovery of mechanical properties qualitatively and quantitatively.

3.4.1 Cracks Characteristics

Surface cracks: The observation of surface crack closure is the most straightforward method to examine self-healing performance after exposure to healing conditions for pre-cracked specimens. The techniques used to evaluate the surface crack closure range from the naked eye to a microscope, such as a magnifier, photographs from a camera, digital microscope, optical microscope, electron microscope, etc. The high-resolution camera or digital single-lens reflex is usually employed to take pictures periodically to record the cracks' development during testing and curing. A high-resolution camera was used by Qiu et al. (2016) to measure the crack width reduction on both sides of the specimen surface as a direct assessment of self-healing. The crack width was measured at a specific location before and after self-healing conditioning. The high-resolution pictures were used to monitor changes in crack width. Photographs from the camera method allow the acquisition of

images during tests, but they cannot provide sufficient details for a specific crack. Likewise, a microscope was used by the vast bulk of researchers. Alghamri et al. (2016) evaluated the surface crack sealing using an optical microscope in various periods. And Liu et al. (2015) quantitatively studied the crack behaviour of the specimens by light microscopy. Implementing the light microscopy technique is simple and inexpensive, and 0.05-0.3 mm cracks can be detected at an improved resolution. Furthermore, some microscopes have been equipped with specific functions to get additional information on self-healing. For instance, fluorescence microscopy has been applied to study the frequency and types of cracks in concrete technology (De Rooij et al., 2013). Fluorescence microscopy is an effective tool for increasing the contrast between space and solid phases, which favors distinguishing capillary porosity, air voids, and cracks from the hydration products and other solids in the cementitious material microstructures. In the bargain, the photographs from the camera and light microscopy are the only methods that can be applied to a specimen without damage during sample preparation. Therefore, these two methods are the most suitable for repeated observations throughout the healing period.

Internal cracks: Industrial X-ray computed tomography (CT) scanning is a non-destructive system used to study the internal structure of materials, combining X-ray images taken from different angles to create cross-sectional 2D images or 3D compositions (Banthia et al., 2014; Zhu et al., 2018). A sample is rotated under the test, and many relative directions are across the sample. Every point of the sample is traversed by different X-rays from different directions. The acquired 2D cross-section images can be used to reconstruct 3D images. Van Tittelboom et al. (2011) and Snoeck et al. (2016) successfully used X-ray computed tomography to discern internal cracks and healing products in self-healing concrete. The self-healing products could be separated from the cementitious matrix by subtracting the reconstructions obtained after the healing period and the reconstructions before healing. The differential volume represented the formed healing products. Besides, Cao et al. (2021) utilized CT scanning technology to investigate the relationship between compressive strength and internal crack formation (e.g., crack width and volume) of cement-fiber-tailings matrix composites. The CT scanning technology enables the exact position and orientation of each individual fiber to be measured. This technology is extremely expensive and has a low availability of equipment, which limits its application. In addition, health and safety hazards are obstacles due to radiation risk. In addition, the electrical method is a non-destructive method to evaluate cracks within a cementitious specimen by measuring its electrical properties. The technique requires highly conductive fibers, such as steel or carbon fibers, to be added to the cementitious materials. Measurement of the impedance values during the fracture process can be used to detect crack propagation by using the frequency-dependent electrical properties of the fiber-reinforced cementitious composite (Ferrara et al., 2018). Ding et al. (2013) evaluated the influence of the combined use of nano-carbon black and carbon fiber as electrically conductive materials in concrete beams to study the relationships among fractional change in resistance, the strain, and the damage degree under bending in the pre-cracking region. Also, Wen & Chung (2007) confirmed that damage self-sensing (to be distinguished from strain self-sensing) by electrical resistance measurement is effective in carbon fiber-reinforced cement below the percolation threshold. This

technique, however, may require dedicated and expensive equipment and a suitable post-processing model to correlate electrical measures with crack width, which are the main disadvantages impeding the wide applications.

3.4.2 Recovery of Mechanical Properties

Resonant frequency: The presence of cracks within cementitious materials impedes the transmission through the matrix, which will, in turn, affect the resonant frequency of cementitious materials. The resonant frequency (RF) measurement of cementitious materials based on ASTM C215-19 "Standard Test Method for Fundamental Transverse, Longitudinal, and Torsional Resonant Frequencies of Concrete Specimens" has been proven to be a promising, non-destructive, and relatively simple technique to determine the extent of damage and rate of self-healing (Yang et al., 2009).

Ultrasonic pulse velocity: The ultrasonic pulse velocity (UPV) test is one of the most widely used methods for evaluating self-healing in cementitious materials based on the procedures from ASTM C597-22 "Standard Test Method for Pulse Velocity Through Concrete." Because the propagation speed of ultrasonic waves in the liquid or gas is slower than in the solid, an increase in transmission time indicates the defects and discontinuities within the cementitious matrix (Xu and Yao, 2014). When the cracks are filled with self-healing products, the propagation time of UPV is reduced, which can be used to demonstrate the self-healing process and to evaluate the effectiveness of self-healing. However, UPV tests are prone to being interfered with by temperature changes and the water in the matrix, affecting the accuracy (Tang et al., 2015).

Uniaxial tensile test: Although the inherent difficulties in performing stable uniaxial tensile tests exist, the uniaxial tensile test has been employed by some researchers to evaluate the effectiveness of self-healing in cementitious materials through the recovery of tensile strength, first cracking strength, stiffness, and tensile strain capacity (Wang et al., 2019). For instance, Liu et al. (2017a and 2017b) used a uniaxial tensile test to evaluate the durability of ECC and the level of self-healing. The stiffness, first cracking strength, ultimate tensile strength, and tensile strain capacity of ECC specimens were determined based on the tensile stress-strain relationships.

Splitting tensile test: The splitting tensile test has been widely used for pre-cracking specimens to introduce cracks for self-healing recovery assessment tests. The splitting tensile test results in strong instability after the post-crack response (Ferrara et al., 2018), but it has been employed to evaluate the mechanical properties of cementitious materials via self-healing. Özbay et al. (2013) studied the self-healing ability of ECCs containing high-volume fly ash, utilizing splitting tensile tests to generate microcracks and evaluate the mechanical recovery. It was shown that the preloaded specimens had a remarkable recovery of the load-carrying capacity, deflection capacity, and stiffness after exposure to continuous moisture and cyclic wet/dry for 60 days.

Bending test: Flexural or bend strength is defined as a material's ability to resist deformation under load. The flexural strength represents the highest stress experienced within the material at its moment of rupture (Boresi et al., 1985). Three-point (Qureshi et al., 2016; Ferrara et al., 2014) and

four-point (Wang et al., 2019; Ali et al., 2017) bending tests are commonly used to determine the flexural strength of a specimen. The bending tests, three- and four-point bending tests, have been commonly adopted to evaluate the self-healing capacity of cementitious materials by examining flexural strength, deflection capacity, and stiffness. The bending test characterizes the behaviour of a material subjected to an external load applied perpendicularly to a longitudinal axis of the material.

Uniaxial compression test: The uniaxial compressive strength (UCS) test has been widely utilized to measure the compressive strength of cementitious materials based on ASTM C39/C39M-21 "Standard Test Method for Compressive Strength of Cylindrical Concrete Specimens." The compressive strength of cementitious materials reflects the integrity of the matrix to some extent, such as the internal porosity and compactness. Thus, a compression test can be used to evaluate the mechanical recovery of cementitious materials via a self-healing process (Zhang et al., 2017; Bundur et al., 2017).

3.4.3 Recovery of Durability Properties

The achievement of self-healing in cementitious materials significantly promotes their durability and prolongs the service life without requiring maintenance and repair. Since cracks directly impact the durability performance of cementitious materials, it is essential to quantitatively evaluate the effectiveness of self-healing capability in engineering practice, especially to assess the recovery of durability performance through self-healing mechanisms. Therefore, different technologies have been proposed for this purpose.

Water permeability test: The decrease in water permeability of self-healed pre-cracked specimens can be used to measure the self-healing capacity. Water permeability tests are usually conducted before and after cracking and healing. Two types of setups can be adopted: a falling head permeability test setup and a constant head permeability test setup (Yang et al., 2009).

Chloride penetration test: The ASTM C1202-22 ''Standard test method for electrical indication of concrete's ability to resist chloride ion penetration", measuring the reduction in the rate of chloride migration, has been widely employed to characterize the recovery of durability performance of cementitious materials through self-healing mechanisms. The method indirectly evaluates resistance to chloride penetration by measuring the quantity of charge passing over a period using an applied electrical potential.

Sorptivity/Absorption test: Sorptivity is related to absorption, with the latter being sometimes used as an indicator of the volume of the capillary pore space or open porosity (Sabir et al., 1998). The dried pre-cracked samples with and without self-healing were placed in a water container as the cracked surface was immersed below the water surface. The samples were weighed at regular time intervals. The results exhibited a clear distinction between the specimens with and without self-healing, illustrating that capillary water absorption tests could also be used to determine crack healing. The testing procedures can be followed as described in ASTM C1585-20, "Standard Test Method for Measurement of Rate of Absorption of Water by Hydraulic-Cement Concretes."

Mercury intrusion porosimetry test: Mercury intrusion porosimetry (MIP) is one of the most widely used methods to evaluate the microstructure of cementitious materials. MIP has been employed to analyze pore size distribution and total porosity of samples in cracked and healed conditions based on the relationship between the amount of mercury flowing into the porous system of the concrete materials and the applied pressure. Healing efficiency can be examined by the reduction of the cumulative pore volume after healing conditions.

3.4.4 Characterization of Self-healing Products

The aforementioned methods are the most intuitive techniques to evaluate a self-healing system. Apart from the quantitative assessment of damage degree or self-healing efficiency, characterizing the chemical or mineral compositions of the crystalline precipitation and morphology of microstructure within the cementitious matrix is also of great importance as an additional method to support the self-healing behaviour. Therefore, contemporary instrumented analytical methods have been successfully employed to characterize the nature of self-healing mineral or chemical products, including X-ray diffraction (XRD), scanning electron microscopy (SEM), energy dispersive X-ray analysis (EDX or EDS), thermogravimetric analysis (TGA), transmission electron microscopy (TEM), Fourier transform infrared spectroscopy (FTIR), etc.

X-ray diffraction (XRD) analysis is the most utilized technique to analyze the compositions of self-healing products. X-ray diffraction is an effective method for crystal structure analysis in the laboratory. The crystal structure of each material is different, and the crystal structure includes parameters such as lattice type and spacing between crystal planes. After irradiating the measured sample with an X-ray of a certain energy, substances in the sample will be stimulated to produce secondary fluorescence X-rays; then, the qualitative analysis of compounds can be conducted by measuring the position of the diffraction angle.

Scanning electron microscopy (SEM) is widely used to analyze the microstructure of healing products. SEM is a kind of scanning on the sample's surface after focusing the electron beam emitted by the electron gun. The composition, morphology, and structure of the sample surface are observed and analyzed by detecting the signal generated by the interaction between the electron and the sample. The interactions between the incident electron and the sample will stimulate secondary electrons, backscattered electrons, absorbed electrons, Auger electrons, cathode fluorescence, and characteristic X-rays. SEM mainly uses secondary electrons, backscattered electrons, and characteristic X-ray signals to analyze the surface characteristics of samples. Moreover, ***energy dispersive spectroscopy (EDS)*** analyses can also be performed to distinguish the main elements present in the healing products. Therefore, SEM-EDS is usually combined to identify the structure, morphology, size, and distribution of crystals (Muhammad et al., 2016).

Thermogravimetric analysis (TGA) is a technique where the mass of a polymer is measured as a function of temperature or time while the sample is subjected to a controlled temperature program in a controlled atmosphere (Charsley and Warrington, 1988). When applied to characterize the self-healing products, TGA refers to a thermal analysis that measures the relationship between the mass

of healing products and the temperature changes under a temperature control program. TGA is usually used to determine the compositions of self-healing products.

A ***transmission electron microscope (TEM)*** is a microscopy technique in which a beam of electrons is transmitted through a specimen to form an image (Wang et al., 2009). The specimen is often an ultrathin section, less than 100nm thick, or a suspension on a grid. TEM has been frequently used in cementitious materials to monitor the crack width changes during the self-healing process, but is scarcely employed to analyze the healing products.

The infrared spectrum of a sample's emission or absorption can be obtained using ***Fourier transform infrared spectroscopy (FTIR)*** by performing a Fourier transform on the data. It is employed to ascertain the molecular structure or recognize chemical species (Araújo et al., 2016). In contrast to the aforementioned analytical techniques, FTIR is more appropriate for analyzing the organic phase. FTIR can provide valuable insights into changes in the different functional groups of the healing products when organic agents are used.

3.5 Conclusions

This chapter of the literature review comprehensively presents the previous studies on the self-healing behaviour and characterization of cementitious materials with a focus on conventional and high-performance concrete, mortar, ECCs, and so forth. The much lower cement content (or much higher water/cement ratio) in CPBs and different particle size distributions between tailings and aggregates signify that the results of current self-healing studies on conventional concrete and cementitious materials are not transferable to CPB materials. In addition, only limited studies were conducted on the investigation of self-healing behaviour in the CPBs of autonomous healing with an adopted low water/cement ratio, which cannot represent the typical CPB mixtures in practice. Moreover, to date, it is clearly recognized from the literature review that no previous studies have been carried out to explore the self-healing (autogenous healing) capacity and behaviour of CPB. Furthermore, the effects of multiphysical (THMC) impacting factors are dominant in the evolution of geotechnical features of the CPB matrix after being placed underground. It is essential to investigate their impacts on the self-healing performance of CPB. Consequently, these research gaps need to be addressed.

3.6 References

Ahn, T. H., & Kishi, T. (2008b). The effect of geo-materials on the autogenous healing behavior of cracked concrete. In Concrete repair, rehabilitation and retrofitting II (pp. 143-144). CRC Press.

Ahn, T. H., & Kishi, T. (2009). Crack healing behaviour of cementitious composite materials incorporating geo-materials. In Proceedings of 2nd International Conference on Self Healing Materials, Chicago, IL, USA (Vol. 28).

Ahn, T. H., & Kishi, T. (2010). Crack self-healing behavior of cementitious composites incorporating various mineral admixtures. Journal of Advanced Concrete Technology, 8(2), 171-186.

Aïtcin, P. C. (2007). Binders for durable and sustainable concrete. CRC Press.

Alghamri, R., Kanellopoulos, A., & Al-Tabbaa, A. (2016). Impregnation and encapsulation of lightweight aggregates for self-healing concrete. Construction and Building Materials, 124, 910-921.

Ali, M. A. E. M., & Nehdi, M. L. (2017). Innovative crack-healing hybrid fiber reinforced engineered cementitious composite. Construction and Building Materials, 150, 689-702.

Araújo, M., Van Vlierberghe, S., Feiteira, J., Graulus, G. J., Van Tittelboom, K., Martins, J. C., ... & De Belie, N. (2016). Cross-linkable polyethers as healing/sealing agents for self-healing of cementitious materials. Materials & Design, 98, 215-222.

Banthia, N., Majdzadeh, F., Wu, J., & Bindiganavile, V. (2014). Fiber synergy in Hybrid Fiber Reinforced Concrete (HyFRC) in flexure and direct shear. Cement and Concrete Composites, 48, 91-97.

Biggs, A. R. (1985). Suberized boundary zones and the chronology of wound response in tree bark. Phytopathology, 75(11), 1191-1195.

Blaiszik, B. J., Kramer, S. L., Olugebefola, S. C., Moore, J. S., Sottos, N. R., & White, S. R. (2010). Self-healing polymers and composites. Annual review of materials research, 40(1), 179-211.

Boresi, A. P., Schmidt, R. J., & Sidebottom, O. M. (1985). Advanced mechanics of materials (Vol. 6). New York: Wiley.

Bundur, Z. B., Kirisits, M. J., & Ferron, R. D. (2017). Use of pre-wetted lightweight fine expanded shale aggregates as internal nutrient reservoirs for microorganisms in bio-mineralized mortar. Cement and Concrete Composites, 84, 167-174.

Cailleux, E., & Pollet, V. (2009). Investigations on the development of self-healing properties in protective coatings for concrete and repair mortars. In Proceedings of the 2nd international conference on self-healing materials, Chicago, IL, USA (Vol. 28, p. 1).

Cao, S., Yilmaz, E., Yin, Z., Xue, G., Song, W., & Sun, L. (2021). CT scanning of internal crack mechanism and strength behavior of cement-fiber-tailings matrix composites. Cement and Concrete Composites, 116, 103865.

Charsley, E. L., & Warrington, S. B. (1988). Industrial applications of compositional analysis by thermogravimetry. ASTM International.

Cremaldi, J. C., & Bhushan, B. (2018). Bioinspired self-healing materials: lessons from nature. Beilstein Journal of Nanotechnology, 9(1), 907-935.

Cuenca, E., & Ferrara, L. (2017). Self-healing capacity of fiber reinforced cementitious composites. State of the art and perspectives. KSCE Journal of Civil Engineering, 21(7), 2777-2789.

Darquennes, A., Olivier, K., Benboudjema, F., & Gagné, R. (2016). Self-healing at early-age, a way to improve the chloride resistance of blast-furnace slag cementitious materials. Construction and Building Materials, 113, 1017-1028.

De Belie, N., Gruyaert, E., Al-Tabbaa, A., Antonaci, P., Baera, C., Bajare, D., ... & Jonkers, H. M. (2018). A review of self-healing concrete for damage management of structures. Advanced materials interfaces, 5(17), 1800074.

De Rooij, M., Van Tittelboom, K., De Belie, N., & Schlangen, E. (Eds.). (2013). Self-healing phenomena in cement-Based materials: state-of-the-art report of RILEM technical committee 221-SHC: self-Healing phenomena in cement-Based materials (Vol. 11). Springer Science & Business Media.

Ding, Y., Chen, Z., Han, Z., Zhang, Y., & Pacheco-Torgal, F. (2013). Nano-carbon black and carbon fiber as conductive materials for the diagnosing of the damage of concrete beam. Construction and Building Materials, 43, 233-241.

Dry, C. (1993). Passive smart materials for sensing and actuation. Journal of intelligent material systems and structures, 4(3), 420-425.
Dry, C. M. (1994). Matrix cracking repair and filling using active and passive modes for smart timed release of chemicals from fibers into cement matrices. Smart Materials and Structures, 3(2), 118.
Dry, C. M. (2000). Three designs for the internal release of sealants, adhesives, and waterproofing chemicals into concrete to reduce permeability. Cement and Concrete Research, 30(12), 1969-1977.
Dry, C., & McMillan, W. (1996). Three-part methylmethacrylate adhesive system as an internal delivery system for smart responsive concrete. Smart Materials and Structures, 5(3), 297.
Duerig, T. W., Melton, K. N., & Stöckel, D. W. C. M. (2013). Engineering aspects of shape memory alloys. Butterworth-heinemann.
Edvardsen, C. (1999). Water permeability and autogenous healing of cracks in concrete. In Innovation in concrete structures: Design and construction (pp. 473-487). Thomas Telford Publishing.
Ferrara, L., Krelani, V., & Carsana, M. (2014). A "fracture testing" based approach to assess crack healing of concrete with and without crystalline admixtures. Construction and Building Materials, 68, 535-551.
Ferrara, L., Krelani, V., & Moretti, F. (2016a). Autogenous healing on the recovery of mechanical performance of High Performance Fibre Reinforced Cementitious Composites (HPFRCCs): Part 2–Correlation between healing of mechanical performance and crack sealing. Cement and Concrete Composites, 73, 299-315.
Ferrara, L., Krelani, V., & Moretti, F. (2016b). On the use of crystalline admixtures in cement based construction materials: from porosity reducers to promoters of self healing. Smart Materials and Structures, 25(8), 084002.
Ferrara, L., Krelani, V., Moretti, F., Flores, M. R., & Ros, P. S. (2017). Effects of autogenous healing on the recovery of mechanical performance of High Performance Fibre Reinforced Cementitious Composites (HPFRCCs): Part 1. Cement and Concrete Composites, 83, 76-100.
Ferrara, L., Van Mullem, T., Alonso, M. C., Antonaci, P., Borg, R. P., Cuenca, E., ... & De Belie, N. (2018). Experimental characterization of the self-healing capacity of cement based materials and its effects on the material performance: A state of the art report by COST Action SARCOS WG2. Construction and Building Materials, 167, 115-142.
Ghosh, S. K. (Ed.). (2009). Self-healing materials: fundamentals, design strategies, and applications (Vol. 18). Weinheim: Wiley-vch.
Glanville, W. H. (1926). The permeability of Portland cement concrete. HM Stationery Office [printed by Harrison and sons, Limited].
Hearn, N. and Morley, C. (1997). Self-sealing property of concrete - Experimental evidence. Materials and Structures, Vol. 30, No. 201, pp. 404-411.
Hemsley, A. R., & Griffiths, P. C. (2000). Architecture in the microcosm: biocolloids, self-assembly and pattern formation. Philosophical Transactions of the Royal Society of London. Series A: Mathematical, Physical and Engineering Sciences, 358(1766), 547-564.
Huang, H., Ye, G., & Damidot, D. (2014). Effect of blast furnace slag on self-healing of microcracks in cementitious materials. Cement and concrete research, 60, 68-82.
Hyde, G. W., & Smith, W. J. (1889). Results of experiments made to determine the permeability of cements and cement mortars. Journal of the Franklin Institute, 128(3), 199-207.

Jaroenratanapirom, D., & Sahamitmongkol, R. (2011). Self-crack closing ability of mortar with different additives. Journal of Metals, Materials and Minerals, 21(1).

Joseph, C., Jefferson, A. D., Isaacs, B., Lark, R., & Gardner, D. (2010). Experimental investigation of adhesive-based self-healing of cementitious materials. Magazine of Concrete Research, 62(11), 831-843.

Kim, J. S., & Schlangen, H. E. J. G. (2011). Self-healing in ECC stimulated by SAP under flexural cyclic load. In ICSHM 2011: Proceedings of the 3rd International Conference on Self-Healing Materials, Bath, UK, 27-29 June 2011.

Kuang, Y., & Ou, J. (2008a). Self-repairing performance of concrete beams strengthened using superelastic SMA wires in combination with adhesives released from hollow fibers. Smart Materials and Structures, 17(2), 025020.

Lee, H. X. D., Wong, H. S., & Buenfeld, N. (2010b). Self-sealing cement-based materials using superabsorbent polymers. In Proceedings of the International RILEM Conference on Use of Superabsorbent Polymers and Other New Additives in Concrete, Lyngby, Denmark (pp. 15-18).

Lee, H. X. D., Wong, H. S., & Buenfeld, N. R. (2010a). Potential of superabsorbent polymer for self-sealing cracks in concrete. Advances in Applied Ceramics, 109(5), 296-302.

Lee, Y. S., & Ryou, J. S. (2016). Crack healing performance of PVA-coated granules made of cement, CSA, and Na2CO3 in the cement matrix. Materials, 9(7), 555.

Li, M., & Li, V. C. (2011). Cracking and healing of engineered cementitious composites under chloride environment. ACI Materials Journal, 108(3), 333.

Li, Q., Li, Z., & Yuan, G. (2012). Effects of elevated temperatures on properties of concrete containing ground granulated blast furnace slag as cementitious material. Construction and Building Materials, 35, 687-692.

Li, V. C., Wu, C., Wang, S., Ogawa, A., & Saito, T. (2002). Interface tailoring for strain-hardening polyvinyl alcohol-engineered cementitious composite (PVA-ECC). Materials Journal, 99(5), 463-472.

Liu, B., Zhang, J. L., Ke, J. L., Deng, X., Dong, B. Q., Han, N. X., & Xing, F. (2015, June). Trigger of self-healing process induced by EC encapsulated mineralization bacterium and healing efficiency in cement paste specimens. In 5th International Conference on Self-Healing Materials (pp. 1-4).

Liu, H., Zhang, Q., Gu, C., Su, H., & Li, V. (2017b). Self-healing of microcracks in Engineered Cementitious Composites under sulfate and chloride environment. Construction and Building Materials, 153, 948-956.

Liu, H., Zhang, Q., Li, V., Su, H., & Gu, C. (2017a). Durability study on engineered cementitious composites (ECC) under sulfate and chloride environment. Construction and Building Materials, 133, 171-181.

Lopez-Tendero, M. J., Diaz, P., Lloris, J. M., & Gamon, C. (2011, June). Optimized hydrogel for application as repairing agents in cement based products. In Proceedings of 3rd International Conference on Self Healing Materials, Bath, UK (Vol. 2729).

Luo, M., Qian, C. X., & Li, R. Y. (2015). Factors affecting crack repairing capacity of bacteria-based self-healing concrete. Construction and building materials, 87, 1-7.

Mihashi, H., Kaneko, Y., Nishiwaki, T., & Otsuka, K. (2000). Fundamental study on development of intelligent concrete characterized by self-healing capability for strength. Transactions of the Japan Concrete Institute, 22, 441-450.

Muhammad, N. Z., Shafaghat, A., Keyvanfar, A., Majid, M. Z. A., Ghoshal, S. K., Yasouj, S. E. M., ... & McCaffer, R. (2016). Tests and methods of evaluating the self-healing efficiency of concrete: A review. Construction and Building Materials, 112, 1123-1132.

Na, S. H., Hama, Y., Taniguchi, M., Katsura, O., Sagawa, T., & Zakaria, M. (2012). Experimental investigation on reaction rate and self-healing ability in fly ash blended cement mixtures. Journal of Advanced Concrete Technology, 10(7), 240-253.

Neville, A. (2002). Autogenous healing-a concrete miracle?. Concrete international, 24(11), 76-82.

Nguyễn, H. H., Choi, J. I., Song, K. I., Song, J. K., Huh, J., & Lee, B. Y. (2018). Self-healing properties of cement-based and alkali-activated slag-based fiber-reinforced composites. Construction and Building Materials, 165, 801-811.

Nishiwaki, T., Sasaki, H., & Sukmin, K. (2015). Experimental study on self-healing effect of FRCC with PVA fibers and additives. J. Ceram. Process. Res, 16(1), 89-94.

Özbay, E., Karahan, O., Lachemi, M., Hossain, K. M., & Atis, C. D. (2013). Dual effectiveness of freezing–thawing and sulfate attack on high-volume slag-incorporated ECC. Composites Part B: Engineering, 45(1), 1384-1390.

Özbay, E., Šahmaran, M., Lachemi, M., & Yücel, H. E. (2013). Self-Healing of Microcracks in High-Volume Fly-Ash-Incorporated Engineered Cementitious Composites. ACI Materials Journal, 110(1).

Qian, C., Chen, H., Ren, L., & Luo, M. (2015). Self-healing of early age cracks in cement-based materials by mineralization of carbonic anhydrase microorganism. Frontiers in microbiology, 6, 1225.

Qiu, J., Tan, H. S., & Yang, E. H. (2016). Coupled effects of crack width, slag content, and conditioning alkalinity on autogenous healing of engineered cementitious composites. Cement and Concrete Composites, 73, 203-212.

Qureshi, T. S., & Al-Tabbaa, A. (2016). Self-healing of drying shrinkage cracks in cement-based materials incorporating reactive MgO. Smart Materials and Structures, 25(8), 084004.

Ramm, W., & Biscoping, M. (1998). Autogenous healing and reinforcement corrosion of water-penetrated separation cracks in reinforced concrete. Nuclear Engineering and Design, 179(2), 191-200.

Roig-Flores, M., Formagini, S., & Serna, P. (2021). Self-healing concrete-What Is it Good For?. Materiales de Construcción, 71(341), e237-e237.

Roig-Flores, M., Pirritano, F., Serna, P., & Ferrara, L. (2016). Effect of crystalline admixtures on the self-healing capability of early-age concrete studied by means of permeability and crack closing tests. Construction and Building Materials, 114, 447-457.

Sabir, B. B., Wild, S., & O'farrell, M. (1998). A water sorptivity test for martar and concrete. Materials and structures, 31(8), 568-574.

Şahmaran, M., Keskin, S. B., Ozerkan, G., & Yaman, I. O. (2008). Self-healing of mechanically-loaded self consolidating concretes with high volumes of fly ash. Cement and Concrete Composites, 30(10), 872-879.

Sahmaran, M., Yildirim, G., Noori, R., ÖZBAY, E., & Lachemi, M. (2015). Repeatability and pervasiveness of self-healing in engineered cementitious composites. ACI Materials Journal, 112(4).

Sakai, Y., Kitagawa, Y., Fukuta, T., & Iiba, M. (2003, August). Experimental study on enhancement of self-restoration of concrete beams using SMA wire. In Smart Structures and Materials 2003: Smart Systems and Nondestructive Evaluation for Civil Infrastructures (Vol. 5057, pp. 178-186). SPIE.

Sherir, M. A., Hossain, K. M., & Lachemi, M. (2017). Development and recovery of mechanical properties of self-healing cementitious composites with MgO expansive agent. Construction and Building Materials, 148, 789-810.
Sisomphon, K., & Copuroglu, O. (2011). Self healing mortars by using different cementitious materials. In Proceedings of the international conference on advances in construction materials through science and engineering, Hong Kong, China (pp. 5-7).
Sisomphon, K., Copuroglu, O., & Koenders, E. A. B. (2012). Self-healing of surface cracks in mortars with expansive additive and crystalline additive. Cement and Concrete Composites, 34(4), 566-574.
Sisomphon, K., Copuroglu, O., & Koenders, E. A. B. (2013). Effect of exposure conditions on self healing behavior of strain hardening cementitious composites incorporating various cementitious materials. Construction and Building Materials, 42, 217-224.
Snoeck, D., Dewanckele, J., Cnudde, V., & De Belie, N. (2016). X-ray computed microtomography to study autogenous healing of cementitious materials promoted by superabsorbent polymers. Cement and Concrete Composites, 65, 83-93.
Snoeck, D., Steuperaert, S., Van Tittelboom, K., Dubruel, P., & De Belie, N. (2012). Visualization of water penetration in cementitious materials with superabsorbent polymers by means of neutron radiography. Cement and Concrete Research, 42(8), 1113-1121.
Snoeck, D., Van Tittelboom, K., Steuperaert, S., Dubruel, P., & De Belie, N. (2014). Self-healing cementitious materials by the combination of microfibres and superabsorbent polymers. Journal of Intelligent Material Systems and Structures, 25(1), 13-24.
Talaiekhozani, A., & Abd Majid, M. Z. (2014). A review of self-healing concrete research development. Journal of Environmental Treatment Techniques, 2(1), 1-11.
Tang, W., Kardani, O., & Cui, H. (2015). Robust evaluation of self-healing efficiency in cementitious materials–A review. Construction and Building Materials, 81, 233-247.
ter Heide, N., & Schlangen, E. (2007, April). Self-healing of early age cracks in concrete. In Proceedings of the First international conference on Self Healing Materials (pp. 18-20). Noordwijk aan Zee The Netherlands.
Termkhajornkit, P., Nawa, T., Yamashiro, Y., & Saito, T. (2009). Self-healing ability of fly ash–cement systems. Cement and concrete composites, 31(3), 195-203.
Thomas, M. D. A. (2007). Optimizing the use of fly ash in concrete (Vol. 5420). Skokie, IL, USA: Portland Cement Association.
Van Breugel, K. (2007, April). Is there a market for self-healing cement-based materials. In Proceedings of the first international conference on self-healing materials (pp. 1-9).
Van Tittelboom, K., & De Belie, N. (2013). Self-healing in cementitious materials—A review. Materials, 6(6), 2182-2217.
Van Tittelboom, K., De Belie, N., Van Loo, D., & Jacobs, P. (2011). Self-healing efficiency of cementitious materials containing tubular capsules filled with healing agent. Cement and Concrete Composites, 33(4), 497-505.
Van Tittelboom, K., Gruyaert, E., Rahier, H., & De Belie, N. (2012). Influence of mix composition on the extent of autogenous crack healing by continued hydration or calcium carbonate formation. Construction and Building Materials, 37, 349-359.
Wang, K., Wang, Y., Wang, Y., Hosono, E., & Zhou, H. (2009). Mesoporous carbon nanofibers for supercapacitor application. The Journal of Physical Chemistry C, 113(3), 1093-1097.
Wang, X. F., Yang, Z. H., Fang, C., Han, N. X., Zhu, G. M., Tang, J. N., & Xing, F. (2019). Evaluation of the mechanical performance recovery of self-healing cementitious materials–

its methods and future development: a review. Construction and Building Materials, 212, 400-421.
Wen, S., & Chung, D. D. L. (2007). Electrical-resistance-based damage self-sensing in carbon fiber reinforced cement. Carbon, 45(4), 710-716.
Woudhuysen, J., & Abley, I. (2004). Why is construction so backward?. Academy Press.
Wu, M., Johannesson, B., & Geiker, M. (2012). A review: Self-healing in cementitious materials and engineered cementitious composite as a self-healing material. Construction and Building Materials, 28(1), 571-583.
Xiang, J., Li, Z., Qiu, J., Wu, N., & Cheng, H. Investigating the potential for porous ceramics as bacterial carrier in self-healing cemented paste backfill. Ceramics International, 49 (2023a), 13490-13500.
Xiang, J., Qiu, J., Yuan, L., Wu, J., & Ma, Z. Characterization and role analysis of bacteria types in self-healing behaviour of cemented paste backfill. J. Build. Eng., 75 (2023b), 106964.
Xu, J., & Yao, W. (2014). Multiscale mechanical quantification of self-healing concrete incorporating non-ureolytic bacteria-based healing agent. Cement and concrete research, 64, 1-10.
Yang, E. H., Yang, Y., & Li, V. C. (2007). Use of high volumes of fly ash to improve ECC mechanical properties and material greenness. ACI materials journal, 104(6), 620.
Yang, Y., Lepech, M. D., Yang, E. H., & Li, V. C. (2009). Autogenous healing of engineered cementitious composites under wet–dry cycles. Cement and Concrete Research, 39(5), 382-390.
Yang, Z., Hollar, J., He, X., & Shi, X. (2011). A self-healing cementitious composite using oil core/silica gel shell microcapsules. Cement and Concrete Composites, 33(4), 506-512.
Yu, J., Lu, C., Leung, C. K., & Li, G. (2017). Mechanical properties of green structural concrete with ultrahigh-volume fly ash. Construction and building materials, 147, 510-518.
Yunovich, M., & Thompson, N. G. (2003). Corrosion of highway bridges: Economic impact and control methodologies. Concrete International, 25(1), 52-57.
Zhang, J., Liu, Y., Feng, T., Zhou, M., Zhao, L., Zhou, A., & Li, Z. (2017). Immobilizing bacteria in expanded perlite for the crack self-healing in concrete. Construction and Building Materials, 148, 610-617.
Zhou, Z. H., Li, Z. Q., Xu, D. Y., & Yu, J. H. (2011). Influence of slag and fly ash on the self-healing ability of concrete. In Advanced materials research (Vol. 306, pp. 1020-1023). Trans Tech Publications Ltd.
Zhu, D. Y., Rong, M. Z., & Zhang, M. Q. (2015). Self-healing polymeric materials based on microencapsulated healing agents: From design to preparation. Progress in Polymer Science, 49, 175-220.
Zhu, J. B., Zhou, T., Liao, Z. Y., Sun, L., Li, X. B., & Chen, R. (2018). Replication of internal defects and investigation of mechanical and fracture behaviour of rock using 3D printing and 3D numerical methods in combination with X-ray computerized tomography. International Journal of Rock Mechanics and Mining Sciences, 106, 198-212.

Chapter 4 Paper I: Investigation of Crack Self-healing Behaviour and Its Impact on Strength and Permeability Recovery in Cemented Paste Tailings

Published in *Powder Technology*, Volume 457, 120834

Weizhou Quan, Mamadou Fall

Department of Civil Engineering, University of Ottawa, Ottawa, Ontario, Canada

Abstract

Cemented paste backfill (CPB, an engineered mixture of tailings, binder, and water), as one of the sustainable technological innovations for mining waste management, is used extensively around the world as a cementitious construction material in underground mines. The induced cracks within the CPB material tend to severely weaken the integrity and mechanical strength of the CPB structures as well as increase their permeability properties, undermining their safety, serviceability, durability, and environmental performance. However, no studies have been conducted to investigate the autogenous self-healing capability and behaviour of CPB. Therefore, this paper presents the results of an experimental study on the autogenous healing behaviour in CPB material to understand the self-healing mechanism and evaluate the self-healing efficiency through the recovery of mechanical and permeation properties. To this end, the CPB specimens were pre-damaged at different initial curing periods (i.e., 3, 7, and 28 days) and at different pre-damage levels (i.e., 30 %, 50 %, 75 %, 90 %, or 100 % of ultimate compressive strength in the pre-peak phase); then cured with self-healing periods of 1, 7, 28 or 90 days. Mechanical and hydraulic conductivity tests were performed on the pre-damaged specimens to monitor the self-healing changes. The results demonstrate that a significant self-healing capability does exist in the CPB materials due to the formed self-healing products from continuous cement hydration interior of the CPB matrix and carbonation of calcium hydroxide. The mechanical strength and hydraulic conductivity of pre-damaged specimens can be restored to similar values of the control specimens after 7 days and 28 days of self-healing periods, respectively. Furthermore, the study also reveals that the CPB specimens with high pre-damage levels (i.e., 75 %, 90 %, or 100 %) can even achieve up to 42 % higher mechanical strengths than the control specimens after 90 days of the self-healing period, indicating that the initiated cracks within the CPB matrix can ameliorate the hydration reactions, favouring the self-healing performance. The results presented in the paper would have significant impacts and practical implications with respect to CPB structure design, mechanical stability, and durability.

Keywords: Tailings; Cemented paste backfill; Self-healing; Mechanical properties; Hydraulic conductivity; Underground mine.

4.1 Introduction

Self-healing, a phenomenon originating from the organisms in nature (i.e., damaged skins of trees and animals can automatically heal without external intervention), has been introduced to automatically repair the cracks in conventional cementitious materials by many researchers (Aıtcin,

2003; Cailleux & Pollet, 2009; De Belie et al., 2018; Ezeoguine, 2022; Ferrara et al., 2017; Gardner et al., 2018; Graybeal, 2006; Li & Herbert, 2012; Li et al., 2009; Mehta, 1999; Qian et al., 2010; Roig-Flores et al., 2016; Van Tittelboom et al., 2010; Van Tittelboom et al., 2011; Wang et al., 2019; Wu et al., 2012; Zollo, 1997). The so-called self-healing can be defined as an ability of a material that is able to heal/repair damages automatically by itself without any external intervention (Ghosh, 2009) or refers to a process that can sense, diagnose, and heal/repair a damaged condition without intervention. Self-healing in the cementitious structure will automatically heal the crack, thus reducing the permeability, restoring the function of the structure, enhancing durability, and prolonging the longevity of service life.

The self-healing behaviour of cracks in fractured structures was initially noticed by the French Academy of Science in 1836 in water retaining structures, culverts, and pipes (Van Breugel, 2007), owing to the inherent self-healing potential in the traditional concrete structure. Traditional concretes are made with a water/cement ratio between 0.4 and 0.55, in which only 70% of cement particles will hydrate during the early curing period, and the remaining 30% of cement will stay unhydrated in the matrix. Once cracks form within the structure, the hydration traction will start again with unhydrated cement particles when exposed to penetrating moisture or water, thus filling the cracks with delayed hydration products to restore the original properties. In the last decades, flourishing research has extended the study of self-healing behaviour from traditional concretes to cementitious materials, such as high-performance fiber-reinforced cementitious composites (HPRFCCs) (Escoffres et al., 2018; Ferrara et al., 2016; Ferrara et al., 2017), ultra-high-performance fiber-reinforced cementitious composites (UHPFRCCs) (Kim et al., 2019; Kwon et al., 2014; Yoo et al., 2020), and engineered cementitious composites (ECCs) (Kan & Shi, 2012; Qian et al., 2010; Yang et al., 2009; Yıldırım et al., 2018) with or without healing agents.

Generally, self-healing approaches in cementitious materials can be roughly divided into two categories: autogenous healing and autonomous healing (Blaiszik et al., 2010; Li & Herbert, 2012; Van Breugel, 2007). Autogenous healing is the self-healing process in which cracks are healed by delayed healing products within the cementitious matrix, and materials are not intentionally added into the matrix or designed for self-healing (Cuenca & Ferrara, 2017), mainly attributed to two chemical mechanisms (Edvardsen, 1999; Ramm & Biscoping, 1998): i) hydration of unhydrated cement particles and ii) dissolution and subsequent carbonation of calcium hydroxide. The cement hydration product, calcium hydroxide $Ca(OH)_2$, precipitates on the crack surfaces, liberating and dissipating Ca^{2+} along the crack surfaces as they dissolve in water. The free Ca^{2+}subsequently reacts with carbonate ion CO_3^{2-} or bicarbonate ion HCO_3^- from dissolved carbon dioxide CO_2 to form the self-healing product calcite $CaCO_3$, growing on both surfaces of the cracks and finally filling the crack gaps (Wu et al., 2012). The chemical process can be described as follows (Edvardsen, 1999):

$$H_2O + CO_2 \Leftrightarrow H_2CO_3 \Leftrightarrow H^+ + HCO_3^- \Leftrightarrow 2H^+ + CO_3^{2-} \quad (4\text{-}1)$$

$$Ca^{2+} + CO_3^{2-} \Leftrightarrow CaCO_3 \quad (4\text{-}2)$$

$$Ca^{2+} + HCO_3^- \Leftrightarrow CaCO_3 + H^+ \quad (4\text{-}3)$$

Apart from the chemical mechanism, the physical mechanism (i.e., swelling of calcium silicate hydrates) and mechanical mechanism (i.e., loose particles broken from the fracture surface or impurities in ingress water) also produce autogenous healing (De Belie et al., 2018). On the other hand, the material used to heal cracks in autonomous healing does not originate from the matrix itself but from other external sources, including directly added or embedded in capsules healing agents from mineral agents (Ahn & Kishi, 2010; Roig-Flores et al., 2016; Sisomphon et al., 2012; Yu et al., 2017), polymer-based agents (Dong et al., 2016; Lee et al., 2016; Snoeck et al., 2014; Van Tittelboom et al., 2016), nanomaterials (Huseien et al., 2019; Qian et al., 2010; Qing et al., 2007; Quercia et al., 2012), shape memory alloy (Duerig et al., 2013; Jefferson et al., 2010; Kuang & Ou, 2008), to bacteria (Seifan et al., 2016; Van Tittelboom et al., 2010; Wang et al., 2014; Wang et al., 2014). The activation methods can be crack propagation, contact with air or water, other agents, and external changes (i.e., temperature and humidity). To date, the feasibility of autonomous healing in a backfill material using embedded bacterial solution has been demonstrated, and the incorporation of a mix of aerobic and anaerobic bacteria has been investigated to enhance self-healing efficacy in polypropylene-fiber reinforced backfill (Xiang et al., 2023a; Xiang et al., 2023b). Notwithstanding, the autonomous healing process is relatively complex and expensive to be applied on a full scale in engineering practice due to its uncontrollable conditions, such as the low survival rate of healing agent carriers during the mixing process, strict nutrient prerequisites for bacterial growth, and intensive cost.

Cemented paste backfill (CPB), as an innovative cementitious material to increase mine productivity, cost-effectively manage mine waste, and contribute to improved health and safety in mining operations from a sustainable perspective, has been extensively studied and used over the last decades (Kesimal et al., 2005; Roshani & Fall, 2020; Yilmaz et al., 2003). CPB, a cementitious engineered mixture consisting of tailings with a solid percentage of 70-85%, binders with typically 3-7%, and water, is mixed in a plant usually located at the surface of the mine site and transported to the underground to fill the extracted cavities or stopes by pumping or gravity, providing ground support and control, a working floor and waste disposal. CPBs must meet certain load requirements to ensure a safe underground working environment for all mining personnel, as mine backfill failures often result in fatalities or injuries. The main geotechnical performance criterion for CPBs is mechanical stability, which is most assessed by uniaxial compressive strength (UCS). Permeability (as defined by hydraulic conductivity) is one of the most important parameters that influence the environmental performance and durability of CPBs (Fall et al., 2009).

As the problem that frequently appears in the aforementioned conventional cementitious materials (i.e., concrete and mortar), cracks can also form in the CPB material or structure as well due to several processes or factors, such as excessive stresses generated by the pressure of the CPB overburden, stresses induced by the closure of rock walls adjacent to or surrounding the CPB structures, rock burst, and shrinkage. The presence of cracks in CPBs tends to weaken the integrity and mechanical strength of the structures as well as increase their permeability properties, thus

severely compromising their safety, serviceability, durability, and environmental performance. These weaknesses have been of deep concern to researchers and practitioners, especially with the current trend of deep mining, where the stresses induced by rock wall closure and the intensity and frequency of rock bursts are higher. In addition, CPB structures vary from a few tens to several hundred meters underground in at least one dimension, which makes manual maintenance and repair of cracks in CPB structures infeasible in practical manners.

It is well known that cementitious materials can have a self-healing capability, as discussed above. However, no studies have been conducted on the self-healing (autogenous healing) ability and behaviour of CPB and its impact on the recovery of mechanical and permeation properties of CPB. Moreover, the lower cement content (or higher water/cement ratio) in CPBs, and different particle size distributions between tailings used in CPB and aggregates utilized in concrete, signify that the results of self-healing studies on traditional concrete and cementitious materials are not transferable to CPB materials. It is therefore necessary to fill this knowledge and technology gap.

Given the research gap, the objectives of this research are to experimentally investigate the self-healing (autogenous healing) behaviour in CPB material, understand the self-healing mechanism, and evaluate the self-healing efficiency of CPB material through its recovery of mechanical and permeation properties.

4.2 Materials and Experimental Program

4.2.1 Materials Used

4.2.1.1 Tailings

Silica tailings (ST), consisting of 99.8% (by weight) quartz SiO_2, which is found to be the dominant mineral in hard rock mines in Canada, were used in this study. The selection of ST is to accurately control the chemical and mineralogical components of the tailings, maintaining a minimum level of uncertainties when studying the isolated impact of mixed components of CPB on its self-healing behaviour. Instead, natural tailings may contain uncontrollable chemical elements (i.e., sulfate ions) and minerals that can react with cement, impacting the outcomes of the study. The ST is analyzed to have a similar grain size distribution to the average of nine Canadian mine natural tailings (NT), as illustrated in Figure 4-1. It is observed that approximately 41-45% of particles in ST and NT are finer than 20 μm, which can be categorized as medium tailings (medium tailings have between 35% and 60% of particles with size less than 20 μm), satisfying the general rule that CPB must contain at least 15% by mass of particles less than 20 μm in diameter (Landriault, 1995). In addition, the physical properties and chemical compositions of ST are shown in Table 4-1 and Table 4-2.

4.2.1.2 Binder and mixing water

Portland cement Type I (PCI), the most frequently used binder in CPB technology, was used as the binder to prepare CPB specimens. The physical and chemical properties of PCI are given in Table 4-3. Additionally, tap water was used to mix with ST and PCI to prepare the CPB mixture.

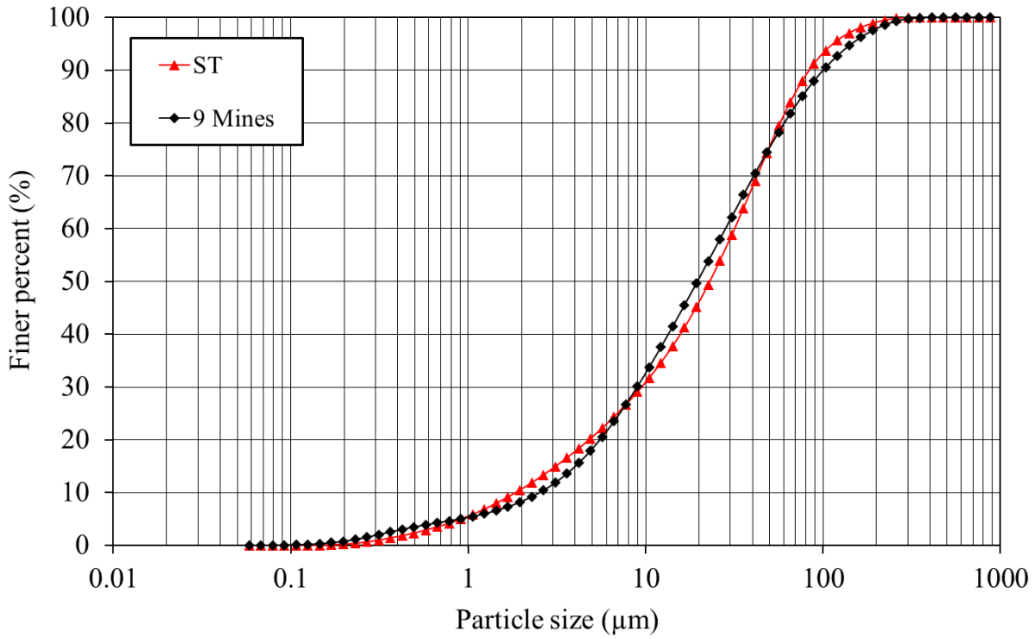

Figure 4-1. Particle size distribution of the used ST along with an average of nine Canadian mines NT.

Table 4-1. Physical properties of the tailings used and the average of nine natural tailings in Canada.

Element	G_s	D_{10}	D_{30}	D_{50}	D_{60}	C_u	C_c
		(μm)					
ST	2.7	1.9	9.0	22.5	31.5	16.6	1.3
Nine NT average	-	1.8	9.1	20.0	30.8	17.1	1.7

G_s: specific gravity; C_u: coefficient of uniformity; C_c: coefficient of curvature.

Table 4-2. Chemical compositions of the used tailings.

Tailings	SiO_2	FeO_3	Al_2O_3	TiO_2	CaO	MgO	Na_2O	K_2O	LOI	pH
	(%)									
ST	99.8	0.035	0.05	0.02	0.01	＜0.01	＜0.01	0.02	0.1	7

LOI: loss on ignition.

Table 4-3. Characteristics of Portland cement type I.

Binder type	MgO	CaO	SiO_2	Al_2O_3	Fe_2O_3	SO_3	R.D.	SSA
	(wt. %)							(m^2/g)
PCI	2.65	62.82	18.03	4.53	2.70	3.82	3.20	1.30

RD: relative density; SSA: specific surface area.

4.2.2 Specimen Preparation and Initial Curing

The required amounts of tailings, PCI, and water were accurately weighed and mixed in a mixer for 7 minutes until a homogenous paste was obtained. The adopted mix proportion of binder (PCI) in this study was 4.5% with a constant water-to-cement ratio (w/c) of 7.35. The consistency of the prepared CPB mixture was measured to be 18 cm by slump tests in accordance with ASTM C143 (ASTM, 2020), which is the most frequently used slump value in CPB preparation, ensuring the pumpability and transportability of the prepared CPB material. Then, the prepared CPB mixtures were poured into cylindrical curing moulds with a size of Φ50×100 mm. The specimens were sealed with caps to avoid water evaporation and cured in ambient conditions with initial curing (IC) periods of 3, 7, and 28 days (i.e., IC3, IC7, and IC28), respectively, for three batches before pre-damaging (see Table 4-4). A total of 240 CPB specimens were prepared to investigate the self-healing behaviour in CPB material.

4.2.3 Initial Crack Introduction

To study the self-healing behaviour of CPB material, various levels of mechanical pre-damage were introduced using the UCS test. The mechanical damage level in CPB or other cementitious materials quantifies the extent to which the material's structure has been compromised due to mechanical forces such as loading, stress, or deformation. It represents the degree of microcracking, fracturing, or structural deformation caused by applied stresses or external forces. The damage level typically ranges from zero (no damage) to one (or 100%), indicating complete failure or maximum structural degradation. The UCS test stands out as the predominant method in CPB practices owing to its simplicity, effectiveness in characterizing the material's response to compressive loading, and seamless integration into routine quality control programs at mining sites. After the initial curing periods, the corresponding compressive strengths were determined in accordance with standard ASTM C39 (ASTM, 2021), and the remaining specimens were loaded to specified pre-damage levels with 0, 30%, 50%, 75%, 90%, or 100% (i.e., control, PC-30%, PC-50%, PC-75%, PC-90% or PC-100%) in the pre-peak phase of their corresponding ultimate UCS values, introducing different levels of crack damage within the specimens. Note that the maximum pre-damage level in the Batch IC3 is 100% of the ultimate UCS, which means the load is increased until reaching the peak stress, intending to investigate the autogenous healing capability of early-age CPB material when a failure occurs. When the applied pre-load reached the target pre-determined load values, the applied load was maintained for one minute and then released, and the pre-damaged specimens were removed to prepare for the self-healing process. Tests were performed in displacement control, using a computer-controlled mechanical press (MTS 10/GL) with a normal loading of 50 kN and at a displacement ratio of 1 mm/min. The axial deformation was automatically measured by using an internal linear variable differential transformer (LVDT) connected to an electronic data acquisition system. The mechanical damage variable (D) can be used to describe the different pre-damage levels, since the damage evolution is caused by the propagation and coalescence of micro-cracks or micro-defects in a material. D is defined as follows (Fall et al., 2009):

$$D=1 - E/E_0 \quad (4\text{-}4)$$

where D is the damage variable, $0 \leq D \leq 1$; E is Young's modulus of damaged CPB; E_0 is the initial Young's modulus of CPB (determined in the elastic range of the stress-strain curve of CPB).

Table 4-4. Experimental program for each batch.

Batch nomenclature	Tailings	PCI content (%)	w/c ratio	Initial curing (day)	Pre-damage level (%)	Self-healing period (day)
IC3	ST	4.50	7.35	3	0, 75%, and 100% of UCS	1 7 28 90
IC7	ST	4.50	7.35	7	0, 30%, 50%, 75%, and 90% of UCS	7 28 90
IC28	ST	4.50	7.35	28	0, 50%, 75%, and 90% of UCS	28 90

4.2.4 Healing Condition

After initial pre-cracks were induced, the pre-damaged specimens were wrapped up with transparent plastic films and stored in ambient conditions (temperature of 20°C) for self-healing curing, together with undamaged control specimens. The self-healing periods, ranging from 1 to 90 days, were determined for the three studied batches based on the cement hydration progression characteristics within the CPB mixture (Benzaazoua et al., 2004; Kesimal et al., 2005). Batch IC3 includes self-healing periods of 1, 7, 28, and 90 days, which are intended to capture both early-stage (rapid hydration) and long-term self-healing mechanisms. Batch IC7 includes 7, 28, and 90 days, omitting the 1-day period to focus on self-healing from a slightly more developed hydration stage. Batch IC28, with self-healing periods of 28 and 90 days, prioritizes the self-healing mechanisms at a more mature stage, where variations due to early hydration are minimized. This selection ensures a comprehensive understanding of self-healing behaviour across different hydration phases of CPB. Note that the studied specimens were pre-damaged on Day 0, marking the start of the self-healing, with subsequent self-healing assessments at Days 1, 7, 28, or 90, respectively. The curing condition without any external interference was intended to simulate the underground condition after CPB being placed and to investigate the inherent self-healing capability of CPB material without any additives. Eliminating external interference is crucial to achieving a fundamental understanding of the self-healing behaviour of CPB and reducing uncertainties in the analysis of the results. Allowing external factors, such as temperature variations, water infiltration, and other conditions typical of underground mines, to influence the self-healing process would obscure insights into the intrinsic, time-dependent self-healing mechanisms of CPB.

Therefore, future studies should address the impact of such external factors on the time-dependent self-healing behaviour of CPB, as this is beyond the scope of the present study.

4.2.5 Testing Methods for Self-healing

4.2.5.1 Crack characteristics

The observation of surface crack closure is the most straightforward method to examine self-healing performance after exposure to healing conditions for pre-damaged specimens. Due to this benefit, a digital microscope of 200X magnification with computer software was utilized as an additional technique to measure the crack width alterations, assessing surface crack closure and supporting other test results. The crack widths were measured from at least 15 positions, including minimum and maximum crack widths on each measuring crack after the initial crack introduction and then at 1-, 7-, 28-, and 90-day self-healing curing period, respectively.

4.2.5.2 Hydraulic property investigation

To monitor the impact of initial pre-cracks induced by mechanical loads and subsequent self-healing behaviour on the hydraulic conductivity of CPB materials, saturated hydraulic conductivity, k, tests were conducted on pre-damaged and healed CPB specimens using a triaxial cell with flexible wall technique in accordance with ASTM 5084 (ASTM, 2016). A constant head method means a known constant hydraulic gradient (10 psi or 69 kPa) between the inflow and outflow was applied for measurement. Full saturation was achieved by applying backpressure after bridging the inflow and outflow burettes until the flow through the specimen became constant. The test for each specimen was repeated twice to ensure the reproducibility of results. The hydraulic conductivity, k, can be calculated as follows:

$$k = \frac{\Delta Q \cdot L}{A \cdot \Delta h \cdot \Delta t} \tag{4-5}$$

where k is hydraulic conductivity, cm/s; ΔQ is the quantity of flow during the certain time interval Δt, taken as the average of inflow and outflow, cm^3; L is the length of the specimen, cm; A is the cross-sectional area of the specimen, cm^2; Δt is the time interval, s; and Δh is the average head loss of across the specimen, cm of water.

The hydraulic conductivity recovery ratio (HCRR) can be determined by:

$$\text{HCRR } (\%) = \frac{k_0 - k_t}{k_0} \times 100\% \tag{4-6}$$

where k_0 is the initial hydraulic conductivity, cm/s, measured after pre-damaging; k_t is the hydraulic conductivity, cm/s, measured after specified self-healing period.

4.2.5.3 Mechanical property investigation

The compressive strength of cementitious materials reflects the integrity of the matrix to some extent, such as the internal porosity and compactness. Thus, a compression test can be used to evaluate the mechanical recovery of cementitious materials via a self-healing process. To determine the strength recovery in CPB materials, the UCS tests were conducted on at least triplicate CPB

specimens in accordance with ASTM C39 (ASTM, 2021) after 1-, 7-, 28-, and 90-day self-healing periods on healed pre-damaged specimens and undamaged control specimens. A computer data acquisition system with a constant deformation rate of 1 mm/min was utilized.

The percentage of UCS dwindled can be calculated by:

$$S_{d\%} = \frac{S_0 - S_{pc}}{S_0} \tag{4-7}$$

where $S_{d\%}$ is the percentage of UCS dwindling, S_0 is the initial compressive strength of undamaged control specimens, and S_{pc} is the compressive strength of pre-damaged specimens.

The relative changes in compressive strength (CCS) of the healed specimens compared to control specimens can be calculated by:

$$CCS(\%) = \frac{S_{healed} - S_{control}}{S_{control}} \tag{4-8}$$

where S_{healed} is the compressive strength of the pre-damaged specimens after a self-healing period, and $S_{control}$ is the compressive strength of undamaged specimens with self-healing condition and period.

4.2.5.4 Microstructural and chemical analysis

The physical properties of CPB material, such as void ratio, porosity, and water content (Ghirian & Fall, 2013), have significant impacts on its mechanical performance. During the self-healing process, the changes in void ratio and porosity of the studied pre-damaged specimens were monitored to support other test results. To investigate the self-healing mechanism within the CPB matrix, the techniques, including X-ray diffraction (XRD), scanning electron microscopy-energy dispersive spectroscopy (SEM-EDS), and thermogravimetric analysis (TGA), were conducted to perform the microstructural and chemical analysis of the studied CPB specimens and self-healing products. Before testing, the CPB specimens were dried in an oven at 45℃ until constant mass to remove the free water within the matrix. After that, small pieces of fragments were collected from the crack's surfaces for SEM-EDS analysis to observe the microstructure and distinguish the main chemical elements present in the self-healing products. Then, the self-healing products were scratched and collected from the healed cracks for the XRD analysis to illustrate the chemical components of self-healing products on the crack surface. Additionally, the powders of control specimens and pre-damaged specimens after self-healing periods were prepared for the TGA analysis to monitor the difference in cement hydration extent. The XRD analysis was performed by Bruker D8 Endeavor equipped with a 1 kW sealed tube Cu Kalpha source (40 kV and 25 mA) and a Lynxeye XE-T 1-D silicon strip detector. The SEM-EDS analysis was carried out using an extremely versatile low-voltage and environmental mode JEOL 6610LV SEM with an attached Oxford INCA large area SDD detector. The TGA analysis was conducted using a Setaram Setsys 24 thermogravimetric analyzer with a heating ramp of 10°C/min starting from room temperature to 1000°C in a Nitrogen atmosphere.

4.3 Results and Discussion

4.3.1 Crack Observation and Characteristics

During the pre-damage process, different levels of pre-damage and generated microcracks or cracks were observed. It was found that the pre-damage levels of PC-30% and PC-50% did not lead to the propagation of cracks in the CPB specimens. As illustrated in Figure 4-2 and also observed by (Fall et al., 2007), the level of mechanical load up to 50% of UCS (i.e., PC-30% and PC-50%) falls in the elastic behaviour zone. However, as the level of mechanical load increases to levels close to the peak region (i.e., PC-75% and PC-90%), the curve begins to exhibit the first non-linear behaviour and micro-cracks can be observed in the CPB specimens (pre-cracked CPB). As the slope of the curve and stress-bearing capacity decrease, the increasing load contributes to the crack propagation in the pre-peak region until reaching peak load (i.e., PC-100%). Therefore, the initiated cracks on the pre-damaged specimens are increasingly visible as the pre-damage level enhances. These observations regarding the absence of cracks in CPBs below a mechanical pre-load of 50% of UCS and their presence and progradation at pre-damage levels of PC-75%, PC-90%, and beyond are consistent with the results presented in Figure 4-3. This figure shows the evolution of the mechanical damage variable (D) in relation to the stress/UCS ratio applied (pre-damage level or mechanical pre-load level) to a CPB sample made of 4.5% PCI and ST. It is clear from this figure that when the stress/UCS ratio is 50% or less (i.e., the load is in the elastic stage of the CPB stress-strain curve), the damage variable D is close to zero ($D < 0.055$), suggesting the absence or negligible presence of micro-cracks or micro-defects in the CPB material. However, for a stress/UCS ratio > 60% (in the plastic stage), a rapid increase of the D variable is observed, indicating rapid generation and propagation of the micro-cracks in the CPB.

The observations of microcracks or cracks in pre-damaged CPB specimens before and after self-healing are shown in Figure 4-4 and Figure 4-5. It is observed that the cracks were completely healed or partially healed as white crystal-like substances formed and filled in the surface cracks after certain self-healing periods. At the current stage of the study, the maximum crack widths that can be completely healed with different initial curing and self-healing periods (listed in Table 4-5) are measured as a direct assessment and representation of autogenous healing capability in the studied CPB material. It is evident from Table 4-5 that the maximum width of completely healed surface cracks increases as the self-healing period extends, regardless of the three batches with different initial curing periods. Notably, the autogenous healing capability of Batch IC3 (younger CPBs) is more pronounced than the other two batches (Table 4-5). For instance, after the same self-healing period of 90 days, crack widths up to 92.9 μm in IC3 can be completely healed, while the batches of IC7 and IC28 exhibit smaller healed crack widths, 67.9 μm and 48.6 μm, respectively. This means that the self-healing capacity of the CPB increases as cracks are generated in the CPB at younger ages. The possible reason for the difference in healing capability is the content of unhydrated cement in the CPB matrix, which dominates the recovery efficiency of self-healing by autogenous healing in pre-damaged specimens. Younger CPBs contain more unhydrated cement particles. To substantiate this assumption or explanation, TGA analysis was performed on the

control specimens after the initial curing periods (i.e., IC3, IC7, and IC28) to determine the extent of cement hydration and to detect the hydration products generated within the CPB matrix at Day 0 before the pre-damage process. Given that, TGA results (see Figure 4-8a) demonstrate that the IC28 specimens display the highest rates of weight change that are associated with rapid weight loss and major phase transformations, namely the dehydration of hydrates, such as C-S-H, carboaluminates, ettringite, and gypsum at 110°C to 200°C (Fall et al., 2010; Noumowe, 1995; Zhou & Glasser, 2001), the decomposition of $Ca(OH)_2$ at 400°C to 500°C (Fall et al., 2010), and the decomposition of $CaCO_3$ at 650°C to 750°C (Anderberg, 1997), indicating the highest degree of hydration, which means the IC28 specimens contain the lowest content of unhydrated cement within the matrix, thus contributing to the poorer surface crack closure. Moreover, the self-healing performance of crack closure becomes diminished with the increasing crack widths, as shown in Figure 4-5. The partially healed cracks illustrate that the healing products produce and grow from both sides of the crack towards the middle, intending to fill the crack gap. Furthermore, it indicates the existence of a capability limit in the autogenous healing for the CPB material. Therefore, crack width is a significant factor affecting the self-healing efficiency of CPB materials, which is consistent with other cementitious materials (Huang et al., 2016; Jiang et al., 2015; Maes et al., 2014; Van Tittelboom et al., 2011; Wu et al., 2012). The narrower, shorter, or shallower cracks have greater potential to be completely healed due to the smaller volume that needs to be filled.

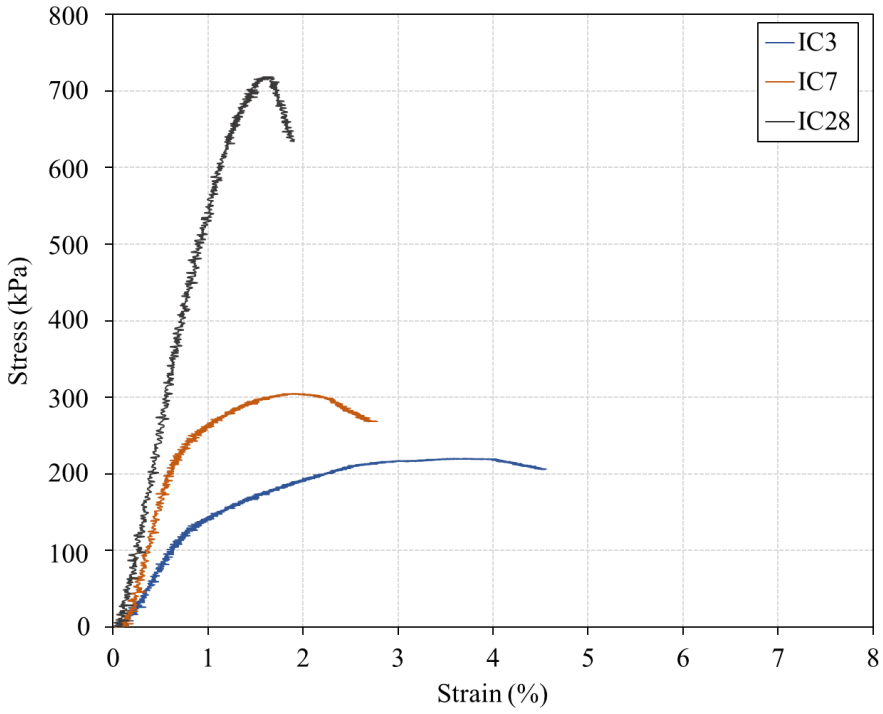

Figure 4-2. Stress-strain characteristics of CPB control specimens with different initial curing periods (initial curing times of IC3, IC7, and IC28 are 3, 7, and 28 days, respectively).

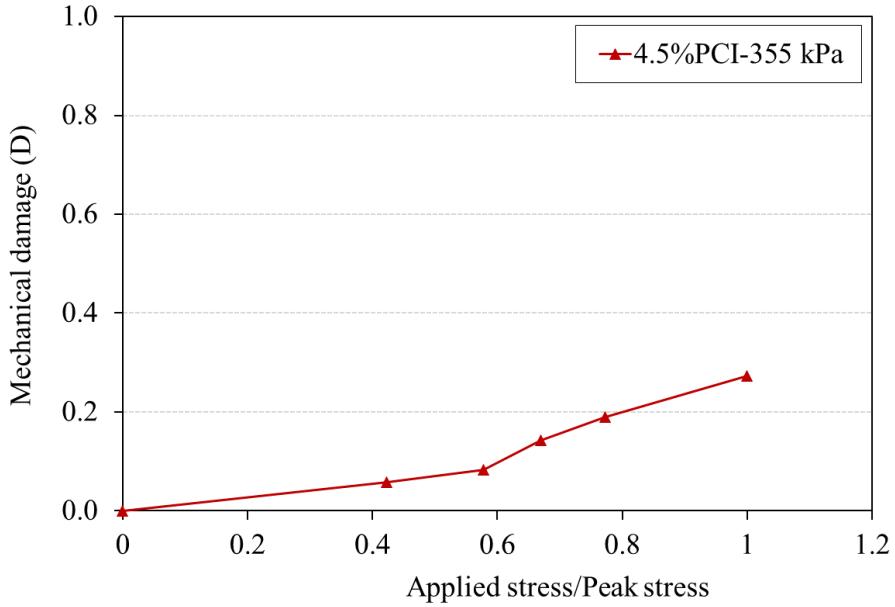

Figure 4-3. Evolution of mechanical damage variable (D) of CPB with a UCS of 355 kPa under different mechanical pre-loads (ratios of applied stress/UCS) or pre-damage levels (data from Fall et al., 2009).

Table 4-5. Maximum crack width healed after certain self-healing periods.

Batch nomenclature	Self-healing period (Day)	Maximum completely healed crack width (μm)
IC3	1	21.3
	7	53.9
	28	75.6
	90	92.9
IC7	7	46.1
	28	56.1
	90	67.9
IC28	28	10.8
	90	48.6

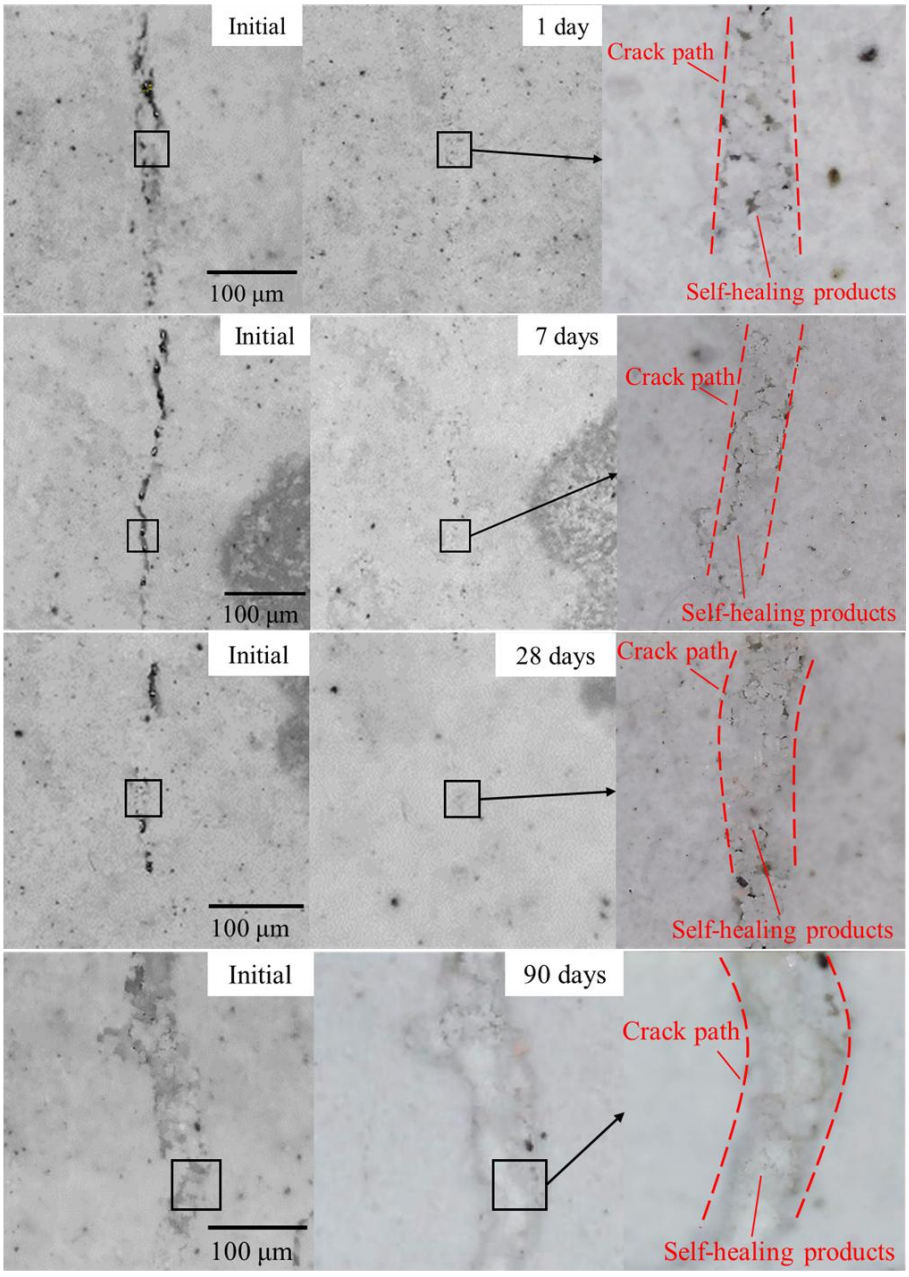
Initial
1 day
Crack path
100 μm
Self-healing products
Initial
7 days
Crack path
100 μm
Self-healing products
Initial
28 days
Crack path
100 μm
Self-healing products
Initial
90 days
Crack path
100 μm
Self-healing products

(A)

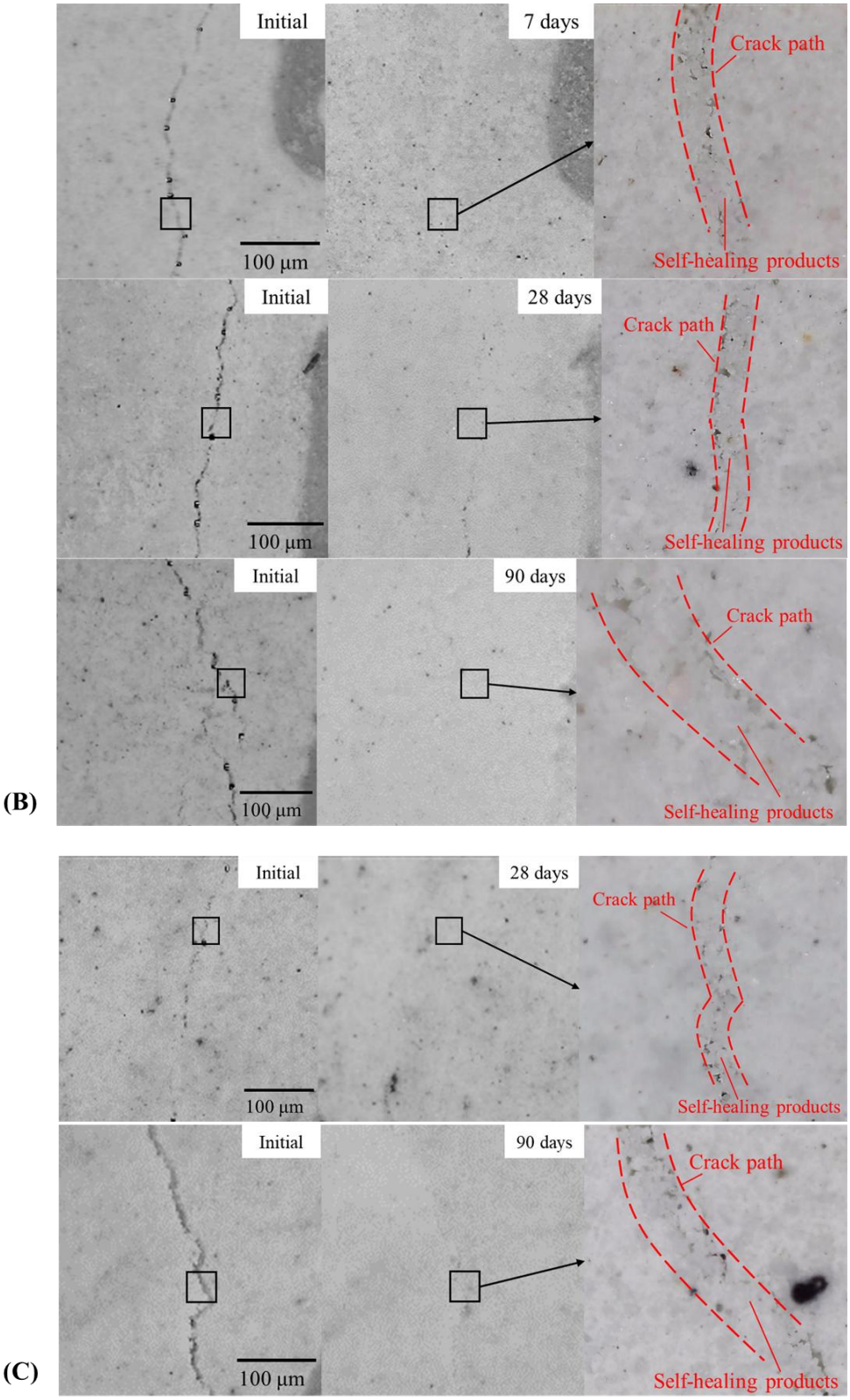

Figure 4-4. Typical observation of complete healing of Batch (A) IC3, (B) IC7, and (C) IC28 after different self-healing periods (1, 7, 28, and 90 days).

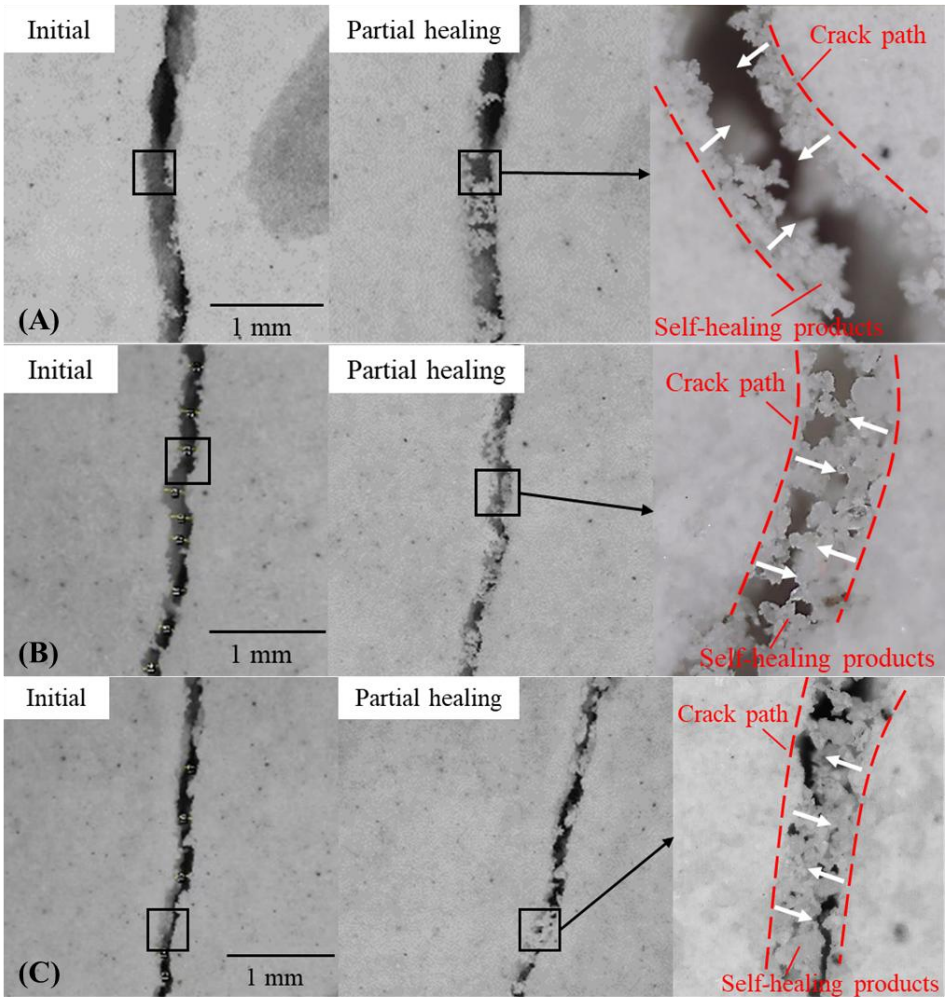

Figure 4-5. Typical observation of partial healing of large cracks in Batch (A) IC3, (B) IC7, and (C) IC28 after a self-healing period of 90 days.

4.3.2 Nature of the Self-healing Products

Apart from the quantitative assessment of damage degree or self-healing efficiency, characterizing the chemical compositions of the crystal-like self-healing products and the morphology of microstructure within the CPB matrix is also of great importance to gain insight into the fundamental mechanisms responsible for the observed self-healing behaviour. Therefore, microstructure analysis techniques, including XRD and SEM-EDS, have been employed to characterize the chemical or mineral natures of the self-healing products.

XRD analysis was conducted on a small amount of crystal-like self-healing products in the powder phase, which were scratched from the healed crack surfaces using a needle. The XRD patterns of self-healing products and regular CPB materials of the control specimen are shown in Figure 4-6. During the scratching procedure, it is impractical to collect only self-healing products from the cracks but contain other substances around the cracks. Due to the silica tailings used in this study, quartz has the most pronounced peaks, undermining the characteristic peaks of other substances.

However, it can be observed at the two-theta degrees range of 25°-65° that the majority difference of the peaks is related to calcite (CC) among the peaks of $Ca(OH)_2$ (CH), C-S-H, C_3S, and C_2S, which indicate that the calcite is more abundant and has higher intensities in self-healing products compared to the regular (control) CPB material when excluding the peaks of quartz, demonstrating that the calcite is the primary self-healing product of the surface cracks of the CPB specimens.

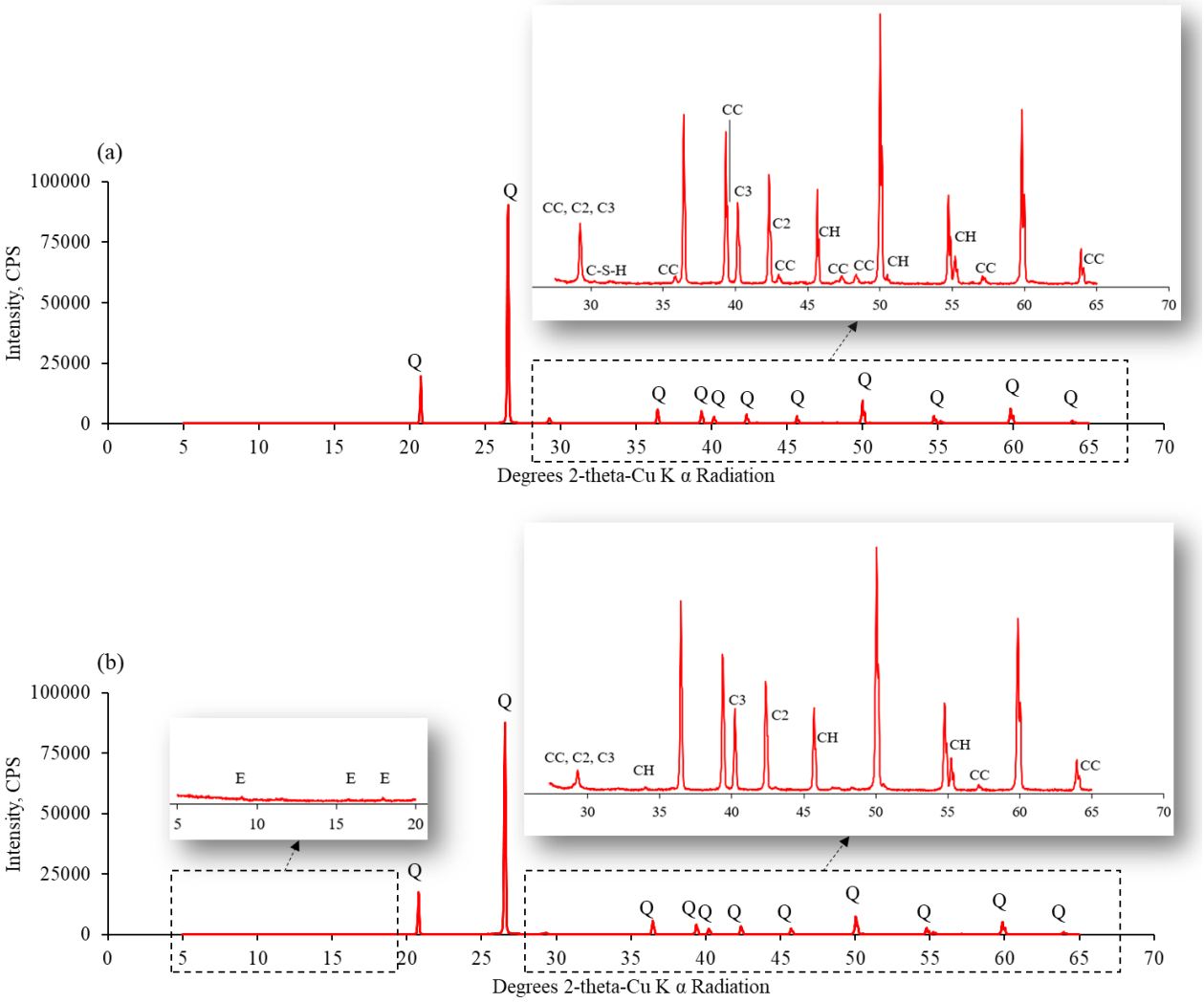

Figure 4-6. XRD result of (a) surface self-healing products and (b) control CPB specimen.

The SEM-EDS analysis was performed on the self-healing products interior of cracks with an approximate depth of 2 mm along the crack gap, intending to capture the microstructure images and identify the chemical natures. Figure 4-7 exhibits the representative SEM-EDS micrographs of different analyzed locations. In all EDS diagrams of different locations, Si shows the highest peaks due to the silica tailings used in the study and its effect cannot be eliminated during the analysis. The detected Cl peak in the self-healing products originated from the used epoxy (shown as dark color in the figures), which was used to integrate the cracks when peeling off and to prevent the powders from contaminating the SEM chamber. Moreover, it is observed that the traces of Ca,

Al, C, and O peaks were clearly detected, suggesting that the combination of C-S-H, $Ca(OH)_2$, and $CaCO_3$ is expected to be the primary self-healing products inside the cracks of CPBs. Nevertheless, it is difficult to rule out the detected self-healing products due to i) the limitation of EDS that adjacent phases may bleed into one another affecting the results (Kan et al., 2010), and ii) the application of epoxy may disarrange the substances inside the cracks during the sample preparation. Therefore, a more precise method to intactly detach the crack should be utilized in future studies.

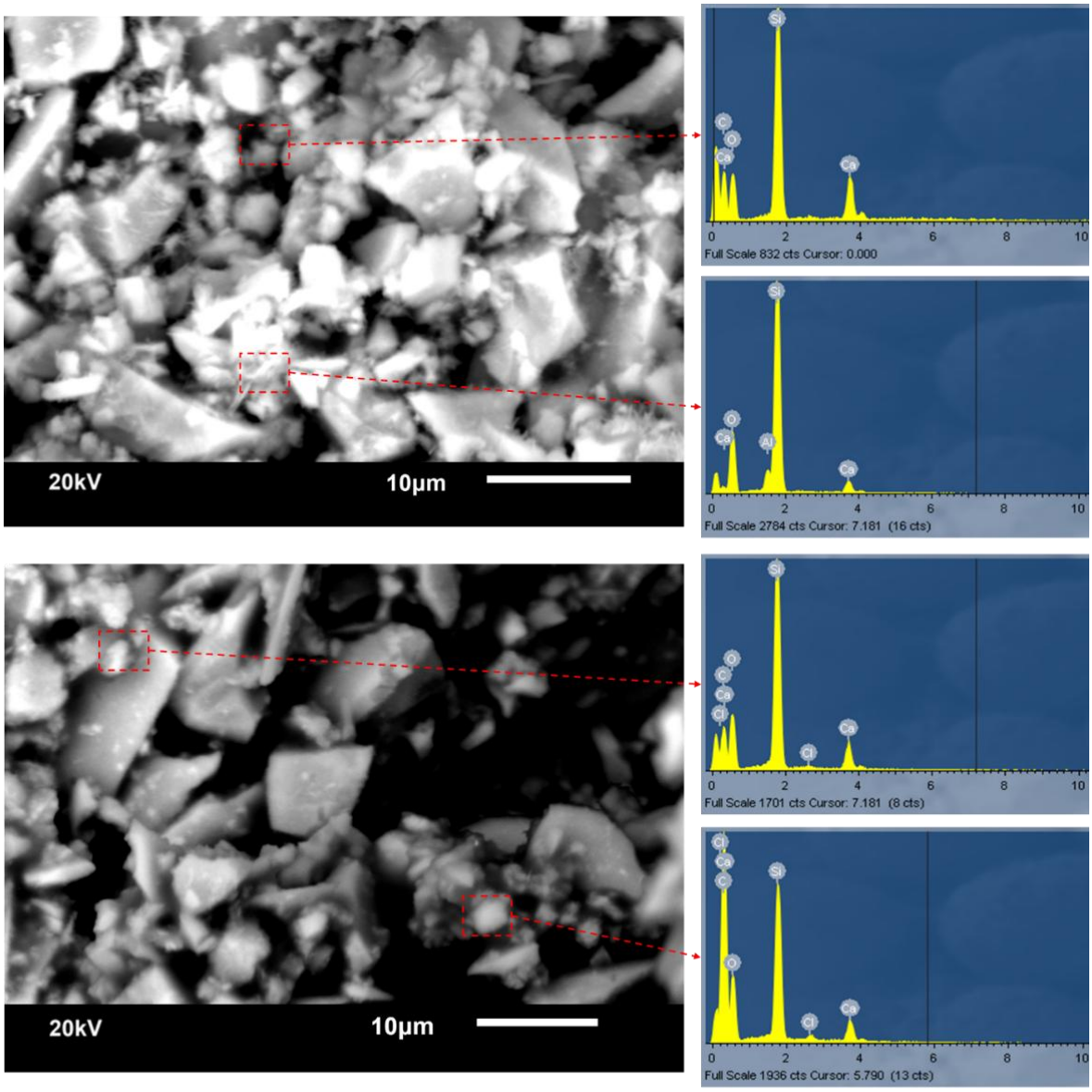

(a) (b)

Figure 4-7. (a) SEM images of the healing products interior of the crack and (b) EDS patterns of the detected self-healed products.

Furthermore, TGA analysis conducted on the powders collected from the interior of both control and pre-cracked specimens revealed a higher extent of cement hydration and carbonation of

$Ca(OH)_2$ in the pre-cracked specimens compared to the controls after the same self-healing periods (Figure 4-8). As demonstrated in Figure 4-8, this finding is evident from the apparent higher weight loss observed in pre-cracked specimens at temperatures of 600-800°C, indicating the decomposition of $CaCO_3$, and at temperatures of 110°C to 200°C, which corresponds to the dehydration of hydrates (i.e., C-S-H). Notably, the TGA results are consistent with the findings obtained from XRD and SEM-EDS analysis, highlighting the strong evidence supporting the primary self-healing products system of CPBs as a combination of C-S-H, $Ca(OH)_2$, and $CaCO_3$. The agreement and consistency among all three microstructure analysis techniques further support that the combination of C-S-H, $Ca(OH)_2$, and $CaCO_3$ is most likely to be the primary self-healing products system of CPBs.

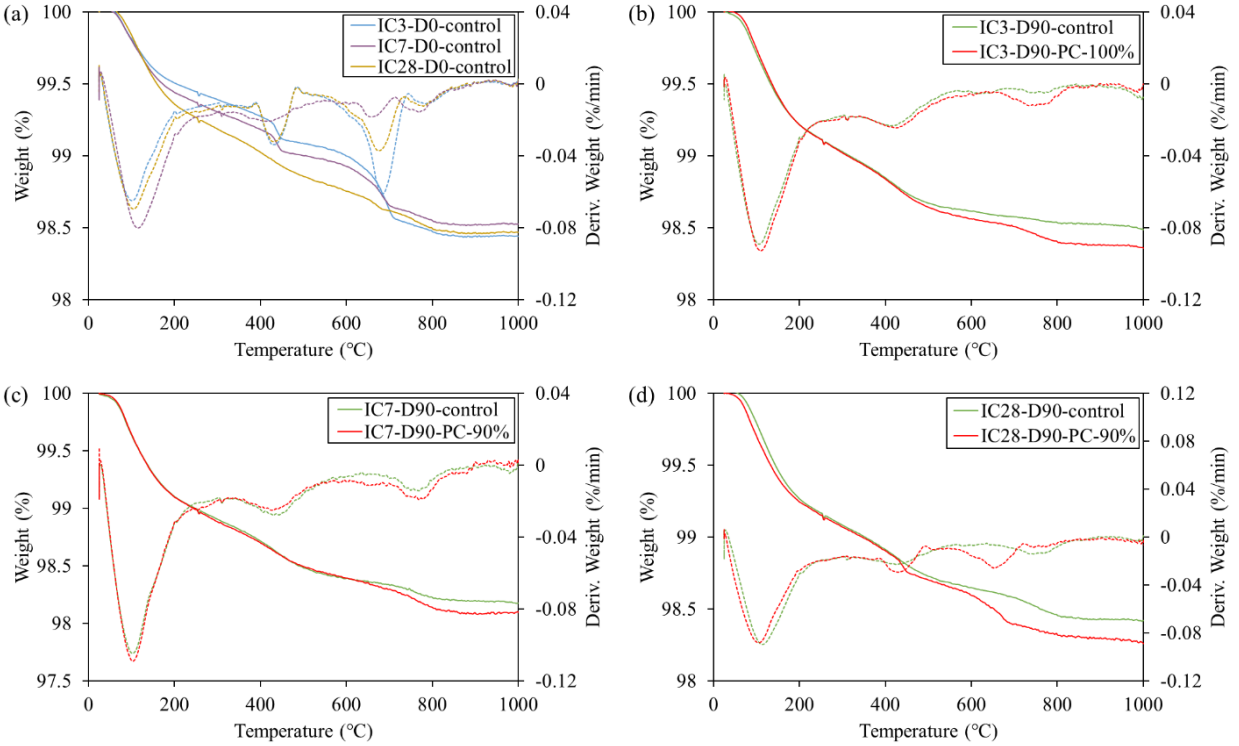

Figure 4-8. TG/DTG analysis of (a) control specimens after the initial curing period and pre-damage impact on cement hydration of Batch (b) IC3, (c) IC7, and (d) IC28 (dashed lines in the graphs represent derived weight (Deriv. Weight)).

4.3.3 Recovery of Compressive Strength

Figure 4-9 illustrates the compressive strength recovery and development of the healed pre-damaged CPB specimens for the Batch (A) IC3, (B) IC7, and (C) IC28 in comparison to the undamaged control specimens over the studied self-healing periods. All control specimens were subjected to the same self-healing conditions as the pre-damaged specimens. Each UCS data point was tested and averaged with at least three specimens.

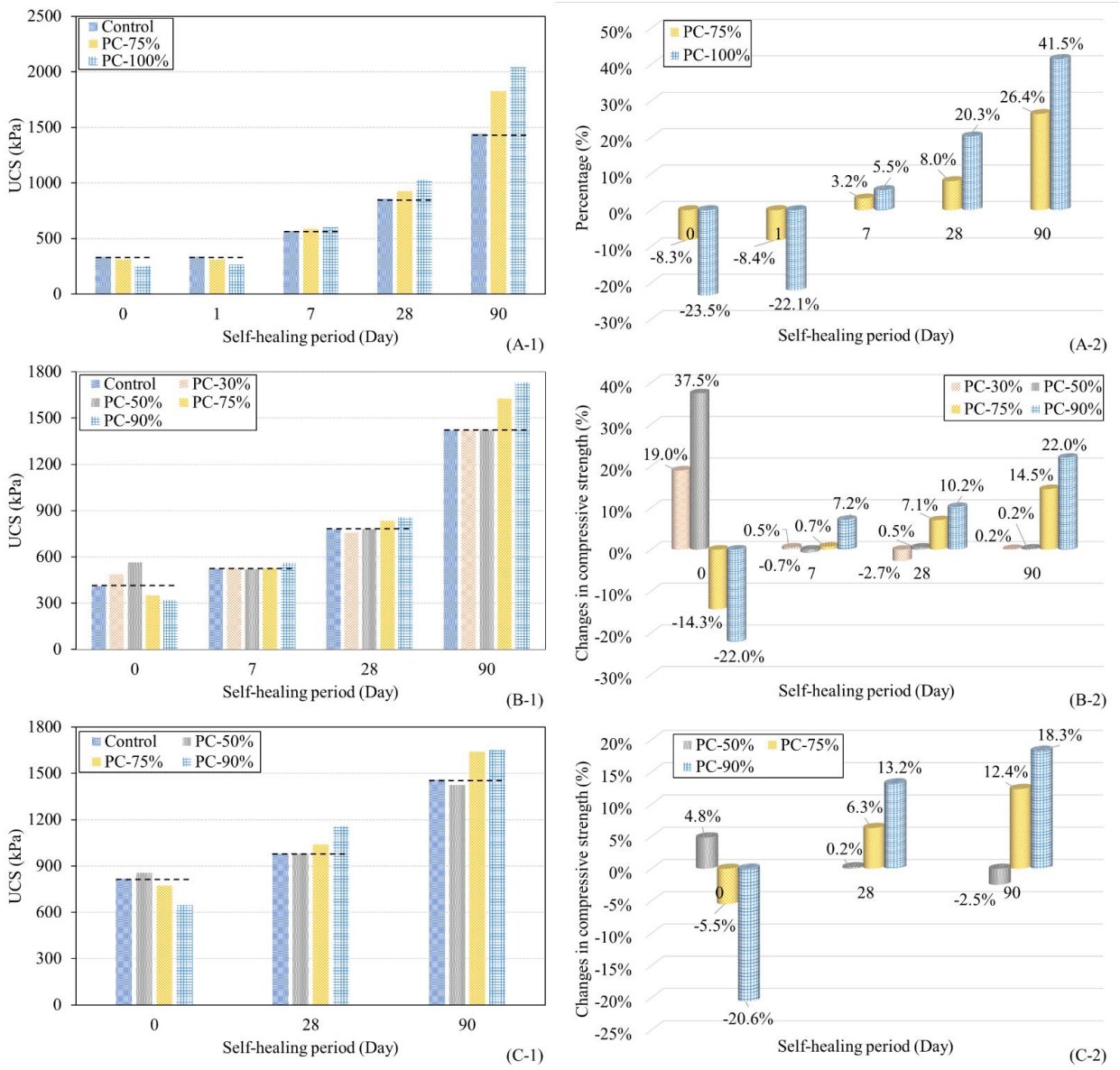

Figure 4-9. Compressive strength recovery of Batch (A) IC3, (B) IC7, and (C) IC28 with different self-healing periods.

The reduction in compressive strength of the pre-damaged specimens prior to self-healing on Day 0 was quantified using the Sd% index, as defined in Eq. 4-7. Similarly, the recovery of compressive strength in the pre-damaged specimens on Day 1, 7, 28, or 90, was assessed using the index of CCS, calculated according to Eq. 4-8. Specifically, it can be observed in Figure 4-9 (B and C) that the specimens pre-damaged at the levels of PC-30% and PC-50% exhibit higher UCS values than the control ones. Moreover, the younger the CPB, the greater the difference in strength. For example, the strength of the CPB specimens from IC7 is up to 37.5% higher than that of the control specimens (Figure 4-9B), while the strength of the IC28-CPB specimens is only 4.9% higher than that of the control. This higher strength of the CPB subjected to pre-damaged levels of 30% and

50% is ascribed to the contracting volumetric behaviour of the CPB material under uniaxial compressive loading (Fall et al., 2009). These CPB specimens were compacted under the pre-damage levels of PC-30% and PC-50%, below which no cracks were observed (D close to zero, see Figure 4-3), and the CPB material became denser and less porous. Higher density and finer pore structure are obviously associated with higher strength of CPBs (Fall et al., 2009; Ghirian & Fall, 2015). This contracting behaviour is stronger in the younger CPB material (Fall et al., 2009). For shorter curing times, CPB becomes softer, i.e., more compressible, due to the low extent of hydration of the cement. In contrast, Figure 4-9 shows that at Day 0 of healing, CPB samples subjected to higher levels of pre-damage (PC-75%, PC-90%, and PC-100%) have lower strength than control samples. For example, the pre-damage level of PC-75% induced an 8.3% and 14.3% reduction in the strength of IC3 and IC7 specimens (Figure 4-9 A-2 and B-2), respectively. Moreover, a 22.0% and 20.6% decline in compressive strength was obtained for the IC7 and IC28 specimens pre-damaged to PC-90% (Figure 4-9 B-2 and C-2), respectively. The pre-damage level of PC-100%, intended to investigate the self-healing ability of the CPB material after failure at an early age, resulted in a 23.5% decrease in the strength of the IC3 samples (Figure 4-9 A-2). This lower strength of pre-damaged CPB specimens at a level of PC-75% or higher and the decrease in strength as the level of pre-damage increases from PC-75% to PC-100% is due to the generation and proliferation of cracks in the CPB specimens. This crack generation and propagation is more intense as the level of pre-damage increases. These statements are consistent with the results of the evolution of the mechanical damage variable (D) of the CPB subjected to different levels of pre-damage, presented in Figure 4-3. This figure shows that the mechanical damage variable, D, which captures crack generation and production, increases rapidly as the pre-damage load (applied stress/UCS) reaches 60% and becomes higher.

Furthermore, Figure 4-9 shows that after 7 days of self-healing and beyond, CPBs subjected to a pre-damage level of PC-30% and PC-50% have nearly similar strengths to those of the controls. In other words, the aforementioned compaction effect induced by the mechanical pre-loads PC-30% and PC-50% dissipates during the self-healing period. This phenomenon can be attributed to the continuous hydration and curing of CPB, which leads to the formation of a more rigid and cohesive microstructure, reducing the influence of initial compaction on strength retention. Additionally, autogenous and drying shrinkage could lead to the formation of microcracks, counteracting the initial densification and the strength gains from initial compaction, thus indicating that the intrinsic material properties dictate long-term strength development (Ghirian & Fall, 2015; Hou et al., 2018; Yan et al., 2022). In addition, from Figure 4-9, it is noticed that 7 days after cracks were initiated (i.e., shown as Day 7 in figures), the pre-cracked specimens (CPBs pre-damaged to PC-75%, PC-90%, and PC-100%) recovered to similar compressive strength values to the control specimens even though the presence of cracks initially (at Day 0) had a negative effect on the strengths. As the self-healing continues, these pre-cracked specimens gradually achieve higher compressive strengths than the control ones. On Day 90 of self-healing, specimens IC3, IC7, and IC28 with the pre-damage level of PC-75% restored strengths 26.5%, 14.5%, and 12.4% higher than the control specimens, respectively. Furthermore, the increase is more pronounced for the specimens with a

higher pre-damage level. For example, after 90 days of self-healing, the strength of specimens IC3 with a pre-damage level of 100% is 41.5% higher than that of the control, while the strength of specimens IC7 and IC28 with a pre-damage level of 90% is 22.0% and 18.3% higher than the controls, respectively. This strength recovery performance is due to the autogenous healing in the CPB material.

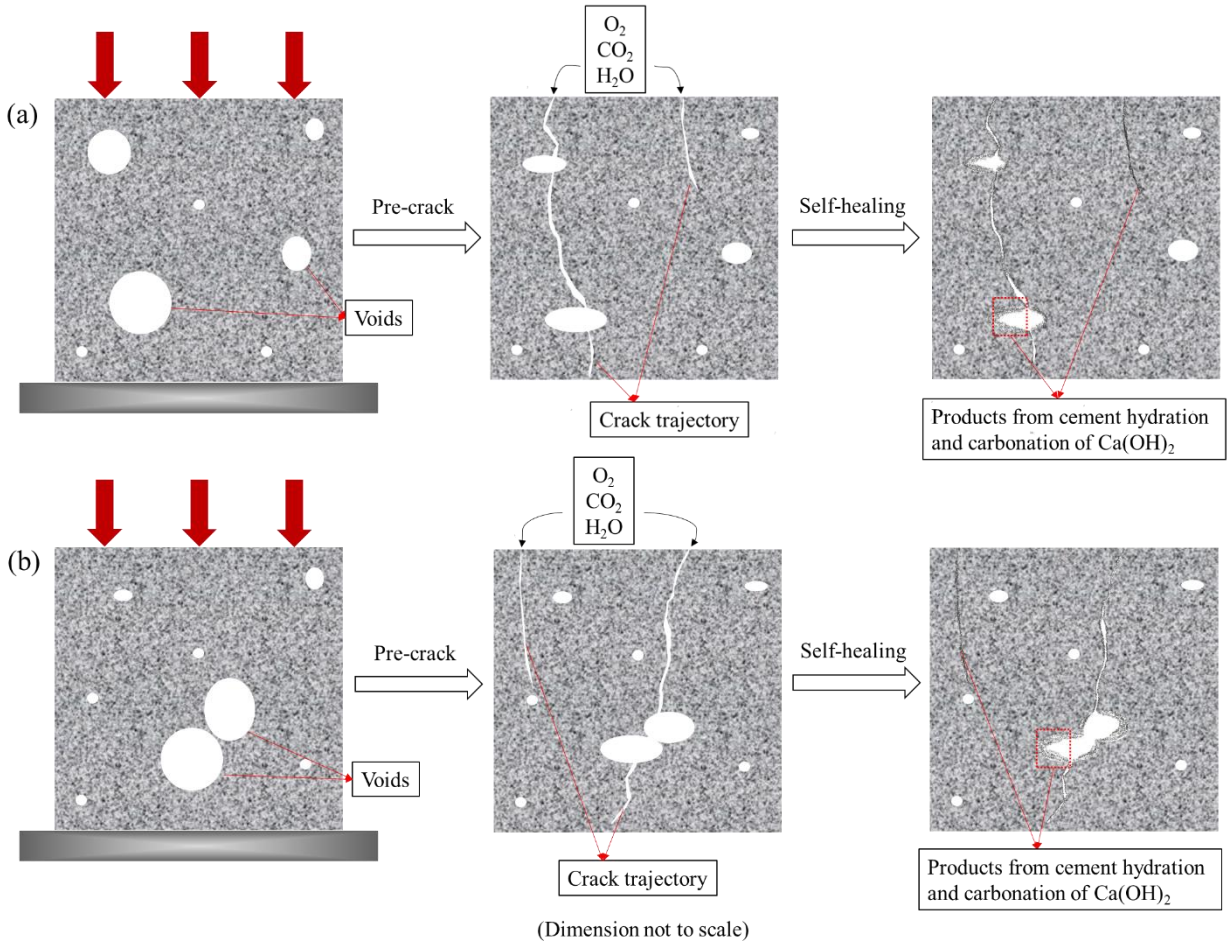

Figure 4-10. Schematic representation of the self-healing mechanism within the CPB matrix with (a) detached pores and (b) interconnected pores.

Autogenous healing is the self-healing process occurring in cementitious materials in which cracks are healed by healing products produced by delayed hydration of unhydrated cement (C-S-H) and carbonation of $CaOH_2$ within the cementitious matrix without intentionally added healing agents (Cuenca & Ferrara, 2017). As demonstrated in Figure 4-8, the continuous cement hydration dominates the self-healing behaviour in the studied early-age CPB specimens, governing the mechanical strength recovery and development. Figure 4-10 illustrates schematically the self-healing mechanism that occurred within the CPB matrix. When the cracks are randomly initiated, the voids inside the CPB matrix will be compacted and interconnected by the cracks, resulting in volume reduction. During the self-healing process, the cracks provide the pathways allowing the

O_2, CO_2, and H_2O to penetrate the CPB matrix, which are the essential elements to accelerate the cement hydration and $Ca(OH)_2$ carbonation (Ghirian & Fall, 2015; Huang et al., 2016; Song et al., 2006). As the self-healing period increases, the continuous cement hydration favors the refinement of the pore structure and decreases the porosity of the CPB materials by allowing the aforementioned autogenous healing products to fill the voids within the CPB matrix (Fall et al., 2009). The refinement of the microstructure with an increasing self-healing period is graphically represented in Figure 4-11 to demonstrate its contribution to the mechanical strength regained with the increasing self-healing period. As the self-healing period elongates, it can be seen that the porosity and void ratio of pre-damaged specimens decrease. As a result of the cement hydration process and the increased production of hydration products, the pore structure becomes more refined over time (Fall & Samb, 2008). Additionally, since the delayed cement hydration products after the pre-damage process have a similar strength to that of the primary hydration products, autogenous healing is capable of restoring the mechanical strength of the CPBs.

One of the interesting findings in the investigation of mechanical strength recovery is that the specimens with pre-damage levels of PC-75%, PC-90%, or PC-100% regained higher compressive strengths than the control specimens after 28 days and 90 days of self-healing periods, indicating that the initiated cracks within the CPB matrix could improve or accelerate the hydration reactions and strength development. In light of the TGA results shown in Figure 4-8 b-d, they display a higher extent of hydration and carbonation of $Ca(OH)_2$ in the pre-cracked CPB specimens than the control ones without cracks after the same 90 days self-healing period. It is observed that the main difference is the higher weight loss of $CaCO_3$ in the pre-cracked specimens at the temperature range of 600-800 °C, denoting the higher content of $CaCO_3$ formed inside the CPB matrix. As the self-healing mechanism discussed previously, the induced cracks provide the pathways allowing more CO_2 to penetrate inside the CPB structure, which contributes to the carbonation reaction from $Ca(OH)_2$ to $CaCO_3$. Even though the amount of generated $CaCO_3$ from the carbonation of $Ca(OH)_2$ is small, it further contributes to the self-healing behaviour and strength recovery as well. A similar performance was also observed for another type of cemented material by Carret et al. (2021). They reported that the dynamic Young's modulus and the compressive and indirect tensile strengths of cement-treated base material samples with pre-crack are higher than those of the samples without pre-crack at an early age.

4.3.4 Analysis of Hydraulic Conductivity Changes

To evaluate the self-healing behaviour of CPBs impacted by the mechanical damage through the permeability performance, the evolution of saturated hydraulic conductivity (k_{sat}) of the different pre-damaged CPB specimens with different initial curing times and self-healing periods is shown in Figure 4-12.

As illustrated in the figure, at Day 0, the low pre-damage levels of PC-30% and PC-50% do not significantly increase the hydraulic conductivity compared to the control specimens due to the volumetric contracting behaviour of the CPB material under uniaxial compressive loading (Fall et al., 2009) and the absence or insignificant generation of cracks in the CPB at these levels of pre-

damage (see Figure 4-3). As the pre-damage level increases to PC-75%, PC-90%, and PC-100% (i.e., above the threshold stress level (Fall et al., 2009), the values of k_{sat} on Day 0 start to increase promptly and significantly. The cracks generated and the deficient pore structure result in rapid water transfer through the CPB matrix, thus leading to high k_{sat} values. This behaviour is more pronounced in the early age IC3 batch due to the lower extent of cement hydration (Figure 4-8a) and the poorer pore structure (Figure 4-11).

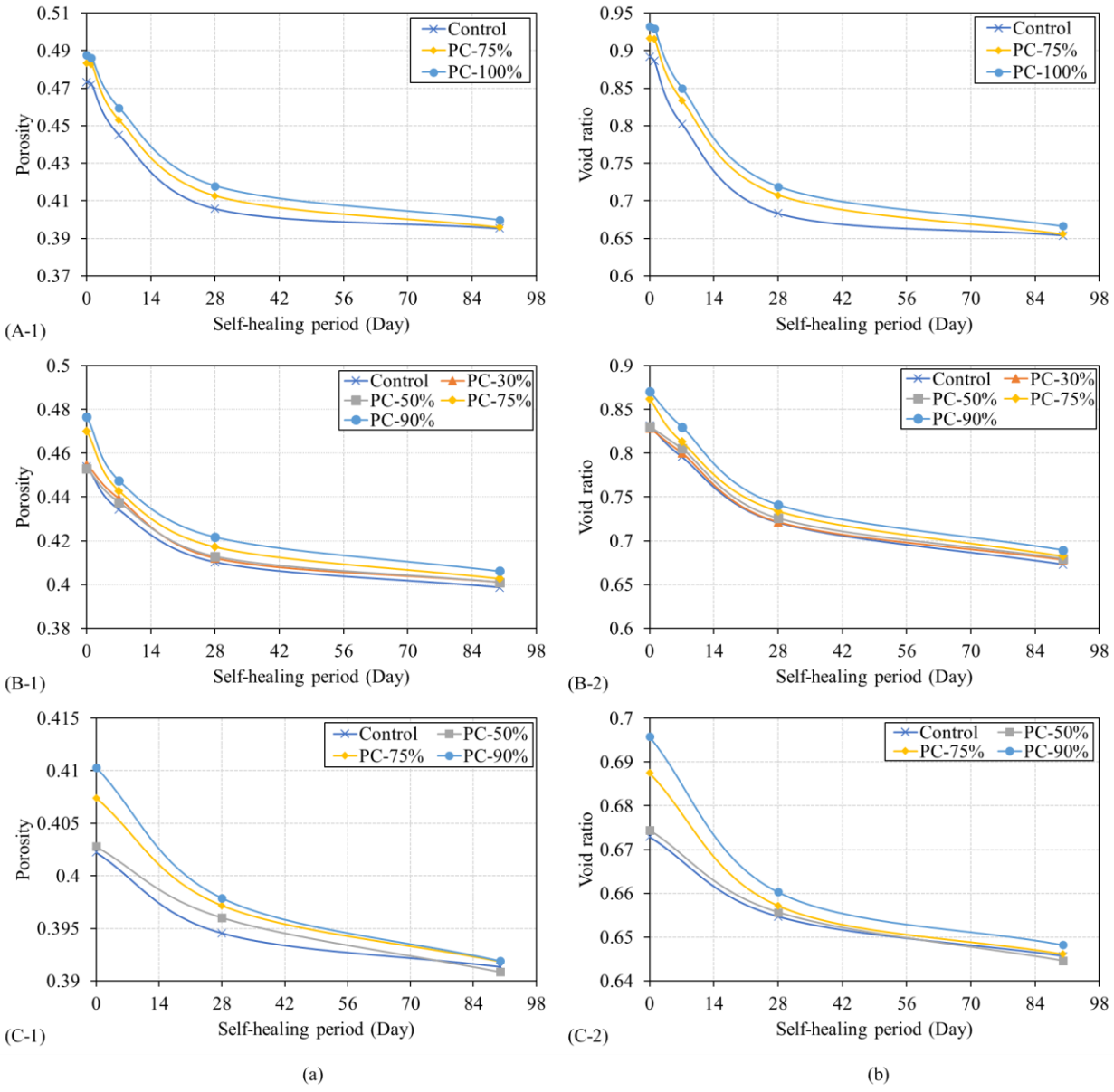

Figure 4-11. (a) Changes of porosity and (b) void ratio with different self-healing periods of pre-damaged specimens in Batch (A) IC3, (B)IC7, and (C) IC28.

In addition, from Figure 4-12, it is clearly observed that, during the self-healing process, the values of k_{sat} decrease with progressive self-healing periods. This decrease in the hydraulic conductivity

is attributed to the aforementioned autogenous healing, which contributes to the continuous cement hydration and carbonation of $Ca(OH)_2$, resulting in the self-healing products of C-S-H, CH, ettringite, $CaCO_3$, etc., to modify the pore structure within the CPB matrix (Bullard et al., 2011; Ercikdi et al., 2009). As the autogenous healing progresses, the produced self-healing products fill in the voids and cracks, resulting in a more refined pore structure within the matrix to block the internal connections, thus decreasing the values of k_{sat}. This explanation is consistent with the corresponding porosity and void ratio results (see Figure 4-11), which exhibit a descending tendency as the self-healing process progresses. In addition, the TGA results are presented in Figure 4-8 to further confirm the higher extent of cement hydration of the specimens with high pre-damage levels. The introduced cracks act as conduits that facilitate the flow of CO_2, O_2, and H_2O into the matrix of CPB, expediting the carbonation of $Ca(OH)_2$ and cement hydration, thus producing more self-healing products to fill the cracks. Furthermore, it is noted that the specimens IC7 and IC28 with PC-75% and PC-90%, respectively, were able to achieve hydraulic conductivity similar to that of the control specimens after 90 days of self-healing; even the IC3 specimens with PC-100% could recover their hydraulic conductivities attributed to the abundant autogenous healing products. According to Eq. 4-6, the hydraulic conductivity recovery ratios (HCRRs) of the specimens with the highest pre-damaging levels, i.e., IC3 (PC-100%), IC7 (PC-90%), and IC28 (PC-90%), are 92.7%, 86.9%, and 70.8%, respectively. The results of HCRRs indicate that the pre-cracked specimens with shorter initial curing time or at an earlier age have a higher capability of autogenous healing than the ones with longer initial curing time. In other words, the extent of cement hydration is more vigorous in the early age pre-cracked specimens which could produce more self-healing products to achieve similar hydraulic conductivities, porosities, and void ratios compared to control specimens, in turn contributing to the higher strength regain during the self-healing process than the control specimens. However, the full recovery of hydraulic conductivity (i.e., HCRR = 100%) was not achieved in the healed pre-damaged CPB specimens over the entire self-healing period. This disparity in hydraulic conductivity is primarily attributed to the presence of unhealed or partially healed macrocracks within the CPB matrix (Quan & Fall, 2025). The limited availability of cement particles in the CPB mixture, which dominates the capability of autogenous healing, restricts the amount of produced self-healing products. As a result, the generated cracks cannot be fully sealed due to insufficient self-healing products, leading to persistently higher hydraulic conductivity even after the self-healing process, particularly in pre-damaged specimens with a longer initial curing period.

4.4 Summary and Conclusions

This paper presents the experimental results of a study aiming to investigate the self-healing behaviour in CPB material. The self-healing mechanism and efficiency have been evaluated via various techniques, including analytical tests of XRD, SEM-EDS, and TGA, and monitoring the recovery of mechanical and permeation properties through the UCS test and hydraulic conductivity test. Based on the results, the following main conclusions can be drawn from the study.

- CPB materials have a high capacity for self-healing. The degree of self-healing depends on the age of the damaged CPB and the degree of mechanical damage. From the direct observation of the cracks by a digital microscope, it is demonstrated that the self-healing of microcracks in CPB material can occur under the ambient exposure condition without external interference and additives. Microcracks generated with a crack width of up to 92.9 μm at the initial curing age of 3 days, i.e., IC3, can be completely healed after a self-healing period of 90 days, which can be explained by the higher content of non-hydrated cement particles, indicating that microcracks initiated at the initial curing age have a greater potential for healing than those at the medium and long curing ages, i.e. IC7 and IC28. In addition, the appearance of partially healed cracks reveals the maximum self-healing capability and limit in the autogenous healing for the studied CPB material in this experimental program.
- The XRD results illustrate that the calcite $CaCO_3$ is the main substance of the white crystal-like self-healing product formed between the surface crack gaps. Then, the SEM-EDS analysis performed on the self-healing products interior of cracks and the TGA result of pre-cracked specimens represent that the combination of C-S-H, $Ca(OH)_2$, and $CaCO_3$ is most likely to be the primary self-healing products inside the cracks of the CPB.
- It is found that the CPB specimens with high pre-damage levels, i.e., PC-75%, -90%, or -100%, can not only restore their compressive strengths similar to the control uncracked specimens after 7 days self-healing period, but they also develop even up to 41.5% higher strengths than the control ones after 90 days self-healing period. This performance is more pronounced for the specimens at an early age with high pre-damage levels. Since the initiated cracks provide the pathways for the flow of O_2, CO_2, and H_2O inside the CPB matrix, the self-healing (autogenous healing) behaviour is dominated by the continuous cement hydration and carbonation of $Ca(OH)_2$. The generated self-healing products gradually refine the initial pore structures, filling the voids as the self-healing progresses, thus decreasing the porosity and void ratio of pre-cracked specimens and contributing to the improvement of the mechanical strength recovery and development. Moreover, the pre-damage levels of PC-30% and PC-50% induce hardly any influence on the compressive strength in contrast to the control specimens, except for the short immediate compaction effect right after the pre-damage procedure.
- The changes in saturated hydraulic conductivity k_{sat} during the self-healing process further demonstrate the self-healing behaviour of CPB material. After 90 days of self-healing, the hydraulic conductivity recovery ratios of 92.7%, 86.9%, and 70.8% are achieved in the highest pre-damaged specimens from IC3, IC7, and IC28, respectively. The early-age pre-cracked specimens have a higher capability of self-healing (autogenous healing), which infers that the pre-cracks stimulate the formation of self-healing products filling the cracks to restore or improve the inherent property.

The self-healing capability of CPB presents significant advantages for mining operations by enhancing the long-term stability, durability, and efficiency of underground backfill structures. The inherent autogenous healing process mitigates the development of microcracks and favours the recovery of permeability and mechanical strength of the CPB matrix through the precipitation of self-healing products, thereby reducing water ingress and structural degradation. This extends the service life of CPB and minimizes the need for costly maintenance or additional reinforcement. Furthermore, self-healing in CPB enhances backfill performance while optimizing material utilization, supporting more sustainable mining practices by reducing material waste and environmental impact. However, as a preliminary investigation into the autogenous healing mechanisms of CPB, this study only incorporated the silica tailings, necessitating further research on the influence of other mineralogical constituents present in natural tailings. Additionally, the controlled laboratory conditions may not fully capture the complex underground mining environment, where factors such as thermal fluctuations, curing stress, and varying hydraulic conditions could influence self-healing behaviour. Future research incorporating these variables would enhance the understanding of self-healing (autogenous healing) applied to the CPB technology.

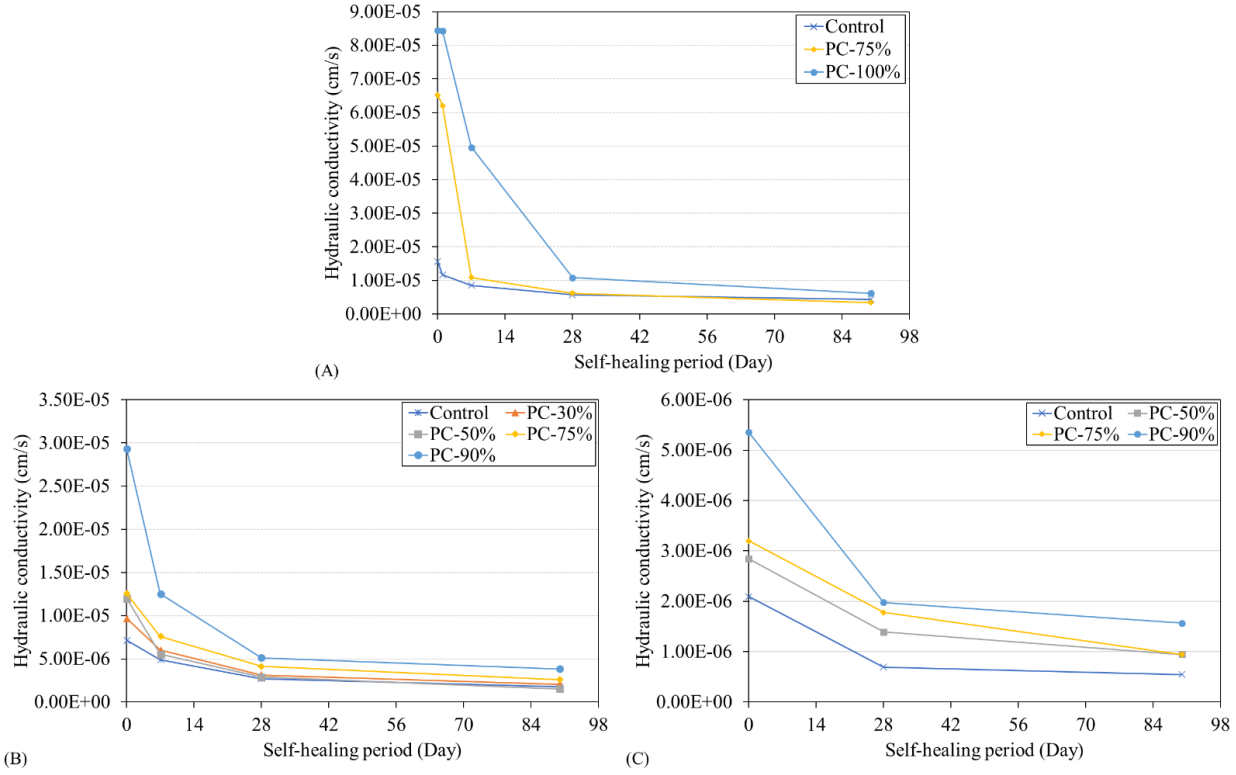

Figure 4-12. Changes of hydraulic conductivity with different self-healing periods of pre-damaged specimens in Batch (A) IC3, (B) IC7, and (C) IC28.

4.5 References

Ahn, T.-H., & Kishi, T. (2010). Crack self-healing behavior of cementitious composites incorporating various mineral admixtures. J. Adv. Concr. Technol., 8, 171-186.

Aıtcin, P. (2003). The durability characteristics of high performance concrete: a review. Cem. Concr. Compos., 25, 409-420.

Anderberg, Y. (1997). Spalling phenomena of HPC and OC. Paper presented at the NIST Workshop on Fire Performance of High Strength Concrete in Gaithersburg.

ASTM. (2016). ASTM D5084-16a. Standard Test Methods for Measurement of Hydraulic Conductivity of Saturated Porous Materials Using a Flexible Wall Permeameter. In. West Conshohocken, PA: ASTM International.

ASTM. (2020). ASTM C143/C143M-20. Standard Test Method for Slump of Hydraulic-Cement Concrete. In. West Conshohocken, PA: ASTM International.

ASTM. (2021). ASTM C39/C39M-21. Standard Test Method for Compressive Strength of Cylindrical Concrete Specimens. In. West Conshohocken, PA: ASTM International.

Benzaazoua, M., Fall, M., & Belem, T. (2004) A contribution to understanding the hardening process of cemented pastefill. Miner. Eng., 17, 141-152.

Blaiszik, B. J., Kramer, S. L., Olugebefola, S. C., Moore, J. S., Sottos, N. R., & White, S. R. (2010) Self-healing polymers and composites. Annu. Rev. Mater. Res., 40, 179-211.

Bullard, J. W., Jennings, H. M., Livingston, R. A., Nonat, A., Scherer, G. W., Schweitzer, J. S., . . . Thomas, J. J. (2011) Mechanisms of cement hydration. Cem. Concr. Res., 41, 1208-1223.

Cailleux, E., & Pollet, V. (2009). Investigations on the development of self-healing properties in protective coatings for concrete and repair mortars. Paper presented at the Proceedings of the 2nd international conference on self-healing materials, Chicago, IL, USA.

Carret, J.-C., Lamothe, S., Hounkponou, S. E., & Carter, A. (2021). Effects of pre-cracking on the early-age mechanical properties of a cement-treated base material mixed and tested in laboratory. Constr. Build. Mater., 303, 124488.

Cuenca, E., & Ferrara, L. (2017). Self-healing capacity of fiber reinforced cementitious composites. State of the art and perspectives. KSCE J. Civ. Eng., 21, 2777-2789.

De Belie, N., Gruyaert, E., Al-Tabbaa, A., Antonaci, P., Baera, C., Bajare, D., . . . Jefferson, T. (2018). A review of self-healing concrete for damage management of structures. Adv. Mater. Interfaces, 5, 1800074.

Dong, B., Fang, G., Ding, W., Liu, Y., Zhang, J., Han, N., & Xing, F. (2016). Self-healing features in cementitious material with urea–formaldehyde/epoxy microcapsules. Constr. Build. Mater., 106, 608-617.

Duerig, T. W., Melton, K., & Stöckel, D. (2013). Engineering aspects of shape memory alloys: Butterworth-heinemann.

Edvardsen, C. (1999). Water permeability and autogenous healing of cracks in concrete. In Innovation in concrete structures: Design and construction (pp. 473-487): Thomas Telford Publishing.

Ercikdi, B., Kesimal, A., Cihangir, F., Deveci, H., & Alp, İ. (2009). Cemented paste backfill of sulphide-rich tailings: Importance of binder type and dosage. Cem. Concr. Compos., 31, 268-274.

Escoffres, P., Desmettre, C., & Charron, J.-P. (2018). Effect of a crystalline admixture on the self-healing capability of high-performance fiber reinforced concretes in service conditions. Constr. Build. Mater., 173, 763-774.

Ezeoguine, K. (2022). Construction statistics, Great Britain: 2021. Retrieved from https://www.ons.gov.uk/businessindustryandtrade/constructionindustry/

Fall, M., Adrien, D., Célestin, J. C., Pokharel, M., & Touré, M. (2009) Saturated hydraulic conductivity of cemented paste backfill. Miner. Eng., 22, 1307-1317.

Fall, M., Belem, T., Samb, S., & Benzaazoua, M. (2007). Experimental characterization of the stress–strain behaviour of cemented paste backfill in compression. J. Mater. Sci., 42, 3914-3922.

Fall, M., Célestin, J., Pokharel, M., & Touré, M. (2010). A contribution to understanding the effects of curing temperature on the mechanical properties of mine cemented tailings backfill. Eng. Geol., 114, 397-413.

Fall, M., & Samb, S. S. (2008). Pore structure of cemented tailings materials under natural or accidental thermal loads. Mater. Charact., 59, 598-605.

Ferrara, L., Krelani, V., & Moretti, F. (2016). Autogenous healing on the recovery of mechanical performance of High Performance Fibre Reinforced Cementitious Composites (HPFRCCs): Part 2–Correlation between healing of mechanical performance and crack sealing. Cem. Concr. Compos., 73, 299-315.

Ferrara, L., Krelani, V., Moretti, F., Flores, M. R., & Ros, P. S. (2017). Effects of autogenous healing on the recovery of mechanical performance of High Performance Fibre Reinforced Cementitious Composites (HPFRCCs): Part 1. Cem. Concr. Compos., 83, 76-100.

Gardner, D., Lark, R., Jefferson, T., & Davies, R. (2018). A survey on problems encountered in current concrete construction and the potential benefits of self-healing cementitious materials. Case Stud. Constr. Mater., 8, 238-247.

Ghirian, A., & Fall, M. (2015). Coupled Behavior of Cemented Paste Backfill at Early Ages. Geotech. Geol. Eng., 33, 1141-1166.

Ghosh, S. K. (2009). Self-healing materials: fundamentals, design strategies, and applications (Vol. 18): Wiley Online Library.

Graybeal, B. A. (2006). Material property characterization of ultra-high performance concrete. Retrieved from https://rosap.ntl.bts.gov/view/dot/38714

Hou, C., Zhu, W., Yan, B., Guan, K., & Du, J. (2018). Influence of binder content on temperature and internal strain evolution of early age cemented tailings backfill. Constr. Build. Mater., 189, 585-593.

Huang, H., Ye, G., Qian, C., & Schlangen, E. (2016). Self-healing in cementitious materials: Materials, methods and service conditions. Mater. Des., 92, 499-511.

Huang, Z., Yilmaz, E., & Cao, S. (2021). Analysis of strength and microstructural characteristics of mine backfills containing fly ash and desulfurized gypsum. Minerals, 11, 409.

Huseien, G. F., Shah, K. W., & Sam, A. R. M. (2019). Sustainability of nanomaterials based self-healing concrete: An all-inclusive insight. J. Build. Eng., 23, 155-171.

Jefferson, A., Joseph, C., Lark, R., Isaacs, B., Dunn, S., & Weager, B. (2010). A new system for crack closure of cementitious materials using shrinkable polymers. Cem. Concr. Res., 40, 795-801.

Jiang, H., Fall, M., Li, Y., & Han, J. (2019). An experimental study on compressive behaviour of cemented rockfill. Constr. Build. Mater., 213, 10-19.

Jiang, Z., Li, W., & Yuan, Z. (2015). Influence of mineral additives and environmental conditions on the self-healing capabilities of cementitious materials. Cem. Concr. Compos., 57, 116-127.

Kan, L.-l., & Shi, H.-s. (2012). Investigation of self-healing behavior of Engineered Cementitious Composites (ECC) materials. Constr. Build. Mater., 29, 348-356.

Kan, L.-L., Shi, H.-S., Sakulich, A. R., & Li, V. C. (2010). Self-Healing Characterization of Engineered Cementitious Composite Materials. ACI Mater. J., 107, 617-624.
Kesimal, A., Yilmaz, E., Ercikdi, B., Alp, I., & Deveci, H. (2005). Effect of properties of tailings and binder on the short-and long-term strength and stability of cemented paste backfill. Mater. Lett., 59, 3703-3709.
Kim, S., Yoo, D.-Y., Kim, M.-J., & Banthia, N. (2019). Self-healing capability of ultra-high-performance fiber-reinforced concrete after exposure to cryogenic temperature. Cem. Concr. Compos., 104, 103335.
Kuang, Y., & Ou, J. (2008). Self-repairing performance of concrete beams strengthened using superelastic SMA wires in combination with adhesives released from hollow fibers. Smart Mater. Struct., 17, 025020.
Kwon, S., Nishiwaki, T., Kikuta, T., & Mihashi, H. (2014). Development of ultra-high-performance hybrid fiber-reinforced cement-based composites. ACI Mater. J., 111, 309.
Landriault, D. (1995). Paste backfill mix design for Canadian underground hard rock mining. Paper presented at the 97th Annual General Meeting of CIM. Rock Mechanics and Strata Control Session. Halifax, Nova Scotia.
Lee, H., Wong, H., & Buenfeld, N. (2016). Self-sealing of cracks in concrete using superabsorbent polymers. Cem. Concr. Res., 79, 194-208.
Li, V. C., & Herbert, E. (2012). Robust self-healing concrete for sustainable infrastructure. J. Adv. Concr. Technol., 10, 207-218.
Li, Z., Leung, C., & Xi, Y. (2009). Structural renovation in concrete: CRC Press.
Maes, M., Van Tittelboom, K., & De Belie, N. (2014). The efficiency of self-healing cementitious materials by means of encapsulated polyurethane in chloride containing environments. Constr. Build. Mater., 71, 528-537.
Mehta, P. K. (1999). Advancements in concrete technology. Concr. Int., 21, 69-76.
Noumowe, A. (1995). Effet de hautes températures (20-600 C) sur le béton: cas particulier du béton a hautes performances. Lyon, INSA,
Orejarena, L., & Fall, M. (2008). Mechanical response of a mine composite material to extreme heat. Bulletin of Engineering Geology and the Environment, 67, 387-396.
Qian, S., Zhou, J., & Schlangen, E. (2010). Influence of curing condition and precracking time on the self-healing behavior of Engineered Cementitious Composites. Cem. Concr. Compos., 32, 686-693.
Qing, Y., Zenan, Z., Deyu, K., & Rongshen, C. (2007). Influence of nano-SiO2 addition on properties of hardened cement paste as compared with silica fume. Constr. Build. Mater., 21, 539-545.
Quan, W., & Fall, M. (2025). Self-Healing Capacity of Cemented Paste Backfill in Response to Internal Sulfate Exposure. Journal of Materials in Civil Engineering, 37(7), 04025192.
Quercia, G., Hüsken, G., & Brouwers, H. (2012). Water demand of amorphous nano silica and its impact on the workability of cement paste. Cem. Concr. Res., 42, 344-357.
Ramm, W., & Biscoping, M. (1998). Autogenous healing and reinforcement corrosion of water-penetrated separation cracks in reinforced concrete. Nucl. Eng. Des., 179, 191-200.
Roig-Flores, M., Pirritano, F., Serna, P., & Ferrara, L. (2016). Effect of crystalline admixtures on the self-healing capability of early-age concrete studied by means of permeability and crack closing tests. Constr. Build. Mater., 114, 447-457.
Roshani, A., & Fall, M. (2020). Rheological properties of cemented paste backfill with nano-silica: Link to curing temperature. Cem. Concr. Compos., 114, 103785.

Seifan, M., Samani, A. K., & Berenjian, A. (2016). Bioconcrete: next generation of self-healing concrete. Appl. Microbiol. Biotechnol., 100, 2591-2602.
Sisomphon, K., Copuroglu, O., & Koenders, E. (2012). Self-healing of surface cracks in mortars with expansive additive and crystalline additive. Cem. Concr. Compos., 34, 566-574.
Snoeck, D., Van Tittelboom, K., Steuperaert, S., Dubruel, P., & De Belie, N. (2014). Self-healing cementitious materials by the combination of microfibres and superabsorbent polymers. J. Intell. Mater. Syst. Struct., 25, 13-24.
Song, H.-W., Kwon, S.-J., Byun, K.-J., & Park, C.-K. (2006). Predicting carbonation in early-aged cracked concrete. Cem. Concr. Res., 36, 979-989.
Van Breugel, K. (2007). Is there a market for self-healing cement-based materials. Paper presented at the Proceedings of the first international conference on self-healing materials.
Van Tittelboom, K., De Belie, N., De Muynck, W., & Verstraete, W. (2010). Use of bacteria to repair cracks in concrete. Cem. Concr. Res., 40, 157-166.
Van Tittelboom, K., De Belie, N., Van Loo, D., & Jacobs, P. (2011). Self-healing efficiency of cementitious materials containing tubular capsules filled with healing agent. Cem. Concr. Compos., 33, 497-505.
Van Tittelboom, K., Wang, J., Araújo, M., Snoeck, D., Gruyaert, E., Debbaut, B., . . . De Belie, N. (2016). Comparison of different approaches for self-healing concrete in a large-scale lab test. Constr. Build. Mater., 107, 125-137. doi:https://doi.org/10.1016/j.conbuildmat.2015.12.186
Wang, J., Dewanckele, J., Cnudde, V., Van Vlierberghe, S., Verstraete, W., & De Belie, N. (2014). X-ray computed tomography proof of bacterial-based self-healing in concrete. Cem. Concr. Compos., 53, 289-304.
Wang, J. Y., Soens, H., Verstraete, W., & De Belie, N. (2014). Self-healing concrete by use of microencapsulated bacterial spores. Cem. Concr. Res., 56, 139-152.
Wang, X. F., Yang, Z. H., Fang, C., Han, N. X., Zhu, G. M., Tang, J. N., & Xing, F. (2019). Evaluation of the mechanical performance recovery of self-healing cementitious materials – its methods and future development: A review. Constr. Build. Mater., 212, 400-421.
Wu, M., Johannesson, B., & Geiker, M. (2012). A review: Self-healing in cementitious materials and engineered cementitious composite as a self-healing material. Constr. Build. Mater., 28, 571-583.
Xiang, J., Li, Z., Qiu, J., Wu, N., & Cheng, H. (2023a). Investigating the potential for porous ceramics as bacterial carrier in self-healing cemented paste backfill. Ceramics International, 49, 13490-13500.
Xiang, J., Qiu, J., Yuan, L., Wu, J., & Ma, Z. (2023b). Characterization and role analysis of bacteria types in self-healing behaviour of cemented paste backfill. J. Build. Eng., 75, 106964.
Yan, B., Jia, H., Yilmaz, E., Lai, X., Shan, P., & Hou, C. (2022). Numerical investigation of creeping rockmass interaction with hardening and shrinking cemented paste backfill. Constr. Build. Mater., 340, 127639.
Yang, Y., Lepech, M. D., Yang, E.-H., & Li, V. C. (2009). Autogenous healing of engineered cementitious composites under wet–dry cycles. Cem. Concr. Res., 39, 382-390.
Yıldırım, G., Khiavi, A. H., Yeşilmen, S., & Şahmaran, M. (2018). Self-healing performance of aged cementitious composites. Cem. Concr. Compos., 87, 172-186.
Yilmaz, E., Kesimal, A., Deveci, H., & Ercikdi, B. (2003). The factors affecting the performance of paste backfill: physical, chemical and mineralogical characterization. Paper presented at the First Engineering Sciences Congress for Young Researcher (MBGAK'03), Istanbul.

Yoo, D.-Y., Shin, W., Chun, B., & Banthia, N. (2020). Assessment of steel fiber corrosion in self-healed ultra-high-performance fiber-reinforced concrete and its effect on tensile performance. Cem. Concr. Res., 133, 106091.
Yu, J., Lu, C., Leung, C. K. Y., & Li, G. (2017). Mechanical properties of green structural concrete with ultrahigh-volume fly ash. Constr. Build. Mater., 147, 510-518.
Zhou, Q., & Glasser, F. P. (2001). Thermal stability and decomposition mechanisms of ettringite at< 120 C. Cem. Concr. Res., 31, 1333-1339.
Zollo, R. F. (1997). Fiber-reinforced concrete: an overview after 30 years of development. Cem. Concr. Compos., 19, 107-122.

Chapter 5 Crack Self-healing Capacity and Performance Recovery of Cemented Paste Backfill Subjected to THMC Factors

5.1 Introduction

Portland cement, which dominates the development of properties within the CPB structure through the bonding of tailings particles and hydration products, also governs and contributes to the performance of the self-healing (autogenous healing) in CPB material, as discussed in Chapter 4. Moreover, CPB structures are exposed to complex and dynamic conditions after being placed underground. These factors interact and influence the properties of CPB, such as strength, permeability, and long-term durability, under different thermal, hydraulic, mechanical, and chemical conditions, as explicated in Chapter 2. However, based on the literature review of previous research work (Chapter 2 and Chapter 3), there are limited previous studies conducted on the self-healing behaviour of CPB, and none of them have addressed the effects of thermal (curing temperature), chemical (sulphate content), hydraulic (drainage) and mechanical (crack-inducing stress) factors on the self-healing behaviour and capacity of CPB.

In this chapter, Section 5.2 investigates the self-healing behaviour of CPB in the presence of different sulphate concentrations. It is demonstrated that the sulphate ions can positively or negatively affect the self-healing efficiency of CPB, depending on the sulphate concentrations and self-healing period. The formation of ettringite and gypsum as the newly introduced components of self-healing products combined with C-S-H, $Ca(OH)_2$, and $CaCO_3$ contributes to the observed self-healing performance. Section 5.3 explores the effects of temperature on the self-healing performance of CPB. The elevated temperatures (up to 50℃ in this study) enhance the self-healing process within the CPB matrix compared to room temperature (20℃), primarily due to accelerated binder hydration and improved degree of cement hydration. However, the low temperature (2℃) induces negligible self-healing performance due to that the low temperature inhibits cement hydration, leading to insufficient self-healing products. Section 5.4 presents the influence of varying drainage conditions on the self-healing behaviour and performance of CPB. Self-healing efficiency is found to be improved as the drainage condition is enhanced, which is attributed to the combined effects of enhanced cement hydration and microstructural refinement. Section 5.5 reveals the autogenous self-healing efficiency of CPB with different crack damage induced by three mechanical pre-cracking methods, including uniaxial compression, triaxial compression, and indirect tensile loading. The specimens pre-cracked under uniaxial and triaxial compression loading exhibit comparably promising self-healing performance attributed to the pronounced autogenous self-healing mechanisms and favourable crack geometries within the matrix. In contrast, the specimens subjected to indirect tensile loading show inferior self-healing efficiency due to the unhealed major cracks destroying the integrity of the matrix. The specific details and findings of these experiments are presented and discussed in sections 5.2, 5.3, 5.4, and 5.5.

5.2 Paper II: Self-Healing Capacity of Cemented Paste Backfill in Response to Internal Sulphate Exposure

Published in *Journal of Materials in Civil Engineering*, Volume 37, Issue 7

Weizhou Quan, Mamadou Fall

Department of Civil Engineering, University of Ottawa, Ottawa, Ontario, Canada

Abstract

This paper experimentally investigates the effect of internal sulphate exposure on the self-healing capacity of cemented paste backfill (CPB). CPB specimens were prepared with different sulphate concentrations of 0, 5,000, 15,000, and 25,000 ppm and cured under ambient conditions for an initial curing period of 7 days. Following the initiation of the cracks within the CPB matrix at various pre-cracking levels (i.e., 0%, 75%, and 90% of ultimate compressive strength in the pre-peak phase), the studied specimens were subjected to various self-healing periods of 7, 28, and 90 days. Self-healing performance was evaluated by observations of crack closure, mechanical strength tests, hydraulic conductivity measurements, and assessments of physical properties (i.e., porosity and void ratio). Self-healing products were identified using X-ray diffraction (XRD), scanning electron microscopy-energy dispersive spectroscopy (SEM-EDS), and thermogravimetric analysis and derivative thermogravimetry (TG/DTG) techniques. The experimental results show that sulphate significantly affects the self-healing performance of CPB. The highly sulphated specimens (i.e., 25,000 and 15,000 ppm) generally exhibit a more pronounced self-healing efficiency in terms of strength and hydraulic conductivity recovery during the first 28 days of self-healing, followed by an opposite performance during the 90 days of the self-healing period. Conversely, specimens with low sulphate concentrations (i.e., 5,000 ppm) consistently displayed positive effects on self-healing performance throughout the entire self-healing duration. The inhibition of cement hydration by sulphate ions and the amount of formed expansive minerals (i.e., ettringite and gypsum) emerged as critical factors underlying these observed behaviours. Furthermore, the combination of ettringite, gypsum, C-S-H, $Ca(OH)_2$, and $CaCO_3$ was identified as the primary self-healing products in the examined specimens. The results presented in the paper hold significant implications for the design, mechanical stability, and durability of CPB structures exposed to sulphate ions, offering valuable guidance for engineering practice.

Keywords: Cemented paste backfill; Self-healing; Sulphate attack; Tailings; Mechanical properties; Hydraulic conductivity.

5.2.1 Introduction

Cemented paste backfill (CPB), an engineered mixture typically consisting of 70-85% of tailings, 3-7% of hydraulic binders, and water, has gained widespread recognition for its application in post-mining backfilling processes (Bull & Fall 2020; Kesimal et al., 2005; Benzaazoua et al., 2004). It serves multiple critical functions, including the establishment of a secure working surface for personnel and machinery, the environmentally sound disposal of mining tailings, and the

enhancement of ore/pillar recovery to boost overall productivity (Ghirian & Fall, 2016). The use of CPB offers the potential to reintegrate up to 60% of the tailings produced by mining operations back into underground cavities. This process effectively minimizes the need for extensive surface tailings impoundments and consequently reduces the costs associated with land reclamation (Yilmaz et al., 2005).

Mechanical strength stands as one of the significant performance criteria of CPB materials from the early to advanced curing ages. In general, achieving adequate mechanical strength is indispensable to meet the demands of dynamic and static loads, ensuring the stability of underground stopes and the surrounding rock formations during various mining activities (i.e., up to 1 MPa is often needed for free-standing walls) (Belem & Benzaazoua, 2007). Failures in CPB integrity can result in significant financial repercussions and regrettably have been associated with fatalities and injuries, an issue observed not only in Canada but also globally. The attainment of robust early strength in CPB materials serves a dual purpose by mitigating the risk of liquefaction and shortening the mining cycle, thereby enhancing productivity and reducing operational costs. Typically, Portland cement predominantly contributes to the strength development within the CPB structure through the hydration products (i.e., calcium-silicate-hydrate, calcium hydroxide, and ettringite), which dominate the mechanical properties of the CPB structure.

Numerous research works have delved into the mechanical properties of CPB materials, alongside the various influential factors at play, such as specimen composition (Wu et al., 2015; Klein & Simon, 2006; Fall et al., 2004), temperature (Walske et al., 2016; Nasir & Fall, 2010; Fall & Samb, 2009), sulphate (Wang et al., 2020; Aldhafeeri & Fall, 2017; Li & Fall, 2016; Ercikdi et al., 2013; Fall & Pokharel, 2010), curing stress and drainage (Ghirian & Fall, 2016; Yilmaz et al., 2014), and chemical and mineral additives (Al-Moselly et al., 2022; Haruna, 2022; Behera et al., 2021; Jiang et al., 2020; Klein & Simon, 2006). Among these factors, sulphate content has emerged as an important aspect significantly impacting CPB properties and structural integrity, which is often associated with strength loss and change in pore characteristics due to internal sulphate attack. Sulphate ions are often present in CPB systems and their introduction can stem from diverse sources (Fall & Pokharel, 2010; Fall & Benzaazoua, 2005;). First, sulphide-rich tailings, typically containing up to 60% sulphide minerals like pyrite, yield sulphate ions through the oxidation of these minerals. Additionally, sulphate can be introduced into the CPB structure through the use of sulfur dioxide/air for cyanide destruction in gold mining. Furthermore, the inclusion of gypsum ($CaSO_4 \cdot 2H_2O$) or anhydrite ($CaSO_4$) to regulate cement setting can introduce trace amounts of sulphate into the CPB mixture. Lastly, mine processing waters employed in CPB mixture preparation may contain substantial sulphate concentrations. The effects of internal sulphate attack on CPB materials have been extensively explored in previous studies. For example, Benzaazoua et al. (1999) investigated the impact of chemical and mineralogical changes on CPB's mechanical strength and highlighted how the presence of sulphides in the tailings led to the dissolution of calcic phases in cement hydrates, compromising strength. (Fall & Pokharel, 2010) suggested that sulphate absorption by C-S-H could lead to the formation of lower-quality C-S-H, thereby undermining CPB strength. Moreover, (Xiapeng et al., 2019) examined the influence of internal sulphate content

on CPB's rheological properties, demonstrating that the yield stress decreases as initial sulphate concentrations increase, while apparent viscosity exhibits the opposite trend. Furthermore, higher initial sulphate concentrations result in reduced self-desiccation rates within the CPB (Li & Fall, 2016). Similarly, the sulphate attack also induces the deterioration of mechanical strength and failure of other cementitious materials, such as concrete (Neville, 2004), mortar (Maes & De Belie, 2014), engineered cementitious composites (ECC) (Liu et al., 2017), and so forth.

In addition to the influence of sulphate content during the curing phase, the formation of cracks within the CPB structures, attributed to various factors, including excessive stresses from CPB overburden, pressure-induced stresses during the closure of adjacent rock walls, rock bursts, and shrinkage, significantly undermines their structural integrity and mechanical strength. These cracks also increase permeability properties, thereby compromising safety, serviceability, durability, and environmental performance. The concept of self-healing (autogenous healing) (Yoo et al., 2020; Yıldırım et al., 2018; Ferrara et al., 2017; Van Tittelboom & De Belie, 2013) has been extensively investigated and implemented in conventional cementitious materials to address crack initiation. The inherent autogenous healing behaviour reduces labor and costs, offering an efficient means to maintain or repair cracks in cementitious infrastructures. When a crack forms, the embedded self-healing system within the cementitious structure automatically initiates healing, reducing permeability, restoring structural function, enhancing durability, and extending service life (Qureshi & Al-Tabbaa, 2020; De Belie et al., 2018). However, research on self-healing capacity in the presence of sulphate conditions remains limited to date. For example, Liu et al. (2017) evaluated the healing of engineered cementitious composites (ECC) exposed to sulphate and chloride environments, assessing the recovery of stiffness, first-crack strength, uniaxial tensile strength, and durability. Their results indicated that the first-crack strength and ultimate tensile strength values were higher for the cracked specimens healed in a sulphate solution compared to those healed in a sulphate and chloride solution or in pure water after 200 days, attributed to improved fiber-matrix interface bond strength facilitated by ettringite and gypsum rather than continuous hydration. Similarly, Niu et al. (2023) also investigated the self-healing performance of fiber-reinforced ECC subjected to Na_2SO_4 and NaCl, Na_2SO_4, and water environments, and concluded that self-healing performance was most robust in Na_2SO_4 environments with the results of the coupling effect of carbonization, secondary hydration, and erosion product fillings after 28 days.

Despite the contributions of previous studies to understanding the self-healing ability and performance of conventional cementitious materials, the understanding of the self-healing ability of CPB is limited. Xiang et al. (2023a) utilized waste porous ceramic (WPC) as a bacterial carrier to embed Sporosarcina pasteurii, achieving self-healing in backfill paste. The results demonstrated that the embedded biosolution could be released from WPC upon crack formation, with initial crack widths of less than 1 mm achieving a 100% self-healing ratio in crack closure after 28 days. Additionally, Xiang et al. (2023b) proposed a bacterial mixture of Sporosarcina pasteurii and Pseudomonads denitrificans pre-embedded in polypropylene-fiber reinforced backfill to enhance the self-healing capacity without the need for additional carriers. These self-healing methods are classified as autonomous healing since the healing does not originate from the matrix itself but

from externally added healing agents (Van Breugel, 2007). Up to this point, no studies have addressed the impact of sulphate on the self-healing (autogenous healing) capacity and behaviour of CPB. Furthermore, findings from studies on the self-healing ability of conventional cementitious materials (e.g., mortars, concrete) cannot be directly applied to CPB due to significant differences in materials and composition. In addition, the sulphate levels within CPB systems can be significantly higher than those typically encountered in conventional concretes or mortars subjected to sulphate attacks. CPB systems may exhibit initial sulphate content ranging from low (<5000 ppm) to very high (25000 ppm). Therefore, this study aims to experimentally investigate the effect of different concentrations of internal sulphate on the self-healing capacity of CPB materials with different self-healing periods.

5.2.2 Materials and Experimental Program

5.2.2.1 Materials

Tailings

Silica tailings (ST), primarily composed of 99.8 wt.% quartz (SiO_2), which is notably abundant in the hard rock mines of Canada, served as the core material in this study. The choice of ST was driven by the need for precise control over the chemical and mineralogical characteristics of the tailings, with the aim of minimizing uncertainties when investigating the isolated impact of mixed components of CPB on its self-healing capacity. This approach diverges from using natural tailings, which may contain uncontrollable chemical constituents (such as sulfides) and minerals capable of interacting with cement, thereby potentially influencing the experimental results. A thorough analysis of ST reveals a grain size distribution comparable to the average of nine natural tailings (NT) samples from Canadian mines, as depicted in Figure 5-1. Notably, approximately 43% of the particles in ST have sizes finer than 20 μm, categorizing them as medium tailings (a category encompassing 35% to 60% of particles smaller than 20 μm), which adhere to the established guideline that CPB should contain at least 15% by mass of such particles. Furthermore, detailed insights into the physical attributes and chemical compositions of ST are presented in Table 5-1 and Table 5-2.

Binder

Portland cement type I (PCI) was used as the binder to prepare CPB specimens with a weight portion of 4.5% in this study. Table 5-3 gives the physical and chemical properties of the PCI.

Mixing water

Tap water was utilized to mix with the tailings and binder. Ferrous sulphate emerges as the predominant sulphate variety detected in cemented backfills. Specific quantities of sulphate salt ($FeSO_4•7H_2O$) with a molecular weight of 278.01 were dissolved into a distinct volume of tap water, leading to the blending water containing a predefined concentration of sulphate, 0 ppm, 5000 ppm, 15000 ppm, and 25000 ppm.

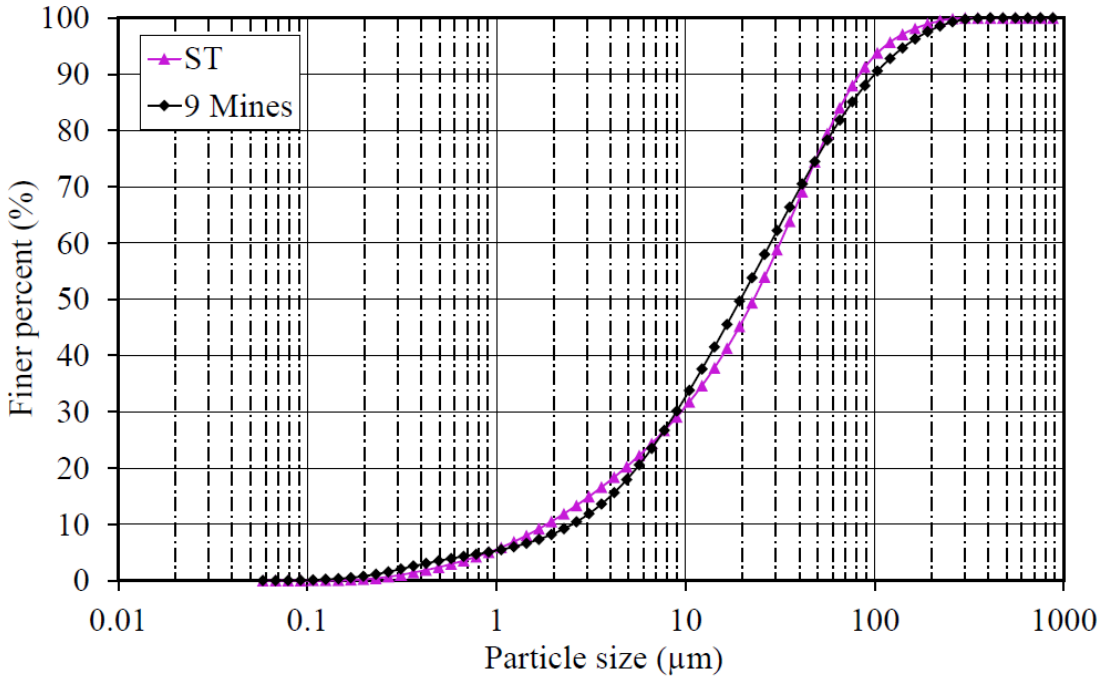

Figure 5-1. Grain size distribution of the used ST and average grain size distribution of tailings from nine Canadian mines.

Table 5-1. Physical properties of the used ST and the average of nine NT in Canada.

Element	G_s	D_{10}	D_{30}	D_{50}	D_{60}	C_u	C_c
		(μm)					
ST	2.7	1.9	9.0	22.5	31.5	16.6	1.3
Nine NT average	-	1.8	9.1	20.0	30.8	17.1	1.7

(G_s: specific gravity; C_u: coefficient of uniformity; C_c: coefficient of curvature)

Table 5-2. Chemical compositions of the used tailings ST.

Tailings	SiO_2	Fe_2O_3	Al_2O_3	TiO_2	CaO	MgO	Na_2O	K_2O
	(wt. %)							
ST	99.8	0.035	0.05	0.02	0.01	＜0.01	＜0.01	0.02

Table 5-3. Characteristic of the used binder PCI.

Binder type	MgO	CaO	SiO_2	Al_2O_3	Fe_20_3	SiO_3	SSA	R.D.
	(wt. %)						(m^2/g)	
PCI	2.65	68.82	18.03	4.53	2.70	3.82	1.30	3.10

R.D.: relative density; SSA: specific surface area.

5.2.2.2 Specimen preparation and initial curing

The designated amounts of tailings, PCI, and blended water with different sulphate concentrations, including 0, 5000, 15000, and 25000 ppm (i.e., SU0, SU5, SU15, and SU25, respectively), were precisely weighed and mixed for 7 minutes in a mixer, achieving a homogenous paste. In this study, a fixed mix proportion of 4.5% binder (PCI) was employed, maintaining a constant water-to-cement ratio (w/c) of 7.35 by weight. To ascertain the workability of the prepared CPB material, the consistency of the mixture was determined through slump tests, adhering to ASTM C143/C143M-20 (ASTM, 2020). The measured slump value, which settled at 18 cm, aligns with the frequently employed benchmark in CPB preparation. Then, the CPB mixtures were poured into cylindrical curing moulds sized at Φ50×100 mm and manual vibration was applied to expel entrapped air within the moulded mixture. The specimens were cap-sealed to prevent water evaporation and subsequently subjected to ambient curing conditions, undergoing an initial curing (IC) period of 7 days prior to pre-cracking (as outlined in Table 5-4). A total of 192 CPB specimens were prepared to investigate the impact of internal sulfate on the self-healing capacity of the CPB material.

5.2.2.3 Initial crack introduction

To evaluate the self-healing capacity of CPB material under the influence of internal sulphate exposure, varying levels of pre-cracking were induced through uniaxial compression. Following the initial curing phase, the initial uniaxial compressive strengths (UCS) were determined according to the guidelines specified in ASTM C39/C39M-21 (ASTM, 2021). Subsequently, the remaining specimens were subjected to specific pre-cracking levels of 0%, 75%, or 90% (i.e., control, PC75%, or PC90%, respectively) during the pre-peak phase of their respective initial UCS values following the procedure illustrated in Figure 5-2, introducing differing levels of crack damage within the specimens. A previous study (Fall et al., 2009) has demonstrated that the initiated cracks on the pre-cracked specimens become visible until the pre-cracking level reaches 75% or above as the mechanical load increases to levels close to the peak region (i.e., PC-75% and PC-90%), the curve begins to exhibit the first non-linear behaviour and cracks can be observed in the CPB specimens. Upon reaching the designated predetermined load thresholds, the applied load was sustained for one minute before being released, marking the conclusion of the pre-cracking process. Then, the pre-cracked specimens were removed to prepare for the self-healing process. The experiments were conducted under displacement control utilizing a computer-controlled mechanical press (MTS 10/GL) with a normal load of 50 kN and a displacement rate of 1 mm/min. Axial deformation was automatically recorded through an internal linear variable differential transformer (LVDT) connected to an electronic data acquisition system.

5.2.2.4 Healing condition

Once initial cracks were generated, the pre-cracked specimens were carefully enveloped using transparent plastic films. These encapsulated pre-cracked specimens, along with undamaged control specimens, were subsequently consigned to an ambient environment (23°C) for a self-healing curing phase. The self-healing environment, devoid of external influences, aimed to

facilitate an examination of the CPB material's self-healing capabilities amidst internal sulphate exposure. In this study, the pre-cracking day is named Day 0, representing the self-healing start day, followed by Day 7, Day 28, and Day 90, representing the early self-healing periods of 7 and 28 days, and the advanced self-healing period of 90 days, respectively. Note that the self-healing periods of Day 0, 7, 28, and 90 correspond to the CPB paste age of 7, 14, 35, and 97 days, respectively.

Table 5-4. Summary of experimental program for each testing batch of CPB specimens.

Batch	PCI content (%)	w/c ratio	Sulphate content (ppm)	Initial curing (day)	Pre-crack level (%)	Self-healing period (day)
SU0	4.50	7.35	0	7	0, 75%, and 90% of UCS	7 28 90
SU5	4.50	7.35	5,000	7	0, 75%, and 90% of UCS	7 28 90
SU15	4.50	7.35	15,000	7	0, 75%, and 90% of UCS	7 28 90
SU25	4.50	7.35	25,000	7	0, 75%, and 90% of UCS	7 28 90

5.2.2.5 Methods for evaluation of self-healing behaviour

Crack characteristics

The self-healing behaviour of crack closure was meticulously monitored and observed employing a digital microscope with a 200× magnification before and after specific predetermined self-healing periods of 0, 7, 28, and 90 days. The digital microscope acquired images of crack alterations at different magnifications, which provided a direct approach to assessing the self-healing behaviour in pre-cracked CPB specimens. The numbers of cracks were counted, and crack widths were analyzed based on at least 15 locations spanning from the narrowest to the widest points of each measured crack. This technique facilitated the quantification of changes in crack width, offering insights into surface crack closure while reinforcing the results of other tests.

Hydraulic property investigation

Given that cracks and sulphate attacks directly impact the durability of CPB, it is essential to quantitatively assess its self-healing capabilities. The self-healing capacity can be evaluated by examining changes in the permeability of pre-cracked specimens that have undergone self-healing. To achieve this, saturated hydraulic conductivity tests were conducted on the CPBs before and after

pre-cracking and healing. These tests used a triaxial cell with a flexible wall technique according to ASTM 5084-16a (ASTM, 2016) to determine their coefficients of permeability or hydraulic conductivity (k). The tests maintained a consistent hydraulic head by applying a constant hydraulic gradient (10 psi or 69 kPa) between the inflow and outflow points for measurement. Full saturation was achieved by applying backpressure until a constant flow rate was maintained through the specimen. Each test was performed twice to ensure the reproducibility of the result. The hydraulic conductivity, k, was calculated as follows:

$$k = \frac{\Delta Q \cdot L}{A \cdot \Delta h \cdot \Delta t} \tag{5-1}$$

where k represents the hydraulic conductivity, cm/s; ΔQ denotes the quantity of flow during a certain time interval Δt, calculated as the average of inflow and outflow, cm^3; L signifies the length of the specimen, cm; A represents the cross-sectional area of the specimen, cm^2; Δt is the time interval, s; and Δh corresponds to the average head loss of across the specimen, cm of water.

The hydraulic conductivity recovery ratio (HCRR) is determined by the following formula:

$$\text{HCRR } (\%) = \frac{k_0 - k_t}{k_0} \times 100\% \tag{5-2}$$

where k_0 is the initial hydraulic conductivity, cm/s, measured after pre-damaging; k_t is the hydraulic conductivity, cm/s, measured after specified self-healing period.

Mechanical property investigation

Mechanical strength is an essential feature of CPB materials, ensuring the stability of underground mine cavities and providing valuable insights into the structural integrity of the CPB matrix. To assess the mechanical strength recovery in CPB, UCS tests were conducted on both control and pre-cracked CPB specimens, following ASTM C39/C39M-21 (ASTM, 2021). These tests were performed at 0, 7, 28, and 90 days of self-healing periods, on both healed pre-cracked specimens and undamaged control specimens. The test was carried out using a computer data acquisition system with a constant deformation rate of 1 mm/min, and each test was replicated three times to verify the reproducibility of the results.

The relative changes in compressive strength (CCS) of the pre-cracked and healed specimens compared to control specimens are calculated as follows:

$$\text{CCS}(\%) = \frac{S_{\text{pre-cracked/healed}} - S_{\text{control}}}{S_{\text{control}}} \tag{5-3}$$

where $S_{pre\text{-}cracked/healed}$ is the UCS of the pre-cracked specimens before or after a self-healing period, and $S_{control}$ is the UCS of undamaged control specimens with self-healing condition and period.

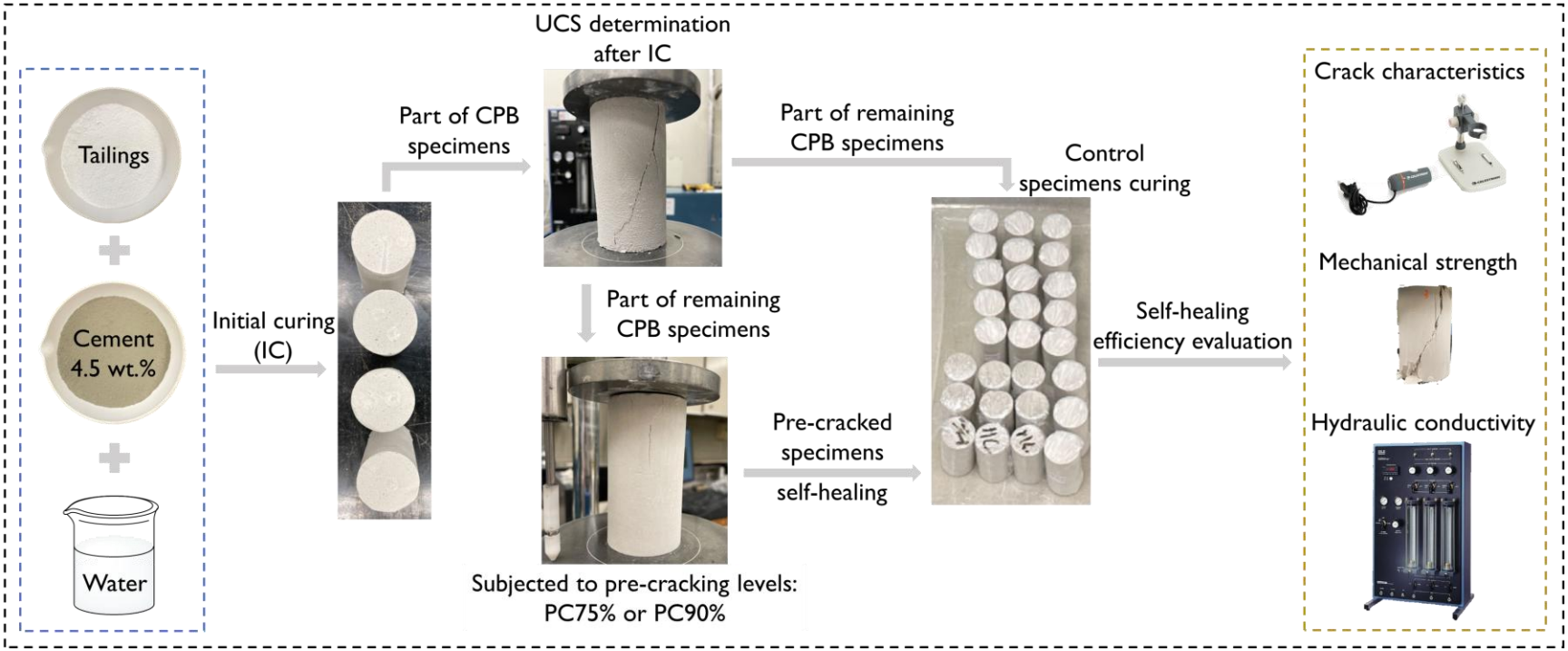

Figure 5-2. Preparation of CPB specimens and experimental tests flow chart.

Microstructural and chemical analysis

The physical properties of CPB material, including void ratio and porosity, significantly affect its mechanical behaviour. These properties were monitored during the self-healing periods at 0, 7, 28, and 90 days in both control and pre-cracked specimens. The observed changes in void ratio and porosity provide crucial supplementary evidence for assessing the internal sulphate influence on self-healing behaviour. In addition to the quantitative assessment of self-healing efficiency, it is vital to characterize the chemical compositions and morphology of the self-healing products to understand the self-healing mechanism better. Microstructural analysis techniques employed included X-ray diffraction (XRD), scanning electron microscopy-energy dispersive spectroscopy (SEM-EDS), and thermal analysis (TG/DTG). The XRD and SEM-EDS analysis allowed us to examine the compositions of CPB self-healing products when exposed to internal sulphate concentrations. Furthermore, the thermal analysis provided insights into binder hydrations under sulphate attack. The XRD analysis was conducted by a Bruker D8 Endeavor equipped with a 1 kW sealed tube Cu Kalpha source (40 kV and 25 mA) and a Lynxeye XE-T 1-D silicon strip detector. SEM-EDS analysis was performed using an environmentally versatile JEOL 6610LV SEM in low voltage mode, featuring an attached Oxford INCA large area SDD detector. Additionally, TG/DTG analysis was carried out using a Setaram Setsys 24 thermogravimetric analyzer, applying a heating ramp of 10°C/minute, commencing from room temperature and reaching up to 1000°C in a nitrogen atmosphere.

5.2.3 Results and Discussion

5.2.3.1 Crack closure observation

During the pre-cracking process, the numbers and widths of generated cracks varied among the CPB specimens with different sulphate concentrations. Specifically, it is observed that the CPB specimens with sulphate concentrations of 25000 and 15000 ppm display a higher number of cracks but with smaller widths compared to specimens with 5000 and 0 ppm sulphate concentrations at the pre-peak phase. This behaviour can be attributed to the enhanced stiffness of CPB specimens, as sulphate concentration increases, leading to a noticeable increase in the slope of the linear portion of stress-strain curves, as illustrated in Figure 5-3. As demonstrated by Fall et al. (2007), microcracks start to be increasingly visible in CPB specimens until the level of mechanical load reaches the first non-linear behaviour. With increasing sulphate concentration, the linear portion of the stress-strain curve accounts for up to 85% of the ascending branch, resulting in a limited first non-linear region before peak stress for microcrack initiation and propagation. Furthermore, the specimens with enhanced stiffness are more resistant to the crack growth, thereby leading to smaller widths of microcracks in the pre-cracked CPB specimens with higher sulphate concentrations.

Figure 5-4 and Figure 5-5 show the representative observations of crack closure in CPB specimens with different initial sulphate concentrations (5000, 15000, and 25000 ppm) after different self-healing periods (7, 28, 90 days). Direct captures from a digital microscope reveal three distinct healing performances among the examined microcracks: complete healing, partial healing, and no healing. It is noticed that abundant self-healing products are produced in the microcracks or along

the crack paths in the complete and partial healing microcracks after the healing periods. Considering the no healing scenario in large cracks (approximately >289.6 μm), it indicates that there is a limitation in the autogenous healing capability of the CPB material under the exposure to sulphate concentrations. Due to the unevenness of crack width, the maximum crack widths of completely healed microcracks (listed in Table 5-5) under the varying conditions of sulphate concentrations and self-healing periods were measured and compared to those of the sulphate-free CPB specimens as a direct assessment and representation of self-healing capability impacted by the internal sulphate exposure. Table 5-5 demonstrates that CPB specimens containing sulphate exhibit generally better crack closure ability, particularly within the self-healing period of 28 days (excluding the instance of 25000 ppm at Day 7). For example, at the Day 7 self-healing period, crack widths of up to 67.8 μm and 62.0 μm are completely healed in pre-cracked specimens with sulphate concentrations of 5000 and 15000 ppm, respectively, representing approximately 47% and 34% improvements compared to sulphate-free specimens. Moreover, at the Day 28 self-healing period, pre-cracked specimens with sulphate concentrations of 5000, 15000, and 25000 ppm demonstrate complete healing of crack widths reaching approximately 81.5 μm, 95.2 μm, and 91.1 μm, respectively. The presence of sulphate ions, as previously demonstrated by Fall & Pokharel (2010), contributes to the decreased CPB internal porosity due to the precipitation of secondary hydrated minerals (i.e., gypsum and ettringite) within the capillary pores and voids, resulting from sulphate ions reacting with calcium hydroxide (CH) and tricalcium aluminate (C_3A). The produced hydration products thereby contribute to the crack closure with the progress of self-healing. However, during the early self-healing stage (Day 7), pre-cracked specimens with a sulphate concentration of 25000 ppm exhibit inferior crack closure performance, attributed to the inhibitory effect of high or excessive sulphate content on binder hydration (Li & Fall, 2018). Furthermore, at the advanced period of self-healing (Day 90), pre-cracked CPB specimens with higher sulphate concentrations, such as 15000 and 25000 ppm, experience compromised crack closure due to sulphate attack induced deterioration, which will be further discussed in subsequent sections.

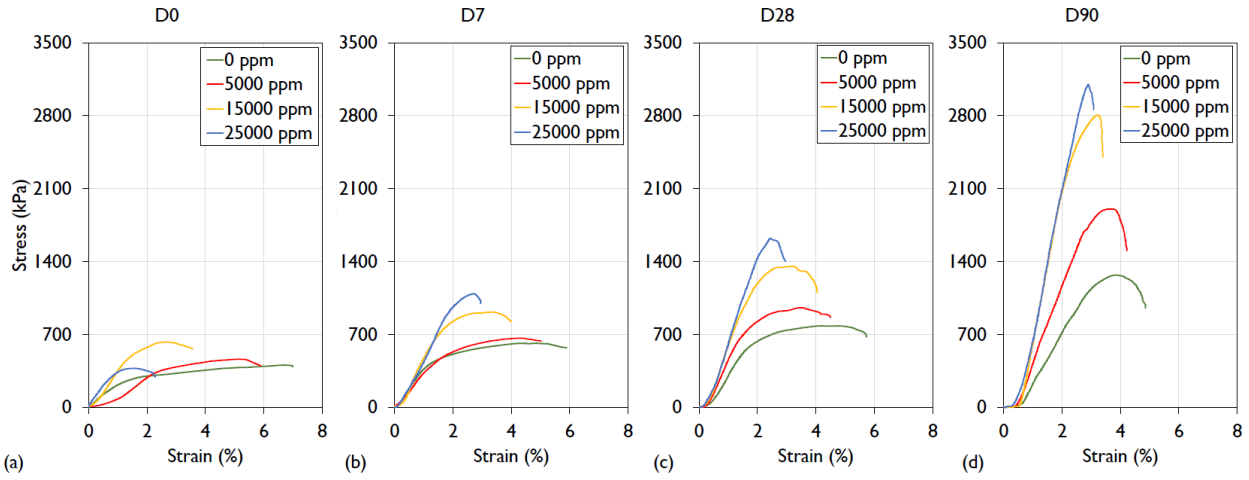

Figure 5-3. Stress-strain characteristics of control CPB specimens with different sulphate concentrations after self-healing period of (a) Day 0, (b) Day 7, (c) Day 28, and (d) Day 90.

5.2.3.2 Nature of the self-healing products with the presence of sulphate

Figure 5-4 and Figure 5-5 exhibit that the microcracks are filled with abundant crystal-like microparticles inside or along the crack path to achieve the crack closure. Previous studies elucidated that sulphate ions interact with cement compounds and hydration products within the CPB matrix (i.e., CH, C_3A, and C-S-H gels), resulting in the formation of secondary hydration products such as ettringite and gypsum (Liu et al., 2019; Xiapeng et al., 2019; Fall & Pokharel, 2010). Therefore, to detail the components of self-healing products in sulphate-containing CPB specimens, XRD, SEM-EDS, and TG/DTG analyses were employed to examine the elemental composition and microstructure.

Figure 5-6 presents the XRD patterns of self-healing products obtained from sulphate-containing and sulphate-free CPB specimens. The spectra are dominated by quartz peaks due to the presence of silica tailings. Previous work (Quan & Fall, 2024) has demonstrated that the primary components of self-healing products in sulphate-free CPB mixtures are a combination of C-S-H, $Ca(OH)_2$, and $CaCO_3$ (refer to Figure 5-6b). However, in the self-healing products from the sulphate-containing CPB specimens, the detection of ettringite and gypsum in the two-theta degrees range of 5°-15° and 30°-35° (refer to Figure 5-6a) highlights the main difference.

In addition, the self-healing products formed inside the microcracks were characterized using SEM-EDS analysis, as illustrated in Figure 5-7. The energy spectrum of the examined area can be obtained to confirm the different types of self-healing products. In all EDS diagrams from different locations, Si shows the highest peaks due to the silica tailings used in the study, and its effect cannot be eliminated during the analysis. The EDS results clearly show the traces of Ca, O, C, Si, and Al peaks, which confirm the presence of the $CaCO_3$, C-S-H, and $Ca(OH)_2$ in self-healing products. In addition, the trace of S is also observed, confirming the formation of ettringite and gypsum with the Ca:S ratios of 2.02 and 1.34, respectively. Moreover, the micrographs further confirm the presence of ettringite and gypsum in conjunction with C-S-H, $Ca(OH)_2$, and $CaCO_3$ as the primary self-healing products in the sulphate-containing CPB specimen to contribute to the crack closure.

Furthermore, Figure 5-8 and Figure 5-9 show the results of thermal analysis (TG/DTG) performed on the CPB specimens with sulphate concentrations of 25000, 5000, and 0 ppm after self-healing periods of 7 and 90 days. Three main thermal decomposition stages can be obviously identified from these figures (Li & Fall, 2016): (a) the dehydration of water molecules in hydrates such as C-S-H, ettringite, gypsum, and carboaluminates at the temperature range of 50-200°C; (b) dehydroxylation of CH at the temperature range of 400-450°C; and (c) decarbonation of calcium carbonate ($CaCO_3$) at the temperature range of 600-750°C. The thermal analysis results reveal the different degrees of cement hydration and secondary hydration in the sulphate-containing and sulphate-free specimens. It can be observed from Figure 5-8 that the pre-cracked specimens with sulphate concentrations exhibit overall higher weight losses than the sulphate-free specimens at the same pre-cracking level and after the same self-healing period. Notably, the weight loss at the temperature range of 50-200°C is more pronounced than in other ranges, suggesting that a higher amount of ettringite and gypsum is produced via the reactions between sulphate ions and C_3A and

CH. Moreover, in the early self-healing period (Day 7), as shown in Figure 5-8a, the CPB specimens with the sulphate concentration of 25000 ppm exhibit a lower weight loss than specimens with the lower sulphate concentration of 5000 ppm at 400-450°C, which means less CH is produced due to the inhibition effect from the high content of sulphate. Conversely, the absence of an inhibition effect in 5000 ppm sulphate concentration favours more rigorous cement hydration, leading to the formation of hydration products CH and $CaCO_3$. As the self-healing progresses to the advanced age (Day 90), as shown in Figure 5-8b, the three main weight losses are pronounced in the specimens with higher sulphate concentration of 25000 ppm, indicating the abundant existence and combination of ettringite, gypsum, C-S-H, $Ca(OH)_2$ and $CaCO_3$ within the CPB matrix. In addition, it can be noticed from Figure 5-9 that the amounts of the produced hydration products significantly vary in the specimens with different sulphate concentrations. Specifically, Figure 5-9a presents comparatively higher weight losses at the temperature ranges of 50-200°C and 600-750°C in the specimens with sulphate concentration of 5000 ppm after the self-healing period of Day 90. This observation suggests that, besides the secondary hydration products ettringite and gypsum, the abundant presence of $CaCO_3$ also contributes to the self-healing performance within the CPB specimens with the sulphate concentration of 5000 ppm. In contrast, ettringite and gypsum apparently dominate the self-healing performance in CPB specimens with the sulphate concentration of 25000 ppm, as observed in Figure 5-9b. Likewise, the XRD results in Figure 5-6a detect comparatively higher intensities of ettringite than gypsum, indicating a larger presence of ettringite in the self-healing products.

Table 5-5. Maximum healed crack width after certain self-healing periods with the existence of sulphate.

Batch nomenclature	Self-healing period (day)	Maximum completely healed crack width (μm)
SU0	7	46.1
	28	56.1
	90	67.9
SU5	7	67.8
	28	81.5
	90	91.0
SU15	7	62.0
	28	95.2
	90	62.8
SU25	7	42.0
	28	91.1
	90	68.4

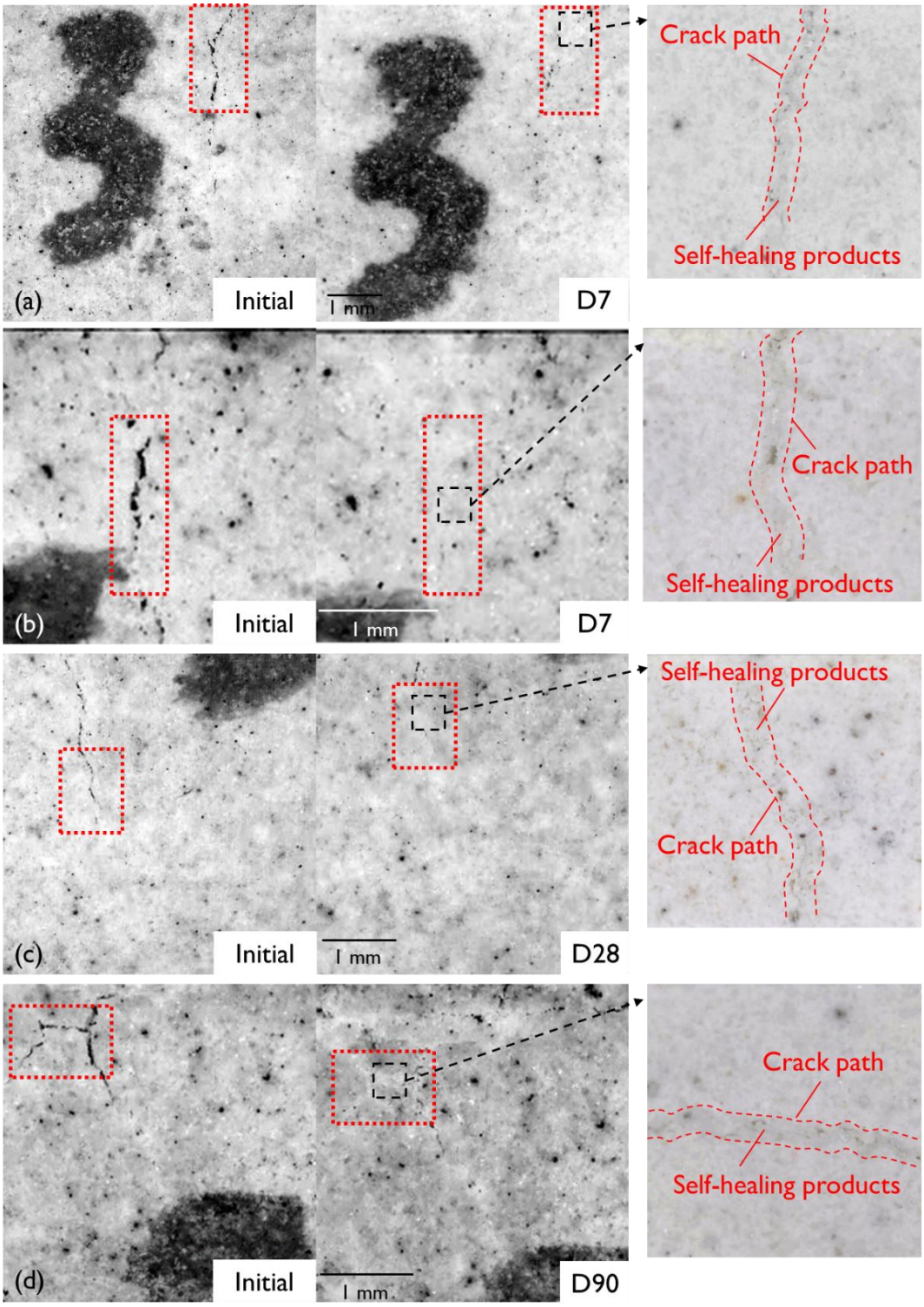

Figure 5-4. Observation of complete healing cracks in CPB specimen with sulphate concentration and self-healing period of (a) 5000 ppm, Day 7; (b) 15000 ppm, Day 7; (c) 25000 ppm, Day 28; and (d) 25000 ppm, Day 90.

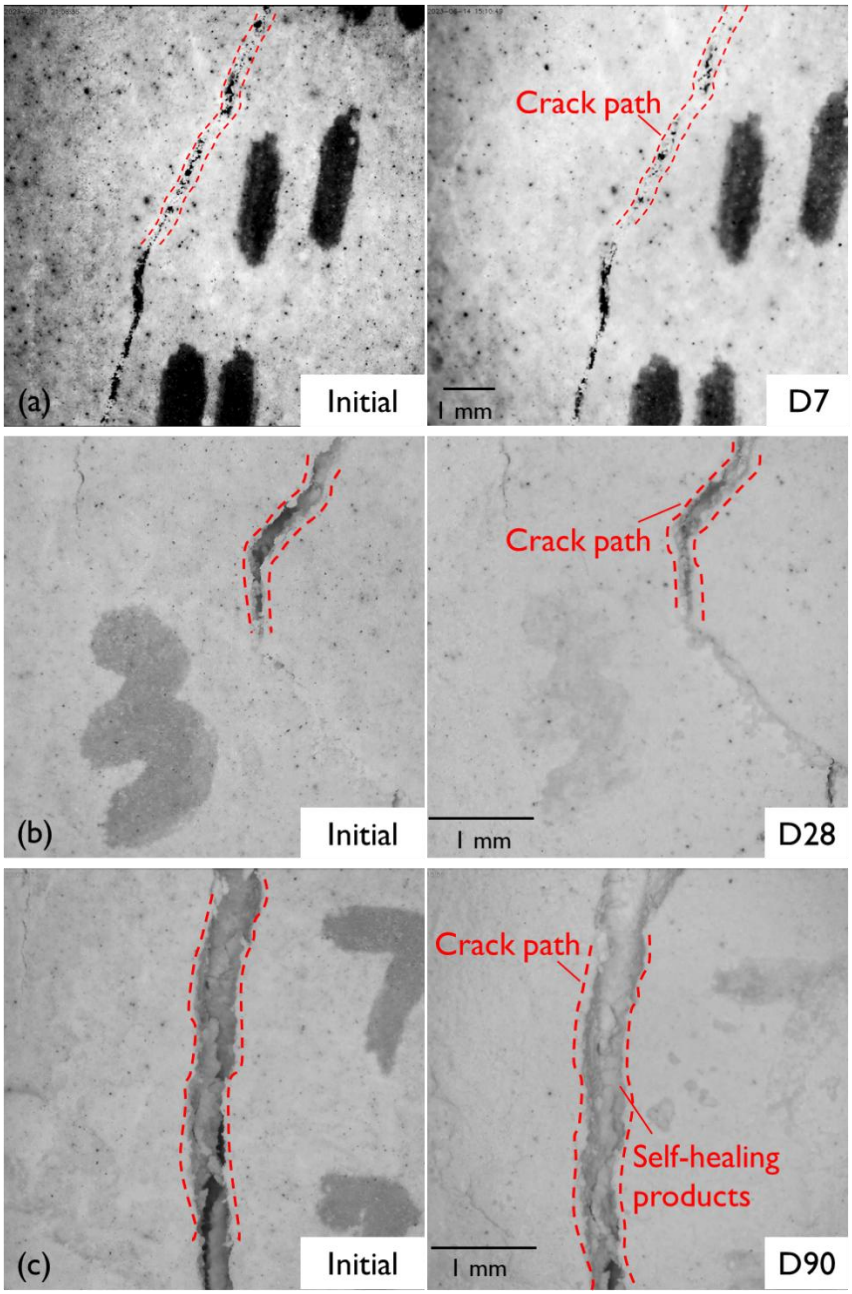

Figure 5-5. Observation of partial healing cracks in CPB specimen with sulphate concentration and self-healing period of (a) 5000 ppm, Day 7; (b) 15000 ppm, Day 28; and (c) 25000 ppm, Day 90.

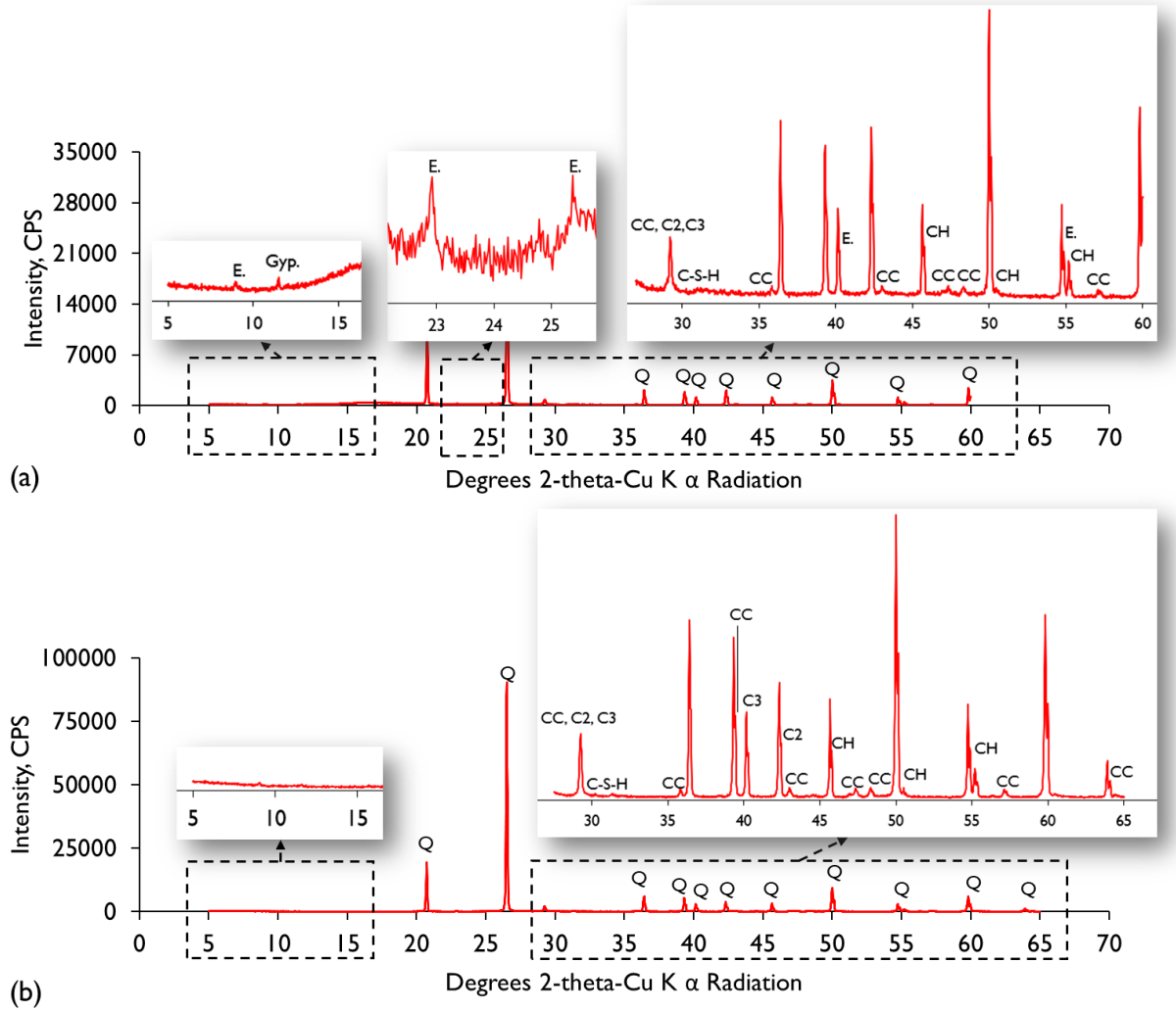

Figure 5-6. XRD patterns of self-healing products collected from (a) CPB specimen with 25000 ppm sulphate concentration after 90 days self-healing period, and (b) sulphate-free CPB specimen after 90 days self-healing period.

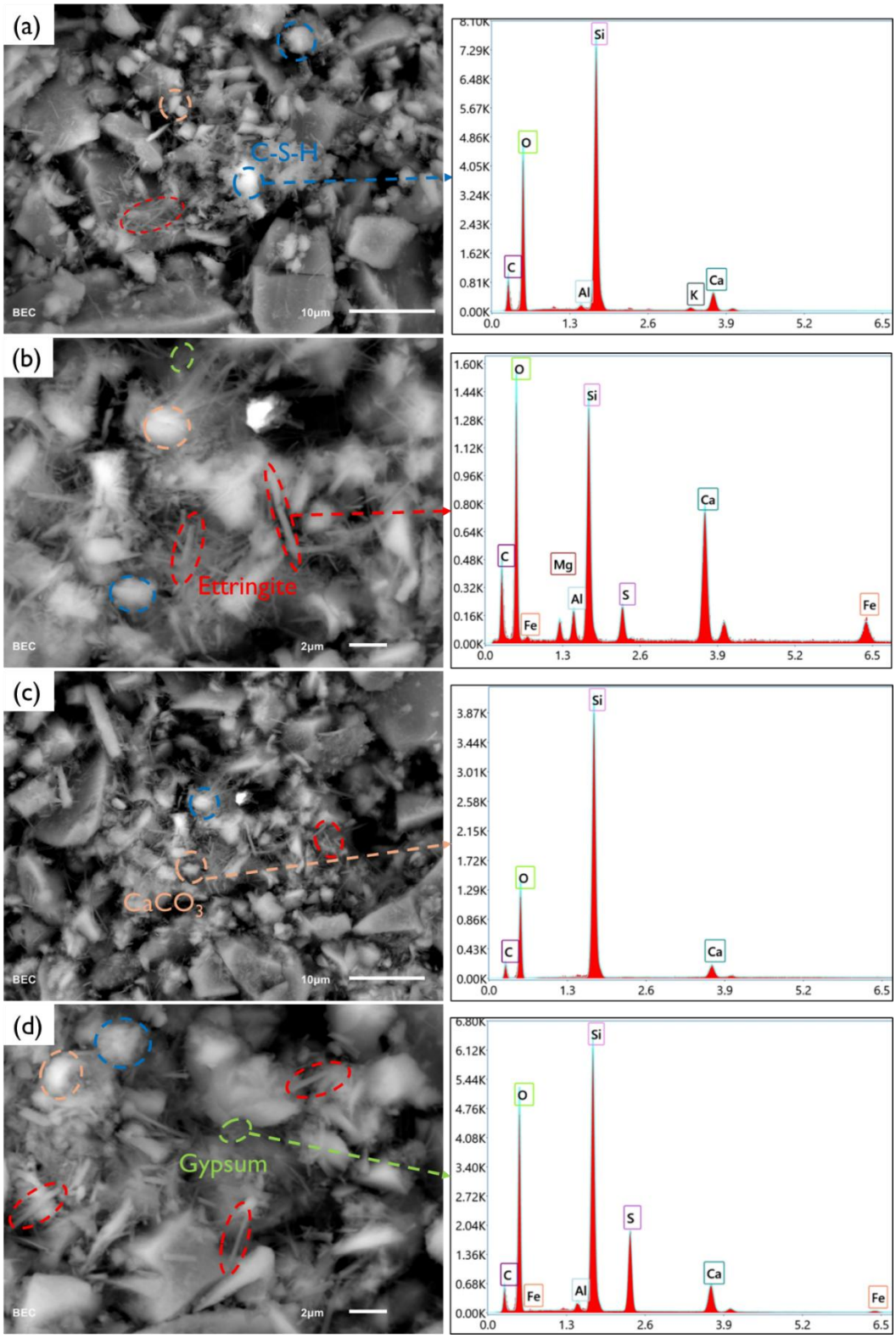

Figure 5-7. SEM-EDS detection of self-healing products inside the cracks after 90 days of self-healing period in the CPB specimen with the sulphate concentration of 5000 ppm (a and b) and 25000 ppm (c and d).

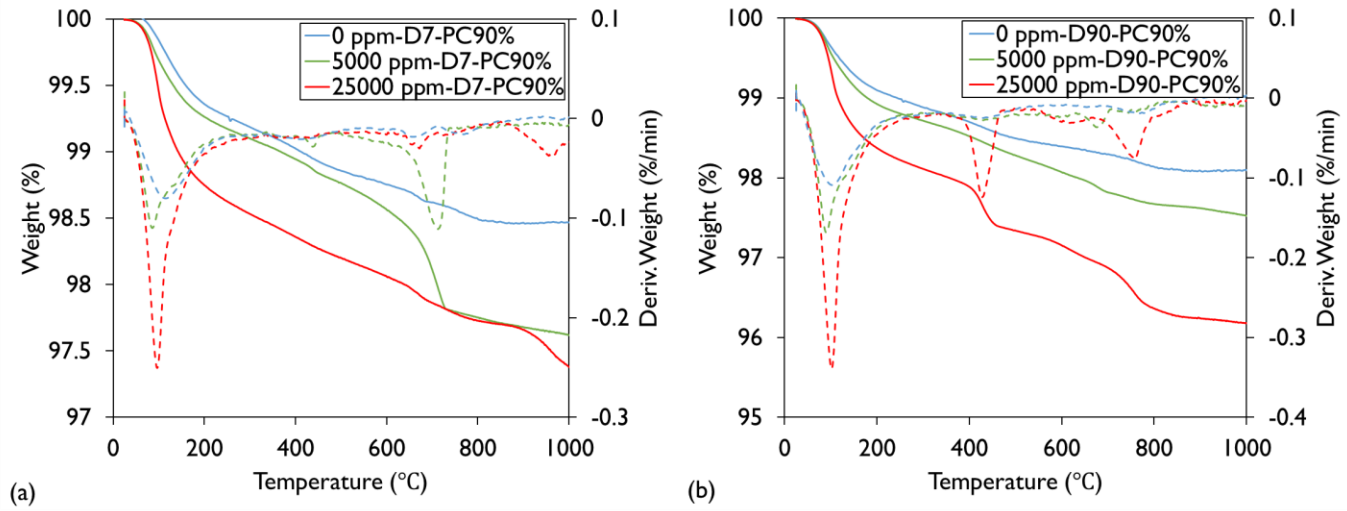

Figure 5-8. TG/DTG comparison of PC90% pre-cracked specimens with the sulphate concentration of 0, 5000, and 25000 ppm at the self-healing period of (a) 7 days and (b) 90 days.

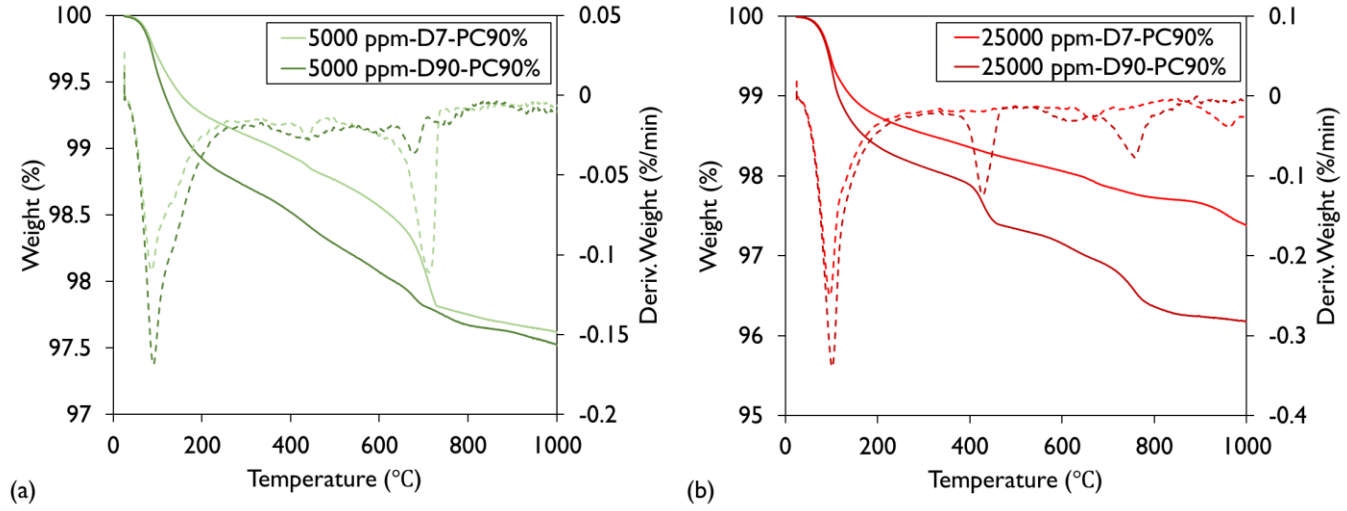

Figure 5-9. TG/DTG comparison of PC90% pre-cracked specimens with the sulphate concentration of (a) 5000 and (b) 25000 ppm after the self-healing period of 7 and 90 days.

5.2.3.3 Mechanical strength recovery

The results regarding the influence of initial sulphate content on the self-healing capacity of CPB to regain its mechanical strength are depicted in Figure 5-10. In this figure, it displays the evolution of UCS and CCS (Eq. 5-3) of pre-cracked specimens with varying initial sulphate concentrations ((a) 0 ppm, (b) 5000 ppm, (c) 15000 ppm, and (d) 25000 ppm) over a self-healing period of up to 90 days, underscoring the significant influence of initial sulphate content on both the evolution of strength in pre-cracked CPBs and the subsequent recovery of mechanical strength. Notably, the impact of initial sulphate content on mechanical strength behaviour and recovery varies depending on the age of the self-healing periods. Distinct differences emerge between early self-healing

periods (28 days or less) and advanced self-healing periods (90 days). Consequently, the following sections will focus on discussing the results of early and advanced self-healing periods.

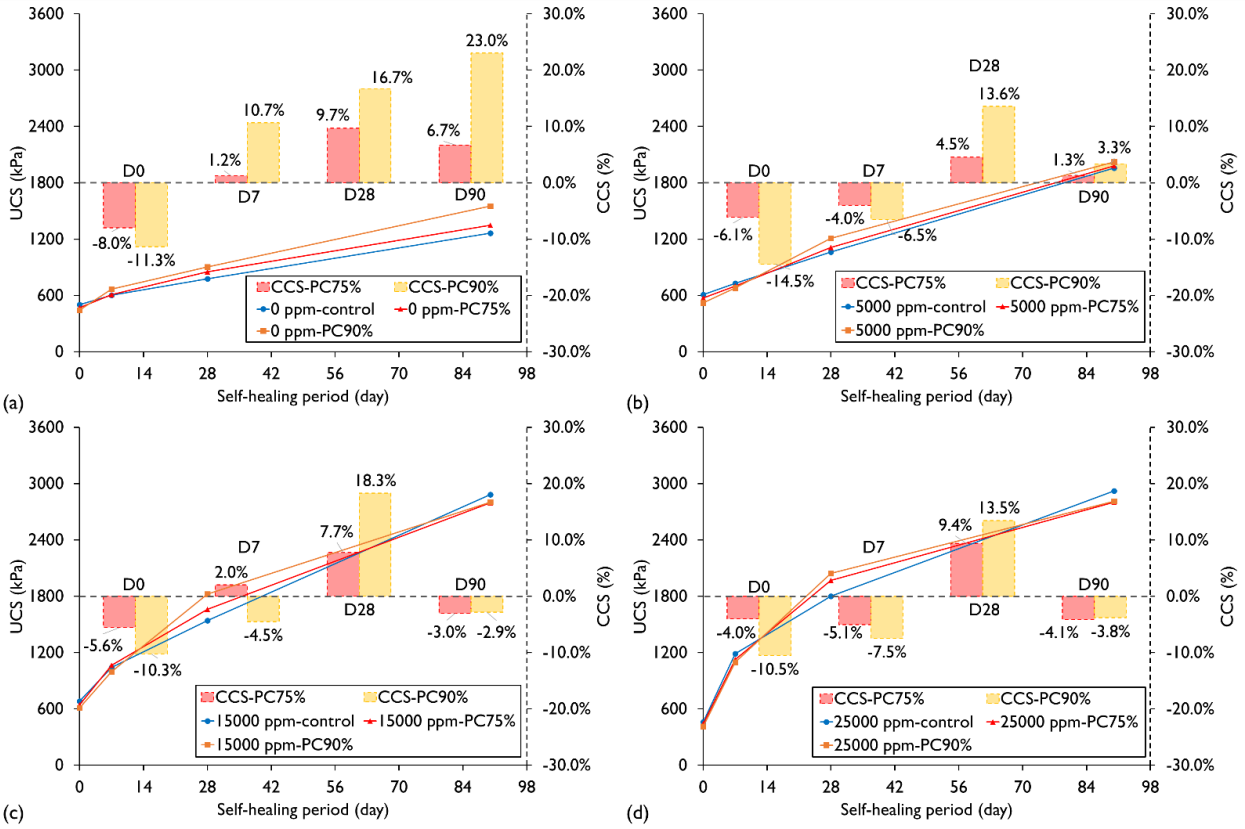

Figure 5-10. Evolution of the UCS and CCS of the studied pre-cracked specimens with different initial sulphate concentrations ((a) 0 ppm, (b) 5000 ppm, (c) 15000 ppm, and (d) 25000 ppm) over self-healing period (D0, D7, D28, and D90: 0, 7, 28 and 90 days of self-healing period, respectively).

Effect of sulphate concentration at early self-healing period

It is observed from Figure 5-10 (b, c) that the control CPB specimens with sulphate concentrations of 15000 and 5000 ppm exhibit higher UCS values in comparison to those without sulphate after the initial curing period. Specifically, they achieve approximately 36% and 21% higher UCS values than the sulphate-free control specimens, respectively. The increase in UCS values can be attributed to the beneficial role of sulphate ions in refining the pore structure of the CPB matrix. When sulphate ions are present within optimal levels, they contribute to the reduction of internal porosity in CPB, thereby enhancing its strength. The secondary hydrated products (i.e., ettringite and gypsum) formed by the reaction of sulphate ions with CH and C_3A fill the empty pores and voids within the CPB matrix (Orejarena & Fall, 2011; Fall & Pokharel, 2010). This argument is supported by the results of porosity (Figure 5-11) and saturated hydraulic conductivity (Figure 5-12) tests performed on control CPBs with various sulphate concentrations. The figures show that the control CPB specimens with sulphate concentrations of 15000 and 5000 ppm have comparatively lower

porosities and permeabilities compared to the control sulphate-free samples due to the refinement of their pore structures. This is in agreement with the SEM observations made in previous studies on the effect of sulphate on CPB that indicate the secondary hydration products precipitate in the pores within the CPB matrix, leading to a decrease in porosity (Pokharel & Fall, 2013). However, the control CPB specimens with 25000 ppm of sulphate show lower strength than the sulphate-free control ones after the initial curing period (Figure 5-10d). This lower strength development is attributed to the inhibition effect of excessively high sulphate concentration on binder hydration. This performance aligns with the previous findings by Xiapeng et al. (2019), which demonstrated that an excessively high sulphate concentration strongly inhibits the early hydration of C_3A. It is also supported by the thermal analysis results conducted on the CPB specimens with 25000 ppm of sulphate concentration at the early self-healing period of Day 7 in Figure 5-9b. The negligible weight losses of CH and $CaCO_3$ decomposition suggest the occurrence of lower binder hydration under the high sulphate concentration.

Furthermore, Figure 5-10 also illustrates the strength recovery and CCS of pre-cracked CPB specimens exposed to various internal sulphate concentrations as the self-healing period progresses, it is generally observed that, irrespective of the pre-cracking level, the presence of sulphate ions benefits the self-healing behaviour during the early self-healing period up to Day 28. The strength development of pre-cracked sulphate-free CPB specimens is also shown in Figure 5-10a for reference. Initially, at Day 0 of self-healing (D0), CPB specimens exhibit lower strength than control specimens after the pre-cracking process. For instance, pre-cracking at PC75% results in an 8.0% reduction in strength, while specimens pre-cracked at PC90% show an 11.3% decline in strength. This decrease in strength observed in pre-cracked CPB specimens correlates with the extent of pre-cracking, where a higher pre-cracking level leads to more pronounced crack generation and propagation within the CPB matrix. These cracks disrupt the integrity of the CPB matrix, thereby contributing to the initial reduction in strength. As the self-healing progresses, it is noticed that the sulphate-free pre-cracked specimens can recover to a similar UCS value as the control specimens or even achieve a higher UCS value than the control ones for the PC90% pre-cracked specimens after the self-healing period of 7 days (D7). The vigorous self-healing behaviour in the sulphate-free specimens during the early stage is mainly attributed to the continuous hydration of unhydrated cement particles within the CPB matrix. The continuous formation of hydration products refines the pore structure and decreases the porosity of the CPB matrix, thereby filling the cracks and capillary voids to contribute to the strength recovery. However, the self-healing performance of the pre-cracked specimens with sulphate concentrations (Figure 5-10b, c, d) is more robust from the self-healing period of 7 days (D7) to 28 days (D28). In Figure 5-10c, it is evident that the PC90% pre-cracked specimens with a sulphate concentration of 15000 ppm show the most significant strength development from D7 to D28, with CCS increasing from -4.5% to 18.3%. Similarly, pre-cracked specimens with sulphate concentrations of 25000 ppm (Figure 5-10d) and 5000 ppm (Figure 5-10b) also exhibit notable strength recoveries during the same period, with CCS increasing from -7.5% to 13.5% and from -6.5% to 13.6%, respectively. The increased CCS values imply that the self-healing behaviour observed in the sulphate-free specimens is also

achieved in the CPB specimens exposed to internal sulphate concentrations, although the self-healing period is slightly delayed. Contrary to previous studies (Yan et al., 2020; Li & Fall, 2016; Pokharel & Fall, 2013; Fall & Pokharel, 2010) that have reported a negative effect of sulphate on other properties of CPB (self-desiccation, strength of undamaged CPB), the presence of sulphate ions here favours the self-healing behaviour within the CPB matrix during the early self-healing period up to Day 28. This performance can be explained by the fact that the precipitation of an adequate amount of secondary hydration products (i.e., ettringite and gypsum) during this period plays a beneficial role in pore filling and microcrack closure in the CPB matrix, thereby positively contributing to the strength of the specimens.

Although the process of crack initiation initially destroys the integrity of the CPB structure, undermining its mechanical strength, the generated cracks can contribute to the progress of self-healing performance. Previous work (Quan & Fall, 2024) has stated that the initiated cracks can provide the pathways for the flow of O_2, CO_2, and H_2O within the CPB matrix, which are essential elements to accelerate the cement hydration and $Ca(OH)_2$ carbonation, thus facilitating the formation of healing products and filling into the cracks to complete the crack closure. Moreover, these generated cracks can provide enough available space to accommodate the precipitation of secondary hydration products, as represented in Figure 5-13. This argument agrees well with the SEM observation in Figure 5-7, where self-healing products are present inside the crack gap, contributing to the crack closure. For example, a 70% larger crack width can be completely healed in the pre-cracked specimen with sulphate concentration of 15000 ppm than in sulphate-free specimens (as listed in Table 5-5). This is because a higher amount of secondary hydration products is produced in the pre-cracked specimens with higher sulphate concentrations to fill the cracks, which in turn refines the pore network and blocks the interconnected pores favouring the strength recovery.

Effect of sulphate concentration at advanced self-healing period

As self-healing continues to the advanced period (Day 90), the sulphate-free pre-cracked CPB specimens exhibit a more pronounced CCS value of up to 23%, as illustrated in Figure 5-10a. The continuous self-healing behaviour can be explained by the aforementioned delayed hydration of unhydrated cement particles and carbonation of $Ca(OH)_2$ within the sulphate-free CPB matrix. The formed hydration products contribute to the continuous refinement of the pore structures, ultimately leading to the regain and development of mechanical strength. This assertion is experimentally supported by the results presented in Figure 5-11a, which demonstrate that the porosity and void ratio of pre-cracked sulphate-free CPB specimens decreases throughout the studied self-healing period. This reduction occurs due to the increased production of hydration products, which fill the cracks and capillary pores.

Similarly, in Figure 5-10b, it is observed that following a self-healing duration of 90 days, the CPB specimens with sulphate concentration of 5000 ppm continue to exhibit positive self-healing characteristics, as evidenced by a continued increase in strength from Day 28 to Day 90. However, it is noteworthy that the rate of strength increase from Day 28 to Day 90 is slower compared to the

early self-healing period (≤ 28 days). For instance, at Day 90, the PC90% pre-cracked specimens demonstrate a CCS value of 3.3%, whereas this value was 13.6% at Day 28. The positive strength recovery observed in the 5000 ppm samples at Day 90 of the self-healing period can be attributed to the lower sulphate concentration compared to the 15000 and 25000 ppm specimens. This lower concentration results in minimal inhibition or no inhibition of cement hydration, allowing for more complete hydration of the cement. Consequently, a greater amount of hydration products precipitate, facilitating the filling of capillary pores and closure of cracks, thereby leading to a further increase in strength. This aligns with the XRD analysis results of the 5000 and 25000 ppm cemented paste samples, depicted in Figure 5-14 a and b, respectively. Notably, Figure 5-14a reveals the absence of dicalcium silicate (C_2S) and tricalcium silicate (C_3S), indicating almost complete cement hydration in the 5000 ppm CPB. Conversely, Figure 5-14b confirms the presence of clinker phases C_3S and C_2S in the 25000 ppm CPB specimen, indicating inhibition of cement hydration in highly sulphated samples. The thermal analysis results in Figure 5-8a also support this argument. In this figure, higher weight losses can be observed at the temperature ranges of 400-450 °C and 600-750 °C, which reveal that more CH and $CaCO_3$ are formed in the CPB specimens with sulphate concentration of 5000 ppm, indicating the occurrence of a higher degree of binder reaction. CPB specimens usually have comparatively high porosity and large capillary pores after a short curing period (i.e., initial curing period of 7 days in this study) (Fall & Samb, 2008). Thus, the presence of sulphate ions combined with the complete binder hydration contributes to the crack closure of microcracks and refinement of the pore structures, resulting in the notable self-healing behaviour of the specimens with 5000 ppm of sulphate concentration at the early self-healing period. Subsequently, more expansive minerals are produced through the secondary hydration reactions at the advanced self-healing period, as illustrated by the thermal analysis in Figure 5-9a. The produced adequate amount of expansive minerals continues to be accommodated within the available cracks and voids, which further facilitates the crack closure and refinement of pore structures. This argument is also supported by the results of previous studies on sulphate effects on the pore structure of CPB (Pokharel & Fall, 2013; Pokharel & Fall, 2011).

However, Figure 5-10 (c, d) indicates that after a self-healing period of 90 days, CPB specimens with higher sulphate concentrations (specifically, 15000 and 25000 ppm) exhibit opposing performance in strength development at the advanced self-healing period (Day 90). Notably, they demonstrate negative values of CCS, indicating that the strengths of pre-cracked specimens with 15000 and 25000 ppm sulphate concentrations are lower than those of their control specimens at the advanced self-healing period of Day 90. The diminished mechanical strength recovery observed in the 15000 and 25000 ppm specimens can be attributed to the cumulative effects of several factors. Firstly, the elevated concentrations of sulphate ions in these specimens, compared to the 5000 ppm specimens, may have facilitated the formation of excessive quantities of expansive minerals such as ettringite and gypsum within the microcracks and capillary pores. This formation occurs through the reaction of sulphate ions with C_3A and CH, respectively. The accumulation of excessive amounts of ettringite and gypsum could have exerted substantial expansive pressure on the walls of preexisting microcracks and capillary pores. Consequently, this pressure might have caused

physical damage to the cemented matrix of the highly sulphated specimens, leading to the generation of new cracks (as represented in Figure 5-13b). Additionally, it may have contributed to the coarsening of the pore structure in the highly sulphated samples compared to the 5000 ppm samples. This pore structure alteration is evidently associated with a decrease in their strength. The results of the thermal analysis performed on the PC90% pre-cracked specimens with sulphate concentrations of 25000, 5000, and 0 ppm after self-healing period of D90, are presented in Figure 5-8b to support this explanation. It can be seen that more expansive minerals are produced in sulphate-containing specimens than in sulphate-free specimens, and that the amount of expansive minerals formed increases as the sulphate concentration increases. In addition, the volumes of the formed ettringite and gypsum are approximately 2.5 times and 1.24 times that of the original reactant, respectively (Liu et al., 2019). The above-mentioned generation of new microcracks and the coarsening of the pore structure of the highly sulphated specimens due to the presence of an excessive amount of expansive minerals are in substantial agreement with the porosity and permeability test results shown in Figure 5-11 and Figure 5-12, respectively. These figures show that after 90 days of self-healing, the porosity and hydraulic conductivity values of the highly sulphated specimens (15000, 25000 ppm) are higher than those of the specimens with 5000 ppm and no sulphate concentration.

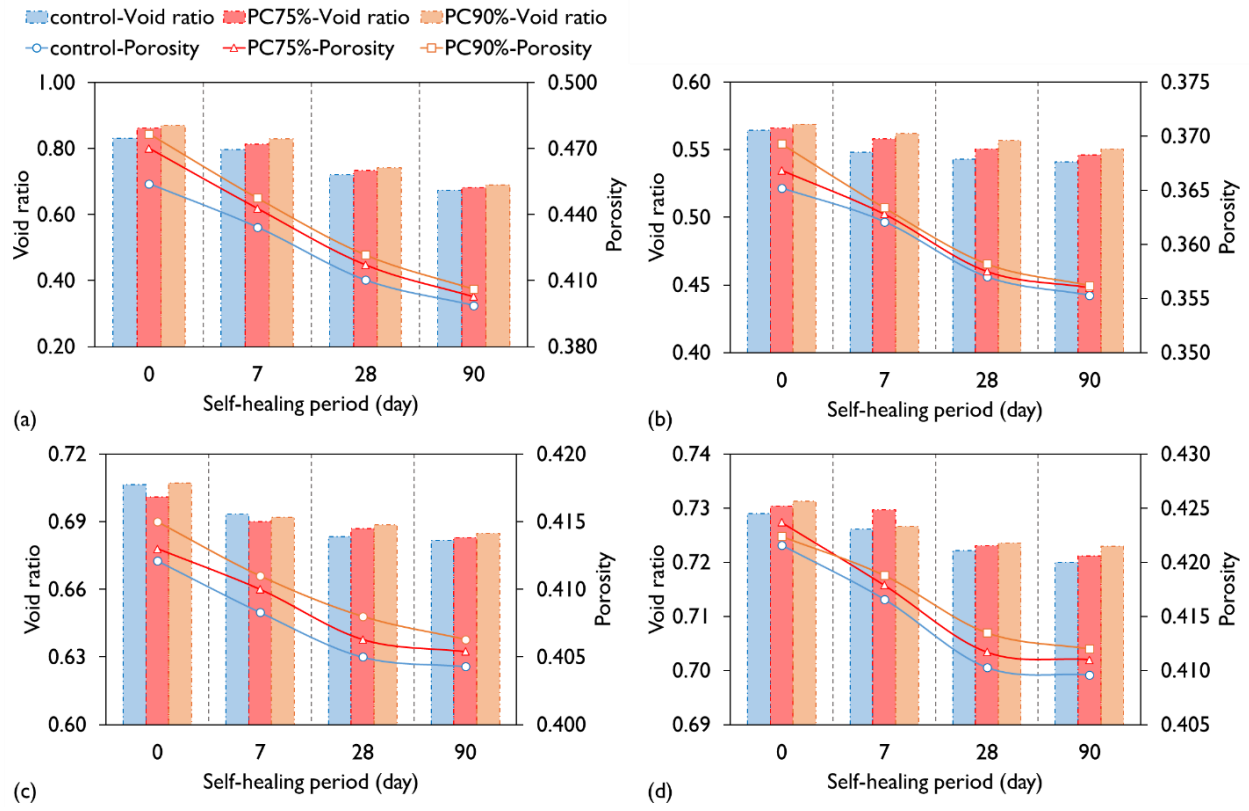

Figure 5-11. Changes of porosity and void ratio of specimens with varying sulphate concentrations (a) 0 ppm, (b) 5000 ppm, (c) 15000 ppm, and (d) 25000 ppm over the self-healing period.

Secondly, sulphate absorption by C-S-H should be considered as an additional factor inducing the diminished self-healing performance of the highly sulphated specimens. As the strength of Portland cementitious materials is dominated by the binding ability of C-S-H, a weaker C-S-H gel would lead to weak strength. A weaker C-S-H gel is usually produced due to the sulphate absorption by C-S-H. The undermined binding ability of C-S-H to other hydration products leads to the slow increase or cessation of strength development (Fall & Pokharel, 2010). This argument can be supported by thermal analysis in Figure 5-8b. In this figure, a significant amount of expansive minerals and CH can be detected in the specimens with 25000 ppm sulphate concentration after the self-healing period of D90. Besides, only a small intensity of gypsum is detected in the self-healing products, as illustrated by XRD analysis in Figure 5-6a. Therefore, the presence of a large amount of CH and a rare amount of gypsum suggests that the sulphate ions remaining in the CPB system are insufficient for the reaction with CH to produce gypsum due to sulphate absorption by C-S-H. The sulphate absorption leads to the formation of additional lower quality C-S-H, thereby contributing to the reduction of CPB strength and deterioration of self-healing performance. This finding is also in agreement with the conclusion of previous studies (Neto et al., 2021; Fall & Pokharel, 2010; Jelenić et al., 1977).

Finally, another contributing factor to the diminished strength recovery performance of the highly sulphated specimens is the presence of elevated sulphate concentrations. This presence reduces the quantity of hydration products precipitated within the pores and cracks of the specimens compared to those with lower (5000 ppm) or no sulphate content. This reduction occurs due to the inhibition of cement hydration at high sulphate concentrations. Consequently, the lower amount of hydration products correlates directly with a reduced ability for self-healing. This inhibitory effect is substantiated by the XRD results outlined in Figure 5-14, as discussed earlier.

5.2.3.4 Pore structure and permeability changes during self-healing of CPB with different sulphate concentrations

Key factors influencing the environmental performance and durability of CPBs include the permeability (hydraulic conductivity) and pore structure, including parameters such as porosity and void ratio. Figure 5-11 and Figure 5-12 show the variations in porosity, void ratio, and saturated hydraulic conductivity (k_{sat}) of the pre-cracked CPB specimens across different sulphate concentrations (0, 5000, 15000, and 25000 ppm) over the self-healing period. In Figure 5-11, it is observed that the porosity and void ratio of the CPB specimens with sulphate are lower than those of sulphate-free specimens after the initial curing period. This performance associated with sulphate concentrations can be explained by the fact that sulphate ions can contribute to the decrease of CPB internal porosity due to the precipitation of secondary hydrated minerals within the capillary pores and voids, as discussed earlier. Moreover, it is noted in Figure 5-11b that the pre-cracked CPB specimens with sulphate concentration of 5000 ppm could achieve the lowest porosity and void ratio. This is due to the absence of an inhibition effect in 5000 ppm sulphate concentration (see Figure 5-14a), which facilitates the formation of hydration products to refine the pore structure (Li & Fall, 2018). This can also be demonstrated by the saturated hydraulic

conductivity of CPB specimens with 5000 ppm of sulphate concentration as shown in Figure 5-12b. It is noticed that the PC90% pre-cracked specimen with sulphate concentration of 5000 ppm exhibits a consistent recovery of saturated hydraulic conductivity with an HCRR value reaching 94.6% after the self-healing period of Day 90. The adequate amount of expansive minerals formed in the cracks and pores results in the refinement of the microstructure, thus, in turn contributing to the hydraulic conductivity recovery and decrease. In the same way, significant recovery of hydraulic conductivity is also observed in the pre-cracked CPB specimens with the sulphate concentration of 15000 during the early self-healing period up to D28. For example, the PC90% pre-cracked specimens achieve an approximately 30% increase in HCRR, indicating a remarkable refinement of the pore structures. This improvement is attributed to the formation of adequate secondary hydration products, which also accounts for the promising self-healing efficiency in mechanical strength as previously discussed. However, as the self-healing progresses to the advanced period, the newly generated cracks caused by excessive pressure start to appear within the CPB matrix with high sulphate concentrations (15000 and 25000 ppm). These newly formed cracks counteract the benefits gained from the microcrack closure and pore filling with expansive minerals. This is illustrated in Figure 5-11 (c, d) and Figure 5-12 (c, d), in which insignificant changes in porosity and void ratio, and saturated hydraulic conductivity can be observed at advanced self-healing periods. The saturated hydraulic conductivity of the control specimen with sulphate concentration of 25000 ppm even increases from the self-healing period of D28 to D90, resulting in an HCRR value of only 59.2%. The increased value of saturated hydraulic conductivity can be caused by the excessive amount of expansive minerals (as illustrated by the thermal analysis in Figure 5-8b). These expansive minerals could have exerted excessive pressure on the pore structure of the CPB specimens with sulphate concentrations of 25000 and 15000 ppm. This pressure would result in the new formation of microcracks, as evidenced by findings from (Pokharel & Fall, 2013), thus undermining the self-healing performance.

Although the CPB specimens with sulphate concentrations of 5000 and 0 ppm demonstrate constantly positive self-healing characteristics as previously discussed, it is noticed that the hydraulic conductivity values of the pre-cracked specimens cannot achieve a complete recovery, obtaining equivalent values as control specimens after the studied self-healing period, as illustrated in Figure 5-12 (a, b). This is due to the existence of macrocracks within the CPB matrix, which significantly impacts the permeability performance of the CPB structure. During the process of crack initiation, the microcracks start to appear when the applied pre-cracking load falls in the plastic zone (the first non-linear deformation region in the strain-stress curve as shown in Figure 5-3). As the pre-cracking level approaches the peak stress region, more microcracks will be generated and gradually connected to form macrocracks within the CPB matrix (Wang et al., 2024; He et al., 2021; Fall et al., 2007). Furthermore, as aforementioned, the self-healing behaviour in CPB specimens is attributed to the continuous hydration of unhydrated cement particles, carbonation of CH, and the formation of secondary hydration products when exposed to internal sulphate. It implies that an insufficient amount of the formed self-healing products limits the crack closure capability of CPB materials, resulting in partial healing or no healing scenarios in the crack

closure as previously discussed. Therefore, the opening of macrocracks in the pre-cracked specimens leads to higher hydraulic conductivity even after the self-healing process.

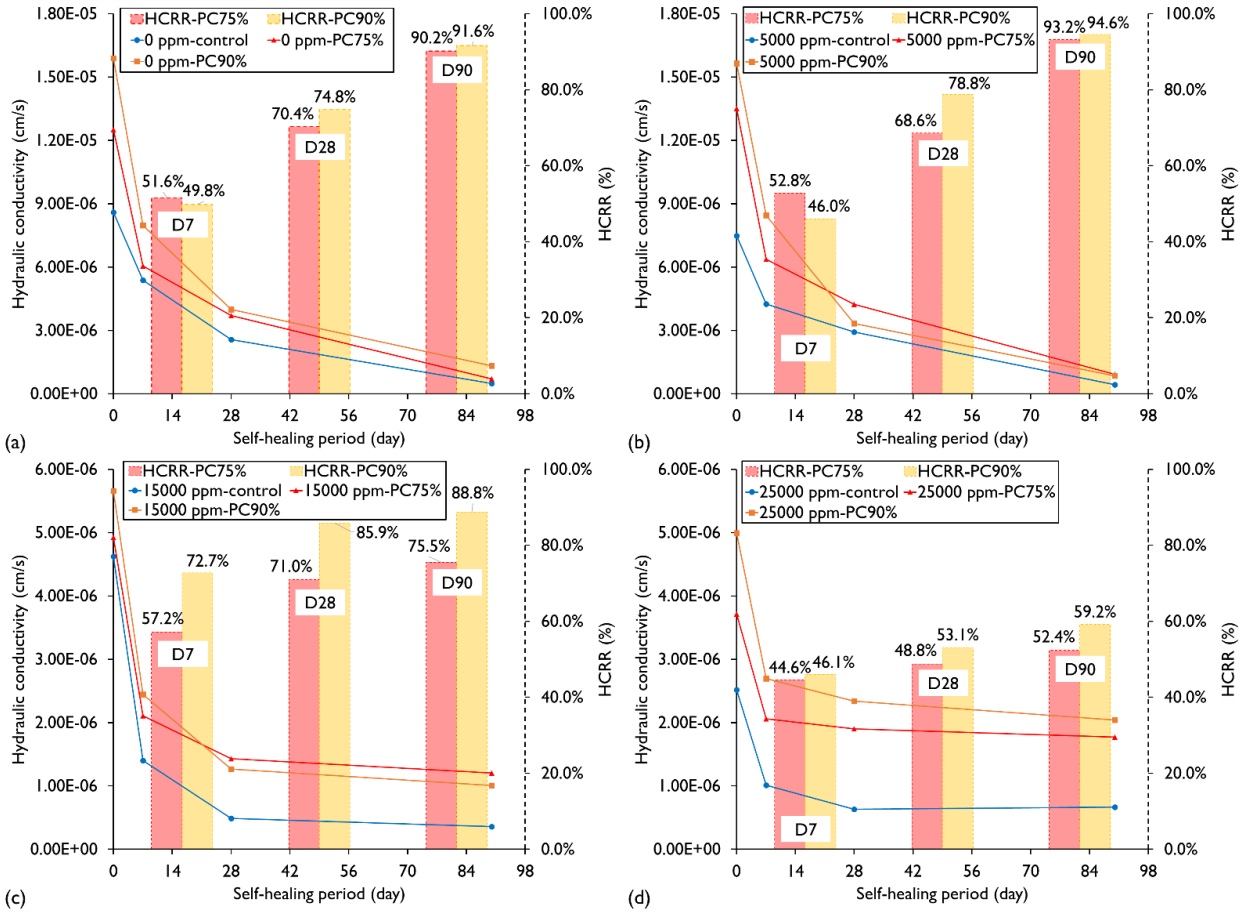

Figure 5-12. Changes of hydraulic conductivity and HCRR of CPB with different sulphate concentrations ((a) 0 ppm, (b) 5000 ppm, (c) 15000 ppm, and (d) 25000 ppm) over self-healing period (D7, D28, and D90: 7, 28 and 90 days of self-healing period, respectively).

5.2.4 Summary and Conclusions

This paper presents the experimental results of a study that investigates the effect of internal sulphate exposure on the self-healing behaviour of CPB mixtures with various self-healing periods (0, 7, 28, and 90 days). Based on the research findings, the following conclusions are determined.

- Sulphate ions within the CPB mixture enhance the self-healing performance in crack closure, particularly in the first 28 days of self-healing, due to the precipitation of secondary hydrated minerals and cement hydration products. As progressing to the 90 days of self-healing period, the pre-cracked specimen with sulphate concentration of 5000 ppm performs a constantly positive impact on crack closure. However, pre-cracked CPB specimens with sulphate concentrations of 15000 and 25000 ppm exhibit diminished performance in crack closure due to sulphate attack induced deterioration.

- The results of analytical techniques reveal that a large amount of ettringite combined with gypsum, C-S-H, $Ca(OH)_2$, and $CaCO_3$ contribute to the crack closure and self-healing performance within the CPB matrix when subjected to the sulphate concentrations. The presence of ettringite and gypsum results from the reactions between C_3A and CH with sulphate ions, while C-S-H and $Ca(OH)_2$ arise from cement hydration and $CaCO_3$ from carbonation.
- All studied sulphate concentrations favour the self-healing performance in mechanical strength of the CPB matrix at the early self-healing period up to Day 28. The PC90% pre-cracked specimens with sulphate concentration of 15000 ppm demonstrate the most significant strength development. The favorable strength recovery is mainly attributed to the precipitation of an adequate amount of secondary hydration and cement hydration products.
- The CPB specimens with sulphate concentration of 5000 ppm maintain a consistently positive self-healing performance in strength recovery over the entire studied self-healing period attributed to the absence of inhibition effect. However, CPB specimens with sulphate concentrations of 15000 and 25000 ppm have an opposite performance at the advanced self-healing period of D90. The negative effect of high sulphate concentrations can be explained by three factors: (i) the physical damage due to the formation of excessive amounts of expansive minerals in the microcracks and capillary pores, (ii) the production of weaker C-S-H gel because of sulphate absorption by C-S-H, and (iii) the lower amount of hydration products due to inhibition of cement hydration at high sulphate concentrations.
- Additionally, saturated hydraulic conductivity shows a self-healing performance similar to mechanical strength. Due to the presence of macrocracks and limited amounts of healing products, the pre-cracked specimens cannot easily achieve a complete recovery in permeability property.

Despite the significant findings of this research and their relevance to CPB technology, the study only explored self-healing periods up to 90 days. The long-term effects of sulphate on self-healing performance over extended periods (e.g., one year or more) remain unknown. Additionally, in the field, backfill structures may be subjected to curing temperatures significantly higher or lower than the room temperatures used in this study. The combined effect of sulphate exposure and varying curing temperatures on self-healing performance has yet to be determined. Furthermore, this research used only synthetic silica tailings composed primarily of quartz for the CPB samples. While quartz is the dominant mineral in many hard rock mine tailings, natural tailings can exhibit a wide variety of mineral compositions. The impact of tailings composed of different minerals on the self-healing performance of CPB under sulphate exposure is still unclear. Future studies should address these knowledge gaps to provide a more comprehensive understanding of self-healing behaviour in CPB systems, ultimately improving their design and durability.

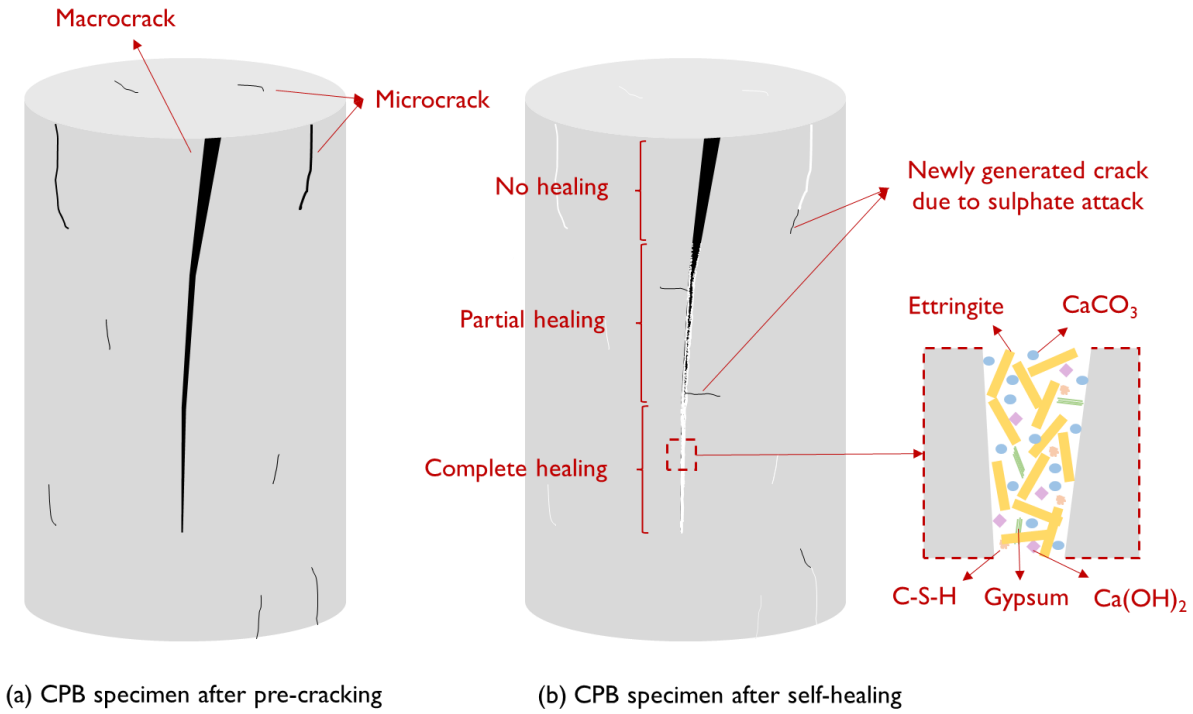

Figure 5-13. Schematic representation of self-healing mechanism subjected to internal sulphate exposure when CPB specimen (a) after pre-cracking, and (b) after self-healing.

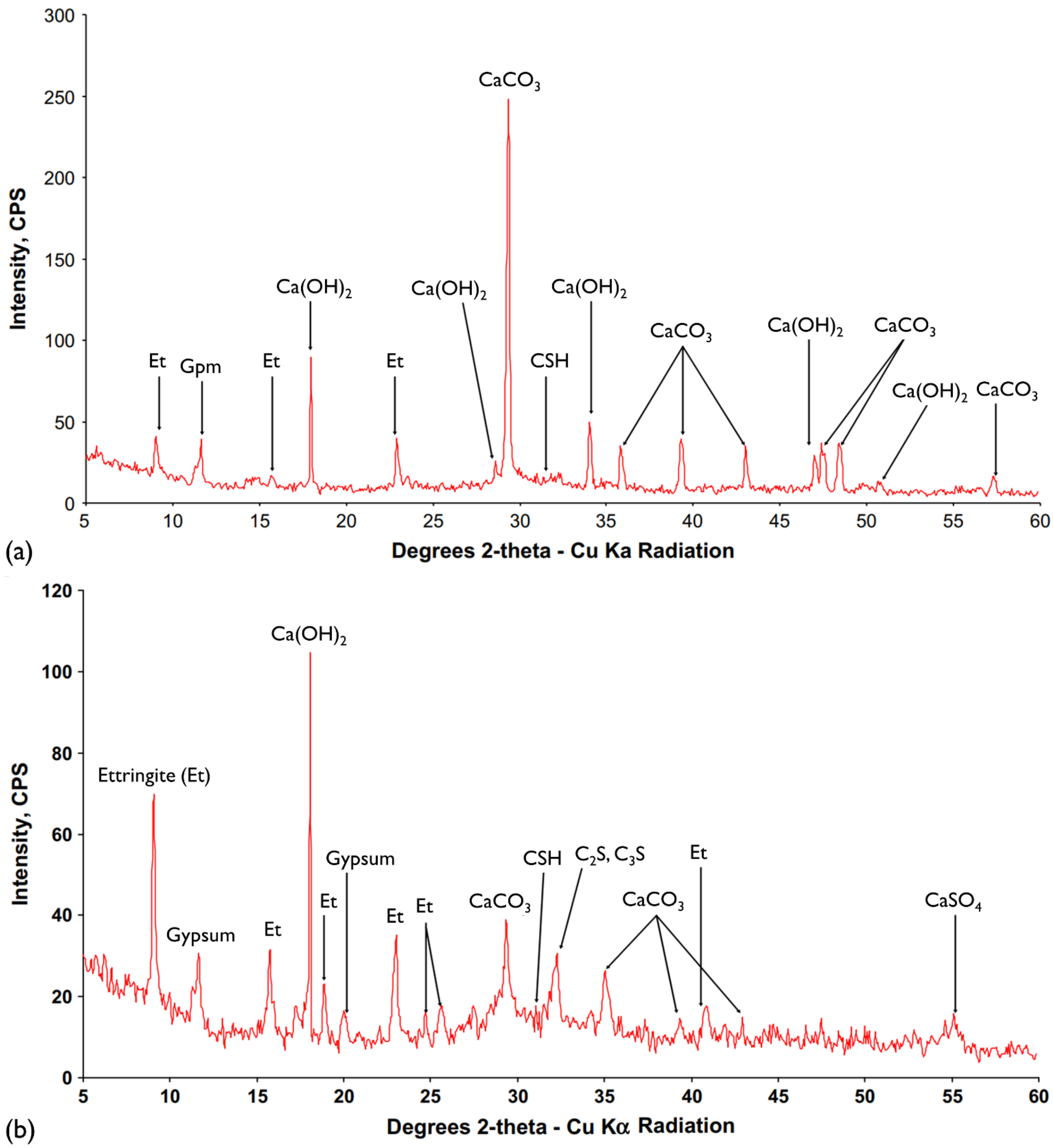

Figure 5-14. XRD results of a) 5000 ppm and b) 25000 ppm mature cement pastes of CPB (Pokharel & Fall, 2013).

5.2.5 References

Aldhafeeri, Z., & Fall, M. Sulphate induced changes in the reactivity of cemented tailings backfill. International Journal of Mineral Processing 166 (2017), 13-23.

Al-Moselly, Z., Fall, M., & Haruna, S. (2022). Further insight into the strength development of cemented paste backfill materials containing polycarboxylate ether-based superplasticizer. Journal of Building Engineering, 47, 103859.

Andrade Neto, J. d. S., De la Torre, A. G., & Kirchheim, A. P. (2021). Effects of sulfates on the hydration of Portland cement – A review. Construction and Building Materials, 279, 122428.

ASTM. (2016). ASTM D5084-16a. Standard Test Methods for Measurement of Hydraulic Conductivity of Saturated Porous Materials Using a Flexible Wall Permeameter. In. West Conshohocken, PA: ASTM International.

ASTM. (2020). ASTM C143/C143M-20. Standard Test Method for Slump of Hydraulic-Cement Concrete. In. West Conshohocken, PA: ASTM International.

ASTM. (2021). ASTM C39/C39M-21. Standard Test Method for Compressive Strength of Cylindrical Concrete Specimens. In. West Conshohocken, PA: ASTM International.

Behera, S. K., Mishra, D. P., Singh, P., Mishra, K., Mandal, S. K., Ghosh, C. N., . . . Mandal, P. K. (2021). Utilization of mill tailings, fly ash and slag as mine paste backfill material: Review and future perspective. Construction and Building Materials, 309, 125120.

Belem, T., & Benzaazoua, M. (2007). Design and Application of Underground Mine Paste Backfill Technology. Geotechnical and Geological Engineering, 26(2), 147-174.

Benzaazoua, M., Fall, M., & Belem, T. (2004). A contribution to understanding the hardening process of cemented pastefill. Minerals Engineering, 17(2), 141-152.

Benzaazoua, M., Ouellet, J., Servant, S., Newman, P., & Verburg, R. (1999). Cementitious backfill with high sulfur content Physical, chemical, and mineralogical characterization. Cement and Concrete Research, 29(5), 719-725.

De Belie, N., Gruyaert, E., Al-Tabbaa, A., Antonaci, P., Baera, C., Bajare, D., . . . Jefferson, T. (2018). A review of self-healing concrete for damage management of structures. Advanced materials interfaces, 5(17), 1800074.

Ercikdi, B., Baki, H., & Izki, M. (2013). Effect of desliming of sulphide-rich mill tailings on the long-term strength of cemented paste backfill. J Environ Manage, 115, 5-13.

Fall, M., Adrien, D., Célestin, J. C., Pokharel, M., & Touré, M. (2009). Saturated hydraulic conductivity of cemented paste backfill. Minerals Engineering, 22(15), 1307-1317.

Fall, M., Belem, T., Samb, S., & Benzaazoua, M. (2007). Experimental characterization of the stress–strain behaviour of cemented paste backfill in compression. Journal of Materials Science, 42(11), 3914-3922.

Fall, M., & Benzaazoua, M. (2005). Modeling the effect of sulphate on strength development of paste backfill and binder mixture optimization. Cement and Concrete Research, 35(2), 301-314.

Fall, M., Benzaazoua, M., & Ouellet, S. (2004). Effect of tailings properties on paste backfill performance. Paper presented at the Proceedings of the 8th International Symposia on Mining with Backfill, Beijing, China.

Fall, M., & Pokharel, M. (2010). Coupled effects of sulphate and temperature on the strength development of cemented tailings backfills: Portland cement-paste backfill. Cement and concrete composites, 32(10), 819-828.

Fall, M., & Samb, S. S. (2008). Pore structure of cemented tailings materials under natural or accidental thermal loads. Materials Characterization, 59(5), 598-605.

Fall, M., & Samb, S. S. (2009). Effect of high temperature on strength and microstructural properties of cemented paste backfill. Fire Safety Journal, 44(4), 642-651.
Ferrara, L., Krelani, V., Moretti, F., Flores, M. R., & Ros, P. S. (2017). Effects of autogenous healing on the recovery of mechanical performance of High Performance Fibre Reinforced Cementitious Composites (HPFRCCs): Part 1. Cement and concrete composites, 83, 76-100.
Ghirian, A., & Fall, M. (2016). Strength evolution and deformation behaviour of cemented paste backfill at early ages: Effect of curing stress, filling strategy and drainage. International Journal of Mining Science and Technology, 26(5), 809-817.
Haruna, S. (2022). Effect of superplasticizer on the performance properties of cemented paste backfill at different curing temperatures. Université d'Ottawa/University of Ottawa,
He, Z., Zhao, K., Yan, Y., Ning, F., Zhou, Y., & Song, Y. (2021). Mechanical response and acoustic emission characteristics of cement paste backfill and rock combination. Construction and Building Materials, 288, 123119.
Jelenić, I., Panović, A., Halle, R., & Gaćeša, T. (1977). Effect of gypsum on the hydration and strength development of commercial portland cements containing alkali sulfates. Cement and Concrete Research, 7(3), 239-245.
Jiang, H., Yi, H., Yilmaz, E., Liu, S., & Qiu, J. (2020). Ultrasonic evaluation of strength properties of cemented paste backfill: Effects of mineral admixture and curing temperature. Ultrasonics, 100, 105983.
Kesimal, A., Yilmaz, E., Ercikdi, B., Alp, I., & Deveci, H. (2005). Effect of properties of tailings and binder on the short-and long-term strength and stability of cemented paste backfill. Materials Letters, 59(28), 3703-3709.
Klein, K., & Simon, D. (2006). Effect of specimen composition on the strength development in cemented paste backfill. Canadian Geotechnical Journal, 43(3), 310-324.
Li, W., & Fall, M. (2016). Sulphate effect on the early age strength and self-desiccation of cemented paste backfill. Construction and Building Materials, 106, 296-304.
Li, W., & Fall, M. (2018). Strength and self-desiccation of slag-cemented paste backfill at early ages: Link to initial sulphate concentration. Cement and concrete composites, 89, 160-168.
Liu, H., Zhang, Q., Gu, C., Su, H., & Li, V. (2017). Self-healing of microcracks in Engineered Cementitious Composites under sulfate and chloride environment. Construction and Building Materials, 153, 948-956.
Liu, H., Zhang, Q., Li, V., Su, H., & Gu, C. (2017). Durability study on engineered cementitious composites (ECC) under sulfate and chloride environment. Construction and Building Materials, 133, 171-181.
Liu, L., Zhu, C., Qi, C., Zhang, B., & Song, K.-I. (2019). A microstructural hydration model for cemented paste backfill considering internal sulfate attacks. Construction and Building Materials, 211, 99-108.
Maes, M., & De Belie, N. (2014). Resistance of concrete and mortar against combined attack of chloride and sodium sulphate. Cement and concrete composites, 53, 59-72.
Nasir, O., & Fall, M. (2010). Coupling binder hydration, temperature and compressive strength development of underground cemented paste backfill at early ages. Tunnelling and Underground Space Technology, 25(1), 9-20.
Neville, A. (2004). The confused world of sulfate attack on concrete. Cement and Concrete Research, 34(8), 1275-1296.

Niu, Y., Han, F., & Liu, Q. (2023). Effect of age and sulfate chloride environment on the Self-Healing performance of the desert sand engineered cementitious composite materials. Construction and Building Materials, 408, 133806.
Orejarena, L., & Fall, M. (2011). Artificial neural network based modeling of the coupled effect of sulphate and temperature on the strength of cemented paste backfill. Canadian Journal of Civil Engineering, 38(1), 100-109.
Pokharel, M., & Fall, M. (2011). Coupled Thermochemical Effects on the Strength Development of Slag-Paste Backfill Materials. Journal of Materials in Civil Engineering, 23(5), 511-525.
Pokharel, M., & Fall, M. (2013). Combined influence of sulphate and temperature on the saturated hydraulic conductivity of hardened cemented paste backfill. Cement and concrete composites, 38, 21-28.
Quan, W., & Fall, M. (2024). Investigation of Inherent Self-Healing Behaviour in Cemented Paste Backfill. Paper presented at the 14th International Symposium on Mining with Backfill, Minefill 2024, Vancouver, Canada.
Qureshi, T., & Al-Tabbaa, A. J. A. f. m. (2020). Self-healing concrete and cementitious materials. 32, 137-144.
Van Breugel, K. (2007). Is there a market for self-healing cement-based materials. Paper presented at the Proceedings of the first international conference on self-healing materials.
Van Tittelboom, K., & De Belie, N. (2013). Self-Healing in Cementitious Materials-A Review. Materials (Basel), 6(6), 2182-2217.
Walske, M. L., McWilliam, H., Doherty, J., & Fourie, A. (2016). Influence of curing temperature and stress conditions on mechanical properties of cementing paste backfill. Canadian Geotechnical Journal, 53(1), 148-161.
Wang, B., Yang, L., Li, Q., Shu, X., & Kang, M. (2024). Mechanical behavior, acoustic emission and principal strain field evolution properties of layered cemented paste backfill under unconfined compression. Construction and Building Materials, 415, 135111.
Wang, Y., Cao, Y., Cui, L., Si, Z., & Wang, H. (2020). Effect of external sulfate attack on the mechanical behavior of cemented paste backfill. Construction and Building Materials, 263, 120968.
Wu, A., Wang, Y., Wang, H., Yin, S., & Miao, X. (2015). Coupled effects of cement type and water quality on the properties of cemented paste backfill. International Journal of Mineral Processing, 143, 65-71.
Xiang, J., Li, Z., Qiu, J., Wu, N., & Cheng, H. (2023a). Investigating the potential for porous ceramics as bacterial carrier in self-healing cemented paste backfill. Ceramics International, 49(9), 13490-13500.
Xiang, J., Qiu, J., Yuan, L., Wu, J., & Ma, Z. (2023b). Characterization and role analysis of bacteria types in self-healing behaviour of cemented paste backfill. Journal of Building Engineering, 75, 106964.
Xiapeng, P., Fall, M., & Haruna, S. (2019). Sulphate induced changes of rheological properties of cemented paste backfill. Minerals Engineering, 141, 105849.
Yan, B., Zhu, W., Hou, C., Yu, Y., & Guan, K. (2020). Effects of coupled sulphate and temperature on internal strain and strength evolution of cemented paste backfill at early age. Construction and Building Materials, 230, 116937.
Yıldırım, G., Khiavi, A. H., Yeşilmen, S., & Şahmaran, M. (2018). Self-healing performance of aged cementitious composites. Cement and concrete composites, 87, 172-186.

Yilmaz, E., Belem, T., & Benzaazoua, M. (2014). Effects of curing and stress conditions on hydromechanical, geotechnical and geochemical properties of cemented paste backfill. Engineering Geology, 168, 23-37.

Yilmaz, E., Kesimal, A., Ercikdi, B., Benzaazoua, M., Belem, T., & Bussière, B. (2005). Short and long terms strength performances of cemented paste backfill. Paper presented at the 19th Int. Mining Congress and Fair of Turkey, MCET2005, Kozan Ofset Matbaacilik, Izmir, Turkey.

Yoo, D.-Y., Shin, W., Chun, B., & Banthia, N. (2020). Assessment of steel fiber corrosion in self-healed ultra-high-performance fiber-reinforced concrete and its effect on tensile performance. Cement and Concrete Research, 133, 106091.

5.3 Paper III: Crack Self-Healing Capacity and Performance Recovery of Cemented Paste Backfill: Influence of Temperature

Published in *Case Studies in Construction Materials*, Volume 21, e04105

Weizhou Quan, Mamadou Fall

Department of Civil Engineering, University of Ottawa, Ottawa, Ontario, Canada

Abstract

Cemented paste backfill (CPB) is an innovative cementitious construction material widely used to stabilize underground mine structures and minimize the mine's environmental impact. Understanding the factors that influence the self-healing efficiency of CPB is essential to optimize its design and improve its durability. In real-world applications, CPB structures are often exposed to varying curing temperatures, which can affect their self-healing ability. However, the specific impact of temperature on the self-healing capacity of CPB is not yet clearly established. This study experimentally investigates the effects of temperature (i.e., 2°C, 20°C, 35°C, and 50°C) on the self-healing performance of CPB. The self-healing efficiency was evaluated through observations of crack closure, mechanical strength tests, hydraulic conductivity measurements, and assessments of physical properties (i.e., porosity and void ratio). The results demonstrate that temperature significantly influences CPB's self-healing performance. Elevated temperatures (35°C and 50°C) enhance the self-healing process within the CPB matrix compared to room temperature (20°C), primarily due to accelerated binder hydration. The pre-cracked CPB specimens can restore their strength and achieve up to approximately 31 % higher strength than uncracked specimens after 28 days of self-healing. However, the pre-cracked specimens cured at low temperature (i.e., 2°C) exhibit low self-healing capacity, particularly at early ages. The low curing temperature significantly delays the onset of the self-healing process in CPB material. Moreover, analytical techniques reveal that an amount of healing products, mainly consisting of C-S-H, $Ca(OH)_2$, and $CaCO_3$, contribute to this promising self-healing performance. The findings from this paper have important practical implications for the design, mechanical stability, and durability of CPB structures, providing valuable insights for engineering practices.

Keywords: Cemented paste backfill; Self-healing; Mine; Tailings; Mechanical properties; Hydraulic conductivity; Temperature.

5.3.1 Introduction

Cemented paste backfill (CPB) has been extensively employed in modern mining operations as an innovative cementitious material for post-mining solid wastes (usually tailings) management from a sustainable and cost-effective perspective (Fall & Benzaazoua, 2005; Yilmaz et al., 2004). The engineered CPB mixture typically consists of dewatered tailings (solid percentage of 70-85%), hydraulic binder (usually 3-7% by weight), and water to achieve a homogeneous paste that is usually prepared in a plant located at the surface of a mine site and transported to the underground filling extracted stopes or cavities (Fall et al., 2005; Benzaazoua et al., 2004). Compared to the

traditional surface mine waste disposal, the CPB technique returns a large amount of waste tailings to the underground, significantly reducing the surface tailings impoundment requirement and eliminating the risk of environmental contamination and dam failure (Saremi & Fall, 2024). In addition, the CPB structure stabilizes the underground structure to minimize the potential geotechnical hazards (i.e., subsidence and rock wall instability) and provides a safe working floor for mining activities (Fall et al., 2010).

To fulfil its role of mine rehabilitation, it is essential for a CPB structure to satisfy the geotechnical requirement of mechanical stability after placement. One of the critical parameters used in practice to evaluate the mechanical performance of a CPB structure is uniaxial compressive strength (USC) since the UCS test is relatively inexpensive, quick, and can be easily incorporated into routine quality control programs at the mine (Vergne, 2000).

From early to advanced curing ages, the properties of designed CPB are significantly affected by thermal (T, i.e., geothermal gradient, hydration heat, heat transfer), hydraulic (H, i.e., suction, pore water pressure (PWP) development, water drainage), mechanical (M, i.e., in-situ stress, CPB self-weight, filling rate and strategy), and chemical processes (C, i.e., binder reactions, contamination dissolution, and precipitation) (Aldhafeeri & Fall, 2017; Cui & Fall, 2015, 2017; Ghirian & Fall, 2014). Among them, thermal load (curing temperature) stands as an important factor impacting CPB mechanical properties and structural integrity, which is often directly associated with binder hydration rate dominating the strength development and pore characteristics. The temperature condition varies in different mines and backfilling structures and is influenced by several critical factors (Fall et al., 2010). First, the depth of mines and geological conditions significantly impact temperatures because of the geothermal gradients. The exposed rock mass is the primary heat load source in any deep-level mining operation, which means those near geothermal sources would experience higher temperature levels with deeper mines. Then, the geographical location of the mine (climate of the region) affects the temperature of the mines situated at relatively shallow depths. In addition, the exothermic hydration of binders in the CPB structure, which is the primary source of heat in the CPB technique, can generate considerable heat during the curing process. The large dimensions of CPB structures can retain heat, and when combined with heat generated during pipeline transportation, the temperature can be substantially elevated within the CPB structure. Furthermore, self-heating from exothermic reactions of sulphide minerals in the backfill or surrounding rock mass can also occur; however, extreme temperatures are infrequent in tailings backfill operations. Lastly, human-induced heat sources, such as machinery and blasting operations, generally have a minor impact on large CPB structures. To date, the effects of temperature on CPB materials have been extensively investigated (Xiu et al., 2022; Chen et al., 2021; Cheng et al., 2020; Fang & Fall, 2018; Wu et al., 2013; Fall et al., 2010; Nasir & Fall, 2010). For example, Fall et al. (2010) evaluated the development of compressive and split tensile strengths, modulus of elasticity, stress-strain behaviour, and microstructure of CPB specimens at different curing times and temperatures from 2℃ to 50℃. The results revealed that the increasing temperature, particularly moderate temperature (<35℃), could contribute to a much better strength development with a reduced binder consumption, and the effect of temperature also depends on the binder type, water-

to-cement ratio, and tailings type. Additionally, Chen et al. (2021) investigated the compressive strength development of CPB samples under similar curing temperatures, and an increasing trend in UCS was observed, with an increase in curing stress and curing temperature due to the acceleration of cement hydration. Furthermore, the shear stress at the interface between early age CPB and rock could also be enhanced with the increasing curing temperature of up to 35°C (Fang & Fall, 2018). However, the increasing temperatures would lead to an increase in yield stress and viscosity of the CPB mixture, which are not favourable to the transportation process (Wu et al., 2013). Accordingly, temperature is a significant variation that should be considered in mine backfill design and operations.

Cracks in CPB structures can be generated when subjected to underground stress conditions. For example, excessive stresses generated by the pressure of the CPB overburden, stresses induced by the closure of rock walls adjacent to or surrounding the CPB structures, rock bursts, or shrinkage could lead to the initiation and propagation of cracks. The presence of cracks will significantly damage the CPB structure integrity, decrease its mechanical strength, and increase its permeability. Thereby, the service life and durability of CPB structures will be severely diminished. Despite the importance of self-healing in extending the longevity of CPB, this area remains largely unexplored, with limited studies investigating self-healing behaviours in CPB. Recent studies (Xiang et al., 2023a; Xiang et al., 2023b) have explored enhancing CPB's self-healing efficacy by embedding a mix of aerobic and anaerobic bacteria in polypropylene-fiber reinforced backfill. Findings suggest this approach can improve the self-healing ratio of cracked backfill. However, introducing bacteria into CPB presents practical challenges in underground mine operations, such as increased costs, increased complexity in CPB quality control and potential environmental concerns. Further work has investigated self-healing (autogenous healing) behaviours in CPB without adding specialized self-healing agents (Quan & Fall, 2024), inspired by the self-healing concept successfully applied to other cementitious materials, such as concrete (De Belie et al., 2018; Neville, 2002), mortar (Suleiman & Nehdi, 2021; De Nardi et al., 2017), high-performance fiber-reinforced cementitious composites (Cuenca & Ferrara, 2017; Ferrara et al., 2017), and engineered cementitious composites (Yang et al., 2011; Yang et al., 2009). This promising self-healing performance in CPB suggests a viable means to repair or mitigate cracks, enhancing durability and extending the structure's service life by initiating a self-repair process upon crack formation.

Nevertheless, the achievement of self-healing in CPB material is mainly attributed to two main mechanisms: i) continuous hydration of unhydrated cement particles, and ii) carbonation of calcium hydroxide, which are likely to be considerably impacted by the temperature variations as aforementioned. Add to that, previous studies on the effects of temperatures on CPB have focused on the properties of intact CPB specimens, but no studies have been carried out to investigate the effect of temperature on the self-healing ability and performance of cracked CPB specimens. Although the effects of temperature on the autogenous healing of conventional cementitious materials (e.g., concrete, mortars) have been studied (e.g., Li et al., 2023; Su et al., 2020; Yang et al., 2009; Reinhardt & Jooss, 2003), these findings cannot be directly applied to CPB materials due to significant differences between CPB and conventional cementitious materials, such as CPB's

lower cement content, CPB's higher water-to-cement ratio and the differing particle size distributions between tailings and aggregates. No studies on the effect of temperature on the self-healing capacity and behaviour of CPB have yet been carried out. Therefore, the primary objective of this study is to experimentally investigate the effects of different temperatures on the self-healing (autogenous healing) capacity and behaviour of CPB material across various self-healing periods.

5.3.2 Materials and Experimental Program

5.3.2.1 Materials

Tailings

To control the mineralogical compositions of tailings and eliminate the uncertainties in experimental results, synthetic silica tailings (ST, 99.8% of which is silicon dioxide) were used to prepare the CPB mixtures because of their pure composition and homologous particle size distribution with the natural tailings (NT) from nine different mines in eastern Canada, as depicted in Figure 5-15. This figure demonstrates that ST has about 45 wt.% fine particles (<20 mm) and can be classified as medium tailings. STs, composed of SiO_2 (99.8%), with Al_2O_3 (0.05%) and Fe_2O_3 (0.035%) as secondary components, are considered to be chemically inert materials (Carraro et al., 2009). In addition, the physical properties of ST are shown in Table 5-6.

Binder and water

General Use (GU) Portland cement, the most common cement in the mining industry, was used as the hydraulic binder to prepare CPB specimens. The chemical compositions of GU cement are CaO (62.82%), SiO_2 (18.03%), Al_2O_3 (4.53%), SO_3 (3.82%), Fe_2O_3 (2.70%), and MgO (2.65%). Additionally, tap water was used to mix with ST and binder to prepare the CPB mixture.

Table 5-6. Physical properties of the tailings used and the average of nine natural tailings in eastern Canada.

Element	G_s	D_{10}	D_{30}	D_{50}	D_{60}	C_u	C_c
		(μm)					
ST	2.7	1.9	9.0	22.5	31.5	16.6	1.3
Nine NT average	-	1.8	9.1	20.0	30.8	17.1	1.7

G_s: specific gravity; C_u: coefficient of uniformity; C_c: coefficient of curvature.

5.3.2.2 Specimen preparation and initial curing

The CPB mixture was prepared by blending the three ingredients in a mixer for 7 minutes until achieving homogeneity with a 4.5 wt.% proportion of binder (GU cement) and a constant water-to-cement ratio (w/c) of 7.35. The slump value of the prepared CPB mixture was measured to be 18 cm by slump tests in accordance with ASTM C143 (ASTM, 2020), ensuring the pumpability and transportability of the prepared CPB material. To prepare specimens for subsequent testing, cylindrical moulds with a size of Φ50×100 mm were used to cast the CPB specimens. Then, the specimens underwent an initial curing (IC) period of 7 days under different curing temperatures of 2℃, 20℃, 35℃, and 50℃ prior to crack initiation (as outlined in Table 5-7). A total of 200 CPB

specimens were prepared in this study to investigate the impact of temperature on the self-healing capacity of the CPB material.

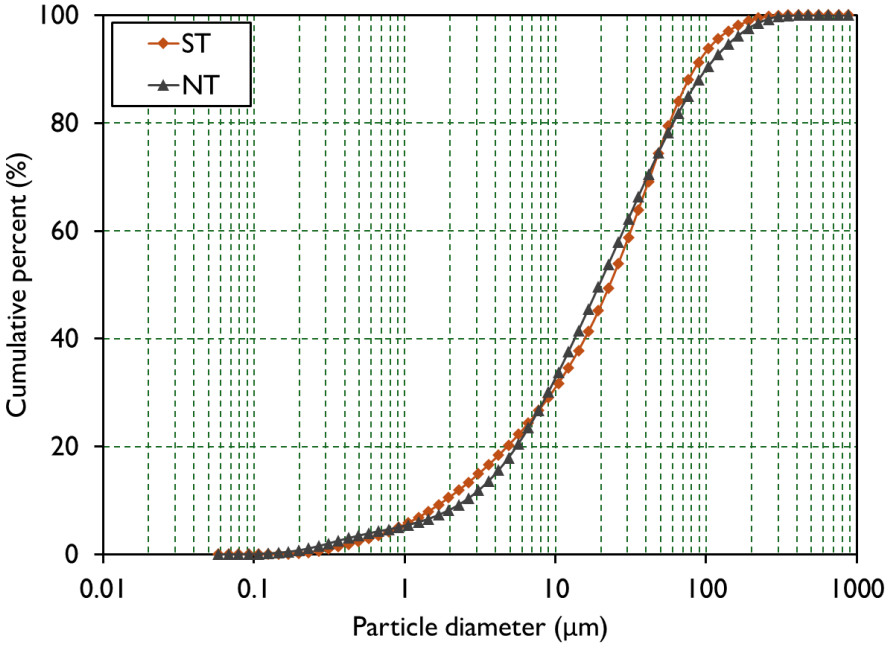

Figure 5-15.Particle size distribution of the used ST along with an average of nine NTs in eastern Canada.

Table 5-7. Mix composition and curing conditions of prepared CPB specimens.

Sample nomenclature	Binder content (wt.%)	w/c ratio	Initial curing (day)	Curing temp. (°C)	Pre-cracking level (%)	Self-healing period (day)
T2	4.50	7.35	7	2	0, 75%, and 90% of UCS after IC	7 28 90
T20	4.50	7.35	7	20	0, 75%, and 90% of UCS after IC	7 28 90
T35	4.50	7.35	7	35	0, 75%, and 90% of UCS after IC	7 28 90
T50	4.50	7.35	7	50	0, 75%, and 90% of UCS after IC	7 28 90

5.3.2.3 Crack Initiation

The uniaxial compressive strength (UCS) tests were conducted on the CPB specimens to determine their compressive strength and to introduce cracks at prescribed different pre-cracking levels according to ASTM C39/C39M-21 (ASTM, 2021). In the first phase, the UCS value of the CPB specimens was determined after the initial curing period. Subsequently, the remaining specimens were subjected to specific pre-cracking levels of 0%, 75%, or 90% (i.e., control, PC75%, or 90%, respectively) of the previously measured compressive strength in the pre-peak regime. After reaching the pre-determined load threshold, the applied load was maintained for one minute for the generation and propagation of cracks. Only when the pre-cracking level reached approximately PC75% or above, the cracks became apparent in CPB specimens. As the enhanced pre-cracking load approaches the peak stress region, the stress-strain curve exhibits its first non-linear behaviour, where microcracks become increasingly visible in CPB specimens. This performance has also been observed in previous works (Quan & Fall, 2024; Fall et al., 2009). Note that control CPB specimens were not subjected to any pre-cracking load (i.e., crack initiation) and were used as reference specimens for the mixtures.

The UCS tests and pre-cracking processes were conducted using a computer-controlled mechanical press (MTS 10/GL) with a normal load of 50 kN and a displacement rate of 1 mm/min under displacement control. Axial deformation was automatically recorded through an internal linear variable differential transformer (LVDT) connected to an electronic data acquisition system.

5.3.2.4 Healing Condition

The pre-cracked CPB specimens, together with uncracked control specimens, were cured under different temperatures of 2°C, 20°C, 35°C, and 50°C for a self-healing curing phase. The self-healing environment without external inference aimed to investigate the self-healing performance of CPB materials exposed to different temperatures. At the end of each self-healing period of 0, 7, 28, and 90 days, the studied specimens were re-tested to determine the self-healing efficiency. In this study, the pre-cracking day is named D0, representing the beginning of self-healing, followed by D7, D28, and D90, representing the self-healing period of 7, 28, and 90 days, respectively.

5.3.2.5 Testing Methods for Self-healing

Crack characteristics

A digital microscope magnified 200 times was employed to observe the crack alterations on the CPB specimens at the end of each self-healing period. The captured images could provide a direct assessment of self-healing behaviour in pre-cracked CPB specimens, providing additional insights into surface crack closure and corroborating the findings of other tests.

Mechanical property investigation

To assess the self-healing efficiency in compressive strength recovery of CPB materials, the UCS tests were conducted on at least triplicate CPB specimens in accordance with ASTM C39/C39M-21 (ASTM, 2021) after 7, 28, and 90 days of self-healing period on both healed pre-cracked

specimens and reference control specimens. A computer data acquisition system was used to maintain a constant deformation rate of 1 mm/min.

The relative changes in compressive strength (CCS_C) of the pre-cracked and healed specimens compared to the control specimens were calculated as follows:

$$CCSc(\%)=\frac{S_{pre\text{-}cracked/healed} - S_{control}}{S_{control}} \quad (5\text{-}4)$$

where $S_{pre\text{-}cracked/healed}$ is the UCS of the pre-cracked specimens before or after a self-healing period, and $S_{control}$ is the UCS of uncracked control specimens subjected to the same self-healing condition and period. It is important to note that Eq. 5-4 is used for all cases where the UCS of the pre-cracked specimen at the initial time of self-healing (D0) is less than or equal to the UCS of the control specimen.

Hydraulic property investigation

Permeability significantly impacts the durability and environmental performance of the CPB structure, and low permeability is essential for controlling water flow, reducing the risk of water ingress, and ensuring operational safety. In addition, low permeability reduces CPB's sensitivity to acid mine drainage and its ability to release contaminants (contaminant leachability) into mining areas and/or groundwater (after mine flooding) (Bull & Fall, 2020). The decrease in permeability of self-healed pre-cracked CPB specimens can reflect the self-healing capacity. Given that, saturated hydraulic conductivity tests were conducted on pre-cracked and healed CPB specimens using a triaxial cell with a flexible wall technique in accordance with ASTM 5084-16a (ASTM, 2016) to quantitatively examine the changes in the permeability of pre-cracked specimens that have experienced self-healing. The hydraulic conductivity, k_{sat}, was then calculated as follows:

$$k_{sat}=\frac{\Delta Q \cdot L}{A \cdot \Delta h \cdot \Delta t} \quad (5\text{-}5)$$

where k represents the hydraulic conductivity, cm/s; ΔQ denotes the quantity of flow during a certain time interval Δt, calculated as the average of inflow and outflow, cm^3; L signifies the length of the specimen, cm; A represents the cross-sectional area of the specimen, cm^2; Δt is the time interval, s; and Δh corresponds to the average head loss of across the specimen, cm of water.

The hydraulic conductivity recovery ratio (HCRR) can be determined by the following formula:

$$HCRR\ (\%) = \frac{k_0 - k_t}{k_0} \times 100\% \quad (5\text{-}6)$$

where k_0 is the initial hydraulic conductivity, cm/s, measured after pre-damaging; k_t is the hydraulic conductivity, cm/s, measured after specified self-healing period.

Microstructural and chemical analysis

A series of analytical techniques, including scanning electron microscopy-energy dispersive spectroscopy (SEM-EDS), thermal analyses (TG/DTG), and mercury intrusion porosimetry (MIP), were employed to characterize the self-healing products and monitor the effect of temperature on

the microstructure of the CPB specimens, which are crucial for understanding the self-healing mechanism. SEM-EDS analysis was performed to examine the compositions of the self-healing products within cracks. Add to that, TG/DTG revealed the different binder hydration degrees between healed pre-cracked and control specimens. Additionally, the MIP tests evaluated the pore size distribution in CPB specimens subjected to different temperatures. Furthermore, the changes in void ratio and porosity of the studied pre-cracked and control specimens were tested over the self-healing period. SEM-EDS analysis was conducted using an environmentally versatile JEOL 6610LV SEM in low voltage mode, featuring an attached Oxford INCA large area SDD detector. TG/DTG analysis was carried out using a Setaram Setsys 24 thermogravimetric analyzer, applying a heating ramp of 10°C/minute from room temperature up to 1000°C in a nitrogen atmosphere. MIP measurements were performed using a Micromeretics AutoPore III 9420 mercury porosimeter.

5.3.3 Results and Discussions

5.3.3.1 Crack closure by self-healing

The self-healing performance of cracks in pre-cracked CPB specimens was observed before and after the self-healing period of 7, 28, and 90 days by using the digital microscope. Figure 5-16 displays the typical observations of crack closure in pre-cracked CPB specimens under different curing temperatures (2℃, 20℃, 35℃, and 50℃) after different self-healing periods (7, 28, 90 days). From this figure, it is clearly seen that abundant white crystal-like self-healing products are precipitated inside the cracks or along the crack paths after specific self-healing periods. The produced healing products contribute to the observed three distinct healing scenarios: complete healing, partial healing, and no healing. The initial crack width of all studied pre-cracked specimens was examined with a range from approximately 11.2 to 622.5 μm. Due to the unevenness of the initiated crack width via compressive loading, the maximum crack widths of completely healed cracks under different healing conditions (i.e., curing temperature and self-healing period) were measured as an indicator of quantitative evaluation of self-healing efficiency in physical crack closure. The experimental findings of the CPB specimens cured at 20℃ (room temperature) are used for reference to compare with other studied temperatures. It is demonstrated in Table 5-8 that the development of crack closure significantly progresses with respect to the curing temperatures and self-healing periods. Specifically, the elevated curing temperature accelerates the crack closure rates, suggesting that a crack with a larger width can be completely healed after the same self-healing period when cured at a higher temperature. For example, the self-healing ability in crack closure can be observed on the reference pre-cracked CPB specimens cured at 20℃, while the crack width up to 56.2 μm can be closed after the self-healing period of 28 days. For the pre-cracked specimens cured at 35℃, crack widths up to 89.7 μm can be completely healed. Furthermore, when the curing temperature increases to 50℃, the complete healing of a larger crack can be achieved with a crack width of up to 120.8 μm. As the self-healing process extends to 90 days, the crack closure becomes enhanced with the maximum completely healed crack width up to 175.3 μm in the pre-cracked specimens cured at 50℃. However, it is noticeable that the self-healing efficiency in crack closure of the pre-cracked specimens cured at 2℃ is negligible at the first 7 days of self-healing, during which complete healing is hardly observed and the residual crack

widths are still as broad as the initial ones. Hence, the self-healing ability of crack closure subjected to varying temperatures is in the order of 50℃ > 35℃ > 20℃ > 2℃ based on the direct observations by microscope. However, Figure 5-16 shows that, regardless of curing temperature, some cracks remain only partially sealed or not sealed at all. This outcome is primarily related to crack width, as larger cracks are less likely to fully self-heal (Quan & Fall, 2024). The self-healing mechanism in cementitious materials relies on narrower cracks, where sufficient precipitation of healing products can effectively seal the opening. Narrower, shorter, or shallower cracks have a higher potential for complete healing due to the smaller volume that requires filling. This indicates a limitation in the autogenous healing capacity of CPB materials, with crack width being a critical factor influencing the self-healing efficiency.

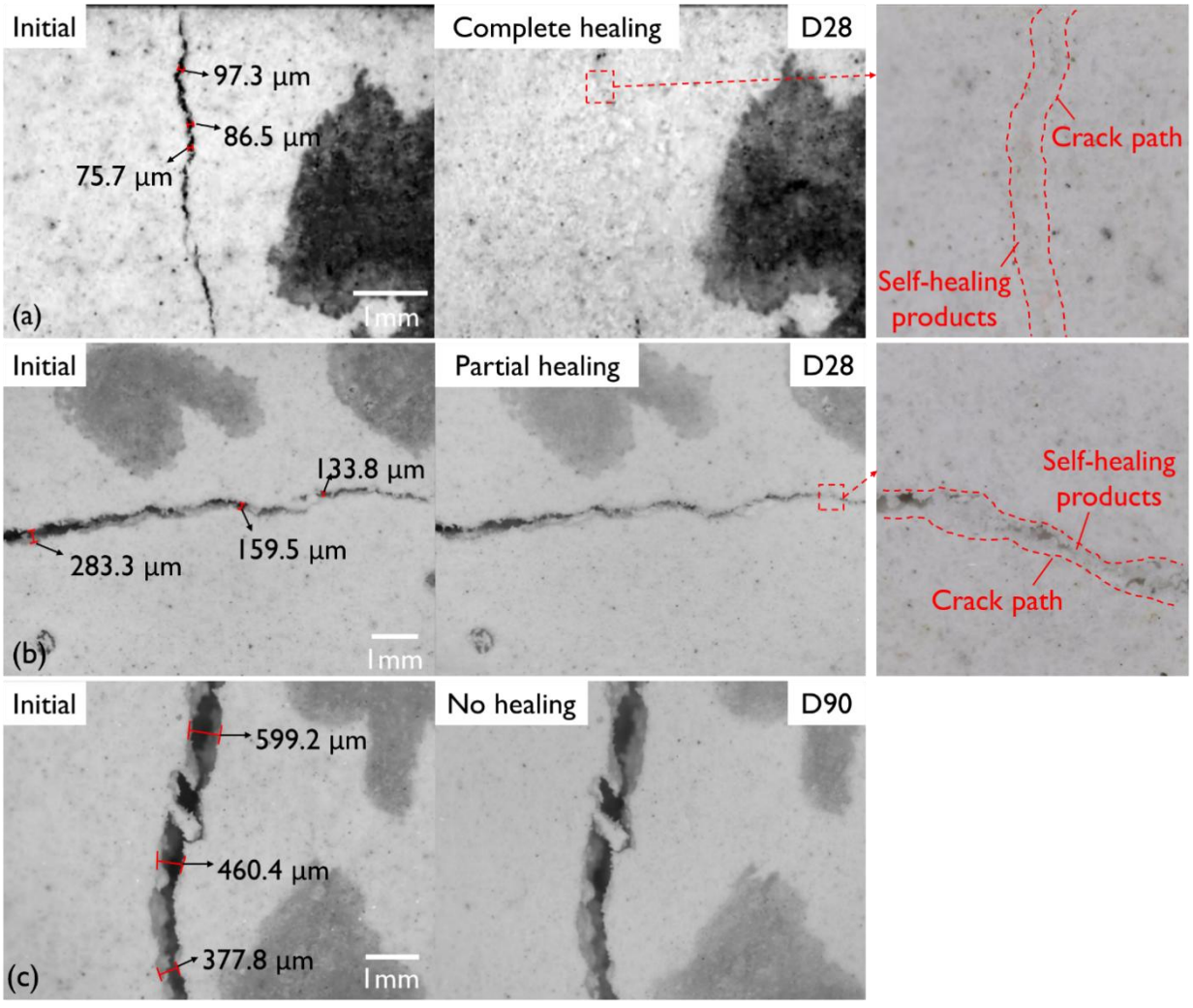

Figure 5-16. Typical observations of crack closure in CPB specimens with curing temperature and self-healing period of (a) 50℃, 28 days, complete healing, (b) 50℃, 28 days, partial healing, and (c) 50℃, 90 days, no healing.

5.3.3.2 Nature of self-healing products

SEM-EDS analysis was employed to investigate the chemical nature of the observed white crystal-like self-healing products inside the cracks. As demonstrated in Figure 5-17, the morphology of the healing products is evident. At least three different locations were analyzed by EDS for each analyzed specimen. According to the energy spectrum analysis as shown in Figure 5-17, it is observed that the traces of Ca, Al, C, and O peaks were clearly detected. Due to the continuous cement hydration, there is no doubt to point out the existence of C-S-H. In addition, the evolution of C:Ca and O:Ca ratios indicates the presence of $Ca(OH)_2$ and $CaCO_3$. The result is consistent with the previous work (Quan & Fall, 2024), the combination of C-S-H, $Ca(OH)_2$, and $CaCO_3$ is the primary self-healing product inside the cracks of the CPB specimens.

5.3.3.3 Mechanical strength change analysis

To analyze the magnitude of strength recovery, UCS tests on both control and healed pre-cracked CPB specimens were conducted. The results of strength recovery efficiency and development over the self-healing periods are presented in Figures 5-18 to 5-21. Figure 5-18 illustrates the impact of curing temperatures on the strength development of control CPB specimens as a function of self-healing periods of 0, 7, 28, and 90 days. Meanwhile, the overall strength distribution under various healing conditions (i.e., temperature, pre-cracking level, and self-healing period) is depicted in Figure 5-19. In addition, Figure 5-20 displays the evolution of UCS and CCS_C in pre-cracked specimens subjected to different curing temperatures of 20℃, 35℃, and 50℃ over a self-healing period of up to 90 days. Figure 5-21 illustrates the evolution of UCS and compressive strength recovery by self-healing of the CPB cured at a temperature of 2℃.

Table 5-8. Maximum healed crack width after specific self-healing periods subjected to different temperatures.

Batch nomenclature*	Self-healing period (day)	Maximum completely healed crack width (μm)
T2	7	-
	28	18.6
	90	33.1
T20	7	45.3
	28	56.2
	90	72.5
T35	7	56.5
	28	89.7
	90	149
T50	7	69.5
	28	120.8
	90	175.3

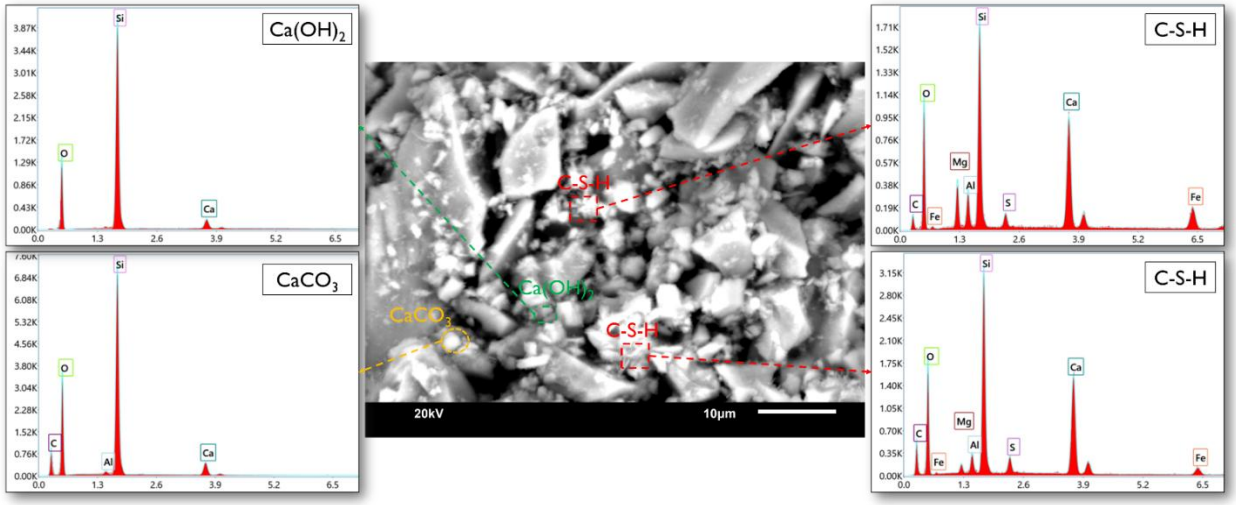

Figure 5-17. SEM-EDS detection of self-healing products inside the cracks of CPB specimen cured at 50°C after 90 days of self-healing period.

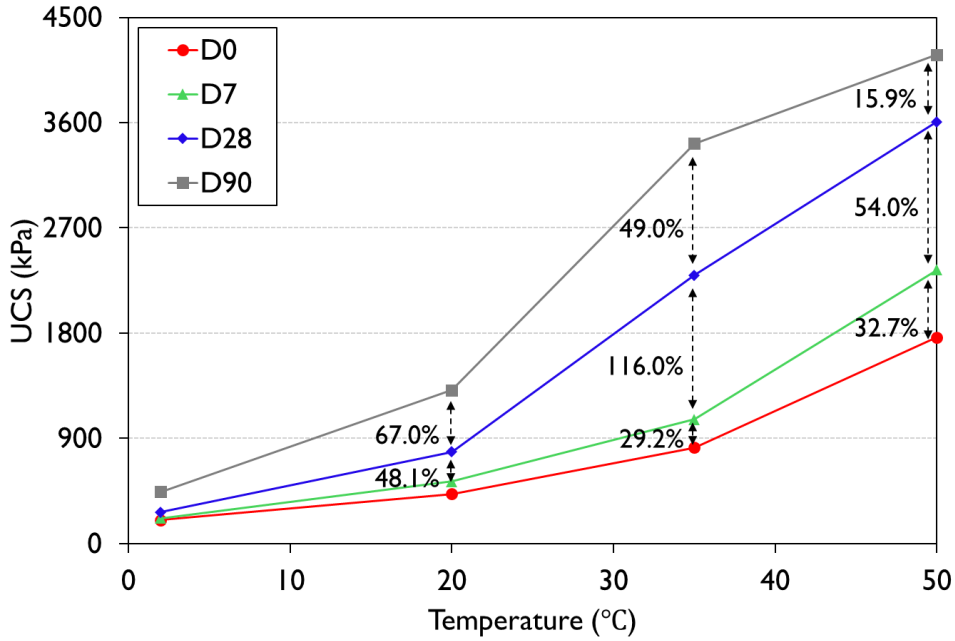

Figure 5-18. Compressive strength development of control CPB specimens under different curing temperatures and healing periods.

Strength development of uncracked control specimens

The results presented in Figure 5-18 obviously show that the strength of the control CPB specimens increases as the curing temperature increases regardless of the curing ages. This increase is more pronounced when the curing temperature (i.e., 35°C, 50°C) is above room temperature (20°C). The sharp increase in strength can be attributed to the fact that a higher temperature accelerates the binder hydration reactions, from which more hydration products (i.e., calcium-silicate-hydrate or

C-S-H, portlandite or CH, ettringite, and gypsum) are generated within the CPB specimens cured at a higher temperature (Bull & Fall, 2020). Thus, the increased amount of C-S-H improves the binding force between particles, favouring strength development (Taylor, 1964). Add to that, the precipitation of hydration products in the empty voids and capillary pores reduces the porosity and refines the pore structure, leading to a denser CPB matrix, which also contributes to the strength gain (Fall et al., 2010). This argument is supported by the thermal analysis results conducted on the CPB specimens cured at 20°C and 35°C at the self-healing period of D7 in Figure 5-22a. Three main thermal decomposition stages at the temperature ranges of 50-200°C, 400-450°C, and 600-750°C can be observed in the figure, which represents the evaporation of water and dehydration of hydration products (i.e., C-S-H, ettringite, gypsum, and carboaluminates), dehydroxylation of CH, and decarbonization of calcium carbonate ($CaCO_3$), respectively. Given that, the CPB specimen cured at 35°C clearly shows a higher weight loss in the first and second range than that of 20°C, indicating that more cement hydration products are generated at a higher curing temperature. Additionally, the rapid increase in hydration products due to higher curing temperatures is also demonstrated by the results of porosity and void ratio tests performed on the control CPB specimens cured at different temperatures (2°C, 20°C, 35°C, and 50°C) as presented in Figure 5-25. The figure shows a decreasing trend in the porosity and void ratio of control CPB specimens as the curing temperature increases due to the refinement of pore structures. This finding of more hydration products with increasing curing temperature is consistent with the previous studies on CPB (Ali et al., 2021; Fang & Fall, 2018; Pokharel & Fall, 2013; Fall et al., 2010) and other cementitious materials (Deschner et al., 2013; Schindler, 2004; Khoury, 1992). Moreover, it is also perceived in Figure 5-18 that the CPB specimens cured at 2°C exhibit the lowest strengths. The reason for this negligible strength development is that due to the inhibition of low temperature on the binder hydration, the formation of hydration products is significantly lower compared to those formed at higher temperatures, thereby resulting in low strength.

Compressive strength recovery by self-healing

At curing temperatures ≥20 °C

Figure 5-19 plots the distribution of the averaged strength value of each specimen subjected to a specific healing regime. It is generally observed that elevated temperatures (temperature ≥20 °C) have a significant effect on self-healing efficiency and the mechanical strength of CPB specimens. Specifically, Figure 5-20 displays the detailed recovery of compressive strength of specimens cured at temperatures ≥20 °C, quantified by means of the index CCS_C, calculated as in Eq. 5-4, for the investigation of temperature effects over the self-healing period. The experimental findings of the CPB specimens cured at 20°C (room temperature), as shown in Figure 5-20a, are used for reference to compare with other studied temperatures. It can be seen that the specimens cured at 20°C can recover to an equivalent UCS value as the control specimens or even achieve higher compressive strength than the control ones for the PC90% pre-cracked specimens after the self-healing period of 7 days (D7). Previous study (Quan & Fall, 2024) has demonstrated that the observed self-healing (autogenous healing) performance within the CPB matrix is mainly attributed to two mechanisms: i) continuous hydration of unhydrated cement particles and ii) carbonation of CH, which enhances

the binding force between particles and decreases the internal porosity, thus refining the pore structure and restore the mechanical strength. This argument is also demonstrated by the thermal analysis results in Figure 5-22b. In the figure, as the self-healing period extends from D7 to D28, the three distinct weight losses that represent the decompositions of hydration products become more pronounced, which indicates that the continuous hydration of unhydrated cement particles significantly benefits the self-healing performance within the CPB matrix. As the self-healing period elongates, the healing performance results in a continuous recovery and increase in compressive strength with the increasing CCS_C values. The increase is more pronounced for the specimens with a higher pre-cracking level. For example, from the self-healing period of 28 days (D28) to 90 days (D90), the specimens with the pre-cracking level of PC90% achieved approximately 13.3% to 20.9% higher UCS values than those of the control specimens. The reason for this supplementary increase in strength is that since the initiated cracks provide the pathways allowing more CO_2 to penetrate the CPB matrix favouring the carbonation of $Ca(OH)_2$, the additional amount of formed calcite $CaCO_3$ further contributes to the self-healing behaviour and strength recovery (Quan & Fall, 2024).

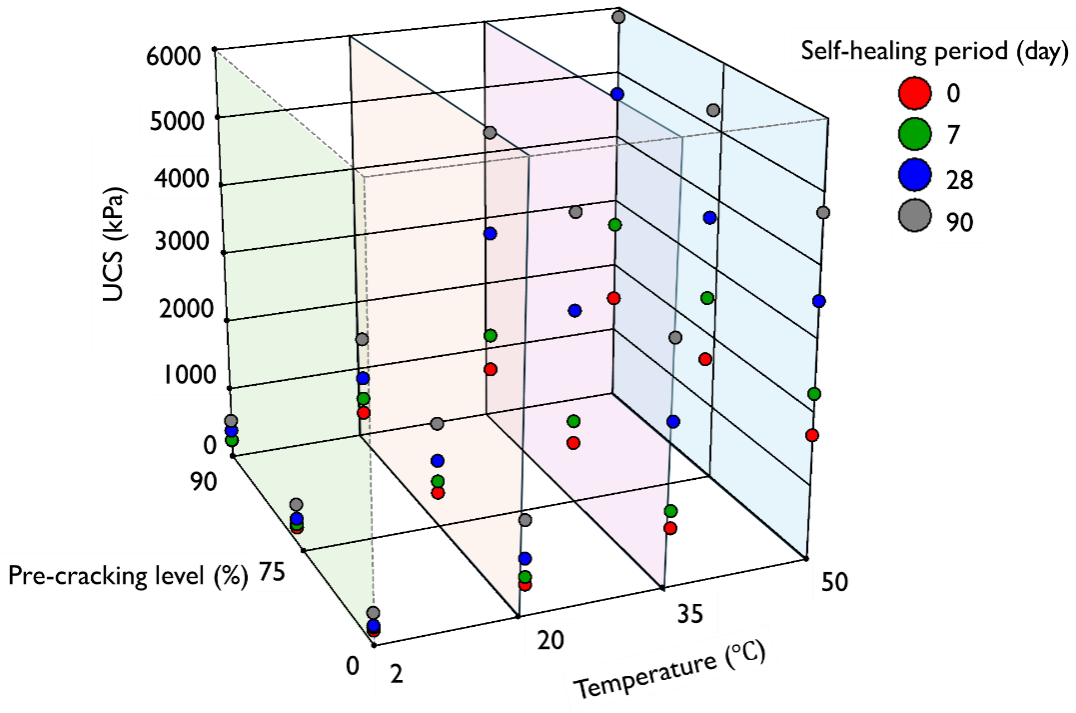

Figure 5-19. Overall comparison of compressive strength recovery and development of pre-cracked CPB specimens subjected to temperature effect.

In addition, the pre-cracked CPB specimens cured at 35°C exhibit a similar but improved self-healing efficiency in strength recovery and development compared to those cured at 20°C, as illustrated in Figure 5-20b. Noticeable increased CCS_C values are observed at the self-healing period of 28 (D28) and 90 days (D90), with CCS_C values of 23.4% and 27.4%, respectively. This increase in strength gain is attributed to the acceleration in cement hydration induced by the

increased curing temperature. The higher curing temperature accelerates the hydration of the unhydrated cement and promotes the formation of more hydration products (i.e., C-S-H, CH, $CaCO_3$, ettringite, and gypsum), as aforementioned and demonstrated in Figure 5-22a. These generated hydration products fill the microcracks to achieve crack closure with a faster healing rate. In other words, microcracks with larger crack widths can be completely healed under higher curing temperatures after the same healing period (as listed in Table 5-8). Likewise, the precipitation of hydration products reduced the volume of capillary pores within the CPB matrix, resulting in a more refined pore structure, which can be considered an additional contributor to the increase in temperature-induced strength of CPB. This argument also agrees well with the results of MIP tests performed on control CPB specimens cured at 2°C, 20°C and 50°C after a self-healing period of 90 days (D90) in Figure 5-23, where the increasing curing temperature delivers a denser microstructure with a finer distribution of the pores and the decreased threshold pore diameter.

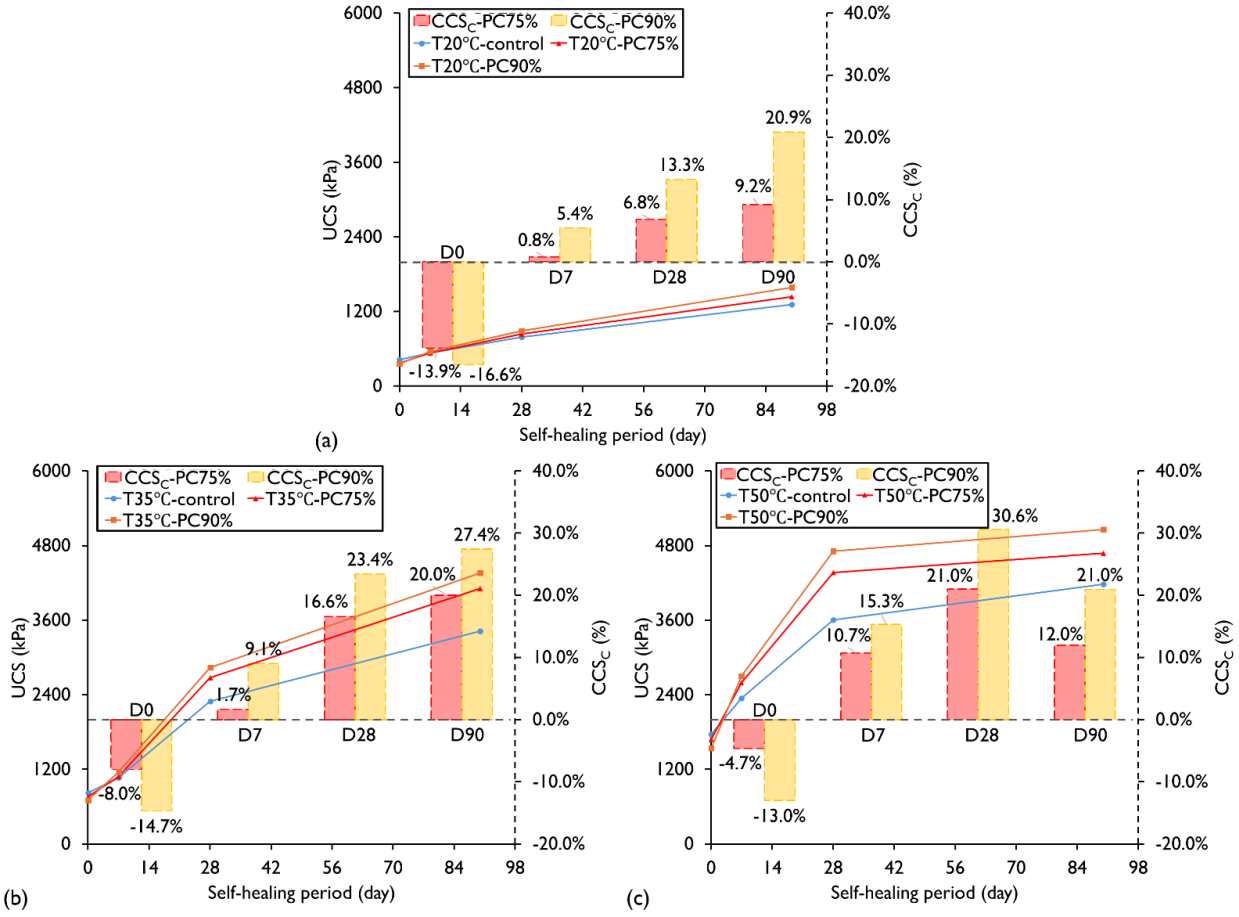

Figure 5-20. Evolution of the UCS and CCS_C of the pre-cracked CPB specimens exposed to different temperatures of (a) 20°C, (b) 35°C, and (c) 50°C over self-healing period (D0, D7, D28, and D90: 0, 7, 28 and 90 days of the self-healing period, respectively).

As the curing temperature elevates to 50°C, a more obvious tendency to a faster self-healing process in case of an increase in temperature can be recognized in Figure 5-20c. Unlikely to the

continuously rigorous self-healing performance for the specimens cured at 20℃ and 35℃ over the studied self-healing period up to 90 days, the CPB specimens cured at 50℃ have a more robust self-healing efficiency up to the self-healing period of 28 days (D28), whereas followed by a lower self-healing rate. Note that the pre-cracked CPB specimens cured at 50℃ achieve higher UCS values than the control specimens after only 7 days self-healing period for both pre-cracking levels. As the self-healing progresses to D28, the specimens with the pre-cracking level of PC90% can even perform 30.6% higher strength than the control ones. In the same way, the elevated curing temperature to 50℃ further accelerates the rate of cement hydration, the produced hydration products fill in the cracks and voids to refine the pore structure and enhance the mechanical strength. While high temperatures accelerate the initial hydration reaction of cement that leads to rapid formation of hydration products, the availability of unhydrated cement particles diminishes, resulting in a slower self-healing efficiency with a CCS_C value of 21% at the advanced self-healing period of 90 days (D90). In contrast to conventional cementitious materials (i.e., concrete and mortar), which usually exhibit an inverse compressive strength development when cured at high temperatures during the advanced curing age due to the cross-effect (Alexander, 1962), the elevated temperature (up to 50°C) can contribute to the continuous refinement of pore structure and strength recovery of the CPB specimens (Fall et al., 2010). Both the results of MIP and porosity tests, as illustrated in Figures Figure 5-23 and Figure 5-25, manifest a decreasing trend of the proportion of macropores and pore structure of control and healed pre-cracked CPB specimens over the self-healing period as the curing temperature increases. This absence of strength inversion can be explained by the dilution effect due to the high w/c ratio of 7.35 within the CPB matrix (Fall et al., 2010). The dilution effect allows more water to react and surround the cement particles than in conventional concrete or mortar, facilitating the diffusion of hydration products farther from the cement grains. This prevents the hydration products from precipitating around the cement grains and impeding further hydration reactions. Furthermore, the thermal analysis results in Figure 5-22d reveal the existence of the additional amount of calcite in the healed pre-cracked specimens cured at 50°C after the advanced self-healing period of 90 days (D90), which further promotes the self-healing efficiency in strength recovery.

It should be noted that although water evaporation from CPB masses in underground mines is generally limited-affecting only shallow depths of the backfill due to the typically high humidity in underground mines and large volume of CPB-very high temperatures, especially in deep mines, can enhance evaporation. Additionally, CPB can release significant heat during cement hydration, which can increase localized evaporation. Excessive evaporation may reduce the water content within the CPB, potentially impacting its self-healing performance, as self-healing processes in cementitious materials rely on the presence of moisture to enable hydration and carbonation reactions. In low-humidity conditions, insufficient moisture can hinder these reactions, leading to incomplete healing (Neville, 2000).

At curing temperature <20 °C

The CPB specimens cured at 2°C (low temperature) exhibit different behaviour compared to those cured at temperatures ≥ 20°C, particularly in terms of initial strength development and the magnitude of strength recovery. The behaviour of these 2°C-cured specimens can be characterized by two main stages: (i) an initial increase in strength due to pre-cracking at D0, and (ii) a low magnitude of strength recovery in the pre-cracked CPB specimens. These stages are discussed in more detail below.

(i) Initial increase in strength due to the pre-cracking at D0

The results indicate that the pre-cracked specimens cured at 2°C initially achieve higher UCS values than the control specimens after the pre-cracking process (at the self-healing period at D0), as shown in Figure 5-21a. This figure illustrates the relative changes in compressive strength (CCS_C) of the pre-cracked and healed specimens compared to the control specimens (which were not initially damaged). It can be observed that immediately after the pre-cracking process, i.e., at self-healing period D0, regardless of the pre-cracking level (PC75% or PC90%), the strength of the pre-cracked specimens at D0 is higher than that of the control specimens. For instance, specimens with a pre-cracking level of PC90% exhibit a 20.7% higher UCS value than the control specimens immediately after the pre-cracking process (Figure 5-21a). This immediate increase in strength, induced by the compaction of CPB specimens, is attributed to the contracting volumetric behaviour of CPB materials under uniaxial compressive loading (Fall et al., 2009). During the pre-cracking process, specimens cured at 2°C experience significant compaction and densification, reducing the volume of voids and pores and enhancing particle interlocking and bonding, which results in improved strength after the pre-cracking process (Ghirian & Fall, 2015; Fall et al., 2009). Figure 5-21a also shows that due to their initial higher strength and the continuous binder hydration in all samples, the strength of the pre-cracked specimens remains consistently higher than that of the control specimens throughout the curing period.

(ii) Low magnitude of strength recovery compared to control specimen at D>0

Given that the strength of the pre-cracked CPB specimens at D0 (i.e., the initial strength of the pre-cracked specimens) is higher than that of the control specimens (uncracked specimens), the calculation of CCS_C is not suitable for evaluating the strength recovery or self-healing efficiency of the pre-cracked specimens cured at 2°C. This conclusion is reached by determining the relative changes in compressive strength ($CCS_{D>0}$) of the pre-cracked specimens at 2°C compared to the control specimens at the same self-healing period (D>0) while taking into account the initial strength increase due to the initial compression of the CPB as described earlier. The relative change was calculated as follows:

$$CCS_{D>0}(\%)=\frac{[S_{D>0} - (S_{D0}-S_{control\ at\ D0})] - S_{control\ at\ D>0}}{S_{control\ at\ D>0}} \quad (5\text{-}7)$$

where $S_{D>0}$ is the UCS of the healed specimens after the self-healing period of 7, 28, and 90 days, and S_{D0} is the UCS of the pre-cracked specimens before self-healing. $S_{control\ at\ D>0}$ represents the UCS of uncracked control specimens subjected to the same self-healing condition and period, and $S_{control\ at\ D0}$ is the UCS of uncracked control specimens at the beginning of the self-healing, i.e., at D0.

Figure 5-21b displays the detailed recovery of compressive strength of the 2°C-specimens quantified by means of the index $CCS_D>0$, calculated as in Eq. 5-7. It can be observed that opposite to the vigorous self-healing behaviour in the pre-cracked CPB specimens cured at temperatures ≥20°C (i.e., 20°C, 35°C, and 50°C) (Figure 5-20), the pre-cracked specimens exhibit a generally minor strength recovery and development when cured at 2°C as illustrated in Figure 5-21b. It is seen that the pre-cracked specimens exhibit similar or lower strengths than the control ones with -0.5% and -4.9% $CCS_D>0$ values of PC75% and PC90% pre-cracked specimens, respectively, after the self-healing period of 7 days (D7), which indicate that the aforementioned immediate increase in strength after the pre-cracking process at D0 cannot be sustained when cured at a low temperature. Moreover, it is noticed that only up to 14.1% value of $CCS_D>0$ is achieved after the self-healing period of 90 days (D90) in the PC75% pre-cracked specimens. This is due to the formation of a low or insufficient amount of hydration products (i.e., C-S-H, which provides binding force between particles) during the healing period. The chemical reactions involved in the hydration process of cement are temperature-dependent, and the low temperature inhibits cement hydration in the CPB specimens, leading to a lower amount of production of hydration products. The insufficient hydration products also impact the crack closure of the pre-cracked specimens cured at 2°C, where no complete crack healing is perceived after a self-healing period of 7 days, as listed in Table 5-8. The table shows that for samples cured at 2°C, only 18.6 and 33.1 μm of the crack width are completely healed after 28 and 90 days of the self-healing period, respectively. This healing performance is significantly inferior to the crack closure observed in the pre-cracked specimens cured at temperatures ≥20°C. The lower amount of cement hydration products in the 2°C-specimens and reduced self-healing capacity are consistent with the MIP results presented in Figure 5-23. This figure shows that the pore structure of the specimens cured at 2°C is much coarser than those cured at ≥20°C after the self-healing period of 90 days. The temperature-dependent increase in pore size is substantially dependent on the hydration process. A lower amount of cement hydration results in fewer hydration products filling the pores of the CPB, leading to a coarser pore structure. Additionally, reduced self-healing leads to more cracks that remain unfilled with hydration products, further contributing to a coarser pore structure. The conclusions drawn from the MIP results are further supported by the findings from hydraulic conductivity tests and porosity/void ratio measurements conducted on the CPB samples, as presented in Figure 5-24 and Figure 5-25, respectively. It can be seen that the insignificant saturated hydraulic conductivity and decrease in porosity of the control and pre-cracked specimens cured at 2°C also imply the occurrence of limited cement hydration and a self-healing process.

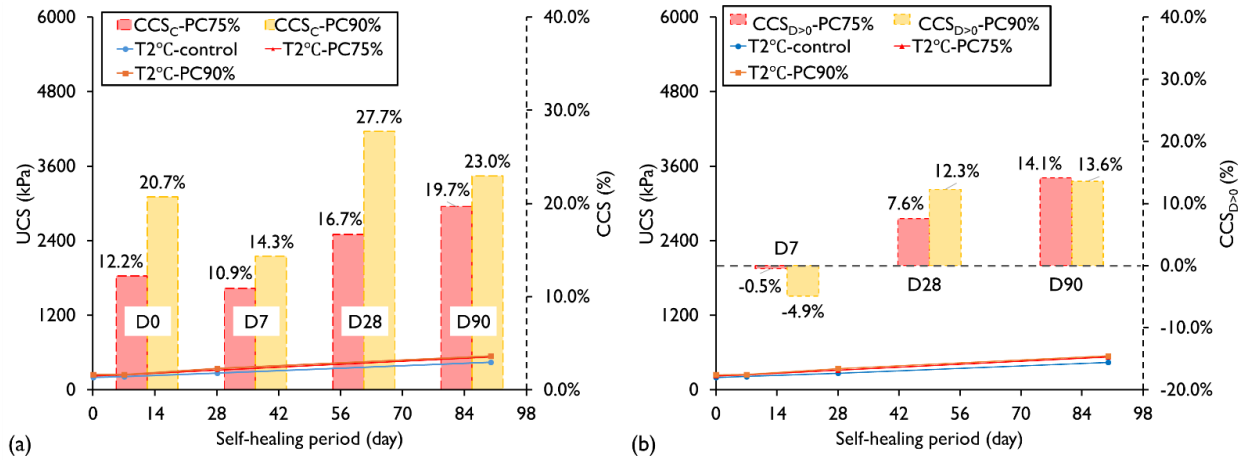

Figure 5-21. Evolution of the UCS along with (a) CCS_C and (b) $CCS_D>0$ of the pre-cracked CPB specimens exposed to the temperature of 2°C over self-healing period (D0, D7, D28, and D90: 0, 7, 28 and 90 days of the self-healing period, respectively).

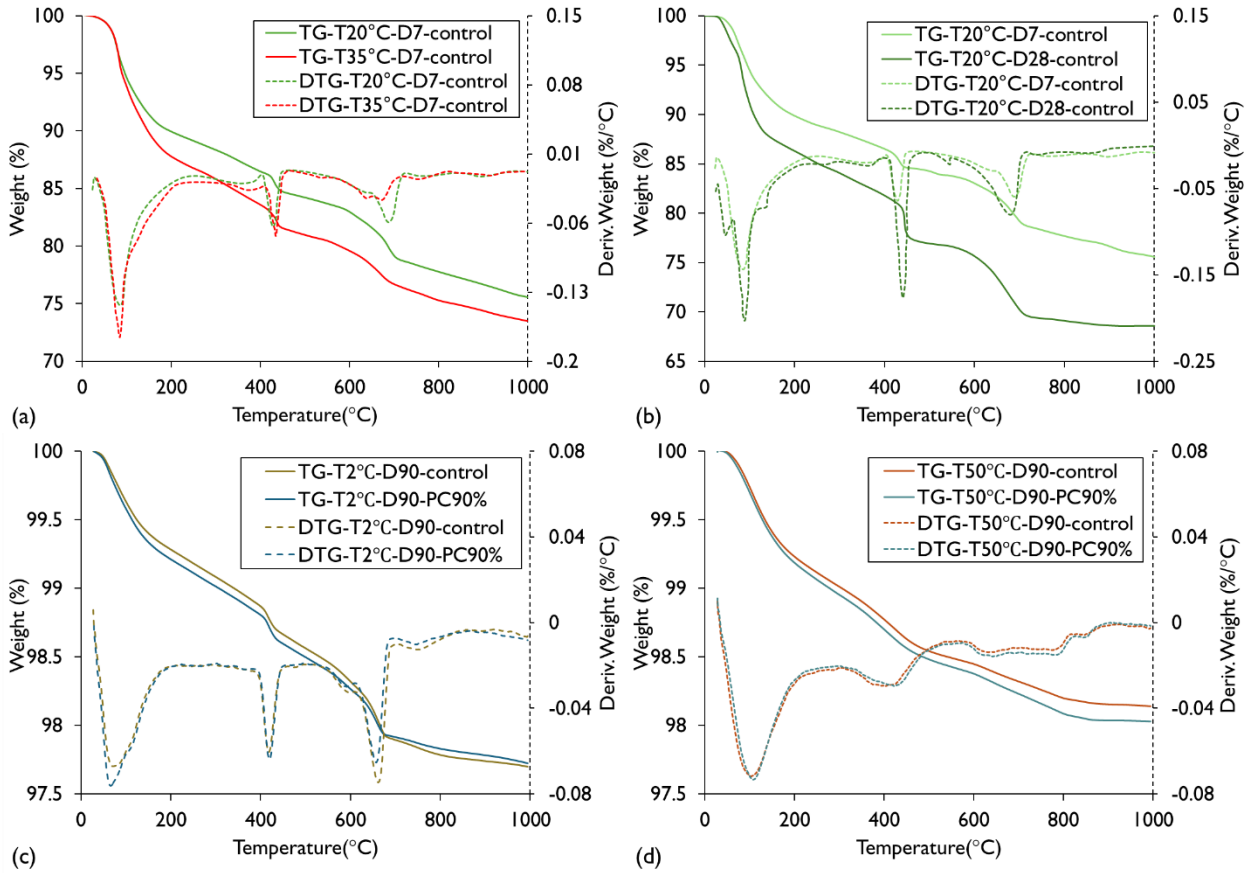

Figure 5-22. TG/DTG comparison of (a) control specimens cured at 20°C and 35°C after self-healing period of 7 days, (b) control specimens cured at 20°C after self-healing period of 7 and 28 days, (c) control and PC90% pre-cracked specimens cured at 2°C after self-healing period of 90 days, and (d) control and PC90% pre-cracked specimens cured at 50°C after self-healing period of 90 days.

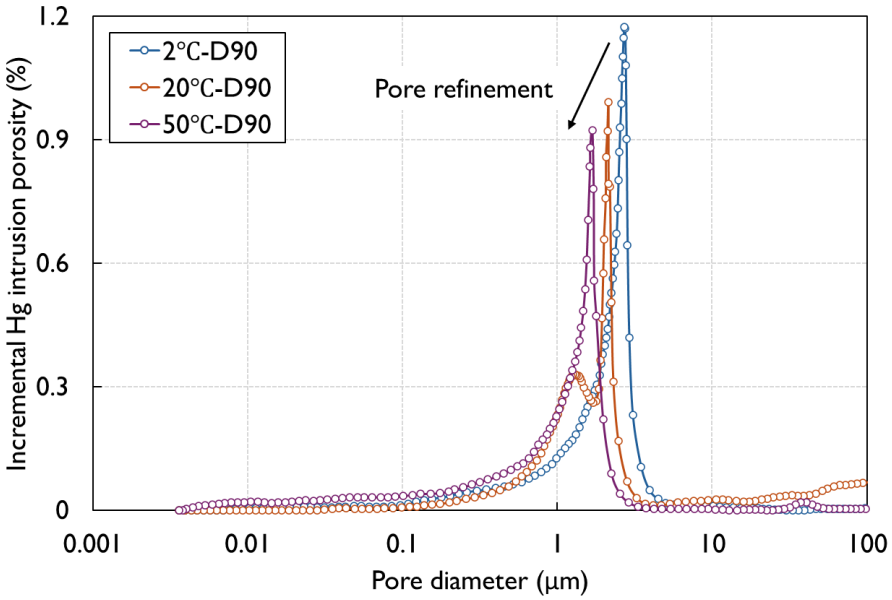

Figure 5-23. MIP pore size distribution of control CPB specimens cured at 2°C, 20°C, and 50°C, respectively, after a self-healing period of 90 days.

5.3.3.4 Analysis of hydraulic conductivity changes

The self-healing efficiency in permeability property of CPB specimens subjected to different temperatures as measured by the change of saturated hydraulic conductivity (k_{sat}) is displayed in Figure 5-24 as a function of the self-healing period. The values on the second y-axis indicate the hydraulic conductivity recovery ratio (HCRR) of the pre-cracked specimens after self-healing compared to the initial scenario. This figure shows that the saturated hydraulic conductivity of the control CPB specimen decreases as the curing temperature increases after the initial curing period. This performance associated with temperature increase is attributed to the previously discussed fact that higher temperatures expedite the cement hydration reactions. The higher amount of generated hydration products accommodates the capillary voids and pores to reduce the internal porosity and refine the pore structure of the CPB matrix, thus delivering a decreased hydraulic conductivity. This has also been demonstrated by the results of porosity and MIP tests performed on control CPBs subjected to different curing temperatures, as shown in Figure 5-23 and Figure 5-25, respectively. The figures show that the control CPB specimens cured under higher temperatures have increasingly lower porosities and finer pore size distribution due to the progressive refinement of their pore structures.

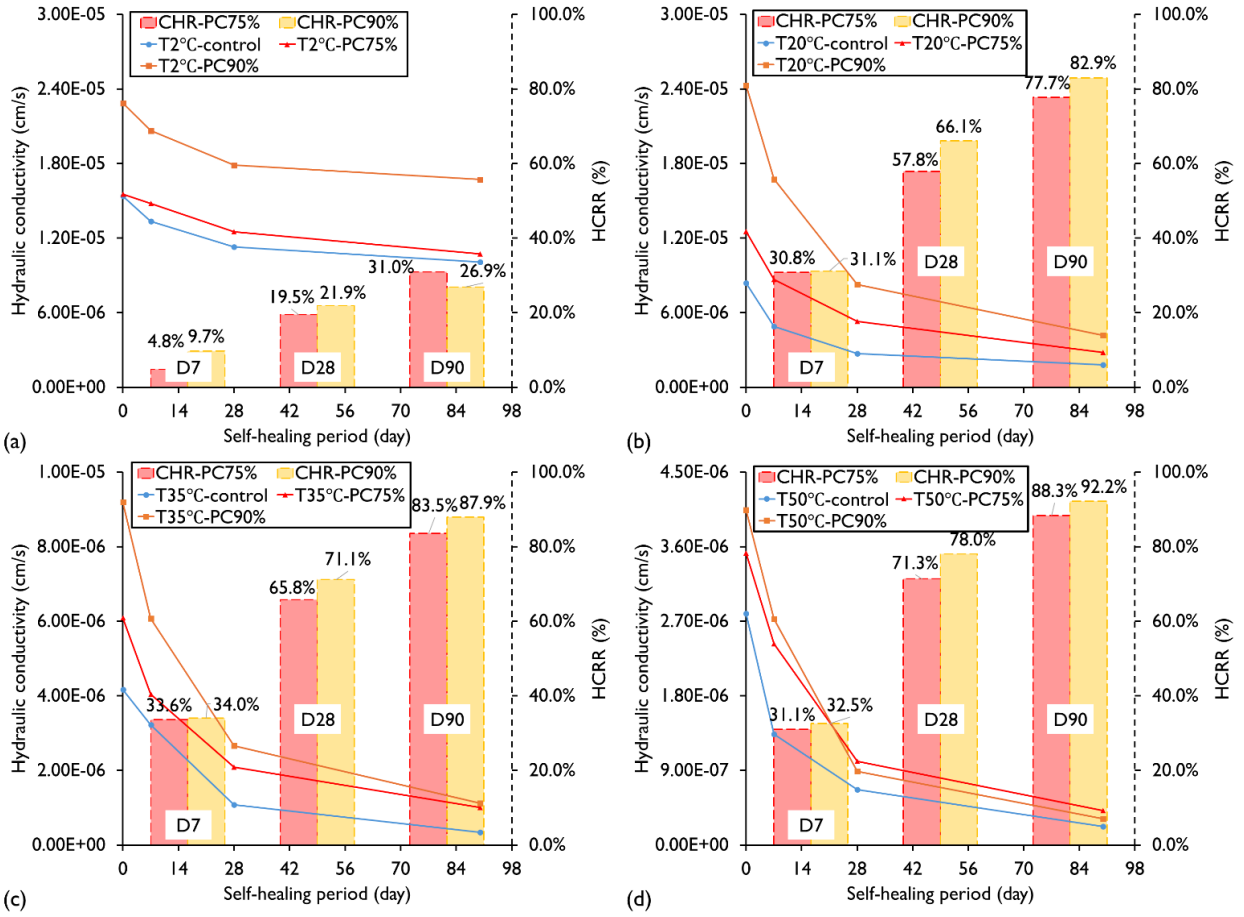

Figure 5-24. Changes of hydraulic conductivity and HCRR of pre-cracked specimens exposed to different temperatures of (a) 2°C, (b) 20°C, (c) 35°C, and (d) 50°C over self-healing period (D7, D28, and D90: 7, 28 and 90 days of self-healing period, respectively).

As the self-healing behaviour occurs, the saturated hydraulic conductivities of pre-cracked CPB specimens decrease with the extension of the self-healing period up to 90 days, regardless of the curing temperature and pre-cracking level. The hydraulic conductivity changes of pre-cracked CPB specimens cured under 20°C (room temperature) are shown in Figure 5-24b for reference. It is seen that the PC90% pre-cracked specimen exhibits a successive recovery of saturated hydraulic conductivity with an HCRR value reaching 82.9% after the self-healing period of Day 90. This decrease in hydraulic conductivity is ascribed to the self-healing process, during which the reactions of continuous cement hydration and carbonation of $Ca(OH)_2$ produce the healing products (i.e., C-S-H, $Ca(OH)_2$, and $CaCO_3$) to fill the cracks and voids and block the internal connections within CPB matrix, thereby resulting in the reduction of porosity and modification of pore structures. When the pre-cracked specimens were cured under 35°C and 50°C, the hydraulic conductivity decreasing rate is faster compared with that of 20°C, with 50°C being the fastest among all studied temperatures. Specifically, the HCRR values of the PC90% pre-cracked specimens reach up to 87.9% and 92.2% when cured at 35°C and 50°C, respectively, after the self-

healing period of D90. Furthermore, the PC90% pre-cracked specimens cured at 50°C exhibit a more robust healing performance during the first 28 days of the self-healing period with an achievement of HCRR value up to 78.0%. The results of HCRR indicate that the elevation of curing temperature significantly enhances the self-healing efficiency in CPBs. In other words, the extent of cement hydration is more vigorous in the pre-cracked specimens cured at higher temperatures, which accelerates the hydration reaction with more production of healing products over the same self-healing period. This argument agrees with the thermal analysis results in Figure 5-22a, where the CPB specimen cured at 35°C presents a higher hydration degree than that of 20°C, suggesting that more cement hydration products are generated at a higher curing temperature to reduce k_{sat}.

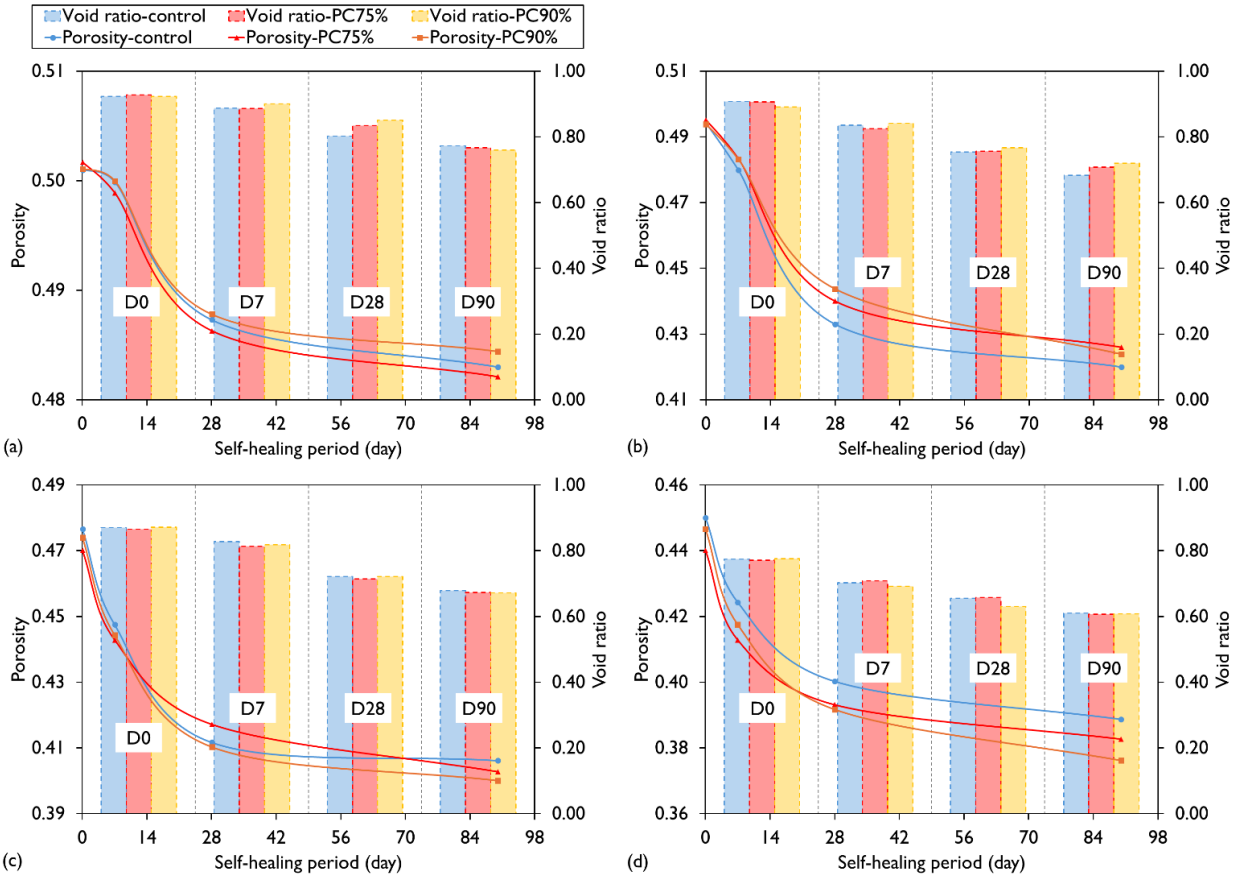

Figure 5-25. Changes of porosity and void ratio of both control and pre-cracked CPB specimens cured at the temperature of (a) 2°C, (b) 20°C, (c) 35°C, and (d) 50°C over the self-healing period (D0, D7, D28, and D90: 0, 7, 28 and 90 days of the self-healing period, respectively).

However, as seen in Figure 5-24a, the pre-cracked specimens cured at a low temperature (2°C) bear comparatively much lower self-healing efficiency in hydraulic conductivity with the achievement of only up to 31.0% HCRR value after a self-healing period of 90 days (D90). This diminished healing performance can be explained by the fact that low temperature induces low reactivity conditions, which impede chemical reactions in cement hydration and the formation of hydration products. Additionally, CPB specimens usually have comparatively high porosity and large

capillary pores after a short curing period (i.e., an initial curing period of 7 days in this study) (Fall & Samb, 2008). Therefore, the lower amount of hydration products is not able to sufficiently fill the cracks and voids to produce a relatively dense cementitious system, resulting in a poor pore structure, which provides an easy path for liquid flow. The observation of poor crack closure at 2°C with the smallest crack width that can be completely healed (as listed in Table 5-8) and the results of MIP tests in Figure 5-23 also support this performance. The rate of binder hydration governed by the curing temperature significantly impacts the refinement of the pore structure of the CPB matrix and is, therefore, responsible for the self-healing efficiency in the recovery of saturated hydraulic conductivity. From the results presented above it can be concluded that low temperatures significantly limit the self-healing capacity of CPB due to slower cement hydration rates and reduced formation of self-healing products. In cold or permafrost regions, this limitation could affect the durability and stability of CPB structures in underground mining operations, as cracks may remain unhealed or only partially healed. This insight suggests that in such regions, additional measures may be needed to enhance CPB's self-healing performance, such as the incorporation of additives that facilitate low-temperature hydration. These considerations are crucial for adapting CPB applications in colder or permafrost areas to ensure the CPB material's resilience and structural integrity in cold mining environments.

5.3.4 Summary and Conclusions

This study comprehensively investigated the effects of varying curing temperatures on the self-healing capacity and performance recovery of pre-cracked CPB specimens. The research focused on four different temperature levels (2°C, 20°C, 35°C, and 50°C) and evaluated the self-healing efficiency through the recovery of mechanical strength, hydraulic conductivity, and crack closure over self-healing periods of 7, 28, and 90 days. Finally, analytical techniques, such as TGA, MIP, and SEM-EDS, are employed to unravel the self-healing mechanisms within CPB specimens. Based on the experimental results and discussions above, the following conclusions can be drawn:

- CPB specimens cured at elevated temperatures (35°C and 50°C) exhibited significantly improved self-healing efficiency and mechanical strength recovery compared to those cured at room temperature (20°C). The enhanced performance is primarily due to the accelerated cement hydration at higher temperatures, leading to the formation of more hydration products within the same self-healing period.
- Among the temperature levels studied, 50°C provided the most robust self-healing efficiency. Particularly, specimens pre-cracked at 90% of their ultimate compressive strength achieved a 30.6 % higher UCS than the control specimens after 28 days of self-healing. However, the availability of unhydrated cement particles decreased over longer periods, resulting in a slower healing rate after 90 days.
- CPB specimens cured at the low temperature of 2°C displayed delayed and inferior self-healing capacity. The low temperature inhibited early cement hydration, resulting in fewer hydration products and limited mechanical strength recovery. This was evident in both the

mechanical strength and hydraulic conductivity recovery, which remained significantly lower compared to specimens cured at higher temperatures.

- Specimens cured at 35℃ and 50℃ also showed faster and more complete recovery of hydraulic conductivity, with a maximum HCRR of 92% observed at 50℃ after 90 days. In contrast, the specimens cured at 2℃ exhibited only up to a 31% recovery in hydraulic conductivity after the same period, further indicating the adverse impact of low temperatures on self-healing.
- The improved rates of unhydrated cement particle hydration and carbonation of calcium hydroxide significantly contribute to the enhanced self-healing efficiency of CPB specimens when exposed to elevated temperatures. A large amount of self-healing products (i.e., C-S-H, $Ca(OH)_2$, $CaCO_3$) facilitates the physical crack closure with a closure ability order of 50℃ >35℃ >20℃ >2℃ based on the direct observations by microscope. Narrower and smaller cracks are more effective and have a higher potential to be completely healed than wider and larger cracks.

In conclusion, this study provides valuable insights into the temperature-dependent self-healing mechanisms of CPB materials. It demonstrates that curing temperature is a critical factor influencing the self-healing capacity and mechanical performance recovery of CPB. The findings underscore the importance of considering curing temperature in the design and implementation of CPB structures, particularly in ensuring long-term mechanical stability and durability in underground mining operations.

This study was conducted under controlled laboratory conditions that may not fully capture the complex environmental and operational conditions present in actual underground mining environments. Factors such as varying humidity, in-situ stresses, and the presence of other chemical constituents could impact the self-healing behaviour of CPB in real-world applications. Thus, a broader investigation into other environmental variables, such as humidity, curing stress or chemical exposure (sulphate ions), may provide a more comprehensive understanding of CPB's self-healing performance. Moreover, future studies could investigate alternative binders or additives that improve self-healing performance at low temperatures, given the constraints observed in our low-temperature experiments. These directions would contribute significantly to refining CPB technology and ensuring its adaptability across diverse mining settings.

5.3.5 References

Aldhafeeri, Z., & Fall, M. (2017). Sulphate induced changes in the reactivity of cemented tailings backfill. International Journal of Mineral Processing, 166, 13-23.

Alexander, K. (1962). Concrete strength, cement hydration and the maturity rule. Aust. J. Appl. Sci., 13, 277-284.

Ali, G., Fall, M., & Alainachi, I. (2021). Time-and temperature-dependence of rheological properties of cemented tailings backfill with sodium silicate. Journal of Materials in Civil Engineering, 33(3), 04020498.

ASTM. (2016). ASTM D5084-16a. Standard Test Methods for Measurement of Hydraulic Conductivity of Saturated Porous Materials Using a Flexible Wall Permeameter. In. West Conshohocken, PA: ASTM International.

ASTM. (2020). ASTM C143/C143M-20. Standard Test Method for Slump of Hydraulic-Cement Concrete. In. West Conshohocken, PA: ASTM International.

ASTM. (2021). ASTM C39/C39M-21. Standard Test Method for Compressive Strength of Cylindrical Concrete Specimens. In. West Conshohocken, PA: ASTM International.

Benzaazoua, M., Fall, M., & Belem, T. (2004). A contribution to understanding the hardening process of cemented pastefill. Minerals Engineering, 17(2), 141-152.

Bull, A. J., & Fall, M. (2020). Curing temperature dependency of the release of arsenic from cemented paste backfill made with Portland cement. Journal of Environmental Management, 269, 110772.

Carraro, J. A. H., Prezzi, M., & Salgado, R. (2009). Shear strength and stiffness of sands containing plastic or nonplastic fines. Journal of geotechnical and geoenvironmental engineering, 135(9), 1167-1178.

Chen, S., Wu, A., Wang, Y., & Wang, W. (2021). Coupled effects of curing stress and curing temperature on mechanical and physical properties of cemented paste backfill. Construction and Building Materials, 273, 121746.

Cheng, H., Wu, S., Li, H., & Zhang, X. (2020). Influence of time and temperature on rheology and flow performance of cemented paste backfill. Construction and Building Materials, 231, 117117.

Cuenca, E., & Ferrara, L. (2017). Self-healing capacity of fiber reinforced cementitious composites. State of the art and perspectives. KSCE Journal of Civil Engineering, 21, 2777-2789.

Cui, L., & Fall, M. (2015). A coupled thermo–hydro-mechanical–chemical model for underground cemented tailings backfill. Tunnelling and Underground Space Technology, 50, 396-414.

Cui, L., & Fall, M. (2017). Modeling of pressure on retaining structures for underground fill mass. Tunnelling and Underground Space Technology, 69, 94-107.

De Belie, N., Gruyaert, E., Al-Tabbaa, A., Antonaci, P., Baera, C., Bajare, D., . . . Jefferson, T. (2018). A review of self-healing concrete for damage management of structures. Advanced materials interfaces, 5(17), 1800074.

De Nardi, C., Cecchi, A., Ferrara, L., Benedetti, A., & Cristofori, D. (2017). Effect of age and level of damage on the autogenous healing of lime mortars. Composites Part B: Engineering, 124, 144-157.

Deschner, F., Lothenbach, B., Winnefeld, F., & Neubauer, J. (2013). Effect of temperature on the hydration of Portland cement blended with siliceous fly ash. Cement and Concrete Research, 52, 169-181.

Fall, M., Adrien, D., Célestin, J., Pokharel, M., & Touré, M. (2009). Saturated hydraulic conductivity of cemented paste backfill. Minerals Engineering, 22(15), 1307-1317.

Fall, M., & Benzaazoua, M. (2005). Modeling the effect of sulphate on strength development of paste backfill and binder mixture optimization. Cement and Concrete Research, 35(2), 301-314.

Fall, M., Benzaazoua, M., & Ouellet, S. (2005). Experimental characterization of the influence of tailings fineness and density on the quality of cemented paste backfill. Minerals Engineering, 18(1), 41-44.

Fall, M., Célestin, J., Pokharel, M., & Touré, M. (2010). A contribution to understanding the effects of curing temperature on the mechanical properties of mine cemented tailings backfill. Engineering Geology, 114(3-4), 397-413.

Fall, M., & Samb, S. (2008). Pore structure of cemented tailings materials under natural or accidental thermal loads. Materials Characterization, 59(5), 598-605.

Fang, K., & Fall, M. (2018). Effects of curing temperature on shear behaviour of cemented paste backfill-rock interface. International Journal of Rock Mechanics and Mining Sciences, 112, 184-192.

Ferrara, L., Krelani, V., Moretti, F., Flores, M. R., & Ros, P. S. (2017). Effects of autogenous healing on the recovery of mechanical performance of High Performance Fibre Reinforced Cementitious Composites (HPFRCCs): Part 1. Cement and concrete composites, 83, 76-100.

Ghirian, A., & Fall, M. (2014). Coupled thermo-hydro-mechanical–chemical behaviour of cemented paste backfill in column experiments: Part II: Mechanical, chemical and microstructural processes and characteristics. Engineering Geology, 170, 11-23.

Ghirian, A., & Fall, M. (2015). Coupled behavior of cemented paste backfill at early ages. Geotechnical and Geological Engineering, 33, 1141-1166.

Khoury, G. (1992). Compressive strength of concrete at high temperatures: a reassessment. Magazine of concrete Research, 44(161), 291-309.

Li, D., Zheng, H., Gu, K., Lang, L., Shi, S., & Chen, B. (2023). Autogenous healing mechanism of cement-based materials. Frontiers of Structural and Civil Engineering, 17(6), 948-963.

Nasir, O., & Fall, M. (2010). Coupling binder hydration, temperature and compressive strength development of underground cemented paste backfill at early ages. Tunnelling and Underground Space Technology, 25(1), 9-20.

Neville, A. (2002). Autogenous healing—a concrete miracle? Concrete International, 24(11), 76-82.

Pokharel, M., & Fall, M. (2013). Combined influence of sulphate and temperature on the saturated hydraulic conductivity of hardened cemented paste backfill. Cement and concrete composites, 38, 21-28.

Quan, W., & Fall, M. (2024). Investigation of Inherent Self-Healing Behaviour in Cemented Paste Backfill. Paper presented at the 14th International Symposium on Mining with Backfill, Minefill 2024, Vancouver, Canada.

Reinhardt, H.-W., & Jooss, M. (2003). Permeability and self-healing of cracked concrete as a function of temperature and crack width. Cement and Concrete Research, 33(7), 981-985.

Saremi, A., & Fall, M. (2024). Self-desiccation behavior of nano-cemented tailings backfill plug: Insights from thermo-mechanical-chemical column experiments. Journal of Materials Research and Technology, 30, 5952-5962.

Schindler, A. K. (2004). Effect of temperature on hydration of cementitious materials. Materials Journal, 101(1), 72-81. doi:10.14359/12990

Su, Y.-F., Huang, C., Jeong, H., Nantung, T., Olek, J., Baah, P., & Lu, N. (2020). Autogenous healing performance of internal curing agent-based self-healing cementitious composite. Cement and concrete composites, 114, 103825.

Suleiman, A., & Nehdi, M. (2021). Effect of autogenous crack self-healing on mechanical strength recovery of cement mortar under various environmental exposure. Scientific Reports, 11(1), 7245.

Taylor, H. F. (1964). The chemistry of cements.

Vergne, J. (2000). Rules of thumb for the hard rock mining industry. Hard rock miner's handbook.

Wu, D., Fall, M., & Cai, S. (2013). Coupling temperature, cement hydration and rheological behaviour of fresh cemented paste backfill. Minerals Engineering, 42, 76-87.

Xiu, Z., Wang, S., Ji, Y., Wang, F., & Ren, F. (2022). Experimental study on the triaxial mechanical behaviors of the Cemented Paste Backfill: Effect of curing time, drainage conditions and curing temperature. Journal of Environmental Management, 301, 113828.

Yang, Y., Lepech, M. D., Yang, E.-H., & Li, V. C. (2009). Autogenous healing of engineered cementitious composites under wet–dry cycles. Cement and Concrete Research, 39(5), 382-390.

Yang, Y., Yang, E.-H., & Li, V. C. (2011). Autogenous healing of engineered cementitious composites at early age. Cement and Concrete Research, 41(2), 176-183.

Yilmaz, E., Kesimal, A., & Ercidi, B. (2004). Strength development of paste backfill simples at Long term using different binders. Paper presented at the Proceedings of 8th symposium MineFill04, China.

5.4 Paper IV: Self-Healing Behaviour of Cemented Paste Backfill in Response to Various Drainage Conditions

Published in *Developments in the Built Environment*, Volume 22, 100648

Weizhou Quan, Mamadou Fall

Department of Civil Engineering, University of Ottawa, Ottawa, Ontario, Canada

Abstract

Cemented paste backfill (CPB) is an innovative mine backfilling method widely used in underground mining operations around the world. In field applications, CPB structures can experience a range of drainage conditions, varying from undrained to fully drained states. However, the influence of these varying drainage conditions on the self-healing behaviour and performance of CPB remains unknown, as no studies to date have addressed this critical knowledge gap. This study addresses this gap by evaluating the self-healing efficiency of CPB under three drainage scenarios: full drainage, partial drainage, and no drainage. Results show that drainage conditions significantly influence self-healing performance, with specimens under partial or full drainage demonstrating superior crack closure and recovery of mechanical and hydraulic properties compared to undrained specimens. These findings enhance understanding of CPB's self-healing mechanisms and offer practical insights for improving the durability and stability of CPB structures in mining applications.

Keywords: Cemented paste backfill; Mine; Self-healing; Tailings; Mechanical properties; Hydraulic conductivity; Drainage condition.

5.4.1 Introduction

Mine waste (i.e., tailings), as the main byproduct of mining activities, has been enormously produced during mining operations and mineral processing (Franks et al., 2011). Approximately 223 billion tonnes (534 billion cubic meters) of waste tailings were present in active, inactive, and abandoned tailings storage facilities (TSFs) as of 2019, with an estimated additional 40 to 50 billion tonnes to be generated over the next five years (World Mine Tailings Futures, 2020). The conventional disposal methods of tailings have substantial potential to induce significant geotechnical and environmental impacts on the communities and ecosystem, such as tailings dam failure (Berghe et al., 2011; Deng et al., 2017), acid mine drainage (AMD) (Kalin et al., 2006; Naidu et al., 2019), etc. The limited tailings impoundment cannot satisfy the deposition of the significantly increasing production of waste tailings. Consequently, cemented paste backfill (CPB) has been extensively used as an innovative technique to manage tailings from a sustainable perspective, which recycles approximately up to 60% of produced tailings into underground extracted stopes/voids (Ercikdi et al., 2015). The application of the CPB technique not only supports the adjacent orebody and underground structure to secure a safe working environment but also improves the mine productivity (Jiang et al., 2020; Kesimal et al., 2005; Yu et al., 2024). CPB is a cementitious mixture that typically consists of dewatered tailings (70-85 wt.%), hydraulic

binders (typically 3-7 wt.%), and processed mine/fresh water to meet certain mechanical requirements after placement fulfilling its role of mine rehabilitation (Benzaazoua et al., 2004; Fall et al., 2005; Haiqiang et al., 2016; Wang et al., 2024).

The fresh CPB mixture is usually prepared in a plant located at the mine ground surface and transported to underground extracted voids by pumping and/or gravity (Belem & Benzaazoua, 2008). Thus, to meet the designed requirements of rheological properties (i.e., flowability), CPBs are always prepared with excessive water to allow easy transportation to designated underground cavities (Haruna & Fall, 2022; Zhao et al., 2020). A high water content (i.e., water-to-cement (w/c) ratio of past backfills is common at 2.5-7 (Ramlochan et al., 2004) enhances the flowability of CPB by reducing its viscosity, thereby facilitating a more fluid and manageable paste. The increased water content lowers the internal friction between the particles within the CPB mixture (reducing the direct contacts between particles) attributed to the lubrication effect of water around the particles, which makes the particles easier to slide past one another (Liu et al., 2020; Simon & Grabinsky, 2013; Zhao et al., 2020), allowing for improved flow characteristics during pumping and distribution, and a more efficient placing process within the underground voids. However, the elevated water content may also adversely impact the mechanical properties and long-term stability of the cured CPB structure. Benzaazoua et al. (2004) stated that the increase in the water content (or slump value) has a negative influence on the mechanical strength of the cemented pastefill due to the dilution rate of the soluble species (i.e., cement dissolution) and precipitation of hydrates. It was concluded that the behaviour of pastefill is influenced not only by the environment in which it is placed, but also by the mixture itself, with the available water playing a critical role. Once placed in the stope, the CPB structure is subjected to coupled thermal (T; i.e., temperature), hydraulic (H; i.e., suction, pore water pressure, degree of saturation, drainage), mechanical (M; i.e., stress, self-weight load), and chemical (C; i.e., contamination dissolution, pore water and binder chemistries) (THMC) processes (Cui & Fall, 2016; Fang et al., 2021; Ghirian & Fall, 2016). Among these, the hydraulic conditions, such as pore water pressure, volumetric water content, and drainage, which are directly associated with the water content, begin to evolve rapidly and have an immediate impact on the development of CPB properties. For example, the drainage conditions of CPB structure can be affected by various factors, such as geological conditions of the mine, groundwater conditions, seepage, drainage pipes, barricade and permeability of CPB materials, drawpoint locations, permeability of the rock mass surrounding the backfill, etc. (El Mkadmi et al., 2014; Ghirian & Fall, 2016; Helinski et al., 2011). If a fresh CPB mixture contains fine tailings and high cement content and the adjacent rock mass is not fractured, the CPB matrix may retain the water without any drainage, representing the almost undrained conditions during its curing. In the same way, if a fresh CPB mixture is prepared by coarse tailings and the surrounding rock mass is highly fractured, the water would drain out at the barricade to achieve full drainage. Numerous studies (Al-Moselly & Fall, 2024; Belem et al., 2006; Cui & Fall, 2016; Fall et al., 2005; Fang et al., 2021; Yin et al., 2012; Zhao et al., 2020) have been conducted to investigate the effect of drainage conditions (water content) on the mechanical and rheological properties of CPB materials. For instance, Belem et al. (2002) conducted a series of experiments using two types of molds under

different applied loads, including molds with a perforated bottom to favour drainage and non-perforated molds to prevent drainage, to identify the possible causes of the differences in mechanical strength of CPB. The primary results revealed that the UCS values of drained specimens are higher than those of the undrained specimens. Moreover, Fang & Fall (2018) found that the drained specimens exhibit higher shear stress at the interface between CPB and rock than the undrained ones, and undrained specimens undergo larger contractions than the drained ones. In addition, Zhao et al. (2020) stated that the yield stress of CPB decreases with an increase in water content regardless of binder type. Furthermore, the water drainage directly affects the changes in volumetric water content (VWC), pore water pressure (PWP), and matrix suction within the CPB matrix, which are essential for initial strength development (Al-Moselly & Fall, 2024; Belem et al., 2002; Fahey et al., 2010; Ghirian & Fall, 2016; Wang et al., 2022; Xiu et al., 2022). These phenomena could be attributed to the settling and hardening processes occurring within the CPB material and the removal of its excess pore water.

As a cementitious material, cracks may also be formed in CPB structures as a similar challenge arises in other cementitious materials (i.e., concrete, mortar, engineered cementitious composites) (Choi et al., 2017; Ohno & Ohtsu, 2010; Yıldırım et al., 2015) due to internal and external factors, such as the pressure of CPB overburden, stresses induced by the closure of rock walls adjacent to or surrounding the CPB structures, shrinkage, loads from mining activities (i.e., machinery), early application of load, uneven load distribution, or rock bursts. The presence of cracks will significantly compromise the CPB structure integrity and its environmental performance. For example, the sensitivity of CPBs to acid mine drainage (AMD) primarily depends on the reactivity of the tailings contained in the CPB. This reactivity not only relies on the types and amount of sulfide minerals present in the CPB, but also on the elements penetrating the CPB matrix through the cracks, such as oxygen and water, which would facilitate the oxidation reactions, thus leading to a loss of mechanical strength and diminishing its durability and serviceability.

Self-healing is a well-documented phenomenon in conventional cementitious materials, referring to their inherent ability to repair cracks automatically without external intervention or diagnosis. Generally, self-healing in these materials is achieved via two mechanisms: autogenous healing and autonomous healing (Li & Herbert, 2012; Van Breugel, 2007). Autogenous healing primarily relies on the delayed hydration of unhydrated cement particles within the cementitious matrix without the intentional addition of self-healing agents (Cuenca & Ferrara, 2017). Conversely, autonomous healing relies on external sources such as embedded or directly added healing agents, such as fibers (Savastano & Agopyan, 1999; Wei et al., 2010), polymer-based agents (Snoeck et al., 2014; Van Tittelboom et al., 2016), nanomaterials (Qian et al., 2010; Quercia et al., 2012), shape memory alloys (Jefferson et al., 2010; Kuang & Ou, 2008), or bacteria (Esaker et al., 2023; Seifan et al., 2016). Water plays a critical role in enhancing self-healing performance in both autogenous and autonomous healing mechanisms (Termkhajornkit et al., 2009; Zhang et al., 2020). For instance, Özbay et al. (2013) demonstrated the effects of sustained flexural loading on the self-healing behaviour of fly ash-incorporated ECC under continuous water, continuous air, and wet/dry cycle exposure conditions. They found that continuous water and wet/dry cycle curing significantly

accelerated crack healing, improved mechanical properties, and reduced permeability, with continuous water conditions yielding the most effective healing due to further hydration. Similarly, Roig-Flores et al. (2015) investigated self-healing in concrete with and without crystalline admixtures under four environmental exposures: water immersion, water contact, humidity chamber, and air exposure. Their results emphasized that water availability is critical for self-healing in both reference and crystalline admixture concretes, with water immersion producing the highest healing rates and achieving complete healing in some cases. In conventional cementitious materials with low w/c ratios (e.g., 0.4-0.55), approximately 10-30% of cement particles remain unhydrated. Upon exposure to water, the hydration process resumes, further producing cement hydration products such as C-S-H and $Ca(OH)_2$. Water also facilitates the dissolution of $Ca(OH)_2$, promoting the formation of calcium carbonate, which contributes to crack filling, pore refinement, and matrix densification (Han et al., 2015; Sahmaran et al., 2015). In the same way, water content significantly impacts autonomous healing. For example, Esaker et al. (2024) examined the autonomous healing performance of a bacteria-based mortar embedded in clay soil under varying water saturation regimes. The findings revealed that fully saturated clay soil conditions enhanced healing performance, as higher water content not only facilitated calcium carbonate precipitation via bacterial metabolism but also supported autogenous healing through the hydration of unhydrated cement particles. Consistent results have been observed for bacteria-based cementitious materials under full water submersion or wet-dry cycles (Hamza et al., 2024; Luo et al., 2015; Zhang et al., 2017).

In contrast, CPB mixtures feature much higher w/c ratios, lower cement content, and finer particle size distributions, making them significantly different from conventional cementitious materials. These differences indicate that self-healing behaviours observed in conventional cementitious materials cannot be directly applied to CPB. Despite the importance of self-healing in extending the durability of CPB, research in this area remains sparse, with only a few studies addressing CPB self-healing behaviour (Quan & Fall, 2024; Xiang et al., 2023a; Xiang et al., 2023b). Furthermore, the influence of drainage conditions (water content) on the autogenous healing capacity of CPB has not been investigated to date. Therefore, this study experimentally investigates the effects of drainage conditions on the autogenous healing capacity and behaviour of CPB material to enhance the comprehensive understanding of the self-healing behaviour of CPB.

5.4.2 Materials and Experimental Program

5.4.2.1 Materials

Tailings

Synthetic silica tailings (ST, primarily composed of SiO_2-99.8%, Al_2O_3-0.05%, and Fe_2O_3-0.035%) were the main constituents used to prepare the CPB mixtures in this experimental program. Its chemically inert property eliminates the uncertainties induced by the uncontrollable variations of the mineralogical compositions in natural tailings and the reactivity of some minerals. Figure 5-26 depicts the comparable particle size distribution of STs to the average of nine natural tailings (NT) samples from eastern Canadian mines. Approximately 43% of the particles in ST have sizes finer

than 20 µm, categorizing them as medium tailings. The use of STs could correlate the results of the experimental work with the actual Canadian mining scenario. Additionally, the physical properties of STs and the average of nine types of Canadian tailings are shown in Table 5-9.

Binder and mixing water

Portland cement Type I (PCI), the most used cement in the mining industry, was used as the hydraulic binder to prepare CPB specimens. The physical and chemical compositions of the PCI are listed in Table 5-10. Additionally, tap water was utilized to mix with the tailings and binder to prepare the CPB mixture.

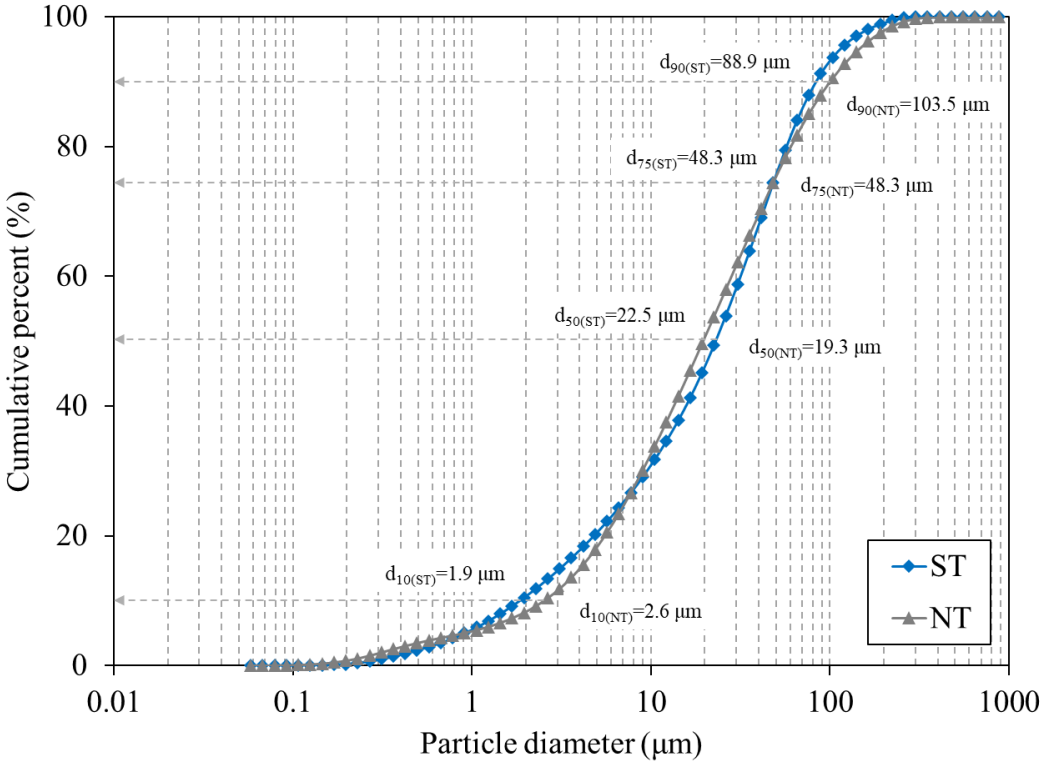

Figure 5-26. Particle size distribution of the used STs along with an average of nine NTs in eastern Canada.

Table 5-9. Physical properties of the used STs and the average of nine NTs in eastern Canada.

Element	G_s	D_{10}	D_{30}	D_{50}	D_{60}	C_u	C_c
		(µm)					
ST	2.7	1.9	9.0	22.5	31.5	16.6	1.3
Nine NT average	-	1.8	9.1	20.0	30.8	17.1	1.7

(G_s: specific gravity; C_u: coefficient of uniformity; C_c: coefficient of curvature)

Table 5-10. Characteristic of the used binder PCI.

Binder type	MgO	CaO	SiO_2	Al_2O_3	Fe_20_3	SO_3	SSA	R.D.
	(wt.%)						(m^2/g)	
PCI	2.65	68.82	18.03	4.53	2.70	3.82	1.30	3.10

RD: relative density; SSA: specific surface area.

5.4.2.2 Specimen preparation and initial curing

The design of CPB specimens in this study is presented in Table 5-11. To prepare the fresh CPB mixture in this study, specific quantities of silica tailings and PCI were weighed and blended in a mechanical mixer for an initial 1-minute dry mixing to ensure uniform distribution of the solid particles. A fixed mix proportion of 4.5 wt.% binder (PCI) by the total weight of solids was adopted. Subsequently, the pre-determined amount of water, calculated based on a constant w/c ratio of 7.35 by weight, was added to the dry mix of tailings and PCI. The mechanical mixing then continued for an additional 7 minutes of wet mixing to achieve a homogeneous CPB mixture. A slump value of 18 cm was determined for the fresh CPB mixture in accordance with ASTM C143 (ASTM, 2020) to ascertain the workability of the prepared CPB materials. This slump value is commonly used in Canadian mine backfill practices and plants. In the field, the drainage conditions of the CPB structure are between full drainage and no drainage, i.e., the CPB mass is partially drained in many field cases. Therefore, three conditions, including full drainage (FD), half drainage (HD), and no drainage (ND), are adopted in this study to incorporate the different drainage conditions, representing the downward axial water drainage. To prepare specimens with the predetermined three different drainage conditions, cylindrical molds (Φ50×100 mm) with perforated bottoms were used to allow the water to bleed from the curing molds for the achievement of fully drained and half-drained specimens casting, while the undrained specimens were prepared in the non-perforated plastic molds to prevent drainage. The drainage water was collected through the funnel below, which connected to the beaker, as illustrated in Figure 5-27. The top of the molds was lid-sealed to prevent water evaporation during the drainage process. According to the pilot testing, approximately 9.8 g of water would drain out from the specimens with full drainage condition when reaching the equilibrium. In this way, the specimens with half drainage were cast under the control of around 4.9 g drainage water. Once the drainage process was completed, the bottom of the molds would be sealed with waterproof silicone sealant to prevent the drainage of extra water from the specimens. Then, the drained and undrained specimens underwent an initial curing (IC) period of 7 days under ambient conditions prior to crack initiation. Note that full drainage does not signify the complete dissipation of pore water pressure (PWP) within the CPB matrix. It refers to the situation where the maximum amount of water has been allowed to drain from the specimen via the perforated bottom of molds.

5.4.2.3 Crack initiation and exposure condition

The CPB specimens were pre-cracked under uniaxial compression loading to introduce cracks of varying numbers and widths to monitor the self-healing behaviour of CPB specimens subjected to

different drainage conditions. To achieve similar pre-damage with constant pre-cracking levels, the initial compressive strength of CPB specimens was determined after the initial curing (IC) phase of 7 days through the uniaxial compressive strength (UCS) tests as per ASTM C39 (ASTM, 2021). In this study, the CPB specimens were subjected to specific pre-cracking levels of 0%, 75%, or 90% (i.e., PC0%, PC75%, or PC90%, respectively) of their respective initial UCS value during the pre-peak phase, making the pre-cracks introduced in CPB specimens in a controlled manner. These pre-cracking levels were determined based on previous studies (Fall et al., 2009; Quan & Fall, 2024) and to simulate varying degrees of compression-induced damage in a practical CPB structure. Note that the specimens subjected to the pre-cracking level of PC0% serve as control specimens with no cracks introduced in this study. When reaching the designated loading thresholds, the applied load was maintained for one minute before being released to allow the generation and propagation of the cracks in CPB specimens. The UCS experiments and pre-cracking process were conducted utilizing a computer-controlled mechanical press (MTS 10/GL) with a normal load of 50 kN and a displacement rate of 1 mm/min under displacement control. Upon unloading, crack characteristics were conducted using a digital microscope with a maximum magnification of 200× to capture the initial cracks before any self-healing performance. After this step, the pre-cracked specimens were encapsulated using plastic films and stored in ambient conditions (23±2°C) along with uncracked (control) specimens for a self-healing curing phase. This isolated self-healing environment aimed to exclude the external impacts and to facilitate the examination of the self-healing capability of CPB materials in relation to drainage conditions. The overall program for mechanical testing and self-healing period is shown in Table 5-11. Note that the pre-cracking day is named Day 0, representing the self-healing start day, followed by Day 7, Day 28, and Day 90, representing the early self-healing periods of 7 and 28 days, and the advanced self-healing period of 90 days, respectively.

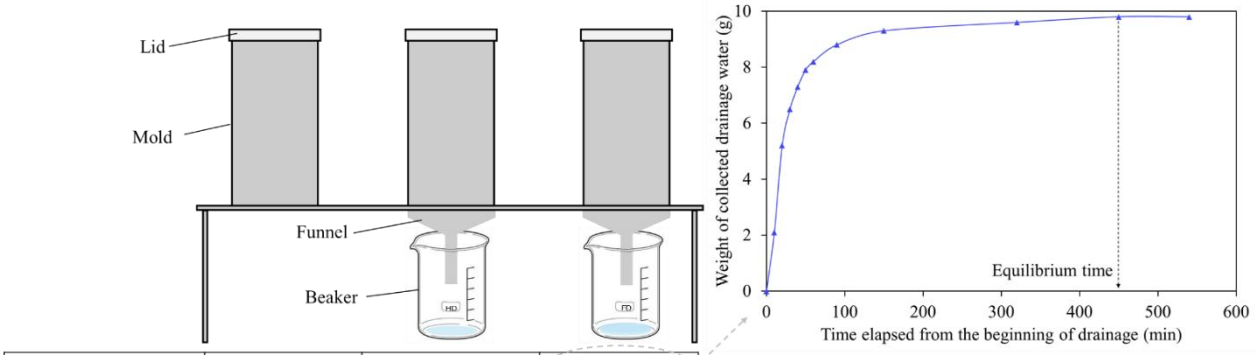

Batch type	No drainage	Half drainage	Full drainage
Collected drainage water (g/specimen)	0	4.9 ± 0.3	9.8 ± 0.3

Figure 5-27. Schematic diagram of the experimental setup representing different drainage conditions of CPB specimens.

Table 5-11. Summary of experimental program for each testing batch of CPB specimens.

Group nomenclature	Binder content (wt.%)	w/c ratio	Initial curing (day)	Drainage condition	Pre-cracking level (%)	Self-healing Period (day)
FD	4.50	7.35	7	Full	0, 75%, and 90% of UCS after IC.	7 28 90
HD	4.50	7.35	7	Half	0, 75%, and 90% of UCS after IC.	7 28 90
ND	4.50	7.35	7	No	0, 75%, and 90% of UCS after IC.	7 28 90

*FD, HD, and ND indicate specimens with drainage conditions of full, half, and no drainage, respectively.

5.4.2.4 Self-healing evaluation methods

Crack characteristics

The surface pre-cracks in CPB specimens were observed using the digital microscope after each specific predetermined self-healing period of 7, 28, and 90 days, which provided a direct approach to visually monitor the self-healing behaviour. The cracks that have the self-healing behaviour were analyzed from the narrowest to the widest points to quantitatively measure the self-healing effect on crack closure.

Mechanical property investigation

To evaluate the self-healing efficiency in terms of mechanical strength recovery, UCS tests were conducted to measure the compressive strength of the CPB specimens at specific self-healing periods based on ASTM C39/C39M-21 (ASTM, 2021). On Day 0 (the pre-cracking day), the initial strengths (denoted as $S_{pre\text{-}cracked}$) of the pre-cracked specimens, subjected to pre-cracking levels of PC75% and PC90%, were measured immediately after the pre-cracking process (prior to the onset of self-healing). Following self-healing periods of Day 7, Day 28, and Day 90, UCS tests were performed on the healed pre-cracked specimens to assess the progression of strength recovery over time (S_{healed}). Additionally, the strengths of reference control specimens (PC0%: $S_{control}$) were measured alongside the pre-cracked specimens at the same self-healing periods as aforementioned. To quantitatively assess strength recovery, the compressive strengths of the pre-cracked or healed pre-cracked specimens were compared to those of the control specimens, with the relative changes in compressive strength (CCS) calculated as follows:

$$CCS(\%)=\frac{S_{pre\text{-}cracked/healed} - S_{control}}{S_{control}} \quad (5\text{-}8)$$

where $S_{pre\text{-}cracked/healed}$ is the UCS of the pre-cracked specimens before or after a self-healing period, and $S_{control}$ is the UCS of uncracked control specimens subjected to the same self-healing condition and period.

The calculated CCS value for each self-healing condition was averaged by at least triplicate CPB specimens to ensure the repeatability of the results. A computer data acquisition system was used to maintain a constant deformation rate of 1 mm/min.

Hydraulic property investigation

To determine whether mechanical pre-damage affects the conductivity and how much self-healing occurred in terms of permeability within the CPB matrix, saturated hydraulic conductivity (k) tests were conducted on both pre-cracked and uncracked CPB specimens before and after healing periods. These tests used a triaxial cell with a flexible wall technique according to ASTM 5084-16a (ASTM, 2016) to determine their coefficients of permeability or hydraulic conductivity. The saturated hydraulic conductivity, k_{sat}, was calculated as follows:

$$k_{sat} = \frac{\Delta Q \cdot L}{A \cdot \Delta h \cdot \Delta t} \tag{5-9}$$

where k represents the hydraulic conductivity, cm/s; ΔQ denotes the quantity of flow during a certain time interval Δt, calculated as the average of inflow and outflow, cm^3; L signifies the length of the specimen, cm; A represents the cross-sectional area of the specimen, cm^2; Δt is the time interval, s; and Δh corresponds to the average head loss of across the specimen, cm of water.

Then, the hydraulic conductivity recovery ratio (HCRR) can be determined by the following formula:

$$\text{HCRR } (\%) = \frac{k_0 - k_t}{k_0} \times 100\% \tag{5-10}$$

where k_0 is the initial hydraulic conductivity, cm/s, measured after pre-cracking; k_t is the hydraulic conductivity, cm/s, measured after specified self-healing period.

Microstructural analysis

After the studied self-healing periods, the self-healing effect on microstructural change and ultimate self-healing products were further analyzed using the following methods:

- X-ray diffraction (XRD) analysis was used to chemically analyze the compositions of self-healing products in the cracks of CPB specimens. The XRD analysis was performed by Bruker D8 Endeavor equipped with a 1 kW sealed tube Cu Kalpha source (40 kV and 25 mA) and a Lynxeye XE-T 1-D silicon strip detector.
- Thermal analyses (TG/DTG) offered insights into the binder hydration of specimens under varying drainage conditions, as well as the differences between healed pre-cracked and control specimens. TG/DTG analysis was conducted using a TA Discovery SDT 650

thermal analyzer, applying a heating ramp of 10°C/minute from room temperature up to 1000°C in a nitrogen atmosphere.

- Mercury intrusion porosimetry (MIP) test evaluated the pore size distribution in CPB specimens subjected to different drainage conditions. MIP measurements were performed using a Micromeretics AutoPore III 9420 mercury porosimeter.
- Furthermore, the physical properties, including porosity and void ratio of the studied pre-cracked and control specimens, were monitored over the self-healing periods through specific gravity tests in accordance with ASTM D854 (ASTM, 2023). The overall porosity (n) is calculated based on the formula: $n=1-(\gamma_d/\gamma_s)$, where γ_d is the dry density, and γ_s is the particle density. Then, the void ratio (e) is derived from the porosity using the equation: $e=n/(1-n)$.

Volumetric water content monitoring

To better understand how water drainage and curing time influence cement hydration within the CPB matrix, the volumetric water content (VWC) was monitored using a 5TE soil moisture sensor for up to 15 days. CPB mixtures were prepared under three drainage conditions (i.e., FD, HD, and ND) and poured into cylindrical plastic molds. The sensor was inserted at the center of the mold to avoid boundary disturbances. Data from the sensor were recorded using an EM50 data logger. The 5TE sensor is capable of measuring VWC in the 0-80% range, with an accuracy of ±0.01 between 1% and 40%, and ±0.15 between 40% and 80%. These results can help explain the progression and intensity of cement hydration, as well as the rheological properties and self-desiccation behaviour influenced by the drainage conditions.

5.4.3 Results and Discussions

5.4.3.1 Recovery of mechanical property through self-healing

Strength development of uncracked control specimens

The influence of different drainage conditions (i.e., full drainage, half drainage, and no drainage) on the mechanical strength development of control CPB specimens is illustrated in Figure 5-28. From this figure, it is observed that the control CPB specimens with full drainage produce consistently higher compressive strengths than those with half drainage and no drainage conditions, regardless of self-healing periods. Specifically, the control CPB specimens with full drainage demonstrate 47.2%, 43.5%, 26.1%, and 29.5% higher UCS values than the specimens with no drainage, and 22.5%, 30.3%, 17.2%, and 15.5% higher UCS values than the ones with half drainage, at the self-healing period of 0, 7, 28, and 90 days, respectively. It is obviously noted that the drainage process significantly contributes to the compressive strength development. This noticeable strength improvement is related to the coupled effects of drainage water, one-dimensional consolidation, and cement hydration (Yilmaz et al., 2014). The drainage of excess water results in a lower w/c ratio within the CPB matrix, which favours the cement hydration and contributes to enhanced mechanical properties (Bentz et al., 2009; Fall et al., 2008). Additionally, the specimens with drainage conditions would develop higher effective stresses during the curing

process due to the dissipation of excess PWP (Ghirian & Fall, 2016). This performance, in turn, enhances the binding between the particles of tailings and hydration products. Furthermore, the drainage would consolidate the CPB pore structure, leading to a reduction in the porosity and void ratio of the CPB matrix. This argument is supported by the results of porosity and void ratio tests performed on the control CPB specimens with different drainage conditions, as presented in Figure 5-29. The figure shows an evident decrease in porosity and void ratio of control CPB specimens with the enhancement of the drainage condition, resulting in a denser CPB matrix. As the hydration reaction continues, the produced hydration products would precipitate in the available voids and capillary pores, thus further refining the pore structure and contributing to the strength development. This argument agrees well with the results of MIP tests performed on control CPB specimens with full and half drainage conditions after the self-healing period of 7 (D7) and 28 days (D28) in Figure 5-30, where the full drainage delivers a finer microstructure and decreased threshold pore diameter at the same self-healing period.

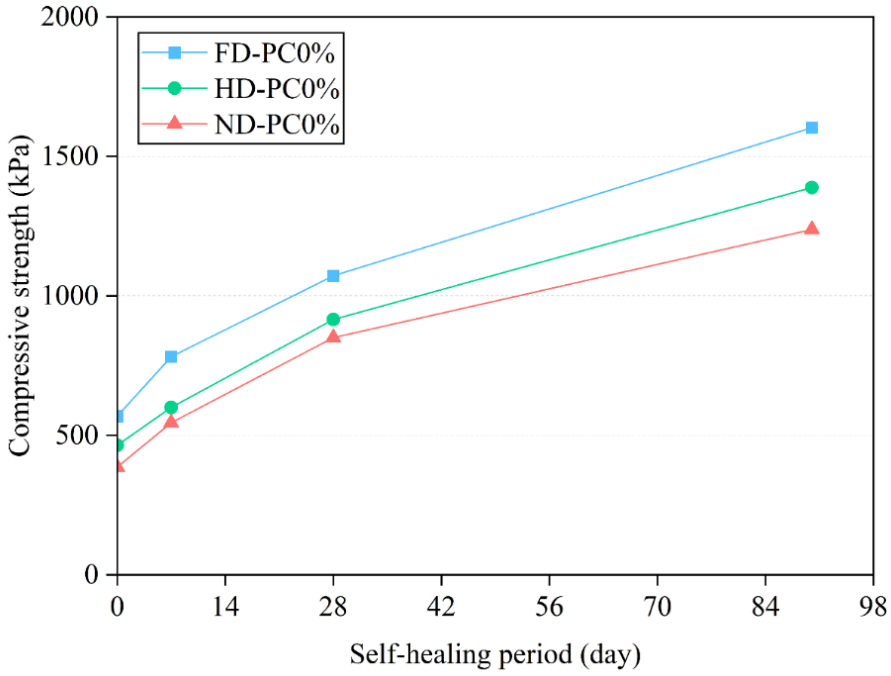

Figure 5-28. Compressive strength development of control CPB specimens with different drainage conditions against elongated healing periods.

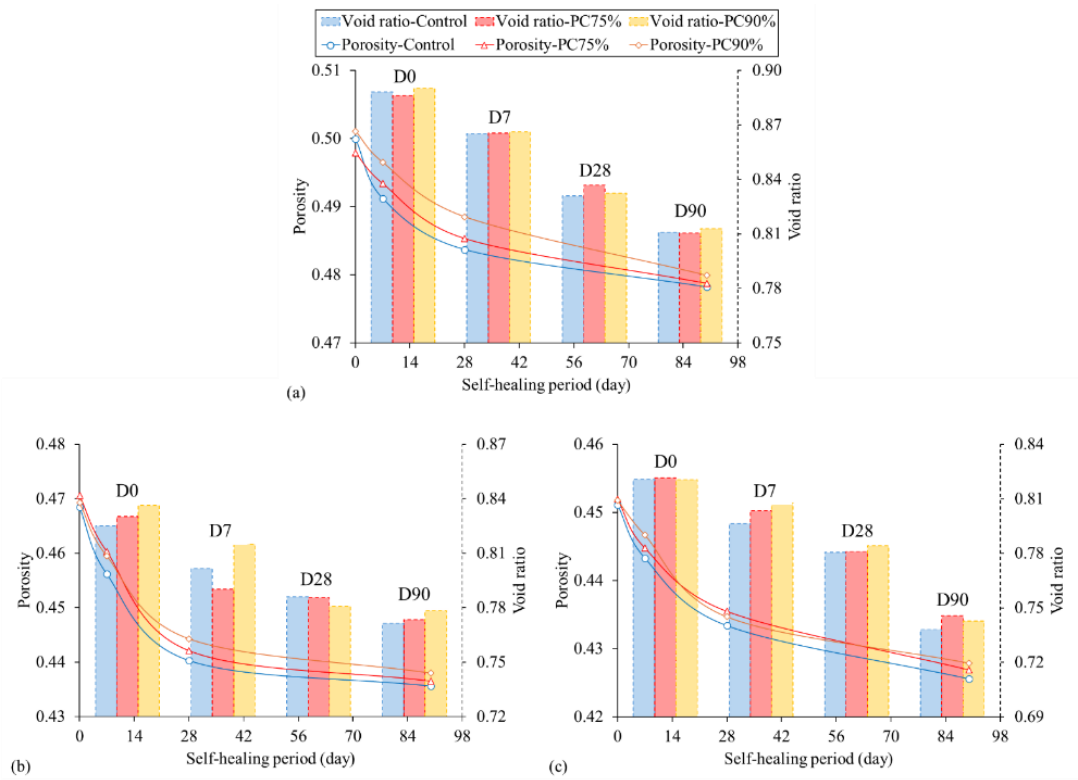

Figure 5-29. Changes of porosity and void ratio of both control and pre-cracked CPB specimens under different drainage conditions of (a) no drainage, (b) half drainage, and (c) full drainage over the self-healing period (D0, D7, D28, and D90: 0, 7, 28 and 90 days of the self-healing period, respectively).

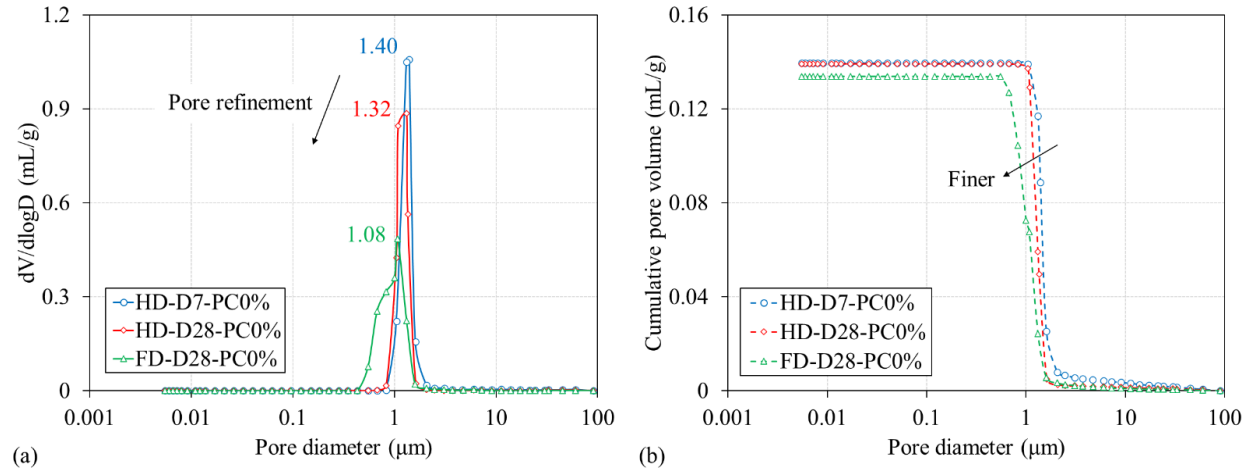

Figure 5-30. Results of MIP test of CPB specimens subjected to full and half drainage conditions over the self-healing period from 7 to 28 days.

Compressive strength recovery and improvement by self-healing

Figure 5-31 represents the mechanical strength variations of pre-cracked CPB specimens compared to the uncracked control ones against the self-healing period up to 90 days when subjected to three drainage conditions (i.e., (a) no drainage, (b) half drainage, and (c) full drainage), underscoring the significant influence of drainage condition on both the evolution of strength in pre-cracked CPBs and the subsequent recovery of mechanical strength. The detailed recovery of compressive strength of pre-cracked specimens is quantified by means of the index CCS, which is defined and calculated as in Eq. 5-8. Generally, it can be seen that the compressive strengths of all pre-cracked CPB specimens gradually recover and improve under all drainage conditions as the self-healing progresses.

Undrained condition (no drainage)

The experimental findings of self-healing efficiency in the CPB specimens with no drainage are illustrated in Figure 5-31a. It is noticed in Figure 5-31a that the pre-cracked specimens with no drainage recover to a comparable and even higher compressive strength as the uncracked control specimens after the self-healing periods of 28 days (D28) with the CCS value up to 6.0% of the PC90% pre-cracked specimens. According to the previous work (Quan & Fall, 2024), two mechanisms, including i) continuous hydration of unhydrated cement particles and ii) carbonation of calcium hydroxide CH, significantly contribute to the observed self-healing behaviour in strength recovery. The produced self-healing products fill into the available microcracks, voids and pores to enhance the binding force between particles and decrease the internal porosity, thus refining the pore structure and restoring the mechanical strength. This argument is supported by the results of XRD analysis as depicted in Figure 5-32, which reveal the absence of dicalcium silicate (C_2S), tricalcium silicate (C_3S), and CH after the self-healing period of 90 days (D90), indicating the contribution of continuous hydration of unhydrated cement particles in the studied CPB specimens. However, in contrast to the previous study (Quan & Fall, 2024), the pre-cracked specimens healed at the ambient condition can usually achieve a similar self-healing performance after the self-healing period of 7 days. This slight delay of self-healing in this study can be attributed to the higher water content in the CPB specimens with no drainage, which decelerates the cement hydration due to the dissolution reactions (Benzaazoua et al., 2004). Excess water increases the water-to-cement (w/c) ratio in CPB, diluting the cement particles and reducing the concentration of calcium and hydroxyl ions in the pore solution. This slows down the formation of hydration products such as calcium silicate hydrate (C-S-H) and calcium hydroxide (CH), which are essential for strength development (Fall et al., 2009). In addition, the presence of excess water reduces the surface energy of the hydration products and weakens the van der Waals bonding among them (Yang et al., 2011), which could delay the precipitation of hydration products and hinder the structural integrity at the early self-healing period. However, as the self-healing progresses to 90 days (D90), the improved strength recovery is obtained in the PC90% pre-cracked specimens with the CCS value of 15.1%, which is even higher than that of PC75% pre-cracked specimens. This prominent increment in strength is not only ascribed to the continuous hydration of unhydrated cement particles, but also to the initially generated cracks that provide the pathways

allowing CO_2 to penetrate the CPB matrix favouring the carbonation of CH. The produced extra amount of calcite $CaCO_3$, in turn, contributes to self-healing behaviour and strength recovery. The thermal analysis results shown in Figure 5-33 can substantiate this argument. This figure reveals three distinct weight loss patterns: i) the loss of free water and dehydration of hydrates such as C-S-H and ettringite in the temperature range of 50°C-200°C; ii) the dihydroxylation of $Ca(OH)_2$ between 400°C and 580°C; and iii) the decomposition of $CaCO_3$ between 600°C and 750°C (e.g., Bhatty, 1991; Fall et al., 2010; Pane and Hansen, 2005). It is evident that the weight loss between 600°C and 750°C, which corresponds to the decarbonization of calcite (e.g., Taylor, 1964; Bhatty, 1991; Sha et al., 1999; Pane and Hansen, 2005; Fall et al., 2010), becomes more pronounced in the healed pre-cracked specimens after the self-healing period of 90 days (D90), indicating the existence of the additional amount of calcite in the healed pre-cracked specimens. Moreover, the high water content in CPB materials benefits the carbonation reactions as well since adequate moisture is required for the dissolution of CO_2 to form carbonic acid (H_2CO_3), which then reacts with calcium ions (Ca^{2+}) to produce $CaCO_3$ (Yıldırım et al., 2018).

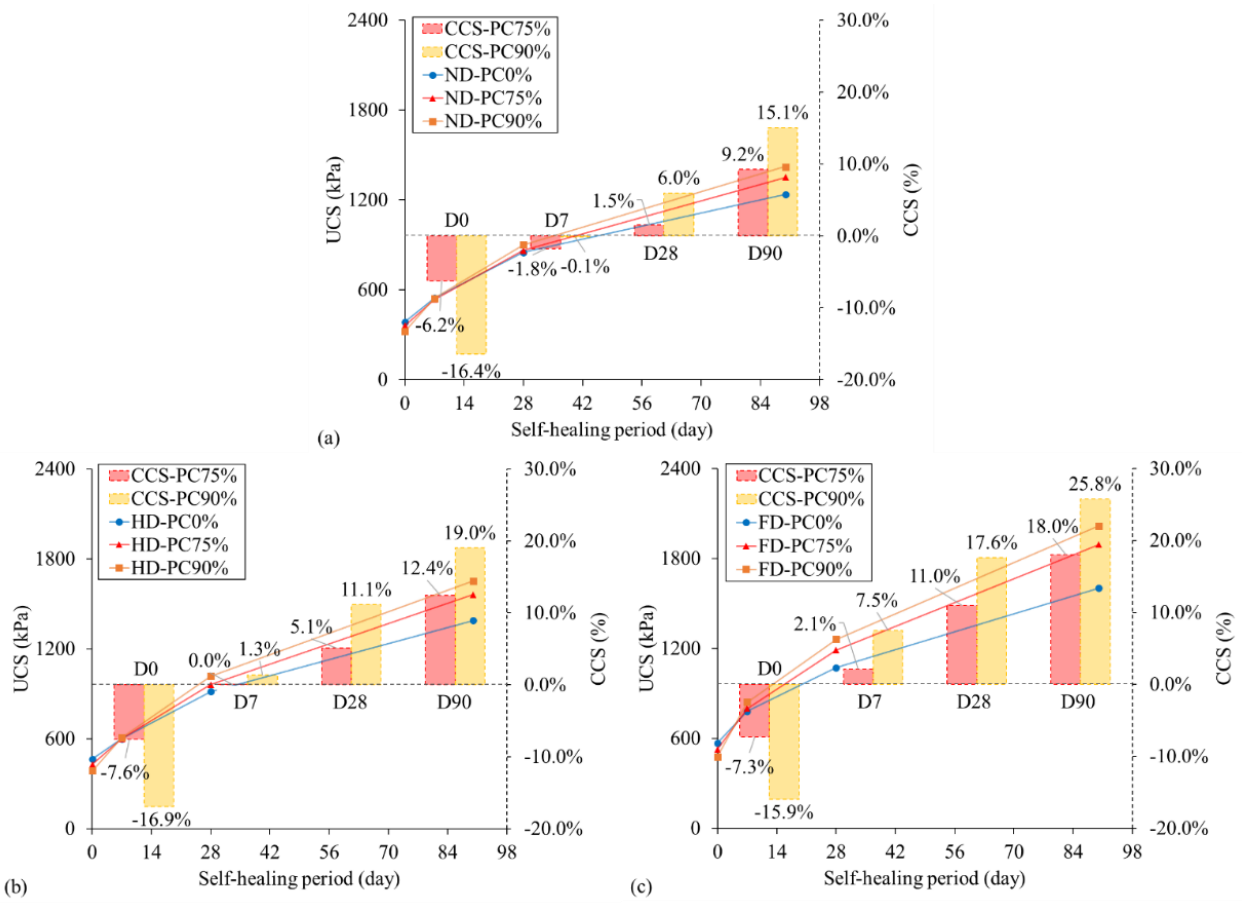

Figure 5-31. Evolution of the UCS and CCS of the studied CPB specimens under different drainage condition of (a) no drainage, (b) half drainage, and (c) full drainage over the self-healing period (D0, D7, D28, and D90: 0, 7, 28 and 90 days of the self-healing period, respectively).

Drained conditions (half drainage and full drainage)

The effect of drainage conditions (i.e., half drainage and full drainage) on the self-healing efficiency of CPB specimens in strength recovery and development are presented in Figure 5-31b and Figure 5-31c, respectively. It is observed that the drained CPB specimens exhibit an enhanced self-healing efficiency compared to those with no drainage (Figure 5-31a). Specifically, the pre-cracked specimens with half or full drainage can recover to equivalent or improved UCS values within the self-healing period of 7 days (D7), demonstrating a faster self-healing rate compared to those with no drainage. In addition, the increased CCS values are observed in the PC90% pre-cracked specimens with half drainage at the self-healing period of 28 (D28) and 90 days (D90), with CCS values of 11.1% and 19.0%, respectively. Furthermore, noticeable CCS values up to 17.6% and 25.8% are achieved in the PC90% pre-cracked specimens with full drainage at the self-healing period of 28 (D28) and 90 days (D90), respectively.

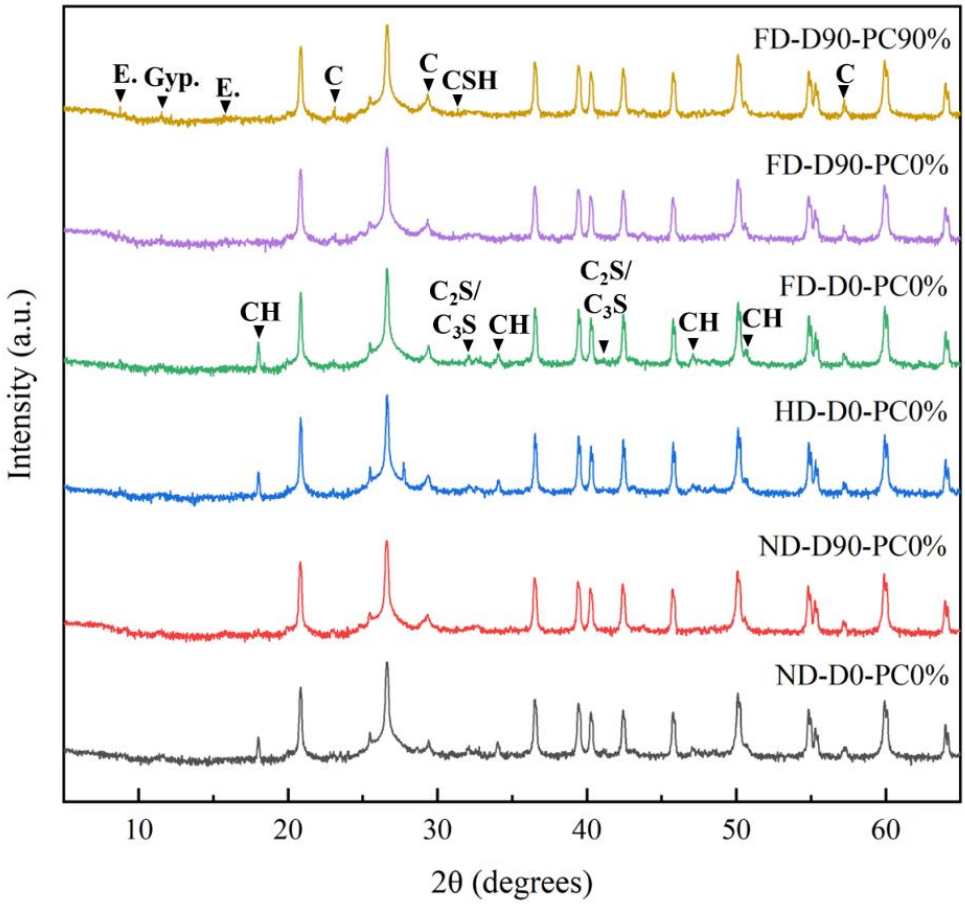

Figure 5-32. Comparison of XRD patterns of control and pre-cracked CPB specimens under different drainage conditions and self-healing periods.

This increased self-healing efficiency in strength recovery is governed by the improved cement hydration and precipitation reaction due to the water drainage, which contributes to the hardening processes within the CPB matrix. In the CPB design, besides the water for cement hydration,

additional water would be added to the mixture to reach the desired consistency, satisfying the pumpability and workability requirements (Benzaazoua et al., 2004). When subjected to drainage conditions, the bleeding of excess water from the fresh CPB mixtures leads to a faster settlement of suspended solids and denser packing of the CPB matrix under the action of self-desiccation, resulting in decreased porosity and void ratio. Figure 5-29 experimentally demonstrated this pore refinement, which shows the results of the porosity and void ratio tests on the control specimens at the self-healing period of D0. The figures show that the control CPB specimens with full drainage and half drainage have comparatively lower porosities compared to those with no drainage due to the refinement of their pore structures. Similar benefits of excess water loss on self-healing performance in strength recovery have also been demonstrated in strain-hardening cementitious composites by Sisomphon et al. (2013), where the water/dry cycle exposure condition resulted in better healing performance compared to submersion in refreshed tap water or tap water. It was suggested that during the drying phase, the evaporation of excess water increased ion concentration within cracks, provided that sufficient water remained in the matrix for reactant interactions, thereby promoting chemical reactions, precipitation, and further hydration. In addition, higher effective stress would develop within the CPB matrix due to the drainage process, which also contributes to the consolidation of the CPB specimens with drainage, thus reducing the volume of voids and pores and enhancing particle interlocking and bonding (Ghirian & Fall, 2016; Matusinović et al., 2003; Yilmaz et al., 2014). After the settlement of solids, the continuous cement hydration consuming the water in the pore spaces will decrease the PWP, leading to the negative PWP inside the CPB specimen and an increase in the effective stress ($\sigma'=\sigma$-PWP, where σ' is the effective stress and σ is the total stress). The solids within the CPB are crowdedly distributed because of the effective stress (Yilmaz et al., 2009). As the hydration products (i.e., C-S-H, CH, ettringite, and gypsum) continuously generate and precipitate in the microcracks and capillary voids, the bonding between the tailings and cement hydrates would be further enhanced, which obviously results in an improved strength recovery in the pre-cracked specimens with drainage after the self-healing process. This porosity reduction or densification is supported by the MIP results presented in Figure 5-30, which shows that CPB specimens with full drainage exhibit a finer pore structure and lower porosity than those with half drainage. This argument is also consistent with the previous findings that higher effective stress enhances the cement curing process, contributing to the development of mechanical strength in porous media (Åhnberg, 2007; Helinski et al., 2011; Rotta et al., 2003). Furthermore, the water drainage results in a lower water content or w/c ratio within the CPB matrix, favouring the cement hydration and precipitation of hydration products. This reduction in water content due to the drainage condition is experimentally supported by the monitoring results of the evolution of VWC, as displayed in Figure 5-34. It can be observed that the VWC climbs up to reach the peak values rapidly regardless of the drainage conditions. This sharp increase in VWC is associated with the formation of voids between the VWC sensor and the CPB mixtures, which are initially filled with water, maintaining the matrix saturated due to the high w/c ratio (7.35) used in the preparation of CPB. Subsequently, a significant decrease is observed around 3.7 hours after casting for the specimens with full drainage and around 6 hours for those with no drainage. This time difference indicates the variations in water movement and

consumption within the CPB mixture due to different drainage conditions. The decrease in VWC is directly related to water consumption through the process of cement hydration (self-desiccation), which is the main factor in specimens without drainage. In contrast, for specimens with drainage, the reduction in VWC is caused by a combination of self-desiccation and water removal through drainage (Al-Moselly & Fall, 2024). During the drainage process, the decreasing water content in the drained specimen results in a denser packing of the particles, leading to the CPB matrix with a reduced overall porosity. In addition, the reduced void volume gives rise to a higher concentration of cement particles, which provides a more specific surface area for hydration reactions, resulting in a faster rate of cement hydration and strength achievement within the specimens with drainage. As hydration products precipitate on the surface of unhydrated cement particles and gradually accommodate the voids, the permeability of CPB is significantly reduced. This reduction delays water transportation and diffusion into the unhydrated cement particles, consequently slowing the rate of water consumption for cement hydration (Cui & Fall, 2020; Helinski et al., 2011). Over time, the VWC value decreases and approaches an asymptote as curing progresses. As a result, the specimens with full drainage conditions exhibit the most pronounced decrease in VWC among the three drainage conditions.

In light of the aforementioned contributors, the pre-cracked specimens with full drainage exhibit the most pronounced self-healing ability among the three studied drainage conditions. For a given pre-cracking level, comparatively less volume of cracks and voids in pre-cracked CPB specimens with drainage need to be healed than those without drainage during the self-healing process due to the denser packing of the CPB matrix. Hence, this refinement of pore structure combined with the accelerated cement hydration contributes to the notable self-healing behaviour of the pre-cracked specimens with drainage over the studied self-healing period. This increase in self-healing efficiency improves with enhanced drainage conditions. The thermal analysis results performed on the PC90% pre-cracked specimens with full drainage and half drainage after the self-healing period of 90 days (D90), are presented in Figure 5-33 to support this capability. It can be seen that more hydration products are formed in the CPB specimens with full drainage than in those with half drainage. In addition to that, this performance is consistent with the results of the MIP tests presented in Figure 5-30, which indicate that CPB specimens with full drainage have a finer pore structure and lower porosity with respect to those with half drainage. Overall, the studied drainage conditions (water loss) enhance the strength recovery of pre-cracked CPB specimens.

In contrast to most studies on cementitious materials such as concrete, mortar, and ECC, where sustained water availability significantly promotes continued hydration and enhances the autogenous healing process due to their high cement content and relatively low w/c ratio (Özbay et al., 2013; Termkhajornkit et al., 2009; Zhang et al., 2020; Roig-Flores et al., 2015), CPB materials benefit from a different condition for autogenous healing. In CPB, the favorable condition is not prolonged water retention, but rather the controlled loss of excess water. The fresh CPB slurry is in a supersaturated state immediately after mixing due to the additional water added to optimize flowability, and remains nearly fully saturated during the initial stage of cement hydration (Wang et al., 2022). The loss of excess water during early curing stages could accelerate the cement

hydration as aforementioned, thereby promoting self-healing behaviour. While water plays a key role in autogenous healing in both CPB and conventional cementitious materials, the underlying mechanism differs: CPB benefits from a balance between initial saturation and subsequent controlled water loss, whereas traditional cementitious materials rely on sustained water availability for optimal healing performance.

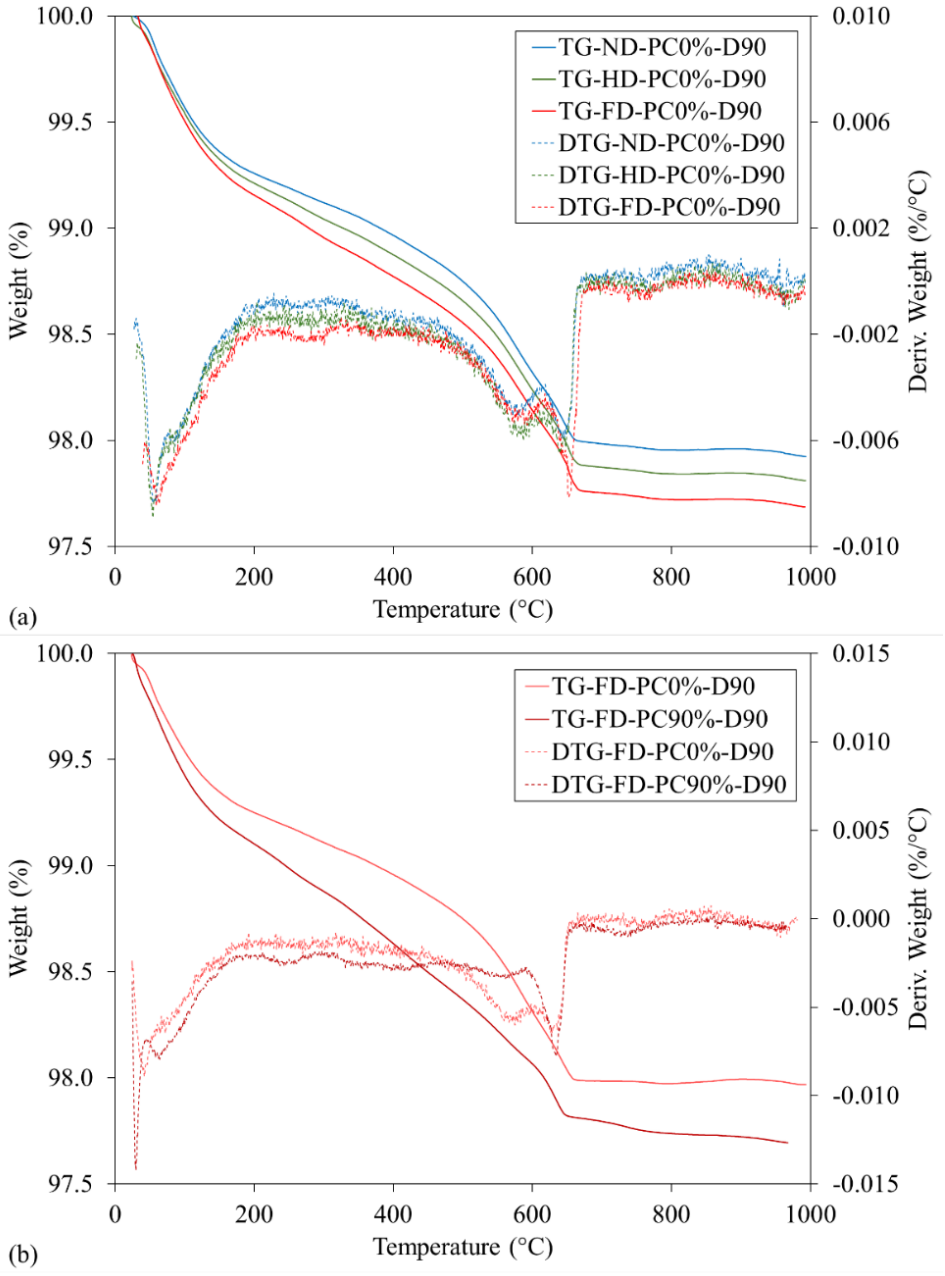

Figure 5-33. TG/DTG comparison of (a) control specimens cured at different drainage conditions after a self-healing period of 90 days, and (b) control and PC90% pre-cracked specimens with full drainage after a self-healing period of 90 days.

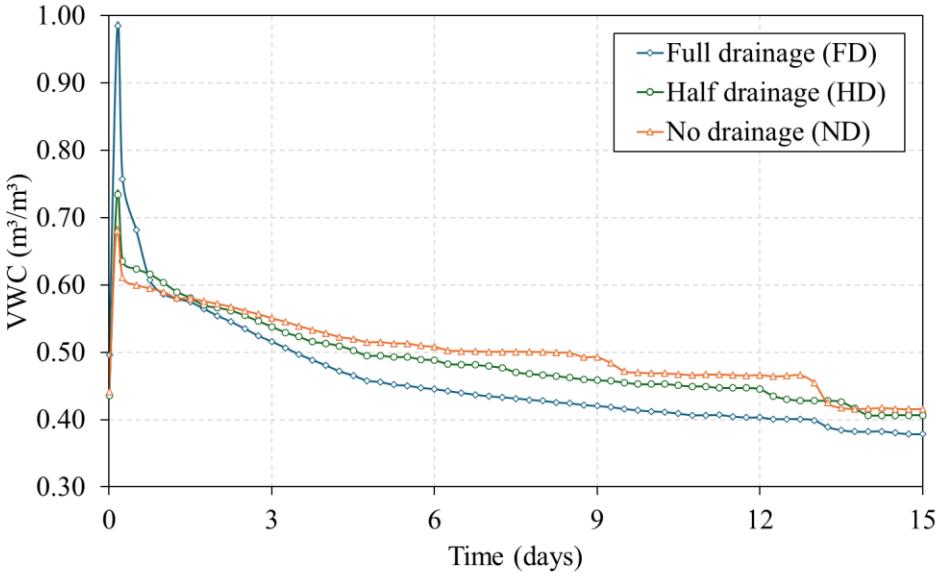

Figure 5-34. Changes in volumetric water content of control CPB specimens under different drainage conditions.

5.4.3.2 Analysis of hydraulic property changes through self-healing

Saturated hydraulic conductivity tests were conducted to determine how the three drainage conditions (i.e., no drainage, half drainage, and full drainage) and pre-cracking levels (i.e., PC0%, PC75%, and PC90%) affect the evolution of permeability in pre-cracked and self-healed CPB specimens over the self-healing period as illustrated in Figure 5-35. The values on the second y-axis show the hydraulic conductivity recovery ratio (HCRR) index of the pre-cracked specimens after self-healing compared to the control specimens by means of Eq. 5-10. Figure 5-35 illustrates that the pre-cracked specimens exhibit higher hydraulic conductivities compared to the control specimens following the pre-cracking process at the self-healing period of D0 irrespective of the drainage conditions. This increase in permeability is attributed to the generation and propagation of interconnected microcrack networks within the CPB specimens (Fall et al., 2009). As the pre-cracking level increases and approaches the peak stress region, some microcracks expand and coalesce to form macrocracks, further exacerbating the permeability (He et al., 2021; Sun et al., 2017). Moreover, as the self-healing progresses, it is observed that the pre-cracked specimens subjected to the studied three drainage conditions can recover their hydraulic conductivity to certain degrees after self-healing process despite the fact that the hydraulic conductivity was initially increased due to the pre-cracking.

Figure 5-35a reveals a continuous recovery performance in hydraulic conductivity of the pre-cracked specimens with no drainage. For example, it is clearly seen that the PC90% pre-cracked specimens exhibit an HCRR value from 28.2% to 78.3% over the self-healing period from 7 days (D7) to 90 days (D90). The observed reduction in permeability due to self-healing is attributed to the continuous hydration of unhydrated cement particles and the carbonation of $Ca(OH)_2$, which generate self-healing products such as C-S-H, $CaCO_3$, and CH (Quan & Fall, 2024). These products

precipitate within cracks and capillary voids, effectively sealing internal pathways and altering the pore structure of the CPB matrix, thereby significantly reducing hydraulic conductivity. In the same way, the pre-cracked specimens with half drainage and full drainage manifest a similar but enhanced self-healing efficiency in hydraulic conductivity, with the HCRR values ascending to 84.9% and 91.3%, as illustrated in Figure 5-35b and Figure 5-35c, respectively. The improved self-healing efficiency is associated with the effect of water drainage, as previously discussed. The densification as a result of water drainage leads to a reduced volume of voids and pores within the CPB matrix. This pore structure refinement is supported by the results of porosity and void ratio tests of the CPB specimens shown in Figure 5-29, where the drainage condition delivers a denser microstructure with lower porosity and void ratio. Furthermore, the reduction in water content due to drainage facilitates cement hydration by minimizing excessive cement dissolution. This leads to increased production and precipitation of hydration products within microcracks and capillary pores, thereby refining the pore structure of the pre-cracked specimens as self-healing progresses. The removal of excess water through drainage effectively lowers the water-to-cement ratio, resulting in a higher concentration of cement particles in the remaining pore solution. This promotes closer contact between cement grains, enhancing the hydration process. The increased proximity of cement particles allows for improved interaction between unhydrated cement grains and water molecules, leading to a faster hydration reaction and more efficient formation of hydration products such as calcium silicate hydrates (C-S-H). This observation is consistent with the XRD analysis of the ND-D0-PC0%, HD-D0-PC0%, and FD-D0-PC0% specimens, which exhibit a progressively higher degree of cement hydration, as shown in Figure 5-29. Notably, specimens subjected to full drainage and half drainage display higher intensities of CH and C-S-H, indicating a greater extent of cement hydration compared to those without drainage. Thus, the higher amount of self-healing products in the pre-cracked specimens with drainage achieves a faster reduction in hydraulic conductivity than those with no drainage given the same self-healing period. Furthermore, it is noted in Figure 5-35b and Figure 5-35c that the self-healing efficiency in permeability is more conspicuous in the specimens with full drainage compared to those with half drainage, indicating that self-healing is improved as the drainage condition enhances. This is because of the phenomenon of higher hydration degree in the specimens with full drainage, as the results of thermal analysis revealed in Figure 5-33. In this figure, the CPB specimen with full drainage clearly shows the most significant weight loss in the first and second range than those with half drainage, indicating that more cement hydration products are generated to fill in the cracks and voids to refine the pore structure, decreasing the hydraulic conductivity. Moreover, the aforementioned more pronounced refinement of pore structure in the specimens with full drainage is also evidenced by the results of MIP tests in Figure 5-30, which depicts the two drainage conditions induced changes in incremental intrusion and the cumulative pore volume of the CPB at the same self-healing period of 28 days (D28). It can be noticed that the CPB specimens exhibit lower threshold pore diameter, representing the range of higher proportions of pore diameters, and cumulative pore volume as the enhancement of drainage condition. For instance, the threshold pore diameter of the specimens with full drainage is 1.08 μm, while that of the specimen with half drainage is 1.32 μm, denoting a more refined pore structure in the specimens with full drainage.

Given that, the full drainage condition stands as the most favourable condition for the self-healing performance in this study.

What's more, it is worth noting that the hydraulic conductivity of the pre-cracked specimens cannot achieve a complete recovery (i.e., HCRR of 100%) as the equivalent k_{sat} as the control specimens after the studied self-healing period, indicating that the self-healing capacity is limited. This is due to the high pre-cracking level (i.e., PC90%) causing the macrocracks (cracks with large crack width) within the CPB matrix, which cannot be completely healed and significantly impacts the permeability performance of the CPB structure. This argument will be discussed in the subsequent section.

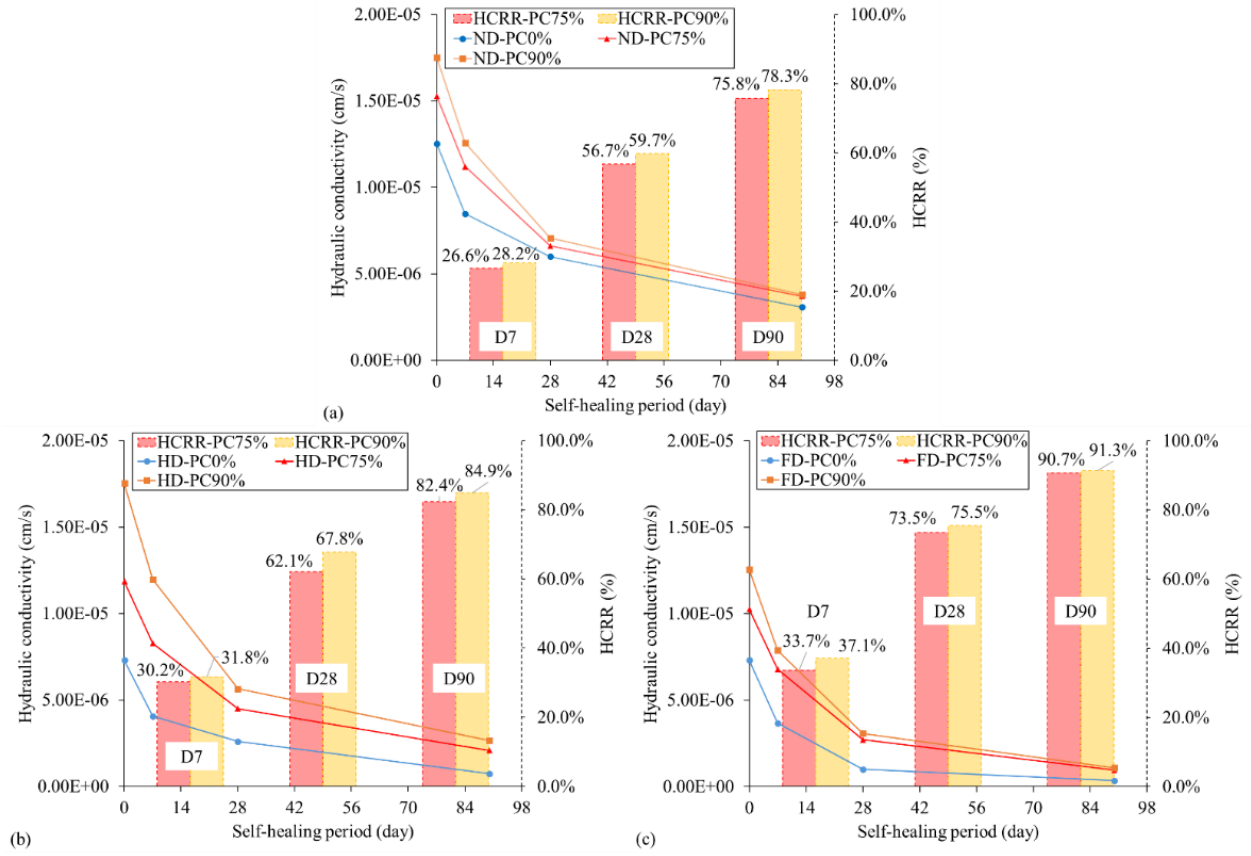

Figure 5-35. Changes of hydraulic conductivity and HCRR of the studied CPB specimens under different drainage conditions of (a) no drainage, (b) half drainage, and (c) full drainage over the self-healing period (D0, D7, D28, and D90: 0, 7, 28 and 90 days of the self-healing period, respectively).

5.4.3.3 Characteristics of self-healed cracks

Crack characteristics of the CPB specimens with different drainage conditions were investigated before being exposed to self-healing and after the self-healing period of 7, 28, and 90 days. In the current study, the measurement of crack width closure is conducted as a direct assessment of self-healing under the studied conditioning regime as a result of the significant variations in crack width

via compressive loading. The typical observation for cracks before and after self-healing is shown in Figure 5-36. From this figure, it can be observed that there are abundant white crystal-like self-healing products produced along the crack lines, contributing to the complete healing of crack closure. Moreover, partial healing and no healing of crack scenarios are also detected on account of the large crack width and the limitation of autogenous healing in the pre-cracked CPB specimens. As demonstrated in the previous study (Quan & Fall, 2024), the substances C-S-H, $CaCO_3$, and $Ca(OH)_2$ from the continuous cement hydration products in conjunction with the carbonation of CH, consist of the self-healing products inside the cracks of the CPB specimens. This is also supported by the results of XRD analysis performed on the self-healing products scratched from the healed pre-cracked specimens with full drainage in this study, as shown in Figure 5-37.

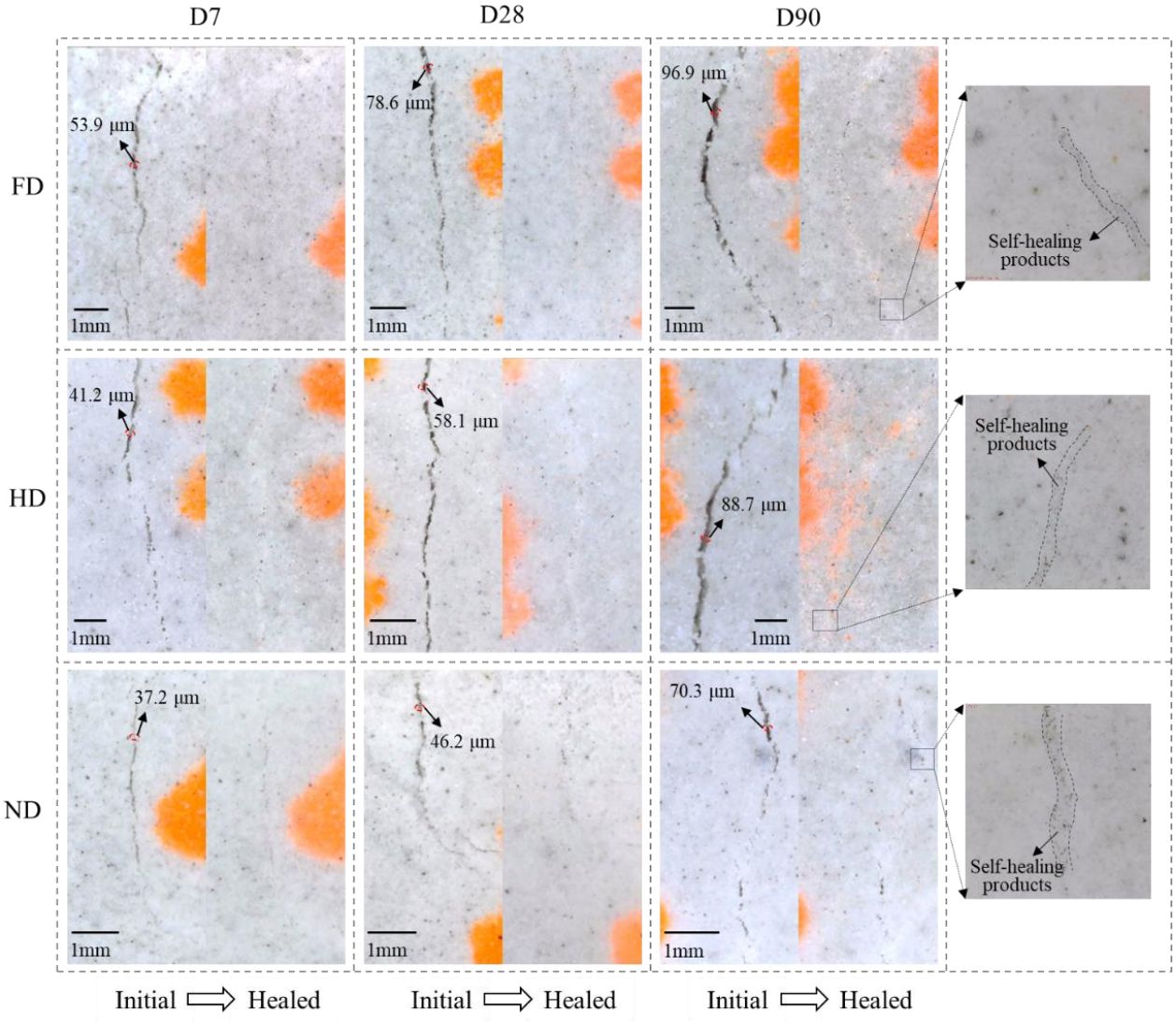

Figure 5-36. Typical observations of crack closure (complete healing) in CPB specimens subjected to different drainage conditions and self-healing periods.

The crack widths of completely healed cracks from all studied specimens over the self-healing period to 90 days were measured and plotted in Figure 5-38 as a quantitative evaluation to compare the effects of drainage conditions on the self-healing ability in crack closure. It can be seen that full drainage exhibits the most favourable drainage condition for self-healing in crack closure, followed by half drainage and no drainage, irrespective of the self-healing periods. For instance, crack widths up to 119.3, 94.9, and 88.7 μm can be completely healed in the pre-cracked specimens with full drainage, half drainage, and no drainage, respectively, after the self-healing period of 90 days. In light of the comparatively lower volume of cracks and voids in pre-cracked CPB specimens with full drainage, these specimens demonstrate the most promising self-healing efficiency in crack closure. This performance aligns with the results of the recovery of mechanical and hydraulic properties, as previously discussed. In addition, as expected, the average healed crack widths increase over the progress of the self-healing period. The average of healed crack widths is lower in all conditions after the self-healing period of 7 days (D7), while significant improvements are observed after the self-healing period of 28 (D28) and 90 days (D90). It is manifested by the results of XRD analysis in Figure 5-32, which reveal that both specimens with full drainage and no drainage demonstrate continuous cement hydration from the self-healing period D0 to D90, aiding in the crack closure over time. Furthermore, the overlaid normal distribution curves show that the healed crack width values generally follow a normal distribution. The points in these groups align well with the bell-shaped normal curve, which suggests a balanced and expected distribution of healed crack widths over time.

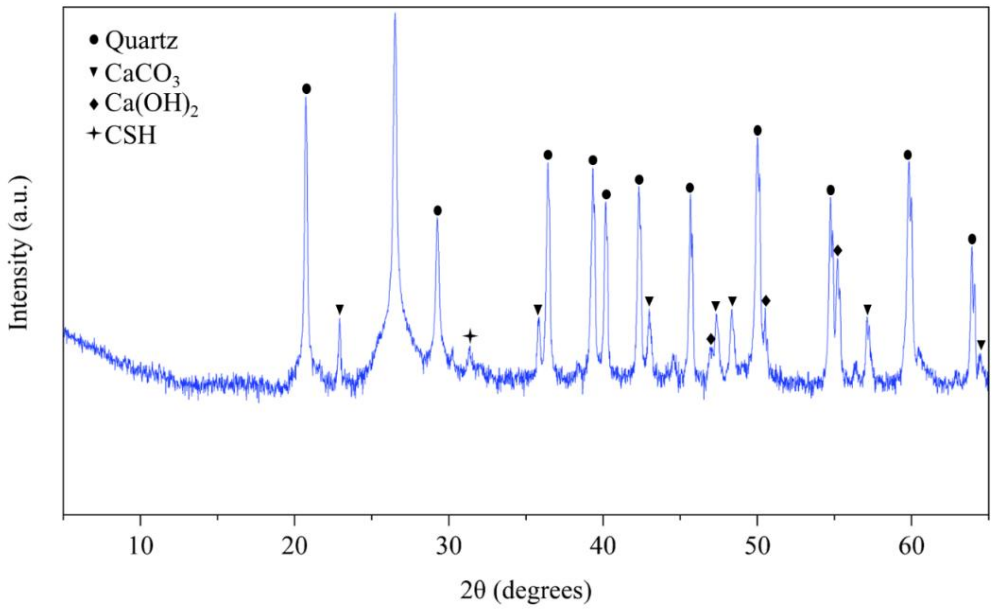

Figure 5-37. XRD patterns of self-healing products collected from pre-cracked CPB specimens after 90 days self-healing period.

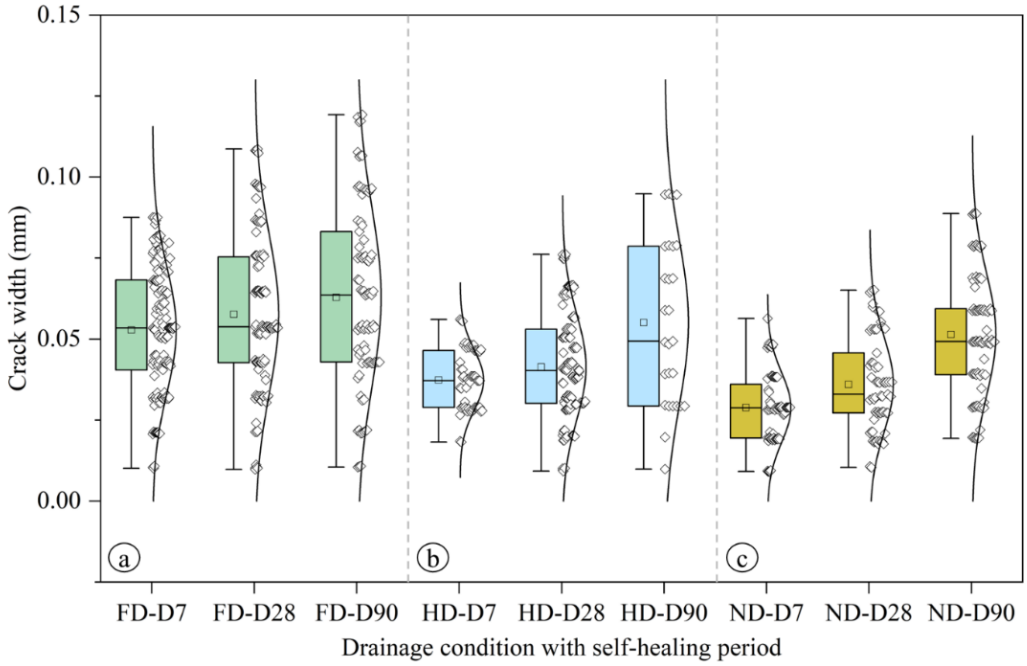

Figure 5-38. Distribution of completely healed crack widths under the drainage condition of (a) full drainage, (b) half drainage, and (c) no drainage.

5.4.4 Summary and Conclusions

The influence of drainage conditions on the self-healing efficiency in the recovery of mechanical strength and hydraulic conductivity, and crack closure of CPB has been investigated in this study, and based on the experimental results, the main conclusions of the study are summarized as follows:

- The uncracked control CPB specimens with full drainage perform consistently higher compressive strengths and lower hydraulic conductivities than those with half drainage and no drainage conditions over the studied self-healing period. The drainage process significantly contributes to the compressive strength development and refinement of pore structure, which is associated with the coupled effects of lower w/c ratio due to drainage of excess water, densification of the matrix, and improved cement hydration reactions.
- The improved cement hydration and precipitation contribute to the hardening processes within the CPB matrix, which benefit self-healing performance in strength recovery of the studied CPB specimens. The pre-cracked CPB specimens with drainage conditions (full and half drainage) have more pronounced self-healing efficiency than those with no drainage. Moreover, this strength enhancement becomes increasingly conspicuous as the drainage condition is enhanced.
- The drainage condition delivers a better evolution of microstructural refinement due to the rearrangement of the solid particles in CPB during the initial curing period, which not only leads to the densification of the matrix reducing the total porosities, but also increases the contact surface area between particles benefiting to the cement hydration, contributing to a

faster reaction and precipitation of healing products and achieving a more efficient recovery in hydraulic conductivity (permeability).

- The pre-cracked CPB specimens with half and full drainage conditions demonstrate an improved self-healing capacity for crack closure compared to those with no drainage condition, with a closure ability order of full drainage> half drainage> no drainage based on the crack characteristics. This improvement is attributed to the large amount of self-healing products (i.e., C-S-H, $Ca(OH)_2$, $CaCO_3$) produced by the improved rates of unhydrated cement particle hydration and carbonation of calcium hydroxide filling available microcracks and capillary voids.

The findings of this study help to better understand the impacts of the drainage conditions on the self-healing capacity of CPB, which provides an essential component to the integrity of self-healing performance investigation of CPB materials. Despite the valuable insights gained, this study utilized only synthetic tailings composed predominantly of quartz. While quartz is the primary mineral in many hard rock mine tailings, natural tailings from different mining sites can exhibit diverse mineralogical compositions. This variability may influence the self-healing behaviour of CPB, potentially limiting the direct generalization of our findings to all mine waste materials. The effects of different mineral compositions on CPB's self-healing performance remain uncertain. To address this limitation, future research should incorporate a broader range of natural mine tailings with varying mineralogical compositions to validate and extend these findings to more diverse field conditions. Additionally, non-destructive techniques such as ultrasonic pulse velocity or resonant frequency testing should be explored in future studies to monitor self-healing progress in the same specimens over multiple self-healing periods. These approaches could provide deeper insights into the kinetics and mechanisms of CPB self-healing. Further research should aim to bridge these knowledge gaps and enhance our understanding of how drainage conditions influence self-healing mechanisms under field-representative conditions.

5.4.5 References

Åhnberg, H. (2007). On yield stresses and the influence of curing stresses on stress paths and strength measured in triaxial testing of stabilized soils. Canadian Geotechnical Journal, 44, 54-66.

Al-Moselly, Z., & Fall, M. (2024). Investigating Pore Water Pressure Development in Paste Backfill Under Conditions Mimicking Field Loading. Geotech. Geol. Eng., 1-24.

ASTM. (2016). ASTM D5084-16a. Standard Test Methods for Measurement of Hydraulic Conductivity of Saturated Porous Materials Using a Flexible Wall Permeameter. In. West Conshohocken, PA: ASTM International.

ASTM. (2020). ASTM C143/C143M-20. Standard Test Method for Slump of Hydraulic-Cement Concrete. In. West Conshohocken, PA: ASTM International.

ASTM. (2021). ASTM C39/C39M-21. Standard Test Method for Compressive Strength of Cylindrical Concrete Specimens. In. West Conshohocken, PA: ASTM International.

ASTM. (2023). ASTM D854-23. Standard Test Methods for Specific Gravity of Soil Solids by the Water Displacement Method. In. West Conshohocken, PA: ASTM International.

Belem, T., & Benzaazoua, M. (2008). Design and application of underground mine paste backfill technology. Geotech. Geol. Eng., 26, 147-174.

Belem, T., Benzaazoua, M., Bussière, B., & Dagenais, A. (2002). Effects of settlement and drainage on strength development within mine paste backfill. In Tailings and Mine Waste 2002 (pp. 139-148): CRC Press.

Belem, T., El Aatar, O., Bussière, B., Benzaazoua, M., Fall, M., & Yilmaz, E. (2006). Characterisation of self-weight consolidated paste backfill. Paper presented at the Paste 2006: Proceedings of the Ninth International Seminar on Paste and Thickened Tailings.

Bentz, D. P., Peltz, M. A., & Winpigler, J. (2009). Early-age properties of cement-based materials. II: Influence of water-to-cement ratio. Journal of materials in civil engineering, 21, 512-517.

Benzaazoua, M., Fall, M., & Belem, T. (2004). A contribution to understanding the hardening process of cemented pastefill. Miner. Eng., 17, 141-152.

Berghe, J.-F. V., Ballard, J., Pirson, M., & Reh, U. (2011). Risks of tailings dams failure. Paper presented at the Proceedings of the 3rd International Symposium on Geotechnical Risk and Safety (ISGSR).

Bhatty, J. I. (1991). A review of the application of thermal analysis to cement-admixture systems. Thermochimica Acta, 189, 313-350.

Choi, S.-G., Wang, K., Wen, Z., & Chu, J. (2017). Mortar crack repair using microbial induced calcite precipitation method. Cem. Concr. Compos., 83, 209-221.

Cuenca, E., & Ferrara, L. (2017). Self-healing capacity of fiber reinforced cementitious composites. State of the art and perspectives. KSCE J. Civ. Eng., 21, 2777-2789.

Cui, L., & Fall, M. (2016). Mechanical and thermal properties of cemented tailings materials at early ages: Influence of initial temperature, curing stress and drainage conditions. Constr. Build. Mater., 125, 553-563.

Cui, L., & Fall, M. (2020). Numerical simulation of consolidation behavior of large hydrating fill mass. International Journal of Concrete Structures and Materials, 14, 23.

Deng, D., Liu, L., Yao, Z., Song, K.-I., & Lao, D. (2017). A practice of ultra-fine tailings disposal as filling material in a gold mine. Journal of Environmental Management, 196, 100-109.

El Mkadmi, N., Aubertin, M., & Li, L. (2014). Effect of drainage and sequential filling on the behavior of backfill in mine stopes. Canadian Geotechnical Journal, 51, 1-15.

Ercikdi, B., Külekci, G., & Yılmaz, T. (2015). Utilization of granulated marble wastes and waste bricks as mineral admixture in cemented paste backfill of sulphide-rich tailings. Constr. Build. Mater., 93, 573-583.
Esaker, M., Hamza, O., & Elliott, D. (2023). Monitoring the bio-self-healing performance of cement mortar incubated within soil and water using electrical resistivity. Constr. Build. Mater., 393, 132109.
Esaker, M., Hamza, O., & Elliott, D. (2024). Bio-self-healing of cementitious mortar incubated within clay soil. Journal of Materials in Civil Engineering, 36, 04023500.
Fahey, M., Helinski, M., & Fourie, A. (2010). Consolidation in accreting sediments: Gibson's solution applied to backfilling of mine stopes. Géotechnique, 60, 877-882.
Fall, M., Adrien, D., Célestin, J., Pokharel, M., & Touré, M. (2009). Saturated hydraulic conductivity of cemented paste backfill. Miner. Eng., 22, 1307-1317.
Fall, M., Benzaazoua, M., & Ouellet, S. (2005). Experimental characterization of the influence of tailings fineness and density on the quality of cemented paste backfill. Miner. Eng., 18, 41-44.
Fall, M., Benzaazoua, M., & Saa, E. (2008). Mix proportioning of underground cemented tailings backfill. Tunnelling and Underground space technology, 23, 80-90.
Fall, M., Célestin, J., Pokharel, M., & Touré, M. (2010). A contribution to understanding the effects of curing temperature on the mechanical properties of mine cemented tailings backfill. Eng. Geol., 114, 397-413.
Fang, K., & Fall, M. (2018). Effects of curing temperature on shear behaviour of cemented paste backfill-rock interface. International Journal of Rock Mechanics and Mining Sciences, 112, 184-192.
Fang, K., Fall, M., & Cui, L. (2021). Thermo-chemo-mechanical cohesive zone model for cemented paste backfill-rock interface. Engineering Fracture Mechanics, 244, 107546.
Franks, D. M., Boger, D. V., Côte, C. M., & Mulligan, D. R. (2011). Sustainable development principles for the disposal of mining and mineral processing wastes. Resources policy, 36, 114-122.
Ghirian, A., & Fall, M. (2016). Strength evolution and deformation behaviour of cemented paste backfill at early ages: Effect of curing stress, filling strategy and drainage. International Journal of Mining Science and Technology, 26, 809-817.
Haiqiang, J., Fall, M., & Cui, L. (2016). Yield stress of cemented paste backfill in sub-zero environments: experimental results. Miner. Eng., 92, 141-150.
Hamza, O., Esaker, M., Abogdera, A., & Elliott, D. (2024). Bio-protection of cementitious materials below ground: The significance of natural soil environments. Developments in the Built Environment, 17, 100331.
Han, B., Wang, Y., Dong, S., Zhang, L., Ding, S., Yu, X., & Ou, J. (2015). Smart concretes and structures: A review. J. Intell. Mater. Syst. Struct., 26, 1303-1345.
Haruna, S., & Fall, M. (2022). Insight into saturated hydraulic conductivity of cemented paste backfill containing polycarboxylate ether-based superplasticizer. Minerals, 12, 93.
He, Z., Zhao, K., Yan, Y., Ning, F., Zhou, Y., & Song, Y. (2021). Mechanical response and acoustic emission characteristics of cement paste backfill and rock combination. Constr. Build. Mater., 288, 123119.
Helinski, M., Fahey, M., & Fourie, A. (2011). Behavior of cemented paste backfill in two mine stopes: measurements and modeling. Journal of geotechnical and geoenvironmental engineering, 137, 171-182.

Jefferson, A., Joseph, C., Lark, R., Isaacs, B., Dunn, S., & Weager, B. (2010). A new system for crack closure of cementitious materials using shrinkable polymers. Cem. Concr. Res., 40, 795-801.
Jiang, H., Fall, M., Yilmaz, E., Li, Y., & Yang, L. (2020). Effect of mineral admixtures on flow properties of fresh cemented paste backfill: Assessment of time dependency and thixotropy. Powder Technology, 372, 258-266.
Kalin, M., Fyson, A., & Wheeler, W. N. (2006). The chemistry of conventional and alternative treatment systems for the neutralization of acid mine drainage. Science of the total environment, 366, 395-408.
Kesimal, A., Yilmaz, E., Ercikdi, B., Alp, I., & Deveci, H. (2005). Effect of properties of tailings and binder on the short-and long-term strength and stability of cemented paste backfill. Mater. Lett., 59, 3703-3709.
Kuang, Y., & Ou, J. (2008). Self-repairing performance of concrete beams strengthened using superelastic SMA wires in combination with adhesives released from hollow fibers. Smart Mater. Struct., 17, 025020.
Li, V. C., & Herbert, E. (2012). Robust self-healing concrete for sustainable infrastructure. J. Adv. Concr. Technol., 10, 207-218.
Liu, L., Mao, X., Xiao, Y., Wang, T., & Nie, M. (2020). Influence of water and rock particle contents on the shear behaviour of a SRM. Transportation Safety and Environment, 2, 29-43.
Luo, M., Qian, C.-x., & Li, R.-y. (2015). Factors affecting crack repairing capacity of bacteria-based self-healing concrete. Constr. Build. Mater., 87, 1-7.
Matusinović, T., Šipušić, J., & Vrbos, N. (2003). Porosity–strength relation in calcium aluminate cement pastes. Cem. Concr. Res., 33, 1801-1806.
Naidu, G., Ryu, S., Thiruvenkatachari, R., Choi, Y., Jeong, S., & Vigneswaran, S. (2019). A critical review on remediation, reuse, and resource recovery from acid mine drainage. Environmental pollution, 247, 1110-1124.
Ohno, K., & Ohtsu, M. (2010). Crack classification in concrete based on acoustic emission. Constr. Build. Mater., 24, 2339-2346.
Özbay, E., Šahmaran, M., Lachemi, M., & Yücel, H. E. (2013). Self-Healing of Microcracks in High-Volume Fly-Ash-Incorporated Engineered Cementitious Composites. ACI Mater. J., 110.
Pane, I., & Hansen, W. (2005). Investigation of blended cement hydration by isothermal calorimetry and thermal analysis. Cem. Concr. Res., 35, 1155-1164.
Qian, S., Zhou, J., & Schlangen, E. (2010). Influence of curing condition and precracking time on the self-healing behavior of Engineered Cementitious Composites. Cem. Concr. Compos., 32, 686-693.
Quan, W., & Fall, M. (2024). Investigation of Inherent Self-Healing Behaviour in Cemented Paste Backfill. Paper presented at the 14th International Symposium on Mining with Backfill, Minefill 2024, Vancouver, Canada.
Quercia, G., Hüsken, G., & Brouwers, H. (2012). Water demand of amorphous nano silica and its impact on the workability of cement paste. Cem. Concr. Res., 42, 344-357.
Ramlochan, T., Grabinsky, M., & Hooton, R. (2004). Microstructural and chemical investigations of cemented paste backfills. Paper presented at the Tailings and Mine Waste.
Roig-Flores, M., Moscato, S., Serna, P., & Ferrara, L. (2015). Self-healing capability of concrete with crystalline admixtures in different environments. Constr. Build. Mater., 86, 1-11.
Rotta, G., Consoli, N., Prietto, P., Coop, M., & Graham, J. (2003). Isotropic yielding in an artificially cemented soil cured under stress. Geotechnique, 53, 493-501.

Sahmaran, M., Yildirim, G., Noori, R., ÖZBAY, E., & Lachemi, M. (2015). Repeatability and pervasiveness of self-healing in engineered cementitious composites. ACI Mater. J., 112.
Savastano Jr, H., & Agopyan, V. (1999). Transition zone studies of vegetable fibre-cement paste composites. Cem. Concr. Compos., 21, 49-57.
Seifan, M., Samani, A. K., & Berenjian, A. (2016). Bioconcrete: next generation of self-healing concrete. Appl. Microbiol. Biotechnol., 100, 2591-2602.
Simon, D., & Grabinsky, M. (2013). Apparent yield stress measurement in cemented paste backfill. International Journal of Mining, Reclamation and Environment, 27, 231-256.
Sisomphon, K., Copuroglu, O., & Koenders, E. (2013). Effect of exposure conditions on self healing behavior of strain hardening cementitious composites incorporating various cementitious materials. Constr. Build. Mater., 42, 217-224.
Snoeck, D., Van Tittelboom, K., Steuperaert, S., Dubruel, P., & De Belie, N. (2014). Self-healing cementitious materials by the combination of microfibres and superabsorbent polymers. J. Intell. Mater. Syst. Struct., 25, 13-24.
Sun, W., Hou, K., Yang, Z., & Wen, Y. (2017). X-ray CT three-dimensional reconstruction and discrete element analysis of the cement paste backfill pore structure under uniaxial compression. Constr. Build. Mater., 138, 69-78.
Termkhajornkit, P., Nawa, T., Yamashiro, Y., & Saito, T. (2009). Self-healing ability of fly ash–cement systems. Cem. Concr. Compos., 31, 195-203.
Van Breugel, K. (2007). Is there a market for self-healing cement-based materials. Paper presented at the Proceedings of the first international conference on self-healing materials.
Van Tittelboom, K., Wang, J., Araújo, M., Snoeck, D., Gruyaert, E., Debbaut, B., . . . De Belie, N. (2016). Comparison of different approaches for self-healing concrete in a large-scale lab test. Constr. Build. Mater., 107, 125-137.
Wang, B., Yang, L., Li, Q., Shu, X., & Kang, M. (2024). Mechanical behavior, acoustic emission and principal strain field evolution properties of layered cemented paste backfill under unconfined compression. Constr. Build. Mater., 415, 135111.
Wang, Y., Na, Q., & Zhang, L. (2022). Monitoring of in-situ properties for cemented tailings backfill that under drainage condition. Constr. Build. Mater., 356, 129254.
Wang, Z., Jiang, H., Fu, Y., Ma, Z., & Wang, X. (2024). Calcined alunite-modified alkali-sulphate-activated slag as a novel binder for high-performance cemented paste backfill. J. Build. Eng., 91, 109687.
Wang, Z., Wang, Y., Cui, L., Bi, C., & Wu, A. (2022). Insight into the isothermal multiphysics processes in cemented paste backfill: Effect of curing time and cement-to-tailings ratio. Constr. Build. Mater., 325, 126739.
Wei, B., Cao, H., & Song, S. (2010). RETRACTED: environmental resistance and mechanical performance of basalt and glass fibers. In: Elsevier.
WorldMineTailingsFutures. (2020). STATE OF WORLD MINE TAILINGS PORTFOLIO 2020. Retrieved from https://worldminetailingsfailures.org/
Xiang, J., Li, Z., Qiu, J., Wu, N., & Cheng, H. (2023a). Investigating the potential for porous ceramics as bacterial carrier in self-healing cemented paste backfill. Ceramics International, 49, 13490-13500.
Xiang, J., Qiu, J., Yuan, L., Wu, J., & Ma, Z. (2023b). Characterization and role analysis of bacteria types in self-healing behaviour of cemented paste backfill. J. Build. Eng., 75, 106964.
Xiu, Z., Wang, S., Ji, Y., Wang, F., & Ren, F. (2022). Experimental study on the triaxial mechanical behaviors of the Cemented Paste Backfill: Effect of curing time, drainage conditions and curing temperature. Journal of Environmental Management, 301, 113828.

Yang, Y., Yang, E.-H., & Li, V. C. (2011). Autogenous healing of engineered cementitious composites at early age. Cem. Concr. Res., 41, 176-183.
Yıldırım, G., Keskin, Ö. K., Keskin, S. B., Şahmaran, M., & Lachemi, M. (2015). A review of intrinsic self-healing capability of engineered cementitious composites: Recovery of transport and mechanical properties. Constr. Build. Mater., 101, 10-21.
Yıldırım, G., Khiavi, A. H., Yeşilmen, S., & Şahmaran, M. (2018). Self-healing performance of aged cementitious composites. Cem. Concr. Compos., 87, 172-186.
Yilmaz, E., Belem, T., & Benzaazoua, M. (2014). Effects of curing and stress conditions on hydromechanical, geotechnical and geochemical properties of cemented paste backfill. Eng. Geol., 168, 23-37.
Yilmaz, E., Benzaazoua, M., Belem, T., & Bussière, B. (2009). Effect of curing under pressure on compressive strength development of cemented paste backfill. Miner. Eng., 22, 772-785.
Yin, S., Wu, A., Hu, K., Wang, Y., & Zhang, Y. (2012). The effect of solid components on the rheological and mechanical properties of cemented paste backfill. Miner. Eng., 35, 61-66.
Yu, S., Jiang, H., Xi, Z., Li, X., Wang, P., & Fu, Y. (2024). Image analysis as a geometry-and integrity-independent tool for predicting strength of cemented tailings backfill using slag-based binder. Constr. Build. Mater., 444, 137867.
Zhang, J., Liu, Y., Feng, T., Zhou, M., Zhao, L., Zhou, A., & Li, Z. (2017). Immobilizing bacteria in expanded perlite for the crack self-healing in concrete. Constr. Build. Mater., 148, 610-617.
Zhang, W., Zheng, Q., Ashour, A., & Han, B. (2020). Self-healing cement concrete composites for resilient infrastructures: A review. Composites Part B: Engineering, 189, 107892.
Zhao, Y., Taheri, A., Karakus, M., Chen, Z., & Deng, A. (2020). Effects of water content, water type and temperature on the rheological behaviour of slag-cement and fly ash-cement paste backfill. International Journal of Mining Science and Technology, 30, 271-278.

5.5 Paper V: Influence of Crack-Inducing Stress Modes on the Self-Healing Efficiency of Cemented Paste Backfill

Submitted for publication

Weizhou Quan, Mamadou Fall

Department of Civil Engineering, University of Ottawa, Ottawa, Ontario, Canada

Abstract

This paper examines the autogenous self-healing behaviour of cemented paste backfill (CPB) with crack damage induced by three distinct stress modes, including uniaxial compression, triaxial compression, and indirect tensile loading, which present common field-relevant stress conditions in underground stopes. Pre-cracked specimens and uncracked controls were subjected to healing periods of up to 90 days and evaluated through mechanical strength recovery, hydraulic conductivity testing, crack characterization, X-ray micro-computed tomography (XR-μCT), and microstructural analyses (SEM-EDS, FTIR, XRD, TG/DTG). Results reveal that specimens pre-cracked under uniaxial and triaxial compression exhibit superior self-healing efficiency, with strength recovery exceeding 15% compared to uncracked controls and permeability reduction surpassing 85-90% after 90 days. These outcomes are attributed to favourable crack geometries, continued cement hydration, and carbonation of $Ca(OH)_2$, leading to the deposition of C-S-H, calcite, and ettringite within cracks. In contrast, disc-shaped specimens subjected to indirect tensile loading developed traversing mode-I cracks with large apertures, limiting healing and resulting in substantially lower strength and permeability recovery. The findings demonstrate that crack type critically governs the self-healing potential of CPB, with confined shear-dominated cracks showing the most efficient closure, while large tensile cracks remain only partially healed. This work advances understanding of stress-dependent self-healing in CPB and provides a scientific basis for predicting the long-term durability and containment performance of backfill structures in subsurface mine conditions.

Keywords: Cemented paste backfill; Autogenous healing; Mine; Tailings; Mechanical properties; Hydraulic conductivity; Mechanical loading

5.5.1 Introduction

As mining operations advance toward deeper underground deposits, tailings production continues to escalate, with recent estimates indicating an annual generation of approximately 16 billion tonnes and a cumulative global inventory exceeding 282 billion tonnes (Global Mining Review, 2023). Cemented paste backfill (CPB) has emerged as an integral component of modern underground mining operations due to its dual role in effective tailings management and ground support. The implementation of CPB significantly reduces reliance on surface tailings storage facilities (TSFs), enhances underground stability, and improves ore recovery from mineralized zones (Qi & Fourie, 2019; Yilmaz & Fall, 2017). CPB is made chiefly from dewatered tailings (70-85 wt.%), hydraulic binders (3-7 wt.%), and either processed mine water or fresh water, which is

delivered to underground stopes as a non-Newtonian slurry through a pipeline system (Benzaazoua et al., 2004; Brackebusch, 1994; Fall et al., 2005). After placement, the CPB structure is required to meet specific mechanical requirements to support the exposed rock mass as a self-supporting structure, thereby minimizing operational interruptions and managing stress redistribution in the surrounding rock (Jafari & Grabinsky, 2021; Sivakugan et al., 2006). In parallel, CPB must also meet durability and environmental requirements by ensuring long-term integrity, containing contaminants, and preventing acid mine drainage (AMD) (Fall et al., 2009).

Upon placement, CPB structures are influenced by a range of intrinsic and extrinsic impacting factors, including tailings characteristics (e.g., particle size distribution, density, mineralogy), binder type and dosage, water geochemistry, temperature, drainage conditions, moisture content, sulphate concentration, in-situ stress, and backfilling strategies (e.g., filling rate and sequence). These factors act independently or interactively to influence the mechanical, durability, and environmental performance of CPB (Cui & Fall, 2015; Ghirian & Fall, 2014). Numerous laboratory and in situ studies have investigated the effects of these variables on CPB behaviour (Fall et al., 2005; Ercikdi et al., 2009; Ghirian & Fall, 2016; Fall & Pokharel, 2010; Helinski et al., 2011; le Roux et al., 2005; Thompson et al., 2012; Wang et al., 2022; Wu et al., 2013; Yilmaz et al., 2014). Among these variables, the role of in-situ stress during curing has received increasing attention. To replicate underground stress environments, various testing apparatuses have been developed (Belem et al., 2002; Cui & Fall, 2016b; Fang & Fall, 2020; Ghirian & Fall, 2016; Guo et al., 2020; Liu & Fall, 2024; Shahsavari et al., 2022; Xu et al., 2019; Yang et al., 2020; Yilmaz et al., 2014; Yilmaz et al., 2009). These systems typically apply vertical stress (self-weight and overburden), horizontal stress (rock wall closure or convergence), and shear stress at CPB-rock or CPB-CPB interfaces. Findings consistently demonstrated that stress applied during curing enhances consolidation and particle rearrangement within the CPB matrix, thereby accelerating binder hydration, promoting additional hydration products, refining the microstructure, increasing mechanical strength, and reducing permeability. This explains why CPB specimens cured under stress-free laboratory conditions often underestimate field strength, even with identical mix designs.

In practice, CPB is subjected to a combination of compressive, tensile, and shear stresses arising from overburden pressure (self-weight, loads from mining activities, overlying rock mass, early loading, or uneven stress distribution), rock mass movement and wall closure, as well as dynamic activities such as blasting-induced vibrations. CPB structures, therefore, experience coupled stress states rather than isolated modes. As mining operations extend to deeper ore bodies, CPB is exposed to substantially higher in-situ stresses, reaching several megapascals in horizontal directions and tens of megapascals vertically (Ouyang et al., 2009; Raffaldi et al., 2019; Seymour et al., 2017). While moderate stresses may enhance strength development, excessive loading can trigger microcracking or structural failure, particularly during early hydration or in the presence of localized weaknesses (Ghirian, 2016; Liu & Fall, 2025; Zhou & Beaudoin, 2003). For instance, a backfill failure at the Lucky Friday Mine was attributed to sudden wall convergence that imposed an average horizontal stress of 3 MPa on the CPB mass (Seymour et al., 2017). Similarly, Liu & Fall (2025) reported that the development of macro-cracks in a 28-day CPB sample cured under

multiaxial stress, culminating in structural failure when vertical and lateral stresses reached 0.61 MPa and 3.75 MPa, respectively. When such loadings interact with intrinsic flaws (e.g., structural defects, shrinkage, or chemical degradation such as sulphate attack), cracks may initiate during curing. The subsequent propagation of cracks compromises both the mechanical integrity and environmental containment of CPB. Indeed, shear, tensile, and mixed-mode (shear-tensile) cracking are common failure mechanisms originating from microstructural defects under stress (Li et al., 1998; Pan et al., 2021). As mines go deeper and stress levels increase, CPB becomes more prone to cracking, undermining its mechanical, durability, and environmental performance.

These facts highlight the critical importance of mitigating or healing cracks in CPB to ensure its mechanical stability, durability, and environmental performance, particularly in deep mining contexts. Autogenous self-healing has emerged as a promising strategy to counteract the detrimental effects of cracking in CPB. Previous studies have examined the influence of healing temperature, drainage, sulphate content, and other factors affecting the autogenous self-healing capability of CPB (Quan & Fall, 2024, 2025a, 2025b). However, all such studies induced cracking via uniaxial compression, which generally produces a mixed tensile-shear crack mode, making it difficult to isolate and compare healing efficiency across distinct crack types. In reality, CPB in stopes is predominantly subjected to multiaxial (triaxial) compressive stress due to confinement by stope walls and arching, with continuous mobilization of interface shear at fill-rock boundaries. Local tensile stresses also arise at free surfaces, underhand spans, and from early-age shrinkage, thermal gradients, blasting, or seismicity, often governing cracking and serviceability. In contrast, uniaxial compression is seldom representative of in-situ conditions. Thus, previous studies based solely on uniaxial loading may not be representative of self-healing behaviour in practice. To date, no studies have examined autogenous self-healing of CPB in cracks induced specifically by shear or tensile stresses.

Moreover, research on conventional cementitious materials, such as mortar, concrete, and engineered cementitious composites (ECC), has often employed controlled loading methods, such as uniaxial tension, splitting, or flexural tests, to generate cracks under well-defined stress states for self-healing evaluation (Choi et al., 2017; Ferrara et al., 2014; Ferrara et al., 2018; Hezhi Liu et al., 2017; Özbay et al., 2013; Qureshi et al., 2016; Sahmaran et al., 2015; Sisomphon et al., 2013; Snoeck & De Belie, 2015). However, the results from conventional concretes cannot be directly transferred to CPB, which differs fundamentally in composition, microstructure, and performance. Even within the broader field of cementitious materials, the role of distinct crack modes in governing autogenous self-healing remains underexplored.

Building upon this gap, this study aims to advance the understanding of autogenous self-healing in CPB by examining the influence of distinct crack modes and the stress types that induce them. In addition to uniaxial compressive loading, which typically generates mixed tensile-shear cracks, two alternative methods are employed: triaxial compression (predominantly generating shear cracks) and indirect (Brazilian) tensile (producing pure tensile cracks) testing. These approaches introduce well-defined crack profiles, enabling systematic evaluation of healing performance. To

assess the self-healing capability, surface crack closure, mechanical strength recovery, and permeability reduction were examined in pre-cracked CPB specimens. The findings provide novel insights into how crack type and stress state influence the autogenous healing performance in CPB, thereby contributing to the design of more durable and environmentally sustainable backfill systems for deep underground mining.

5.5.2 Materials and Experimental Program

5.5.2.1 Materials

Tailings

Silica tailings (ST), characterized by a high quartz content (99.8% of SiO_2) and commonly present in Canadian hard rock mine tailings, served as the primary material for CPB specimen preparation. The relatively high purity and chemically inert nature of ST aim to minimize the uncertainties associated with the reactive mineralogical compositions in natural tailings (NT). Additionally, approximately 45 wt.% of ST comprises fine particles with sizes below 20 μm, falling within the range of medium tailings. Its particle size distribution closely resembles that of NTs from nine different mines in eastern Canada, as shown in Figure 5-39. The close agreement in particle size distributions supports the use of ST as a realistic proxy for Canadian mining contexts. Table 5-12 and Table 5-13 summarize the mineralogical and physical properties of ST, respectively.

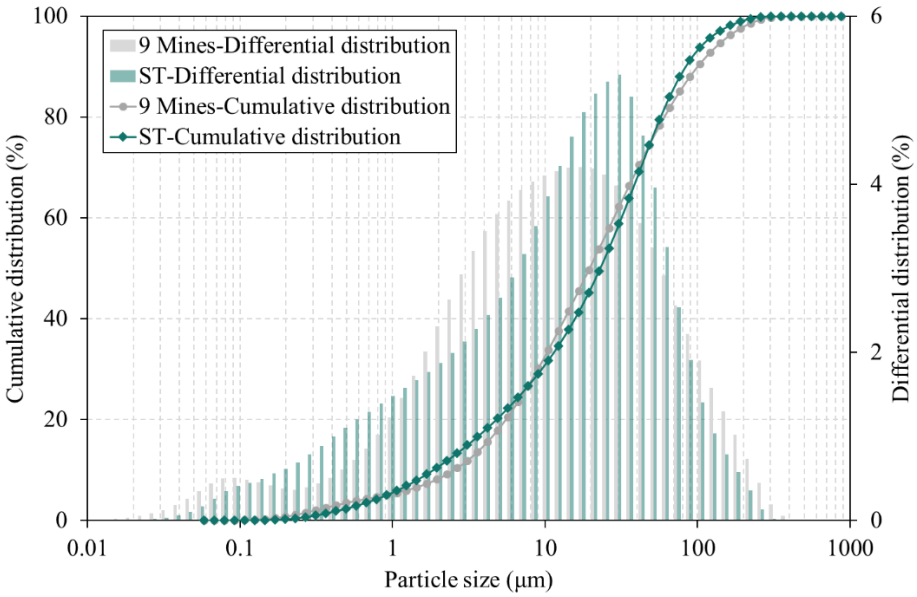

Figure 5-39. Gradation curve of the ST compared with the average gradation of nine natural tailings (NT) from eastern Canada.

Binder and Water

Type I Portland cement (PCI), also commonly referred to as General Use (GU) cement, was selected as the hydraulic binder for preparing the CPB specimens, reflecting its widespread adoption in mining applications. The GU cement used here consisted of CaO, SiO_2, Al_2O_3, SO_3, Fe_2O_3, and MgO, with respective proportions of 62.82%, 18.03%, 4.53%, 3.82%, 2.70%, and

2.65%. Potable tap water served as the mixing water for combining the ST with the cement to produce backfill mixtures.

Table 5-12. Mineralogical constituents of the utilized tailings.

Tailings	SiO_2	FeO_3	Al_2O_3	TiO_2	CaO	MgO	Na_2O	K_2O	LOI
	(%)								
ST	99.8	0.035	0.05	0.02	0.01	< 0.01	< 0.01	0.02	0.1

LOI: loss on ignition.

Table 5-13. Physical characteristics of ST alongside the average of nine natural tailings from Eastern Canada.

Element	G_s	D_{10}	D_{30}	D_{50}	D_{60}	C_u	C_c
		(μm)					
ST	2.7	1.9	9.0	22.5	31.5	16.6	1.3
9 mines average	-	1.8	9.1	20.0	30.8	17.1	1.7

G_s: specific gravity; C_u: coefficient of uniformity; C_c: coefficient of curvature.

5.5.2.2 Specimen preparation and initial curing

Silica tailings and PCI were batched to yield a binder content of 4.5 wt.% with respect to the solid mass. The dry constituents were premixed for ~1 min in a mechanical mixer to disperse fines uniformly, after which water was added to reach a fixed w/c of 7.35. Mechanical mixing then proceeded for 7 min, ensuring a homogeneous paste was achieved. The workability of the fresh CPB mixture was evaluated using the slump test according to ASTM C143 (ASTM, 2020a), yielding a slump value of 18 cm, which aligns with common practices in Canadian mine backfill operations. Specimens intended for subsequent testing were cast in molds with a dimension of Φ50×100 mm. A 7-day initial curing (IC) stage under ambient laboratory conditions was applied to the specimens before crack introduction, as outlined in Table 5-14. For indirect tensile stress testing, disc specimens were prepared by cutting the central portion of the previously cast specimens, maintaining a thickness-to-diameter (t/d) ratio of approximately 0.6 to ensure consistency after the initial curing period, as illustrated in Figure 5-40c.

5.5.2.3 Crack initiation

Following the initial curing phase, a subset of the CPB specimens was stored as uncracked control specimens and maintained under continued curing conditions. The remaining specimens then underwent a controlled pre-cracking process to introduce defined levels of crack damage in preparation for subsequent self-healing investigations. To investigate the influence of stress conditions and crack modes on self-healing efficiency, three mechanical testing methods commonly used in CPB mechanical property evaluation were employed: uniaxial compression, triaxial compression, and indirect (Brazilian) tensile testing, as illustrated in Figure 5-40. These tests were selected to represent crack-inducing stresses dominated by compressive stress (CS),

shear stress (SS), and tensile stress (TS), respectively, thereby enabling the generation of distinct and well-characterized crack damage profiles for subsequent healing analysis.

Table 5-14. Experimental summary of the studied CPB specimens, including mix design, curing/healing conditions, and testing methods.

Sample nomenclature	Binder content (wt.%)	w/c ratio	Initial curing (day)	Pre-cracking method	Pre-cracking level	Self-healing period (day)
Self-healing behaviour of CPB with crack damage induced by uniaxial compression loading						
CS	4.5	7.35	7	Uniaxial compression test	75% and 90% of compressive stress	7 28 90
Self-healing behaviour of CPB with crack damage induced by triaxial compression loading						
SS	4.5	7.35	7	Triaxial compression test	75% and 90% of deviator stress	7 28 90
Self-healing behaviour of CPB with crack damage induced by indirect tensile loading						
TS	4.5	7.35	7	Indirect tensile test	90% and 100% of tensile stress	7 28 90

For the CS-induced cracking scenario, the initial strengths of CPB specimens were determined through uniaxial compressive strength (UCS) testing after the IC period in compliance with ASTM C39/C39M-21 (ASTM, 2021). Based on these values, the specimens were then loaded to 75% and 90% of their UCS values (designated as CS-PC75% and CS-PC90%, respectively) to induce controlled pre-cracking before reaching the peak stress stage. The load was maintained for one minute to allow crack initiation and propagation within the CPB matrix. These specific pre-cracking levels were adopted in accordance with previous findings (Quan & Fall, 2025a), which demonstrated that surface-visible cracks typically occur at or beyond 75% of UCS. It was observed that the PC75% pre-cracking level predominantly produced tensile cracks, whereas the PC90% pre-cracking level resulted in a combination of tensile and shear cracks. In terms of the SS-induced cracking condition, an analogous pre-cracking procedure, represented by SS-PC75% and SS-PC90%, was adopted, while the reference stress was the peak deviator stress obtained from triaxial compression tests. The pre-cracking process was conducted within a triaxial testing cell (Figure 5-40b), where the effective confining pressure for the specimens was provided by a Tri-Flex 2 hydraulic pressure system. During the shear stress pre-cracking process, specimens enclosed in rubber membranes were placed in a pressure chamber and subjected to a confining pressure (σ_3 = 120 kPa) using hydraulic water. This pressure was determined based on a confinement ratio of 0.25, defined as the ratio of confining stress to UCS. A vertical load was then applied to perform triaxial compression tests under undrained conditions in accordance with ASTM D4767-11 (ASTM,

2020b). This procedure primarily induced major shear cracks with occasional tensile cracking. Both UCS and triaxial pre-cracking processes were conducted subjected to a displacement-controlled regime at a steady rate of 1 mm/min. Furthermore, regarding the TS-induced cracking scenario, indirect tensile tests were carried out on the disc specimens utilizing a compressive testing system with flat loading plates, following ASTM D3967-23 (ASTM, 2023), with a displacement-controlled loading rate of 0.2 mm/min. This method resulted in the formation of dominant tensile cracks initiating from the center of the specimens. All mechanical loading procedures were implemented on a servo-controlled mechanical press (MTS 10/GL, 50 kN capacity). Axial displacement was recorded using an internal linear variable differential transformer (LVDT) connected to an automated data acquisition system.

5.5.2.4 Healing condition

During the self-healing curing phase, the pre-cracked CPB specimens were individually wrapped in plastic film and stored alongside the uncracked control specimens under ambient conditions. This controlled self-healing exposure condition aimed to minimize external interference, thereby reducing uncertainties in the subsequent analysis. Such conditions ensured a consistent environment for evaluating the intrinsic autogenous self-healing behaviour and efficiency of CPB materials with different stress-induced crack damage mechanisms. In this study, the day on which pre-cracking was completed was designated as D0, marking the completion of pre-cracking and the initiation of the self-healing period. Subsequent self-healing periods were defined as D7, D28, and D90, representing short-term (7 and 28 days) and long-term (90 days) self-healing phases, respectively. Notably, these self-healing periods corresponded to CPB paste ages of 7, 14, 35, and 97 days for D0, D7, D28, and D90, respectively.

5.5.2.5 Testing method for self-healing

Evaluation of mechanical property

The mechanical strength recovery due to self-healing was assessed through uniaxial compression, triaxial compression, and indirect tensile tests, performed on at least three specimens per condition. To evaluate the recovery of uniaxial compressive, deviator, and tensile stresses, tests were carried out on pre-cracked specimens (pre- and post-healing) as well as uncracked control specimens at self-healing periods of 0, 7, 28, and 90 days. An index, referred to as Changes in Mechanical Strength (CMS), was defined for quantitative evaluation of self-healing efficiency in terms of strength recovery, based on the differences in strength between the pre-cracked and the corresponding control specimens. CMS is calculated as follows:

$$\mathrm{CMS}(\%)=\frac{S_{\text{pre-cracked/healed}} - S_{\text{control}}}{S_{\text{control}}} \tag{5-11}$$

where $S_{pre\text{-}cracked/healed}$ represents the strength of pre-cracked specimens before or after the self-healing period, and $S_{control}$ corresponds to the strength of uncracked control specimens exposed to the identical self-healing regime and duration. Note that strength in these calculations refers to UCS, deviator stress, or tensile stress, depending on the test performed.

Evaluation of permeability property: hydraulic conductivity test

Low permeability is often associated with the durability of CPB structures, as it minimizes the risk of fluid (water, air) ingress, acid mine drainage (AMD), and contaminant release into groundwater systems. Saturated hydraulic conductivity (k_{sat}) measurements of CPB specimens with different crack-induced damage were measured to evaluate permeability recovery and to reflect the internal crack self-healing. The hydraulic conductivity tests were performed on pre-cracked specimens (pre- and post-healing) and control specimens employing a triaxial cell equipped with a flexible wall following the procedures specified in ASTM D5084-16a (ASTM, 2016). The Hydraulic Conductivity Recovery Ratio (HCRR) is defined to quantify the improvement in permeability by comparing the hydraulic conductivity of pre-cracked specimens pre- and post-healing stage:

$$\text{HCRR } (\%) = \frac{k_0 - k_t}{k_0} \times 100\% \tag{5-12}$$

where k_0 represents the initial hydraulic conductivity, cm/s, before healing; k_t is the hydraulic conductivity, cm/s, measured after specified self-healing period.

Crack characteristics

Crack morphology parameters were monitored to complement the results from the mechanical and permeability tests. Surface crack closure of pre-cracked CPB specimens was assessed using a portable digital microscope (200× magnification), enabling direct visualization and measurement of healed crack widths as an indicator of autogenous healing performance. For disc specimens subjected to TS loading, where prominent cracks were present, crack areas were quantified to track changes in crack size during the self-healing period.

To investigate internal crack geometry, X-ray micro-computed tomography (XR-μCT) scanning was performed on SS-PC and TS-PC specimens using a SkyScan high-resolution scanner with analytical settings of 130 kV voltage, 61 μA current, 1350 ms exposure time, and 25 μm resolution. During scanning, the specimen was illuminated by an X-ray beam, which attenuated as it passed through different phases of the CPB matrix. This attenuation allowed the acquisition of 2D cross-sectional projections at rotation steps of 0.25° or 0.3° (Flannery et al., 1987). In the raw images, two primary phases can be distinguished: (i) air-filled regions (cracks and pores) appearing black, and (ii) the solid CPB matrix (cement hydrates and tailings in dark gray, unhydrated cement in light gray). Reconstruction of 3D structures from the 2D attenuation slices, along with numerical segmentation, was performed using ImageJ software. This enabled high-resolution visualization and analysis of crack morphology, distribution, propagation, and potential self-healing behaviour within the CPB structure. For enhanced interpretability, segmented images were rendered with the solid matrix displayed in white, while cracks and pores were pseudo-colored in blue-purple to clearly distinguish them from the solid phase.

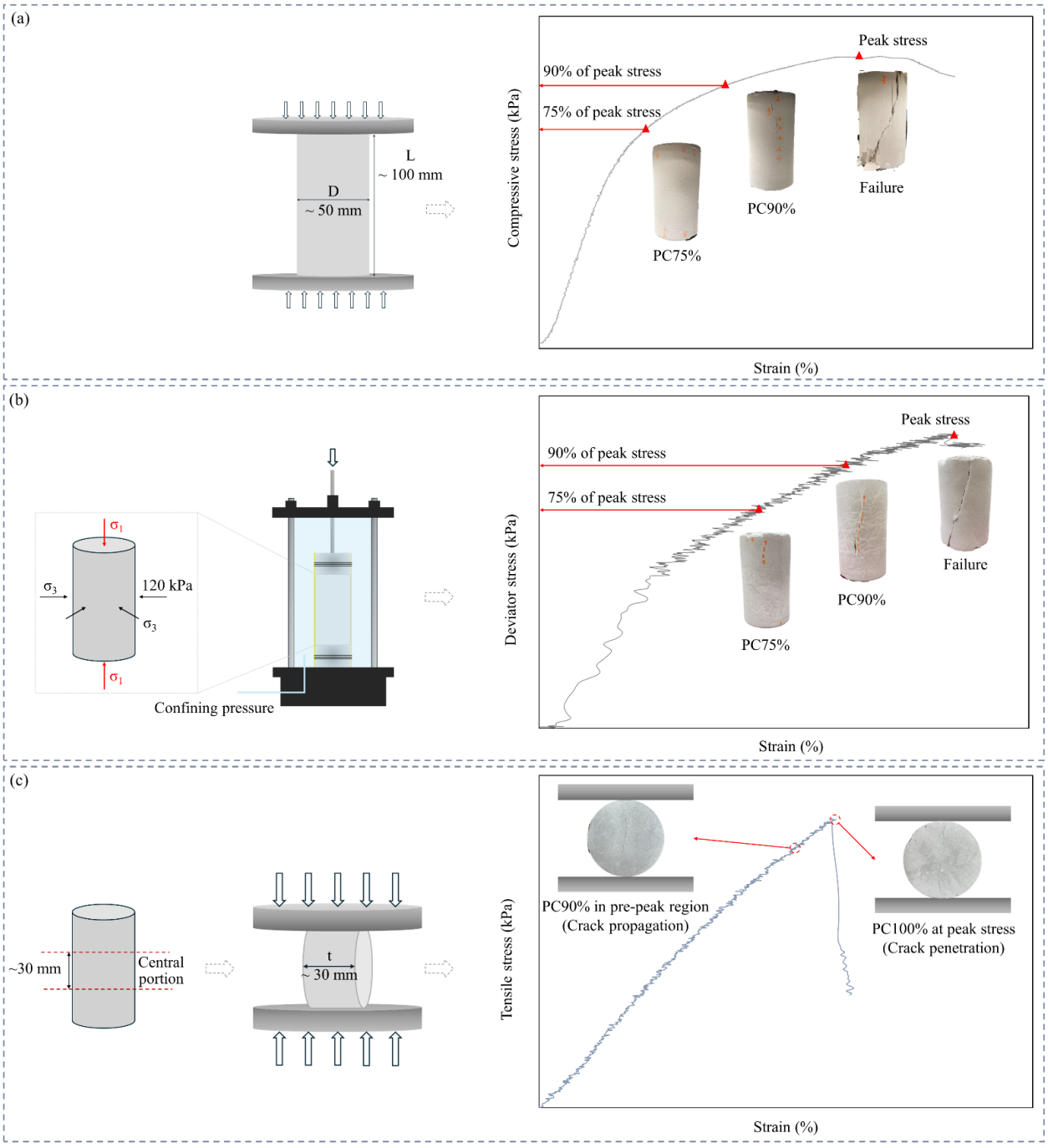

Figure 5-40. Pre-cracking process by employing (a) uniaxial compression loading, (b) triaxial compression loading, and (c) indirect tensile loading.

Microstructural analysis

Scanning electron microscopy (SEM) equipped with energy dispersive spectroscopy (EDS), thermogravimetric analysis (TG/DTG), X-ray diffraction (XRD), and Fourier transform infrared spectroscopy (FTIR) were employed to characterize the self-healing products and hydration behaviour of the studied CPB specimens. A JEOL 6610LV SEM with environmental operation

capability, operating at low voltage and equipped with an Oxford INCA large-area SDD detector, was used for SEM-EDS characterization. The analysis aimed to observe the morphology of self-healing products and to determine their elemental compositions. Complementary chemical characterization was performed using XRD and FTIR to identify the crystalline and functional groups present in the self-healing products. XRD analyses were carried out with a Bruker D8 Endeavor diffractometer, and FTIR spectra were detected utilizing a Thermo Scientific Nicolet 6700 spectrometer. In addition, TG/DTG analyses were conducted using Mettler Toledo TGA 2 to investigate the thermal decomposition behaviour and hydration products of healed and control CPB specimens. The thermal tests were conducted under nitrogen with a heating rate of 10 °C/min to a maximum temperature of 1000 °C, providing insights into the binder hydration mechanisms influenced by pre-cracking and subsequent self-healing.

5.5.3 Results and Discussion

5.5.3.1 Nature of self-healing products

As illustrated in Figure 5-41, direct microscopic observations reveal the progressive formation and accumulation of crystal-like self-healing products precipitating and growing along the surfaces of cracks over the self-healing period. These products gradually fill the crack openings, leading to apparent closure throughout the self-healing period from D0 to D90. To further characterize the chemical composition and elucidate the autogenous healing mechanisms, the self-healing materials formed in pre-cracked specimens exposed to the different crack-inducing stress conditions following 90 days of self-healing were analyzed using FTIR spectroscopy, as shown in Figure 5-42a. As seen in the FTIR spectral profiles, the characteristic absorption peaks at 694 cm^{-1} and 1083 cm^{-1} associated with asymmetrical Si-O bending vibrations, and at 777 cm^{-1} and 796 cm^{-1} attributed to symmetric Si-O-Si stretching vibrations, are identified as features of quartz present in the silica tailings. Notably, the peaks at 694 cm^{-1} and 1083 cm^{-1} are not only indicative of quartz but also suggest the formation of silicate (C-S-H) (Sari et al., 2023; Sun et al., 2022). In addition, the absorption band at 451 cm^{-1}, corresponding to Si-O bending vibrations, further supports the formation of C-S-H within the self-healing products (Feng et al., 2023; Wang et al., 2021). The presence of carbonate phases is confirmed by peaks at 875 cm^{-1} and 1442 cm^{-1}, representing out-of-plane bending and asymmetric C-O stretching vibrations of CO_3^{2-}, respectively. These peaks indicate the formation of calcite, a product of $Ca(OH)_2$ carbonation within the CPB matrix (dos Santos et al., 2021; Sun et al., 2022). Furthermore, an absorption band near 1162 cm^{-1} is attributed to the S-O asymmetric stretching vibration of SO_4^{2-}, confirming the presence of ettringite (Sari et al., 2023). Collectively, the FTIR spectra clearly demonstrate that C-S-H, calcite, and ettringite constitute the primary components of the self-healing products formed within the cracks. These findings are further corroborated by XRD analysis in Figure 5-42b, which confirms the presence of the same aforementioned crystalline phases. Moreover, SEM-EDS characterization of the self-healing products, as shown in Figure 5-43, supports these conclusions by revealing the corresponding morphologies and elemental compositions. Together, the FTIR, XRD, and SEM-EDS results confirm that continued cement hydration and carbonation of $Ca(OH)_2$ are the dominant

mechanisms governing the autogenous self-healing behaviour observed in pre-cracked CPB specimens, irrespective of the type of crack-inducing stress. These mechanisms are consistent with those reported in prior studies on conventional CPB systems (Quan & Fall, 2025a, 2025b).

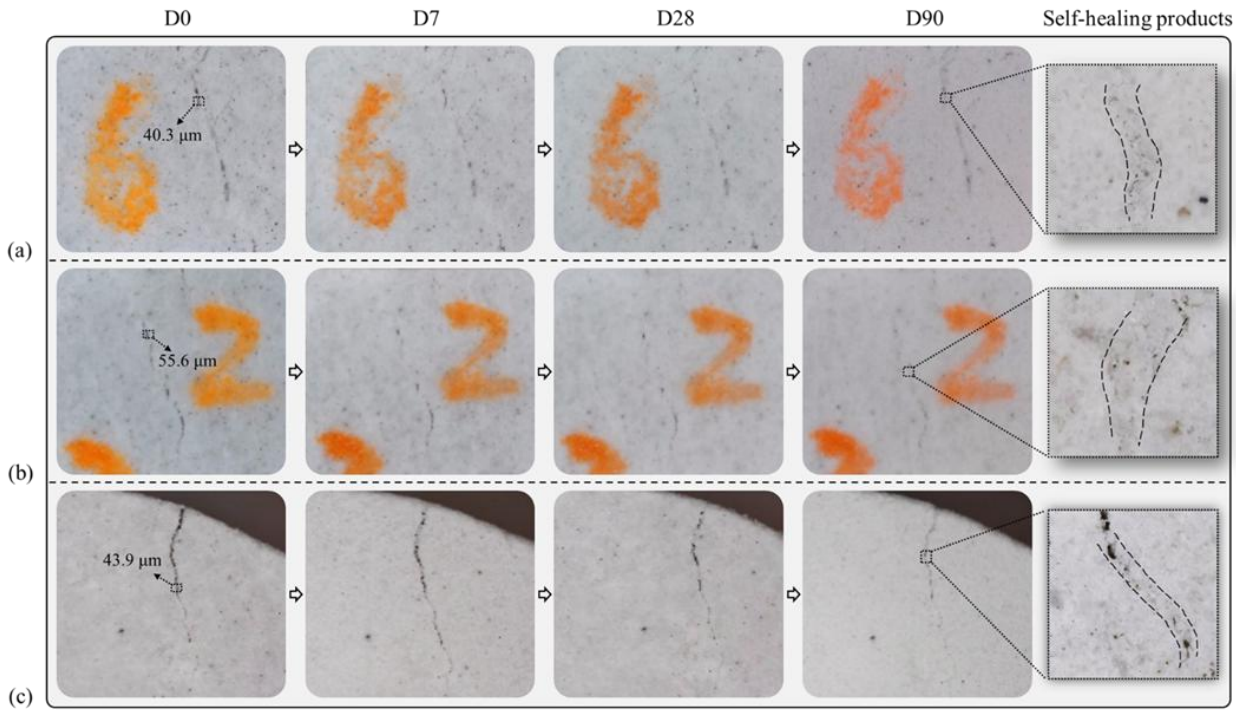

Figure 5-41. Typical surface crack closure observed throughout the self-healing period from 0 to 90 days in pre-cracked specimens subjected to (a) triaxial compression, (b) uniaxial compression, and (c) indirect tensile loading.

5.5.3.2 Crack characteristics through self-healing

The crack characteristics of pre-cracked cylinder and disc specimens subjected to three crack-inducing stresses/methods were assessed by evaluating the average crack widths, maximum healed crack widths, and reductions in crack area before and/or after the self-healing periods. As self-healing products precipitate and bridge the crack gaps, visible surface crack widths are reduced, resulting in the development of continuous and compact specimen surfaces as exemplified by complete healing in Figure 5-41. In particular, Figure 5-41 shows a steady decrease in crack width from D0 to D90. This progressive crack closure behaviour demonstrates the autogenous self-healing capability of the CPB matrix and its potential to restore surface integrity without external intervention. In addition, specimens exhibiting large crack widths were analyzed under partial and no healing conditions, demonstrating the limited effectiveness of autogenous self-healing in such pre-cracked CPB specimens. To quantitatively evaluate the self-healing of surface crack closure under the three crack-inducing stresses, the crack widths with complete healing were measured and summarized in Table 5-15 for all studied specimens after the designated self-healing periods. Evidently, the pre-cracked specimens, regardless of the crack-inducing method, exhibit overall comparable crack closure performance in healed crack widths as the healing progress advances.

This consistent performance is attributed to the identical mix design used for all CPB specimens, ensuring the same cement content, which dominates the autogenous self-healing of CPB materials. Consequently, similar surface crack closure behaviour is observed when specimens are subjected to the same pre-cracking age and self-healing conditions.

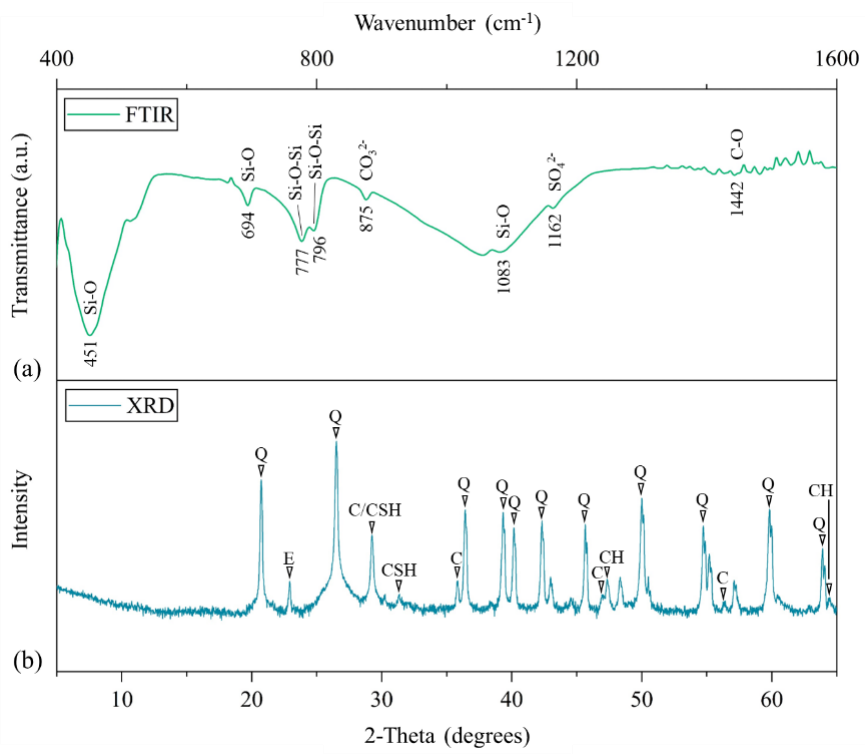

Figure 5-42. (a) FTIR and (b) XRD curves of self-healing products extracted from pre-cracked specimens.

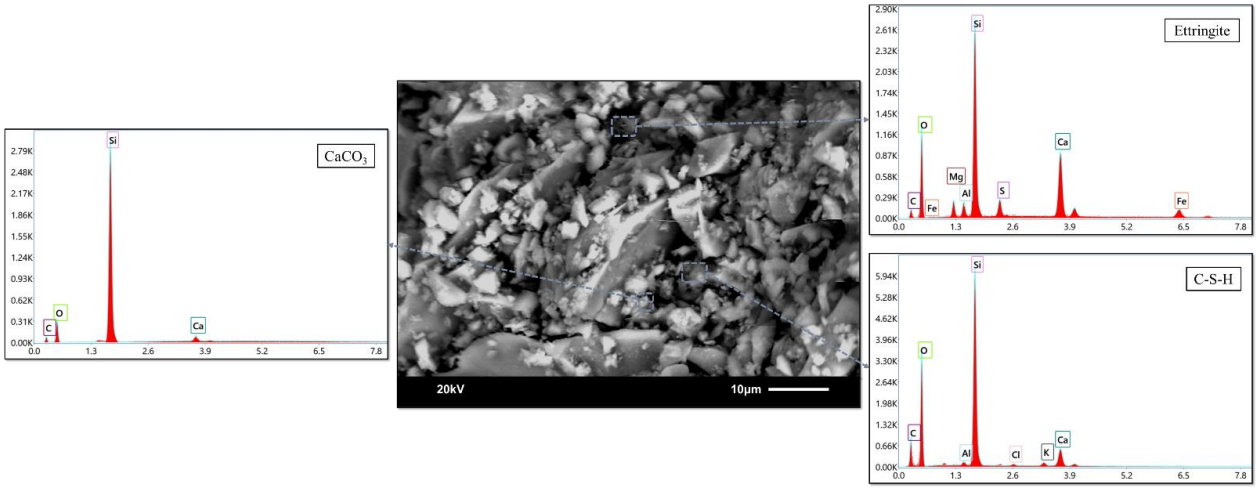

Figure 5-43. SEM-EDS characterization of the crack surface in a CS pre-cracked specimen after a 90-day self-healing period.

Table 5-15. Maximum healed surface crack width on specimens subjected to different crack-inducing methods after specific self-healing periods.

Batch nomenclature*	Self-healing period (day)	Maximum completely healed crack width (μm)
CS-PC	7	48.6
	28	60.4
	90	75.5
SS-PC	7	45.1
	28	61.0
	90	73.1
TS-PC	7	50.9
	28	66.0
	90	80.2

*CS-PC, SS-PC, and TS-PC indicate specimens pre-cracking by uniaxial compression, triaxial compression, and indirect tensile loading, respectively.

It is important to note that multiple cracking patterns are observed in the studied specimens subjected to the three crack-inducing stresses, which reveal variations in the self-healing performance among different crack types. In the cylinder specimens under uniaxial compression, crack propagation typically involves a combination of tensile and shear cracks, as shown in Figure 5-44ab. At the pre-cracking level of CS-PC75%, axial compression combined with lateral tensile stresses predominantly induces vertical tensile splitting cracks parallel to the loading axis. These tensile cracks are relatively clean and open, with clearly visible gaps. As the pre-cracking level increases to CS-PC90%, stress concentrations around flaws facilitate the formation of inclined shear cracks, resulting in a combination of tensile and shear crack types. While shear cracks are primarily governed by sliding displacement, they also exhibit narrow, irregular openings due to localized dilation (Figure 5-44b). In contrast, the crack patterns in cylinder specimens under triaxial compression differ significantly due to the lateral confining pressure. At the pre-cracking level of SS-P90%, microcracks become more pronounced, with orientations influenced by the combined compressive and shear stress conditions. Vertical tensile splitting cracks are largely suppressed, and crack propagation is dominated by the formation of inclined shear cracks, typically oriented at approximately 15-30 degrees to the loading axis. Some shear cracks remain narrow and irregular, with minimal apertures due to the restraining effect of confining pressure, resulting in less open shear cracks (Figure 5-44ef). Despite the confining pressure restricting the crack opening, Figure 5-44g reveals the localized dilation zones where microcrack coalescence and particle interlocking induce measurable apertures (Cui & Fall, 2016a; Jafari et al., 2021; Jouanna, 1993; Kadin & Rychahivskyy, 2012; Liu et al., 2025). The dilation behaviour is further supported by the XR-μCT images of the shear cracks formed at different specimen depths under the pre-cracking level of SS-PC90% in Figure 5-45, revealing that the dilated regions become more pronounced near the mid-height of the specimen with the increase of crack opening. On the other hand, in disc specimens

subjected to indirect tensile loading, the mode-I tensile cracks are formed under the indirect tensile test, where a transverse tensile stress field develops perpendicular to the applied load (Figure 5-44d). During pre-cracking, the major visible tensile cracks typically initiate near the center of the disc, exhibiting the largest aperture and gradually tapering toward the edges. These cracks are uniform, clean, and more accessible compared to shear cracks, illustrating the differences in crack morphology induced by distinct loading conditions.

The three crack-inducing methods generate cracks with different geometries and apertures, which significantly influence the crack closure performance during self-healing. The indirect tensile test produces major continuous tensile cracks with wide and uniform openings, allowing self-healing analysis in crack widths ranging from 14.3 to 163.0 μm. The observations over the 90-day self-healing indicate that the crack portions near the two ends of the major crack and secondary cracks typically achieve full closure with healed crack widths reaching up to 80.2 μm, as summarized in Table 5-15. The self-healing products generated within cracks, such as CaCO3 from the carbonation of $Ca(OH)_2$ and additional hydrates from continued cement hydration, possess a solid volume that progressively fills and bridges the crack cavity. The presence of crack openings provides the essential space for the precipitation and growth of the self-healing products, which in turn facilitates the crack closure process. In addition, the crack with apertures could act as pathways for the reactants, such as CO_2 and water, to interact more effectively on the crack surfaces, promoting the self-healing process. As the self-healing products accumulate, their volume growth gradually reduces the crack aperture and leads to surface crack closure. However, the quantity of self-healing products is primarily restricted by the amount of remaining unhydrated cement within the matrix (Quan & Fall, 2024; Qureshi & Al-Tabbaa, 2020; Rajczakowska et al., 2019; Wu et al., 2012). The large crack width (e.g., near the middle of major cracks) may experience partial or no healing due to the insufficient healing products to fill the entire crack cavity as shown in Figure 5-46a, even when sufficient space exists for the healing products precipitation. A quantitative representation of the surface crack healing process is provided in Figure 5-47, showing the average reduction in crack area for TS-PC100% disc specimens over the self-healing period. The initial crack images were first imported into ImageJ, followed by binary image processing to segment the crack regions. The total crack area was then computed by selecting the crack region of interest (ROI) and calculating its area based on the calibrated pixel-to-length ratio as shown in Figure 5-46b. This procedure was repeated for all healing stages using the same threshold settings to ensure consistency. A notable reduction of crack area is achieved during the first 28-day healing period, followed by a slower closure rate until the end of 90-day self-healing. The overall approximately 26.6% reduction in crack area after 90 days of self-healing demonstrates the effectiveness of the autogenous self-healing mechanism in surface crack closure. Similarly, the tensile surface cracks in the specimens subjected to uniaxial compression also exhibit the effective crack closure with comparable healed crack width reaching 75.5 μm after 90 days of self-healing (Table 5-15), attributed to the open and accessible geometry of the tensile cracks. Although tensile cracks are dominant in the CS-PC75% and CS-PC90% specimens, shear cracks may develop combinedly to form a mixed-mode (shear-tensile) crack. These shear cracks generally retain partially open due to

localized dilation (Chemenda et al., 2011; Dodd & Bai, 2012; Meng et al., 2024), resulting in the irregular and discontinuous crack geometries compared to the relatively uniform tensile cracks. Given the consistent availability of unhydrated cement, the healing efficiency in crack closure is more effective in shear cracks with narrow widths, attributed to the physical infilling of self-healing products. This phenomenon becomes even more pronounced for the shear cracks generated under the triaxial compression, where the confining pressure during the crack formation produces compacted shear bands with minimal dilation, resulting in the cracks with partial closure of smaller apertures by sliding and relatively smaller crack cavities (Figure 5-44e-g). The initial crack widths in SS-PC pre-cracked specimens were measured to range between approximately 9.6 and 125.9 μm (excluding fracture-falling areas), which is smaller than that generated by other crack-inducing methods. The localized dilation along the inclined shear planes provides the pathways for the self-healing interactions with CO_2 and water, where the self-healing products effectively can precipitate and accommodate to benefit the crack closure performance in cracks with narrower apertures. As demonstrated in Table 5-15, the crack widths up to 73.1 μm are completely healed after 90 days of self-healing. Visual inspection suggests that, in some cases, it is difficult to distinguish true crack closure from the formation of self-healing products along sliding shear cracks, as the opposing crack surfaces are tightly compressed and in direct contact.

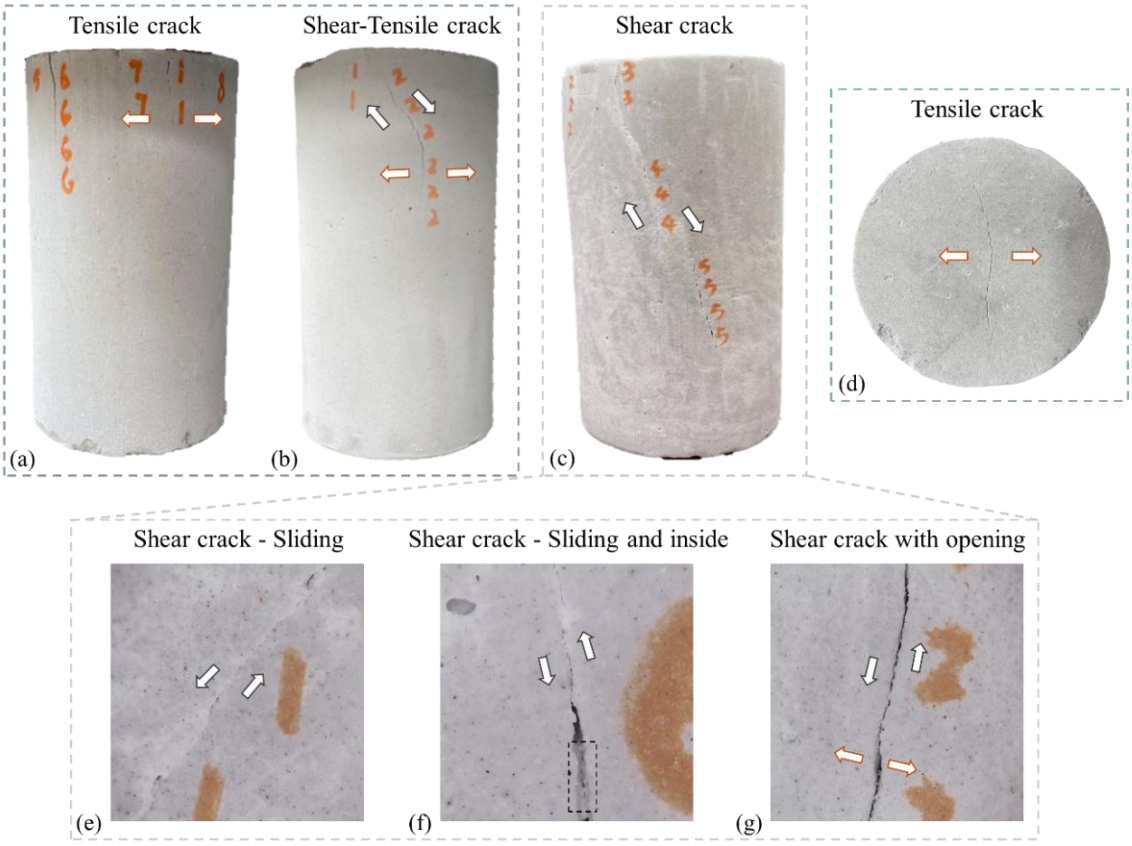

Figure 5-44. Typical crack type and propagation patterns during pre-cracking process subjected to uniaxial compression (a-b), triaxial compression (c, e-g), and indirect tensile (d) tests.

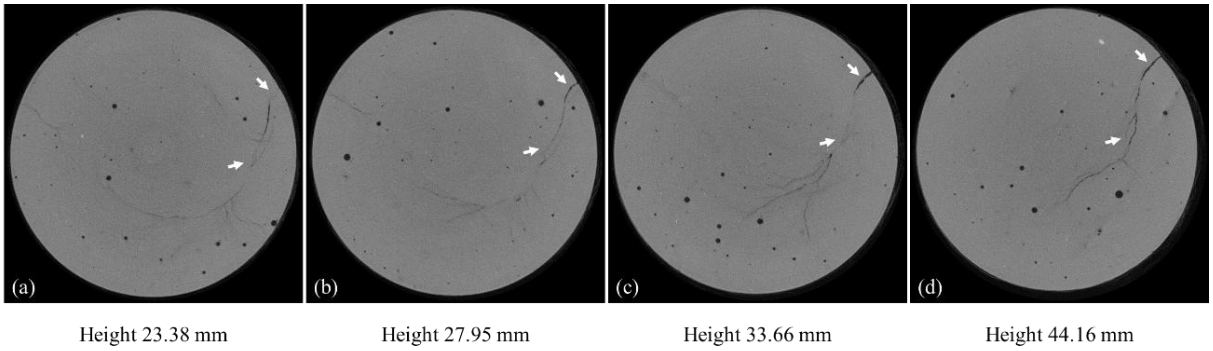

Figure 5-45. XR-μCT scanning of crack patterns at different heights of the SS-PC90% specimen.

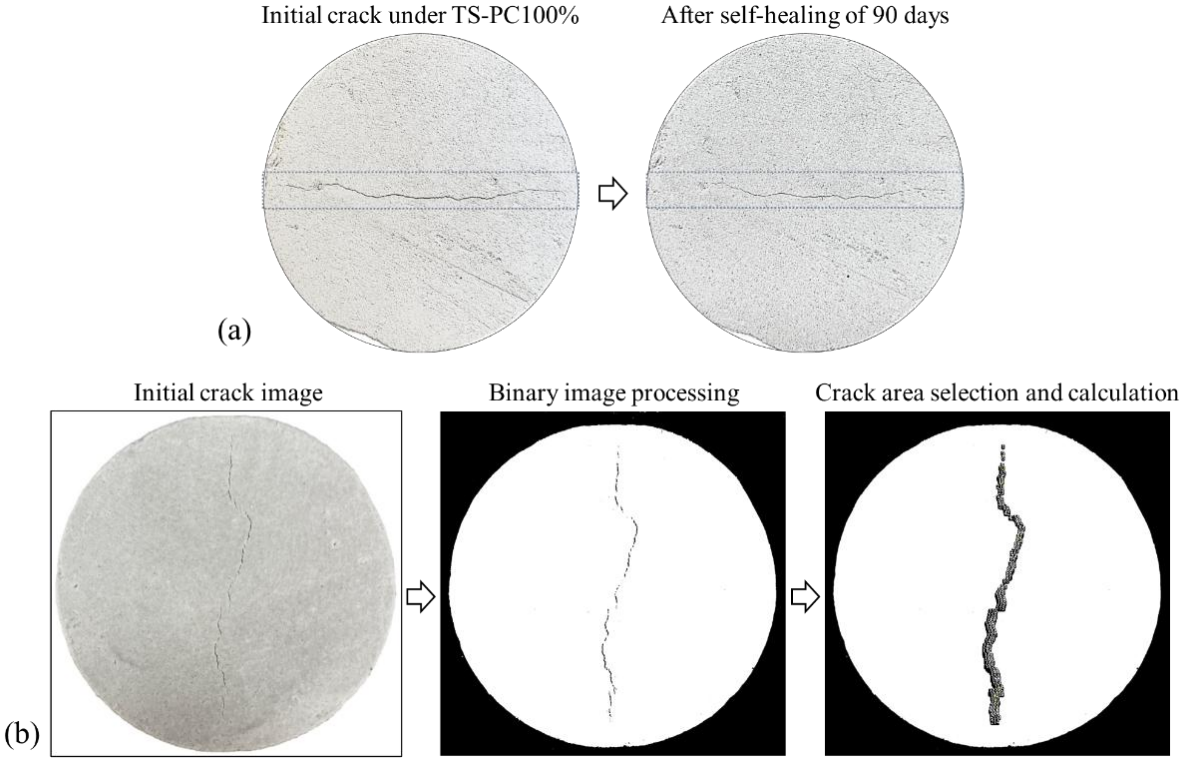

Figure 5-46. (a) Typical observation of crack closure on disc specimen following 90 days of self-healing, and (b) image processing for crack area detection and calculation.

Therefore, the observations across the three crack-inducing methods manifest that the crack type critically governs the autogenous self-healing performance of surface crack closure in the CPB matrix. Tensile cracks feature open, continuous, and relatively smooth crack surfaces that facilitate the transportation of CO_2 and water and provide sufficient space for the deposition of self-healing products. However, the large apertures of these cracks pose a limitation for complete crack closure, since the quantity of self-healing products is inadequate to bridge the entire crack width. In contrast, shear cracks formed under triaxial compression loading are more prone to near-complete closure within the specific capacity during the self-healing period, as shear cracks are characterized by

narrower apertures and irregular, interlocked surfaces, resulting in smaller crack cavities that can be effectively filled by the accumulating self-healing products.

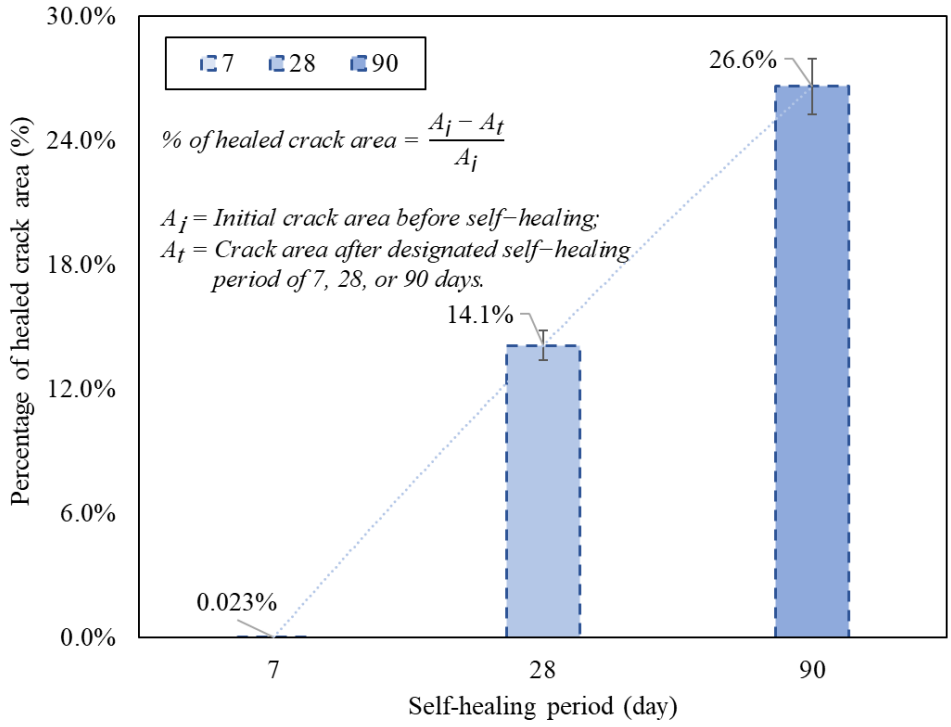

Figure 5-47. Average crack area reduction of disc specimens with cracks induced via indirect tensile test at the pre-cracking level of TS-PC100% over the self-healing period.

5.5.3.3 Mechanical strength recovery

The self-healing efficiency of CPB cylinder and disc specimens subjected to the three crack-inducing methods is evaluated based on their corresponding mechanical strengths: (a) uniaxial compressive strength, (b) deviator stress, and (c) tensile stress, as presented in Figure 5-48. To quantify the recovery efficiency, the CMS index (Eq. 5-11) is employed, which relates the strength of healed specimens to their uncracked control counterparts over the self-healing duration. It is generally observed in Figure 5-48 that the pre-cracked CPB specimens progressively regain their mechanical strength as the self-healing proceeds.

Figure 5-48a demonstrates the efficiency of self-healing process in pre-cracked specimens subjected to uniaxial compression. The results reveal that the CS-PC75% specimens recover nearly the strength of the control (uncracked) specimens, whereas the CS-PC90% specimens exceed the controls, achieving a CCS value of 6.2% at the early stage of self-healing (7 days). Notably, this value continues to increase with time, attaining 17.7% after 90 days of self-healing. This pronounced compressive strength recovery is primarily ascribed to the two dominant autogenous healing mechanisms in the CPB matrix, namely: i) continued hydration of unhydrated cement particles and ii) carbonation of calcium hydroxide (Quan & Fall, 2025a). Evidence from the thermal analysis conducted in this study provides additional support for these mechanisms, presented in

Figure 5-49a. Specifically, three distinct weight loss regions are observed at 100-200°C, 400-500°C, and 600-750°C, corresponding to the decomposition of cement hydration products C-S-H, calcium hydroxide, and calcite, respectively (Fall et al., 2010; Pane & Hansen, 2005). These weight losses become more pronounced with the progression of the self-healing period from 7 to 28 days in the CS-PC0% specimens, inferring that continued cement hydration significantly contributes to the self-healing process in CPB. In addition to the chemical healing processes, the mechanical conditions associated with uniaxial compression also play an important role in strength recovery. As aforementioned, the cracks induced under the uniaxial compression loading typically involve a combination of predominantly axial tensile cracks and inclined shear cracks. During the self-healing phase, microcracks can be gradually filled by the self-healing products generated through continued cement hydration and carbonation reactions. Of particular interest are the shear cracks, many of which remain partially closed or tightly aligned due to residual compressive stress after unloading from the pre-cracking process (Kang et al., 1990; Tchuindjang et al., 2018; Zhou et al., 2018). The relatively smaller crack apertures ($\leq$ 111.7 μm) allow the more effective precipitation and deposition of the self-healing materials within the cracks and voids, bridging the crack gaps and enhancing the particle bonding. Furthermore, as seen in Figure 5-49a, the greater weight losses observed in CS-PC90% specimens compared to uncracked CS-PC0% specimens after 90 days of self-healing indicate more extensive cement hydration and carbonation in the pre-cracked specimens. This enhancement can be attributed to the geometry of the crack network, which provides the pathways of transportation of CO_2 and water within the matrix, both of which are essential for the chemical healing reactions. The ingress of CO_2 facilitates the carbonation reaction of calcium hydroxide to calcite, further contributing to the crack filling (Qian et al., 2010; Yıldırım et al., 2018). In the same way, the introduced cracks increase the surface area due to the generation of new crack surfaces, which enhances the air/fluid transport pathways and allows the evaporation of excess water from the CPB matrix during the self-healing phase. The high water content is usually adopted during the preparation to meet the designed flowability requirements of the backfill mixture; however, this can adversely impact the strength development due to the dilution effect on cement particles and delayed precipitation (Baănt & Raftshol, 1982; Bisschop & van Mier, 2008; Bisschop & Wittel, 2011). The evaporation of water through cracks reduces the water content (e.g., the average water content of CS-PC0%, CS-PC75%, and CS-PC90% is 25.91%, 25.48%, and 24.53%, respectively, after 28 days of self-healing in this study), decreasing the water-to-cement (w/c) ratio in the pre-cracked CPB specimens, which benefits the cement hydration and further results in the relatively larger quantity of self-healing products to expedite the crack filling, thereby enhancing the recovery of compressive strength (Bentz et al., 2009; Fall et al., 2009; Yilmaz et al., 2009).

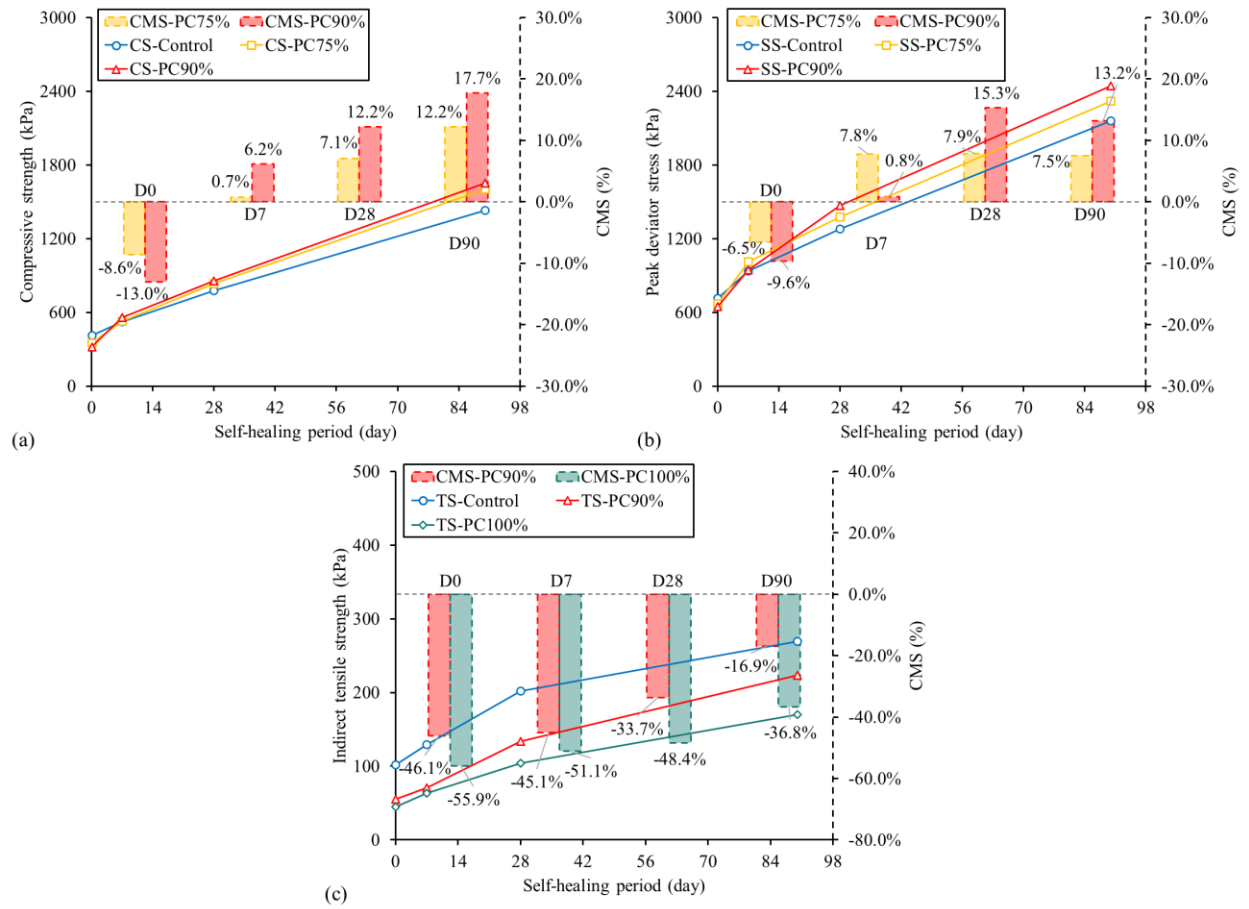

Figure 5-48. Evolution of mechanical strength and CMS for pre-cracked CPB specimens subjected to pre-cracking process of (a) uniaxial compression, (b) triaxial compression, and (c) indirect tensile over the self-healing periods of 0, 7, 28, and 90 days.

Similarly, the specimens subjected to the triaxial compression pre-cracking exhibit comparably promising mechanical strength recovery throughout the entire self-healing period as depicted in Figure 5-48b. Specifically, both SS-PC75% and SS-PC90% specimens recover their strengths compared to the control specimens within the first 7-day healing period. Over the course of 90 days, the SS-PC90% specimens achieve approximately 13.2% to 15.3% higher deviator stress than the controls. This noticeable self-healing efficiency is also driven by the ongoing hydration of residual unhydrated cement particles. Evidence for this mechanism is provided by the results of thermal analysis observed in Figure 5-49b, where the three characteristic weight losses associated with hydration products decomposition are increasingly pronounced from 28 to 90 days for SS-PC90% specimens. Moreover, the confined geometry of the crack network in the SS-PC specimens contributes to the favourable conditions for the precipitation of self-healing products. During triaxial compression pre-cracking, the applied confining pressure suppresses the tensile crack propagation and narrows the crack apertures of the major shear cracks, which often remain partially closed and/or under compression (Ewy & Cook, 1990; Lockner & Madden, 1991), limiting the crack propagation and branching. The 3D reconstruction of XR-µCT scanning of an SS-PC90%

specimen shown in Figure 5-50 further confirms that the internal crack network remains localized, with the dominant shear cracks failing to penetrate the entire cross-section of the specimen. Instead, cracks are concentrated within specific shear bands, while large portions of the surrounding matrix remain intact and structurally continuous, which also provides additional resistance of the specimens through the friction between the crack surfaces (Fall et al., 2007). In addition, the crack network benefits the internal hydration processes in a manner similar to that observed in CS-PC specimens as previously discussed. This is again validated by the thermal analysis in Figure 5-49b, which reveals an enhanced extent of both hydration and carbonation in the SS-PC90% specimens compared with the SS-PC0% specimens following 90 days of self-healing. The combination of narrow crack apertures and partial physical crack closure not only enables self-healing products to efficiently occupy the available cavities but also increases the direct contact between rough crack surfaces, enhancing the nucleation and growth of self-healing products. As a result, the synergy between favourable crack morphology under confined conditions and intrinsic chemical healing reactions enables SS-PC specimens to recover their load-bearing capacity within a relatively short self-healing period. Notably, the underground CPB backfill structures are typically subjected to triaxial loading conditions, where the vertical loads from overlying rock masses are accompanied by lateral confinement imposed by surrounding rock masses (Jafari et al., 2021; Liu et al., 2025; Yang et al., 2020). Therefore, the triaxial compression pre-cracking loading provides a more realistic and reliable evaluation of the self-healing efficiency in mechanical strength recovery of the backfill matrices performed underground.

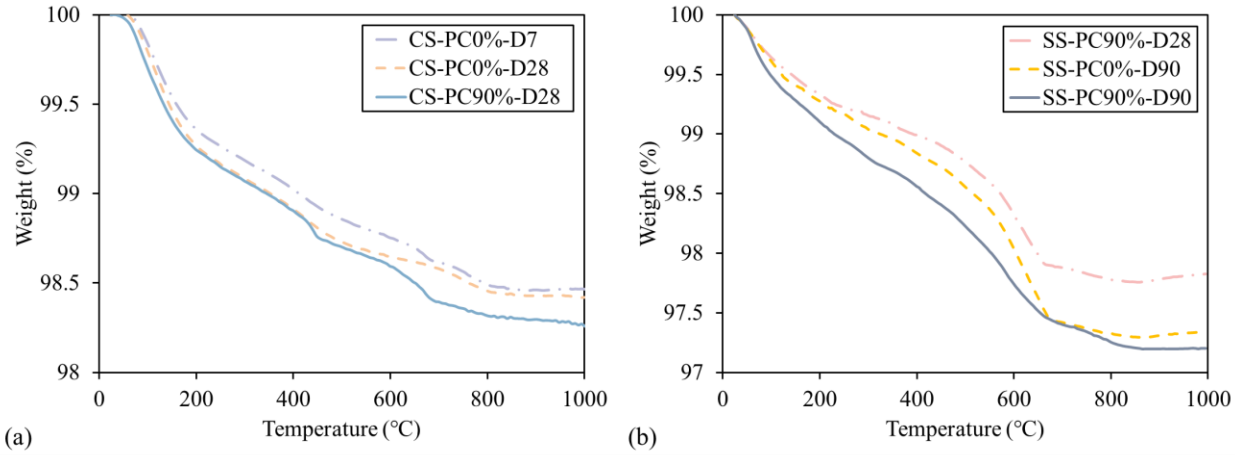

Figure 5-49. TG/DTG analyses of (a) CS-PC specimens subjected to 7 and 28 days of self-healing, and (b) SS-PC specimens following 28 and 90 days of self-healing.

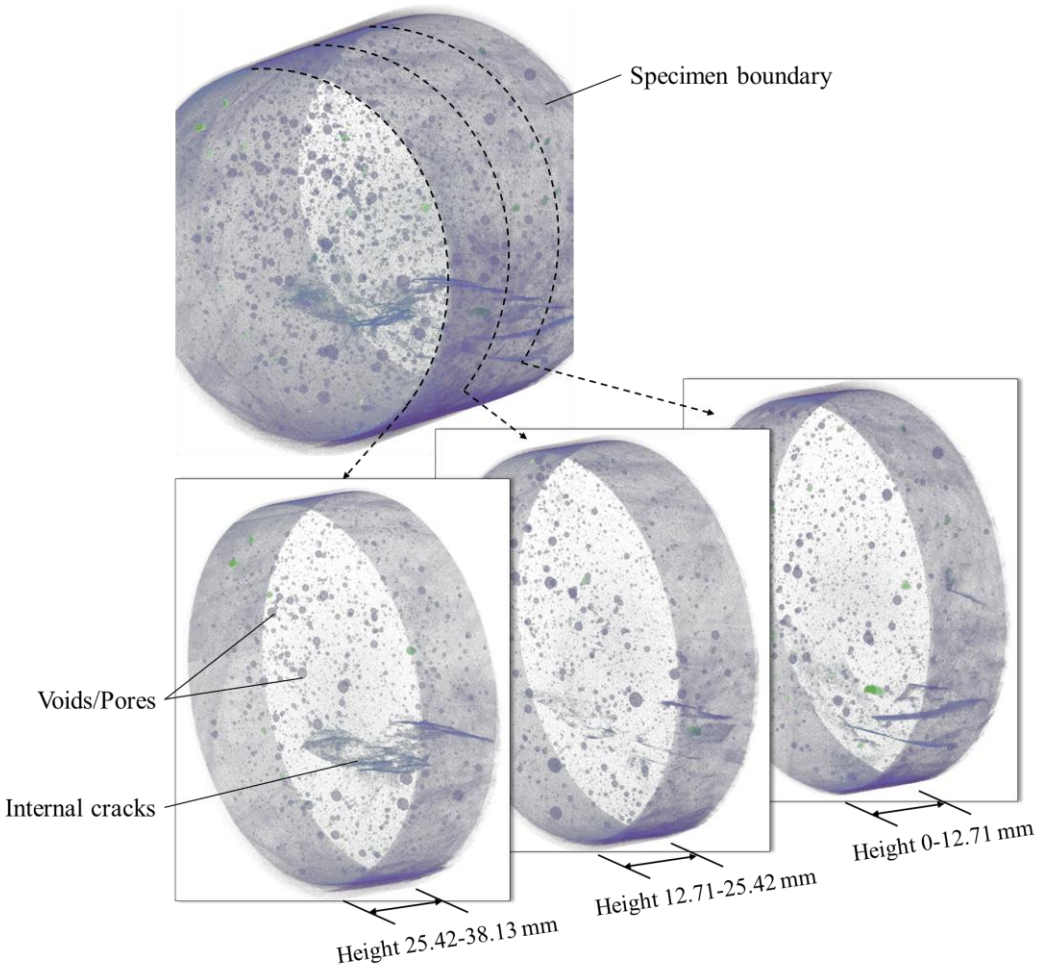

Figure 5-50. 3D reconstruction of the SS-PC90% specimen with overall view and segmented views of the divided three parts showing internal crack geometry.

In contrast, the specimens subjected to the indirect tensile loading display a notably limited self-healing efficiency in tensile strength restoration as presented in Figure 5-48c. Although both TS-PC90% and TS-PC100% specimens demonstrate increasing CMS values with prolonged self-healing after 90 days, the ultimate recovered tensile strengths remain significantly lower than those of the uncracked control specimens with the CMS values of -16.9% and -36.8%, respectively. This inferior healing efficiency is primarily attributed to the crack geometry generated in the disc-shaped specimens under tension. The indirect tensile pre-cracking loading produces dominant mode I tensile cracks that propagate nearly perpendicular to the applied compression load due to the concentrated tensile stress along the horizontal diameter and the intrinsically low tensile strength of CPB materials. As can be seen in Figure 5-51, XR-μCT scanning of the TS-PC100% specimen confirms that the major crack almost penetrates the entire disc, splitting the specimen into two segments. This traverse tensile crack substantially compromises the structural integrity of the disc-shaped specimen, leaving the two cracked surfaces largely unconfined and physically separated after the pre-cracking process. Despite the crack closure was observed at the microcracks and along

the edges of the major cracks, the large width especially close to the central portion of the cracks, which typically represents the widest aperture (up to ~163.0 μm in TS-PC100% specimens) due to stress concentration along the disc diameter, remains largely unclosed and mechanically disconnected after cracking, reflecting the limitation of autogenous self-healing effectiveness of the CPB materials with relatively low cement content compared to the conventional cementitious materials. The insufficient precipitation of self-healing products is unable to effectively bridge the crack gaps, thus inhibiting the physical contact and cohesive bonding between crack surfaces. Furthermore, the self-healing products, such as calcite and calcium hydroxide, are mechanically weaker than C-S-H gels, and even the C-S-H gels formed within the cracks lack the degree of interlocking and structural continuity as that found in the uncracked control specimens (Qian et al., 2010). Therefore, the healed regions exhibit poor stress transfer capability due to the relatively weak interfacial bonding, a limitation further exacerbated by the absence of external confinement during the healing phase in disc-shaped specimens.

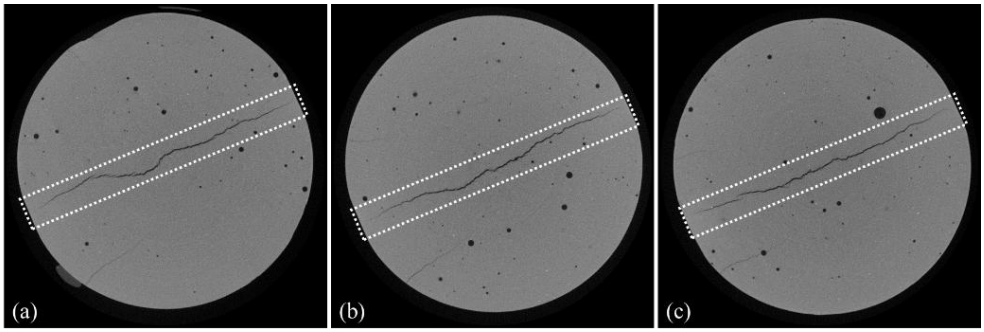

Figure 5-51. Cross-sectional 2D scans of the TS-PC100% specimen at three different heights illustrating the traversing major tensile cracks.

5.5.3.4 Hydraulic conductivity recovery

The development and morphology of cracks dominantly impact the permeability of the CPB matrix, as they reflect the internal connectivity and continuity of the crack network induced by mechanical loading (Fall et al., 2009). Changes in permeability were assessed through saturated hydraulic conductivity (k_{sat}) tests on specimens subjected to the three different crack-inducing methods. This testing approach enables the evaluation of healing efficiency in permeability by using the index HCRR, defined in Eq. 5-12, as illustrated in Figure 5-52.

Figure 5-52a manifests the variations of hydraulic conductivity in the specimens subjected to uniaxial compression loading, and their corresponding healing efficiency across the self-healing period. At the initial self-healing (D0), the pre-cracked specimens show elevated hydraulic conductivity compared to the uncracked control specimens, indicating increased crack-induced permeability after the pre-cracking process. This increase becomes more pronounced as the pre-cracking level progresses from CS-PC75% to CS-PC90%. Under uniaxial compression, axial tensile microcracks typically develop at the CS-PC75% level. As the pre-cracking level elevates to CS-PC90%, these microcracks further expand into macrocracks, and additional shear cracks

emerge around initial structural defects. This progression results in an interconnected network of tensile and shear cracks, which facilitates water flow and consequently leads to elevated hydraulic conductivity. Moreover, the crack-induced permeability is observed to recover with an obvious decreasing tendency in Figure 5-52a, with HCRR values reaching up to 86.6% in CS-PC90% specimens as the self-healing continues to 90 days. This self-healing performance in hydraulic conductivity can be explained by the previously discussed chemical healing processes of continued cement hydration and carbonation reactions. The newly generated self-healing products deposit and fill the crack gaps and voids to block the internal flow paths and refine the microstructure of the specimen matrix, which significantly contributes to the permeability recovery.

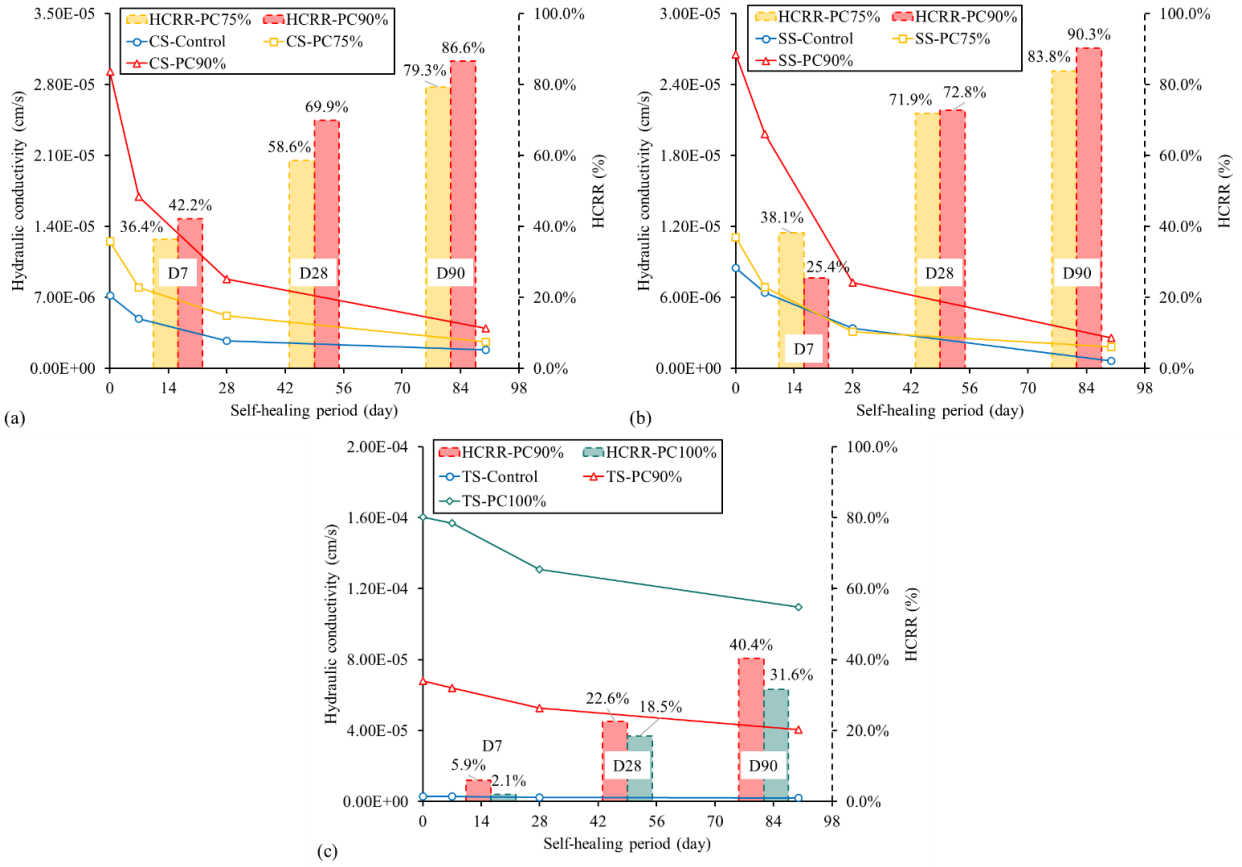

Figure 5-52. Evolution of hydraulic conductivity and HCRR of the pre-cracked CPB specimens subjected to pre-cracking process of (a) uniaxial compression, (b) triaxial compression, and (c) indirect tensile over the self-healing periods of 0, 7, 28, and 90 days.

In the same way, a more effective recovery in permeability can be noticed in the specimens subjected to triaxial compression loading, as demonstrated in Figure 5-52b, with the HCRR value reaching 90.3% in SS-PC90% specimens after a self-healing period of 90 days. This relatively enhanced self-healing performance in permeability recovery is attributed to the combined effects of the favourable crack morphology developed under confined conditions and the chemical self-healing mechanisms. Cracks formed during the triaxial compression loading are typically associated with the shear failure and are characterized predominantly by shear cracks, accompanied

by minor suppressed tensile cracks. At the pre-cracking level of SS-PC75%, the pre-cracked specimens exhibit only a minor increase in the hydraulic conductivity compared to the uncracked controls immediately after the pre-cracking process, as the cracks remain partially closed and/or compressed, lacking the open connectivity necessary for effective water flow. Despite the occurrence of localized dilation leading to the escalation in the hydraulic conductivity with the pre-cracking level reaching SS-PC90%, the pre-cracked specimens subjected to triaxial compression loading still show relatively lower hydraulic conductivity than those subjected to uniaxial compression loading under the same pre-cracking level. This can be attributed to the presence of confinement during the triaxial compression loading, which not only limits the overall number of cracks but also results in major shear cracks with small apertures (Figure 5-50). As a result, the favourable crack geometry leads to smaller crack volumes that need to be healed, thus enabling more effective crack infilling by self-healing products under the same CPB mixing composition. On the other hand, since both pre-cracked CS-PC and SS-PC specimens contain the same cement content, they possess a comparable potential capability for autogenous self-healing through continued chemical hydration processes. However, due to the relatively smaller crack volumes present in SS-PC specimens compared to CS-PC specimens, the chemical healing process can operate more efficiently within SS-PC specimens, ultimately resulting in an enhanced recovery performance in permeability.

However, the pre-cracked specimens subjected to the indirect tensile loading feature comparatively inferior self-healing performance in permeability recovery as seen in Figure 5-52c. As aforementioned, the indirect tensile loading generates dominant tensile cracks that propagate along the vertical plane perpendicular to the applied compression, resulting in the large open apertures (Figure 5-51). This through-crack establishes instantaneous and direct hydraulic connectivity between the two sides of the disc-shaped specimens, resulting in a dramatic surge in hydraulic conductivity after being subjected to the pre-cracking process. While the chemical self-healing processes initiate the deposition of self-healing products along the crack surfaces, the limitation of the autogenous healing capacity is insufficient to form a complete bridge across the large crack apertures and the extensive traverse crack morphology. This observation is supported by the 3D reconstruction from XR-μCT scanning of a TS-PC100% specimen following 90 days of self-healing in Figure 5-54, which illustrates that the central region of the major crack remains largely unhealed due to the initial large crack aperture and relatively inadequate quantity of self-healing products. Hence, the unhealed region can hardly resist the water flow, ultimately resulting in only marginal permeability recovery with HCRR values of 40.4% and 31.6% for TS-PC90% and TS-PC100% specimens after 90 days of self-healing.

5.5.3.5 Detection of self-healing through CT scanning

The production of self-healing products progressively precipitates within the generated microcracks and narrow regions to bridge the crack gaps as the self-healing advances, resulting in the physical crack closure, blockage of the crack network, and mechanical bonding across the fractured interface. The self-healing efficiency in the mechanical and permeability of pre-cracked CPB is dominated not only by the surface cracks but also by the internal crack geometry within the

specimen matrix. Figure 5-53 illustrates the typical crack morphology of a representative disc-shaped TS-PC100% specimen, where Crack A propagates through both sides of the specimen, with an overall crack aperture range of 19.1 to 77.6 μm. Comparison of the pre- (a) and post-healing (b) images demonstrates a complete surface closure of Crack A, which serves as a critical first indicator of autogenous self-healing, implying deposition of healing products or restoration of surface continuity at the exposed crack interface. To further explore the internal crack morphology following self-healing, 3D volumetric reconstructions from XR-μCT scanning are analyzed in Figure 5-54a. Notably, in the representative disc-shaped specimen, the surface regions of Crack A exhibit no discernible signs of cracking after the healing period in the outer zones of the specimen (i.e., height 0-10.73 mm and 21.46-32.19 mm from either surface, Figure 5-54bd), suggesting complete surface bridging and deposition of healing products. Faint grayscale discontinuities are, however, detected in the deep internal crack region of the specimen (i.e., height 10.73-21.46 mm, Figure 5-54c), indicating the presence of residual cracks after healing. The interface between the previously separated crack faces becomes increasingly indistinct and morphologically irregular after the self-healing period, as observed in both 2D observations and 3D volume renderings. This blurred appearance can be indicative of the gradual deposition and accumulation of self-healing products within the crack cavity, which effectively bridges the crack surfaces. The transition from a sharply defined crack boundary to a diffuse interface indicates that discrete discontinuities have been progressively filled, thereby leading to a reduction in crack continuity and reflecting the self-healing performance of the interior of the CPB matrix. This internal healing pattern aligns with observations in other conventional cementitious systems, wherein crack closure typically initiates at outer surfaces, where ionic transport is more favourable, particularly for carbonation reactions, and gradually progresses inward into the internal regions of the crack (Fan & Li, 2014; Huang et al., 2013). Given that autogenous self-healing is governed by the availability of unhydrated cement particles, the self-healing behaviour is more effective and often complete in regions with narrower cracks or microcrack networks. In contrast, wider cracks, especially those formed with large openings or severe dilation, tend to exhibit partial or no closure, where an open void may remain toward the core of the crack, undermining the healing efficiency in the restoration of mechanical and permeability properties.

The combination of 2D visual disappearance of the surface crack, 3D detection of the absence of internal crack features near the outer surfaces, and localized persistence of central cracking provides a comprehensive picture of significant self-healing performance inside the CPB matrix. However, it is important to acknowledge the limitations associated with the current imaging and analysis approach when interpreting the observed self-healing behaviour. Due to the relatively large size of the scanned specimens (approximately a diameter of 50 mm and scanned height of 30-45 mm) and the limited resolution of the XR-μCT scanning (i.e., 25 μm), it was difficult to distinctly differentiate the self-healing products from the surrounding CPB matrix at this microscale. As a result, though the visual closure of cracks, particularly in the surface and near-surface regions, was clearly identifiable, the precise extent and continuity of the healing products within the crack interior remain uncertain. This limitation complicates the full quantification of the volumetric

integration of self-healing products with the overall matrix. In particular, for internal cracks with small apertures or located deep within the specimen, the contrast between partially healed and unhealed zones may fall below the detection threshold, potentially leading to underestimation or overinterpretation of the healing extent. Future research is therefore needed to address these challenges by employing finer-resolution imaging (e.g., < 10μm), such as micro-CT with smaller cored specimens (in several mm) or advanced phase-contrast imaging conducted before and after self-healing. Such approaches could allow more precise segmentation of self-healing products from the matrix to further elucidate the relationship between visual crack closure and mechanical strength or permeability recovery (Gong et al., 2022; Snoeck et al., 2016; Suleiman & Nehdi, 2018; Suleiman et al., 2019; Wang et al., 2014).

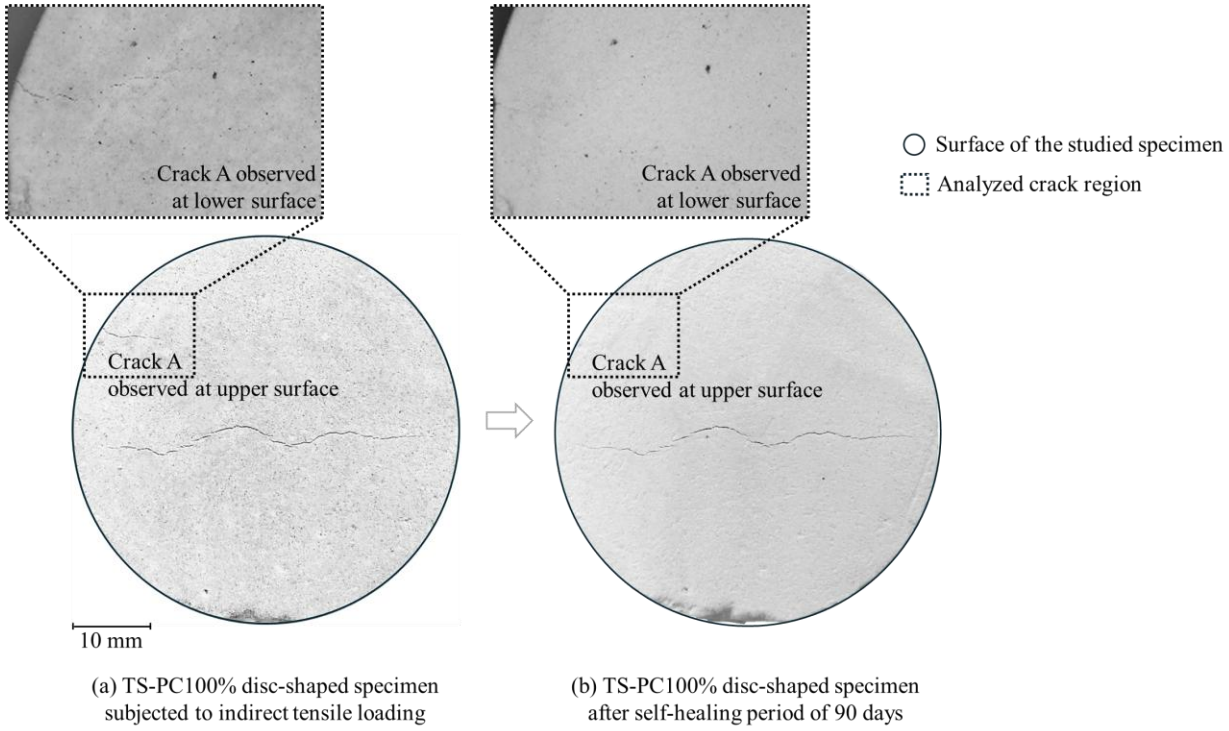

Figure 5-53. Surface crack morphology of the TS-PC100% specimen (a) before self-healing and (b) after a self-healing period of 90 days.

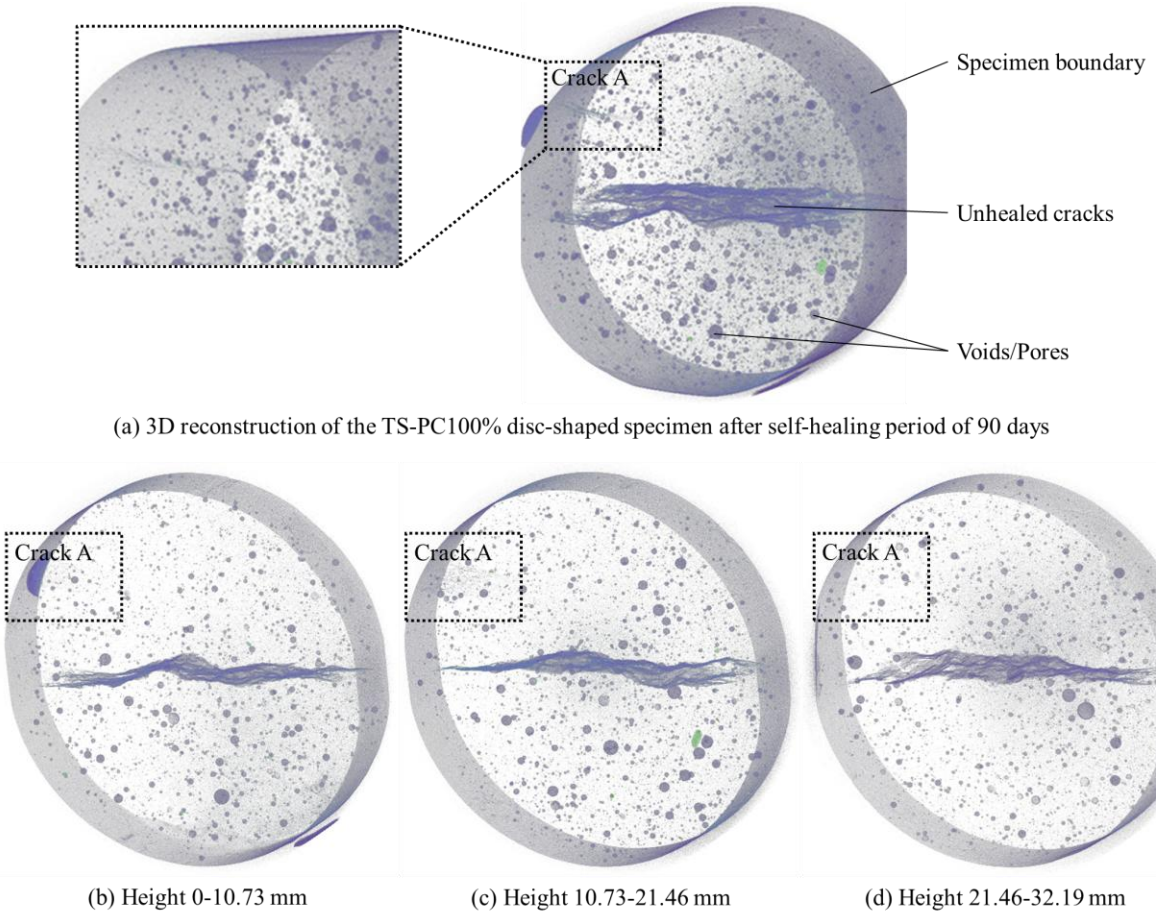

Figure 5-54. 3D reconstruction of the TS-PC100% specimen with (a) overall view of the specimen, and (b-d) segmented views of the three parts illustrating the internal crack geometry after self-healing period of 90 days.

5.5.4 Summary and Conclusions

This study investigates the autogenous self-healing behaviour of CPB subjected to cracks induced by three stress modes commonly encountered in underground mining environments: uniaxial compression, triaxial compression, and indirect tensile loadings. The experimental program combined mechanical strength recovery tests, hydraulic conductivity measurements, crack characterization, and detailed microstructural analyses (i.e., XR-μCT, TG/DTG, XRD, FTIR, and SEM-EDS) to evaluate the efficiency and mechanisms of self-healing over a 90-day self-healing period. The key findings of this study are summarized as follows:

- Regardless of the crack types, the progressive formation and deposition of crystal-like self-healing products gradually fill and bridge the crack gaps, effectively reducing the crack widths and contributing to the rehabilitation of the continuous and compact specimen surfaces over the designated self-healing period up to 90 days. C-S-H, $CaCO_3$, and ettringite constitute the primary self-healing products, formed as a result of continued cement hydration and carbonation of $Ca(OH)_2$.

- Distinct crack geometries develop under different mechanical loading conditions. Disc-shaped specimens subjected to indirect tensile loading exhibit pure tensile cracks, typically featuring the widest apertures near the center that gradually taper toward the edges. Cylindrical specimens under uniaxial compression display a combination of clean, open tensile and narrow shear cracks resulting from localized dilation. In contrast, triaxial compression loading, with the presence of confining pressure, suppresses tensile crack formation, producing a crack pattern dominated by inclined shear cracks with partially closed or narrow openings influenced by localized dilation.
- A crack network provides pathways for the transport of CO_2 and water, facilitating the self-healing process. Given consistent binder content, which governs the autogenous self-healing capability of the CPB matrix, the shear cracks and narrow tensile microcracks are more prone to near-complete closure due to their smaller crack volumes requiring less filling. In contrast, the large cracks limit the complete crack closure because the available self-healing products are insufficient to bridge the entire crack width, resulting in partial and/or no closure.
- Both pre-cracked specimens subjected to uniaxial compression and triaxial compression loading exhibit comparably promising self-healing efficiencies in strength recovery with CMSs exceeding 15%. The presence of a crack network not only promotes the transportation of CO_2 and water but also enables the evaporation of excess water, decreasing the w/c ratio of CPB. This reduction improves cement hydration, thereby benefiting the healing efficiency in mechanical strength. Furthermore, the favourable crack geometry (i.e., partially closed and narrow aperture shear cracks) induced by the triaxial compression allows the self-healing products to fill cavities more efficiently and promote the direct contact between the rough crack surfaces, generating additional resistance from friction and further strengthening the healing efficiency. However, as the traverse tensile crack destroys the structural integrity of the disc-shaped specimen subjected to the indirect tensile loading, inferior healing efficiency in strength is observed due to the remaining largely unclosed and mechanically disconnected crack after healing.
- A similar healing performance to that observed in mechanical strength recovery is evident in the hydraulic conductivity of specimens subjected to uniaxial and triaxial compression loadings. The self-healing products occupy the crack and voids to block the internal connections and enhance the microstructure of the CPB matrix, thereby contributing to the recovery of the permeability. In contrast, as the unhealed regions maintain the direct hydraulic connectivity between the two sides of the disc-shaped specimens with cracks induced by indirect tensile loading, the deficient healing performance is only achieved within the disc-shaped specimens.
- Triaxial compression loading more closely represents the in-situ stress conditions of underground backfill structures, where lateral confinement from surrounding rock masses restricts deformation. This crack-inducing loading condition therefore delivers a more

representative assessment of the self-healing behaviour of CPB under field-relevant stress states, providing a valuable basis for correlating laboratory findings with field performance.

- The results underscore the critical role of crack type in controlling the sustained durability and containment performance of CPB structures in deep mines. Designs and operational practices that minimize tensile crack formation while promoting confined compressive stress states are more likely to ensure efficient self-healing and sustained stability of underground backfill.

In summary, the findings contribute to a new mechanistic understanding of the stress-dependent self-healing behaviour of CPB. By clarifying the links between crack mode, healing efficiency, and microstructural processes, the findings contribute to advancing predictive models and sustainable design strategies for durable mine backfill systems. Despite the novel contributions of this study, several research gaps remain that merit further investigation. Future investigations should explicitly quantify groundwater inflow effects and coupled THMC-cyclic loading on healing across crack modes. Longer-term studies with varied binders/tailings, mechanistic modeling that links crack geometry to precipitation kinetics, and in-situ validation in backfilled stopes are also recommended.

5.5.5 References

ASTM. (2016). ASTM D5084-16a. Standard Test Methods for Measurement of Hydraulic Conductivity of Saturated Porous Materials Using a Flexible Wall Permeameter. In. West Conshohocken, PA: ASTM International.

ASTM. (2020a). ASTM C143/C143M-20. Standard Test Method for Slump of Hydraulic-Cement Concrete. In. West Conshohocken, PA: ASTM International.

ASTM. (2020b). ASTM D4767-11(2020). Standard Test Method for Consolidated Undrained Triaxial Compression Test for Cohesive Soils. In. West Conshohocken, PA: ASTM International.

ASTM. (2021). ASTM C39/C39M-21. Standard Test Method for Compressive Strength of Cylindrical Concrete Specimens. In. West Conshohocken, PA: ASTM International.

ASTM. (2023). ASTM D3967-23. Standard Test Method for Splitting Tensile Strength of Intact Rock Core Specimens with Flat Loading Platens. In. West Conshohocken, PA: ASTM International.

Baănt, Z. P., & Raftshol, W. J. (1982). Effect of cracking in drying and shrinkage specimens. Cem. Concr. Res., 12, 209-226.

Belem, T., Benzaazoua, M., Bussière, B., & Dagenais, A. (2002). Effects of settlement and drainage on strength development within mine paste backfill. In Tailings and Mine Waste 2002 (pp. 139-148): CRC Press.

Bentz, D. P., Peltz, M. A., & Winpigler, J. (2009). Early-age properties of cement-based materials. II: Influence of water-to-cement ratio. Journal of materials in civil engineering, 21, 512-517.

Benzaazoua, M., Fall, M., & Belem, T. (2004). A contribution to understanding the hardening process of cemented pastefill. Miner. Eng., 17, 141-152.

Bisschop, J., & van Mier, J. G. (2008). Effect of aggregates and microcracks on the drying rate of cementitious composites. Cem. Concr. Res., 38, 1190-1196.

Bisschop, J., & Wittel, F. K. (2011). Contraction gradient induced microcracking in hardened cement paste. Cem. Concr. Compos., 33, 466-473.
Brackebusch, F. (1994). Basics of paste backfill systems. Mining Engineering (Littleton, Colorado);(United States), 46.
Chemenda, A., Nguyen, S. H., Petit, J. P., & Ambre, J. (2011). Mode I cracking versus dilatancy banding: Experimental constraints on the mechanisms of extension fracturing. Journal of Geophysical Research: Solid Earth, 116.
Choi, S.-G., Wang, K., Wen, Z., & Chu, J. (2017). Mortar crack repair using microbial induced calcite precipitation method. Cem. Concr. Compos., 83, 209-221.
Cui, L., & Fall, M. (2015). A coupled thermo–hydro-mechanical–chemical model for underground cemented tailings backfill. Tunnelling and Underground Space Technology, 50, 396-414.
Cui, L., & Fall, M. (2016a). An evolutive elasto-plastic model for cemented paste backfill. Computers and Geotechnics, 71, 19-29.
Cui, L., & Fall, M. (2016b). Mechanical and thermal properties of cemented tailings materials at early ages: Influence of initial temperature, curing stress and drainage conditions. Constr. Build. Mater., 125, 553-563.
Dodd, B., & Bai, Y. (2012). Adiabatic shear localization: frontiers and advances: Elsevier.
dos Santos, V. H. J. M., Pontin, D., Ponzi, G. G. D., e Stepanha, A. S. d. G., Martel, R. B., Schütz, M. K., . . . Dalla Vecchia, F. (2021). Application of Fourier Transform infrared spectroscopy (FTIR) coupled with multivariate regression for calcium carbonate (CaCO3) quantification in cement. Constr. Build. Mater., 313, 125413.
Ercikdi, B., Kesimal, A., Cihangir, F., Deveci, H., & Alp, İ. (2009). Cemented paste backfill of sulphide-rich tailings: Importance of binder type and dosage. Cem. Concr. Compos., 31, 268-274.
Ewy, R., & Cook, N. (1990). Deformation and fracture around cylindrical openings in rock—II. Initiation, growth and interaction of fractures. Paper presented at the International journal of rock mechanics and mining sciences & geomechanics abstracts.
Fall, M., Adrien, D., Célestin, J., Pokharel, M., & Touré, M. (2009). Saturated hydraulic conductivity of cemented paste backfill. Miner. Eng., 22, 1307-1317.
Fall, M., Belem, T., Samb, S., & Benzaazoua, M. (2007). Experimental characterization of the stress–strain behaviour of cemented paste backfill in compression. J. Mater. Sci., 42, 3914-3922.
Fall, M., Benzaazoua, M., & Ouellet, S. (2005). Experimental characterization of the influence of tailings fineness and density on the quality of cemented paste backfill. Miner. Eng., 18, 41-44.
Fall, M., Célestin, J., Pokharel, M., & Touré, M. (2010). A contribution to understanding the effects of curing temperature on the mechanical properties of mine cemented tailings backfill. Eng. Geol., 114, 397-413.
Fall, M., & Pokharel, M. (2010). Coupled effects of sulphate and temperature on the strength development of cemented tailings backfills: Portland cement-paste backfill. Cem. Concr. Compos., 32, 819-828.
Fan, S., & Li, M. (2014). X-ray computed microtomography of three-dimensional microcracks and self-healing in engineered cementitious composites. Smart Mater. Struct., 24, 015021.
Fang, K., & Fall, M. (2020). Shear behavior of the interface between rock and cemented backfill: effect of curing stress, drainage condition and backfilling rate. Rock Mechanics and Rock Engineering, 53, 325-336.

Feng, Y., Qi, W., Zhao, Q., Huang, Y., Ren, Q., Qi, W., & Kong, F. (2023). Synthesis and characterization of cemented paste backfill: Reuse of multiple solid wastes. Journal of Cleaner Production, 383, 135376.

Ferrara, L., Krelani, V., & Carsana, M. (2014). A “fracture testing” based approach to assess crack healing of concrete with and without crystalline admixtures. Constr. Build. Mater., 68, 535-551.

Ferrara, L., Van Mullem, T., Alonso, M. C., Antonaci, P., Borg, R. P., Cuenca, E., . . . Roig-Flores, M. (2018). Experimental characterization of the self-healing capacity of cement based materials and its effects on the material performance: A state of the art report by COST Action SARCOS WG2. Constr. Build. Mater., 167, 115-142.

Flannery, B. P., Deckman, H. W., Roberge, W. G., & D'Amico, K. L. (1987). Three-dimensional X-ray microtomography. Science, 237, 1439-1444.

Ghirian, A. (2016). Coupled thermo-hydro-mechanical-chemical (THMC) processes in cemented tailings backfill structures and implications for their engineering design. Université d'Ottawa/University of Ottawa,

Ghirian, A., & Fall, M. (2014). Coupled thermo-hydro-mechanical–chemical behaviour of cemented paste backfill in column experiments: Part II: Mechanical, chemical and microstructural processes and characteristics. Eng. Geol., 170, 11-23.

Ghirian, A., & Fall, M. (2016). Strength evolution and deformation behaviour of cemented paste backfill at early ages: Effect of curing stress, filling strategy and drainage. International Journal of Mining Science and Technology, 26, 809-817.

GlobalMiningReview. (2023). Clean TeQ accelerates expansion into global mine tailings management. Retrieved from https://www.globalminingreview.com/mining/14112023/clean-teq-accelerates-expansion-into-global-mine-tailings-management/

Gong, P., Zhang, C., Wu, Z., Zhang, G., Mei, K., Gao, Q., & Cheng, X. (2022). Study on the effect of CaCO3 whiskers on carbonized self-healing cracks of cement paste: Application in CCUS cementing. Constr. Build. Mater., 321, 126368.

Guo, S., Fall, M., & Haruna, S. (2020). Interface shear behavior of cementing underground mine backfill. International Journal of Geomechanics, 20, 04020230.

Helinski, M., Fahey, M., & Fourie, A. (2011). Behavior of cemented paste backfill in two mine stopes: measurements and modeling. Journal of geotechnical and geoenvironmental engineering, 137, 171-182.

Huang, H., Ye, G., & Damidot, D. (2013). Characterization and quantification of self-healing behaviors of microcracks due to further hydration in cement paste. Cem. Concr. Res., 52, 71-81.

Jafari, M., & Grabinsky, M. (2021). Effect of hydration on failure surface evolution of low sulfide content cemented paste backfill. International Journal of Rock Mechanics and Mining Sciences, 144, 104749.

Jafari, M., Shahsavari, M., & Grabinsky, M. (2021). Drained triaxial compressive shear response of cemented paste backfill (CPB). Rock Mechanics and Rock Engineering, 54, 3309-3325.

Jouanna, P. (1993). A summary of field test methods in fractured rocks. Flow and Contaminant Transport in Fractured Rock, 437-544.

Kadin, Y., & Rychahivskyy, A. (2012). Modeling of surface cracks in rolling contact. Materials Science and Engineering: A, 541, 143-151.

Kang, K. J., Song, J. H., & Earmme, Y. Y. (1990). Fatigue crack growth and closure behaviour through a compressive residual stress field. Fatigue & Fracture of Engineering Materials & Structures, 13, 1-13.
le Roux, K., Bawden, W. F., & Grabinsky, M. F. (2005). Field properties of cemented paste backfill at the Golden Giant mine. Mining Technology, 114, 65-80.
Li, V. C., Lim, Y. M., & Chan, Y.-W. (1998). Feasibility study of a passive smart self-healing cementitious composite. Composites Part B: Engineering, 29, 819-827.
Liu, H., & Fall, M. (2024). Testing the properties of cemented tailings backfill under multiaxial compressive loading. Constr. Build. Mater., 421, 135682.
Liu, H., & Fall, M. (2025). Experimental investigation of the microstructural and mechanical response of cemented tailings backfill to rockwall closure.
Liu, H., Zhang, Q., Gu, C., Su, H., & Li, V. (2017). Self-healing of microcracks in Engineered Cementitious Composites under sulfate and chloride environment. Constr. Build. Mater., 153, 948-956.
Liu, S., Fall, M., & Haruna, S. (2025). Understanding the Triaxial Behavior of Cemented Tailings Backfill Reinforced with Fibers. International Journal of Geomechanics, 25, 04025078.
Lockner, D. A., & Madden, T. R. (1991). A multiple-crack model of brittle fracture: 1. Non-time-dependent simulations. Journal of Geophysical Research: Solid Earth, 96, 19623-19642.
Meng, F., Yue, Z., Li, M., Han, J., Cai, Q., Wang, W., . . . Zhang, C. (2024). Frictional sliding behaviour of rough fracture in granite under true triaxial loading with implications for fault reactivation. Rock Mechanics and Rock Engineering, 57, 197-217.
Ouyang, Z.-h., Li, C.-h., Xu, W.-c., & Li, H.-j. (2009). Measurements of in situ stress and mining-induced stress in Beiminghe Iron Mine of China. Journal of Central South University of Technology, 16, 85-90.
Özbay, E., Sahmaran, M., Yücel, H. E., Erdem, T. K., Lachemi, M., & Li, V. C. (2013). Effect of sustained flexural loading on self-healing of engineered cementitious composites. J. Adv. Concr. Technol., 11, 167-179.
Pan, A., Jafari, M., Guo, L., & Grabinsky, M. (2021). Hybrid failure of cemented paste backfill. Minerals, 11, 1141.
Pane, I., & Hansen, W. (2005). Investigation of blended cement hydration by isothermal calorimetry and thermal analysis. Cem. Concr. Res., 35, 1155-1164.
Qi, C., & Fourie, A. (2019). Cemented paste backfill for mineral tailings management: Review and future perspectives. Miner. Eng., 144, 106025.
Qian, S., Zhou, J., & Schlangen, E. (2010). Influence of curing condition and precracking time on the self-healing behavior of Engineered Cementitious Composites. Cem. Concr. Compos., 32, 686-693.
Quan, W., & Fall, M. (2024). Temperature-driven crack self-healing and performance recovery in cemented tailings materials. Case Stud. Constr. Mater., 21, e04105.
Quan, W., & Fall, M. (2025a). Investigation of crack self-healing behaviour and its impact on strength and permeability recovery in cemented paste tailings. Powder Technology, 457, 120834.
Quan, W., & Fall, M. (2025b). Self-healing responses of cementitious tailings materials to changing drainage conditions. Developments in the Built Environment, 22, 100648.
Qureshi, T., & Al-Tabbaa, A. (2020). Self-Healing Concrete and Cementitious Materials. Advanced functional materials, 191.

Qureshi, T., Kanellopoulos, A., & Al-Tabbaa, A. (2016). Encapsulation of expansive powder minerals within a concentric glass capsule system for self-healing concrete. Constr. Build. Mater., 121, 629-643.
Raffaldi, M. J., Seymour, J. B., Richardson, J., Zahl, E., & Board, M. (2019). Cemented paste backfill geomechanics at a narrow-vein underhand cut-and-fill mine. Rock mechanics and rock engineering, 52, 4925-4940.
Rajczakowska, M., Habermehl-Cwirzen, K., Hedlund, H., & Cwirzen, A. (2019). Autogenous self-healing: a better solution for concrete. Journal of Materials in Civil Engineering, 31, 03119001.
Sahmaran, M., Yildirim, G., Noori, R., ÖZBAY, E., & Lachemi, M. (2015). Repeatability and pervasiveness of self-healing in engineered cementitious composites. ACI Mater. J., 112.
Sari, M., Yilmaz, E., & Kasap, T. (2023). Long-term ageing characteristics of cemented paste backfill: Usability of sand as a partial substitute of hazardous tailings. Journal of Cleaner Production, 401, 136723.
Seymour, J., Raffaldi, M., Abraham, H., Johnson, J., & Zahl, E. (2017). Monitoring the in situ performance of cemented paste backfill at the Lucky Friday Mine. Paper presented at the Proceedings of Minefill.
Shahsavari, M., Jafari, M., & Grabinsky, M. (2022). Influence of load path and effective stress on one-dimensional deformation of cemented paste backfill (CPB) during deposition and curing. Geotech. Geol. Eng., 1-20.
Sisomphon, K., Copuroglu, O., & Koenders, E. (2013). Effect of exposure conditions on self healing behavior of strain hardening cementitious composites incorporating various cementitious materials. Constr. Build. Mater., 42, 217-224.
Sivakugan, N., Rankine, R., Rankine, K., & Rankine, K. (2006). Geotechnical considerations in mine backfilling in Australia. Journal of Cleaner Production, 14, 1168-1175.
Snoeck, D., & De Belie, N. (2015). From straw in bricks to modern use of microfibers in cementitious composites for improved autogenous healing–A review. Constr. Build. Mater., 95, 774-787.
Snoeck, D., Dewanckele, J., Cnudde, V., & De Belie, N. (2016). X-ray computed microtomography to study autogenous healing of cementitious materials promoted by superabsorbent polymers. Cem. Concr. Compos., 65, 83-93.
Suleiman, A., & Nehdi, M. (2018). Effect of environmental exposure on autogenous self-healing of cracked cement-based materials. Cem. Concr. Res., 111, 197-208.
Suleiman, A. R., Nelson, A. J., & Nehdi, M. L. (2019). Visualization and quantification of crack self-healing in cement-based materials incorporating different minerals. Cem. Concr. Compos., 103, 49-58.
Sun, X., Liu, J., Qiu, J., Wu, P., & Zhao, Y. (2022). Alkali activation of blast furnace slag using a carbonate-calcium carbide residue alkaline mixture to prepare cemented paste backfill. Constr. Build. Mater., 320, 126234.
Tchuindjang, D., Fricke, W., & Vormwald, M. (2018). Numerical analysis of residual stresses and crack closure during cyclic loading of a longitudinal gusset. Engineering fracture mechanics, 198, 65-78.
Thompson, B. D., Bawden, W. F., & Grabinsky, M. (2012). In situ measurements of cemented paste backfill at the Cayeli Mine. Canadian Geotechnical Journal, 49, 755-772.
Wang, C.-l., Ren, Z.-z., Huo, Z.-k., Zheng, Y.-c., Tian, X.-p., Zhang, K.-f., & Zhao, G.-f. (2021). Properties and hydration characteristics of mine cemented paste backfill material

containing secondary smelting water-granulated nickel slag. Alexandria Engineering Journal, 60, 4961-4971.
Wang, J., Dewanckele, J., Cnudde, V., Van Vlierberghe, S., Verstraete, W., & De Belie, N. (2014). X-ray computed tomography proof of bacterial-based self-healing in concrete. Cem. Concr. Compos., 53, 289-304.
Wang, Y., Na, Q., & Zhang, L. (2022). Monitoring of in-situ properties for cemented tailings backfill that under drainage condition. Constr. Build. Mater., 356, 129254.
Wu, D., Fall, M., & Cai, S. (2013). Coupling temperature, cement hydration and rheological behaviour of fresh cemented paste backfill. Miner. Eng., 42, 76-87.
Wu, M., Johannesson, B., & Geiker, M. (2012). A review: Self-healing in cementitious materials and engineered cementitious composite as a self-healing material. Constr. Build. Mater., 28, 571-583.
Xu, X., Fall, M., Alainachi, I., & Fang, K. (2019). Characterisation of fibre-reinforced backfill/rock interface through direct shear tests. Geotechnical Research, 7, 11-25.
Yang, C., Yang, P., Lv, W.-s., & Wang, Z.-k. (2020). Mechanical performance of confined consolidation on the strength development of cemented paste backfill. Geotech. Geol. Eng., 38, 1097-1110.
Yang, L., Xu, W., Yilmaz, E., Wang, Q., & Qiu, J. (2020). A combined experimental and numerical study on the triaxial and dynamic compression behavior of cemented tailings backfill. Engineering Structures, 219, 110957.
Yıldırım, G., Khiavi, A. H., Yeşilmen, S., & Şahmaran, M. (2018). Self-healing performance of aged cementitious composites. Cem. Concr. Compos., 87, 172-186.
Yilmaz, E., Belem, T., & Benzaazoua, M. (2014). Effects of curing and stress conditions on hydromechanical, geotechnical and geochemical properties of cemented paste backfill. Eng. Geol., 168, 23-37.
Yilmaz, E., Benzaazoua, M., Belem, T., & Bussière, B. (2009). Effect of curing under pressure on compressive strength development of cemented paste backfill. Miner. Eng., 22, 772-785.
Yilmaz, E., & Fall, M. (2017). Introduction to paste tailings management: Springer.
Zhou, Q., & Beaudoin, J. J. (2003). Effect of applied hydrostatic stress on the hydration of Portland cement and C3S. Advances in cement research, 15, 9-16.
Zhou, X.-P., Zhang, J.-Z., & Wong, L. N. Y. (2018). Experimental study on the growth, coalescence and wrapping behaviors of 3D cross-embedded flaws under uniaxial compression. Rock mechanics and rock engineering, 51, 1379-1400.

Chapter 6 Paper VI: Effect of Blast Furnace Slag and Fly Ash on Autogenous Self-healing in Tailings-Based Cementitious Composites

Submitted for publication

Weizhou Quan, Mamadou Fall

Department of Civil Engineering, University of Ottawa, Ottawa, Ontario, Canada

Abstract

The incorporation of supplementary cementitious materials (SCMs), such as blast furnace slag (BFS) and fly ash (FA), provides a promising strategy to optimize cemented paste backfill (CPB) by reducing operational costs, enhancing durability, and reducing the carbon footprint. This study systematically investigates the effects of partially replacing cement with BFS or FA on the autogenous self-healing behaviour of the CPB system. Four binder blend ratios (i.e., cement/SCM ratio of 100/0, 80/20, 50/50, and 20/80) were evaluated based on crack closure observations, uniaxial compressive strength, hydraulic conductivity, and porosity-related parameters. Results show that the appropriate BFS contents promote self-healing efficiency at early and long-term healing stages compared with cement-only CPB, attributed to the secondary latent hydraulic reactions between BFS and calcium hydroxide, leading to the formation of C-(A)-S-H gels and microstructural densification. The pre-cracked PCI/BFS:50/50 specimens exhibited the highest healing efficiency at 28 days of self-healing, with strength exceeding the uncracked control by 17.2% and hydraulic conductivity recovery reaching 81.8%, whereas at 90 days, superior long-term performance was observed for the PCI/BFS 80/20 mixture, achieving a 21.4% strength increase relative to the uncracked control and 96.2% recovery in hydraulic conductivity. In contrast, FA incorporation resulted in progressively reduced self-healing efficiency with increasing FA content due to its intrinsic physical characteristics and delayed pozzolanic reactivity. While the PCI/FA 80/20 mixture recovered strength comparable to the uncracked control, higher FA contents (50/50 and 20/80) exhibited significantly inferior strength recovery (13.3% and 23.2% lower than controls, respectively) and limited hydraulic conductivity recovery. Across both SCM systems, the formation and sufficiency of self-healing products, such as C-(A)-S-H, calcite, and ettringite, primarily govern the overall self-healing performance. These findings provide critical insights for designing CPB with improved autogenous self-healing capacity and optimized binder formulations for field applications.

Keywords: Cemented paste backfill; Blast furnace slag; Fly ash; Autogenous self-healing; Microstructure; Hydraulic conductivity; Mechanical strength

6.1 Introduction

Mining, as a fundamental engineering discipline, has played a crucial role in the advancement of civilization, modernization, and economic development of many nations across the world. As surface and near-surface mineral resources become increasingly depleted, the increasing consumption and demand for minerals are driving the industry toward deeper mining operations,

with depths exceeding 4 kilometers, as exemplified by the Mponeng Gold Mine in South Africa, currently recognized as the deepest mine globally (Dong et al., 2019; Manzi et al., 2015; Ranjith et al., 2017). Consequently, vast quantities of mining waste have been generated during the mining activities and mineral processing, primarily in the form of processed tailings. An estimated 13 billion tonnes of tailings are produced annually, and this figure continues to increase, making tailings the largest waste stream globally (Franks et al., 2021; UNEP, 2020; Valenta et al., 2023).

Surface tailings disposal, such as in tailings dams or ponds, presents significant geotechnical hazards and environmental risks to nearby communities and ecosystems, such as mine tailings dust, tailings dam failures, acid mine drainage (AMD), cave-ins, ground subsidence, and underground void collapses (Azam & Li, 2010; Ighalo et al., 2022; Kratzsch, 2012; Rico et al., 2008). Rising public awareness, along with the enforcement of stricter regulations, is compelling the mining industry to implement more efficient and sustainable techniques for the management of waste tailings. As a result, the industry has developed underground tailings disposal methods, including cemented hydraulic, rock, and paste backfills, which not only stabilize underground mined-out voids (stopes) but also provide an efficient solution for tailings disposal (Grice, 1998; Sveinson, 1999). Among these, cemented paste backfill (CPB) has gained prominence as an advanced engineered solution and is extensively used in modern mining operations, particularly in Canada and Australia (Fall & Benzaazoua, 2005; Kesimal et al., 2005). Its widespread adoption is driven by several advantages, including enhanced support for surrounding rock masses and underground structures, improved safety in underground working environments, reduced reliance on surface tailings storage, and increased overall mine productivity (Grice, 1998).

CPB is a cementitious material formulated from typically 70-85 wt.% of dewatered tailings, 3-7 wt.% of hydraulic binder, and either processed mine water or fresh water (Fall & Benzaazoua, 2005; Qi & Fourie, 2019). Once placed underground, CPB must meet certain load-bearing requirements to ensure a safe working environment while also exhibiting low permeability to act as a barrier against oxygen diffusion and underground water seepage to mitigate the formation of AMD, contributing to the long-term stability and durability of the backfill structure. The mechanical and permeability properties of CPB are predominantly governed by the hydraulic binder, with Portland cement (PC) commonly employed as the primary binder in CPB formulations (Fall et al., 2009). These properties development is largely associated with the generation of hydration products, including calcium silicate hydrates (C-S-H), ettringite, and calcium hydroxide (CH), which act as the binding agents between particles. In general, higher cement content leads to increased strength and reduced permeability. However, backfilling operations account for approximately 20% of total mine operating costs, with PC consumption representing up to 75% of backfilling expenses (Hassani et al., 2007; Grice, 1998). Furthermore, PC is vulnerable to sulfate attack when sulfide-rich tailings are used, which can hinder strength development in CPB structures (Ercikdi et al., 2009; Fall & Pokharel, 2010). Moreover, the production of PC accounts for approximately 5-8% of global anthropogenic CO2 emissions (Damtoft et al., 2008). To address these challenges, there is a growing trend toward the partial replacement of PC with more cost-effective and environmentally sustainable SCMs, such as BFS and FA. This substitution not only reduces

backfilling costs but also mitigates the environmental impact of PC production, particularly by lowering carbon dioxide (CO2) emissions (Ogunmakinde et al., 2022).

BFS and FA are by-products of industrial processes and are classified as solid waste materials. FA, typically characterized by its spherical shape and smooth texture, is lighter and finer compared to BFS, which exhibits a sub-rounded to angular morphology with distinct asperities and edges (Behera et al., 2020a; Behera et al., 2021; Sinsiri et al., 2010). Both materials are commonly used as SCMs in paste backfill and primarily consist of SiO_2, Fe_2O_3, Al_2O_3, TiO_2, K_2O, CaO, SO_3, P_2O_5, MgO, and Na_2O (Behera et al., 2021; Kar, 2021). The lime saturation factor (LSF), quantified by the ratio of lime to the combined contents of silica, alumina, and iron oxide, determines their suitability as partial replacements for PC in mine backfill applications (Behera et al., 2020b). Owing to their distinct chemical, physical, and pozzolanic properties, numerous studies (Arachchilage et al., 2023; Behera et al., 2020b; Behera et al., 2020a; Jiang et al., 2020a; Jiang et al., 2020b; Kesimal et al., 2005; Li & Fall, 2018; Xiao et al., 2021; Yilmaz et al., 2011b; Yilmaz et al., 2011a) have explored the incorporation of BFS and FA as partial PC replacements to enhance the engineering performance of CPB, including strength development, microstructural refinement, and resistance to sulfate attack. Jiang et al. (2020a) reported that replacing cement with alkali-activated slag significantly improved strength after 28-day curing, achieving uniaxial compressive strength (UCS) values of 3 MPa with an 8% binder content. Similarly, Yilmaz et al. (2011a) observed that increasing binder content (i.e., cement-to-slag ratio of 20:80 wt.%) led to porosity refinement and a reduction in average pore diameter due to the formation of additional hydration products. The partial replacement of PC with FA has also been demonstrated to enhance strength by improving the interfacial bonding between tailings particles and binder hydration products (Zhao et al., 2020; Zhou et al., 2021). Qi et al. (2015) investigated the early-age compressive strength and microstructural characteristics of CPB containing FA and found that higher FA content reduced porosity and improved strength due to its high pozzolanic activity and reduced presence of large pores. Additionally, the high pozzolanic content of FA enhances resistance to sulfate attack, thereby contributing to the long-term stability of CPB, particularly when sulfide-rich tailings are used (Kesimal et al., 2005). However, variations in coal sources, power plant combustion efficiency, and metal extraction processes lead to inconsistencies in the physical and chemical properties of BFS and FA, which may adversely affect the performance of CPB (Behera et al., 2021). Jiang et al. (2020b) noted that an increased substitution of PC with slag led to a substantial reduction in UCS at all curing ages owing to the relatively low pozzolanic reactivity of slag. Similarly, Yilmaz et al. (2011b) reported that CPB containing FA exhibited lower UCS values at early curing ages (up to 28 days). Klein & Simon (2006) further indicated that a 70:30 PC:FA binder blend contributed minimally to strength development during the first year of curing. These findings highlight the need for careful selection and optimization of SCMs to attain the desired performance in CPB applications.

In the field, various internal and external factors, such as initial structural defects, shrinkage, sulfate attack, overburden pressure, stresses from surrounding rock closure or ground movement, and uneven load distribution, can induce cracks in CPB structures during curing. The propagation of

these cracks compromises both the structural integrity and environmental performance of CPB. Autogenous self-healing has been introduced and explored in the CPB materials as a promising solution to mitigate these challenges, enabling the restoration of mechanical strength and permeability of cracked CPB samples, primarily resulting from two mechanisms: (i) continued hydration of cement particles and (ii) carbonation of CH (Quan & Fall, 2024, 2025a). However, the healing mechanism and efficiency of CPB when incorporating BFS or FA as a mineral additive remain unclear, as reaction conditions within cracks differ from those in the bulk CPB matrix. In conventional cementitious materials, FA enhances long-term strength through pozzolanic reactions, while its secondary hydration promotes self-healing, particularly in shrinkage-induced cracks (Termkhajornkit et al., 2009; Thomas, 2007). Similarly, BFS improves resistance to chloride and sulfate attacks, with unreacted particles providing significant self-healing potential over time. Studies have also shown that slag-rich cement pastes and alkali-activated slag-based composites exhibit superior crack-sealing properties, improving durability and reducing permeability (Darquennes et al., 2016; Huang et al., 2014; Nguyễn et al., 2018). However, the properties of CPB differ significantly from conventional cementitious materials due to its much lower cement content, higher water-to-binder (w/b) ratio, and finer particle gradation, limiting the direct applicability of existing findings. Hence, this work experimentally evaluates how BFS and FA influence the autogenous self-healing capacity and response of CPB, clarifying its underlying healing mechanisms.

6.2 Materials and Methods

6.2.1 Materials

6.2.1.1 Tailings

The mineralogical composition and physical properties of tailings vary depending on different ore types and metallurgical processes. To minimize uncertainties associated with the variable composition and reactivity of natural tailings, synthetic silica tailings (ST) supplied by U.S. Silica in Katy, Texas, were utilized in the formulation of CPB mixtures for this study. ST consists of 99.8% quartz (SiO_2), the dominant mineral in many Canadian hard rock mine tailings, along with minor amounts of Al_2O_3 (0.05%) and Fe_2O_3 (0.035%). Due to its chemically inert nature, ST ensures consistency in experimental results. Containing roughly 43 wt.% of particles smaller than 20 μm, ST is categorized as medium tailings and its particle size distribution (PSD) is comparable to that of the average natural tailings (NT) obtained from nine mines in eastern Canada, as shown in Figure 6-1. Table 6-1 presents the physical properties of ST alongside the average values of the nine Canadian mine tailings.

6.2.1.2 Hydraulic binders and mixing water

The binders used in this study for CPB preparation included Portland cement Type I (PCI), granulated blast furnace slag (BFS), and Type C fly ash (FA). PCI, the most commonly used binder in the mining industry, served as the primary binder. The BFS (S80 grade) was supplied by Lafarge Canada Inc. and primarily comprised 41.14% CaO, 34.43% SiO_2, 10.98% MgO, and 9.54% Al_2O_3. Given that, the quality coefficient [$Kq=(CaO+ Al_2O_3+MgO)/(SiO_2)$] is determined to be 1.7, which

can be considered as good hydraulic activity (Burciaga-Díaz & Betancourt-Castillo, 2018; Jiang et al., 2020a). The FA was a commercial product from ENX Inc., with a main composition of 38.06% SiO_2, 21.47% CaO, 19.45% Al_2O_3, 5.58% MgO, and 5.33% Fe_2O_3 (as shown in Table 6-2). Figure 6-1 illustrates the PSDs of these three binders, while Table 6-2 summarizes their chemical and physical properties. The chemical composition analysis was conducted using X-ray fluorescence (XRF), and the specific surface areas of the materials were determined by gas physisorption using the Brunauer-Emmett-Teller (BET) method. Tap water was employed to prepare fresh CPB mixtures.

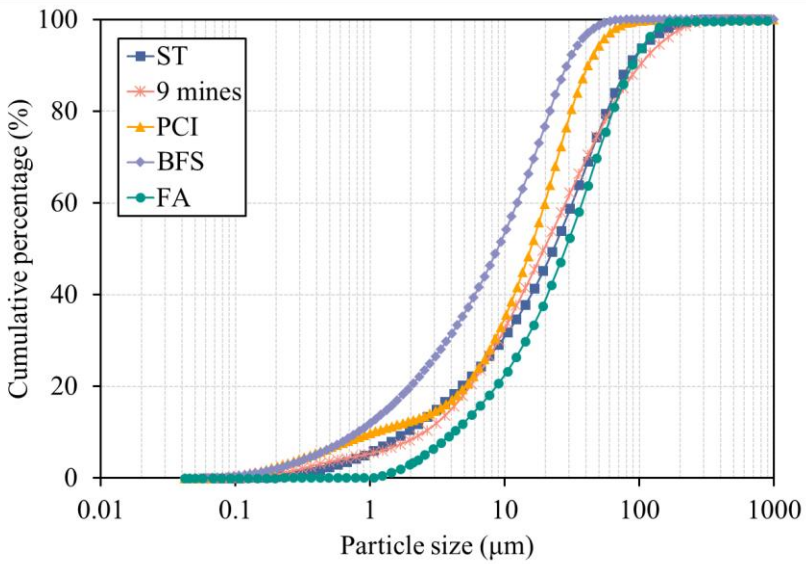

Figure 6-1. Particle size distribution curves of raw materials: silica tailings (ST), Portland cement type I (PCI), granulated blast furnace slag (BFS), and fly ash (FA).

Table 6-1. Physical characteristics of the STs and the average of nine NTs in eastern Canada.

Element	G_s	D_{10}	D_{30}	D_{50}	D_{60}	C_u	C_c
		(μm)					
ST	2.7	1.9	9.0	22.5	31.5	16.6	1.3
Nine NT average	-	1.8	9.1	20.0	30.8	17.1	1.7

G_s: specific gravity; C_u: coefficient of uniformity; C_c: coefficient of curvature.

Table 6-2. Characteristics of the used binders.

Binder type	MgO	CaO	SiO_2	Al_2O_3	Fe_2O_3	SO_3	SSA
	(%)						(m^2/g)
PCI	2.65	68.82	18.03	4.53	2.70	3.82	1.26
BFS	10.98	41.14	34.32	9.54	-	3.87	5.80
FA	5.58	21.47	38.06	19.45	5.33	2.70	2.20

SSA: specific surface area.

Table 6-3. Summary of experimental program for each testing batch of CPB specimens.

Sample nomenclature	Binder content (wt.%)	PCI in Binder (wt.%)	BFS in Binder (wt.%)	FA in Binder (wt.%)	w/b ratio	IC (day)	PC level	Self-healing period (day)
Self-healing behaviour in CPB with the addition of BFS								
PCI-BFS	4.5	100	0	0	7.35	7	90% of UCS after IC	7, 28, and 90 days
		80	20	0				
		50	50	0				
		20	80	0				
Self-healing behaviour in CPB with the addition of FA								
PCI-FA	4.5	100	0	0	7.35	7	90% of UCS after IC	7, 28, and 90 days
		80	0	20				
		50	0	50				
		20	0	80				

6.2.2 Specimen Preparation and Initial Curing

The experimental program comprised two batches of CPB specimens to examine the self-healing response of PCI/BFS and PCI/FA binder systems. Five cement-to-additive (c/a) ratios were examined, i.e., 100/0, 80/20, 50/50, and 20/80 by weight, while maintaining a fixed total binder content of 4.5 wt.%. As outlined in Table 6-3, precise quantities of solid materials, including ST, PCI, BFS, or FA, were weighed and subjected to a 1-minute dry mixing in a mechanical mixer to ensure uniform particle distribution. Subsequently, the required mixing water was then added to achieve a water-to-binder (w/b) ratio of 7.35, followed by wet mixing for 7 minutes until obtaining a homogeneous CPB mixture. It is noteworthy that such relatively w/b ratios, compared to conventional concrete or mortar, are typically employed in CPB to provide adequate fluidity and pumpability, enabling efficient underground transport and complete filling of mine stopes despite the low binder content. Fresh materials were cast into cylindrical molds (50 mm diameter × 100 mm height) for subsequent testing. All specimens underwent 7 days of initial curing (IC) at ambient laboratory conditions prior to crack introduction. In total, 290 cylinders were prepared to assess how mineral additives influence the self-healing capacity of CPB.

6.2.3 Crack Initiation and Exposure Condition

The initial compressive strength of the cast CPB specimens was determined after the 7-day initial curing phase using uniaxial compressive strength (UCS) tests in accordance with ASTM C39 (ASTM, 2021). Previous studies (Fall et al., 2009; Quan & Fall, 2025b) suggest that microcracks begin to initiate and propagate under the uniaxial compression loading when the applied load reaches approximately 75% or beyond of the UCS of CPB specimens. In this study, CPB specimens were subjected to a controlled pre-cracking level of 90% of their respective initial UCS values (i.e., PC90%) in the pre-peak phase. Upon reaching the designated loading threshold, the applied load was held for one minute before being released to facilitate the formation and propagation of micro- and macro-cracks within the CPB matrix. All loading was performed on a computer-controlled MTS 10/GL frame operated at a displacement rate of 1 mm/min, with a normal load setting of 50 kN. Companion control specimens (PC0%) were not subjected to any pre-loading and served as references for subsequent comparisons.

Immediately after pre-cracking, each specimen was imaged with a digital microscope (up to 200×) to document crack geometry before any healing could occur. The pre-cracked samples were then sealed in plastic film and stored at 23±2℃ alongside uncracked controls for the self-healing (cracked) and concurrent curing (controls) phases. This sealed, ambient-temperature conditioning limits moisture exchange and other exogenous influences, allowing the intrinsic autogenous healing of CPB to be isolated and interpreted with reduced uncertainty. In this study, the day of pre-cracking was designated as D0, marking the initiation of self-healing. Subsequent evaluations were conducted on D7, D28, and D90 to assess self-healing efficiency over 7, 28, and 90 days, respectively (hereafter referred to as the ‘self-healing period’) of the pre-cracked specimens. For clarity and ease of comparison, the corresponding uncracked control specimens were labeled as ‘curing period’ of D0, D7, D28, and D90. Both the pre-cracked and control specimens share the

same total paste age of 0+7, 7+7, 28+7, and 90+7 days at the respective self-healing or curing periods of 0, 7, 28, and 90 days. The overall experimental program is summarized in Table 6-3.

6.2.4 Self-healing Performance Evaluation

The self-healing performance of CPB or tailings-based cementitious composites is evaluated using parameters that directly reflect the recovery of both structural integrity and durability; in particular, compressive strength restoration quantifies the regained load-bearing capacity, while reductions in hydraulic conductivity capture the re-establishment of matrix impermeability and refinement of transport pathways. In addition, crack closure observations and microstructural analyses corroborate the formation and filling of healing products within cracks and voids, providing widely recognized and reliable indicators of autogenous self-healing effectiveness in cementitious materials.

6.2.4.1 Mechanical property

To evaluate the self-healing efficiency in terms of mechanical performance, UCS tests were conducted on the pre-cracked CPB specimens after self-healing periods of 7, 28, and 90 days based on ASTM C39/C39M-21 standard (ASTM, 2021). The recovered strength of the healed pre-cracked specimens was compared to both the pre-cracked specimens prior to healing and the uncracked reference control specimens. All tests were performed in triplicate to ensure the reproducibility and reliability of the results. To quantitatively assess the strength recovery, a healing index, termed the relative change in compressive strength (CCS), was introduced. This index reflects the degree of mechanical restoration and is calculated using the following equation:

$$\mathrm{CCS}(\%)=\frac{S_{\text{pre-cracked/healed}} - S_{\text{control}}}{S_{\text{control}}} \tag{6-1}$$

where $S_{pre\text{-}cracked}$ represents the initial UCS of the pre-cracked specimens measured at D0 (immediately after the pre-cracking process), S_{healed} denotes the UCS value of healed pre-cracked specimens at the designated self-healing period, and $S_{control}$ represents the UCS of uncracked control specimens tested under identical self-healing conditions and periods.

6.2.4.2 Permeability property

Permeability is a critical parameter in CPB applications, as it governs the migration of water, contaminants, and other fluids through the backfill matrix, which in turn, directly affects the long-term performance, durability, and environmental containment capacity of CPB structures. In this study, saturated hydraulic conductivity, which quantifies the rate of water flow through a saturated CPB matrix and serves as a key indicator of the permeability and integrity of the material, was adopted to assess the evolution of transport properties throughout the self-healing period. Hydraulic conductivity tests were performed on pre-cracked and control (uncracked) CPB specimens pre- and post-healing. The tests employed a triaxial cell with a flexible wall technique in accordance with ASTM D5084-16a (ASTM, 2016). The saturated hydraulic conductivity, k_{sat}, was calculated as follows:

$$k_{sat}=\frac{\Delta Q \cdot L}{A \cdot \Delta h \cdot \Delta t} \quad (6\text{-}2)$$

where k represents the hydraulic conductivity, cm/s; ΔQ denotes the quantity of flow during a certain time interval Δt, calculated as the average of inflow and outflow, cm^3; L signifies the length of the specimen, cm; A represents the cross-sectional area of the specimen, cm^2; Δt is the time interval, s; and Δh corresponds to the average head loss of across the specimen, cm of water.

To quantify the self-healing efficiency in terms of permeability, a hydraulic conductivity recovery ratio (HCRR) was defined and calculated as follows:

$$\text{HCRR } (\%) = \frac{k_0 - k_t}{k_0} \times 100\% \quad (6\text{-}3)$$

where k_0 denotes the initial hydraulic conductivity, cm/s, measured immediately after pre-cracking; k_t refers to the hydraulic conductivity, cm/s, measured following a given self-healing period.

6.2.4.3 Crack characteristics

In addition to mechanical and permeability evaluations, visual inspections of the pre-cracks in CPB specimens were carried out pre- and post-healing process using a digital microscope. For each designated self-healing period, crack images were captured from the specimens used in the aforementioned tests. The characteristics of microcracks (i.e., the healed crack widths) were measured from a defined observation surface, and the values were reported as averages to represent the extent of visible crack closure over the self-healing duration.

6.2.4.4 Microstructural analysis

To elucidate the self-healing mechanisms in CPB specimens incorporating mineral additives, advanced analytical techniques, including scanning electron microscopy with energy dispersive spectroscopy (SEM-EDS), thermal analysis (TG/DTG), X-ray diffraction (XRD), Mercury intrusion porosimetry (MIP), and Fourier transform infrared spectroscopy (FTIR), were employed. SEM-EDS was performed using a JEOL 6610LV SEM in low-voltage mode, equipped with an Oxford INCA large-area SDD detector, to characterize the microstructural morphology and elemental composition of healing products formed within cracks of BFS- and FA-incorporated CPB. XRD analyses were conducted using a Bruker D8 Endeavor diffractometer with a 1 kW sealed-tube Cu Kα radiation source (40 kV, 25 mA) and a Lynxeye XE-T 1D detector, facilitating the identification of crystalline phases associated with mineral additive-induced hydration products. MIP measurements were performed using a Micromeretics AutoPore III 9420 mercury porosimeter to assess the pore size distribution in CPB specimens with two binder systems. FTIR spectroscopy, performed on a Thermo Scientific Nicolet 6700 instrument, was used to detect the formation of functional groups indicative of self-healing products. In addition, TG/DTG analysis using a Mettler Toledo TGA 2 thermal analyzer was conducted under a nitrogen atmosphere, with a heating rate of 10 °C/min up to 1000 °C. This thermal profiling revealed the influence of varying contents of BFS and FA on the binder hydration behaviour and the development of healing phases. Furthermore,

porosity and void ratio of the studied specimens were monitored over time during self-healing and computed from specific gravity tests following ASTM D854 (2023).

6.3 Experimental Results and Discussion

6.3.1 Effect of BFS Incorporation on Self-healing Efficiency

6.3.1.1 Compressive strength development and recovery behaviour

Strength development of uncracked control specimens

The compressive strength development of PCI/BFS uncracked control specimens with varying BFS contents is illustrated in Figure 6-2a. As shown, the compressive strength increases with an extended curing period, regardless of BFS dosage. However, the influence of BFS content on strength development significantly varies along the curing periods.

Following the initial curing phase (at D0 of the curing period), the PCI/BFS:50/50 and 20/80 specimens exhibit approximately 23% and 5% higher initial compressive strength, respectively, compared to the PCI/BFS:100/0 reference specimens (Figure 6-2a). This strength enhancement is partially a result of the filler effect of BFS due to its smaller particle size relative to the STs, as shown in Figure 6-1. The finer BFS particles can accommodate voids between cement and/or tailings grains, refining the microstructure of the PCI/BFS matrix and enhancing its early mechanical properties (Escalante et al., 2001; Manmohan & Mehta, 1981). In addition to the simultaneous binder hydration, the precipitation of hydration products further densifies the packing of the specimen matrix, contributing to strength development. This argument is supported by the results of porosity and void ratio tests on the control PCI/BFS specimens. As is seen in Figure 6-3a, the incorporation of BFS leads to an evident reduction in both parameters, particularly as the BFS content increases. These performances are consistent with previous findings (Fall & Pokharel, 2010; Pokharel & Fall, 2011; Xiao et al., 2021). Moreover, in specimens with high BFS content (i.e., ≥ 50%), the alkaline environment generated by cement hydration (with a minimum pH of ≥12.3 in PCI/BFS:20/80) can initiate early latent hydraulic reactions in PCI/BFS system, which contribute to the formation of secondary C-S-H and enable early strength development, even as the PCI content decreases due to BFS replacement. Previous studies have demonstrated that even modest levels of alkaline activators can promote the early hydration of fine slag, with a pore solution pH of approximately 12 being sufficient to initiate slag activation, which is evidenced by measurable heat evolution and the formation of C-S-H and other hydration products (Bijen, 1996; Lim & Wee, 2000; Xu et al., 2022). In contrast, the limited BFS content in the PCI/BFS:80/20 specimen does not provide a sufficient filler effect to enhance particle packing, nor is the dosage high enough to engage in effective early-age hydration. Moreover, the relatively high PCI contents in both the PCI/BFS:80/20 and 100/0 specimens promote the rapid formation of cement hydration products, which precipitate on the surfaces of cement and/or slag particles. This leads to the development of a hydration product coating that hinders the water contact, thereby slowing the progression of hydration in the early stage, thus exhibiting comparatively lower early-age strength development (Ghirian & Fall, 2015; Hewlett & Liska, 2019).

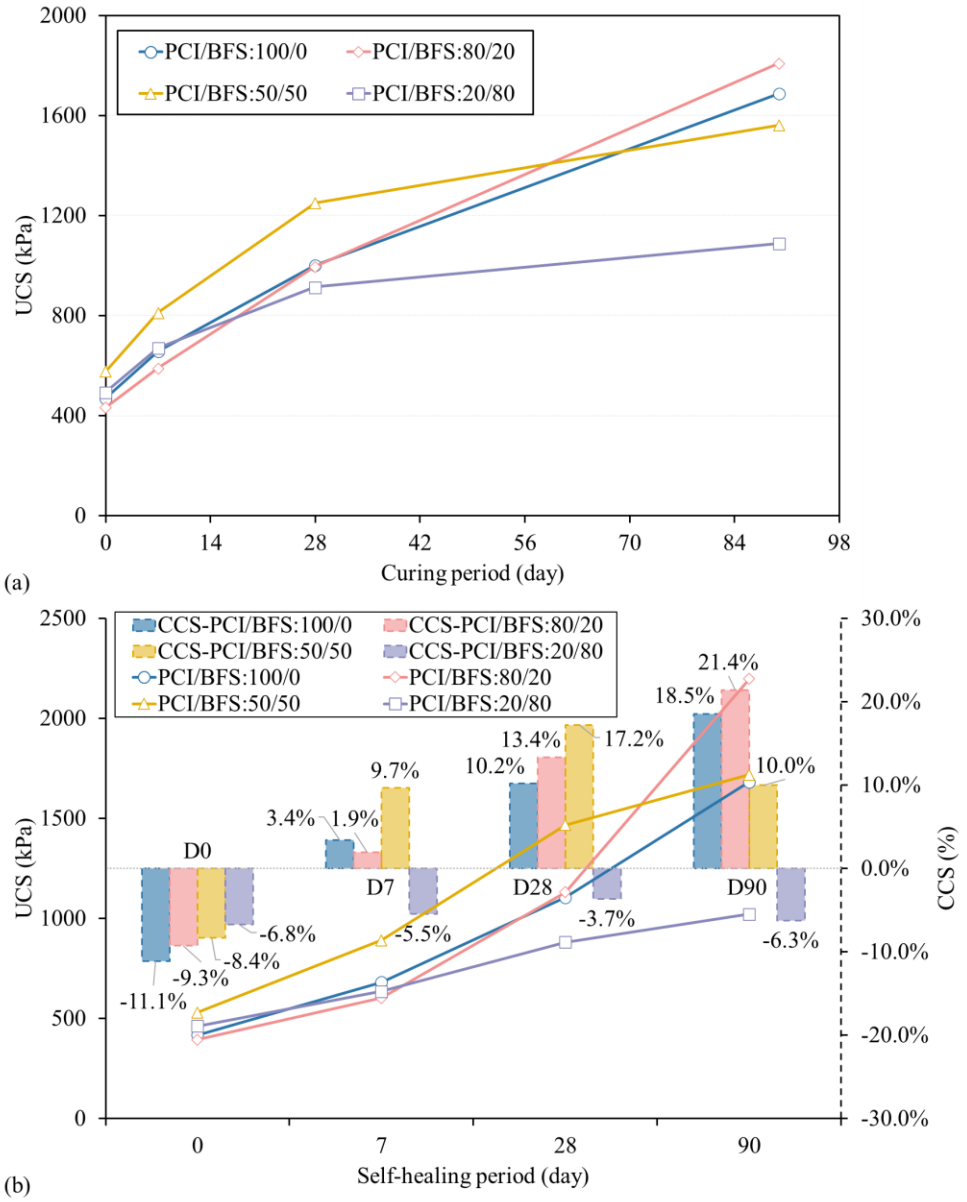

Figure 6-2. (a) UCS development of uncracked control PCI/BFS specimens, and (b) development of UCS and CCS in pre-cracked PCI/BFS specimens during self-healing periods of 0, 7, 28, and 90 days.

By the time the self-healing period reaches 28 days (i.e., paste age of 35 days), the strength profiles of PCI/BFS specimens begin to shift. The PCI/BFS:50/50 control specimens achieve the highest compressive strength, indicating an optimal synergy between cement hydration and slag activation. BFS does not react directly with water but is instead activated by CH, which is a byproduct of cement hydration. Therefore, cement not only facilitates its own hydration but also contributes to the necessary alkaline environment, primarily through CH, for activating the latent hydraulic properties of BFS. These coupled reactions promote the generation of hydration phases, including C-S-H, ettringite, and CH, within the microstructure-refined matrix, delivering a denser and more

refined pore structure (Fall et al., 2009). As evidenced in Figure 6-3a, a noticeable decrease in the porosity of the PCI/BFS:50/50 control specimen can be observed between D7 and D28. Add to that, MIP results in Figure 6-4 further confirm this finding; at 28 days, the PCI/BFS:50/50 mix exhibits a finer microstructure and a reduced threshold pore diameter compared to PCI/BFS:100/0. Meanwhile, the PCI/BFS:80/20 and 100/0 specimens continue to gain strength through sustained binder hydration. However, the PCI/BFS:20/80 specimens exhibit almost a plateau in strength development. This is likely due to the limited PCI content, which constrains the cement hydration and amount of available CH for activating the large proportion of BFS (Taylor, 1997), resulting in a significant portion of the BFS likely remaining unreacted and limiting further strength development.

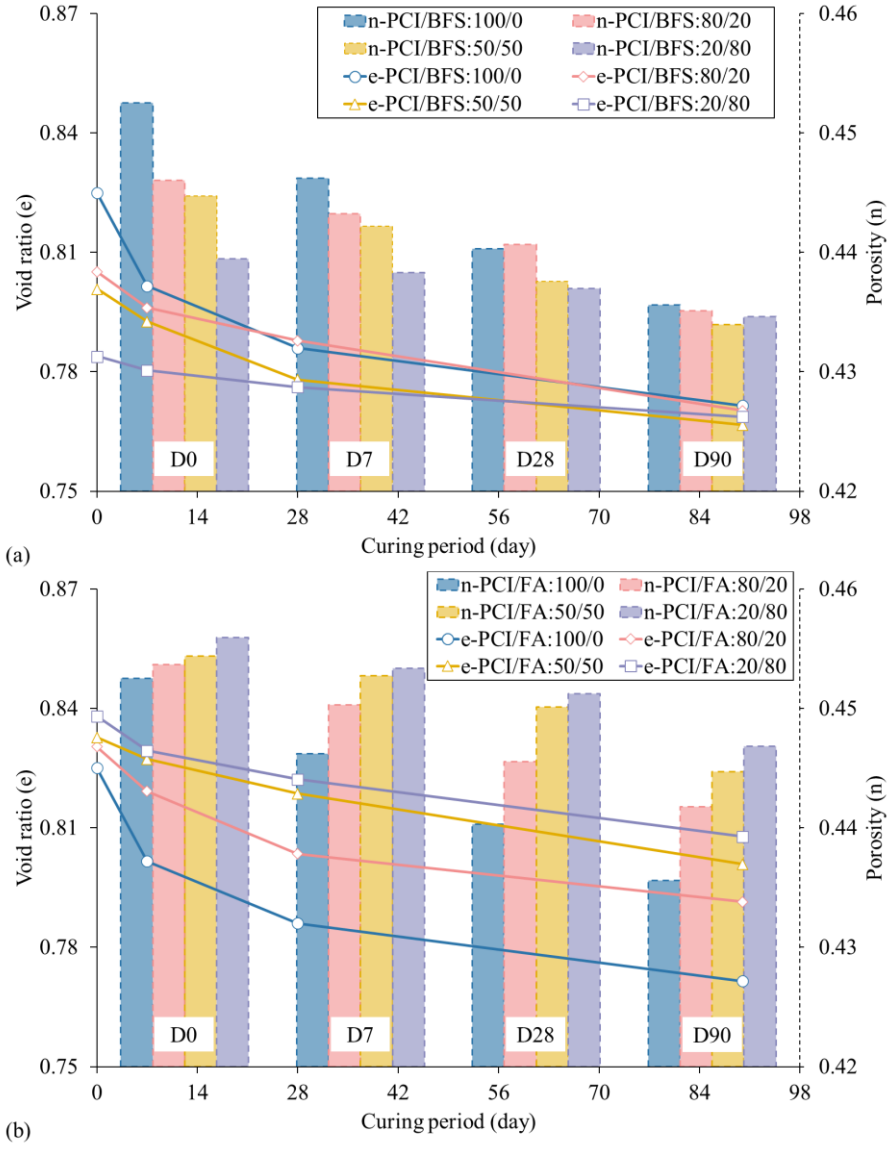

Figure 6-3. Variations in porosity (n) and void ratio (e) in CPB specimens containing different dosages of (a) BFS and (b) FA over self-healing periods of 0, 7, 28, and 90 days.

At the extended self-healing period of 90 days (i.e., paste age of 97 days), the PCI/BFS:80/20 control specimens attain the highest compressive strength among all other mixes, as seen in Figure 6-2a. This long-term strength development results from continuous cement hydration and a delayed activation of slag. The appropriate BFS content, combined with residual cement, allows continued generation of both primary and secondary hydration products, which densify the matrix and significantly enhance strength. Thermal analysis supports this interpretation. As shown in Figure 5a, the PCI/BFS:80/20 specimens exhibit relatively higher weight loss ranging from 50 °C to 200 °C compared to other mixes, indicating a higher extent of binder hydration and increased generation of hydrates, particularly C-S-H, ettringite, and carboaluminates (Bhatty, 1991; Pane & Hansen, 2005). These hydration products enhance particle bonding, thereby contributing to strength development. In contrast, the PCI/BFS:100/0 specimens, which lack supplementary cementitious material, show lower long-term strength despite the continuous cement hydration. The PCI/BFS:50/50 mix, though strong at earlier ages, may have reached a plateau in reactivity, with most of its CH consumed and limited residual cement available to sustain further hydration. For the PCI/BFS:20/80 mix, the low cement content results in insufficient CH generation and an inadequately alkaline environment for prolonged BFS activation, thus limiting long-term strength gain.

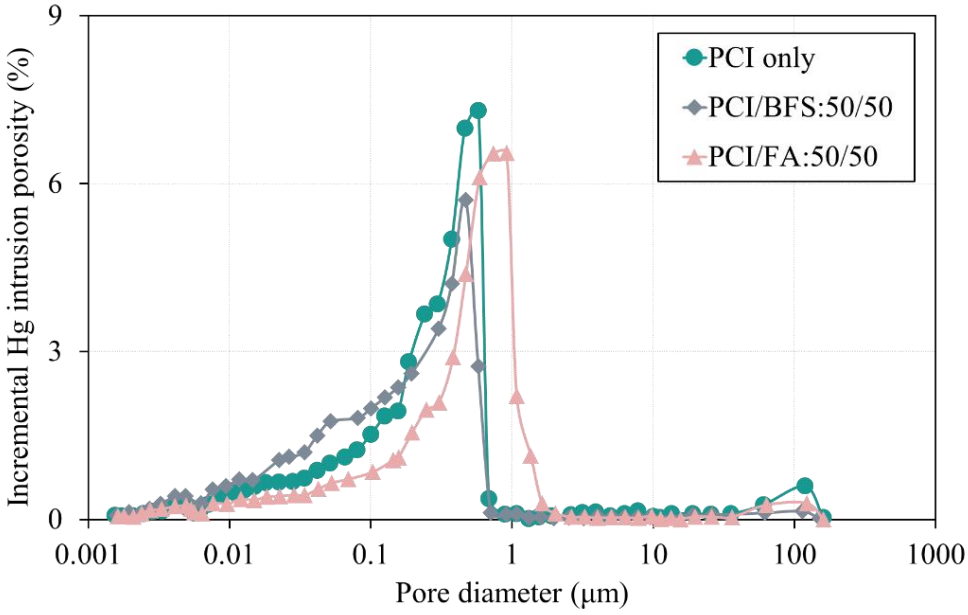

Figure 6-4. Pore size distributions of CPB specimens consisted of PCI only, PCI/BFS:50/50, and PCI/FA:50/50 at a paste age of 28 days.

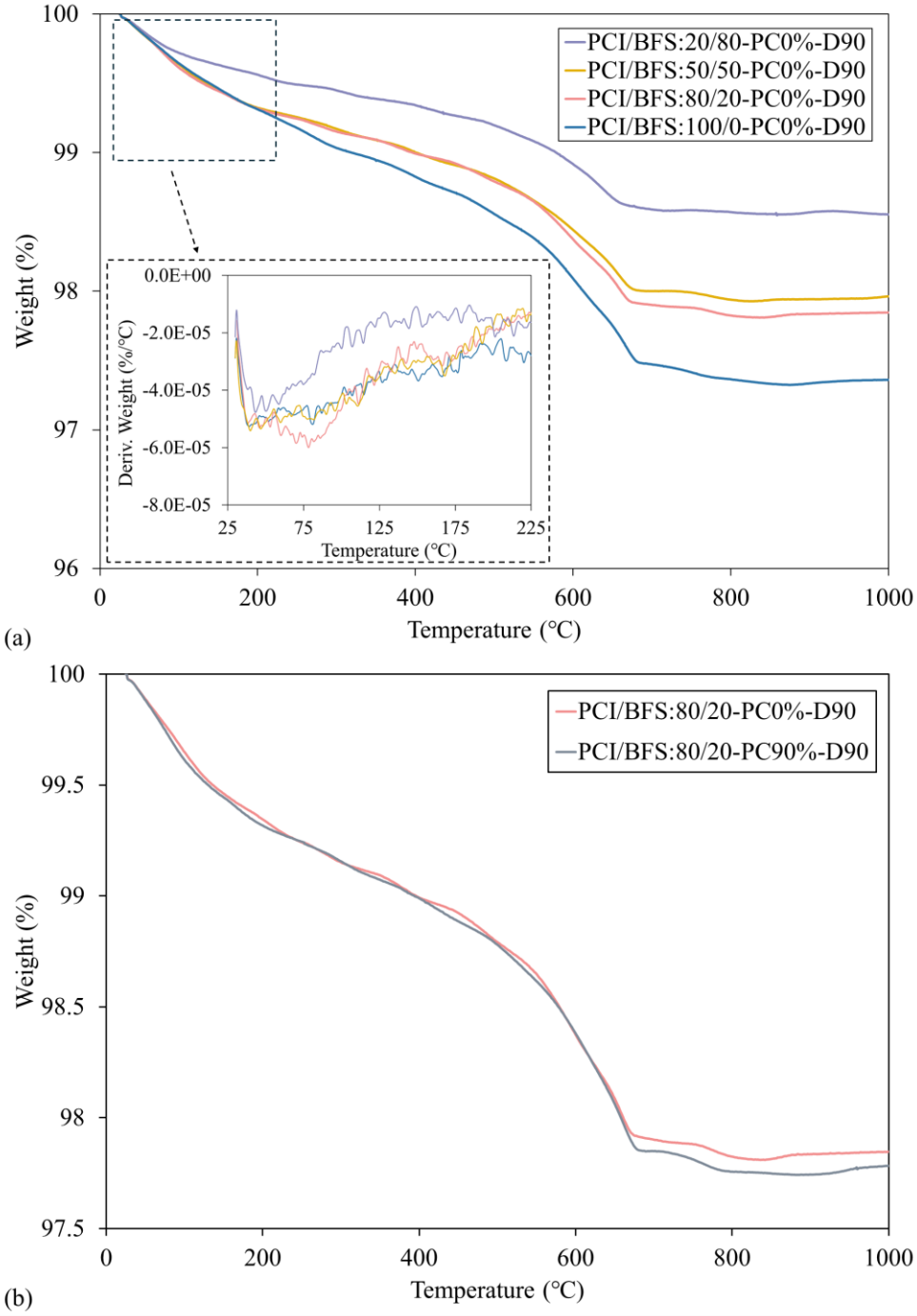

Figure 6-5. Comparison of TG/DTG profiles for (a) control (PC0%) PCI/BFS specimens, and (b) control and PC90% pre-cracked PCI/BFS:80/20 specimens after 90 days of self-healing.

Strength recovery of pre-cracked specimens through self-healing

Regarding the influence of BFS on the self-healing efficiency in strength, Figure 6-2b represents the compressive strength variations of pre-cracked PCI/BFS specimens in comparison with their uncracked control specimens over the self-healing period up to 90 days. The index change in compressive strength (CCS), defined and determined as in Eq. 6-1, is utilized to quantify the self-

healing efficiency and is shown on the right axis of the figure. Overall, most pre-cracked PCI/BFS specimens exhibit gradual strength and improved recovery as the self-healing time progresses, reflected by positive CCS values. The exception is the PCI/BFS:20/80 mixture, which presents negative CCS values, indicating a net loss of strength relative to its uncracked control specimens.

The PCI/BFS:100/0 specimens, which contain only PCI as the binder, demonstrate a self-healing performance comparable to that reported in previous studies (Quan & Fall, 2025b, 2025c). It is shown in Figure 6-2b that the compressive strength of pre-cracked PCI/BFS:100/0 specimens is nearly restored to that of the uncracked controls within only 7-day self-healing. This favourable healing performance results from two primary processes: (i) continued hydration of unhydrated cement particles, producing C-S-H and CH, and (ii) carbonation of CH, forming $CaCO_3$ (Quan & Fall, 2025a). The generated healing products precipitate within the cracks, pores and voids to fill and bridge the space gaps between the particles, which facilitates the crack closure and the pore structure refinement, thereby resulting in the restoration of strength (Quan & Fall, 2025c). With increasing self-healing duration, the continued formation of healing products further enhances both strength and stiffness of the pre-cracked specimens, and the CCS values reach 10.2% and 18.5% subsequent to 28- and 90-day self-healing period, respectively.

The introduction of BFS into the CPB matrix at proper content (i.e., PCI/BFS:80/20) generally improves self-healing capability in strength recovery, particularly during the 28- (intermediate) and 90-days (advanced) self-healing periods, as clearly shown in Figure 6-2b. Although the limited filler effect from the small amount of BFS and the delayed hydration process result in less effective early hydration after initial curing, the pre-cracked PCI/BFS:80/20 specimens still achieve compressive strength comparable to their controls after 7 days of self-healing, primarily due to continued binder hydrations and relatively enhanced internal porosity. The high cement content not only supports the aforementioned hydration mechanisms but also elevates the electrolyte concentration in the pore solution and reduces water content. These changes decrease the thickness of diffuse double layers (DDL), thereby effectively increasing the pH of the matrix (Ali et al., 2021; Mojid, 2011; Nägele, 1986). A higher pH environment facilitates the slag activation, promoting the secondary hydration and production of C-S-H within microcracks and pores, thereby enhancing the particle bonding and strength recovery (Sun et al., 2022; Ye & Radlińska, 2016). This healing behaviour becomes more pronounced as the self-healing progresses. From 28 days onward, PCI/BFS:80/20 specimens outperform PCI/BFS:100/0 in self-healing efficiency with an achievement of CCS value of 13.4%. Furthermore, continuous cement hydration and slag activation, coupled with refined microstructure, allow the pre-cracked PCI/BFS:80/20 specimens to obtain the greatest self-healing efficiency among all mixes with a CCS value of 21.4% at the 90-day self-healing stage. The abundant CH from cement hydration enables continued pozzolanic reactions with BFS, resulting in the production of C-S-H gels which benefits the strength restoration. This is corroborated by thermal analysis results in Figure 6-5a, which exhibits the PCI/BFS:80/20 specimens having the greatest weight loss at temperatures between 50 °C and 200 °C, indicating the highest degree of hydration. In other words, the substitution of BFS for PCI does not diminish the healing efficiency; on the contrary, it enhances the healing performance with

appropriate content. This improvement is attributed to the hydration reactions driven by the latent hydraulic activity of BFS, which promote the continuous formation of self-healing products within the crack network. In addition, the thermal analysis in Figure 6-5b reveals relatively overall greater weight loss for the pre-cracked PCI/BFS:80/20 specimens compared to the controls, which suggests that the presence of cracks could facilitate the hydration and carbonation reactions, further strengthening the long-term self-healing. This supplementary improvement in healed strength is largely associated with the initiated cracks which act as the channels for air/fluid transport, allowing the evaporation of extra water from CPB specimen matrix, thus promoting the hydration degree with relatively larger production of hydrates (Bisschop & Wittel, 2011; Quan & Fall, 2025a; Zhao et al., 2020).

When the BFS content is increased to 50% (i.e., PCI/BFS:50/50), a more effective self-healing performance is recognized through the initial 28-day self-healing period, as observed in Figure 6-2b. Note that the pre-cracked PCI/BFS:50/50 specimens achieve higher healed strengths than those of their controls after only 7 days of healing. The most pronounced healing efficiency is achieved at 28 days of self-healing, with a CCS value rising to 17.2%. This augmented performance results from the synergistic interactions between cement hydration and slag activation. Upon water exposure, tricalcium silicate (C_3S) and dicalcium silicate (C_2S) in PCI react to produce C-S-H and CH. The accumulation of CH provides an alkaline environment that activates BFS, which then reacts to produce C-S-H through secondary hydration (Niu et al., 2002). XRD patterns presented in Figure 6-6 reveal that the PCI/BFS:50/50 specimens exhibit comparable intensities of hydration products as PCI/BFS:100/0 specimens and higher than PCI/BFS:80/20 specimens, suggesting the promising formation of self-healing products. Additionally, the filler effect of BFS results in denser packing and reduced void volumes at the same pre-cracking level, further contributing to the notable healing performance given similar or higher amounts of self-healing products. However, healing efficiency is observed to slightly diminish upon prolonging the self-healing period to 90 days, primarily due to the depletion of cement and CH (Pokharel & Fall, 2011; Taylor, 1997). Nonetheless, a satisfactory CCS value of 10.0% is still attained.

In contrast, specimens with high BFS content (i.e., PCI/BFS:20/80) exhibit inferior self-healing performance, as shown in Figure 6-2b. It can be seen that the pre-cracked PCI/BFS:20/80 specimens are unable to achieve full recovery in compressive strength, consistently remaining lower than the control specimens over the self-healing period, as indicated by the negative CCS values across all healing ages. Initially, the filler effect resulting from the high BFS content favours bridging the gaps between tailings and/or PCI particles. This densified packing pattern enhances interparticle friction and produces the finest pore structure among the studied mixes, contributing to an initial strength increase. However, despite the integration of binder hydration, the pre-cracked PCI/BFS:20/80 specimens exhibit limited healing performance. The reduced availability of PCI leads to a decrease in CH production and a lower alkaline environment, both of which are crucial for activating and hydrating BFS. This insufficient activation restricts the secondary formation of C-S-H required to bridge and bond the crack gaps, thereby limiting the long-term strength recovery. Moreover, the amount of C-S-H produced solely from PCI hydration is inadequate to sustain

prolonged self-healing. Carbonation reaction, which acts as one of the main autogenous healing mechanisms, is also diminished as CH is consumed by the excessive unreacted BFS. As a result, healing efficiency is compromised with increasing BFS content and decreasing PCI proportion. This observed trend is confirmed by the thermal analysis results in Figure 6-5a, which presents less weight loss of decompositions in the PCI/BFS:20/80 specimens, indicating the insufficient formation of healing products within the matrix.

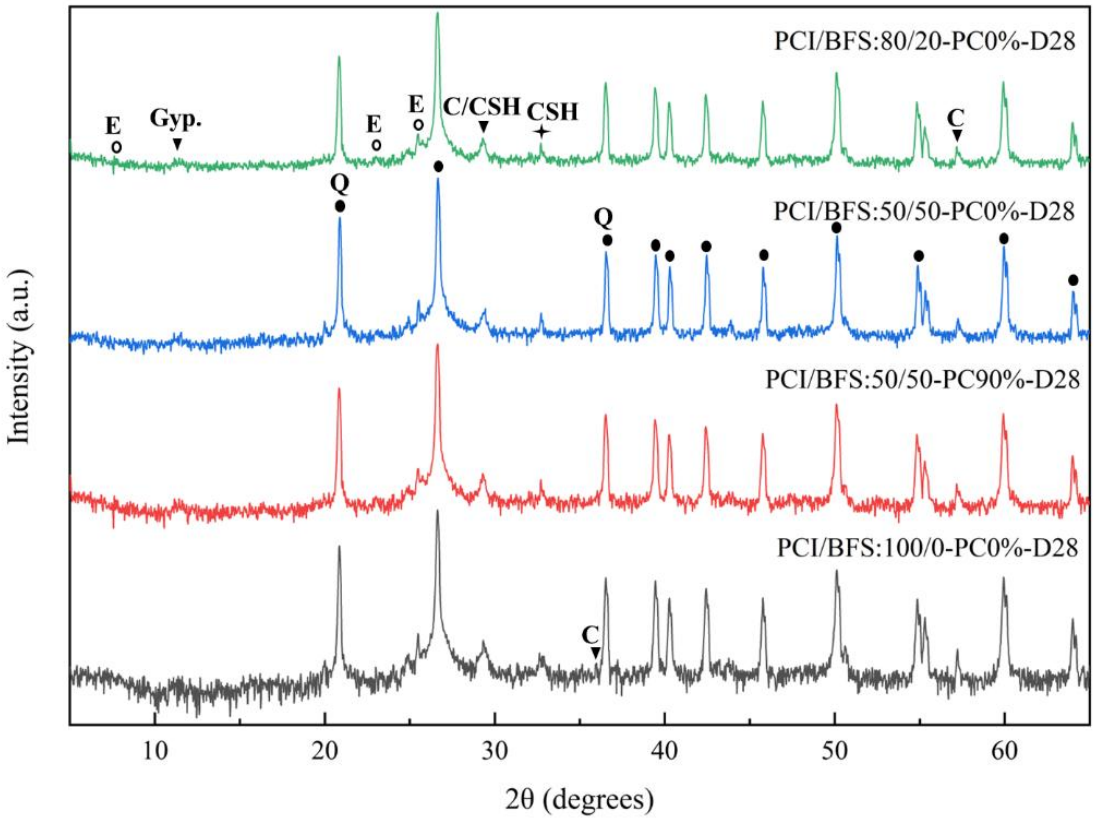

Figure 6-6. Comparison of XRD patterns of control and pre-cracked PCI/BFS specimens after a self-healing period of 28 days (Q: Quartz; E: ettringite; Gyp.: gypsum; C-S-H: calcium-silicate-hydrate; C: calcite).

6.3.1.2 Hydraulic conductivity

Changes in saturated hydraulic conductivity (k_{sat}) were measured to evaluate the impact of BFS incorporation on the self-healing efficiency in the permeability of the CPB matrix. Figure 6-7a presents the evolution of hydraulic conductivity in uncracked PCI/BFS control specimens with varying BFS contents over the curing period. The healing efficiency in terms of permeability for the pre-cracked PCI/BFS specimens was quantitatively assessed using Eq. 6-3, relative to the control specimens, and is expressed as the hydraulic conductivity recovery ratio (HCRR), shown on the secondary y-axis in Figure 6-7b.

As seen in Figure 6-7a, k_{sat} of the uncracked PCI/BFS control specimens decreases with the progression of self-healing (paste age), irrespective of the BFS contents. This reduction in

hydraulic conductivity is associated with the continued binder hydrations of PCI and/or BFS, which produce the hydration products, such as ettringite, C-S-H, CH, and calcite, to fill the crack network and available voids, leading to a refined pore structure and diminished internal porosity, thereby contributing to the gradual decrease in hydraulic conductivity (Fall et al., 2009). Evidence from the results of porosity tests conducted on the PCI/BFS control specimens in Figure 6-3 confirms this argument, manifesting a decline in both parameters due to the microstructural enhancement. Notably, the introduction of BFS into the CPB matrix results in a notable decrease in hydraulic conductivity, with the PCI/BFS:100/0 specimens exhibiting the highest permeability throughout the entire study period. This enhancement from BFS results primarily from the combined influence of its filler effect and pozzolanic reactivity. The fine BFS particles physically occupy the voids and pores between the larger PCI and tailings grains to decrease the internal porosity, resulting in a denser particle distribution (Sohn & Moreland, 1968; Fall et al., 2009). Moreover, as the hydration progresses, the cement hydration and pozzolanic reaction between BFS and CH generate additional hydration products, particularly C-S-H gels. These products further densify the matrix by filling capillary pores and decreasing pore connectivity, ultimately lowering the hydraulic conductivity of PCI/BFS specimens. This microstructural refinement is corroborated by MIP test results on the control specimens, as illustrated in Figure 6-4. The figure shows that the threshold pore diameter of the PCI/BFS:50/50 specimens is 0.47 μm, which is smaller than that of the PCI/BFS:100/0 specimens (0.58 μm), indicating lower cumulative pore volume and a more refined microstructure in the BFS-incorporated system.

The presence of BFS contributes not only to the recovery of mechanical performance but also to the permeability restoration, which is crucial for minimizing fluid migration and ensuring the long-term durability of the backfill structure. Figure 6-7b illustrates the gradual restoration of the hydraulic conductivity in the pre-cracked PCI/BFS samples. At the onset of the self-healing period (D0), the hydraulic conductivity of pre-cracked samples exceeds that of uncracked controls. This increase is attributed to the formation of crack networks (i.e., both micro- and macro-cracks) within the CPB matrix as a result of the pre-cracking process, which serve as preferential pathways for fluid flow and thereby exacerbate permeability (Fall et al., 2009). However, as the self-healing process initiates, the pre-cracked specimens progressively recover their hydraulic conductivity. For the reference specimens without BFS (i.e., PCI/BFS:100/0), the observed reduction in hydraulic conductivity is primarily governed by two mechanisms: cement hydration and carbonation of CH (Quan and Fall, 2025). These processes facilitate the progressive deposition of healing products within cracks and capillary voids, which modify the pore structure and promote crack closure. As a result, internal pore connectivity is reduced, leading to a gradual decrease in permeability. Correspondingly, the HCRR value increases from 36.7% at 7 days to 90.1% at 90 days, reflecting the effectiveness of these autogenous healing mechanisms over time. Moreover, the presence of BFS imposes varying impacts on the healing efficiency in hydraulic conductivity, depending on the BFS dosage and the duration of the self-healing. As illustrated in Figure 6-7b, the pre-cracked PCI/BFS:50/50 specimens exhibit the most pronounced healing rate and efficiency in hydraulic conductivity during the first 28 days, achieving an HCRR value of 81.8%. As aforementioned,

cement hydration provides a sufficient concentration of CH, establishing a highly alkaline environment within the matrix. When combined with an adequate BFS dosage, this environment effectively activates the pozzolanic reaction of BFS. The resulting generation of additional C-S-H gels fills the available pores and cracks, and, together with the initial filler effect of BFS, leads to a significant improvement in healing efficiency. This enhanced performance is supported by the XRD results shown in Figure 6-6. Add to that, the high specific surface area (SSA) of BFS (i.e., 5.8 m^2/g in Table 6-2) also plays a significant role in enhancing its hydration behaviour within the PCI/BFS system. A larger SSA provides more reactive sites for interaction with the alkaline pore solution, especially with CH produced from cement hydration. This promotes the initial dissolution of the amorphous glassy phase of BFS, thereby accelerating the formation of secondary hydration products (Briki et al., 2021; Yilmaz et al., 2011a). However, it is important to note that this beneficial effect is highly dependent on the availability of CH to activate the BFS. As the cement depletes within the matrix, the PCI/BFS:50/50 specimens exhibit a slower healing rate due to insufficient CH concentration during the extended 90-day self-healing period. In comparison, the PCI/BFS:80/20 pre-cracked specimens demonstrate the highest long-term healing efficiency among the mixes, achieving an HCRR of 96.2%. This is attributed to their relatively higher cement content, which ensures a sustained provision of CH to activate the smaller proportion of BFS, thus enabling continued pozzolanic reactions. In the absence of external alkali sources, the cement phase governs the development of the CPB system, as BFS activation depends on CH generated through cement hydration. Thermal analysis results shown in Figure 6-5 corroborate this, with the PCI/BFS:80/20 pre-cracked specimens exhibiting the largest weight loss in the 50-200 °C range, indicating the precipitation of higher quantity of C-S-H, ettringite, and carboaluminates, which fill internal crack cavities and block crack networks, thereby restoring the permeability.

In contrast, the PCI/BFS:20/80 pre-cracked specimens exhibit diminished self-healing performance in hydraulic conductivity recovery. Although the high BFS content initially contributes to a densified matrix with the lowest porosity, which results in comparatively smaller volumes of cracks and voids to be filled at the same pre-cracking level, the limited hydration products from both cement and BFS fail to provide effective healing performance. This reduced healing efficiency is consistent with the lower amount of hydrates detected, as shown in Figure 6-5a, where the PCI/BFS:20/80 specimens exhibit the smallest weight losses among all mixes tested. Furthermore, the insufficient formation of healing products weakens the capability for crack closure, as illustrated in Figure 6-12, where PCI/BFS:20/80 pre-cracked specimens display a comparatively smaller maximum crack width closure throughout the studied self-healing period. Therefore, the presence of unhealed cracks governs the permeability of the matrix, leading to the diminished self-healing performance observed in these specimens.

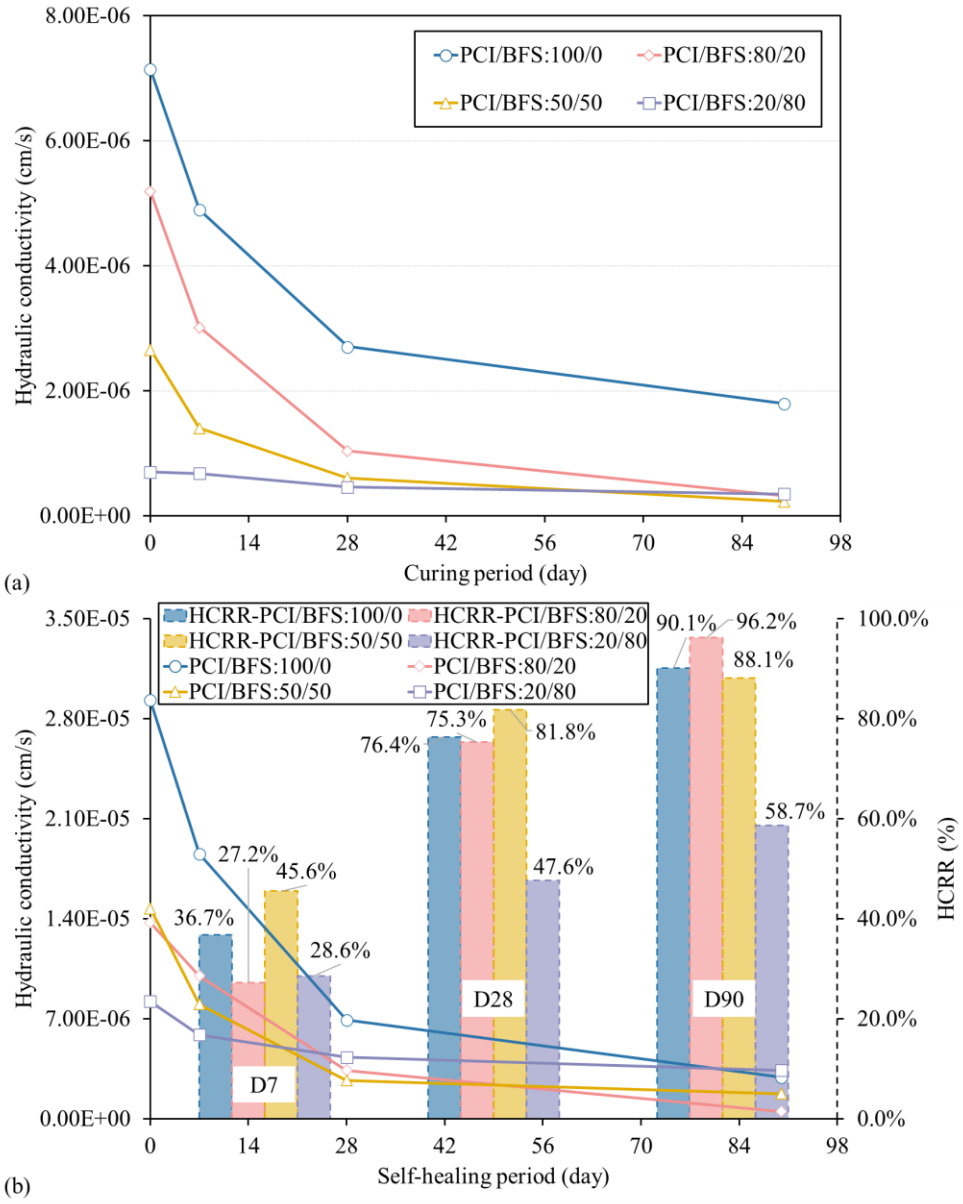

Figure 6-7. (a) Hydraulic conductivity changes of uncracked control PCI/BFS specimens, and (b) hydraulic conductivity and HCRR variations in pre-cracked PCI/BFS specimens throughout self-healing periods of 0, 7, 28, and 90 days.

6.3.2 Effect of FA Incorporation on Self-healing Efficiency

6.3.2.1 Compressive strength development and recovery behaviour

Figure 6-8a depicts the development of compressive strength in uncracked PCI/FA control specimens as a function of FA content and curing period. A continuous increase in strength is observed for all PCI/FA specimens throughout the curing period, regardless of the FA contents. This strength development is primarily due to the active binder hydrations over time, during which the precipitation of hydration products, including C-S-H, ettringite, and CH, progressively accommodates the capillary pores and voids within the matrix, thus leading to the pore structure

refinement (Taylor, 1997). The corresponding reduction in porosity and void ratio of the specimens is illustrated in Figure 6-3b. The accumulation of hydration products strengthens interparticle bonding, improving compressive strength. However, partial substitution of PCI by FA leads to a noticeable reduction in strength. The compressive strength decreases with increasing FA content. Specifically, after the initial curing phase, the PCI/FA:80/20, 50/50, and 20/80 specimens experience approximately 22%, 52%, and 68% reduction in compressive strength, respectively, compared to the reference PCI/FA:100/0 specimens. Correspondingly, the incorporation of FA into the CPB matrix generally undermines the self-healing efficiency as displayed in Figure 6-8b, especially in the PCI/FA:50/50 and 20/80 specimens. Following 7-days self-healing period, the pre-cracked PCI/FA:80/20 and 50/50 specimens barely recover their strength relative to the control ones. With the extended self-healing to 28 and 90 days, the pre-cracked PCI/FA:80/20 specimens still exhibit reduced healing efficiency, with CCS values remaining below those of PCI/FA:100/0 specimens. The pre-cracked PCI/FA:50/50 and 20/80 specimens even demonstrate significantly inferior strength recovery, with CCS values decreasing to -13.3% and -23.2% following a 90-day self-healing. It is noted that immediately following the pre-cracking (namely, at D0), the pre-cracked PCI/FA specimens exhibit higher strength compared with their respective control specimens. The transient strength gain, resulting from compaction of CPB specimens under uniaxial loading, can be attributed to the volumetric contraction behaviour of CPB materials, as elucidated in (Fall et al., 2009; Quan & Fall, 2024). To exclude this effect, the CCS of PCI/FA specimens is determined using the following equation:

$$\text{CCS}\ (\%)=\frac{[S_{D>0}-(S_{D0}-S_{\text{control at D0}})]-S_{\text{control at D>0}}}{S_{\text{control at D>0}}} \tag{6-4}$$

where $S_{D>0}$ represents the UCS values of healed specimens following self-healing duration of 7, 28, and 90 days, S_{D0} denotes the UCS values of the pre-cracked samples immediately after pre-cracking, $S_{control\ at\ D>0}$ corresponds to the strength of uncracked control specimens exposed to the identical self-healing regime and duration, and $S_{control\ at\ D0}$ is the UCS of uncracked control samples at D0.

PCI/FA system shares similar interaction mechanisms between the mineral admixture and cement particles to those observed in the PCI/BFS system. The initial cement hydration produces C-S-H gels and CH, which establishes the alkaline environment for the secondary reaction between CH and FA particles to produce C-S-H (Biernacki et al., 2001; Taylor, 1997; Wang, 2014). However, despite this conceptual similarity, the PCI/FA system differs in its reaction mechanisms and performance characteristics. Its impacts on the observed diminished strength development and recovery can be ascribed to three main attributors, including physical effect, dilution effect, and chemical effect (Wang & Lee, 2010; Narmluk & Nawa, 2011; Wang, 2014).

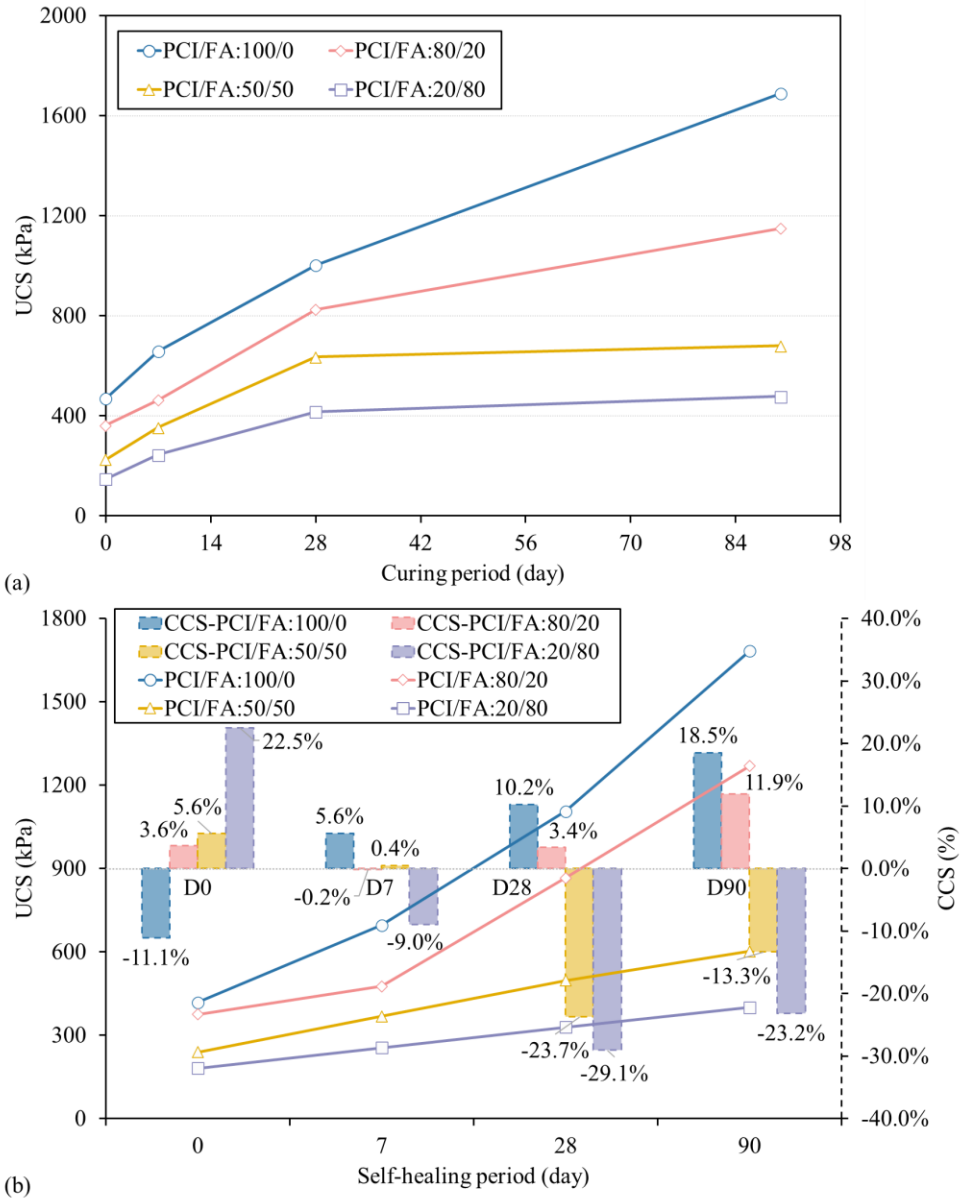

Figure 6-8. (a) UCS development of uncracked control PCI/FA specimens during curing periods, and (b) UCS and CCS progression in pre-cracked PCI/FA specimens during self-healing at 0, 7, 28, and 90 days.

As shown in Figure 6-1, the utilized FA exhibits a particle size distribution comparable to the tailings in the coarse range, with a limited proportion of fine particles that restricts its effectiveness as a micro-filler in the PCI/FA system. Unlike finer binders (i.e., PCI or BFS), which can occupy the spaces between coarse tailings particles and promote the microstructural packing, the introduction of FA induces limited microstructural refinement, leading to increased interconnected pores and internal porosity. Additionally, the spherical morphology and relatively lower surface roughness of FA particles may reduce the interparticle friction and mechanical interlocking, leading to a less cohesive microstructure. This coarseness of PCI/FA specimens is corroborated by the

microstructural measurements of the control PCI/FA specimens in Figure 6-3b, which demonstrate an increasing trend in porosity and void ratio with rising FA content. Furthermore, FA particles can absorb calcium ions (Ca^{2+}) or physically block active sites on cement grains, thereby retarding the cement hydration and delaying the formation of hydration products. This behaviour manifests as slower strength development and elevated porosity (Akmalaiuly et al., 2023; Sakai et al., 2005). This retardation effect becomes more pronounced at higher FA contents or when the alkali availability is limited due to reduced PCI content (i.e., in PCI/FA:50/50 and 20/80 systems). On the other hand, FA particles also serve as heterogeneous nucleation sites, which can facilitate the precipitation of hydration products by providing surfaces for crystal growth (Takemoto, 1980; Xu et al., 1993). However, the retardation influence tends to dominate during early ages, especially with high FA contents before the onset of pozzolanic activity. Due to the limited hydration in the PCI/FA system, a more porous structure develops, compromising matrix integrity and leading to diminished strength development and recovery (Chindasiriphan et al., 2020; Zhang et al., 2014). This performance aligns with the pore size distribution obtained from MIP measurements shown in Figure 6-4, where PCI/FA:50/50 specimens reveal a coarser pore structure compared to PCI-only and PCI/BFS:50/50 specimens. As a consequence, a larger volume of unhealed cracks persists in the pre-cracked PCI/FA specimens due to insufficient formation of healing products, ultimately impairing the self-healing efficiency.

The dilution effect, correlated with the hydration processes within the matrix, remains a significant factor contributing to the diminished self-healing performance in strength recovery. Substituting a portion of PCI with FA decreases the amount of early-reactive material, resulting in diminished generation of hydration products, especially C-S-H gels that bond particles during the self-healing period. Since the early strength recovery predominantly relies on the presence and continuity of these hydration products, the reduced PCI limits the formation of a mechanically stable microstructure. In addition, the dilution of PCI also decreases the CH availability from cement hydration, which is essential for the activation of FA pozzolanic reaction, thus impeding hydration even after a 90-day self-healing period. This trend is supported by thermal analysis results of PCI/FA control specimens (Figure 6-9a), where increasing FA content corresponds to decreased weight loss at characteristic hydration peaks, indicating fewer hydration products. Furthermore, an increment in the content of FA involves a reduction in the content of PCI and, consequently, an elevated w/b ratio within the PCI/FA system. It is well acknowledged that a moderate increase in w/b ratio can improve the cement hydration degree in conventional cementitious materials (e.g., concrete, mortar, and ECC) with relatively low w/b ratios (e.g., 0.4-0.55), which in turn facilitates the pozzolanic activity of FA with the improved availability of CH (Sahmaran et al., 2013; Termkhajornkit et al., 2009; Wang, 2014; Xu et al., 1993). However, the elevated water content (w/b ratio) adversely affects the mechanical performance of the CPB materials, which are usually formulated with high water content to ensure flowability, as a result of the dilution of soluble components and slower formation of hydration products (Bentz et al., 2009; Benzaazoua et al., 2004; Fall et al., 2009). Excess water content reduces the concentrations of Ca^{2+} and OH^- ions in the pore solution by diluting cement particles, which decelerates the formation and precipitation of

hydration products, such as C-S-H and CH. Hence, the retarded cement hydration and pozzolanic reactivity compromise the structural integrity, negatively impacting the self-healing efficiency. The effects of w/b ratio on the self-healing efficiency of CPB materials have been elucidated in the previous work (Quan & Fall, 2025b).

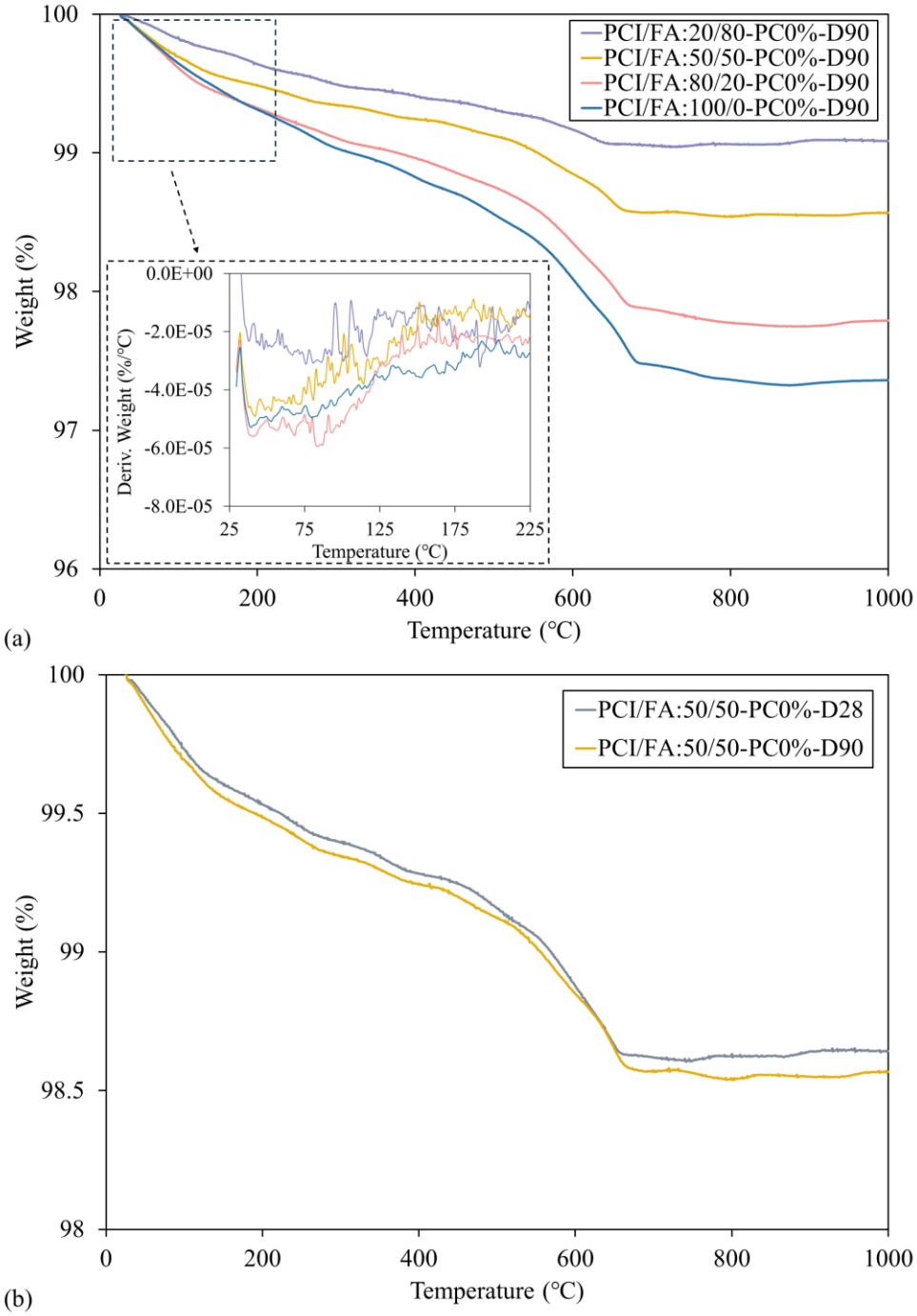

Figure 6-9. Comparison of TG/DTG curves for (a) control (PC0%) PCI/FA specimens at 90 days of self-healing, and (b) control PCI/FA:50/50 specimens at 28 and 90 days.

The chemical effects of FA involved in the healing behaviour of the CPB system are mainly governed by its reactions with CH and intrinsically pozzolanic reactivity. FA typically exhibits a prolonged initial dormant period because of its slower reaction kinetics, which are influenced by its physical characteristics (Taylor, 1997). Unlike the hydration process of PCI, which begins the hydration reactions upon contact with water, the pozzolanic reaction of FA requires the presence of CH from cement hydration, especially in the absence of external alkali sources. The availability of CH from cement hydration thus controls the contribution of secondary pozzolanic activity of FA to the overall self-healing efficiency. Consequently, the coupled impacts result in the limited pozzolanic reaction and minimal contribution to the formation of binder hydrates for the self-healing process. Add to that, the activation of FA typically requires a pH above 13 to initiate pozzolanic reactions (Klein & Simon, 2006); however, a threshold not reached in the PCI/FA specimens studied here (i.e., measured pH values of 12.2, 12.1, and 11.8 for PCI/FA:80/20, 50/50, and 20/80, respectively). Notably, Figure 6-8b reveals an improvement in strength recovery for pre-cracked PCI/FA:50/50 and 20/80 specimens between 28 and 90 days of self-healing, with CCR values increasing from -23.7% to 13.3% and from -29.1% to -23.2%, respectively. Although some C-S-H gels are produced within the matrix, the less C-S-H gels have insufficient agglomeration effect to bridge the crack network, and these pre-cracked specimens still perform significantly impaired mechanical bearing-capability after a 90-day self-healing period. This behaviour is corroborated by thermal analysis results in Figure 6-9a, which show significantly fewer hydrates in the PCI/FA:50/50 and 20/80 specimens, as evidenced by their lower weight losses compared with the specimens with none or lower dosages of FA. These findings imply that a longer self-healing duration and supply of CH would be necessary for the substantial strength recovery in PCI/FA systems, particularly at higher FA contents where CH availability is limited. From a practical perspective, the extended self-healing period and low self-healing efficiency are undesirable for mining operations as additional reinforcement of backfill structure may be required, potentially prolonging mining cycles and increasing operational complexity and costs.

6.3.2.2 Hydraulic conductivity

Figure 6-10a presents the evolution of saturated hydraulic conductivity (k_{sat}) in uncracked control PCI/FA specimens over the curing period. As can be seen, all mixes display a progressive reduction in k_{sat} as the curing period extends, irrespective of FA content, attributable to the accumulation of hydration products within capillary voids, which progressively lowers the internal porosity of the matrix to decrease the permeability. This trend aligns with the concurrent decrease in porosity and void ratio observed in Figure 6-3b. However, it is noted that PCI/FA specimens (i.e., PCI/FA:80/20, 50/50, and 20/80) consistently display higher k_{sat} values than the PCI/FA:100/0 reference, with the difference becoming more pronounced at higher FA contents. Figure 6-10b demonstrates the influence of FA incorporation on the healing efficiency in k_{sat} of pre-cracked PCI/FA specimens, determined through the hydraulic conductivity recovery ratio (defined as HCRR, Eq. 6-3) relative to the initial pre-cracked scenario. The results show that the FA addition significantly reduces the self-healing efficiency in permeability recovery. For instance, a light FA content (i.e., PCI/FA:80/20) decreases the HCRR from 90.1% to 68.9% compared to the specimens without FA (i.e.,

PCI/FA:100/0) following 90-day self-healing. At high FA content, PCI/FA:20/80 specimens reach only 32.3% HCRR subsequent to a 90-day self-healing period, representing the minimal self-healing performance among all mixes. This adverse effect is primarily ascribed to the combined influences of physical characteristics, dilution effect, and delayed pozzolanic reactivity of FA, as discussed previously.

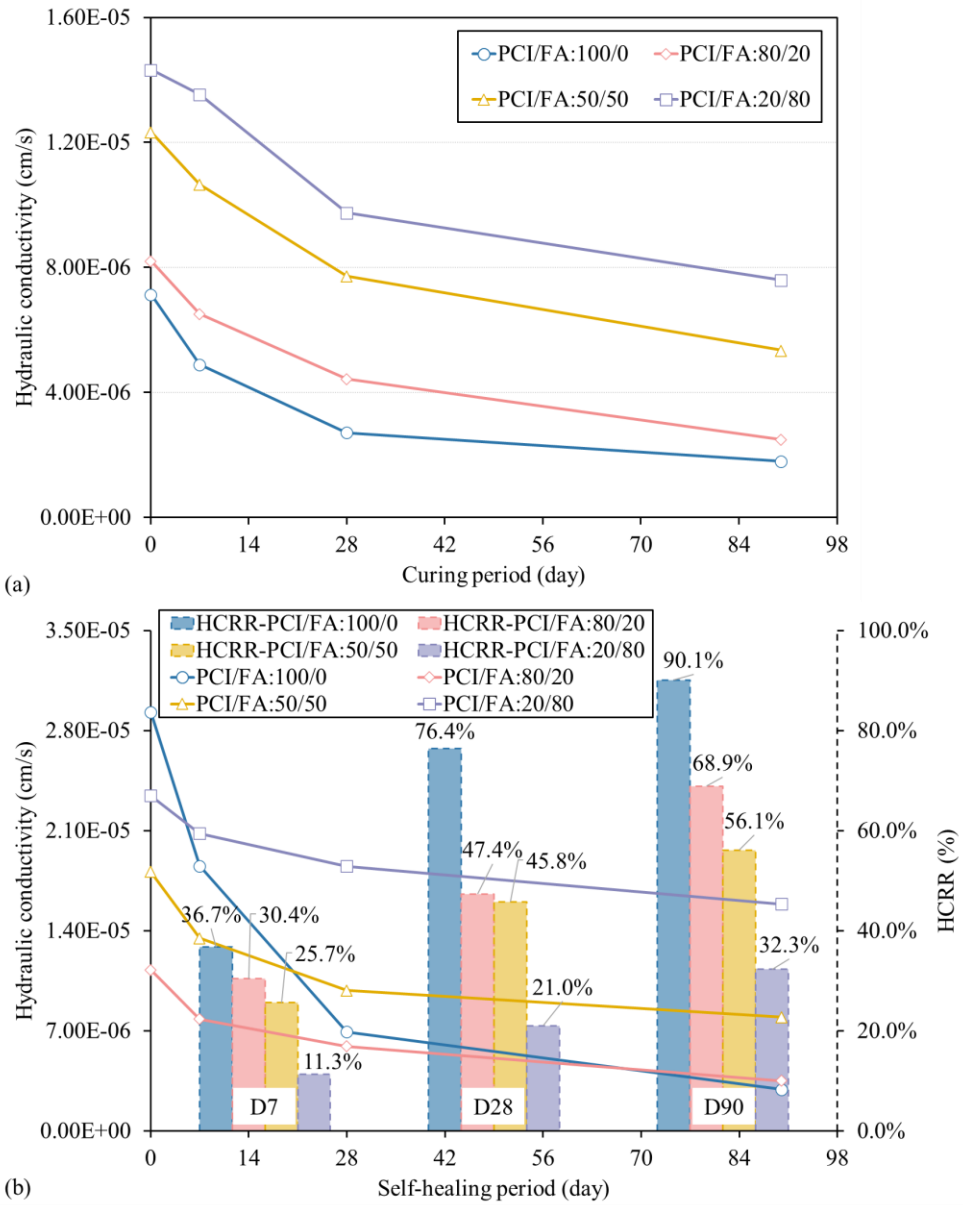

Figure 6-10. (a) Hydraulic conductivity changes of uncracked control PCI/FA specimens, and (b) hydraulic conductivity and HCRR variations in pre-cracked PCI/FA specimens throughout self-healing periods of 0, 7, 28, and 90 days.

Hydraulic conductivity is directly related to the interconnected porosity and void network, which act as pathways for fluid transport within the matrix. Due to the ineffective filler effect of FA, its incorporation disrupts particle distribution and packing patterns of the specimen matrix, resulting

in increased porosity and the formation of larger unfilled voids between particles. As shown in Figure 6-3b and Figure 6-4, the PCI/FA specimens exhibit a progressively more porous microstructure with increasing FA content. This increased porosity could enhance the connectivity between generated microcracks and voids during the pre-cracking process, producing a larger total crack volume that must be filled during the self-healing phase for the same level of pre-cracking. Furthermore, replacing PCI with FA elevates the w/b ratio, making more water available for cement hydration but simultaneously inducing a dilution effect that decelerates and delays hydration, thereby hindering the precipitation of hydrates and the microstructure refinement. Add to that, the intrinsically slower pozzolanic reactivity of FA further restricts the self-healing potential, even in the presence of CH, while the reduced PCI content constrains the total quantity of hydration products available for crack closure and void filling. This reduction is reflected in the progressive attenuation in weight loss across the entire examined temperature range in Figure 6-9, indicating a declining formation of hydration products with increasing FA dosage. As a result of these combined effects, the healing products generated during the self-healing period are insufficient to close cracks and fill interconnected voids, particularly those of larger width, leading to the persistence of unhealed pathways within the matrix and consequently high hydraulic conductivity in pre-cracked PCI/FA specimens, even after 90 days of self-healing.

6.3.3 Characteristics of Self-healing Cracks

6.3.3.1 Crack closure through self-healing

Figure 6-11 presents the representative microscopic observations of crack closure in pre-cracked specimens with different binder types and dosages before and after the designated self-healing periods of 7, 28, and 90 days. Figure 6-11(a-c) illustrates crack closure in the PCI/BFS system, whereas Figure 6-11(d-f) depicts crack closure in the PCI/FA system. Across all specimens, self-healing products are observed precipitating within surface cracks, progressively filling the pre-introduced crack gaps and, in some cases, achieving complete closure. However, partial or no closure is also documented in specimens containing larger cracks, reflecting the intrinsic limitations of autogenous healing in CPB systems. In these cases, the quantity of self-healing products generated is insufficient to bridge and fill the larger crack widths, consistent with the mechanistic constraints discussed earlier. These distinct closure scenarios align with previous findings for CPB matrices under varying healing conditions (Quan & Fall, 2024, 2025a).

To quantitatively assess and compare the healing performance in crack closure of CPB specimens with different binder types and dosages across the investigated self-healing periods, the widths of fully closed cracks are measured and plotted in Figure 6-12 for all specimens subjected to various healing regimes. It can be seen in Figure 6-12a that crack closure in the PCI/BFS system is strongly influenced by both BFS content and healing duration. In general, the pre-cracked PCI/BFS:80/20 and 50/50 specimens exhibit overall comparable surface crack closure performance to the PCI/BFS:100/0 reference specimens across the studied healing periods. This robust healing performance in surface crack closure can be ascribed to the synergistic contributions of cement hydration, CH carbonation, and slag activation, which collectively lead to accelerated production

of the healing products occupying the crack gaps. However, as healing extended to 90 days, the progressive consumption of CH and cement during hydration slows the rate of healing product formation, thereby reducing crack closure efficiency. For example, the pre-cracked PCI/BFS:80/20 specimens display a comparable crack closure capability, with a maximum healed crack width of 68.8 μm, to that of the reference PCI/BFS:100/0 specimens (i.e., with a maximum healed crack width of 66.2 μm), suggesting that the efficiency in crack closure in PCI/BFS:80/20 specimens is less pronounced than the healing efficiency observed in mechanical strength and permeability recovery, as discussed in Section 6.3.1. This discrepancy reflects the nature of surface crack closure, which is primarily governed by calcite precipitation through CH carbonation (Sisomphon et al., 2012; Sun et al., 2022). In BFS-containing mixtures, a substantial portion of CH is consumed during secondary pozzolanic reactions to form C-S-H gels, thereby reducing the available CH for the carbonation and limiting calcite formation. Consequently, excessive BFS content (e.g., PCI/BFS:20/80) results in the diminished crack closure performance, with the smallest healed crack widths. The reduced cement content in these mixtures constrains both CH availability and the alkaline environment, which are unfavourable for the activation and hydration of BFS. Even though the filler effect of BFS may contribute to early-age properties, the insufficient generation of healing products ultimately hinders the progression of self-healing within the matrix.

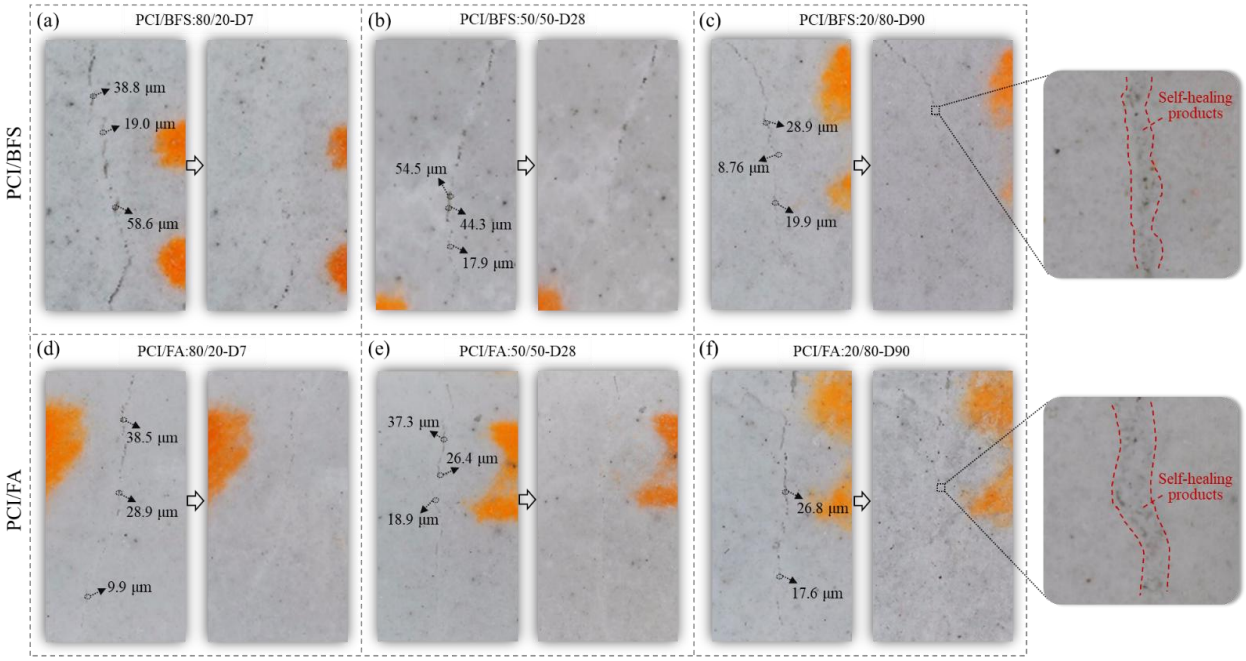

Figure 6-11. Representative images of crack healing in CPB specimens with varying BFS (a-c) and FA (d-f) binder dosages at different self-healing periods.

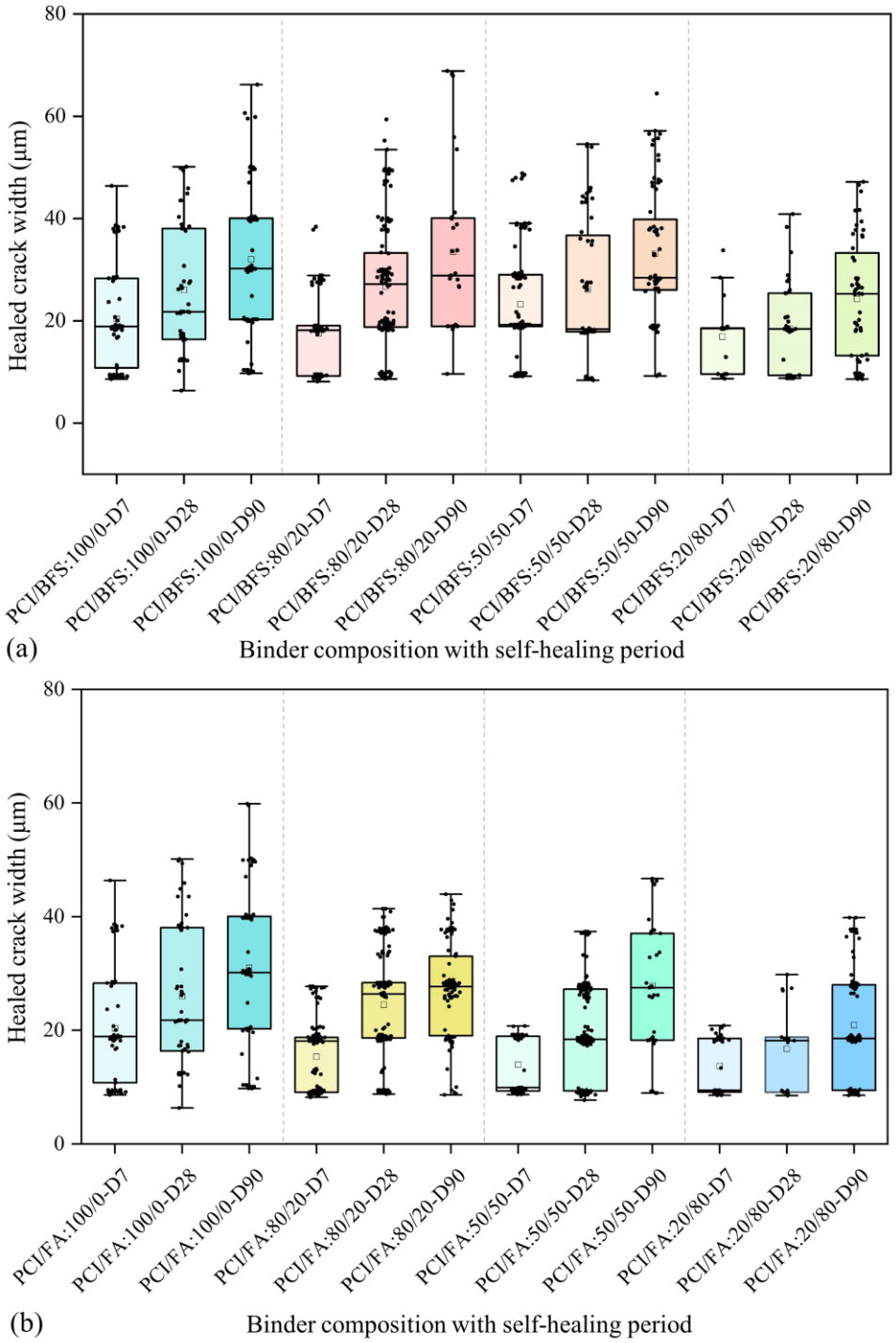

Figure 6-12. Distribution of surface completely healed crack widths on CPB specimens with varying contents of (a) BFS and (b) FA, along with progression of self-healing.

An apparent decline in self-healing efficiency for crack closure is evident in Figure 6-12b with the introduction of FA into the CPB matrix. This deterioration in healing performance becomes particularly pronounced as the FA content increases. The reduced performance can be explained by the combined influence of the physical characteristics of FA, the dilution effect, and its delayed

pozzolanic reactivity, as previously discussed. Owing to the spherical morphology and relatively inert surface of FA particles, their incorporation increases the internal porosity of PCI/FA specimens, resulting in a more porous structure with less cohesion between the particles. Under pre-cracking, microcracks in such a matrix are more susceptible to propagation and interconnection with pre-existing voids, producing larger unfilled spaces within the crack path. Moreover, the inherently slow pozzolanic reactivity of FA contributes to the limited hydration reactions within the studied self-healing period, which implies that the self-healing process is primarily governed by cement hydration within the PCI/FA system. As a result, substituting PCI with FA decreases the available proportion of cement, thereby leading to limited production of healing products and weakening the crack-filling capability. In addition, the reduced PCI content denotes the increase in w/b ratio at a constant binder content, which dilutes the cement particles and slows both the hydration and the precipitation processes of hydrates. This further impedes the rate and extent of self-healing product formation, thereby limiting the crack closure efficiency.

6.3.3.2 Nature comparison of self-healing products

The observed self-healing behaviour in crack closure, as well as the restoration of compressive strength and hydraulic conductivity in the studied PCI/BFS and PCI/FA specimens, can be ascribed to the progressive formation of self-healing products within cracks and voids. To elucidate the compositional differences in these products resulting from BFS or FA incorporation in the CPB system, a combination of analytical techniques, including XRD, FTIR, and SEM-EDS, was employed.

Figure 6-13 presents the XRD patterns of the self-healing products collected from the PCI/BFS, PCI/FA, and PCI-only specimens. Although sampling was targeted at healed cracks, it is practically unavoidable to include portions of the surrounding paste, particularly quartz originating from tailings, BFS, and FA. In the PCI-only specimens (i.e., PCI/BFS:100/0 and PCI/FA:100/0), the dominant self-healing materials, C-S-H, $Ca(OH)_2$, ettringite, and calcite (the latter especially for surface crack), arise primarily from continued cement hydration coupled with carbonation of CH (Quan & Fall, 2025a). As previously discussed, the incorporation of BFS and FA enables secondary reactions with CH to form additional C-(A)-S-H via latent hydraulic and pozzolanic activity, respectively, supplementing cement hydration and contributing to self-healing. In the PCI/BFS system, the characteristic peaks of C-(A)-S-H, ettringite, calcite, and gypsum are clearly evident in the self-healing products. Notably, the higher C-(A)-S-H peak intensity relative to PCI-only specimens correlates with the improved strength and permeability recovery observed in PCI/BFS:80/20 and PCI/BFS:50/50. The detection of a small amount of gypsum in the PCI/BFS specimen most likely indicates a prolonged hydration process, which contributes to the long-term self-healing performance observed in the PCI/BFS:80/20 specimens due to the incomplete hydration of aluminate phases. Moreover, the PCI/FA system displays similar phase assemblages, with more intense gypsum peaks and detectable $Ca(OH)_2$. The presence of unconsumed gypsum and $Ca(OH)_2$ indicates slower hydration kinetics and extended dormant behaviour, aligning with the reduced self-healing efficiency previously noted for FA-containing specimens.

FTIR analysis was also conducted to validate the composition of the self-healing products in the CPB systems with the three different binder types, as shown in Figure 6-14. The absorption peaks located at approximately 451 cm^{-1} and 966 cm^{-1} correspond to the bending vibrations and asymmetric stretching vibrations of Si-O bonds in the silicate tetrahedra SO_4^{4-}, respectively, which are associated with the primary binding phase of C-(A)-S-H (Feng et al., 2023; Hu et al., 2024; Wang et al., 2021). Compared with the self-healing products from the PCI-only specimens, the PCI/BFS specimens show a slight increase in the intensity of these peaks, whereas the PCI/FA specimens exhibit a slight decrease. This variation reflects differences in the degree of silicate polymerization, which in turn suggests variations in the quantity of C-(A)-S-H formed through hydration reactions. These findings are consistent with the previously discussed trends in self-healing efficiency. In addition, the absorption peaks observed at 694 cm^{-1} and 1083 cm^{-1} can be attributed to asymmetrical Si-O bending vibrations and the bands at 777 cm^{-1} and 796 cm^{-1} are related to the symmetric Si-O-Si stretching vibrations, both of which are the typical characteristics of quartz (Hu et al., 2024; Sari et al., 2023; Sun et al., 2022). In the same way, the absorption peak at 875 cm^{-1} is indicative of the bending vibration of CO_3^{2-}, revealing the formation of calcite in the self-healing products (Sun et al., 2022). Furthermore, the absorption band at 1162 cm^{-1} corresponds to the S-O asymmetric stretching vibration of SO_4^{2-}, signifying the presence of ettringite in the matrix (Sari et al., 2023; Zhang et al., 2022).

The morphology of self-healing products was further characterized by SEM-EDS analysis conducted on the crack surface to validate their compositions. Figure 6-15 and Figure 6-16 show the results for the PCI/BFS:50/50 and PCI/FA:50/50 system, respectively, after 90 days of self-healing period. The EDS spectra indicate the presence of primary self-healing products of C-(A)-S-H, calcite, and ettringite, in both CPB mixing systems, as evidenced by the detected Ca, O, Al, S, and Si peaks. It is clearly visible in Figure 6-15 that the PCI/BFS system exhibits a relatively denser distribution of C-(A)-S-H gels in the capillary voids, which is in line with the aforementioned results of XRD, FTIR, and thermal analysis. Note that the detection of primary product C-(A)-S-H gel rather than pure C-S-H is attributed to the incorporation of aluminum released from BFS and FA into the silicate gel structure. While C-(A)-S-H and C-S-H cannot be distinctly differentiated due to their similar morphology and overlapping elemental signals, both contribute to binding the solid particles, which governs the development of mechanical strength and overall stability of the CPB matrix. In contrast, the presence of partially reacted and/or unreacted FA particles in Figure 6-16 suggests the comparatively inferior self-healing efficiency in the PCI/FA system due to the insufficient formation of healing products during the studied self-healing period up to 90 days.

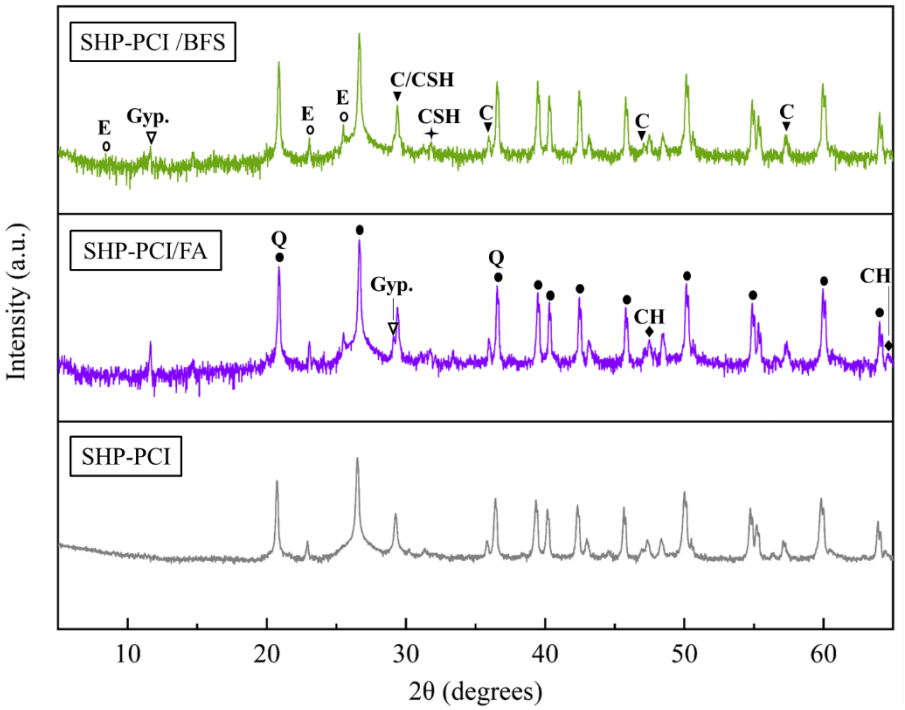

Figure 6-13. XRD profiles of collected self-healing products from PCI/BFS, PCI/FA, and PCI specimens following 90 days of self-healing (Q: Quartz; E.: ettringite; Gyp.: gypsum; C: calcite; CH: calcium hydroxide; SHP: self-healing products).

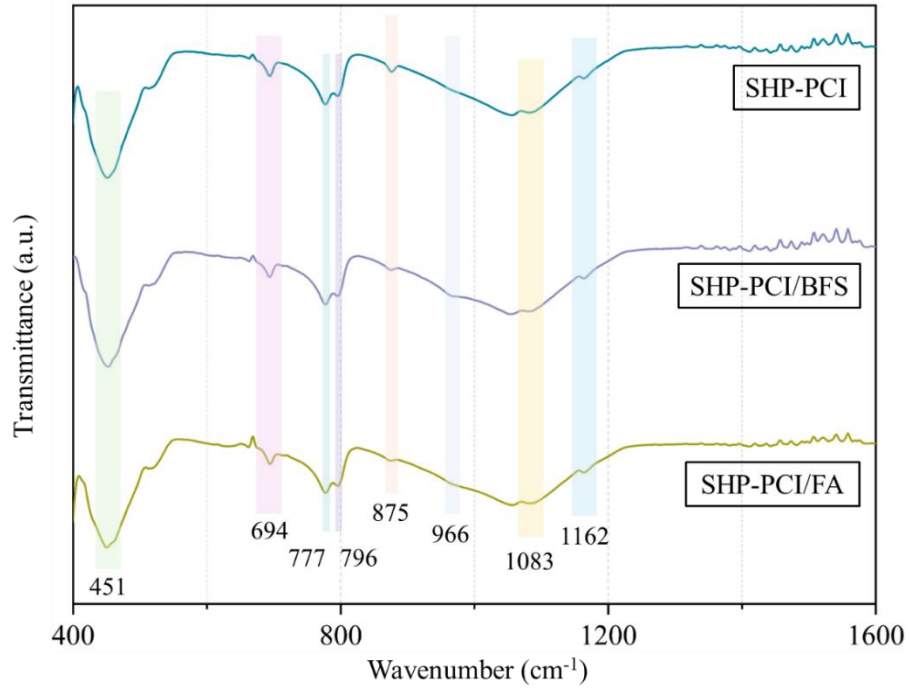

Figure 6-14. FTIR curves of collected self-healing products from PCI/BFS, PCI/FA, and PCI specimens following 90 days of self-healing.

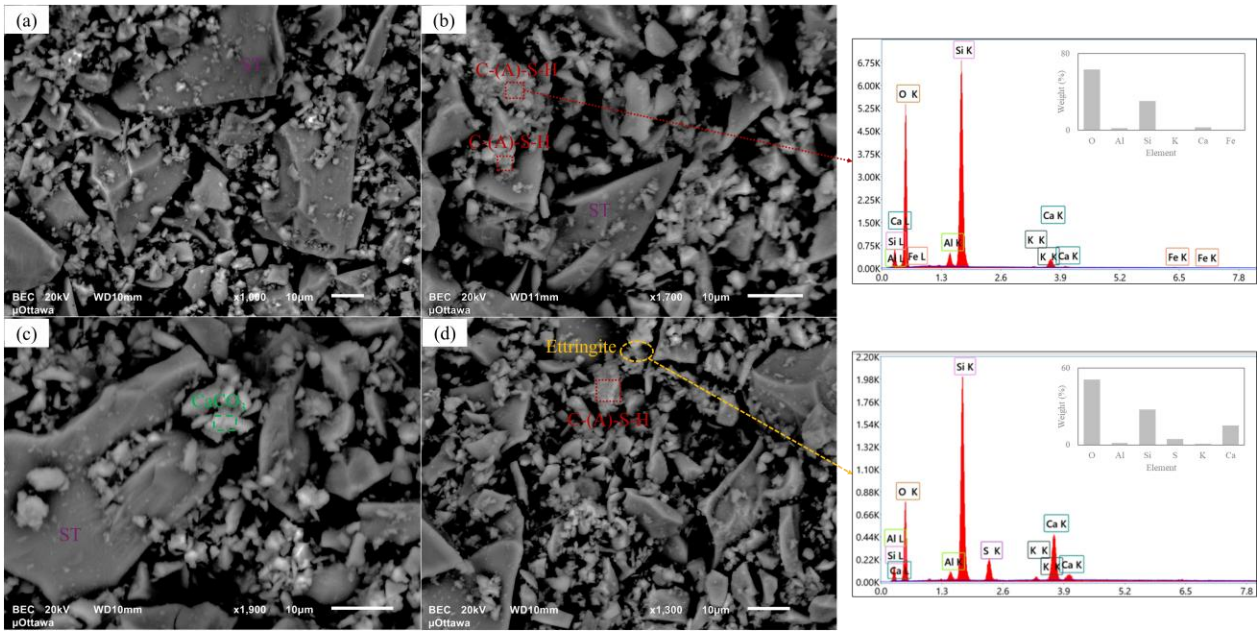

Figure 6-15. SEM-EDS characterization of self-healing products within cracks of PCI/BFS:50/50 specimens following a 90-day self-healing period at multiple locations.

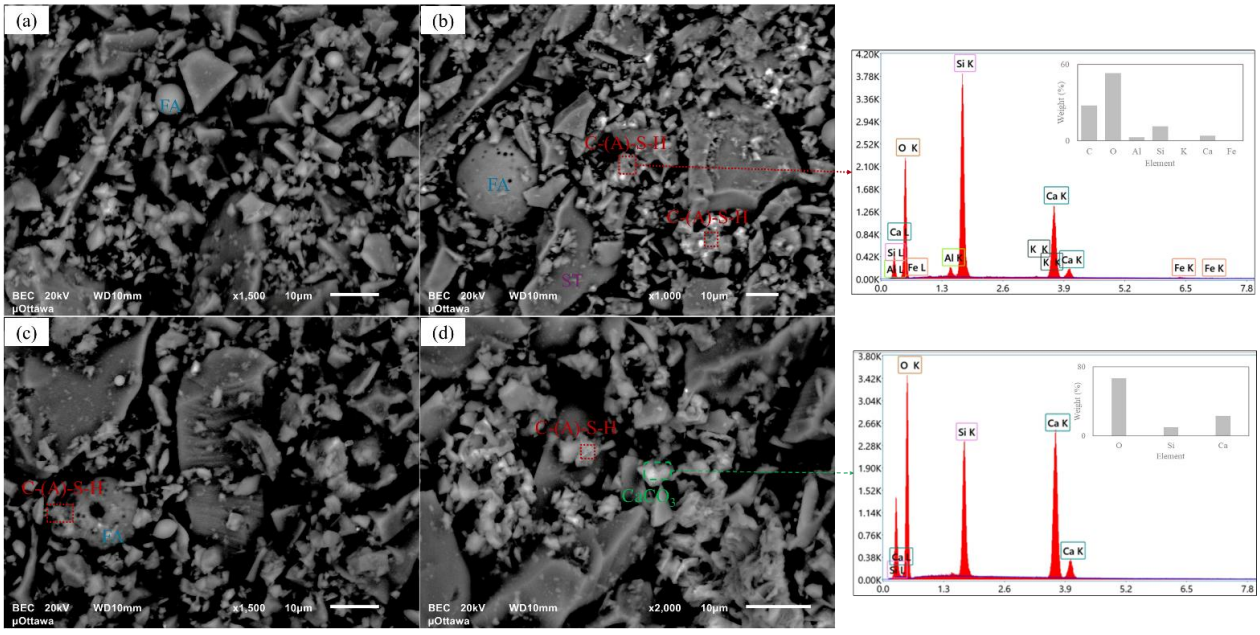

Figure 6-16. SEM-EDS characterization of self-healing products within cracks of PCI/FA:50/50 specimens following a 90-day self-healing period at multiple locations.

6.3.4 Comparison of the Effects of Two SCMs on Self-Healing Performance

The incorporation of SCMs, including BFS and FA, distinctly influences the self-healing performance of the CPB system through their contributions to binder hydration mechanisms and microstructural modifications, which arise from differences in their chemical reactivity and physical characteristics.

BFS is a latent hydraulic material that readily reacts in a calcium-rich environment, particularly in the presence of CH generated from cement hydration, thereby contributing to both early and sustained strength development. Its relatively fine particle size and angular morphology enhance particle packing, promoting a denser matrix formation with smaller pore volume and reduced hydraulic conductivity. This microstructural refinement not only enhances mechanical performance but also promotes self-healing behaviour, as unreacted slag particles continue to hydrate over time, precipitating C-(A)-S-H within cracks and voids. However, the influence of BFS on self-healing efficiency is significantly influenced by its dosage and the available cement in the CPB system, particularly in the absence of external alkali or activators. In this study, a 50% replacement of PCI with BFS (i.e., PCI/BFS:50/50) significantly enhances self-healing performance during the early to medium self-healing periods (7 to 28 days). This improvement is attributed to the synergistic effect of robust cement hydration and latent hydraulic activity, attributed to the sufficient availability of CH and reactive BFS, which facilitates the generation of additional healing products, contributing to crack closure and restoration of mechanical strength and permeability. Furthermore, a moderate reduction in BFS content (i.e., PCI/BFS:80/20) demonstrates even more pronounced self-healing behaviour over extended periods. The relatively higher cement content in this mix sustains the availability of CH, thereby supporting continued slag activation and prolonged pozzolanic reactions within the matrix. Conversely, the PCI/BFS:20/80 mix, with low cement content, limits CH production, which impedes slag activation and suppresses the healing mechanisms associated with continuous cement hydration, thus diminishing the mechanical and permeability-related self-healing efficiencies.

In contrast, the addition of FA significantly reduced the self-healing efficiency in the CPB system in this study, primarily due to its physical characteristics, dilution effect, and delayed pozzolanic reactivity. The similar particle size distribution between FA and the STs compromises the particle packing efficiency within the matrix, increasing voids, crack volumes, porosity, and permeability. Higher FA replacement levels also elevate the w/b ratio, which adversely affects the development of mechanical and permeability properties. This effect arises from the dilution of cement content, which weakens cement hydration and reduces the precipitation of hydration products. Additionally, the reduced cement content limits the production of CH, thereby lowering the internal pH below the threshold required to activate the pozzolanic reaction of FA. The suboptimal chemical environment delays both cement hydration and the pozzolanic contribution of FA, ultimately resulting in reduced self-healing capability in terms of both strength recovery and permeability restoration.

It is important to emphasize that interactions between cement, tailings, and SCMs (BFS or FA) are highly dependent on their physical (e.g., fineness, morphology) and chemical (e.g., mineralogical composition, glass content) properties. These characteristics are largely determined by manufacturing processes, which in turn are influenced by factors such as coal source variability and combustion efficiency for FA, and metallurgical extraction methods for BFS (Behera et al., 2021; Fall et al., 2010; Maltais & Marchand, 1997). Such inherent heterogeneity can lead to

variability in hydration mechanisms and self-healing behaviour, potentially resulting in inconsistent performance within CPB systems.

6.4 Summary and Conclusions

This study investigates the autogenous self-healing behaviour of CPB systems with the incorporation of SCMs, specifically BFS and FA, into the binder matrix. The evaluation considers the evolution of compressive strength, hydraulic conductivity, internal porosity, crack closure, and the formation and composition of self-healing products over a 90-day self-healing period. Based on the experimental results, the following conclusions can be drawn:

- The incorporation of BFS exerts a dual effect on the PCI/BFS system, dependent on BFS content and self-healing duration. During the early to medium self-healing period (i.e., 7 and 28 days), the PCI/BFS:50/50 specimens exhibit the highest self-healing efficiency among all studied mixes, achieving CCS values of 9.7% and 17.2%, respectively. This enhancement can be attributed to the synergistic contributions of cement hydration, activation of BFS latent hydraulic reactions, which promote the formation of additional C-(A)-S-H and result in a refined microstructure. The accumulation of these hydration products effectively fills cracks and voids, promoting the recovery of both mechanical strength and permeability. Due to the reduced availability of unhydrated cement grains and CH, the healing rate of PCI/BFS:50/50 mixture gradually decreases. As the self-healing period extends to 90 days, the PCI/BFS:80/20 specimens demonstrate more sustained long-term self-healing performance with CCS and HCRR values reaching 21.4% and 96.2%, as the higher cement content ensures sufficient availability of CH, which is essential for the BFS latent hydraulic activity.

- The utilized BFS significantly refines the pore structures within the PCI/BFS specimens as its finer particle sizes effectively fill voids between solid constituents. This microstructural refinement becomes increasingly pronounced with increasing BFS content. However, excessive replacement of PCI (e.g., PCI/BFS:20/80) limits the available cement within the matrix, constraining the primary self-healing mechanisms (i.e., cement hydration and carbonation) and restricting the secondary latent hydraulic activation of BFS due to insufficient CH, thereby diminishing the overall self-healing capacity with the ultimate recovered strengths remaining lower than that of uncracked controls and hydraulic conductivity recovery reaching only 58.7%.

- The incorporation of FA considerably undermines the self-healing capacity of the PCI/FA system, with only the PCI/FA:80/20 specimens exhibiting relatively satisfactory healing performance, achieving CCS and HCRR values of 11.9% and 68.9%, respectively, compared with 18.5% and 90.1% for the PCI-only CPB. Its inherent physical characteristics and dormant pozzolanic reactivity contribute to a more porous microstructure, initially compromising matrix stability. Although FA can react with CH to form C-(A)-S-H, its delayed reactivity results in a substantial portion remaining unreacted or slowly reacting,

even in the presence of sufficient CH. This effect, coupled with the increased w/b ratio, further hinders cement hydration and the precipitation of binder hydrates. Increasing FA content further deteriorates the healing efficiency as the amount of early-reactive cement decreases, leading to insufficient healing capacity to restore mechanical strength and permeability. As a result, the PCI/FA:20/80 mixture exhibits negligible strength recovery with a CCS of -23.2% and only 32.3% permeability recovery after 90 days of self-healing.

- The observed self-healing performance in both PCI/BFS and PCI/FA systems is primarily ascribed to the formation of C-(A)-S-H, calcite, and ettringite within cracks and voids. In the PCI/BFS system, the abundant C-(A)-S-H generated via binder hydrations substantially benefits the recovery of strength and permeability, while the calcite is mainly responsible for the surface crack closure. The PCI/FA system exhibits limited hydration, reflected by the relatively higher presence of gypsum and $Ca(OH)_2$ in the self-healing products, suggesting the potential for extended long-term self-healing, albeit with slower efficacy.
- The autogenous self-healing approach has been demonstrated as a promising method to mitigate cracking in the CPB matrix and enhance its long-term durability. The incorporation of SCMs could tackle budgetary constraints by reducing the backfill operational costs and lowering the carbon footprint of mines through reduced Portland cement usage in CPB systems. Accordingly, the findings of this study have direct implications for practical CPB design and application, offering quantitative guidance for the selection of binder type and replacement level to balance short- and long-term autogenous self-healing capacity, enhancing the performance and sustainability of backfill systems.

Despite the significant findings and insights obtained from this study, it is important to acknowledge certain limitations. Only one type of BFS and FA was investigated, whereas in practice, the physical (e.g., fineness, morphology) and chemical (e.g., mineralogical composition, glass content) characteristics of SCMs can vary considerably. Such variations may predominantly affect their interactions with the selected PCI and silica-based tailings used in this study. Moreover, the mineralogical compositions of tailings differ substantially across mining sites, which may limit the direct applicability of these results to all types of mine wastes. Therefore, it is recommended that laboratory-scale testing be conducted for site-specific paste fill formulations to ensure optimal self-healing performance before full-scale implementation. Furthermore, given the superior self-healing performance observed in the PCI/BFS system, future studies could explore the incorporation of an external source of alkali (e.g., alkali activators or engineered triggers) to sustain or enhance BFS activation beyond what is achievable through cement hydration alone, potentially further improving the self-healing capability of CPB.

6.5 References

Akmalaiuly, K., Berdikul, N., Pundienė, I., & Pranckevičienė, J. (2023) The effect of mechanical activation of fly ash on cement-based materials hydration and hardened state properties. Materials, 16, 2959.

Ali, G., Fall, M., & Alainachi, I. (2021) Time-and temperature-dependence of rheological properties of cemented tailings backfill with sodium silicate. Journal of Materials in Civil Engineering, 33, 04020498.

Arachchilage, C. B., Fan, C., Zhao, J., Huang, G., & Liu, W. V. (2023) A machine learning model to predict unconfined compressive strength of alkali-activated slag-based cemented paste backfill. Journal of Rock Mechanics and Geotechnical Engineering, 15, 2803-2815.

ASTM. (2016). ASTM D5084-16a. Standard Test Methods for Measurement of Hydraulic Conductivity of Saturated Porous Materials Using a Flexible Wall Permeameter. In. West Conshohocken, PA: ASTM International.

ASTM. (2021). ASTM C39/C39M-21. Standard Test Method for Compressive Strength of Cylindrical Concrete Specimens. In. West Conshohocken, PA: ASTM International.

ASTM. (2023). ASTM D854-23. Standard Test Methods for Specific Gravity of Soil Solids by the Water Displacement Method. In. West Conshohocken, PA: ASTM International.

Azam, S., & Li, Q. (2010) Tailings dam failures: a review of the last one hundred years. Geotechnical news, 28, 50-54.

Behera, S., Ghosh, C., Mishra, D., Singh, P., Mishra, K., Buragohain, J., & Mandal, P. K. (2020b) Strength development and microstructural investigation of lead-zinc mill tailings based paste backfill with fly ash as alternative binder. Cem. Concr. Compos., 109, 103553.

Behera, S., Ghosh, C., Mishra, K., Mishra, D., Singh, P., Mandal, P., . . . Sethi, M. (2020a) Utilisation of lead–zinc mill tailings and slag as paste backfill materials. Environmental Earth Sciences, 79, 1-18.

Behera, S., Mishra, D., Singh, P., Mishra, K., Mandal, S. K., Ghosh, C., . . . Mandal, P. K. (2021) Utilization of mill tailings, fly ash and slag as mine paste backfill material: Review and future perspective. Constr. Build. Mater., 309, 125120.

Bentz, D. P., Peltz, M. A., & Winpigler, J. (2009) Early-age properties of cement-based materials. II: Influence of water-to-cement ratio. Journal of materials in civil engineering, 21, 512-517.

Benzaazoua, M., Fall, M., & Belem, T. (2004) A contribution to understanding the hardening process of cemented pastefill. Miner. Eng., 17, 141-152.

Bhatty, J. I. (1991) A review of the application of thermal analysis to cement-admixture systems. Thermochimica Acta, 189, 313-350.

Biernacki, J. J., Williams, P. J., & Stutzman, P. E. (2001) Kinetics of reaction of calcium hydroxide and fly ash. ACI Mater. J., 98, 340-349.

Bijen, J. (1996) Benefits of slag and fly ash. Constr. Build. Mater., 10, 309-314.

Bisschop, J., & Wittel, F. K. (2011) Contraction gradient induced microcracking in hardened cement paste. Cem. Concr. Compos., 33, 466-473.

Briki, Y., Zajac, M., Haha, M. B., & Scrivener, K. (2021) Factors affecting the reactivity of slag at early and late ages. Cem. Concr. Res., 150, 106604.

Burciaga-Díaz, O., & Betancourt-Castillo, I. (2018) Characterization of novel blast-furnace slag cement pastes and mortars activated with a reactive mixture of MgO-NaOH. Cem. Concr. Res., 105, 54-63.

Chindasiriphan, P., Yokota, H., & Pimpakan, P. (2020) Effect of fly ash and superabsorbent polymer on concrete self-healing ability. Constr. Build. Mater., 233, 116975.
Damtoft, J. S., Lukasik, J., Herfort, D., Sorrentino, D., & Gartner, E. M. (2008) Sustainable development and climate change initiatives. Cem. Concr. Res., 38, 115-127.
Darquennes, A., Olivier, K., Benboudjema, F., & Gagné, R. (2016) Self-healing at early-age, a way to improve the chloride resistance of blast-furnace slag cementitious materials. Constr. Build. Mater., 113, 1017-1028.
Dong, L., Tong, X., Li, X., Zhou, J., Wang, S., & Liu, B. (2019) Some developments and new insights of environmental problems and deep mining strategy for cleaner production in mines. Journal of Cleaner Production, 210, 1562-1578.
Ercikdi, B., Kesimal, A., Cihangir, F., Deveci, H., & Alp, İ. (2009) Cemented paste backfill of sulphide-rich tailings: Importance of binder type and dosage. Cem. Concr. Compos., 31, 268-274.
Escalante, J., Gomez, L., Johal, K., Mendoza, G., Mancha, H., & Mendez, J. (2001) Reactivity of blast-furnace slag in Portland cement blends hydrated under different conditions. Cem. Concr. Res., 31, 1403-1409.
Fall, M., Adrien, D., Célestin, J., Pokharel, M., & Touré, M. (2009) Saturated hydraulic conductivity of cemented paste backfill. Miner. Eng., 22, 1307-1317.
Fall, M., & Benzaazoua, M. (2005) Modeling the effect of sulphate on strength development of paste backfill and binder mixture optimization. Cem. Concr. Res., 35, 301-314.
Fall, M., Célestin, J., Pokharel, M., & Touré, M. (2010) A contribution to understanding the effects of curing temperature on the mechanical properties of mine cemented tailings backfill. Eng. Geol., 114, 397-413.
Fall, M., & Pokharel, M. (2010) Coupled effects of sulphate and temperature on the strength development of cemented tailings backfills: Portland cement-paste backfill. Cem. Concr. Compos., 32, 819-828.
Feng, Y., Qi, W., Zhao, Q., Huang, Y., Ren, Q., Qi, W., & Kong, F. (2023) Synthesis and characterization of cemented paste backfill: Reuse of multiple solid wastes. Journal of Cleaner Production, 383, 135376.
Franks, D. M., Stringer, M., Torres-Cruz, L. A., Baker, E., Valenta, R., Thygesen, K., . . . Barrie, S. (2021) Tailings facility disclosures reveal stability risks. Scientific reports, 11, 5353.
Ghirian, A., & Fall, M. (2015) Coupled behavior of cemented paste backfill at early ages. Geotech. Geol. Eng., 33, 1141-1166.
Grice, T. (1998) Underground mining with backfill. 2nd Annual Summit œ Mine Tailings Disposal Systems, Brisbane, Nov, 696, 24-25.
Hassani, F., Razavi, S., & Isagon, I. (2007) A study of physical and mechanical behaviour of gelfill. CIM Bull, 100.
Hewlett, P., & Liska, M. (2019). Lea's chemistry of cement and concrete: Butterworth-Heinemann.
Hu, Y., Hu, R., Zhang, B., & Han, B. (2024) Research on mechanical properties and mix proportion design of solid waste-based cemented paste backfill. Case Stud. Constr. Mater., 21, e03618.
Huang, H., Ye, G., & Damidot, D. (2014) Effect of blast furnace slag on self-healing of microcracks in cementitious materials. Cem. Concr. Res., 60, 68-82.
Ighalo, J. O., Kurniawan, S. B., Iwuozor, K. O., Aniagor, C. O., Ajala, O. J., Oba, S. N., . . . Igwegbe, C. A. (2022) A review of treatment technologies for the mitigation of the toxic environmental effects of acid mine drainage (AMD). Process Safety and Environmental Protection, 157, 37-58.

Jiang, H., Han, J., Li, Y., Yilmaz, E., Sun, Q., & Liu, J. (2020a) Relationship between ultrasonic pulse velocity and uniaxial compressive strength for cemented paste backfill with alkali-activated slag. Nondestructive Testing and Evaluation, 35, 359-377.
Jiang, H., Yi, H., Yilmaz, E., Liu, S., & Qiu, J. (2020b) Ultrasonic evaluation of strength properties of cemented paste backfill: Effects of mineral admixture and curing temperature. Ultrasonics, 100, 105983.
Kar, K. K. (2021). Handbook of fly ash: Butterworth-Heinemann.
Kesimal, A., Yilmaz, E., Ercikdi, B., Alp, I., & Deveci, H. (2005) Effect of properties of tailings and binder on the short-and long-term strength and stability of cemented paste backfill. Mater. Lett., 59, 3703-3709.
Klein, K., & Simon, D. (2006) Effect of specimen composition on the strength development in cemented paste backfill. Canadian geotechnical journal, 43, 310-324.
Kratzsch, H. (2012). Mining subsidence engineering: Springer Science & Business Media.
Li, W., & Fall, M. (2018) Strength and self-desiccation of slag-cemented paste backfill at early ages: Link to initial sulphate concentration. Cem. Concr. Compos., 89, 160-168.
Lim, S., & Wee, T. (2000) Autogenous shrinkage of ground-granulated blast-furnace slag concrete. Materials Journal, 97, 587-593.
Maltais, Y., & Marchand, J. (1997) Influence of curing temperature on cement hydration and mechanical strength development of fly ash mortars. Cem. Concr. Res., 27, 1009-1020.
Manmohan, D., & Mehta, P. (1981) Influence of pozzolanic, slag, and chemical admixtures on pore size distribution and permeability of hardened cement pastes. Cement, Concrete, and Aggregates, 3, 63-67.
Manzi, M., Cooper, G., Malehmir, A., Durrheim, R., & Nkosi, Z. (2015) Integrated interpretation of 3D seismic data to enhance the detection of the gold-bearing reef: Mponeng Gold mine, Witwatersrand Basin (South Africa). Geophysical Prospecting, 63, 881-902.
Mojid, M. A. (2011). Diffuse double layer (DDL). In Encyclopedia of agrophysics (pp. 213-214): Springer.
Nägele, E. (1986) The Zeta-potential of cement: Part II: Effect of pH-value. Cem. Concr. Res., 16, 853-863.
Narmluk, M., & Nawa, T. (2011) Effect of fly ash on the kinetics of Portland cement hydration at different curing temperatures. Cem. Concr. Res., 41, 579-589.
Nguyễn, H. H., Choi, J.-I., Song, K.-I., Song, J.-K., Huh, J., & Lee, B. Y. (2018) Self-healing properties of cement-based and alkali-activated slag-based fiber-reinforced composites. Constr. Build. Mater., 165, 801-811.
Niu, Q., Feng, N., Yang, J., & Zheng, X. (2002) Effect of superfine slag powder on cement properties. Cem. Concr. Res., 32, 615-621.
Ogunmakinde, O. E., Egbelakin, T., & Sher, W. (2022) Contributions of the circular economy to the UN sustainable development goals through sustainable construction. Resources, Conservation and Recycling, 178, 106023.
Pane, I., & Hansen, W. (2005) Investigation of blended cement hydration by isothermal calorimetry and thermal analysis. Cem. Concr. Res., 35, 1155-1164.
Pokharel, M., & Fall, M. (2011) Coupled Thermochemical Effects on the Strength Development of Slag-Paste Backfill Materials. Journal of Materials in Civil Engineering, 23, 511-525.
Qi, C., & Fourie, A. (2019) Cemented paste backfill for mineral tailings management: Review and future perspectives. Miner. Eng., 144, 106025.
Qi, T., Feng, G., Zhang, Y., Guo, J., & Guo, Y.-x. (2015) Effects of fly ash content on properties of cement paste backfilling. Journal of Residuals Science & Technology, 12, 133-141.

Quan, W., & Fall, M. (2024) Temperature-driven crack self-healing and performance recovery in cemented tailings materials. Case Stud. Constr. Mater., 21, e04105.
Quan, W., & Fall, M. (2025a) Investigation of crack self-healing behaviour and its impact on strength and permeability recovery in cemented paste tailings. Powder Technology, 457, 120834.
Quan, W., & Fall, M. (2025b) Self-healing responses of cementitious tailings materials to changing drainage conditions. Developments in the Built Environment, 22, 100648.
Ranjith, P. G., Zhao, J., Ju, M., De Silva, R. V., Rathnaweera, T. D., & Bandara, A. K. (2017) Opportunities and challenges in deep mining: a brief review. Engineering, 3, 546-551.
Rico, M., Benito, G., Salgueiro, A., Díez-Herrero, A., & Pereira, H. (2008) Reported tailings dam failures: a review of the European incidents in the worldwide context. Journal of hazardous materials, 152, 846-852.
Sahmaran, M., Yildirim, G., & Erdem, T. K. (2013) Self-healing capability of cementitious composites incorporating different supplementary cementitious materials. Cem. Concr. Compos., 35, 89-101.
Sakai, E., Miyahara, S., Ohsawa, S., Lee, S.-H., & Daimon, M. (2005) Hydration of fly ash cement. Cem. Concr. Res., 35, 1135-1140.
Sari, M., Yilmaz, E., & Kasap, T. (2023) Long-term ageing characteristics of cemented paste backfill: Usability of sand as a partial substitute of hazardous tailings. Journal of Cleaner Production, 401, 136723.
Sinsiri, T., Chindaprasirt, P., & Jaturapitakkul, C. (2010) Influence of fly ash fineness and shape on the porosity and permeability of blended cement pastes. International Journal of Minerals, Metallurgy, and Materials, 17, 683-690.
Sisomphon, K., Copuroglu, O., & Koenders, E. (2012) Self-healing of surface cracks in mortars with expansive additive and crystalline additive. Cem. Concr. Compos., 34, 566-574.
Sohn, H. Y., & Moreland, C. (1968) The effect of particle size distribution on packing density. The Canadian Journal of Chemical Engineering, 46, 162-167.
Sun, B., Ye, G., & De Schutter, G. (2022) A review: Reaction mechanism and strength of slag and fly ash-based alkali-activated materials. Constr. Build. Mater., 326, 126843.
Sun, J., Kong, K. H., Lye, C. Q., & Quek, S. T. (2022) Effect of ground granulated blast furnace slag on cement hydration and autogenous healing of concrete. Constr. Build. Mater., 315, 125365.
Sun, X., Liu, J., Qiu, J., Wu, P., & Zhao, Y. (2022) Alkali activation of blast furnace slag using a carbonate-calcium carbide residue alkaline mixture to prepare cemented paste backfill. Constr. Build. Mater., 320, 126234.
Sveinson, S. (1999). Characterisation of tailings for paste backfill system design. University of British Columbia,
Takemoto, K. (1980). Hydration of pozzolanic cements. Paper presented at the Proc. 7th International congress on the chemistry of cements, 1980.
Taylor, H. F. (1997). Cement chemistry (Vol. 2): Thomas Telford London.
Termkhajornkit, P., Nawa, T., Yamashiro, Y., & Saito, T. (2009) Self-healing ability of fly ash–cement systems. Cem. Concr. Compos., 31, 195-203.
Thomas, M. (2007). Optimizing the use of fly ash in concrete (Vol. 5420): Portland Cement Association Skokie, IL, USA.
UNEP. (2020). Global Industry Standard on Tailings Management. Retrieved from https://www.unep.org/resources/report/global-industry-standard-tailings-management

Valenta, R. K., Lèbre, É., Antonio, C., Franks, D. M., Jokovic, V., Micklethwaite, S., . . . Segura-Salazar, J. (2023) Decarbonisation to drive dramatic increase in mining waste–Options for reduction. Resources, Conservation and Recycling, 190, 106859.

Wang, C.-l., Ren, Z.-z., Huo, Z.-k., Zheng, Y.-c., Tian, X.-p., Zhang, K.-f., & Zhao, G.-f. (2021) Properties and hydration characteristics of mine cemented paste backfill material containing secondary smelting water-granulated nickel slag. Alexandria Engineering Journal, 60, 4961-4971.

Wang, X.-Y. (2014) Effect of fly ash on properties evolution of cement based materials. Constr. Build. Mater., 69, 32-40.

Wang, X.-Y., & Lee, H.-S. (2010) Simulation of a temperature rise in concrete incorporating fly ash or slag. Materials and Structures, 43, 737-754.

Xiao, B., Fall, M., & Roshani, A. (2021) Towards understanding the rheological properties of slag-cemented paste backfill. International Journal of Mining, Reclamation and Environment, 35, 268-290.

Xu, A., Sarkar, S., & Nilsson, L.-O. (1993) Effect of fly ash on the microstructure of cement mortar. Materials and Structures, 26, 414-424.

Xu, D., Zhang, D., Wang, D., & Qi, G. (2022) Effects of GGBFS on hydration and carbonation process, microstructure, and mechanical properties of NHL-based materials. J. Build. Eng., 60, 105149.

Ye, H., & Radlińska, A. (2016) Fly ash-slag interaction during alkaline activation: Influence of activators on phase assemblage and microstructure formation. Constr. Build. Mater., 122, 594-606.

Yilmaz, E., Belem, T., Benzaazoua, M., Kesimal, A., Ercikdi, B., & Cihangir, F. (2011b) Use of high-density paste bacfill for safe disposal of copper/zinc mine tailings. Gospodarka Surowcami Mineralnymi-Mineral Resources Management, 81-94-81-94.

Yilmaz, E., Belem, T., Bussière, B., & Benzaazoua, M. (2011a) Relationships between microstructural properties and compressive strength of consolidated and unconsolidated cemented paste backfills. Cem. Concr. Compos., 33, 702-715.

Zhang, F., Li, Y., Zhang, J., Gui, X., Zhu, X., & Zhao, C. (2022) Effects of slag-based cementitious material on the mechanical behavior and heavy metal immobilization of mine tailings based cemented paste backfill. Heliyon, 8.

Zhang, Z., Qian, S., & Ma, H. (2014) Investigating mechanical properties and self-healing behavior of micro-cracked ECC with different volume of fly ash. Constr. Build. Mater., 52, 17-23.

Zhao, Y., Taheri, A., Karakus, M., Chen, Z., & Deng, A. (2020) Effects of water content, water type and temperature on the rheological behaviour of slag-cement and fly ash-cement paste backfill. International Journal of Mining Science and Technology, 30, 271-278.

Zhou, N., Dong, C., Zhang, J., Meng, G., & Cheng, Q. (2021) Influences of mine water on the properties of construction and demolition waste-based cemented paste backfill. Constr. Build. Mater., 313, 125492.

Chapter 7 Integration of Results and Discussions

7.1 Introduction

The implementation of CPB is recognized as an effective strategy for minimizing the environmental footprint of mining activities while providing structural support to underground excavations. However, the progressive development of cracks within CPB structures can significantly compromise their integrity and serviceability, undermining safety and long-term durability. In this research, the autogenous self-healing method has been investigated to restore the mechanical and permeability characteristics of CPB under multiphysical conditions, addressing the crack challenges. Specifically, Section 7.2 synthesizes representative results, presenting the fundamental mechanisms and behaviour of self-healing in CPB. Additionally, this section includes complementary results from CPB materials incorporating natural tailings to demonstrate the feasibility and effectiveness of self-healing in broader practical mining backfill scenarios. Furthermore, Section 7.3 provides a comparative summary of Chapters 5 and 6, presenting the influence of multiphysical factors (i.e., healing/curing temperature, drainage condition, crack-inducing stress, sulphate concentration, and mineral additives) on the self-healing behaviour and efficiency of CPB.

7.2 Research Result Synthesis and Discussion

The investigation of autogenous self-healing in CPB is inspired by the concept of self-healing, which has been successfully applied to conventional cementitious materials (e.g., concrete, mortar, engineered cementitious composites, etc.). In this research, the incorporation of silica tailings (STs) is scientifically valid and representative of the tailings used to prepare CPB materials in practice. The STs are produced through the identical crushing and grinding production processes as natural tailings (NT), originating from natural rocks of the same geological source. Moreover, STs satisfy industrial requirements for paste tailings, specifically containing at least 15 wt.% of particles finer than 20 μm. Their dominant quartz composition reflects the major mineralogical constituent of tailings produced from many Canadian hard-rock mines and other hard-rock mining operations worldwide, making STs highly representative of the natural tailings commonly employed in paste technology. Accordingly, STs have been widely adopted as a representative substitute for NTs in numerous experimental investigations on paste tailings and CPB systems, which enable the accurate control of the mineralogical components of the tailings, minimizing uncertainties when investigating the intrinsic self-healing performance of CPB.

The obtained results and findings reveal a promising autogenous self-healing performance in CPB under the ambient exposure condition without external interference and healing additives, which is primarily attributed to two main fundamental mechanisms: (i) continuous hydration of unhydrated cement particles, and (ii) carbonation of calcium hydroxide.

Firstly, the formation of crystal-like healing products (e.g., C-S-H, $CaCO_3$, ettringite, and $Ca(OH)_2$) contributes to the crack closure through the precipitation inside the cracks or along the crack paths, resulting in three distinct healing scenarios: complete healing, partial healing, and no healing as

represented in Figure 7-1. Notably, the extent of healing is strongly influenced by the initial crack width and geometry; narrower, shorter, and shallower cracks demonstrate a higher potential of complete crack closure due to the smaller volume that requires filling. Larger cracks, on the other hand, often remain partially or completely unhealed, indicating the limitations of inherent autogenous healing in CPB, with crack width being a critical factor influencing the self-healing efficiency.

Secondly, the studied pre-cracked CPB specimens can recover/restore their mechanical strengths comparable to the uncracked ones generally after only approximately 7 days of self-healing period, regardless of the initial pre-cracking levels under certain healing conditions. This strength restoration is attributed to the continuous hydration of unhydrated cement particles. At an extended self-healing period (i.e., 90 days), the healed pre-cracked specimens surpassed the strength of the uncracked controls, especially those pre-cracked at earlier curing ages when more unhydrated cement remained. Add to that, as hydration progresses and the availability of unreacted cement diminishes, the carbonation of calcium hydroxide becomes the dominant healing mechanism at the advanced self-healing period. The presence of cracks provides pathways for the transport of O_2, CO_2, and H_2O inside the CPB matrix, which are essential for facilitating the hydration reactions and self-healing mechanisms. The generated healing products gradually refine the initial pore structures, filling the cracks and voids as the self-healing progresses, thus decreasing the porosity and void ratio of pre-cracked specimens and contributing to the mechanical strength recovery and development.

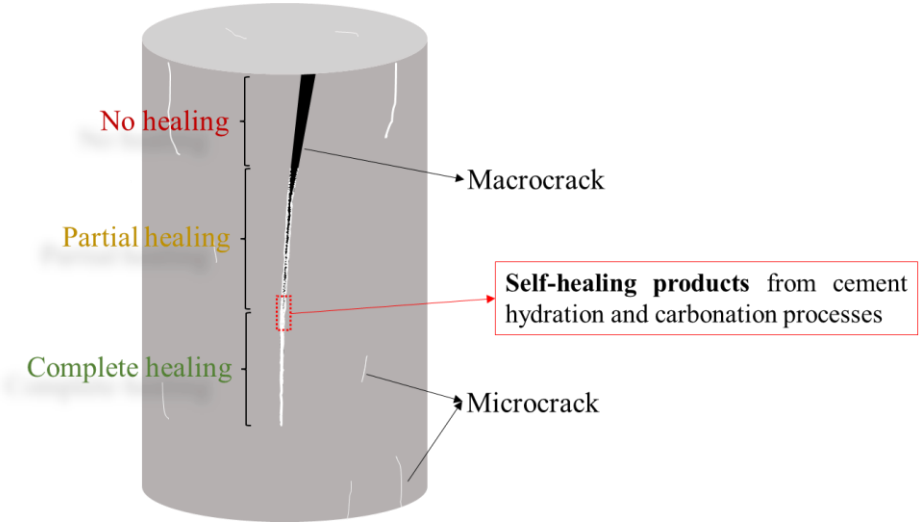

Figure 7-1. Schematic representation of three healing scenarios with precipitation of healing products.

Thirdly, as the autogenous healing progresses, the healing products precipitate and fill in the voids and cracks, resulting in a more refined pore structure within the matrix to block the internal connections, thus decreasing the hydraulic conductivity (permeability) of the pre-cracked CPB specimens. It is noted that the full recovery of hydraulic conductivity cannot be achieved due to

the presence of unhealed or partially healed macrocracks within the CPB matrix. The limited availability of cement particles in the CPB mixture, which dominates the capability of autogenous healing, restricts the amount of the produced self-healing products. As a result, the generated macrocracks cannot be fully healed due to insufficient self-healing products.

Complementary tests were also conducted on CPB prepared with NTs sourced from a Canadian polymetallic mine to further validate the representativeness of STs with the introduction of different PSDs and mineralogical compositions, as shown in Figure 7-2 and Figure 7-3, respectively. This natural variability reflects more realistic conditions of CPB performance in field applications. Compared to silica tailings, the considered NTs exhibit a significantly broader and coarser particle size distribution, indicating the coexistence of both fine and coarse fractions (Figure 7-2). Additionally, the chemical composition of the NTs is markedly more heterogeneous, rendering the material chemically active and potentially reactive in cementitious environments (Figure 7-3). Of particular significance is the detection of 0.26 wt.% sulphur, which suggests the presence of sulphate-bearing minerals in the tailings. NT-CPB specimens were subjected to an initial curing (IC) period of 3 days prior to crack induction. A single pre-cracking level (PC100%) was employed, followed by self-healing periods of 1, 7, 28, and 90 days under ambient exposure conditions. The experimental program was designed to mirror that of Batch IC3 using silica tailings, as described in Chapter 4.

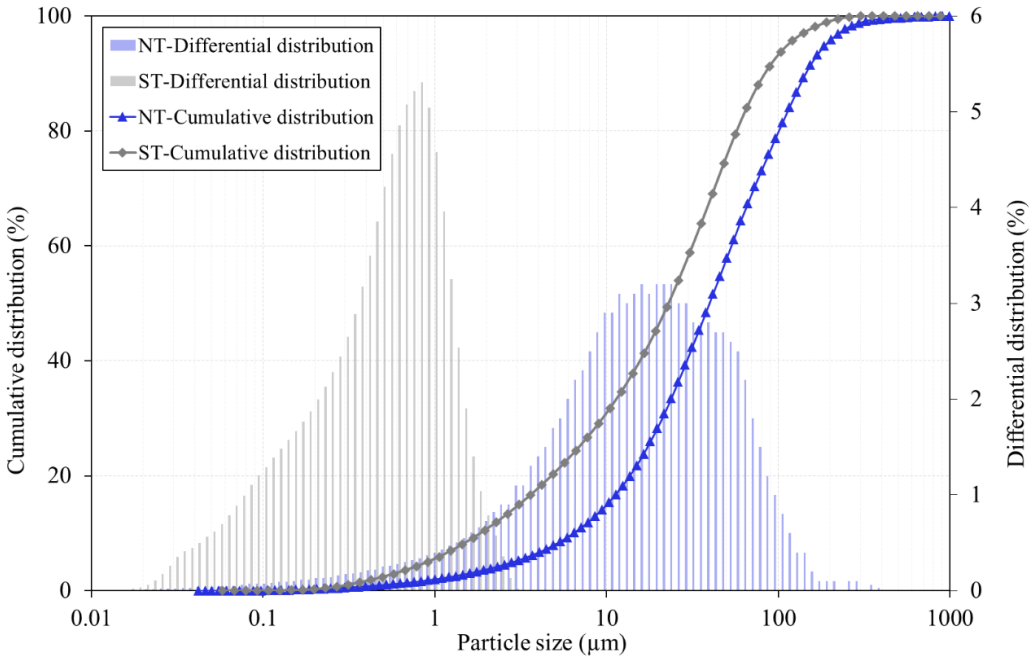

Figure 7-2. Comparison of particle size distributions between natural tailings and silica tailings.

The NT-CPB specimens exhibit consistent self-healing behaviour, as evidenced by crack closure, and partial to substantial recovery of mechanical strength and permeability properties. In addition to the two determined self-healing mechanisms: (i) continued hydration of unhydrated cement particles and (ii) carbonation of calcium hydroxide, the self-healing efficiency of NT-CPB

specimens is also significantly dominated by the sulphate-influenced self-healing processes with the formation of secondary hydration products, ettringite and gypsum (as elucidated in Section 5.2 and summarized in Section 7.3.4).

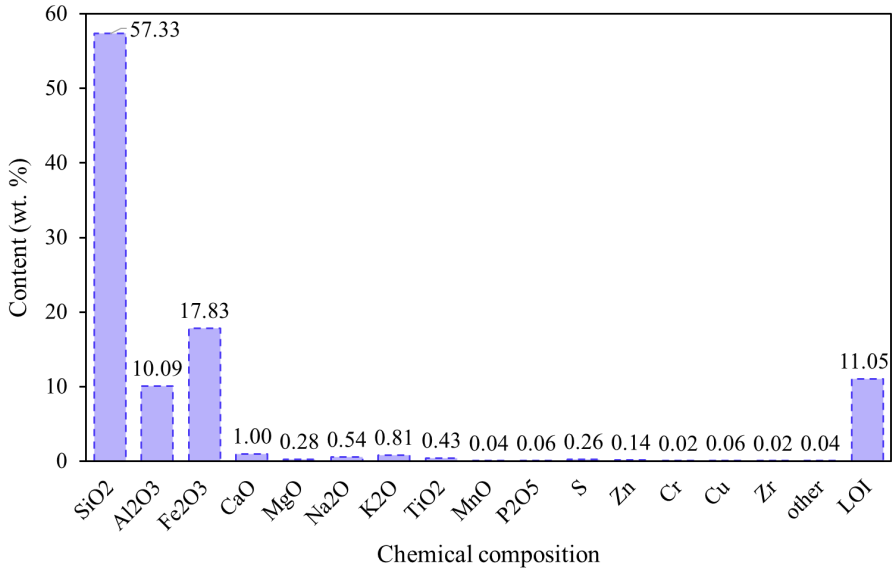

Figure 7-3. Chemical compositions of the used polymetallic mine tailings.

During the self-healing period up to 28 days, the NT-CPB specimens exhibit three distinct crack closure scenarios: complete healing, partial healing, and no healing, depending on factors such as crack width, healing duration, and the reactivity of the tailings (Figure 7-5). Morphological observations reveal the appearance of a rust-like coloration on the specimen surfaces at 28 days, likely due to the oxidation of pyrite present in the tailings. Notably, both compressive strength and hydraulic conductivity demonstrate substantial recovery over this period (Figure 7-4). This improvement is primarily attributed to the formation and precipitation of cement hydration and secondary products (i.e., ettringite, gypsum, C-S-H, $Ca(OH)_2$, and $CaCO_3$), which fill the cracks and voids, thereby refining the microstructure and enhancing both strength and permeability. However, as healing progresses into the advanced period (i.e., 90 days), the recovery trends for compressive strength and hydraulic conductivity begin to diverge. Specifically, healing indices such as the CCS and HCRR show a declining trend, which correlates with the visual observation of newly formed or extended cracks in the NT-CPB specimens (Figure 7-5f and Figure 7-6), compromising the structural integrity of the matrix. In addition, it is noted in Figure 7-6 that some "break-out" features accompanied by new cracks exhibit on the surface of the specimens filled by white crystalline materials. SEM-EDS analysis identified these infills as ettringite (Figure 7-7). As previously discussed in Section 5.2, the excessive formation of expansive minerals such as ettringite, whose volume is approximately 2.5 times that of the original reactants, can exert substantial internal pressure within pre-existing microcracks and capillary pores. This expansion results in physical damage to the CPB matrix, manifesting as newly generated cracks (i.e., Figure 7-5 and Figure 7-6) and ultimately compromising long-term healing performance. In addition,

weaker C-S-H gels are usually produced due to the sulphate absorption by C-S-H, leading to the undermined ability to bind hydration/solid particles, thus diminishing the self-healing efficiency.

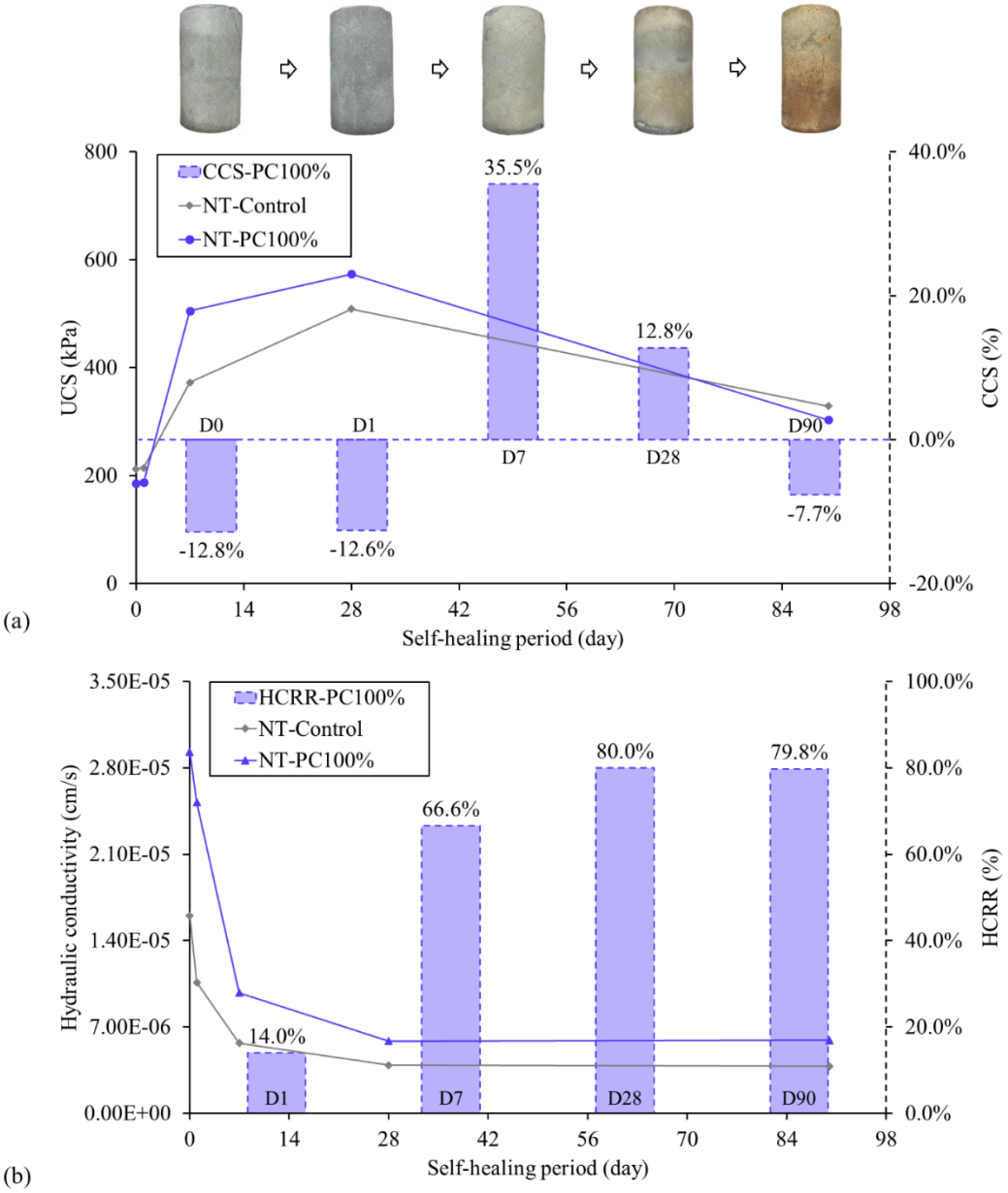

Figure 7-4. Recovery of (a) compressive strength and (b) hydraulic conductivity of natural tailings incorporated in CPB specimens over the self-healing period.

Despite the inherent variability in PSDs and mineralogical compositions, the NT-CPB specimens exhibit consistent self-healing (autogenous healing) behaviour with those obtained from ST-based CPB. This consistency confirms that the use of STs is not only a scientifically sound approach for studying CPB self-healing mechanisms but also one that reliably reflects the performance of NTs under realistic field conditions. It is important to note that due to the variability in the geochemical and mineralogical properties of different tailings, tailored strategies are essential to optimize the

healing efficiency. For example, in sulphide-rich tailings where sulphate attack poses a risk to long-term performance, the use of additives such as slag may help mitigate sulphate-related damage and promote more durable self-healing behaviour.

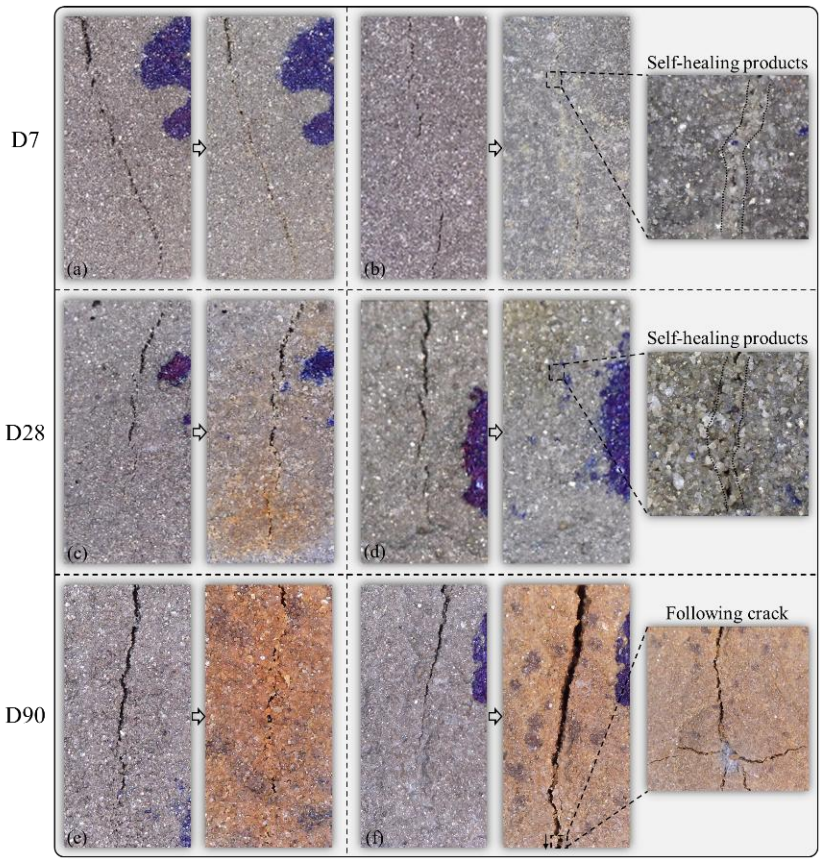

Figure 7-5. Typical observations of crack closure and self-healing products.

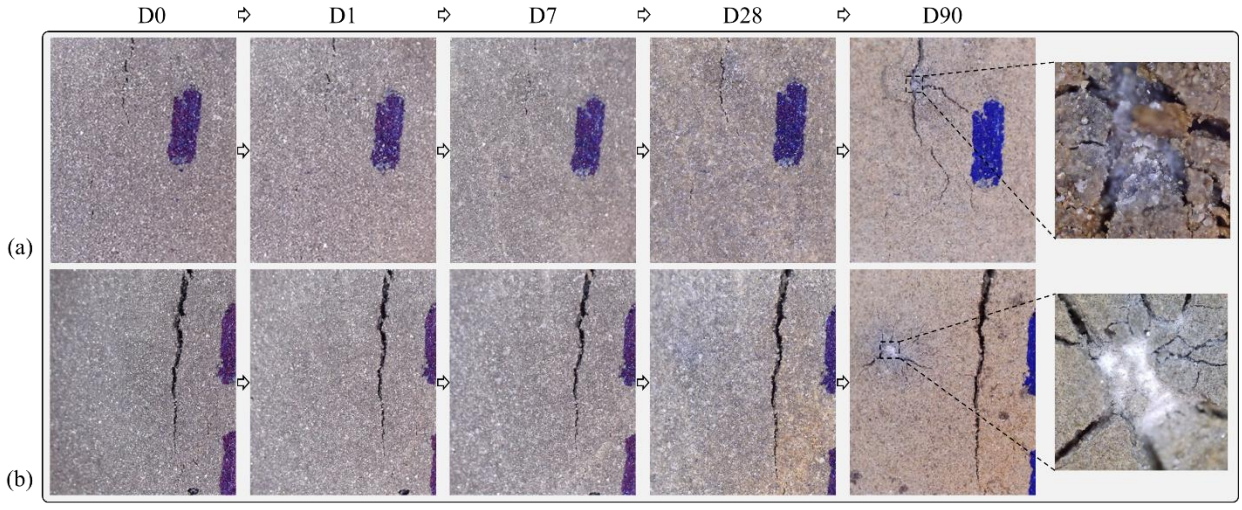

Figure 7-6. Appearance of the “break-out” features accompanied by new cracks on the specimen surface.

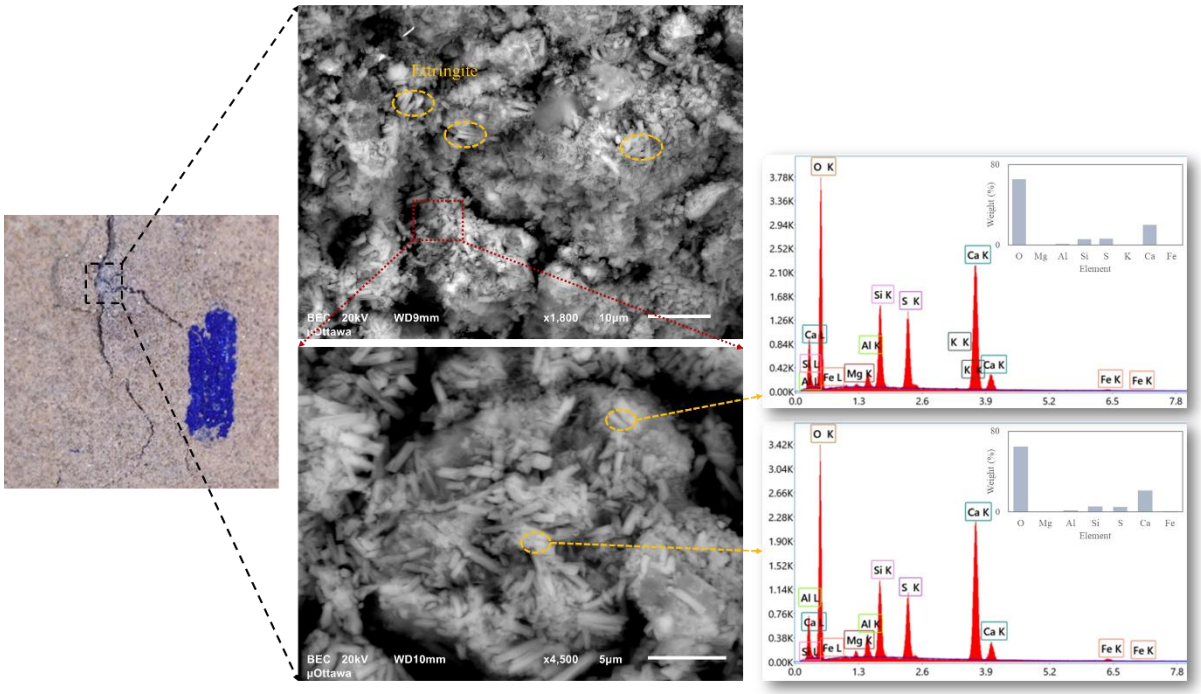

Figure 7-7. SEM-EDS detection of infilled products in the "break-out".

7.3 Role of Multiphysical Factors on Self-healing Behaviour of CPB

7.3.1 Effect of Thermal Factor

Temperature variation within CPB structures arises primarily from two sources: (i) external heat exchange with the surrounding rock mass or atmosphere via heat conduction and/or advection, and (ii) internal heat generation due to exothermic reactions from cement hydration and/or the oxidation of sulphide minerals (Fall et al., 2010). As presented in Section 5.3, the efficiency of the primary self-healing mechanisms in CPB (continued hydration of unhydrated cement particles and the carbonation of calcium hydroxide) is markedly influenced by exposure temperature, with tested ranges including 2, 20, 35, and 50°C.

At low temperatures (e.g., 2°C), CPB specimens exhibit delayed and significantly diminished self-healing performance. This is attributed to the temperature sensitivity of cement hydration reactions, which proceed at a reduced rate under cold conditions due to the inhibition effect. As a result, insufficient hydration products are generated, leading to minimal recovery in mechanical and permeability properties. Poor crack closure is particularly evident in specimens exposed to these cold curing conditions. Conversely, elevated temperatures (e.g., ≥20°C) substantially improve the self-healing capacity of CPB. Increased healing temperature accelerates cement hydration and facilitates the greater formation of healing products (i.e., C-S-H, $CaCO_3$, $Ca(OH)_2$) given the same self-healing period. These products contribute to more efficient crack closure and even larger crack widths. The refined pore structure also leads to a denser microstructure, which enhances compressive strength recovery and reduces hydraulic conductivity over the self-healing period.

Notably, at 50°C, no strength inversion or adverse cross-over effects are observed. This phenomenon is likely mitigated by the dilution effect arising from the high water content in the CPB matrix, which supports sustained hydration and healing reactions. However, the availability of unhydrated cement particles decreases over longer periods, resulting in a slower healing rate after a self-healing period of 90 days.

Overall, temperature is a critical factor influencing the self-healing capacity of CPB. In cold or permafrost regions, where cracks may remain unhealed or only partially healed, it may be necessary to adopt supplementary measures, such as incorporating additives that facilitate low-temperature hydration to ensure resilience and structural integrity in cold mining environments. In contrast, in deep underground mines where temperatures are elevated, the combination of ambient heat and exothermic hydration could induce localized evaporation. Excessive evaporation under such conditions may lead to moisture loss, potentially impeding the long-term self-healing efficiency, as self-healing processes in cementitious materials require moisture to enable hydration and carbonation reactions. The findings underscore the necessity of considering thermal conditions in the design and implementation of CPB structures. Tailoring the self-healing strategy to site-specific temperature profiles is essential to ensure long-term structural integrity, mechanical resilience, and durability of CPB structures in diverse mining environments.

7.3.2 Effect of Hydraulic Factor

Hydraulic conditions, such as pore water pressure, volumetric water content, and drainage, evolve rapidly following CPB placement and exert immediate influence on the development of its properties. Once CPB is placed underground, drainage begins to occur, governed primarily by site-specific factors, including geological formations, groundwater conditions, seepage, barricade, and permeability of CPB materials, permeability of the rock mass surrounding the backfill structure, etc. In practice, CPB structures often experience drainage conditions that fall between the two extremes of full drainage and no drainage; thus, the drainage environment is typically considered partially drained under field conditions. Therefore, Section 5.4 systematically assesses the effects of three downward axial drainage conditions on the autogenous healing capacity and behaviour of CPB material.

For undrained specimens, the dominant self-healing mechanisms remain consistent with those previously identified, including i) continuous hydration of unhydrated cement particles and ii) carbonation of calcium hydroxide. However, a slight delay in the onset of healing is observed during the early self-healing period. This is primarily due to dilution effects and dissolution reactions that slow cement hydration. Specifically, the use of additional mixing water to ensure CPB pumpability increases the w/c ratio, which in turn dilutes cement particle concentration and reduces the availability of calcium and hydroxyl ions within the pore solution. This impedes the early formation of hydration products necessary for healing. Moreover, the excess water reduces surface energy and weakens van der Waals forces between hydration products (Yang et al., 2011), thereby delaying their precipitation and negatively affecting microstructural development and property recovery. In contrast, drained specimens (i.e., under full or half drainage conditions)

exhibit significantly enhanced self-healing efficiency and faster healing rates. These improvements are attributed to the synergistic effects of water drainage, one-dimensional consolidation, and optimized hydration conditions. Drainage enables excess water to bleed from the fresh CPB matrix, promoting the settlement of suspended solids and facilitating denser particle packing through self-desiccation. This leads to a refined pore structure and reductions in both porosity and void ratio. Simultaneously, the reduction in pore water pressure increases the effective stress within the matrix, enhancing consolidation and interparticle bonding, particularly between tailings and hydration products. Furthermore, the improved hydraulic environment accelerates cement hydration owing to the reduced w/c ratio. As hydration reactions proceed, water is consumed, further reducing pore water pressure and increasing effective stress. This fosters concentrated precipitation of hydration healing products within cracks and capillary voids, contributing to crack closure and a more cohesive microstructure. The localized healing products serve not only to heal microcracks but also to reinforce the particle-matrix interface, thereby improving self-healing efficiency in mechanical strength recovery and permeability reduction under drainage conditions.

Effective water management, particularly during early-stage curing, can significantly enhance healing efficiency and structural performance. In field applications, optimizing drainage pathways and tailoring backfill mixture designs to site-specific hydraulic conditions may offer a practical strategy for improving the long-term durability and integrity of CPB structures.

7.3.3 Effect of Mechanical Factor

Upon displacement into underground, CPB structures are subjected to a variety of in situ stress conditions, such as self-weight, overlying rock mass, mining-induced stresses, rock mass movement, or rock wall closure, which can impose compressive, tensile, and shear stresses on the CPB structures, introducing the different cracking pattern/crack damage, such as shear, tensile, and mixed-mode (shear-tensile) cracks (Li et al., 1998; Pan et al., 2021). To replicate these stress conditions, multiple crack-inducing approaches are adopted. In addition to the conventional uniaxial compression method, which typically produces mixed tensile-shear crack patterns, two alternative loading (pre-cracking) methods were employed, including i) triaxial compression, which predominantly generates shear cracks under confined stress states, and ii) indirect tensile (Brazilian) testing, which produces pure tensile cracks across the disc specimens. These methods enable the controlled introduction of diverse crack geometries and damage profiles. Section 5.5 explores how different crack types and their associated stress conditions influence the autogenous self-healing capacity of CPB materials.

The pre-cracked CPB specimens under uniaxial compression loading demonstrate a promising self-healing performance in mechanical and permeability recoveries. The pronounced self-healing performance can be primarily attributed to two previously identified self-healing mechanisms, including i) continued hydration of unhydrated cement particles and ii) carbonation of calcium hydroxide. Both mechanisms produce solid self-healing products that deposit along the crack surfaces and within crack voids, thereby bridging the crack gaps and restoring interparticle bonding. Beyond these chemical processes, the mechanical conditions associated with uniaxial compression

loading also play a significant role in the healing process. The crack morphology generated under uniaxial compression is generally a combination of axial tensile and inclined shear cracks. After the pre-cracking, the shear cracks tend to remain tightly compressed or partially closed, resulting in relatively narrow apertures compared with the wider tensile cracks. Such geometries provide a favourable environment for self-healing, as smaller crack widths enhance the efficiency of precipitation, deposition, and densification of self-healing products, which accelerate crack closure and strengthen particle bonding. Similarly, the pre-cracked specimens subjected to the triaxial compression loading perform comparably promising healing efficiency in mechanical recovery and enhanced healing efficiency in permeability. In the same way, besides the chemical self-healing mechanisms, the combined effects of the favourable crack morphology under confined conditions promote the healing efficiency. The triaxial compression loading restricts the crack propagation and branching, resulting in the suppressed tensile cracks and shear cracks that remained partially closed and/or under compression. This confinement yields narrower crack apertures and a localized crack network that collectively provide favourable conditions for self-healing. Furthermore, the geometry of the crack networks facilitates the ingress of CO_2, which improves the carbonation of calcium hydroxide to calcite, contributing to the crack filling. And the crack pathways allow the evaporation of excess water from the CPB matrix during the self-healing phase, which reduces the local w/c ratio to enhance the cement hydration and precipitation of self-healing products, further improving mechanical integrity and microstructural refinement.

However, the pre-cracked specimens subjected to the indirect tensile loading show a significantly limited self-healing efficiency, which is attributed to the crack geometry generated in the disc-shaped specimens under tension. The indirect tensile pre-cracking loading produces dominant mode I tensile cracks that almost traverse the entire disc with large crack apertures, splitting the specimen into two segments, which considerably undermines the structural integrity of the disc-shaped specimen. Given the limitation of the autogenous self-healing capacity of the CPB materials, the insufficient self-healing products fail to effectively bridge the wide crack gaps, leaving the cracks largely unclosed and exhibiting slight mechanical reconnection or permeability improvement after self-healing.

7.3.4 Effect of Chemical Factor

The presence of sulphate ions in CPB systems is a critical factor affecting the long-term durability and chemical stability of backfill structures. Sulphate ions, which commonly originate from sulphide-rich tailings, the use of sulfur dioxide/air in cyanide destruction processes, the incorporation of gypsum ($CaSO_4 \cdot 2H_2O$) or anhydrite ($CaSO_4$) to regulate cement setting, and mine process waters, can initiate internal sulphate attack within the CPB matrix. These reactions are often associated with strength degradation and alterations in pore structure (Fall & Pokharel, 2010; Fall & Benzaazoua, 2005).

In the context of self-healing, however, the role of sulphate ions can be dual in nature. On the one hand, excessive sulphate concentrations may hinder the self-healing process by disrupting the microstructural integrity and inhibiting cement hydration. On the other hand, under controlled

concentrations, sulphate ions can contribute positively to the self-healing mechanism by forming additional solid phases that fill cracks and refine the pore network. The self-healing performance is governed by not only the previously determined mechanisms, but also the secondary hydrated products (i.e., ettringite and gypsum) formed by the reaction of sulphate ions with CH and C_3A, resulting in a combination of self-healing products: ettringite, gypsum, C-S-H, $Ca(OH)_2$, and $CaCO_3$.

The impact of varying sulphate concentrations, ranging from low (<5000 ppm) to very high (25000 ppm), on the self-healing capacity of CPB is elucidated in Section 5.2. During the early self-healing period (up to 28 days), the presence of sulphate ions is found to enhance healing performance, particularly in specimens exposed to 15,000 ppm, which exhibit the most robust healing efficiency between 7 and 28 days. However, a delayed healing response is observed at the highest concentration of 25,000 ppm, attributed to the inhibitory effect of excessive sulphate on binder hydration. This favourable self-healing performance is primarily due to the beneficial precipitation of secondary phases (ettringite and gypsum), which effectively fill microcracks and refine the internal pore network. Additionally, the availability of pre-crack spaces provides sufficient space to accommodate these expansive products, as illustrated in Figure 5-13, further enhancing the healing efficiency. These adverse effects can be attributed to three main factors: (i) physical damage from excessive formation of expansive minerals (ettringite and gypsum) in microcracks and capillary pores; (ii) production of weaker C-S-H gel because of sulphate absorption by C-S-H; and (iii) reduced amount of hydration products due to the inhibition of cement hydration at high sulphate concentrations. Conversely, specimens exposed to 5,000 ppm sulphate maintain a positive healing trajectory. At this lower concentration, cement hydration is not significantly inhibited, enabling the continued formation of hydration products and the effective healing of cracks and pores, thereby enhancing the self-healing efficiency.

These findings are particularly relevant in mining environments with prevalent sulphate exposure, where the intrinsic self-healing ability of CPB may mitigate the adverse effects of sulphate attack on structural stability and environmental performance, contributing to safer underground operations and helping minimize the long-term environmental risks associated with tailings and mine backfill systems.

7.3.5 Effect of Mineral Additives

Portland cement (PC) has been the most widely used hydraulic binder in the mining industry for the preparation of CPB mixtures, as its hydration process primarily governs the development of mechanical and durability properties in CPB structures. However, the relatively high cost of PC and the environmental footprint of its production have motivated increasing use of SCMs, particularly BFS and FA, to partially replace PC. Such substitutions not only lower binder-related costs but also mitigate the environmental impact of PC production by lowering CO_2 emissions (Andrew, 2018). In addition, the incorporation of SCMs contributes to the modification of CPB properties through their distinct chemical reactivity and physical characteristics. Therefore,

Chapter 6 elucidates the effects of incorporating BFS and FA as mineral additives on the autogenous self-healing efficiency of CPB materials.

The influence of BFS on CPB self-healing is primarily attributed to its latent hydraulic activity and physical characteristics. In calcium-rich environments, BFS reacts with CH released from cement hydration to generate additional C-(A)-S-H phases, which progressively fill and bridge microcracks. At appropriate replacement levels (e.g., at PCI/BFS:50/50 and PCI/BFS:80/20), this synergistic interaction between cement hydration and BFS activation enhances both early- and long-term self-healing efficiency, contributing to crack closure and improved recovery of mechanical and permeability properties. In addition, the relatively fine PSD and angular morphology of BFS enhance the particle packing within the CPB matrix, reduce porosity, and further benefit the self-healing performance. However, excessive BFS replacement (e.g., PCI/BFS:20/80) can limit CH availability, thereby hindering both slag activation and continued cement hydration associated with self-healing reactions, which ultimately diminishes the self-healing efficiency of CPB. In contrast, the incorporation of FA generally exhibits a detrimental effect on the self-healing efficiency of CPB, ascribed to the physical characteristics, dilution effect, and delayed pozzolanic reactivity of the utilized FA. The comparable PSDs between FA and the STs compromise the particle packing efficiency within the matrix, which increases the internal voids and porosity, leading to more continuous and larger cracks requiring greater self-healing products to achieve closure. Moreover, the prolonged initial dormant period, because of its slower reaction kinetics and reduced cement content, induces a suboptimal chemical environment for the self-healing processes. Hence, the increasing content of FA also elevates the effective w/c ratio within the CPB matrix, which adversely affects the development of mechanical and permeability properties. This effect arises from the dilution of cement content, which weakens cement hydration and reduces the precipitation of hydration products.

It is noteworthy that in the absence of external activators, the self-healing performance of BFS- and FA-bearing CPB is governed by the intrinsic interactions among cement, tailings, and the SCMs. These interactions are strongly dependent on the physical (e.g., fineness, morphology) and chemical (e.g., mineralogical composition, glass content) characteristics of the SCMs. Such properties, however, are not uniform and largely depend on their production processes, for example, coal source variability and combustion efficiency for FA, and metallurgical extraction methods for BFS (Maltais & Marchand, 1997; Behera et al., 2021). Consequently, the inherent heterogeneity of SCMs can lead to inconsistent hydration reactions and variable self-healing behaviour in CPB. This emphasizes the necessity of site-specific laboratory evaluations of SCM types and proportions to ensure optimal self-healing performance in practical backfilling applications.

7.4 Novel Contributions of the Research

This doctoral research represents the first comprehensive and systematic investigation of the autogenous self-healing behaviour of cemented paste backfill (CPB), an essential yet previously unexplored property of this material system that plays a critical role in underground mine stability and sustainability. While self-healing has been extensively studied in conventional cementitious

materials such as concrete and mortar, no prior studies have characterized or quantified self-healing in CPB, whose distinct composition (low binder content, high tailings fraction, and variable THMC conditions) fundamentally differentiates it from traditional cement-based materials. The novelty of this work lies in its integrated experimental framework, multiphysical coupling perspective, and mechanistic interpretation of autogenous healing processes within CPB. The main contributions can be summarized as follows.

(a) *First demonstration of autogenous self-healing in CPB*

This research provides the first direct experimental evidence that CPB possesses a measurable autogenous self-healing capability. Through controlled pre-cracking, healing, and re-testing procedures, the study demonstrates that CPB can partially or fully close micro- and macro-cracks, recover a substantial portion of its mechanical strength, and significantly reduce its hydraulic conductivity without any external healing agents. The healing is shown to result primarily from continued binder hydration, dissolution-precipitation reactions, and the formation of crystalline products such as C-S-H, $CaCO_3$, $Ca(OH)_2$, ettringite, and gypsum. This finding fundamentally extends the current understanding of CPB durability by introducing self-healing as an intrinsic performance mechanism.

(b) *Development of a unified experimental methodology for CPB self-healing evaluation*

A robust and reproducible experimental framework was established to evaluate self-healing efficiency through a combination of macroscopic performance recovery tests (uniaxial compressive strength, tensile and shear strength, and hydraulic conductivity) and microscopic/microchemical characterizations (e.g., SEM-EDS, XRD, TG/DTG, FTIR, MIP, and XR-μCT). This integrated methodology enables multi-scale assessment of healing processes and provides the first standardized protocol for quantifying self-healing performance in CPB under different environmental and mechanical conditions.

(c) *Comprehensive assessment of multiphysical (THMC) effects on CPB self-healing*

A key novelty of this doctoral research lies in its systematic and integrative evaluation of the thermal, hydraulic, mechanical, and chemical (THMC) factors that simultaneously govern the self-healing performance of CPB. This is the first study to decouple and then interrelate these multiphysical influences through a series of controlled laboratory investigations designed to replicate realistic underground mine environments. The resulting framework provides a mechanistic understanding of how each factor independently and interactively affects the kinetics, extent, and durability of the autogenous healing process in CPB.

- *Thermal (**T**) effects:* Temperature exerts a dominant control over the rate and extent of CPB self-healing by influencing hydration and carbonation reactions within the cementitious matrix. The experimental results demonstrate that elevated curing temperatures (35-50 °C), representative of deep-mine thermal conditions, markedly accelerate the dissolution of anhydrous cement phases and enhance the secondary hydration of unreacted clinker grains, leading to the formation of abundant C-S-H and CH. These reactions promote rapid crack infilling and densification of the microstructure, resulting in faster and more complete recovery

of compressive strength and permeability. Conversely, low temperatures near 2 °C, which are analogous to permafrost or cold-mine environments, retard hydration kinetics and suppress the precipitation of healing products, yielding minimal crack closure or property recovery even after extended healing periods. This quantification of thermal sensitivity offers the first evidence-based guideline for predicting self-healing efficiency across temperature gradients encountered in Canadian and international underground mines.

- *Hydraulic (**H**) effects:* The study establishes the critical role of hydraulic boundary conditions, specifically water drainage and saturation state, in governing self-healing efficiency. Controlled experiments under full, partial, and no drainage scenarios revealed that drainage enhances healing through two coupled mechanisms: (i) facilitating the continuous supply and redistribution of pore water necessary for ongoing hydration and ion migration, and (ii) enabling the removal of excess water that could otherwise inhibit hydration or promote leaching. Full-drainage conditions led to significant reductions in porosity and hydraulic conductivity, accompanied by the precipitation of self-healing products within microcracks. In contrast, undrained conditions produced limited healing due to stagnant pore water chemistry and restricted ionic exchange. These findings provide a mechanistic explanation for field observations that CPB placed in well-drained stopes tends to exhibit superior long-term stability and reduced permeability.

- *Mechanical (**M**) effects:* Another major contribution of this research is the first comparative assessment of self-healing in CPB subjected to cracks induced under distinct loading regimes, including uniaxial compression, triaxial shear, and indirect tensile stress. The results demonstrate that the geometry, orientation, and confinement of cracks generated under different stress states strongly influence healing outcomes. Shear and confined compression cracks, characterized by narrow apertures and tortuous paths, provide favourable geometries for product precipitation and crack bridging, thereby exhibiting high healing efficiency. In contrast, tensile cracks, which are wider and less confined, show limited closure due to the reduced likelihood of contact between crack surfaces and slower diffusion of healing reactants. This mechanistic insight is crucial for understanding how in-situ stress regimes and mining-induced loading conditions influence the self-repair potential of CPB in deep mines.

- *Chemical (**C**) effects:* The influence of the internal chemical environment, especially sulphate concentration, on CPB self-healing was also investigated for the first time. The study revealed a dual or "threshold" effect: at low to moderate sulphate concentrations (≤ 5,000 ppm), sulphate ions stimulate additional ettringite and gypsum formation within cracks, enhancing sealing and densification. However, at higher concentrations (≥25,000 ppm), excessive sulphate ingress leads to expansive reactions, microcracking, and partial degradation of previously healed zones, thereby compromising mechanical recovery. This nuanced understanding of sulphate-driven healing and deterioration underscores the importance of chemical compatibility between backfill composition and mine water chemistry.

- *Integrated implications:* Together, these results demonstrate that self-healing in CPB is governed by the interactions among THMC processes, where favourable combinations of temperature, drainage, stress confinement, and moderate chemical environment promote synergistic healing responses. The comprehensive THMC framework developed in this study establishes a predictive, mechanistic basis for assessing CPB durability under field-relevant multiphysical conditions. It provides a mechanistic basis to bridge the gap between laboratory-scale healing observations and large-scale mine performance assessment, thereby enabling engineers to design self-healing backfill systems optimized for site-specific thermal, hydraulic, mechanical, and chemical environments.

(d) *Discovery of the role of mineral additives in autogenous healing*

The study pioneers the evaluation of supplementary cementitious materials (SCMs), specifically blast furnace slag and fly ash, and elucidates their influence on the intrinsic autogenous self-healing capacity of CPB. Their impacts arise from differences in chemical reactivity and physical characteristics. The results show that the appropriate selection of SCM type and the optimization of SCM replacement ratios can enhance hydration kinetics, pore structure refinement, and precipitation of healing products, which collectively improve strength and permeability recovery. This introduces a new pathway for designing low-carbon, self-healing CPB formulations with improved sustainability and durability.

(e) *Establishment of microstructural and mechanistic models of self-healing in CPB*

By integrating experimental evidence from chemical, mineralogical, and microstructural analyses, this thesis develops conceptual models describing the mechanisms and stages of autogenous self-healing in CPB under varying THMC conditions. These models elucidate the interplay between crack geometry, moisture state, and chemical reactions that control the nucleation and growth of healing products within cracks and pores. The models serve as a scientific foundation for future numerical simulations and predictive design tools for self-healing backfill systems.

(f) *Practical implications for design, maintenance, and sustainability of backfill structures*

This research provides the first science-based framework for integrating self-healing into CPB design practice. The findings demonstrate how controlling curing temperature, drainage, binder composition, and exposure chemistry can significantly enhance the long-term integrity and environmental performance of CPB structures in underground mines. The proposed insights contribute to reducing binder consumption and extending service life, thereby supporting cost-effective, low-carbon, and resilient mine backfilling strategies.

In summary, this Ph.D. work transforms the understanding of cemented paste backfill from a passive load-bearing material to a self-adaptive, self-healing system capable of automatic recovery from damage. The originality lies not only in discovering and quantifying this phenomenon but also in establishing the mechanistic, methodological, and practical foundations for its application in sustainable underground mining and geo-infrastructure design.

7.5 References

Maltais, Y., & Marchand, J. (1997) Influence of curing temperature on cement hydration and mechanical strength development of fly ash mortars. Cem. Concr. Res., 27, 1009-1020.

Behera, S., Mishra, D., Singh, P., Mishra, K., Mandal, S. K., Ghosh, C., . . . Mandal, P. K. (2021) Utilization of mill tailings, fly ash and slag as mine paste backfill material: Review and future perspective. Constr. Build. Mater., 309, 125120.

Ogunmakinde, O. E., Egbelakin, T., & Sher, W. (2022) Contributions of the circular economy to the UN sustainable development goals through sustainable construction. Resources, Conservation and Recycling, 178, 106023.

Andrew, R. M. (2018). Global CO2 emissions from cement production. Earth System Science Data, 10(1), 195-217.

Fall, M., & Pokharel, M. (2010). Coupled effects of sulphate and temperature on the strength development of cemented tailings backfills: Portland cement-paste backfill. Cement and concrete composites, 32(10), 819-828.

Fall, M., & Benzaazoua, M. (2005). Modeling the effect of sulphate on strength development of paste backfill and binder mixture optimization. Cement and Concrete Research, 35(2), 301-314.

Fall, M., Célestin, J. C., Pokharel, M., & Touré, M. (2010). A contribution to understanding the effects of curing temperature on the mechanical properties of mine cemented tailings backfill. Engineering Geology, 114(3-4), 397-413.

Yang, Y., Yang, E. H., & Li, V. C. (2011). Autogenous healing of engineered cementitious composites at early age. Cement and concrete research, 41(2), 176-183.

Li, V. C., Lim, Y. M., & Chan, Y.-W. (1998). Feasibility study of a passive smart self-healing cementitious composite. Composites Part B: Engineering, 29, 819-827.

Pan, A., Jafari, M., Guo, L., & Grabinsky, M. (2021) Hybrid failure of cemented paste backfill. Minerals, 11, 1141.

Chapter 8 Conclusions and Recommendations

8.1 General Conclusions

The main objective of this research is to explore the self-healing (autogenous healing) behaviour of CPB materials and investigate its self-healing efficiency under multiphysical impacting factors or conditions. To demonstrate the achievement of autogenous self-healing behaviour in CPB materials, a preliminary experimental study was first conducted to explore the impacts of age of cracking, pre-cracking levels, crack widths, and self-healing periods on the healing performance. Thereafter, a systematic experimental program, including the effects of thermal (i.e., curing/healing temperature), hydraulic (i.e., drainage condition), mechanical (i.e., different crack-inducing stresses), chemical (i.e., sulphate content), as well as addition of mineral additives (i.e., BFS and FA), was performed to provide a comprehensive understanding of the autogenous self-healing performance and the evolution of the healing efficiency through the observations of crack closure, mechanical properties recovery, permeability property recovery, assessments of physical and microstructural properties changes, and characteristics of self-healing products. Additionally, a type of natural tailings was incorporated into the preparation of CPB specimens to introduce practical challenges from natural variability in tailings, reflecting the autogenous self-healing behaviour in realistic formulations of CPB applications. Finally, the promising autogenous self-healing capability was demonstrated in the CPB materials. The findings provide important practical implications for the design and maintenance of the stability and durability of CPB structures. The following conclusions can be drawn from the obtained results.

- CPBs demonstrate promising autogenous self-healing behaviour in the restoration of mechanical and permeability properties through two primary mechanisms: continued hydration of unhydrated cement particles and carbonation of calcium hydroxide. Continued hydration predominantly facilitates crack closure within the internal matrix, while carbonation mainly contributes to surface crack closure. The primary identified self-healing products include C-S-H, ettringite, calcite, and calcium hydroxide, with the relative quantities of each varying according to the healing conditions.
- Three distinct crack healing scenarios are observed, including complete healing, partial healing, and no healing, which are highly dependent on the availability of self-healing products and the crack geometry. Partial and no healing scenarios reflect the intrinsic limitations of autogenous self-healing in the CPB matrix, where the cement content plays a critical role in determining the maximum achievable healing capacity.
- Younger CPBs, in which cracks form at early ages, exhibit more pronounced autogenous healing capability due to the higher content of unhydrated cement particles, indicating a greater potential for autogenous self-healing.
- The generation of cracks initially compromises the mechanical strength and increases the permeability of the CPB matrix. During the self-healing phase, the crack network provides the pathways facilitating the ingress of carbon dioxide and evaporation of excessive water within

the CPB matrix, which in turn promotes the carbonation and cement hydration processes, thereby benefiting the self-healing mechanisms.

- Healing/curing temperatures have a significant impact on the autogenous healing efficiency of CPBs. Elevated temperatures up to 50 °C, as examined in this study, accelerate cement hydration, resulting in the formation of a greater quantity of self-healing products within the same self-healing period and shortening the overall healing duration. Conversely, low temperatures, such as 2 °C, substantially delay and diminish the self-healing performance by inhibiting cement hydration and limiting the production of self-healing products.
- Drainage of excessive water from the CPB matrix significantly enhances the self-healing efficiency. The drainage process delivers a promoted evolution of microstructural refinement ascribed to the rearrangement of solids, which results in the matrix densification with reduced total porosity and increases the contact surface area, benefiting the continued cement hydration. Coupled with the lowered w/c ratio resulting from excess water drainage, the self-healing processes are significantly improved with faster reaction and precipitation of healing products, achieving more efficient recovery.
- Sulphate exerts dual impacts on the autogenous self-healing behaviour, depending on the sulphate concentration and self-healing period, which governs the formation of secondary expansive hydrated minerals (i.e., ettringite and gypsum) and cement hydration products in the sulphate-CPB system. CPB specimens with 5,000 ppm sulphate concentration perform consistently positive self-healing behaviour through the entire studied self-healing period up to 90 days, attributed to the absence of inhibition effect and production of an adequate amount of secondary hydrates. In contrast, highly sulfated specimens (i.e., 25,000 and 15,000 ppm) demonstrate initially enhanced self-healing efficiency during the first 28 days, followed by an opposite performance during the 90 days of the self-healing period. The negative effect is associated with i) physical damage (new cracks) due to the formation of excessive amounts of expansive minerals, ii) production of weaker C-S-H gels because of sulphate absorption by C-S-H, and iii) reduced amount of hydration products due to inhibition of cement hydration at high sulphate concentrations.
- The CPB specimens pre-cracked under uniaxial compression, triaxial compression, and indirect tensile loading exhibit mixed tensile-shear, predominantly shear, and pure tensile crack patterns, respectively. The synergy between the induced crack morphology within the matrix and chemical self-healing reactions (i.e., continued cement hydration and carbonation) emerges as a critical factor underlying the observed self-healing efficiency. Specimens subjected to uniaxial compression and triaxial compression loading show comparably promising self-healing efficiencies. The partially closed and narrow aperture shear cracks allow the self-healing products to fill cavities more efficiently and promote the direct contact between the rough crack surfaces compared to large tensile cracks, generating additional resistance from friction and benefiting the healing efficiency. In contrast, in disc-shaped specimens subjected to indirect tensile loading, the traverse tensile cracks compromise structural integrity, resulting

in largely unclosed and mechanically disconnected cracks after healing, which leads to inferior self-healing efficiency.

- The incorporation of SCMs, including BFS and FA, affects the self-healing performance of the CPB system through their contributions to binder hydration mechanisms and microstructural modifications, which depend on their chemical reactivity and physical characteristics. Appropriate dosages of BFS (e.g., PCI/BFS:80/20 and PCI/BFS:50/50) promote the self-healing efficiency compared to the PCI-only CPB system at early or long-term self-healing period via secondary latent hydraulic reactions between BFS and calcium hydroxide, and the associated microstructural densification. However, excessive replacement of PCI (e.g., PCI/BFS:20/80) limits the available cement within the matrix, constraining the primary self-healing mechanisms.
- The incorporation of FA substantially undermines the self-healing capacity of the PCI/FA system, with only the PCI/FA:80/20 specimens exhibiting relatively satisfactory healing performance, whereas increasing the FA proportion leads to inferior self-healing due to the combined effects of dormant pozzolanic reactivity, dilution of cement content, and inherent physical characteristics of FA.
- Autogenous self-healing can generally restore the mechanical properties of the studied CPB matrices after the self-healing period of 7 or 28 days, with further strength improvement observed after 90 days under specific healing conditions, mainly attributed to the enhanced binder hydrations, which strengthen the matrix and improve interparticle bonding. However, complete restoration of permeability (hydraulic conductivity) is rarely achieved through an autogenous self-healing process, as the limited binder content constrains the quantity of self-healing products available to fill all micro- and macro-cracks.
- By considering and integrating the autogenous self-healing, the durability, stability, and resilience of the designed CPB can be significantly enhanced, contributing to safer, more cost-effective, and sustainable mining practices. Furthermore, the self-healing property is able to favour the environmental performance by minimizing leaching and contamination risks associated with cracked backfill structures.

8.2 Research Limitations and Recommendations for Future Studies

Based on the findings of this research, the following recommendations are proposed for further investigation.

- The CPB structure is exposed to various conditions once placed underground, which is directly related to the healing conditions during the self-healing phase. Since a single healing exposure condition was adopted in this study, future investigations should broaden the scope to various exposure conditions representative of field application, such as wet/dry cycles, freeze/thaw cycles, healing under stresses, etc.

- The synergistic effects among THMC factors, such as coupled chemical-thermal, hydro-mechanical, and other interactions, could be further investigated to improve the understanding of their interactive impacts on the healing performance of CPB.
- It would be beneficial to link the crack geometry/damage from various pre-cracking levels to the corresponding self-healing efficiencies, which could favour the prediction of recovery of the properties.
- The selection of mineral additives should be based on each specific tailings/slurry. The effects of the incorporation of BFS and FA on the self-healing efficiency are not fully revealed, and future studies could adopt the external CH supply and a more extended self-healing period to maximize the latent hydraulic potential of BFS and the pozzolanic activity of FA on the healing.
- Non-destructive techniques, such as ultrasonic pulse velocity or resonant frequency testing, could be explored in future studies to monitor the progression of self-healing within the same specimens over multiple self-healing periods.
- As tailings characterization varies between mines, it is essential to conduct laboratory testing for site-specific backfill formulations. Future research should incorporate a broader range of mine tailings with different characteristics to extend these findings to diverse field conditions.
- Given the limitation of the autogenous self-healing capacity in CPB, an autonomous healing method can be incorporated by externally adding healing agents, such as superabsorbent polymers, nanomaterials, etc., to explore their potential contributions to enhance the healing efficiency.